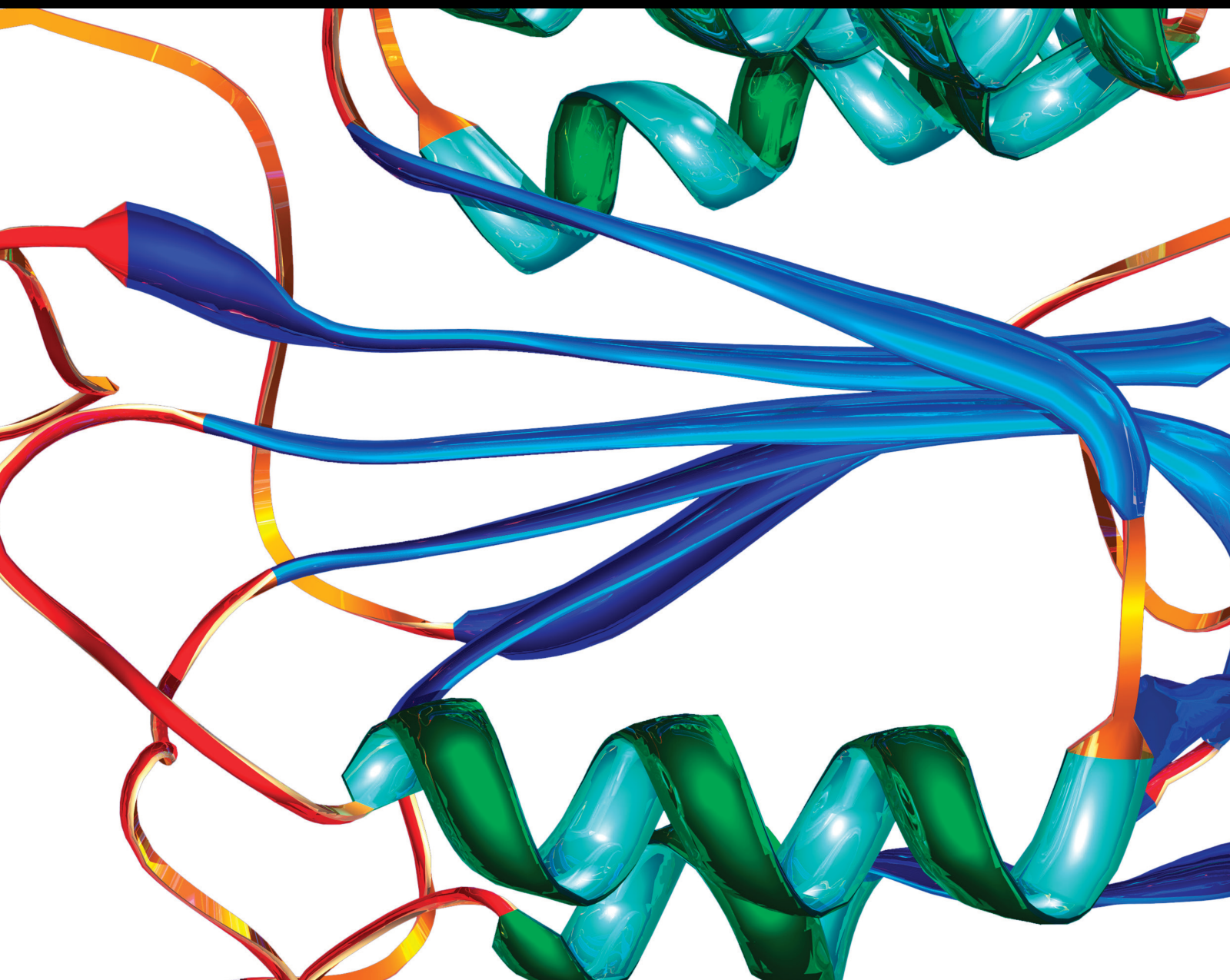


Disease Markers

Forensic and Clinical Applications of Biomarkers of Cardiovascular Disease

Lead Guest Editor: Francesco Busardò

Guest Editors: Simona Pichini





Forensic and Clinical Applications of Biomarkers of Cardiovascular Disease

Disease Markers

Forensic and Clinical Applications of Biomarkers of Cardiovascular Disease

Lead Guest Editor: Francesco Busardò

Guest Editors: Simona Pichini



Copyright © 2022 Hindawi Limited. All rights reserved.

This is a special issue published in "Disease Markers." All articles are open access articles distributed under the Creative Commons Attribution License, which permits unrestricted use, distribution, and reproduction in any medium, provided the original work is properly cited.

Chief Editor

Paola Gazzaniga, Italy

Associate Editors


Donald H. Chace , USA
Mariann Harangi, Hungary
Hubertus Himmerich , United Kingdom
Yi-Chia Huang , Taiwan
Giuseppe Murdaca , Italy
Irene Rebelo , Portugal

Academic Editors

Muhammad Abdel Ghafar, Egypt
George Agrogiannis, Greece
Mojgan Alaeddini, Iran
Atif Ali Hashmi , Pakistan
Cornelia Amalinei , Romania
Pasquale Ambrosino , Italy
Paul Ashwood, USA
Faryal Mehwish Awan , Pakistan
Atif Baig , Malaysia
Valeria Barresi , Italy
Lalit Batra , USA
Francesca Belardinilli, Italy
Elisa Belluzzi , Italy
Laura Bergantini , Italy
Sourav Bhattacharya, USA
Anna Birková , Slovakia
Giulia Bivona , Italy
Luisella Bocchio-Chiavetto , Italy
Francesco Paolo Busardó , Italy
Andrea Cabrera-Pastor , Spain
Paolo Cameli , Italy
Chiara Caselli , Italy
Jin Chai, China
Qixing Chen, China
Shaoqiu Chen, USA
Xiangmei Chen, China
Carlo Chiarla , Italy
Marcello Ciaccio , Italy
Luciano Colangelo , Italy
Alexandru Corlateanu, Moldova
Miriana D'Alessandro , Saint Vincent and the Grenadines
Waaqo B. Daddacha, USA
Xi-jian Dai , China
Maria Dalamaga , Greece


Serena Del Turco , Italy
Jiang Du, USA
Xing Du , China
Benoit Dugue , France
Paulina Dumnicka , Poland
Nashwa El-Khazragy , Egypt
Zhe Fan , China
Rudy Foddis, Italy
Serena Fragiotta , Italy
Helge Frieling , Germany
Alain J. Gelibter, Italy
Matteo Giulietti , Italy
Damjan Glavač , Slovenia
Alvaro González , Spain
Rohit Gundamaraju, USA
Emilia Hadziyannis , Greece
Michael Hawkes, Canada
Shih-Ping Hsu , Taiwan
Menghao Huang , USA
Shu-Hong Huang , China
Xuan Huang , China
Ding-Sheng Jiang , China
Esteban Jorge Galarza , Mexico
Mohamed Gomaa Kamel, Japan
Michalis V. Karamouzis, Greece
Muhammad Babar Khawar, Pakistan
Young-Kug Kim , Republic of Korea
Mallikarjuna Korivi , China
Arun Kumar , India
Jinan Li , USA
Peng-fei Li , China
Yiping Li , China
Michael Lichtenauer , Austria
Daniela Ligi, Italy
Hui Liu, China
Jin-Hui Liu, China
Ying Liu , USA
Zhengwen Liu , China
César López-Camarillo, Mexico
Xin Luo , USA
Zhiwen Luo, China
Valentina Magri, Italy
Michele Malaguarnera , Italy
Erminia Manfrin , Italy
Utpender Manne, USA


Alexander G. Mathioudakis, United Kingdom


Andrea Maugeri , Italy

Prasenjit Mitra , India

Ekansh Mittal , USA

Hiroshi Miyamoto , USA

Naoshad Muhammad , USA

Chiara Nicolazzo , Italy

Xing Niu , China

Dong Pan , USA

Dr.Krupakar Parthasarathy, India

Robert Pichler , Austria

Dimitri Poddighe , Kazakhstan

Roberta Rizzo , Italy


Maddalena Ruggieri, Italy

Tamal Sadhukhan, USA


Pier P. Sainaghi , Italy


Cristian Scheau, Romania


Jens-Christian Schewe, Germany

Alexandra Scholze , Denmark

Shabana , Pakistan

Anja Hviid Simonsen , Denmark

Eric A. Singer , USA

Daniele Sola , Italy


Timo Sorsa , Finland


Yaying Sun , China

Mohammad Tarique , USA

Jayaraman Tharmalingam, USA


Sowjanya Thatikonda , USA

Stamatios E. Theocharis , Greece

Tilman Todenhöfer , Germany

Anil Tomar, India

Alok Tripathi, India

Drenka Trivanović , Germany

Natacha Turck , Switzerland

Azizah Ugusman , Malaysia

Shailendra K. Verma, USA

Aristidis S. Veskoukis, Greece

Arianna Vignini, Italy

Jincheng Wang, Japan


Zhongqiu Xie, USA


Yuzhen Xu, China

Zhijie Xu , China


Guan-Jun Yang , China

Yan Yang , USA

Chengwu Zeng , China

Jun Zhang Zhang , USA

Qun Zhang, China








Changli Zhou , USA

Heng Zhou , China



Jian-Guo Zhou, China

Contents

MicroRNA-146: Biomarker and Mediator of Cardiovascular Disease

Fatemeh Sadat Mahdavi , Shayan Mardi , Sareh Mohammadi , Sarina Ansari , Somayeh Yaslianifard , Parviz Fallah , and Sayed-Hamidreza Mozhgani 
Review Article (13 pages), Article ID 7767598, Volume 2022 (2022)

Neutrophil to Lymphocyte Ratio as a Biomarker for Predicting the Coronary Artery Abnormality in Kawasaki Disease: A Meta-Analysis

Shirin Sarejloo, Matin Moallem Shahri, Pouria Azami, Alec Clark, Ethan Hass, Maryam Salimi , Brandon Lucke-Wold, Shahram Sadeghvand, and Shokoufeh Khanzadeh 
Review Article (11 pages), Article ID 6421543, Volume 2022 (2022)



Investigation of Statin Medication Use in Elderly Patients with Cardiovascular Disease on Regular Physical Examination and the Relationship with Glucolipid Metabolism and Adverse Cardiovascular Prognosis

Chang Liu, Rui Ma, Daifeng Gao, Bin Hu, Xiaolei Yin, Zhipeng Liu, Hu Lin , and Zhenhua Zhang 
Research Article (5 pages), Article ID 8714392, Volume 2022 (2022)




Diagnostic and Prognostic Significance of microRNA-208a in Acute Myocardial Infarction

Sheng Chen, Xin Hong, Yong Wu , and Ziguo Chen 
Research Article (8 pages), Article ID 7030722, Volume 2022 (2022)

The ceRNA Crosstalk between mRNAs and lncRNAs in Diabetes Myocardial Infarction

Yun Zhou , Chengjun Zhou, Lilong Wei, Chengwu Han, and Yongtong Cao 
Research Article (12 pages), Article ID 4283534, Volume 2022 (2022)

Targeting Circulating lncRNA ENST00000538705.1 Relieves Acute Coronary Syndrome via Modulating ALOX15

Hao Chen , Shiwei Huang, Fanlu Guan, Sisi Han, Fanhao Ye, Xun Li , and Liyi You 
Research Article (24 pages), Article ID 8208471, Volume 2022 (2022)

Knockdown of ILK Alleviates High Glucose-Induced Damage of H9C2 Cells through TLR4/MyD88/NF- κ B Pathway

Qiang Yin, Zhendong Li, and Shaoying Lu 
Research Article (9 pages), Article ID 6205190, Volume 2022 (2022)

Association between Cystatin C and Cardiac Function in Acute Myocardial Infarction Patients: A Real-World Analysis

Bowen Lou , Yongbai Luo, Haoxuan Zhang, Haoyu Wu, Gulinigaer Tuerhong Jiang, Hui Liu, Kejia Kan, Xiang Hao, Lizhe Sun, Zuyi Yuan , and Jianqing She 
Research Article (12 pages), Article ID 7267937, Volume 2022 (2022)




The Relationship between Intracarotid Plaque Neovascularization and Lp (a) and Lp-PLA2 in Elderly Patients with Carotid Plaque Stenosis

Chang Sun , Na Xi, Zhijun Sun, Xinxin Zhang, Xiaowei Wang, Huiyang Cao, and Xiaowei Jia 
Research Article (6 pages), Article ID 6154675, Volume 2022 (2022)


Paraoxonase-1 (PON-1) Arylesterase Activity Levels in Patients with Coronary Artery Disease: A Meta-Analysis

Marco Zuin , Alessandro Trentini , Judit Marsillach , Andrea D'Amuri , Cristina Bosi , Loris Roncon , Angelina Passaro , Giovanni Zuliani , Mike Mackness , and Carlo Cervellati 
Research Article (9 pages), Article ID 4264314, Volume 2022 (2022)


Pyroptosis Patterns Are Involved in Immune Microenvironment Regulation of Dilated Cardiomyopathy

Kexin Wang , Zhan Lv, Chenggang Fang, Chengkai Xu, Zhimin Yu , Liuming Gao, and Yanggan Wang 
Research Article (15 pages), Article ID 4627845, Volume 2022 (2022)



Ferroptosis-Specific Inhibitor Ferrostatin-1 Relieves H₂O₂-Induced Redox Imbalance in Primary Cardiomyocytes through the Nrf2/ARE Pathway

Chaofeng Sun, Fang Peng, Jianfei Li, Xudong Cui, Xin Qiao, and Wangliang Zhu 
Research Article (10 pages), Article ID 4539932, Volume 2022 (2022)


LINC00460 Stimulates the Proliferation of Vascular Endothelial Cells by Downregulating miRNA-24-3p

Ruofei Jia, Xingxing Yuan, Chengzhi Yang, Jing Han, Xiaojing Cao, Zheng Qin, Jing Nan, and Zening Jin 
Research Article (7 pages), Article ID 2524156, Volume 2022 (2022)


Effects of Escin on Oxidative Stress and Apoptosis of H9c2 Cells Induced by H₂O₂

Peng Qiao, Baokun Zhang, Xueni Liu , Jie Xu, and Xuehan Li 
Research Article (12 pages), Article ID 7765353, Volume 2022 (2022)

lncRNA ROR and miR-125b Predict the Prognosis in Heart Failure Combined Acute Renal Failure

Qianlong Xue, Lipeng Yang, Jia Wang, Linlin Li, Hui Wang, and Ying He 
Research Article (6 pages), Article ID 6853939, Volume 2022 (2022)

Death-Associated Protein Kinase 1 (DAPK1) Protects against Myocardial Injury Induced by Myocardial Infarction in Rats via Inhibition of Inflammation and Oxidative Stress

Jun Zhang , Jing Zhang, Bo Zhou, Xiaojing Jiang, Yanrong Tang, and Zhenzhen Zhang
Research Article (14 pages), Article ID 9651092, Volume 2022 (2022)

Genetic Polymorphism of Matrix Metalloproteinase-9 and Susceptibility to Myocardial Infarction: A Meta-Analysis


Beili Feng and Hengdong Li 
Research Article (8 pages), Article ID 5507153, Volume 2022 (2022)

Simvastatin Improves Myocardial Ischemia Reperfusion Injury through KLF-Regulated Alleviation of Inflammation


Tingju Wei, Jun Li, Guowei Fu, Hui Zhao, Chen Huang, Xiaohua Zhu, Gongcheng Huang, and Jing Xu 
Research Article (6 pages), Article ID 7878602, Volume 2022 (2022)

Contents


Valsartan Regulates PI3K/AKT Pathways through lncRNA GASL1 to Improve Isoproterenol-Induced Heart Failure

Jian Zhou, Xiujuan Duan, Jibing Wang, Yunhong Feng, and Jiangyong Yuan 
Research Article (8 pages), Article ID 1447399, Volume 2022 (2022)


Potential Effects of Metformin on the Vitality, Invasion, and Migration of Human Vascular Smooth Muscle Cells via Downregulating lncRNA-ATB

Wei Jia, Yue Zhou, Lina Sun, Jianlong Liu, Zhiyuan Cheng, and Shuofang Zhao 
Research Article (8 pages), Article ID 7480199, Volume 2022 (2022)


MiR-218 Promotes Adriamycin-Induced H9C2 Apoptosis by Inhibiting Stress-Associated Endoplasmic Reticulum Protein 1

Qinghua Chen, Gang Chen, and Shuofang Zhao 
Research Article (10 pages), Article ID 6881103, Volume 2022 (2022)


Relationship between Expression of Plasma lncRNA-HEIH and Prognosis in Patients with Coronary Artery Disease

Zhenying Zhang, Sushuang Nan, Xiujuan Duan, Lizhong Wang, Xiaojing Sun, and Haiying Zheng 
Research Article (5 pages), Article ID 5662080, Volume 2021 (2021)


Effects of Long Noncoding RNA HOTAIR Targeting miR-138 on Inflammatory Response and Oxidative Stress in Rat Cardiomyocytes Induced by Hypoxia and Reoxygenation

Guofeng Wang , Qi Wang, and Weixue Xu
Research Article (11 pages), Article ID 4273274, Volume 2021 (2021)


Serum Levels of lncRNA CCHE1 and TCF21 in Patients with Coronary Artery Disease and Their Clinical Significances

Miaomiao Liu , Ying Zhang, Xiantong Cao, and Xue Wang
Research Article (6 pages), Article ID 8526144, Volume 2021 (2021)



miRNA-19b-3p Stimulates Cardiomyocyte Apoptosis Induced by Myocardial Ischemia Reperfusion via Downregulating PTEN

Ke Li, Xujie Ya, Xiujuan Duan, Yang Li, and Xuefeng Lin 
Research Article (7 pages), Article ID 9956666, Volume 2021 (2021)


miRNA-576 Alleviates the Malignant Progression of Atherosclerosis through Downregulating KLF5

Jing Wang, Lihui Zhang, Ting Wang, Caige Li, Lijing Jiao, Zhansheng Zhao, and Yongjun Li 
Research Article (8 pages), Article ID 5450685, Volume 2021 (2021)

Cox-2 Antagonizes the Protective Effect of Sevoflurane on Hypoxia/Reoxygenation-Induced Cardiomyocyte Apoptosis through Inhibiting the Akt Pathway


Chunyan Guo, Lei Zhang, Yaoxing Gao, Junzhi Sun, Lingling Fan, Yuguang Bai, Jing Zhang, Gaowa Naren, Jiwen Yang , and Libiao Li 
Research Article (6 pages), Article ID 4114593, Volume 2021 (2021)

MicroRNA-146-5p Promotes Pulmonary Artery Endothelial Cell Proliferation under Hypoxic Conditions through Regulating USP3

Wei Zhang , Yujuan Qi, and Bo Wu


Research Article (8 pages), Article ID 3668422, Volume 2021 (2021)

MicroRNA-383-5p Regulates Oxidative Stress in Mice with Acute Myocardial Infarction through the AMPK Signaling Pathway via PFKM

Linlin Gao, Zhongbao Ruan, and Gecai Chen 


Research Article (9 pages), Article ID 8587535, Volume 2021 (2021)

Protective Effect of Fasudil on Hydrogen Peroxide-Induced Oxidative Stress Injury of H9C2 Cardiomyocytes

Yu Zhang , Shanxin Liu, Xiaochun Li, and Jian Ye

Research Article (9 pages), Article ID 8177705, Volume 2021 (2021)

Regulatory Mechanism of LINC00152 on Aggravating Heart Failure through Triggering Fibrosis in an Infarcted Myocardium

Lizhong Song, Xiujuan Duan, Xiaojuan Zeng, Xinglian Duan, and Li Li 


Research Article (7 pages), Article ID 2607358, Volume 2021 (2021)

Tanshinone IIA Improves Ventricular Remodeling following Cardiac Infarction by Regulating miR-205-3p

Peng Qiao, Jie Xu, Xueni Liu, and Xuehan Li 


Research Article (6 pages), Article ID 8740831, Volume 2021 (2021)

N-Acetylcysteine Slows Down Cardiac Pathological Remodeling by Inhibiting Cardiac Fibroblast Proliferation and Collagen Synthesis

Jin Zhou, Jing Xu, Shan Sun, Mengyuan Guo, Peng Li, and Aijuan Cheng 


Research Article (10 pages), Article ID 3625662, Volume 2021 (2021)

miR-190-5p Alleviates Myocardial Ischemia-Reperfusion Injury by Targeting PHLPP1

Yangxue Li, Zhibo Li, Jiagen Liu, Yihang Liu, and Guobin Miao 


Research Article (11 pages), Article ID 8709298, Volume 2021 (2021)

RRM2 Improves Cardiomyocyte Proliferation after Myocardial Ischemia Reperfusion Injury through the Hippo-YAP Pathway

Huamin Yu, Haiyan Tang, Chaochao Deng, Qing Lin, Peng Yu, Shaowen Chen, and Jingming Ruan 

Research Article (10 pages), Article ID 5089872, Volume 2021 (2021)








FOXC2 Alleviates Myocardial Ischemia-Reperfusion Injury in Rats through Regulating Nrf2/HO-1 Signaling Pathway

Rui Wang , Yonggang Wu, and Shoutao Jiang

Research Article (9 pages), Article ID 9628521, Volume 2021 (2021)

Review Article

MicroRNA-146: Biomarker and Mediator of Cardiovascular Disease

Fatemeh Sadat Mahdavi ¹, Shayan Mardi ¹, Sareh Mohammadi ², Sarina Ansari ¹,
Somayeh Yaslianifard ³, Parviz Fallah ⁴, and Sayed-Hamidreza Mozhgani ^{3,5}

¹Student Research Committee, School of Medicine, Alborz University of Medical Sciences, Karaj, Iran

²Cardiovascular Research Center, Alborz University of Medical Sciences, Karaj, Iran

³Department of Microbiology, School of Medicine, Alborz University of Medical Sciences, Karaj, Iran

⁴Department of Laboratory Science, School of Allied Medicine, Alborz University of Medical Sciences, Karaj, Iran

⁵Noncommunicable Disease Research Center, Alborz University of Medical Sciences, Karaj, Iran

Correspondence should be addressed to Sayed-Hamidreza Mozhgani; hamidrezamozhgani@gmail.com

Received 17 February 2022; Accepted 15 September 2022; Published 11 October 2022

Academic Editor: Simona Pichini

Copyright © 2022 Fatemeh Sadat Mahdavi et al. This is an open access article distributed under the Creative Commons Attribution License, which permits unrestricted use, distribution, and reproduction in any medium, provided the original work is properly cited.

Cardiovascular diseases (CVDs) are the prime cause of morbidity and mortality worldwide. Although noticeable progress has been made in the diagnosis, prognosis, and treatment, there is still a critical demand for new diagnostic biomarkers and novel therapeutic interventions to reduce this disease incidence. Many investigations have been conducted on the regulatory effects of microRNAs in cardiovascular diseases. miRNA circulating serum level changes are correlated with several CVDs. In addition, there is growing evidence representing the potential role of miRNAs as diagnostic biomarkers or potential therapeutic targets for CVD. Preliminary studies identified the prominent role of miR-146 in host defense, innate immunity, and different immunological diseases by regulating cytokine production and innate immunity modification in bacterial infections. However, more recently, it was also associated with CVD development. miR-146 has received much attention, with positive results in most studies. Research demonstrated the crucial role of this molecule in the pathogenesis of cardiac disease and related mechanisms. As a result, many potential applications of miR-146 are expected. In this paper, we provide an overview of recent studies highlighting the role of miR-146 in CVD, focusing on CAD (coronary artery disease), cardiomyopathy, and MI (myocardial infarction) in particular and discussing its current scientific state, and use a prognostic biomarker as a therapeutic agent for cardiovascular diseases.

1. Introduction

Despite significant advances and improvements in preventive care, diagnostic tools, and treatments, cardiovascular diseases (CVDs) are still a significant cause of mortality and morbidity. They have imposed a significant burden on the health care system [1]. CVD consists of various disorders associated with cardiomyocytes, conduction system of the heart, coronary artery diseases (CAD), and congenital disabilities [2]. As a subtype of CAD, myocar-

dial infarction is the necrosis of the myocardium, secondary to the prolonged lack of oxygen supply [3–5].

The occurrence and progression of CVD usually result from many risk factors, including genetic, epigenetic, and environmental factors. Eight WHO's targeted risk factors for reduction by 2025 are smoking, hypertension, diabetes, dyslipidemia, obesity, diet, alcohol, and sedentary lifestyle [6, 7]. According to the high mortality and disability rate of CVD, better knowledge of risk factors would probably help us quickly detect those with an increased risk of CVD

development and improve patient outcomes and survival. In attempts to diagnose and treat CVD early, noncoding RNAs (ncRNAs) have recently attracted more attention [8, 9].

The role of miR-146 in host defense, innate immunity, and immunological diseases has been mentioned by various researchers. It links the innate immune to oncogenic transformation and is involved in inflammation, innate immunity, and cancer. For example, downregulation of miR-146b in lung cancer [10], increased expression of miR-146a/b in metastatic human breast cancer cells [11], and mitochondrial functions regulation have been reported earlier.

miR-146 plays a central role in many inflammatory processes [12]. Studies showed that *in vitro* treatment of miR-146a may induce the expression of proinflammatory factors such as TNF- α , NF- κ B p65, and MCP-1, which are essential transcription factors in atherosclerosis [13]. Palomer et al. showed critical functions in miR-146a in myocardial dysfunction and progression of HF. miR-146a suppresses MMP-9 by affecting *c-Fos* and decreasing the *c-Fos/AP-1* pathway [14]. As shown in Figure 1, through its inhibitory effect on TLR4, miR-146 decreases AP-1 in the cell nucleus, diminishes cytokine production, and suppresses inflammation. In most cardiac diseases, inflammation leads to the death of cardiomyocytes and reduced cardiac contraction capacity [15]. In this condition, the tissue level of miR-146 is increased to suppress the inflammation through negative autoregulation. Various research were conducted according to these mechanisms to determine the diagnostic capacity of these biomarkers.

A study by Oerlemans et al. on the serum level of miR-146 in ACS patients showed that the serum level of this biomarker had significantly increased in non-ST segment elevation MI (NSTEMI) and unstable angina compared to non-ACS patients. Moreover, the serum level of miR-146 is higher in NSTEMI patients than in unstable angina patients [16]. Furthermore, Arroyo et al.'s study showed that the miRNA was effective on ACS in AF (atrial fibrillation) through neutrophil extracellular trap formation [17].

As it is evident, pharmacological inhibition of TNF- α promotes the function of myocardium cells during HF [18]. Studies reported the elevation of miR-146a transcript levels in the ventricular tissue of transgenic mice, with specific TNF- α overexpression in the myocardium and a human origin cardiomyocyte cell line (AC16) exposed to TNF- α . Target genes of miR-146a were remarkably reduced after miR-146a overexpression or TNF- α treatment [14]. Also, *in vivo* studies using a lentivirus expressing miR-146a (LmiR-146a) have shown that miR-146a is essential in preventing sepsis-induced NF- κ B signaling and the generation of inflammatory cytokines as well as the inhibition of IRAK and TRAF6 expression in the myocardium. Therefore, it leads to heart dysfunction secondary to sepsis [19], indicating the role of miR-146a as a novel therapeutic tool in inflammatory-associated cardiac disorders [14]. However, studies have not proven the diagnostic value of this marker [20].

Numerous studies have been conducted on miR-146 genotypes and their relationship with different diseases

[21–23]. For example, Chen et al. showed an enormous increase in MI and other CADs risk by the CC genotype [24]. In contrast, further research demonstrates the association of miR-146a rs2910164 C>G genotype and low ACS risk [25]. These results depend highly on the study population, and studying in new communities can lead to different outcomes. A study by Kim et al. on hypertensive patients and the GG genotype control group demonstrated a significant association of miR-146a C>G genotype distributions with this disease [25]. Another polymorphism of this miRNA is rs2431697. Studies on CAD patients have shown that the wild type of rs2910164 and mutant type of rs2431697 are more frequent [26].

The association of ischemic stroke and mentioned polymorphisms has also been discussed separately. For example, Zhu et al. stated that the risk of ischemic stroke might increase by miR-149 T>C and miR-146a C>G polymorphisms, which might be mainly associated with an increased risk of large artery atherosclerosis stroke [27]. Zha et al. examined the allele frequencies and stated a significant association between the genotype and allele frequency of the miR-146a gene loci rs2910164 G/C and rs57095329 A/G. Also, they suggest that genotype GG of rs2910164 G/C and allele A of rs57095329 A/G are risk factors for coronary artery lesions [28].

No previous published literature has brought together the role of miR-146 on each type of CVD. In the current review, the most recent studies have been discussed, highlighting the role of miR-146 in CVD, focusing on CAD, cardiomyopathy, and MI in particular, and providing an overview of its current scientific state and use as a prognostic biomarker as well as a therapeutic agent for cardiovascular diseases. Therefore, we provide a comprehensive conclusion of the potential role of miR-146 and its relevance to different types of CVD to fill the gaps in previous studies.

In order to perform a comparative study on the effect of miR-146 on heart diseases, PubMed, the Institute for Scientific Information (ISI), Scopus, and EMBASE were searched using the following keywords:

))))))hsa-mir-146) OR miR-146, human) OR microRNA-146, human) OR hsa-mir-146b) OR hsa-mir-146a) AND (((((Heart failure) OR Cardiomyopathy) OR Myocardial infarction) OR Coronary artery diseases).

Articles were screened by title, abstract, and, eventually, the main text. Cross-sectional studies reporting descriptive data in English were included. The retrieval literature publication date was before Jan 24, 2022. The analysis did not include review articles, opinion pieces, or letters that did not include original data. The following information was extracted from each study: the authors, year, type of disease, microRNA subtype, clinical appliance, study design, study size, and source tissue. Finally, a total of 43 eligible articles were selected for further consideration.

2. Acute Myocardial Infarction

Although the acute myocardial infarction (AMI) diagnosis is made with an overview of the patient's history, symptoms, signs, ECG, and physical examination, cardiac biomarkers

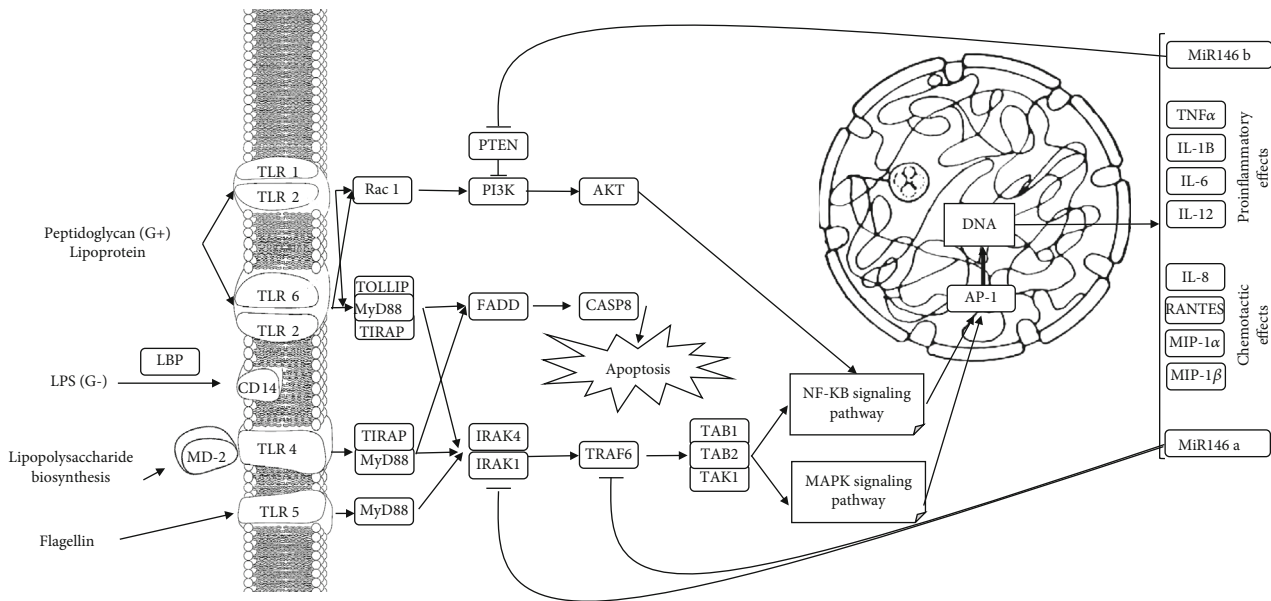


FIGURE 1: By identifying inflammatory molecules, a cascade of intermediate molecules is created, and depending on the type of activated receptor, the cell may become apoptotic or produce proinflammatory and chemotactic molecules. Inflammatory molecules activate both the MAPK signaling and NF- κ B signaling pathways, eventually increasing the production of inflammatory and chemotactic interleukins by affecting DNA. As shown, miR-146a and miR-146b exhibit their anti-inflammatory properties in relatively different pathways.

are still an essential diagnostic factor in AMI cases [29]. Troponin and its two isoforms, I and T, are widely used as specific lab tests to diagnose the disease. Research has shown that, despite this test's high specificity for myocardial injury, troponin isoforms are not highly sensitive. Also, troponin measurements in patients with STEMI are not of immediate value, and the treatment plan should still be based on a rapid troponin check, the patient's clinical symptoms, and ECG.

Studies suggest new promising biomarkers for AMI diagnosis, one of which is miRNAs [30] (Table 1). Although miR-146 plays a significant role in cardiac diseases, studies on the diagnostic value of this marker have not been promising. Xue et al. showed that circulating miR-146a can be used as biomarkers for AMI diagnosis [31]. In contrast, Corsten et al. stated that the detectable release of microRNA-208b and microRNA-499 has been seen in cardiac damage, but no significant elevation in plasma levels of miR-146 has been seen in AMI patients [20]. Also, the results of a study by Bukauskas et al. showed that although plasma levels of miR-146a-5p in STEMI patients were 4.048-fold lower than the control group, the AUC of this microRNA is less than 0.8 and is classified as a fair predictor [32].

The different results of the above studies are probably due to different methods. In the study of Xue et al., blood samples were taken from all patients in the first 4 hours, including 14 patients with STEMI and 17 with NSTEMI.

Treatment of AMI is based on two general pillars, reducing the load on the heart and restoring blood flow to the infarcted area. Despite the positive results of emergency reperfusion, this leads to the spread of inflammatory molecules throughout the heart muscle, apoptosis of myocardial cells, and thus an increase in the size of the infarct location. Nowadays, there are several approaches to controlling MI-induced I/R injury, including inhibiting leukocyte accumula-

tion, complement inhibition (e.g., pexelizumab), and inhibition of mPTP. Unfortunately, none of the available methods can completely prevent I/R injury [33]. In 2015, Liu et al. showed that cells exposed to inflammation attempted to reduce neutrophil activity and suppress inflammation by increasing the secretion of miR-146a. The results of this study identify miR-146a as a prognostic and therapeutic target in myocardial I/R injury [34].

On the other hand, Shu et al. showed that Troxerutin could significantly control myocardial ischemia or reperfusion injury by inhibiting miR-146a-5p [35]. Due to study limitations and the fact that all studies have been limited to animal and cellular research, the need for more extensive research in clinical settings is strongly felt. Considering the role of miR-146a in the liver and renal I/R injury and the results of the mentioned articles, the prognostic and therapeutic use of this microRNA in managing this condition will probably be adequate.

A critical cause of death due to AMI is various complications such as left ventricular remodeling (LVR) or ventricular rupture. Studies have shown that the main mechanisms involved in causing these complications are immune pathways such as TLR and NF- κ B-mediated pathways, and due to the regulatory role of miR-146 on these pathways (Figure 1), different studies have been done in this regard. For example, Zhao et al. reported that miR-146b mediated vascular inflammation and apoptosis in MI patients [36].

The most critical steps in managing left ventricular remodeling (LVR) patients are determining prognosis and preventive measures by blood volume management and administering angiotensin-converting enzyme (ACE) inhibitors and vasodilators such as NO to prevent cardiovascular events such as cardiogenic shock [37]. So far, several factors have been suggested for determining prognosis, including C-

TABLE 1: Descriptive overview of the data extracted from the reviewed studies on the diagnostic application of miR-146a on cardiovascular disease.

Author	Year	Disease	Study design	Participant	Tissue source	Method	MicroRNA	Result	Reference
Oerlemans et al.	2012	ACS	Case-control	332	Serum	QRT-PCR	miR-146a	↑	[16]
Corsten et al.	2010	MI	Case-control	68	Plasma	QRT-PCR	miR-146	—	[20]
Xue et al.	2019	AMI	Case-control	58	Blood	QRT-PCR	miR-146a	↑	[31]
Bukauskas et al.	2019	MI	Case-control	114	Blood	QRT-PCR	miR-146a	↑	[32]
Xie J et al.	2018	CM	In vivo	60	Mice	QRT-PCR	miR-146a	↑	[43]
Besler et al.	2016	CM	In vitro	98	Heart biopsy	QRT-PCR	miR-146b	—	[44]
Gumus et al.	2018	ARM	Case-control	71	Plasma	QRT-PCR	miR-146a-5p	—	[45]
Szczebra et al.	2018	PPCM	Case-control	12	Serum	miRNA cards	miR-146a	↑	[54]
Haghikia et al.	2013	PPCM	Case-control	134	Plasma	QRT-PCR	miR-146a	↑	[55]
Horie et al.	2010	CM	In vivo	N/A	C57BL/6 mice	QRT-PCR	miR-146a	↑	[58]
Beg et al.	2017	HF	Case-control	60	Plasma	QRT-PCR	miR-146a	↑	[74]
Gao et al.	2015	SICD	In vivo	N/A	Mice	QRT-PCR	miR-146a	—	[85]

reactive protein (CRP), creatinine kinase MB (CK-MB), troponin I plasma levels, eGFR, and LV ejection fraction [38], but these factors are not accurate enough; and new prognostic factors are required. Liu et al. in 2015 studied prognostic factors for LVR and showed that the miR-146a assessment for five days following MI could significantly predict LVR development (AUC = 0.818) [39]. Unfortunately, extensive studies have not been conducted in this area, and further clinical studies are needed (Table 2).

Ventricular rupture (VR) is one of the most acute cardiac complications requiring rapid surgical measures to prevent the patient's death. Therefore, predicting this event is very important. Various research have been done on the role of miR-146a on VR. For example, a study by Zidar et al. on tissue specimens from 50 patients who expired due to MI showed that measurement of serum level of miR-146a could be used in 2-7 days post MI as a prognostic factor for VR incidence in MI patients [40]. Research on the role of this microRNA in VR is minimal, and conclusions need to be studied. Nevertheless, it can be expected that AMI patients with higher levels of miR-146 are more likely to develop MI complications than other patients.

3. Myocarditis

Myocarditis is defined as myocardial inflammation associated with cardiac dysfunction, which may be due to viral, bacterial infections, or the body's autoimmune reaction. Despite various diagnostic modalities, the definite diagnosis still depends on endomyocardial biopsy, and the detection of inflammatory infiltrates in specimens according to the Dallas criteria.

Due to the difficulties in diagnosing viral myocarditis (VM), diagnostic factors have been considered. Different studies investigate the role of miR-146 in this disease; for example, cellular research conducted by Chen et al. reports that miR-146b upregulation is associated with VM by targeting ITCH. They also noted that overexpression of this miRNA is responsible for cytokine and chemokine excessive secretion, which enhances myocardial inflammation by

weakening the NF- κ B pathway feedback signaling. Furthermore, specific immunosuppressive agents may control the inflammatory response [41]. In return, studies on the serum level of this miRNA have shown no significant elevation of this factor in VM patients compared to the control group, which probably reduces its use as a diagnostic factor [20].

Another cause of myocarditis is sepsis. Sepsis is a life-threatening organ dysfunction caused by the host's dysregulated immune response to infection [42]. Considering the role of miR-146a in immune processes, especially TLR4-mediated pathways, XIE et al. examined the changes in this miRNA by injecting bacterial LPS into 60 healthy mice. This study showed that miR-146a might inhibit the TLR4/NF- κ B signaling pathway through negative feedback mechanisms, thereby reducing the complications of sepsis-induced cardiomyopathy [43]. Therefore, inhibition of this miRNA can be considered a promising therapeutic approach. However, similar to the results seen in VM, the diagnostic value of this microRNA in other types of myocarditis is also not significant. For example, results of the study by Besler et al. demonstrated no significant difference concerning miR-146b levels between sepsis-induced cardiomyopathies patients and controls [44]. Also, Gumus et al. showed that the serum levels of miR-146a were similar between the acute rheumatic myocarditis (ARM) patient and control groups [45].

Due to the minimal results, mir146a could be used as a therapeutic target in various types of myocarditis. However, the preliminary results of the above studies show that the diagnostic use of this factor is not very promising due to the deficient serum level of this microRNA in patients with myocarditis. Further studies are needed to lighten whether these miRNAs might be helpful as therapeutic targets.

4. Cardiomyopathy

A heterogeneous group of myocardial diseases associated with electromechanical dysfunctions is classified as cardiomyopathies. These patients usually exhibit inappropriate ventricular hypertrophy or dilatation and are due to a variety

TABLE 2: Descriptive overview of the data extracted from the reviewed studies on the prognostic application of miR-146a on cardiovascular disease.

Author	Year	Disease	Study design	Participant	Tissue source	Method	MicroRNA	Reference
Arroyo et al.	2018	AF	Case-control	463	Mice, plasma	QRT-PCR/TaqMan analysis	miR-146a	[17]
Chen et al.	2014	MI	Case-control	1808	Blood	PCR-LDR	miR-146a Rs2910164	[24]
Wang et al.	2017	CAD	Case-control	721	Blood	Matrix-assisted laser desorption/ionization time-of-flight mass spectrometry Sequenom Massarray system	miR-146a Rs2431697/ Rs2910164	[26]
Zhu et al.	2018	MI	Case-control	774	Blood	PCR-RFLP	miR-146a (C>G)	[27]
Zha et al.	2019	KD	Case-control	246	Blood	PCR-sequence-based typing	miR-146a Rs2910164 G/C, Rs57095329 A/G, Rs6864584 T/C	[28]
Liu et al.	2015	IRI	In vitro	N/A	HUVEC	QRT-PCR	miR-146a/b	[34]
Liu et al.	2015	LVR	Cohort	198	Plasma	QRT-PCR	miR-146a	[38]
Zidar et al.	2011	VR	In vitro	50	Biopsy	QRT-PCR	miR-146a	[40]
Feng et al.	2017	DC	Case-control	N/A	HCMEC, mice	QRT-PCR	miR-146a	[48]
Alipoor et al.	2016	DC	Case-control	375	Blood	PCR-RFLP	miR-146a	[49]
Yang et al.	2011	Ath	In vitro	N/A	Cell line, ATCC	Luciferase assay, Western blot, rescue assay	miR-146a	[63]
Cheng et al.	2013	Ath	In vitro/ in vivo	N/A	HUVEC, mice	HUR immunoprecipitation, Western blot, ELISA	miR-146a/b	[65]
Raitoharju et al.	2011	Ath	In vitro	50	Blood, mice	QRT-PCR, Illumina's expression BEADCHIP	miR-146 a/b	[66]
Li et al.	2015	Ath	In vitro/ in vivo	N/A	Blood, mice	RT-PCR	miR-146a	[68]

of causes that frequently are genetic [46]. Diagnosis of cardiomyopathy can be made with various diagnostic techniques, including chest X-ray, treadmill stress test, ECG, cardiac catheterization, echocardiogram, and blood tests. Blood factors such as B-type natriuretic peptide (BNP) are used in cardiomyopathy diagnosis. New studies point to the diagnostic potential of miR-146 in multiple causes of cardiomyopathy.

Type 2 diabetes (T2D) is prevalent with various cardiac complications. Due to the progressive nature and cardiac complications of T2D, early diagnosis and treatment of diabetic cardiomyopathy (DC) are essential. Studies have demonstrated that the plasma level of miR-146 is associated with cardiac complications of diabetes, including DC [47]. Feng et al. showed that miR-146a is reduced in endothelial cells exposed to high glucose, which leads to the activation of NF- κ B, thus, other inflammatory molecules. The protective effect of miR-146a on functional and structural alterations in DC through preventing inflammatory changes [48] (Table 3).

Nevertheless, an increase in miR-146a in T2D patients has been reported by some studies. For example, Alipoor et al. suggested that higher levels of miR-146a, especially rs2910164 polymorphism, might increase the risk of T2D and its cardiac complications [49]. The apparent difference in the above results is probably due to the different roles of this microRNA in different cells. The study by Feng et al. clearly shows that endothelial cells experience a decrease in miR-146 cellular levels due to exposure to high glucose levels, resulting in intracellular inflammatory processes. Nevertheless, the role of miR-146 in diabetes is not limited to endothelial cells. Studies have shown that the deregulation of microRNAs in peripheral blood mononuclear cells (PBMC) plays a more critical role in the pathogenesis of the disease [50]. Probably what increases the risk of T2D in people with higher plasma levels of miR-146 (or different polymorphisms) is the inflammatory processes involved in PBMCs, not endothelial cells.

Despite the different results of the studies, the role of miR-146 in the pathogenesis of DC is undeniable, and most

TABLE 3: Descriptive overview of the data extracted from the reviewed studies on the therapeutic application of miR-146a on cardiovascular disease.

Author	Year	Disease	Study design	Participant	Tissue source	Method	MicroRNA	Result	Reference
Palomer et al.	2015	N/A	In vivo	N/A	Mice, AC16 cells	QRT-PCR	miR-146a	—	[14]
Shu et al.	2018	IRI	In vivo	N/A	Rat	QRT-PCR	miR-146a-5p	—	[35]
Zhao L et al.	2019	MI	In vivo	12	Rat	QRT-PCR	miR-146b	↓	[36]
Chen et al.	2015	VM	In vitro	16	Heart biopsy	QRT-PCR	miR-146b	↑	[41]
Halkein J	2013	PPCM	In vivo	N/A	CKO mice	QRT-PCR	miR-146a	↑	[53]
Costantino et al.	2015	DC	In vivo	9	C57/B6 mice	QRT-PCR	miR-146a	↑	[60]
Guo et al.	2010	ACS	In vitro	91	Blood	QRT-PCR,	miR-146a	↓	[71]
Chouvarine et al.	2019	Hypoxia	In vivo	N/A	Rat	QRT-PCR	miR-146b	↓	[75]
Heggermont et al.	2014	HF	In vivo	N/A	Mice	QRT-PCR	miR-146a	—	[76]
Oh et al.	2018	HF	In vivo	N/A	Mice	QRT-PCR	miR-146a	—	[77]
Huang et al.	2016	AMI	In vivo	N/A	Mice	QRT-PCR	miR-146a	—	[79]
Huang et al.	2019	AMI	In vitro	N/A	Endothelial cell	QRT-PCR	miR-146a	—	[80]
Desjarlais et al.	2019	AMI	In vivo	N/A	Mice	QRT-PCR	miR-146b	—	[81]
Seo et al.	2017	IRI	In vitro	N/A	HMSCS	QRT-PCR	miR-146a	—	[84]
Heggermont et al.	2012	Cardiac hypertrophy	In vivo	N/A	Mice	QRT-PCR	miR-146a	—	[87]
Widmer-Teske et al.	2012	AMI	In vitro/ in vivo	N/A	Mice, endothelial cell	QRT-PCR	miR-146a	—	[88]

patients with DC show abnormal (and mostly high) amounts of this microRNA, but no valid studies have been performed on the diagnostic value of miR-146 for DC.

Early diagnosis of peripartum cardiomyopathy (PPCM) is vital due to the relatively high prevalence (about 1 in 2000 cases) and the need for prompt treatment. Studies have cited various pathophysiological models for the disease, including increased cardiac susceptibility to myocarditis in pregnancy, cross-reactivity of antiuterine antibodies to the heart muscle, or oxidative stress due to prolactin breakdown [51, 52]. As stated by Halkein et al., the absence of STAT3 or PGC1 in cardiomyocytes leads to the decreased expression of the ROS scavenger MnSOD in these cells [53]. Decreased MnSOD levels accumulate ROS and increase and activate Cathepsin D, which is secreted from cardiomyocytes into the interstitial space. Cathepsin D cleaves PRL to generate an antiangiogenic 16-kDa fragment, 16K PRL. 16K PRL stimulates endothelial cells to activate NF- κ B through an unknown mechanism that increases miR-146a levels. miR-146a decreases NRAS levels and inhibits angiogenesis. It also transits to cardiomyocytes in exosomes to reduce ERBB4

levels, resulting in a slower cardiac metabolism (Figure 2). Also, Szczerba et al. showed that in the third trimester of physiological pregnancy, the serum level of miR-146a increases by 70%, which is probably related to its cardiac protective effects against volume overload [54]. This increase led to further inhibition of ERBB4 in PPCM patients and decreased cardiac metabolism.

Due to the significant role of miR-146a in PPCM pathogenesis, different studies have been conducted on the serum level of miR-146a. Haghikia et al. demonstrated the increased serum levels of Cathepsin D, an enzyme that generates 16 kDa prolactin, miR-146a, N-terminal-pro-brain-natriuretic peptide, and asymmetric dimethylarginine emerged as biomarkers for PPCM [55]. This highly specific biomarker profile can help clinicians detect early-stage PPCM patients and provide appropriate treatment. Overall, the above studies showed that miR-146 physiologically protects the heart against pregnancy overload, but its excessive increase, with a severe decrease in cardiac metabolism, leads to PPCM in high-risk individuals. Therefore, with advances in studies and confirmation of the role of 16 kDa prolactin in

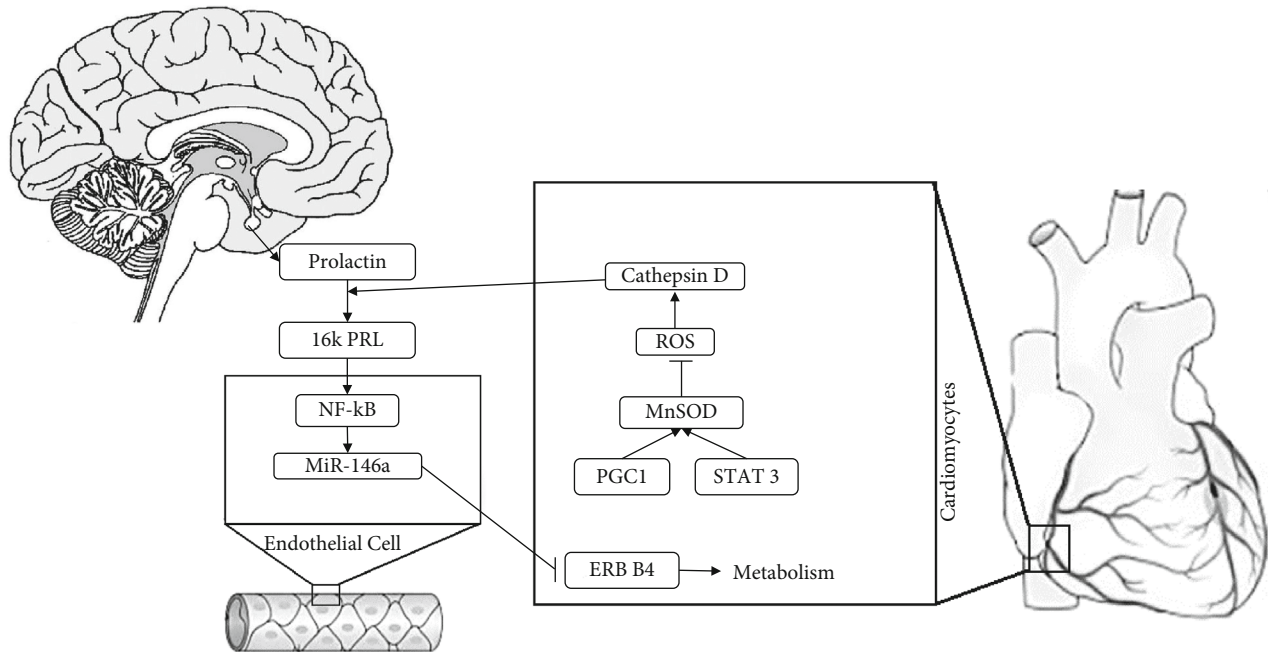


FIGURE 2: Pregnancy leads to volume overload physiologically, increasing the preload. In PPCM, cardiomyocytes become inflamed due to overwork and produce MnSOD. By inhibiting ROS, cathepsin D increases and enters the bloodstream. On the other hand, during pregnancy, a lot of prolactin is present in the bloodstream, which breaks into 16K PRL by cathepsin D. 16K PRL also affects endothelial cells and leads to the production of miR-146a. Eventually, this molecule disrupts the metabolism of heart cells by affecting cardiomyocytes and inhibiting ErbB-4.

diagnosing PPCM, it can be hoped that PPCM can be managed in the early stages by periodical measurement of this factor in high-risk mothers.

Various studies show the therapeutic potential of miR-146A in cardiomyopathies caused by different etiologies, such as DOX-induced cardiomyopathy and DC.

Doxorubicin (DOX) is an effective anticancer agent. However, its dose-dependent cardiotoxic effects have limited its use. Studies have shown a significant reduction in ErbB4 expression after DOX treatment [56]. Neuregulin-1-ErbB signaling is an essential pathway for normal cardiac function in adults. The inhibition of this pathway by DOX can cause changes in myocardial structure, which can develop into severe and irreversible cardiomyopathy [57]. As shown in Figure 3, the overexpression of miR-146 by DOX can lead to ErbB4 inhibition, which may cause structural problems in myocardiocytes. Therefore, developing new therapeutic strategies based on NRG-1, such as the delivery of nucleotides that inhibit miR-146a, can be promising for treating doxorubicin-induced cardiomyopathy [58].

Considering the role of miR-146 in DC pathogenesis, several studies have focused on the therapeutic capabilities of this microRNA. Randomized clinical trials have shown that even with intensive glycemic control, cardiac complications of T2D cannot be prevented entirely. Costantino et al.'s results indicate that hyperglycemia triggered maladaptive signatures in cardiomyocytes, a phenomenon known as metabolic memory [59], which persisted even after restoring glucose to normal levels. One of the dysregulated miRNAs is miR-146a [60]. This means that miR-146 could be a new therapeutic target in preventing DC. Despite these data,

determining this microRNA's exact function in T2D and thus defining treatment strategies based on it requires extensive cell-molecular studies considering the role of this molecule in cardiomyocytes, endothelial cells, and PBMCs.

5. Atherosclerosis

Atherosclerosis is the main reason for morbidity and mortality in the Western world. It can cause different complications, such as hypertension, dyslipidemia, and diabetes. Proper management of atherosclerosis can improve the function of endothelial cells and prevent its many complications. For this reason, ACE inhibitors, statins, β blockers, and antiplatelet drugs (aspirin, clopidogrel) are often prescribed [61]. Recent studies have suggested new anti-inflammatory approaches for treating atherosclerosis [62].

Different reports suggest that miR-146a could have a significant effect on the reduction of the intracellular cholesterol content of lipid-loaded macrophages [63]. For example, a study reported that miR-146a intravascular injection mimics the protective effects of apoE in both *Ldlr*^{-/-} and *ApoE*^{-/-}; *Ldlr*^{-/-} atherosclerotic mouse models can be considered a novel potential therapeutic strategy [64].

miR-146a produces atheroprotective properties. miR-146a and miR-146b expression are induced in a delayed kinetic manner in ECs by cytokines such as IL-1 β and TNF- α , coinciding with inflammatory gene expression resolution [65]. Cytokine responsiveness in ECs inhibited by overexpression of miR-146a indicates its participation in limiting EC inflammatory signaling by the negative feedback mechanism. Studies showed that the expression of miR-146a

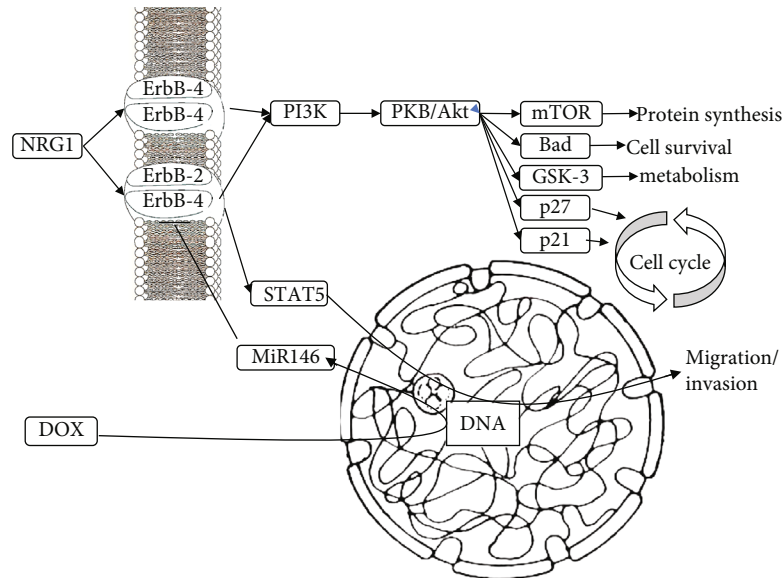


FIGURE 3: DOX increases the production of miR-146, which reduces cancer cell migration and adhesion. However, higher doses of DOX cause complete inhibition of ErbB-4, affect the PI3K pathway in heart cells, and cause cardiomyopathy by affecting the cell cycle and metabolism. Therefore, developing new therapeutic strategies, such as delivering nucleotides that inhibit miR-146a, can be promising for treating doxorubicin-induced cardiomyopathy.

is also increased in atherosclerotic plaques in mice and humans [66], directly targeting RNA-binding protein (HuR), and miR-146a repressed both MAPK and NF- κ B signaling pathways that inhibit endothelial nitric oxide synthase (eNOS). Also, targeting upstream adaptor proteins IRAK1/2 and TRAF6, the EC adhesion molecules induction is repressed by miR-146a [67]. Contrary to miR-181b, which has a more selective inhibitory role in EC NF- κ B signaling pathway, in both macrophages and ECs, the NF- κ B signaling pathway is inhibited by miR-146a [68].

To reduce macrophages, ApoE overexpression in ApoE $-/-$ macrophages induces the expression of miR-146a. Also, miR-146a systemic delivery mimics significantly reduce the progression of atherosclerotic lesions. However, along with having an anti-inflammatory role in regulating a range of immune cells (macrophages, T cells, and dendritic cells), miR-146a may also take more part in limiting inflammatory stimuli. Nevertheless, miR-146, another significant cytokine-responsive miRNA in a negative feedback manner, helps in EC inflammation repression [69].

Similarly, in an NF- κ B-dependent manner, induction of miR-146a/b in macrophages is involved in resolving inflammation by limiting the cytokine signaling and TLR. It is indicated that apolipoprotein E (apoE), a protein with antiatherosclerotic characteristics, induces the miR-146a expression in macrophages and dumps the inflammatory responses of macrophages in vitro and in vivo. Also, studies suggest that miR-146a may regulate the maturation and secretion of proinflammatory cytokines in dendritic cells by targeting CD40L in ox-LDL-stimulated dendritic cells [68, 70].

In general, due to the anti-inflammatory function of this molecule and various studies, the induction of miR-146 is

one of the most promising therapeutic approaches for managing atherosclerotic complications.

Acute coronary syndrome (ACS) is one of the most severe complications of atherosclerosis. In ASC patients, the Th1 activity level is high, which is the consequence of arteriosclerosis activity. Studies have reported that in patients with ACS, the elevation of miR-146a expression level strongly increases the activity of the Th1 cells. Moreover, miR-146a increases proinflammatory factor (TNF- α , MCP-1, and NF- κ B p65) expression, which plays a vital role in atherosclerosis and ASC progression [71]. Cholesterol crystallization may also be prevented by cholesteryl ester hydrolase inhibition, which converts cholesteryl esters to free cholesterol. In return, ACAT-1 inhibition triggers the promotion of cholesterol crystallization, increased atheroma volume, and major cardiovascular events [72]. Overexpression of miR-146a is considered beneficial in preventing atherosclerosis and its treatment. Although more studies are needed to clarify this issue, miR-146a could be a novel promising regulatory factor in Th1 differentiation and a new therapeutic target for atherosclerosis and ACS [73].

6. Heart Failure

Recent studies claim that HF disease can be diagnosed by evaluating the level of miR-146. For example, a study by Beg et al. states that the body begins to produce circulating exosomal miR-146a to counteract the effects of systemic inflammation resulting from HF [74]. As a result, the circulating exosomal miR-146a can be used as a diagnostic biomarker in HF.

Molecular studies have achieved new mechanisms in the pathogenesis of HF. According to most of these studies,

miR-146 is considered a critical factor in the pathogenesis of different types of HF. For example, Chouvarine et al. showed that hypoxia could lead to ventricular dysfunction and eventually death by activating the miR-146b-TRAF6-IL-6/CCL2 (MCP-1) pathway [75]; on the other hand, results of research by Heggermont et al. showed that pressure overload leads to decreasing the level of dihydrolipoyl succinyltransferase (DLST) by increasing the level of miR-146a and consequently disrupts the pathway of oxidative metabolism in cardiomyocytes [76]. Oh et al. also showed that this increased level of miR-146a could lead to reduced SUMO1 (small ubiquitin-like modifier 1) expression and SERCA2a (sarcoplasmic reticulum Ca²⁺-ATPase) SUMOylation in human and animal HF models [77].

Eventually, both studies suggest miR-146a as an essential factor in the course of heart hypertrophy. These results are significant because they consider miR-146a a therapeutic target in HF. Although investigating the association between HF and miR-146a requires further studies, the inhibition of miR-146a may help prevent hypertrophy and HF.

7. Future Directions and Potential of miR146 as a Therapeutic Target in CVD

There is a long way before miRNAs can be clinically used in CVD. Research on different miRNAs promised changes in diagnosing and treating these diseases. miR-146 has received much attention, with positive results in most studies. Researches show that this molecule has played a significant role in the pathogenesis of cardiac disease and its related mechanisms. As a result, many potential applications of miR-146 are expected. These potential applications can be examined in three sections: induction, inhibition, and diagnosis.

Secondary to hypoxia and ischemia of a particular tissue, the process of cell apoptosis begins rapidly and leads to irreversible complications. These complications are critical in myocardial tissue, and even with the elimination of hypoxia and the restoration of blood flow to the tissue, the chances of HF and mortality are significantly increased due to apoptosis of cardiac cells [78]. Different studies have been performed in this area, and most of them show that increasing the level of miR-146 (directly or indirectly) leads to a reduction in secondary apoptosis to hypoxia and can somewhat prevent an irreversible complication of MI [79]. With increasing studies and research in this area, the induction of miR-146 may be one of the first approaches to managing MI patients in the future. On the other hand, researches show that miR-146 can have a good effect on myocardial tissue angiogenesis and rapid blood flow to the infarct area by increasing the migration, penetration, and proliferation of coronary artery endothelial cells [80]. This effect of increased angiogenesis is significant in patients with hypercholesterolemia. In these patients, ischemic tissue angiogenesis occurs much less frequently and later than in healthy individuals, making hypercholesterolemia patients more prone to recurrent MI and secondary failure. The research results show that the administration of miR-146b to patients with hypercholesterolemia can accelerate angiogenesis [81]. If future studies confirm

these results, miR-146b can significantly reduce the recovery process of heart tissue.

The primary treatment for MI is to increase blood flow with reperfusion methods such as PCI and coronary artery bypass grafting (CABG). Nevertheless, one of the major problems patients face after vascular occlusion and reperfusion is ischemia-reperfusion injury (IRI). Due to ischemia, the tissue is deprived of oxygen and nutrients, resulting in a significant accumulation of inflammatory cytokines. With reperfusion and drainage of retained blood into the bloodstream, cytokines reach other heart parts, causing inflammation and oxidative damage throughout the heart muscle [82].

The treatments to prevent this problem mostly had minimal results and various side effects [83]. One of the treatments is the transplantation of human mesenchymal stem cells (hMSCs). Despite the acceptable results, transplantation of hMSCs may be destroyed by the effects of hypoxia, resulting in treatment failure. Seo et al. show that increasing the level of miR-146 in combination with this treatment significantly increases the survival of hMSCs and, consequently, the efficacy of this method [84]. In contrast, some researchers claim that the self-induction of miR-146 without the help of any additional treatments will protect the myocardium against IRI complications [34].

Another potential therapeutic effect of this miRNA is its protective effect against polymicrobial sepsis. Different research results show that using miR-146 in a preventive way will reduce the cardiac complication of sepsis, such as ICMs [85].

Simultaneously with the widespread use of miRNAs, research has been done on their inhibition, production, and activity. One of the ways to inhibit miRNAs is to use antagomirs. Antagomirs are particular synthetic molecules initially introduced as silencing agents of miRNAs in 2005. One of the unique characteristics of this molecule is that it inhibits a specific miRNA [86]. There are many clinical uses for this selective inhibition. For example, Heggermont et al., by studying the pathogenesis of pressure overload-induced cardiac hypertrophy and its secondary HF, found that it played a crucial role in miR-146 and showed that by inhibiting this miRNA and thus overexpression of its target, dihydrolipoyl succinyl transferase has the ability of heart cells to protect against ventricular dysfunctions [87].

Also, Widmer-Teske et al. indicated that miR-146a acts as a critical regulator of endothelial cell angiogenesis during myocardial regeneration. These results suggest that miR-146a may represent an attractive target for future therapeutic interventions to treat ischemic heart disease [88].

One of the considered applications for miRNAs is their diagnostic usage. This application is specifically for cardiac patients because of the rapid course and severe prognosis of these diseases if not treated in time. Research has shown that the serum level of miR-146 could effectively diagnose MI and prevent LVR or ventricular rupture [38, 40]. miR-146a also reduces inflammation and inhibits complications of sepsis-induced cardiomyopathy by inhibiting the TLR4/NF- κ B signaling pathway [43].

Evaluating the molecular level of miR-146 could lead to broader diagnoses in sensitive groups of society. Research

has shown that the serum level of miR-146 among patients with diabetic cardiomyopathy and PPCM is higher. Critical needs for diagnosis and earlier treatment of these two diseases can be expected by measuring the periodical level of miRNA of pregnant and cardiac patients. Common cardiomyopathy in these groups will be identified faster and have a better prognosis in treating the patients [54, 60].

Another issue for miR-146 diagnosis is the presence of various polymorphisms of this miRNA. Numerous associations have been reported between polymorphism and the presence or absence of specific cardiac diseases. For example, possibly carriers' mutant type (T allele) of rs2431697 and wild type (C allele) of rs2910164 have a lower risk of developing ACS [25, 28]. Despite the impressive results and the ability of this method to diagnose diseases even before the onset of the first symptoms, the results are highly dependent on the study population; the results may be completely different or even contradictory in other study samples. For this reason, this field will be highly considered in the personal medicine approaches, and a wide range of applications can be expected.

8. Conclusion

In conclusion, heart diseases are known as one of the deadliest diseases in most societies, and new research has been able to prevent or treat many of these cases by offering new approaches. In recent years, the discovery of microRNAs has revolutionized the medical sciences, and researchers have since devised various applications for these molecules. Meanwhile, miR-146 has attracted much attention with its essential role in inflammatory processes. Dysregulation of the levels of this microRNA is seen in most heart diseases, but in some of these diseases, such as viral myocarditis or diabetic and prepartum cardiomyopathies, the role of this microRNA is very prominent. In this article, we have tried to gather and review all the studies that point to the correlation between miR-146 and heart disease to provide a more comprehensive view of the progress made and the research paths ahead.

Abbreviations

CVDs:	Cardiovascular diseases
CAD:	Coronary artery diseases
MI:	Myocardial infarction
ncRNAs:	Noncoding RNAs
mRNAs:	Messenger RNAs
miRNAs:	MicroRNAs
TRAF6:	Tumor necrosis factor receptor-associated factor 6
IRAK1:	Interleukin 1 receptor-associated kinase 1
TLR:	Toll-like receptor
NF- κ B:	Nuclear factor κ -light chain
Tregs:	Regulatory T cells
TCR:	T-cell receptor
HF:	Heart failure
LmiR-146a:	Lentivirus expressing miR-146a
STEMI:	ST segment elevation myocardial infarction

NSTEMI:	Non-ST segment elevation myocardial infarction
ACS:	Acute coronary syndrome
AMI:	Acute myocardial infarction
ECG:	Electrocardiogram
LVR:	Left ventricular remodeling
ACE:	Angiotensin-converting enzyme
CRP:	C-reactive protein
VR:	Ventricular rupture
eGFR:	Estimated glomerular filtration rate
AF:	Atrial fibrillation
VM:	Viral myocarditis
ARM:	Rheumatic myocarditis
DOX:	Doxorubicin
T2D:	Type 2 diabetes
DC:	Diabetic cardiomyopathy
PBMC:	Peripheral blood mononuclear cells
PPCM:	Peripartum cardiomyopathy
EC:	Endothelial cells
SMC:	Smooth muscle cells
eNOS:	Endothelial nitric oxide synthase
apoE:	Apolipoprotein E
DLST:	Dihydrolipoyl succinyl transferase
CABG:	Coronary artery bypass grafting
hMSCs:	Human mesenchymal stem cells
SUMO1:	Small ubiquitin-like modifier 1
SERCa2A:	Sarcoplasmic reticulum Ca ²⁺ -ATPase
MCP-1:	Monocyte chemoattractant protein-1
TNF- α :	Tumor necrosis factor alpha
KD:	Kawasaki disease
IRI:	Ischemia-reperfusion injury
SICM:	Sepsis-induced cardiomyopathy
Ath:	Atherosclerosis

Data Availability

No data have been submitted to any open-access databases. All data supporting the study are presented in the manuscript or available upon request.

Disclosure

The full article was not posted or published elsewhere.

Conflicts of Interest

The authors have no conflicts of interest to declare that they are relevant to the content of this article.

Authors' Contributions

The authors confirm contributions to the paper as follows: study conception and design were done by ShM, FM, and HM; data collection was done by FM, HM, SaM, SA, and SY; analysis and interpretation of results were done by ShM, FM, and PF; draft manuscript preparation was done by ShM, FM, and HM. All authors reviewed the results and approved the final version of the manuscript. Fatemeh

Sadat Mahdavi and Shayan Mardi are co-first authors and contributed equally to this article.

References



- [1] A. Timmis, N. Townsend, C. P. Gale et al., "European Society of Cardiology: cardiovascular disease statistics 2019," *European heart journal*, vol. 41, no. 1, pp. 12–85, 2020.
- [2] I. Tzoulaki, P. Elliott, V. Kontis, and M. Ezzati, "Worldwide exposures to cardiovascular risk factors and associated health effects: current knowledge and data gaps," *Circulation*, vol. 133, no. 23, pp. 2314–2333, 2016.
- [3] S. B atkai and T. Thum, "MicroRNAs in hypertension: mechanisms and therapeutic targets," *Current hypertension reports*, vol. 14, no. 1, pp. 79–87, 2012.
- [4] G. Iacomino and A. Siani, "Role of microRNAs in obesity and obesity-related diseases," *Genes & nutrition*, vol. 12, no. 1, p. 23, 2017.
- [5] D. Sayed, C. Hong, I.-Y. Chen, J. Lypowy, and M. Abdellatif, "MicroRNAs play an essential role in the development of cardiac hypertrophy," *Circulation research*, vol. 100, no. 3, pp. 416–424, 2007.
- [6] W. H. Organization, *Global Action Plan for the Prevention and Control of Noncommunicable Diseases*, World Health Organization, 2013.
- [7] C. A. MacRae and R. S. Vasan, "The future of genetics and genomics: closing the phenotype gap in precision medicine," *Circulation*, vol. 133, no. 25, pp. 2634–2639, 2016.
- [8] Y. Lu, J. Boer, R. M. Barsova et al., "TGFB1 genetic polymorphisms and coronary heart disease risk: a meta-analysis," *BMC Medical Genetics*, vol. 13, no. 1, p. 39, 2012.
- [9] S. Sayols-Baixeras, C. Llu s-Ganella, G. Lucas, and R. Elosua, "Pathogenesis of coronary artery disease: focus on genetic risk factors and identification of genetic variants," *The application of clinical genetics*, vol. 7, p. 15, 2014.
- [10] C. Backes, E. Meese, H.-P. Lenhof, and A. Keller, "A dictionary on microRNAs and their putative target pathways," *Nucleic acids research*, vol. 38, no. 13, pp. 4476–4486, 2010.
- [11] D. Bhaumik, G. Scott, S. Schokrpur, C. Patil, J. Campisi, and C. Benz, "Expression of microRNA-146 suppresses NF- B activity with reduction of metastatic potential in breast cancer cells," *Oncogene*, vol. 27, no. 42, pp. 5643–5647, 2008.
- [12] D. Bhaumik, G. K. Scott, S. Schokrpur et al., "MicroRNAs miR-146a/b negatively modulate the senescence-associated inflammatory mediators IL-6 and IL-8," *Aging*, vol. 1, no. 4, pp. 402–411, 2009.
- [13] A. Tahamtan, M. Teymoori-Rad, B. Nakstad, and V. Salimi, "Anti-inflammatory microRNAs and their potential for inflammatory diseases treatment," *Frontiers in immunology*, vol. 9, p. 1377, 2018.
- [14] X. Palomer, E. Capdevila-Busquets, G. Botteri et al., "miR-146a targets Fos expression in human cardiac cells," *Disease models & mechanisms*, vol. 8, no. 9, pp. 1081–1091, 2015.
- [15] G. Kania, P. Blyszczuk, and U. Eriksson, "Mechanisms of cardiac fibrosis in inflammatory heart disease," *Trends in cardiovascular medicine*, vol. 19, no. 8, pp. 247–252, 2009.
- [16] M. I. Oerlemans, A. Mosterd, M. S. Dekker et al., "Early assessment of acute coronary syndromes in the emergency department: the potential diagnostic value of circulating microRNAs," *EMBO molecular medicine*, vol. 4, no. 11, pp. 1176–1185, 2012.
- [17] A. B. Arroyo, A. M. de Los Reyes-Garc a, J. M. Rivera-Caravaca et al., "miR-146a regulates neutrophil extracellular trap formation that predicts adverse cardiovascular events in patients with atrial fibrillation," *Arteriosclerosis, thrombosis, and vascular biology*, vol. 38, no. 4, pp. 892–902, 2018.
- [18] A. Isic, M. Scharin T ang, E. Haugen, and M. Fu, "TNF -antagonist neither improve cardiac remodelling or cardiac function at early stage of heart failure in diabetic rats," *Autoimmunity*, vol. 41, no. 6, pp. 473–477, 2008.
- [19] H.-M. Lee, T. S. Kim, and E.-K. Jo, "miR-146 and miR-125 in the regulation of innate immunity and inflammation," *BMB reports*, vol. 49, no. 6, pp. 311–318, 2016.
- [20] M. F. Corsten, R. Dennert, S. Jochems et al., "Circulating microRNA-208b and microRNA-499 reflect myocardial damage in cardiovascular Disease," *Genetics*, vol. 3, no. 6, pp. 499–506, 2010.
- [21] P. Ramkaran, S. Khan, A. Phulukdaree, D. Moodley, and A. A. Chuturgoon, "miR-146a polymorphism influences levels of miR-146a, IRAK-1, and TRAF-6 in young patients with coronary artery disease," *Cell biochemistry and biophysics*, vol. 68, no. 2, pp. 259–266, 2014.
- [22] T. Xu, Y. Zhu, Q.-K. Wei et al., "A functional polymorphism in the miR-146a gene is associated with the risk for hepatocellular carcinoma," *Carcinogenesis*, vol. 29, no. 11, pp. 2126–2131, 2008.
- [23] C. Yue, M. Wang, B. Ding et al., "Polymorphism of the pre-miR-146a is associated with risk of cervical cancer in a Chinese population," *Gynecologic oncology*, vol. 122, no. 1, pp. 33–37, 2011.
- [24] C. Chen, H. Hong, L. Chen, X. Shi, Y. Chen, and Q. Weng, "Association of microRNA polymorphisms with the risk of myocardial infarction in a Chinese population," *The Tohoku journal of experimental medicine*, vol. 233, no. 2, pp. 89–94, 2014.
- [25] S. Huang, Z. Lv, Q. Deng et al., "A genetic variant in pre-miR-146a (rs2910164 C > G) is associated with the decreased risk of acute coronary syndrome in a Chinese population," *The Tohoku journal of experimental medicine*, vol. 237, no. 3, pp. 227–233, 2015.
- [26] Y. Wang, X. Wang, Z. Li et al., "Two single nucleotide polymorphisms (rs2431697 and rs2910164) of miR-146a are associated with risk of coronary artery disease," *International journal of environmental research and public health*, vol. 14, no. 5, p. 514, 2017.
- [27] X. Zhu, R. Hou, A. Ma, S. Yang, and X. Pan, "Associations of miR-146a, miR-149, miR-196a2, and miR-499 polymorphisms with ischemic stroke in the Northern Chinese Han population," *Medical science monitor: international medical journal of experimental and clinical research*, vol. 24, pp. 7366–7374, 2018.
- [28] L. Zha, S. Li, X. Liu et al., "Association of miR-146a gene polymorphism at loci rs2910164 G/C, rs57095329 A/G, and rs6864584 T/C with susceptibility to Kawasaki disease in Chinese children," *Pediatric cardiology*, vol. 40, no. 3, pp. 504–512, 2019.
- [29] C. P. McCarthy, M. Vaduganathan, and J. L. Januzzi, "Type 2 myocardial infarction—diagnosis, prognosis, and treatment," *Journal of the American Medical Association*, vol. 320, no. 5, pp. 433–434, 2018.
- [30] S. Aydin, K. Ugur, S. Aydin,  . Sahin, and M. Yardim, "Biomarkers in acute myocardial infarction: current perspectives," *Vascular health and risk management*, vol. 15, pp. 1–10, 2019.

- [31] S. Xue, W. Zhu, D. Liu et al., "Circulating miR-26a-1, miR-146a and miR-199a-1 are potential candidate biomarkers for acute myocardial infarction," *Molecular Medicine*, vol. 25, no. 1, pp. 1–12, 2019.
- [32] T. Bukauskas, R. Mickus, D. Cereskevicius, and A. Macas, "Value of serum miR-23a, miR-30d, and miR-146a biomarkers in ST-elevation myocardial infarction," *Medical science monitor: international medical journal of experimental and clinical research*, vol. 25, pp. 3925–3932, 2019.
- [33] A. T. Turer and J. A. Hill, "Pathogenesis of myocardial ischemia-reperfusion injury and rationale for therapy," *The American journal of cardiology*, vol. 106, no. 3, pp. 360–368, 2010.
- [34] R. R. Liu, J. Li, J. Y. Gong et al., "MicroRNA-141 regulates the expression level of ICAM-1 on endothelium to decrease myocardial ischemia-reperfusion injury," *American Journal of Physiology-Heart and Circulatory Physiology*, vol. 309, no. 8, pp. H1303–H1313, 2015.
- [35] L. Shu, W. Zhang, G. Huang et al., "Trolox attenuates myocardial cell apoptosis following myocardial ischemia-reperfusion injury through inhibition of miR-146a-5p expression," *Journal of cellular physiology*, vol. 234, no. 6, pp. 9274–9282, 2019.
- [36] L. Zhao, X. R. Yang, and X. Han, "MicroRNA-146b induces the PI3K/Akt/NF- κ B signaling pathway to reduce vascular inflammation and apoptosis in myocardial infarction by targeting PTEN," *Experimental and therapeutic medicine*, vol. 17, no. 2, pp. 1171–1181, 2019.
- [37] E. Braunwald and M. A. Pfeffer, "Ventricular enlargement and remodeling following acute myocardial infarction: mechanisms and management," *The American journal of cardiology*, vol. 68, no. 14, pp. 1–6, 1991.
- [38] Y. Maekawa, T. Anzai, T. Yoshikawa et al., "Prognostic significance of peripheral monocytes after reperfused acute myocardial infarction: a possible role for left ventricular remodeling," *Journal of the American College of Cardiology*, vol. 39, no. 2, pp. 241–246, 2002.
- [39] X. Liu, Y. Dong, S. Chen et al., "Circulating microRNA-146a and microRNA-21 predict left ventricular remodeling after ST-elevation myocardial infarction," *Cardiology*, vol. 132, no. 4, pp. 233–241, 2015.
- [40] N. Zidar, E. Boštjančič, D. Glavač, and D. Štajer, "MicroRNAs, innate immunity and ventricular rupture in human myocardial infarction," *Disease markers*, vol. 31, no. 5, 265 pages, 2011.
- [41] Z. G. Chen, H. Liu, J. B. Zhang, S. L. Zhang, L. H. Zhao, and W. Q. Liang, "Upregulated microRNA-214 enhances cardiac injury by targeting ITC1 during coxsackievirus infection," *Molecular Medicine Reports*, vol. 12, no. 1, pp. 1258–1264, 2015.
- [42] F. Haddad, G. Berry, R. L. Doyle, P. Martineau, T.-K. Leung, and N. Racine, "Active bacterial myocarditis: a case report and review of the literature," *The Journal of heart and lung transplantation*, vol. 26, no. 7, pp. 745–749, 2007.
- [43] J. Xie, L. Zhang, X. Fan, X. Dong, Z. Zhang, and W. Fan, "MicroRNA-146a improves sepsis-induced cardiomyopathy by regulating the TLR-4/NF- κ B signaling pathway," *Experimental and Therapeutic Medicine*, vol. 18, no. 1, pp. 779–785, 2019.
- [44] C. Besler, D. Urban, S. Watzka et al., "Endomyocardial miR-133a levels correlate with myocardial inflammation, improved left ventricular function, and clinical outcome in patients with inflammatory cardiomyopathy," *European Journal of Heart Failure*, vol. 18, no. 12, pp. 1442–1451, 2016.
- [45] G. Gumus, D. Giray, O. Bobusoglu, L. Tamer, D. Karpuz, and O. Hallioglu, "MicroRNA values in children with rheumatic carditis: a preliminary study," *Rheumatology international*, vol. 38, no. 7, pp. 1199–1205, 2018.
- [46] E. Braunwald, "Cardiomyopathies," *Circulation research*, vol. 121, no. 7, pp. 711–721, 2017.
- [47] M. Böni-Schnetzler and D. T. Meier, "Islet inflammation in type 2 diabetes," in *Seminars in immunopathology*, Springer, 2019.
- [48] B. Feng, S. Chen, A. D. Gordon, and S. Chakrabarti, "miR-146a mediates inflammatory changes and fibrosis in the heart in diabetes," *Journal of molecular and cellular cardiology*, vol. 105, pp. 70–76, 2017.
- [49] B. Alipoor, R. Meshkani, H. Ghaedi, Z. Sharifi, G. Panahi, and T. Golmohammadi, "Association of miR-146a rs2910164 and miR-149 rs2292832 variants with susceptibility to type 2 diabetes," *Clinical Laboratory*, vol. 62, no. 8, pp. 1553–1561, 2016.
- [50] C. V. Collares, A. F. Evangelista, D. J. Xavier et al., "Identifying common and specific microRNAs expressed in peripheral blood mononuclear cell of type 1, type 2, and gestational diabetes mellitus patients," *BMC research notes*, vol. 6, no. 1, p. 491, 2013.
- [51] Z. Arany and U. Elkayam, "Peripartum cardiomyopathy," *Circulation*, vol. 133, no. 14, pp. 1397–1409, 2016.
- [52] J. Triebel, C. Clapp, G. Martínez de la Escalera, and T. Bertsch, "Remarks on the prolactin hypothesis of peripartum cardiomyopathy," *Frontiers in Endocrinology*, vol. 8, article 77, 2017.
- [53] J. Halkein, S. P. Tabruyn, M. Ricke-Hoch et al., "MicroRNA-146a is a therapeutic target and biomarker for peripartum cardiomyopathy," *The Journal of clinical investigation*, vol. 123, no. 5, pp. 2143–2154, 2013.
- [54] E. Szczerba, A. Zajkowska, A. Bochowicz et al., "Rise in antifibrotic and decrease in profibrotic microRNA protect the heart against fibrosis during pregnancy: a preliminary study," *Advances in Clinical and Experimental Medicine*, vol. 27, no. 7, pp. 867–872, 2018.
- [55] A. Haghikia, E. Podewski, E. Libhaber et al., "Phenotyping and outcome on contemporary management in a German cohort of patients with peripartum cardiomyopathy," *Basic research in cardiology*, vol. 108, no. 4, p. 366, 2013.
- [56] C. W. Hoeger, C. Turissini, and A. Asnani, "Doxorubicin cardiotoxicity: pathophysiology updates," *Current Treatment Options in Cardiovascular Medicine*, vol. 22, no. 11, pp. 1–17, 2020.
- [57] K. Renu, V. G. Abilash, P. B. TP, and S. Arunachalam, "Molecular mechanism of doxorubicin-induced cardiomyopathy—an update," *European journal of pharmacology*, vol. 818, pp. 241–253, 2018.
- [58] T. Horie, K. Ono, H. Nishi et al., "Acute doxorubicin cardiotoxicity is associated with miR-146a-induced inhibition of the neuregulin-ErbB pathway," *Cardiovascular Research*, vol. 87, no. 4, pp. 656–664, 2010.
- [59] R. Testa, A. R. Bonfigli, F. Prattichizzo, L. La Sala, V. De Nigris, and A. Ceriello, "The "metabolic memory" theory and the early treatment of hyperglycemia in prevention of diabetic complications," *Nutrients*, vol. 9, no. 5, p. 437, 2017.

- [60] S. Costantino, F. Paneni, T. F. Lüscher, and F. Cosentino, "MicroRNA profiling unveils hyperglycaemic memory in the diabetic heart," *European heart journal*, vol. 37, no. 6, pp. 572–576, 2016.
- [61] M. Aziz and K. Yadav, "Pathogenesis of atherosclerosis a review," *Medical & Clinical Reviews*, vol. 2, no. 3, pp. 1–6, 2016.
- [62] F. Spannella, F. Giulietti, C. Di Pentima, and R. Sarzani, "Prevalence and control of dyslipidemia in patients referred for high blood pressure: the disregarded "double-trouble" lipid profile in overweight/obese," *Advances in therapy*, vol. 36, no. 6, pp. 1426–1437, 2019.
- [63] K. Yang, Y. S. He, X. Q. Wang et al., "miR-146a inhibits oxidized low-density lipoprotein-induced lipid accumulation and inflammatory response via targeting toll-like receptor 4," *FEBS letters*, vol. 585, no. 6, pp. 854–860, 2011.
- [64] A. P. Landstrom, D. Dobrev, and X. H. Wehrens, "Calcium signaling and cardiac arrhythmias," *Circulation research*, vol. 120, no. 12, pp. 1969–1993, 2017.
- [65] H. S. Cheng, N. Sivachandran, A. Lau et al., "MicroRNA-146 represses endothelial activation by inhibiting pro-inflammatory pathways," *EMBO molecular medicine*, vol. 5, no. 7, pp. 1017–1034, 2013.
- [66] E. Raitoharju, L.-P. Lyytikäinen, M. Levula et al., "miR-21, miR-210, miR-34a, and miR-146a/b are up-regulated in human atherosclerotic plaques in the Tampere vascular study," *Atherosclerosis*, vol. 219, no. 1, pp. 211–217, 2011.
- [67] R. Gareus, E. Kotsaki, S. Xanthoulea et al., "Endothelial cell-specific NF- κ B inhibition protects mice from atherosclerosis," *Cell metabolism*, vol. 8, no. 5, pp. 372–383, 2008.
- [68] K. Li, D. Ching, F. S. Luk, and R. L. Raffai, "Apolipoprotein E enhances microRNA-146a in monocytes and macrophages to suppress nuclear factor- κ B-driven inflammation and atherosclerosis," *Circulation research*, vol. 117, no. 1, pp. e1–e11, 2015.
- [69] R. Saba, D. L. Sorensen, and S. A. Booth, "MicroRNA-146a: a dominant, negative regulator of the innate immune response," *Frontiers in immunology*, vol. 5, p. 578, 2014.
- [70] X. Sun, B. Icli, A. K. Wara et al., "MicroRNA-181b regulates NF- κ B-mediated vascular inflammation," *The Journal of clinical investigation*, vol. 122, no. 6, pp. 1973–1990, 2012.
- [71] M. Guo, X. Mao, Q. Ji et al., "miR-146a in PBMCs modulates Th1 function in patients with acute coronary syndrome," *Immunology and cell biology*, vol. 88, no. 5, pp. 555–564, 2010.
- [72] M. C. Meuwese, E. de Groot, R. Duivenvoorden et al., "ACAT inhibition and progression of carotid atherosclerosis in patients with familial hypercholesterolemia: the CAPTIVATE randomized trial," *Journal of the American Medical Association*, vol. 301, no. 11, pp. 1131–1139, 2009.
- [73] A. Shahriar, G. G. Shiva, B. Ghader, J. Farhad, A. Hosein, and H. Parsa, "The dual role of mir-146a in metastasis and disease progression," *Biomedicine & Pharmacotherapy*, vol. 126, article 110099, 2020.
- [74] F. Beg, R. Wang, Z. Saeed et al., "Circulating free and exosomal microRNAs as biomarkers of systemic response to heart failure," *Journal of the American College of Cardiology*, vol. 69, no. 11, p. 689, 2017.
- [75] P. Chouvarine, E. Legchenko, J. Geldner, C. Riehle, and G. Hansmann, "Hypoxia drives cardiac miRNAs and inflammation in the right and left ventricle," *Journal of Molecular Medicine*, vol. 97, no. 10, pp. 1427–1438, 2019.
- [76] W. Heggermont, A. P. Papageorgiou, A. Quaegebeur et al., "MicroRNA-146a interferes with TCA cycle flux via DLST and rewires cardiomyocyte metabolism in hypertensive heart failure," *European Journal of Heart Failure*, vol. 16, p. 102, 2014.
- [77] J. G. Oh, S. Watanabe, A. Lee et al., "miR-146a suppresses SUMO1 expression and induces cardiac dysfunction in maladaptive hypertrophy," *Circulation research*, vol. 123, no. 6, pp. 673–685, 2018.
- [78] F. J. Giordano, "Oxygen, oxidative stress, hypoxia, and heart failure," *The Journal of clinical investigation*, vol. 115, no. 3, pp. 500–508, 2005.
- [79] W. Huang, S.-S. Tian, P.-Z. Hang, C. Sun, J. Guo, and Z.-M. Du, "Combination of microRNA-21 and microRNA-146a attenuates cardiac dysfunction and apoptosis during acute myocardial infarction in mice," *Molecular Therapy-Nucleic Acids*, vol. 5, article e296, 2016.
- [80] H.-T. Huang, F. Wang, S.-G. Ding, Y.-B. Tian, Y.-M. Xu, and C.-J. Zhong, "Overexpression of miRNA-146A promoting the proliferation and angiogenesis of human coronary artery endothelial cells via NF2," *Acta Medica Mediterranea*, vol. 35, no. 1, pp. 109–116, 2019.
- [81] M. Desjarlais, S. Dussault, F. Rivard et al., "Forced expression of microRNA-146b reduces TRAF6-dependent inflammation and improves ischemia-induced neovascularization in hypercholesterolemic conditions," *Atherosclerosis*, vol. 289, pp. 73–84, 2019.
- [82] M.-y. Wu, G.-t. Yiang, W.-T. Liao et al., "Current mechanistic concepts in ischemia and reperfusion injury," *Cellular Physiology and Biochemistry*, vol. 46, no. 4, pp. 1650–1667, 2018.
- [83] G. Heusch, "Treatment of myocardial ischemia/reperfusion injury by ischemic and pharmacological postconditioning," *Comprehensive Physiology*, vol. 5, no. 3, pp. 1123–1145, 2011.
- [84] H.-H. Seo, S.-Y. Lee, C. Y. Lee et al., "Exogenous miRNA-146a enhances the therapeutic efficacy of human mesenchymal stem cells by increasing vascular endothelial growth factor secretion in the ischemia/reperfusion-injured heart," *Journal of vascular research*, vol. 54, no. 2, pp. 100–108, 2017.
- [85] M. Gao, X. Wang, X. Zhang et al., "Attenuation of cardiac dysfunction in polymicrobial sepsis by microRNA-146a is mediated via targeting of IRAK1 and TRAF6 expression," *The Journal of Immunology*, vol. 195, no. 2, pp. 672–682, 2015.
- [86] J. Krützfeldt, N. Rajewsky, R. Braich et al., "Silencing of microRNAs in vivo with 'antagomirs,'" *Nature*, vol. 438, no. 7068, pp. 685–689, 2005.
- [87] W. Heggermont, A. P. Papageorgiou, P. Carai et al., "MicroRNA 146a: new kid on the block in the pathophysiology of cardiac hypertrophy and a promising therapeutic target," *Acta Cardiologica*, vol. 67, no. 1, p. 120, 2012.
- [88] R. Widmer-Teske, K. Kueppers, W. Bielenberg et al., *Role of miR-146a in angiogenesis and myocardial regeneration*, American Heart Association, 2012.

Review Article

Neutrophil to Lymphocyte Ratio as a Biomarker for Predicting the Coronary Artery Abnormality in Kawasaki Disease: A Meta-Analysis

Shirin Sarejloo,¹ Matin Moallem Shahri,² Pouria Azami,¹ Alec Clark,³ Ethan Hass,³ Maryam Salimi ,⁴ Brandon Lucke-Wold,⁵ Shahram Sadeghvand,⁶ and Shokoufeh Khanzadeh ⁷

¹Cardiovascular Research Center, Shiraz University of Medical Sciences, Shiraz, Iran

²Department of Thoracic Surgery, Thoracic Surgery Research Center, School of Medicine, Mashhad University of Medical Sciences, Mashhad, Iran

³University of Central Florida College of Medicine, USA

⁴Bone and Joint Diseases Research Center, Shiraz University of Medical Sciences, Shiraz, Iran

⁵Department of Neurosurgery, University of Florida, Gainesville, Florida, USA

⁶Pediatric Health Research Center, Tabriz University of Medical Sciences, Tabriz, Iran

⁷Student Research Committee, Tabriz University of Medical Sciences, Tabriz, Iran

Correspondence should be addressed to Shokoufeh Khanzadeh; shokoufehkhazadeh2@yahoo.com

Received 13 April 2022; Revised 24 August 2022; Accepted 20 September 2022; Published 11 October 2022

Academic Editor: Simona Pichini

Copyright © 2022 Shirin Sarejloo et al. This is an open access article distributed under the Creative Commons Attribution License, which permits unrestricted use, distribution, and reproduction in any medium, provided the original work is properly cited.

We conducted a systematic review and meta-analysis on the relationship between the neutrophil to lymphocyte ratio (NLR) and coronary artery abnormalities (CAA) in patients with Kawasaki disease (KD), according to the Preferred Reporting Items for Systematic Reviews and Meta-Analyses (PRISMA) statements. We searched PubMed, Scopus, Web of Science, Embase, TRIP, Google Scholar, and ProQuest up to the 8th of August 2022. This was done to retrieve eligible studies. No date or language limitations were considered in this study. Methodology quality assessment was conducted according to the Newcastle–Ottawa scale (NOS). Standard mean difference (SMD) and its 95% confidence interval (CI) were used to depict the pooled continuous variables. Finally, 17 articles with 6334 KD patients, of whom 1328 developed CAA, were enrolled in this meta-analysis. NLR level was significantly higher in KD patients with CAA compared to those without CAA (SMD=0.81; 95% CI=0.05–1.57, $P=0.03$). In addition, NLR level was significantly higher in patients with coronary artery aneurysms than those without coronary artery aneurysms (SMD=2.29; 95% CI=0.18–4.41, $P=0.03$). However, no significant association between NLR and coronary artery dilation was observed in this meta-analysis (SMD=0.56; 95% CI=-0.86–1.99). There was no publication bias for the pooled SMD of NLR for coronary artery abnormality in KD (Egger's test $P=0.82$; Begg's test $P=0.32$). The NLR may be useful in monitoring CAA development in these patients and may further imply a mechanistic role in potential inflammation that mediates this process.

1. Introduction

Kawasaki disease (KD) is an acute, febrile vasculitis that occurs predominantly in children under 5 years old. It presents with a classic presentation that may include erythema of the palms and soles, maculopapular rash, conjunctival injection, oral mucosal abnormalities, and cervical lymph-

adenopathy [1]. Coronary artery abnormalities (CAA) have been identified in a subset of KD patients. One of the major complications is dilation of one or more arteries. This varies from minor arteries to large (or giant) CA aneurysms [1]. While dilations of the CAs have been found to regress in most cases, large aneurysms have demonstrated a tendency to persist for years, predisposing to rupture [2]. Further,

identification of large aneurysms in childhood has been associated with a significantly increased risk of developing adverse cardiac events in adulthood, including unstable angina pectoris and myocardial infarction [3]. The prevalence of large CA aneurysms in KD has diminished in recent decades, with studies reporting 0.1-0.5% incidence among KD cases since the introduction of intravenous gamma globulin (IVGG) treatment [4, 5]. Despite this downward trend, it is estimated that 5% of myocardial infarction cases in adults under 40 years old in the United States are caused as a consequence of the sequelae of KD [6].

No one etiology has been identified for KD or related CAA, although genetic and environmental factors have been speculated [1]. Elevations of proinflammatory blood markers during the acute phase of KD [7] suggest that a dysregulation of the inflammatory response is involved in the disease progression. The degree of this dysregulation may also determine the risk of developing CA aneurysms, as arterial wall infiltration by immune cells like neutrophils is an early pathological finding of KD-related CAA. This is followed by predominantly lymphocytic infiltrates in the subacute phase [8, 9].

Neutrophil to lymphocyte ratio (NLR) analysis of the peripheral blood is becoming a popular, cost-effective tool for the clinical assessment of inflammatory involvement in a wide variety of diseases [10, 11]. Neutrophils mediate non-specific inflammation by combating pathogens and releasing proinflammatory cytokines when recruited to the tissues. When neutrophilic recruitment becomes abnormally high, leukocytosis can be identified, as in KD [12]. Conversely, lymphocytes carry out functions of adaptive immunity by targeting the response rather than promoting nonspecific inflammation. There is growing evidence that both innate and adaptive immune cells mediate the systemic and tissue-specific effects of KD-like CA aneurysms [9]. In light of this, several studies have suggested that NLR calculation may aid in the clinical assessment of the inflammatory aspect of KD, serving as a metric for risk stratification and prediction for adverse cardiac events in adulthood [13–26].

Herein, we conducted a systematic review and meta-analysis on the relationship between NLR and CAA in KD patients. To the best of our knowledge, this is the first systematic review and meta-analysis on this topic.

2. Method

This systematic review was performed according to the Preferred Reporting Items for Systematic Reviews and Meta-Analyses (PRISMA) statements. Two investigators conducted study selection, data extraction, and quality assessment steps separately.

2.1. Study Selection. We searched PubMed, Scopus, Web of Science, Cochrane library, ScienceDirect, Embase, ProQuest, TRIP, and the Google Scholar up to the 8th August 2022 to retrieve eligible studies. The literature search was performed using the following keywords: “neutrophil to lymphocyte ratio,” “neutrophil-to-lymphocyte ratio,” or “NLR” in com-

ination with “coronary” and “Kawasaki.” The exact search strategy of each database is shown as supplementary file A. Moreover, the reference list of the relevant articles was also screened to determine additional studies. No date or language limitations were considered in this study.

2.2. Inclusion Criteria. The inclusion criteria were as follows: (i) case-control or cross-sectional design; (ii) peer-reviewed full-text publications; (iii) reporting the blood NLR data as mean \pm SD or median [range or interquartile range]; (iv) comparing KD patients with and without CAA including those with aneurysms and dilation.

2.3. Exclusion Criteria. The exclusion criteria were as follows: (i) data were unavailable or only reported in abstracts; (ii) articles were submitted by the same authors or institution which might have overlapping patients; (iii) duplicate publications; (iv) reviews, editorials, meeting abstracts, case reports, and non-comparative studies.

2.4. Data Extraction. The extracted information included the name of the first author, publication year, study design, country, number of patients in case and control groups, and the values of NLR in each group.

2.5. Methodology Quality Assessment. Methodologic quality assessment was conducted according to the Newcastle–Ottawa scale (NOS) with a score range of 0–9 points, and high quality was defined as a score of ≥ 6 .

2.6. Statistical Analysis. The statistical analysis was performed by using STATA version 12.0 (Stata Corporation, College Station, TX, USA). Standard mean difference (SMD) and its 95% confidence interval (CI) were used to depict the pooled continuous variables. In addition, the Cochrane Q test (χ^2) and I^2 test were used to evaluate statistical heterogeneity among the studies; if significant heterogeneity existed among included studies ($P < 0.05$ and $I^2 \geq 50\%$), a random-effect model was used; otherwise, the fixed-effect model was conducted. The publication bias was assessed using the funnel plot, Egger test, and Begg test. A two-tailed $P < 0.05$ was considered statistically significant.

3. Results

3.1. Study Selection. The flow chart diagram of the study selection is shown in Figure 1. A total of 1349 articles were yielded through a primary study search. Of these studies, 28 were from PubMed, 124 from Scopus, 30 from WOS, 824 from Google Scholar, 147 from Embase, 51 from ProQuest, 49 from TRIP database, 93 from ScienceDirect, and three from other sources. Among the studies, 196 articles were removed because of duplication, and 1055 publications were excluded due to reviews, meeting abstracts, no reporting on NLR data, and not being pertinent to CAA after screening the title and abstract. Thus, the remaining 98 articles were left for the full-text review. Of the 98 studies, 11 articles were removed because they were reviews, 39 were removed due to the lack of available data on NLR, and 31

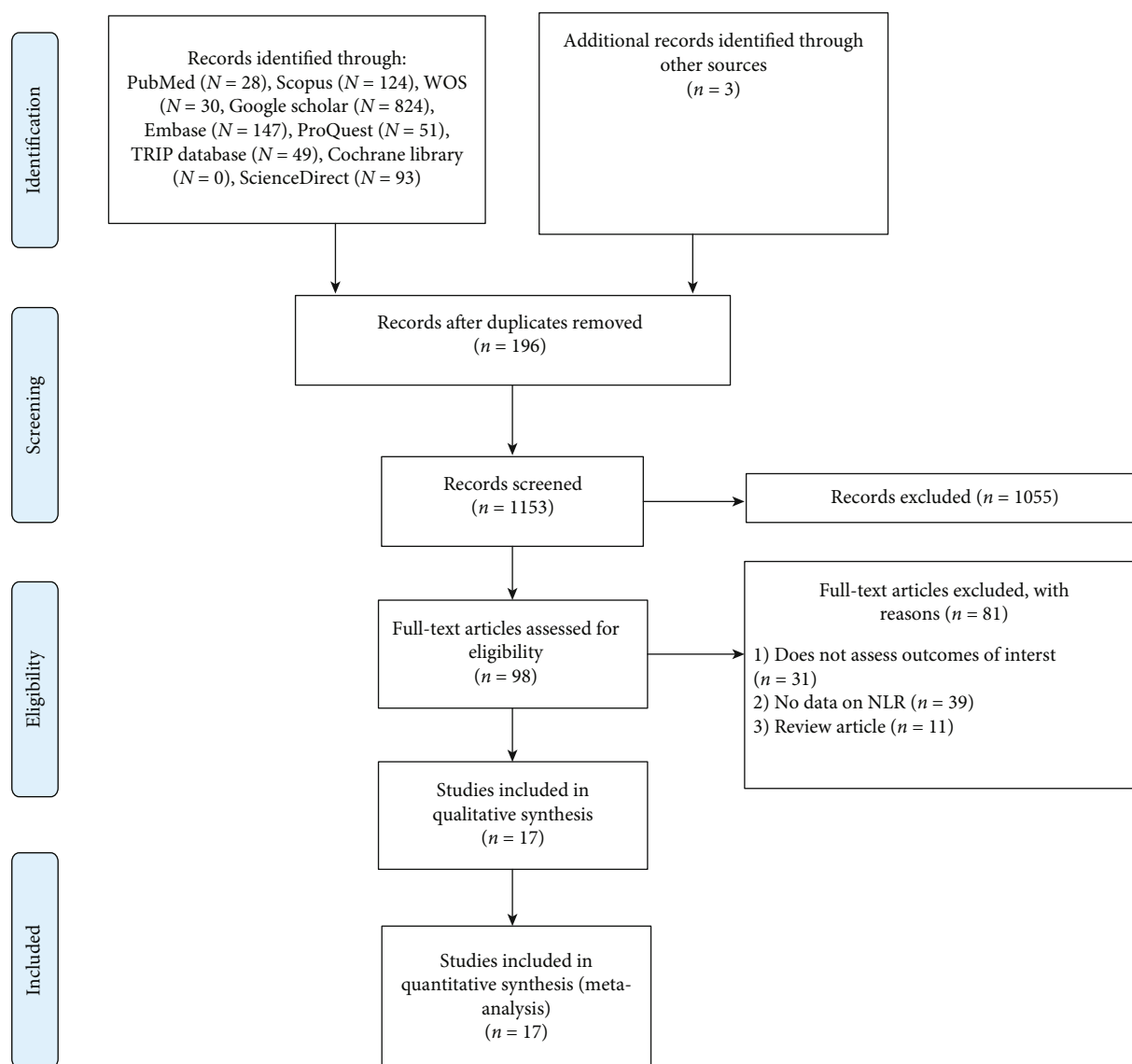


FIGURE 1: Flow chart of search and study selection.

were excluded because they did not assess outcomes of interest.

Finally, 17 articles with 6334 KD patients, of whom 1328 developed CAA, were enrolled in this meta-analysis [13–29]. The list of included studies is shown in supplementary file B.

3.2. Characteristics of Included Studies. All the selected studies were published from 2015 to 2021. Of 17 articles, seven came from China [21, 22, 24, 26–29], four from Korea [16, 19, 20, 25], three from Turkey [13, 17, 18], one from Japan [23], one from Taiwan [14], and one from Thailand [15]. Sixteen studies were retrospective [13–23, 25–29], and one study was prospective [24]. Twelve studies were written in English [13–17, 19–25], one in Turkish [18], and two studies in Chinese [26, 29]. Sixteen studies were published as journal articles [13–21, 23–29] and one study as a preprint [21]. The basic characteristics and data of interest in the eligible studies are summarized in Table 1. The demographic data of

samples included in the meta-analysis is shown in Table 2. Moreover, the methodological quality of the included articles was assessed according to NOS, and the scores ranged from 5 to 8. This indicates that the quality of selected studies was moderate to high.

3.3. The Association of NLR with Coronary Artery Abnormality in Kawasaki Disease. A total of 14 studies [13, 14, 16–26, 29] involving 5952 KD patients, of whom 1218 developed CAA, were included in the meta-analysis. Random-effect model was applied since significant heterogeneity was present ($I^2 = 99.0\%$; $P < 0.001$). From the results of our meta-analysis, NLR level was significantly higher in KD patients with CAA compared to those without CAA (SMD = 0.81; 95% CI = 0.05–1.57, $P = 0.03$, Figure 2).

3.4. The Association of NLR with Coronary Artery Aneurysm in Kawasaki Disease. A total of six studies [15, 19–21, 27, 28]

TABLE 1: General characteristic of included studies.

Author	Year	Country	Design	CAA group		Total	Non-CAA group				NOS score	
				N	NLR		N	NLR	CA aneurysm	CA dilation		N
Demir	2015	Turkey	R	49	1.50±1.28	26	2.02±1.63	–	–	–	–	5
Ha2	2015	Korea	R	525	1.20±0.07	62	2.21±0.49	15	4.72±1.72	47	1.39±0.22	7
Youn	2016	Korea	R	168	1.71±1.40	52	2.72±3.79	–	–	–	–	8
Cho	2017	Korea	R	158	4.78±4.88	38	4.15±3.50	–	–	–	–	7
Ha1	2017	Korea	R	613	3.27±2.48	69	3.75±3.81	15	6.53±7.37	54	2.98±2.83	6
Bozlu	2018	Turkey	R	43	3.59±3.41	15	2.99±2.83	–	–	–	–	5
Chantasiriwan	2018	Thailand	R	162	–	–	4.16±7.18	55	4.56±8.52	–	–	6
Hua	2018	China	R	1606	2.60±2.30	523	2.03±2.00	–	–	–	–	8
Nakada	2018	Japan	R	197	4.05±8.42	4	6.52±12.71	–	–	–	–	7
Gokce	2019	Turkey	R	114	2.17±1.14	39	2.29±2.51	–	–	–	–	6
Chang	2020	Taiwan	R	238	2.73±0.15	127	3.95±0.39	–	–	–	–	6
PengYoun	2020	China	R	513	2.63±2.28	67	3.40±2.50	–	–	–	–	7
Hu	2021	China	R	326	2.22±2.28	94	1.72±1.66	40	1.81±1.69	47	1.64±1.63	7
Yang	2021	China	P	28	4.20±3.80	38	2.40±2.50	–	–	–	–	6
Haiyan	2022	China	R	–	–	41	1.30± 1.02	37	1.93± 2.09	–	–	7
Liu	2022	China	R	–	–	69	5.52± 4.52	18	6.42± 3.67	–	–	7
Yanfei	2022	China	R	64	4.5± 5.1	156	3.1± 2.6	–	–	–	–	6

N: number; NLR: neutrophil to lymphocyte ratio; R: retrospective; P: prospective; CAA: coronary artery abnormality.

with 1916 KD patients, of whom 180 developed coronary artery aneurysm, were included in this meta-analysis. The heterogeneity tests showed the extinction of significant heterogeneity ($I^2 = 99.3\%$; $P < 0.001$), so the random-effect model was used. The results suggested that NLR level was significantly higher in patients with coronary artery aneurysms (SMD = 2.29; 95% CI = 0.18–4.41, $P = 0.03$, Figure 3) than in those without coronary artery aneurysms.

3.5. The Association of NLR with Coronary Artery Dilation in Kawasaki Disease. Three articles with 1612 KD patients [19–21], of whom 148 developed coronary artery dilation, were also included for the meta-analysis regarding the association between NLR and coronary artery dilation in KD. The random-effect model was used because of the extinction of significant heterogeneity in the heterogeneity tests ($I^2 = 98.5\%$; $P < 0.001$). However, no significant association between NLR and coronary artery dilation was observed in this meta-analysis (SMD = 0.56; 95% CI = -0.86–1.99, Figure 4).

3.6. Publication Bias. The assessment of publication bias of the included studies was performed using Begg's and Egger's tests. From the results of the publication bias test, we found that there was no evidence of publication bias for the pooled SMD of NLR for coronary artery abnormality in KD (Egger's test, $P = 0.82$; Begg's test, $P = 0.32$, Figure 5).

4. Discussion

The outcome of this study demonstrates that KD patients with CAA had significantly elevated levels of NLR compared to those without CAA. Statistically significant elevations in NLR were also demonstrated in patients with coronary

artery aneurysms compared with those without CAA. No significant elevations in NLR were demonstrated in those with coronary artery dilation compared to those without CAA and those with coronary artery aneurysms (Figure 6). Thus, results from this study suggest that the NLR may be useful in monitoring CAA development in these patients and may further imply a mechanistic role in inflammation that mediates this process.

4.1. Prognostic Value of NLR Related to Long-Term Sequelae of KD. The most severe and frequent complication of KD is the development of coronary artery involvement. The recent introduction of treatment with IVIG has reduced this problem. Despite treatment with intravenous gamma globulin, 2% to 4% of patients have coronary abnormalities or develop coronary aneurysms [30]. Those with giant aneurysms are at risk for stenosis and myocardial ischemia/infarction, which requires systemic anticoagulation with frequent follow-up. This predisposes to frequent stress testing and coronary angiography. In rare cases, patients will have coronary artery bypass grafting. Those with less severe coronary involvement need antiplatelet therapy and infrequent noninvasive testing [31]. Patients with normal echos after the acute phase are not treated, but the future impact of the disease is not certain, particularly in adult-onset coronary artery disease [32]. NLR might be associated with CAA and might predict long-term cardiovascular risk in KD patients, so it can help clinicians in the risk stratification of these patients. This aids in the development of diagnostic and therapeutic modalities to prevent mortality and morbidity in such patients.

4.2. NLR and Inflammation. It is well-known that neutrophils play a critical role in the incitement of the

TABLE 2: Demographic data of samples included in the meta-analysis.

Author	Sample size	CAA group		Non-CAA group		Total sample	
		Age *	Male percentage	Age*	Male percentage	Age*	Male percentage
Demir	75	31± 44	73%	36 ±44	55%	34 ±46	61%
Ha2	587	27.73± 3.19	82.3%	34.32± 0.99	55%	–	–
Youn	220	32.56± 29.40	69%	24.91± 19.47	61%	–	63%
Cho	196	–	–	–	–	32± 21	59%
Ha1	682	–	–	–	–	30.0 (14.0-46.0)	57.9%
Bozlu	58	–	–	–	–	52.56±22.99	60%
Chantasiriwan	217	14[3-168]	60%	18[2-79]	64%	–	–
Hua	2129	19 [9–33]	69%	23 [11–47]	59%	–	–
Nakada	201	39.5 [20–62]	75%	24 [2–159]	50%	24 [2–159]	51%
Gokce	153	28 [15–46]	69%	27 [15–47]	64%	–	–
Chang	365	1.4[0.7–2.4]	72%	1.5[0.8–2.6]	54%	–	–
PengYoun	580	34.4± 30.1	70%	28.4± 22.5	65%	–	–
Hu	420	–	70%	–	59%	2.4 years[2 months-11 years]	62%
Yang	66	2.1 ± 1.3	66%	2.5 ± 1.5	61%	–	–
Haiyan	78	2.4 (1.8-3.7)	51.4%	3.0 (2.0-4.9)	65.9%	–	–
Liu	87	35.44 ± 36.71	78%	36.77 ± 22.54	75%	36.49 ± 25.86	76%
Yanfei	220	3 ± 2	69	2.9 ± 2.1	58	–	–

SD: standard deviation; CAA: coronary artery abnormality. *Expressed as mean ± SD or median (IQR) or median [range]. All ages are expressed as months, except for Haiyan and Chang.

proinflammatory response in the body, including both acute and chronic inflammatory states [12, 33, 34]. Furthermore, a reduction in lymphocyte count is commonly seen during proinflammatory states due to the modulatory role that lymphocytes play in these states [35]. Thus, the inverse relationship between neutrophils and lymphocytes makes the NLR a potentially optimal marker in proinflammatory states or conditions, such as CAA in KD patients.

As it pertains to the development of CAA in KD patients, a proposed mechanism of action that has been backed by significant evidence is the direct increased inflammatory response leading to arterial dilation and subsequent aneurysm formation. Several inflammatory cytokines have now been linked to this phenomenon, including IL-6, IL-8, TNF- α , IFN- γ , and C-reactive protein (CRP) [36–39]. Research has demonstrated that neutrophils routinely respond to several signaling pathways on the biochemical level, ultimately leading to the direct production of several of these cytokines [40, 41]. These cytokines manifest the inflammatory state by several mechanisms, including endothelial dysfunction and collagen destruction. This leads to the compromised structural integrity of coronary arteries, which directly contributes to intimal thickening and compromised laminar blood flow, eventual thrombosis, or aneurysm development [42]. Thus, neutrophils may be involved in both the initial incitement of and propagation of inflammation in the setting of disease progression. In either case, the NLR appears to be a prime candidate for a reliable inflammatory marker in these conditions.

4.3. NLR and Arterial Abnormalities. Potential mechanisms by which the NLR can incite CAA development in KD patients can be divided into neutrophil-derived and lymphocyte-derived etiologies.

Neutrophils have been, and have largely remained, the main mediator of the development of CAA seen in KD patients [43]. Researchers suspect that neutrophils begin to infiltrate the coronary arteries at approximately 1-2 weeks after the development of KD, which are then replaced by monocytes. With the eventual resolution of inflammation after approximately two months after fever onset, aneurysm formation occurs [43]. Several studies have highlighted the significant increase in neutrophil count seen in these patients that distinguish it from other viral etiologies [44, 45]. In more recent years, the role of neutrophils in the development of CAA in KD patients has been further characterized. Necrotizing arteritis has been described as a neutrophil-mediated process characterized by the gradual destruction of the adventitia of the endothelium. Both the onset and completion occur within the first two weeks consistent with fever period [46]. Neutrophil extracellular traps (NETs) are a mechanism specific to neutrophils. It is characterized by morphological changes that facilitate the trapping of pathogens by both oxidative and non-oxidative mechanisms [47]. NETs have now been demonstrated to play a role in inflammation in several autoimmune diseases, such as rheumatoid arthritis, systemic lupus erythematosus (SLE), and anti-neutrophilic cytoplasmic antibody- (ANCA-) associated vasculitis [48]. Even more recently, evidence of NET production in preclinical models mimicking KD conditions

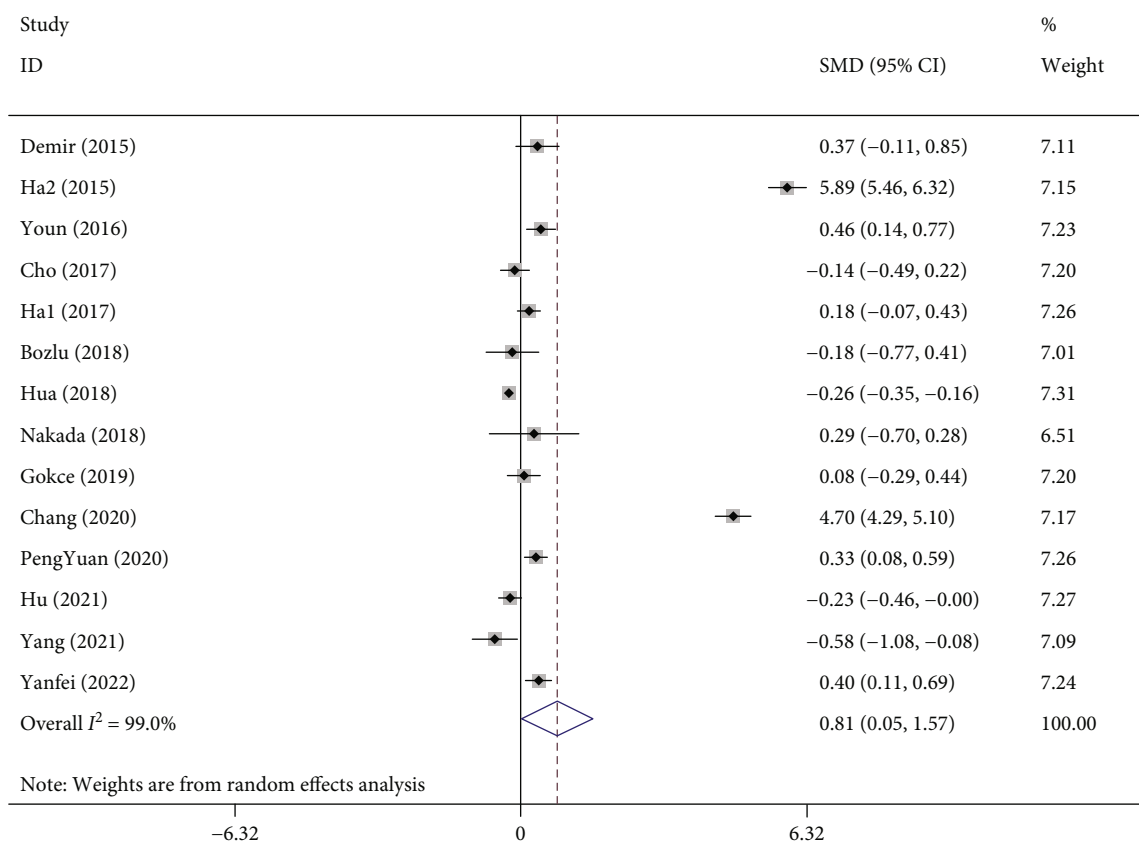


FIGURE 2: Meta-analysis of differences in NLR level between Kawasaki patients with coronary artery abnormality and those without coronary artery abnormality.

and clinical models exposed to KD serum has been demonstrated [49, 50]. Vascular endothelial growth factor (VEGF) production has also been hypothesized as a mechanism by which CAA develops, with the early production of VEGF in the acute phase seen predominately by neutrophils. In the chronic phase, production is seen predominately by mononuclear cells [51]. The exact etiology of this relationship is unclear but likely due, at least in part, to vascular injury and remodeling [51]. Furthermore, increased neutrophil respiratory burst, a marker of neutrophil activation, has been demonstrated in KD patients with CAA compared to healthy controls or KD patients without CAA [52]. This adds credence to the assertion that neutrophils are not only produced in increased quantities in this context but likely play a more active role in the pathogenesis of CAA.

Evidence for the mechanistic role of neutrophils in CAA development is most convincing in the acute phase of KD (1-2 weeks). Indeed, it has been shown that neutrophils infiltrate coronary arteries in KD most rapidly in the early stage of the disease, with peaks in macrophage and lymphocytes later in the disease course [53]. However, in the subacute and chronic phases, evidence for the role of other cells, particularly lymphocytes, is amassing [42]. A decrease in lymphocyte count is typically seen with systemic inflammatory responses [35]. Thus, as a condition where systemic inflammatory responses are seen, KD would logically be expected to manifest with a decreased lymphocyte count. However,

studies in the context of CAA in KD tend to demonstrate an increase in lymphocyte response, particularly T-lymphocyte activation. This remains the main mediator of CAA in the post-acute phase of KD [54–56]. A concurrent type I interferon response has also been characterized alongside this T-lymphocyte activation, which some have speculated as potentially due to a presently unidentified infectious (i.e., viral) cause [54]. Interestingly, recent studies have also suggested a role of lymphocytes and even macrophages in the pathogenesis of CAA in the acute phase of the disease, with demonstrated transmural infiltration of primarily CD8 T lymphocytes and macrophages mainly demonstrated in the adventitial layer [57].

Although this has been purported to be a potential cause, a viral or bacterial etiology for KD has yet to be identified. Given that these findings seem to conflict on a superficial level with the logical assumption that lymphopenia, rather than lymphocytosis, would be seen in KD, a further explanation in the context of the results of this study is warranted. Firstly, the results of the aforementioned study mention that the evidence for the T-lymphocyte activation in KD is most significant in subacute or chronic KD cases [54]. If this is the case, then the lymphopenia most associated with systemic inflammatory responses would likely predominate in the acute phase of KD. Since lymphopenia would further increase the NLR in the setting of acute disease, and the classic clinical presentation is well-known

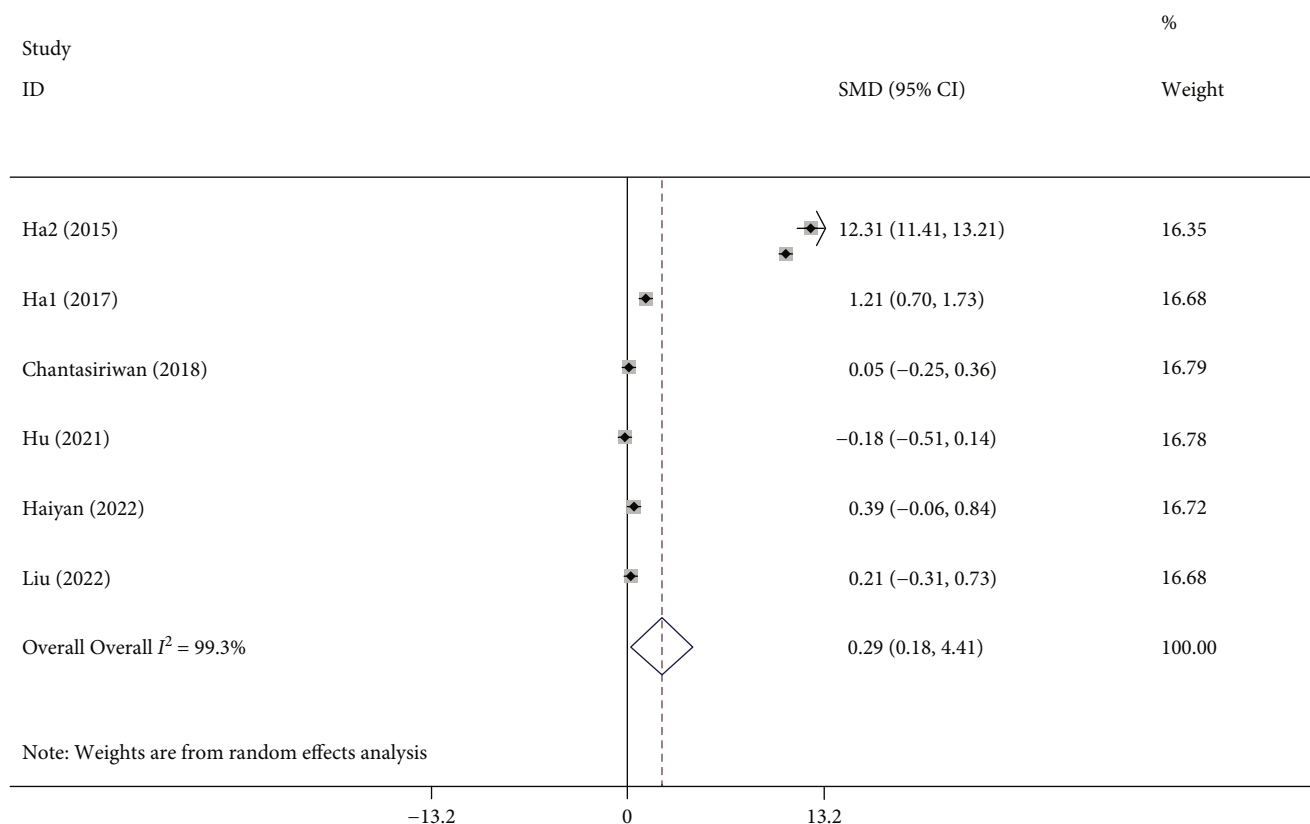


FIGURE 3: Meta-analysis of differences in NLR level between Kawasaki patients with coronary artery aneurysm and those with normal coronary arteries.

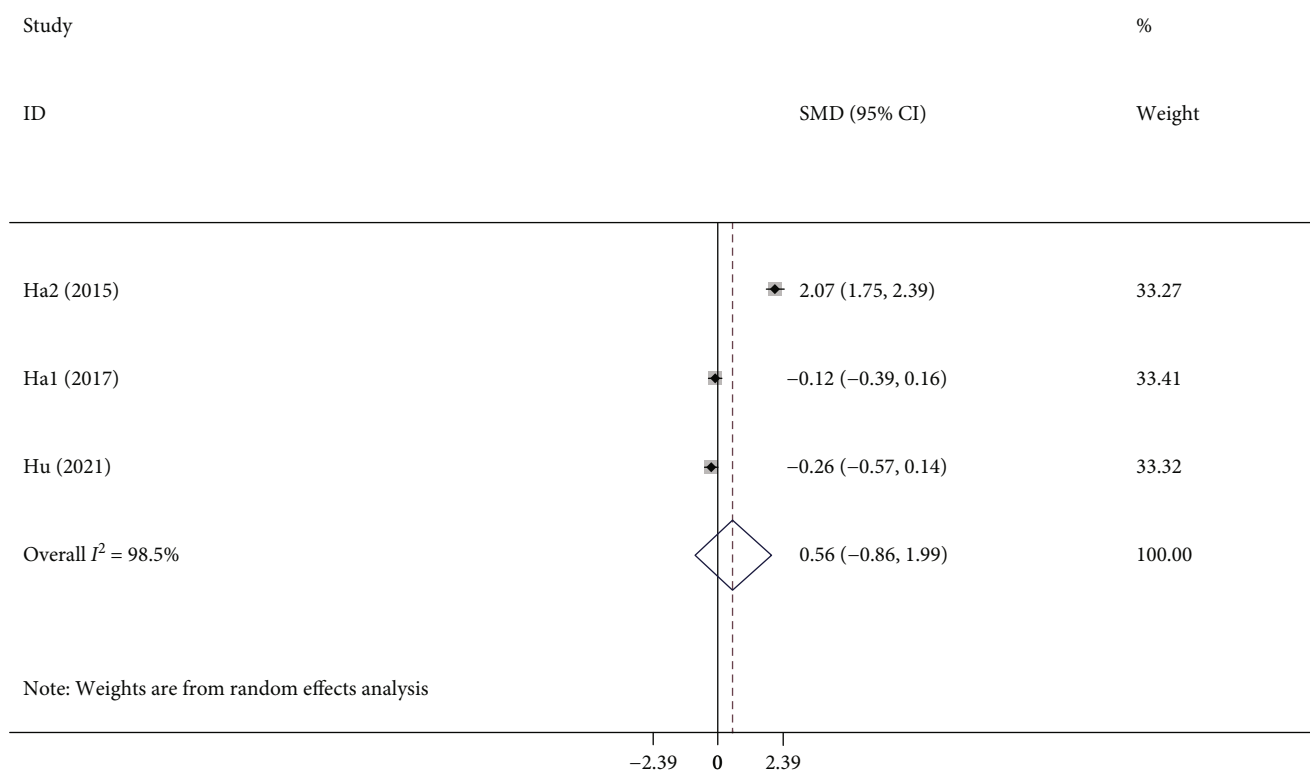


FIGURE 4: Meta-analysis of differences in NLR level between Kawasaki patients with coronary artery dilation and those with normal coronary artery.

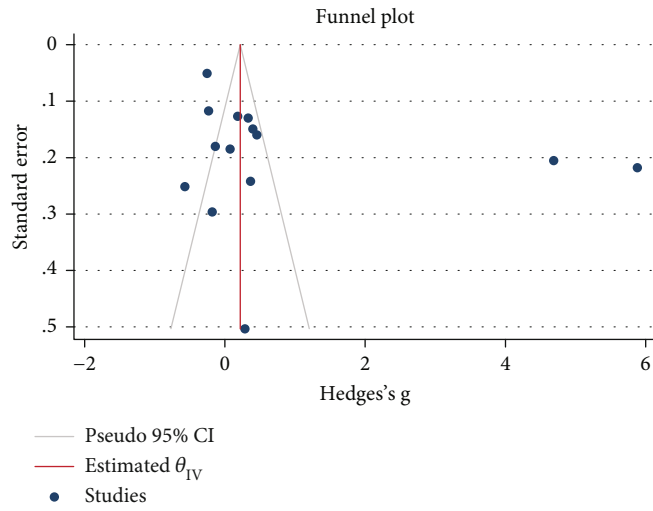


FIGURE 5: Funnel plot assessing publication bias.

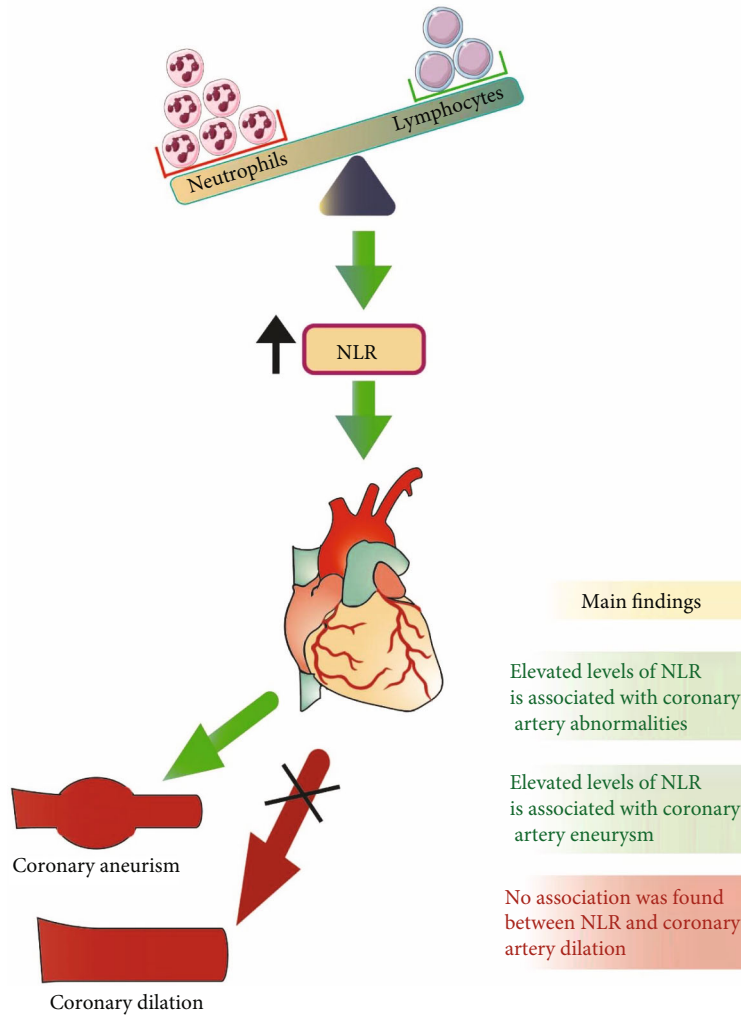


FIGURE 6: Main findings of the study.

and easily identifiable in the clinical setting, this would strengthen the case for using NLR as a screening marker for CAA in KD patients upon the patient's initial presentation. Moreover, it is also possible that even if lymphocytosis is present in these patients, the relative increase in neutrophil count may be much larger than the marginal increase in lymphocyte count, thus elevating the NLR regardless.

4.4. Biomarker Usage and Pharmacologic Insights. The utility of the NLR as a predictive biomarker for the development of CAA has been demonstrated in recent years, with one study reporting an $\text{NLR} > 3.5$ as an independent risk factor for developing CAA in KD patients [14]. One study also showed that an IL-10 level greater than 8 pg/dL displayed a sensitivity of 75% and specificity of 64.4% when predicting the concurrent development of coronary artery lesions before intravenous immunoglobulin (IVIG) administration [37]. After IVIG administration, an IL-6 level greater than 10 pg/mL had a sensitivity of 67.9% and a specificity of 81.7% for predicting the presence of coronary artery lesions, and an IL-10 level greater than 6 pg/mL had a sensitivity of 53.6% and specificity of 86% for predicting the presence of coronary artery lesions [37].

Research has also demonstrated that IVIG given early in the course of disease showed a quicker reduction in circulating neutrophils and a decrease in coronary artery lesion formation compared to patients who received aspirin only or those who received IVIG later in the disease course [14]. This not only demonstrates the potential efficacy of IVIG in reducing the CAA sequelae but also implies a mediating relationship between increased neutrophil count and CAA development. Moreover, IVIG administration can decrease several cytokines, including IL-6, IL-10, TNF- α , and IFN- γ , in patients with KD [37, 38]. In patients with concurrent CAA, the response of certain cytokine levels to IVIG may vary, with one study showing that levels of TNF- α may slightly increase in KD patients with coronary artery lesions compared to greatly decreased levels seen in KD patients without coronary artery lesions [37]. Furthermore, a recent meta-analysis demonstrated the potential diagnostic utility of the NLR as an independent predictor for IVIG-resistant KD. Namely, the NLR was shown to have a sensitivity of 66% and a specificity of 71% for predicting IVIG resistance in these patients [58]. These findings increase the credibility of the NLR in overall context for KD, demonstrating that it can serve as a useful tool in predicting response to first-line treatment as well as in predicting outcomes.

Given the results of these studies, the role that the NLR may play in diagnosing CAA in KD patients is promising. It can be used to develop medications aimed at reducing neutrophil count and activation and prevent long-term complications.

4.5. Limitation. The findings of this report are subject to some limitations. First, heterogeneity in studies was greater than expected due to various treatment regimens, duration of recorded stays, center protocols, different study populations, timing of blood tests from which NLR was calculated, and different study designs. Second, several of the studies are

limited by bias, whether selection or publication, which should be considered. Third, the effect size for several of the tests was limited to a few studies. Thereby widespread adoption and applicability are again a concern warranting further investigation.

5. Conclusion

In conclusion, results from our study demonstrate that patients with KD and concurrent CAA had elevated levels of NLR compared to KD patients without CAA. NLR represents a unique inflammatory marker whose elevation in CAA implicates immune system imbalance in the pathogenesis of the disease. Further, our findings support NLR to be a promising biomarker that can be readily integrated into clinical settings to aid in the prediction and prevention of CAA. Given the implications for its role in inflammation, the NLR may be a useful tool for early monitoring in these patients. Evidence suggests that it may be most useful in the acute phase of the disease. This evidence also warrants investigation into new drug targets for developing novel medications. With the development of new biomarkers and therapeutic modalities, we can better prevent and treat CAA in KD with an emphasis on decreasing long-term morbidity and mortality.

Data Availability

All data generated or analyzed during this study are included in this published article.

Conflicts of Interest

The authors declare that there is no conflict of interest regarding the publication of this article.

Supplementary Materials

The exact search strategy of each database is shown as supplementary file A. The list of included studies is shown in supplementary file B. (*Supplementary Materials*)

References

- [1] B. W. McCrindle, A. H. Rowley, J. W. Newburger et al., "Diagnosis, Treatment, and Long-Term Management of Kawasaki Disease: A Scientific Statement for Health Professionals From the American Heart Association," *Circulation*, vol. 135, no. 17, pp. e927–e999, 2017.
- [2] N. Advani, S. Sastroasmoro, T. Ontoseno, and C. S. Uiterwaal, "Long-term outcome of coronary artery dilatation in Kawasaki disease," *Annals of Pediatric Cardiology*, vol. 11, no. 2, pp. 125–129, 2018.
- [3] M. Miura, T. Kobayashi, T. Kaneko et al., "Association of Severity of Coronary Artery Aneurysms in Patients With Kawasaki Disease and Risk of Later Coronary Events," *JAMA Pediatrics*, vol. 172, no. 5, article e180030, 2018.
- [4] Y. Tang, X. Gao, J. Shen, L. Sun, and W. Yan, "Epidemiological and Clinical Characteristics of Kawasaki Disease and Factors Associated with Coronary Artery Abnormalities in East China: Nine Years Experience," *Journal of Tropical Pediatrics*, vol. 62, no. 2, pp. 86–93, 2016.

- [5] H. Masuda, R. Ae, T.-a. Koshimizu et al., "Epidemiology and Risk Factors for Giant Coronary Artery Aneurysms Identified After Acute Kawasaki Disease," *Pediatric Cardiology*, vol. 42, no. 4, pp. 969–977, 2021.
- [6] L. B. Daniels, M. S. Tjajadi, H. H. Walford et al., "Prevalence of Kawasaki Disease in Young Adults With Suspected Myocardial Ischemia," *Circulation*, vol. 125, no. 20, pp. 2447–2453, 2012.
- [7] H. Chaudhary, J. Nameirakpam, R. Kumrah et al., "Biomarkers for Kawasaki Disease: Clinical Utility and the Challenges Ahead," *Frontiers in Pediatrics*, vol. 7, 2019.
- [8] K. Takahashi, T. Oharaseki, and Y. Yokouchi, "Histopathological aspects of cardiovascular lesions in Kawasaki disease," *International Journal of Rheumatic Diseases*, vol. 21, no. 1, pp. 31–35, 2018.
- [9] S. Menikou, P. R. Langford, and M. Levin, "Kawasaki Disease: The Role of Immune Complexes Revisited," *Frontiers in Immunology*, vol. 10, 2019.
- [10] R. Zahorec, "Neutrophil-to-lymphocyte ratio, past, present and future perspectives," *Bratislava Medical Journal*, vol. 122, no. 7, pp. 474–488, 2021.
- [11] S. Takeshita, Y. Kawamura, T. Kanai, Y. Yoshida, Y. Tsujita, and S. Nonoyama, "The Role of Neutrophil Activation in the Pathogenesis of Kawasaki Disease," *Pediatric Infectious Diseases: Open Access*, vol. 3, no. 1, 2018.
- [12] E. Kolaczowska and P. Kubes, "Neutrophil recruitment and function in health and inflammation," *Nature Reviews. Immunology*, vol. 13, no. 3, pp. 159–175, 2013.
- [13] G. Bozlu, D. Karpuz, O. Hallioglu, S. Unal, and N. Kuyucu, "Relationship between mean platelet volume-to-lymphocyte ratio and coronary artery abnormalities in Kawasaki disease," *Cardiology in the Young*, vol. 28, no. 6, pp. 832–836, 2018.
- [14] L. S. Chang, Y. J. Lin, J. H. Yan, M. M. H. Guo, M. H. Lo, and H. C. Kuo, "Neutrophil-to-lymphocyte ratio and scoring system for predicting coronary artery lesions of Kawasaki disease," *BMC Pediatrics*, vol. 20, no. 1, p. 398, 2020.
- [15] N. Chantasiriwan, S. Silvilairat, K. Makonkawkeyoon, Y. Pongprot, and R. Sittiwangkul, "Predictors of intravenous immunoglobulin resistance and coronary artery aneurysm in patients with Kawasaki disease," *Paediatrics and international child health*, vol. 38, no. 3, pp. 209–212, 2018.
- [16] H. J. Cho, S. Y. Bak, S. Y. Kim et al., "High neutrophil : lymphocyte ratio is associated with refractory Kawasaki disease," *Pediatrics International*, vol. 59, no. 6, pp. 669–674, 2017.
- [17] F. Demir, C. Karadeniz, R. Ozdemir et al., "Usefulness of Neutrophil to Lymphocyte Ratio in Prediction of Coronary Artery Lesions in Patients with Kawasaki Disease," *Balkan Medical Journal*, vol. 32, no. 4, pp. 371–376, 2015.
- [18] Z. G. Gayretli Aydın and G. Tanır, "Kawasaki Hastalığında Koroner Arter Tulumunun Belirlenmesinde Lenfosit Monosit Oranının Değeri Kawasaki Hastalığı: Lenfosit Monosit Oranı," *Medical Journal of Bakirkoy*, vol. 15, no. 2, 2019.
- [19] K. S. Ha, G. Y. Jang, J. H. Lee, K. C. Lee, and C. S. Son, "Laboratory Markers in Incomplete Kawasaki Disease according to Coronary Artery Outcome," *Korean Circulation Journal*, vol. 48, no. 4, pp. 287–295, 2018.
- [20] K. S. Ha, J. Lee, G. Y. Jang et al., "Value of neutrophil-lymphocyte ratio in predicting outcomes in Kawasaki disease," *The American Journal of Cardiology*, vol. 116, no. 2, pp. 301–306, 2015.
- [21] J. Hu and W. Ren, *Analysis of Risk Factors of Kawasaki Disease With Coronary Artery Lesions*, 2021.
- [22] W. Hua, F. Ma, Y. Wang et al., "A new scoring system to predict Kawasaki disease with coronary artery lesions," *Clinical Rheumatology*, vol. 38, no. 4, pp. 1099–1107, 2019.
- [23] T. Nakada, "Acute phase treatment for prevention of coronary artery stenosis caused in Kawasaki disease: a single center retrospective study," *Journal of Advanced Research in Medicine*, vol. 5, no. 4, pp. 1–7, 2018.
- [24] M. Yang, H. Weng, Q. Pei, F. Jing, and Q. Yi, "The Relationship between Retinol-Binding Protein 4 and Markers of Inflammation and Thrombogenesis in Children with Kawasaki Disease," *Mediators of Inflammation*, vol. 2021, Article ID 7029514, 7 pages, 2021.
- [25] S. E. Youn, H. Y. Ju, K. S. Lee, S. H. Cha, M. Y. Han, and K. L. Yoon, "Severe Skin Lesions or Arthritis May be Associated with Coronary Artery Lesions in Kawasaki Disease," *Pediatric Infection and Vaccine*, vol. 23, no. 2, pp. 102–108, 2016.
- [26] C. Pengli et al., "Predictive value of systemic immune-inflammatory index for coronary dilation in children with Kawasaki disease," *Chinese Journal of Immunology*, vol. 36, no. 16, p. 2003, 2020.
- [27] G. Haiyan, L. Jianming, T. Suqian, Q. Dong, L. Shuang, and Z. Jin, "Blood routine risk factors for coronary artery aneurysm in infants younger than 8 months with Kawasaki disease," *BMC Pediatrics*, vol. 22, no. 1, pp. 1–8, 2022.
- [28] J. Liu, Y. Huang, C. Chen, D. Su, S. Qin, and Y. Pang, "Risk Factors for Resistance to Intravenous Immunoglobulin Treatment and Coronary Artery Abnormalities in a Chinese Pediatric Population With Kawasaki Disease: A Retrospective Cohort Study," *Frontiers in Pediatrics*, vol. 10, 2022.
- [29] Y. Yanfei and Z. Liping, "The diagnostic value of heart rate variability index and neutrophil-to-lymphocyte ratio in children with Kawasaki disease complicated with coronary artery disease," *e-journal of developmental medicine*, vol. 10, no. 3, pp. 174–181, 2022.
- [30] H. Hamada, H. Suzuki, Y. Onouchi et al., "Efficacy of primary treatment with immunoglobulin plus CYCLOSPORINE for prevention of coronary artery abnormalities in Kawasaki disease PATIENTS predicted to be at increased risk of IVIG NON- RESPONSE (KAICA STUDY): a CONTROLLED, PHASE 3, RANDOMISED, open-label, BLINDED-ENDPOINTS trial," *The Lancet*, vol. 58, Supplement_2, pp. 1128–1137, 2019.
- [31] J. P. Griffin, A. R. Powell, P. H. Bhagat, A. H. Bartlett, and S. M. Rotolo, "A Preliminary, Single-Center Retrospective Chart Review of Infusion Times of Intravenous Immune Globulin in Kawasaki Disease and Clinical Outcomes," *The Journal of Pediatric Pharmacology and Therapeutics*, vol. 27, no. 5, pp. 415–418, 2022.
- [32] E. Liu, J. Gonzalez, and A. Siu, "Use of premedication with intravenous immune globulin in Kawasaki disease: A retrospective review," *Pediatric Allergy and Immunology*, vol. 32, no. 4, pp. 750–755, 2021.
- [33] C. Silvestre-Roig, Z. G. Fridlender, M. Glogauer, and P. Scapini, "Neutrophil Diversity in Health and Disease," *Trends in Immunology*, vol. 40, no. 7, pp. 565–583, 2019.
- [34] P. X. Liew and P. Kubes, "The Neutrophil's Role During Health and Disease," *Physiological Reviews*, vol. 99, no. 2, pp. 1223–1248, 2019.
- [35] J. Núñez, G. Miñana, V. Bodí et al., "Low lymphocyte count and cardiovascular diseases," *Current Medicinal Chemistry*, vol. 18, no. 21, pp. 3226–3233, 2011.

- [36] C. Y. Lin, C. C. Lin, B. Hwang, and B. N. Chiang, "Cytokines predict coronary aneurysm formation in Kawasaki disease patients," *European Journal of Pediatrics*, vol. 152, no. 4, pp. 309–312, 1993.
- [37] Y. Wang, W. Wang, F. Gong et al., "Evaluation of intravenous immunoglobulin resistance and coronary artery lesions in relation to Th1/Th2 cytokine profiles in patients with Kawasaki disease," *Arthritis and Rheumatism*, vol. 65, no. 3, pp. 805–814, 2013.
- [38] A. Nandi, P. Pal, and S. Basu, "A comparison of serum IL6 and CRP levels with respect to coronary changes and treatment response in Kawasaki disease patients: a prospective study," *Rheumatology International*, vol. 39, no. 10, pp. 1797–1801, 2019.
- [39] M. Shimizu, M. Mizuta, M. Usami et al., "Clinical significance of serum soluble TNF receptor II level and soluble TNF receptor II/I ratio as indicators of coronary artery lesion development in Kawasaki disease," *Cytokine*, vol. 108, pp. 168–172, 2018.
- [40] C. Rosales, "Neutrophil: A Cell with Many Roles in Inflammation or Several Cell Types?," *Frontiers in Physiology*, vol. 9, p. 113, 2018.
- [41] W. M. Nauseef and N. Borregaard, "Neutrophils at work," *Nature Immunology*, vol. 15, no. 7, pp. 602–611, 2014.
- [42] D. Zhang, L. Liu, X. Huang, and J. Tian, "Insights Into Coronary Artery Lesions in Kawasaki Disease," *Frontiers in Pediatrics*, vol. 8, p. 493, 2020.
- [43] S. Amano, F. Hazama, H. Kubagawa, K. Tasaka, H. Haebara, and Y. Hamashima, "General pathology of Kawasaki disease. On the morphological alterations corresponding to the clinical manifestations," *Acta Pathologica Japonica*, vol. 30, no. 5, pp. 681–694, 1980.
- [44] S. J. Popper, V. E. Watson, C. Shimizu, J. T. Kanegaye, J. C. Burns, and D. A. Relman, "Gene transcript abundance profiles distinguish Kawasaki disease from adenovirus infection," *The Journal of Infectious Diseases*, vol. 200, no. 4, pp. 657–666, 2009.
- [45] S. J. Popper, C. Shimizu, H. Shike et al., "Gene-expression patterns reveal underlying biological processes in Kawasaki disease," *Genome Biology*, vol. 8, no. 12, p. R261, 2007.
- [46] J. M. Orenstein, S. T. Shulman, L. M. Fox et al., "Three linked vasculopathic processes characterize Kawasaki disease: a light and transmission electron microscopic study," *PLoS One*, vol. 7, no. 6, article e38998, 2012.
- [47] M. Zawrotniak and M. Rapala-Kozik, "Neutrophil extracellular traps (NETs) - formation and implications," *Acta Biochimica Polonica*, vol. 60, no. 3, pp. 277–284, 2013.
- [48] E. Fousert, R. Toes, and J. Desai, "Neutrophil Extracellular Traps (NETs) Take the Central Stage in Driving Autoimmune Responses," *Cell*, vol. 9, no. 4, 2020.
- [49] M. Noval Rivas and M. Arditi, "Kawasaki disease: pathophysiology and insights from mouse models," *Nature Reviews Rheumatology*, vol. 16, no. 7, pp. 391–405, 2020.
- [50] K. Yamashita, A. Takaori-Kondo, and K. Mizugishi, "Exaggerated neutrophil extracellular trap formation in Kawasaki disease: a key phenomenon behind the outbreak in western countries?," *Annals of the Rheumatic Diseases*, vol. 81, no. 9, p. e177, 2022.
- [51] Y. Hamamichi, F. Ichida, X. Yu et al., "Neutrophils and mononuclear cells express vascular endothelial growth factor in acute Kawasaki disease: its possible role in progression of coronary artery lesions," *Pediatric Research*, vol. 49, no. 1, pp. 74–80, 2001.
- [52] J. Hu, W. Qian, Z. Yu et al., "Increased Neutrophil Respiratory Burst Predicts the Risk of Coronary Artery Lesion in Kawasaki Disease," *Frontiers in Pediatrics*, vol. 8, p. 391, 2020.
- [53] K. Takahashi, T. Oharaseki, S. Naoe, M. Wakayama, and Y. Yokouchi, "Neutrophilic involvement in the damage to coronary arteries in acute stage of Kawasaki disease," *Pediatrics International*, vol. 47, no. 3, pp. 305–310, 2005.
- [54] A. H. Rowley, K. M. Wylie, K. Y. Kim et al., "The transcriptional profile of coronary arteritis in Kawasaki disease," *BMC Genomics*, vol. 16, p. 1076, 2015.
- [55] Y. Onouchi, T. Gunji, J. C. Burns et al., "ITPKC functional polymorphism associated with Kawasaki disease susceptibility and formation of coronary artery aneurysms," *Nature Genetics*, vol. 40, no. 1, pp. 35–42, 2008.
- [56] Y. Onouchi, K. Ozaki, J. C. Buns et al., "Common variants in CASP3 confer susceptibility to Kawasaki disease," *Human Molecular Genetics*, vol. 19, no. 14, pp. 2898–2906, 2010.
- [57] T. J. Brown, S. E. Crawford, M. L. Cornwall, F. Garcia, S. T. Shulman, and A. H. Rowley, "CD8 T lymphocytes and macrophages infiltrate coronary artery aneurysms in acute Kawasaki disease," *The Journal of Infectious Diseases*, vol. 184, no. 7, pp. 940–943, 2001.
- [58] Z. Onouchi, K. Hamaoka, S. Ozawa, K. Sakata, N. Kiyosawa, and H. Ito, "Neutropenia in the acute phase of Kawasaki disease and prevention of coronary artery aneurysm," *Pediatrics International*, vol. 51, no. 4, pp. 448–452, 2009.

Research Article

Investigation of Statin Medication Use in Elderly Patients with Cardiovascular Disease on Regular Physical Examination and the Relationship with Glucolipid Metabolism and Adverse Cardiovascular Prognosis

Chang Liu,¹ Rui Ma,² Daifeng Gao,³ Bin Hu,⁴ Xiaolei Yin,⁵ Zhipeng Liu,⁶ Hu Lin ,⁶ and Zhenhua Zhang ⁷

¹Physical Examination Center, The 305th Hospital of the PLA, Beijing, China

²Department of Pharmacy, The 305th Hospital of the PLA, Beijing, China

³Department of Geriatric Medicine, Health Division of Guard Bureau, Joint Staff of the Central Military Commission, Beijing, China

⁴Department of Stomatology, The 305th Hospital of the PLA, Beijing, China

⁵Department of Ophthalmology, The 305th Hospital of the PLA, Beijing, China

⁶Department of Medical Administration, The 305th Hospital of the PLA, Beijing, China

⁷Department of Gastroenterology, The 305th Hospital of the PLA, Beijing, China

Correspondence should be addressed to Hu Lin; zq13661210507@163.com and Zhenhua Zhang; whfz2@163.com

Received 21 April 2022; Revised 28 May 2022; Accepted 31 May 2022; Published 16 June 2022

Academic Editor: Francesco Busardò

Copyright © 2022 Chang Liu et al. This is an open access article distributed under the Creative Commons Attribution License, which permits unrestricted use, distribution, and reproduction in any medium, provided the original work is properly cited.

Our purpose of this study was to investigate the use of statins in elderly patients with cardiovascular diseases during regular physical examination and to analyze the relationship between statins and glucose and lipid metabolism and adverse cardiovascular prognosis. From January 2019 to December 2021, 2121 elderly patients with cardiovascular disease underwent regular physical examination as the study subjects to investigate the use and intensity of statins. The patients were divided into the dosing group ($n = 1848$) and the nondosing group ($n = 273$) according to whether they were taking statins or not. The cardiac function, glucose and lipid metabolism indexes, and cardiovascular adverse events were compared between the two groups. Statin use in elderly patients with cardiovascular disease was 87.13% (1848/2121). The intensity of statin use decreased with age ($P < 0.05$); the left ventricular ejection fraction (LVEF) was greater in the medicated group than in the nonmedicated group, and the left ventricular end-diastolic internal diameter (LVDd) and left ventricular end-systolic internal diameter (LVDs) were smaller than in the nonmedicated group ($P < 0.05$). The total cholesterol (TC), triglyceride (TG), low-density lipoprotein cholesterol (LDL-C), and fasting blood glucose (FBG) levels were lower in the medicated group than in the nonmedicated group, the high-density lipoprotein cholesterol (HDL-C) levels were higher than in the nonmedicated group, and the glycated hemoglobin (HbA1c) values were lower than in the nonmedicated group ($P < 0.05$). The overall incidence of cardiovascular adverse events in the medicated group was lower than that in the nonmedicated group ($P < 0.05$). Statin use was higher in elderly patients with cardiovascular disease; the intensity of drug use decreased with age. The patients' cardiac function, glucose metabolism, and prognosis were significantly improved after statin treatment.

1. Introduction

Cardiovascular diseases are caused by atherosclerosis, including coronary heart disease, stroke, and peripheral vascular disease. It is now clinically recognized that disorders of lipid

metabolism are an important factor in the development of cardiovascular disease [1]. Statins are commonly used lipid-lowering drugs that not only lower lipid levels but also have the functions of antioxidant, inhibition of cardiac hypertrophy, and inhibition of neuroendocrine hyperactivation [2, 3].

Related reports also point out that statins can improve endothelial cell function, restore autonomic function, and prevent abnormal myocardial perfusion due to microvascular spasm [4]. Most of the current clinical evidence on the benefits of statins and drug safety comes from nonelderly patients, and there are few studies on statin use in elderly patients. Therefore, this study investigated statin medication use in elderly patients with cardiovascular disease through regular physical examination. We also analyzed the relationship between statin use and glucolipid metabolism as well as adverse cardiovascular prognosis. This study will further provide a clinical basis for the use of statins in elderly patients.

2. Patients and Methods

2.1. Patients. This study was approved by the ethics committee of The 305th Hospital of the PLA. All participants signed written informed consents before the study. 2,121 elderly patients with cardiovascular disease who had regular physical examination from January 2019 to December 2021 were enrolled as the study population. The inclusion criteria were as follows: (i) patients that met the diagnostic criteria of Practical Cardiology on cardiovascular diseases [5]; (ii) patients' age were ≥ 60 years; and (iii) those with complete clinical data. Exclusion criteria were as follows: (i) patients with combined malignant neoplastic diseases; (ii) patients with combined liver and kidney insufficiency; (iii) patients with alcoholism or history of drug abuse; and (iv) patients with combined infectious diseases.

2.2. Methods. Patients were counted on atorvastatin, rosuvastatin, simvastatin, fluvastatin and pitavastatin, and the intensity of use. The intensity of use was based on the relevant guidelines [6], with high intensity being 20 mg of rosuvastatin and 40-80 mg of atorvastatin; medium intensity being 10-40 mg of atorvastatin, 5-20 mg of rosuvastatin, 2-4 mg of pitavastatin, 80 mg of fluvastatin, and 20-40 mg of simvastatin; and low intensity being doses below medium intensity.

The hospital information system was used to inquire about the patients' age, gender, smoking history, drinking history, and other general data and past medical history such as hypertension history and diabetes history.

Vivid-7 Doppler color echocardiography of GE company was used to determine left ventricular end dimension (LVDD), left ventricular end systolic dimension (LVDs), and left ventricular ejection fraction (LVEF).

3 mL of fasting venous blood was collected from the patients within 24 hours after enrollment, and the total cholesterol (TC), triglyceride (TG), low-density lipoprotein cholesterol (LDL-C), high-density lipoprotein cholesterol (HDL-C), fasting blood glucose (FBG), and glycosylated hemoglobin A1c (HbA1c) levels were measured using Beckman Coulter DXC800 system.

The incidence of major cardiovascular adverse events such as acute myocardial infarction and heart failure in the two groups was statistically analyzed.

2.3. Observation Index. The use of statins and the dose of statins were counted, and the patients were divided into a med-

icated group and a nonmedicated group according to whether they were taking statins or not. The cardiac function, glucose and lipid metabolism indexes, and the occurrence of cardiovascular adverse events were compared between the two groups.

2.4. Statistical Analysis. Statistical Product and Service Solutions (SPSS) 23.0 (IBM, Armonk, NY, USA) was applied for statistical analysis. Independent sample *t*-test was used for comparison between the groups for measurement data obeying normal distribution and was used for comparison within the groups, all expressed as $(\bar{x} \pm s)$. Count data were tested by χ^2 and expressed as rate (%), $P < 0.05$ indicates statistical difference.

3. Results

3.1. Statin Use in Elderly Patients with Cardiovascular Disease. The use rate of statins in elderly patients with cardiovascular disease was 87.13% (1848/2121). There was no significant difference in the use of statins in patients of different ages ($P > 0.05$) (Table 1); the intensity of statin use in patients decreased with increasing age ($P < 0.05$) (Table 1).

3.2. Clinical Data of Patients in Nonmedicated Group. The patients were divided into medicated group ($n = 1848$) and nonmedicated group ($n = 273$) according to whether they took statins or not. There was no significant difference in clinical data between the two groups ($P > 0.05$) (Table 2).

3.3. Cardiac Function Indexes in the Nonmedicated Group. The LVEF value in the medicated group was greater than that in the nonmedicated group, and the LVDs and LVDD values were less than those in the nonmedicated group ($P < 0.05$) (Table 3).

3.4. Glucose and Lipid Metabolism Indexes in the Nonmedicated Group. The levels of TG, TC, LDL-C, and FBG in the medicated group were lower than those in the nonmedicated group, the level of HDL-C was higher than that in the nonmedicated group, and the HbA1c value was lower than that in the nonmedicated group ($P < 0.05$) (Table 4).

3.5. The Incidence of Cardiovascular Adverse Events in the Nonmedicated Group. The total incidence of cardiovascular adverse events in the medicated group was lower than that in the nonmedicated group ($P < 0.05$) (Table 5).

4. Discussion

At present, it is believed that improving lipid metabolism disorders is the key to the treatment of cardiovascular diseases. Statins can inhibit cholesterol synthase to play a lipid-lowering role and are widely used in cardiovascular diseases. Decreased function of various organs and changes in statin metabolism in elderly patients have led to few clinical reports on statin use in elderly patients. In this study, we analyzed the use of statins in elderly patients and found that the use of other statins was 87.13%, which was slightly higher than that in the study [7]. This may be related to the higher treatment compliance of patients with regular

TABLE 1: Analysis of statin use in elderly patients with cardiovascular disease.

Item	60-69 years (<i>n</i> = 795)	70-79 years (<i>n</i> = 637)	≥80 years (<i>n</i> = 689)
Type of drug			
Atorvastatin calcium	330 (41.51)	260 (40.82)	285 (41.36)
Rosuvastatin calcium	322 (40.50)	254 (39.87)	276 (40.06)
Simvastatin	33 (4.15)	29 (4.55)	28 (4.06)
Fluvastatin	9 (1.13)	7 (1.10)	6 (0.87)
Pitavastatin	4 (0.5)	3 (0.47)	2 (0.29)
Drug intensity			
Low-intensity statin	171 (21.51)	214 (33.59)	543 (78.81)
Moderate-intensity statin	525 (66.04)	337 (52.90)	54 (7.84)
High-intensity statin	2 (0.25)	2 (0.31)	0 (0.00)
Total	698 (87.80)	553 (86.81)	597 (86.65)

Note: Comparison of statin intensity among the three groups, $P < 0.05$.

TABLE 2: Comparison of clinical data of medicated group.

Classification	Administration group (<i>n</i> = 1848)	Unmedicated group (<i>n</i> = 273)	X^2/t	<i>P</i>
Age (years)	73.65 ± 6.09	73.52 ± 6.58	0.326	0.745
Gender: male (case)	1168 (63.20)	159 (58.24)	2.500	0.114
BMI (body mass index) (kg/m ²)	22.34 ± 2.06	22.19 ± 2.24	1.110	0.267
Complicated with hypertension (<i>n</i>)	1083 (58.60)	147 (53.85)	2.120	0.137
Complicated with hyperlipidemia (case)	629 (34.04)	78 (28.57)	3.197	0.074
Complicated with diabetes (case)	417 (22.56)	53 (19.41)	1.369	0.242
Smoking history (case)	563 (30.47)	97 (35.53)	2.848	0.092
Alcohol history (case)	438 (23.70)	57 (20.88)	1.059	0.303

TABLE 3: Comparison of cardiac function indicators in the medicated group.

Group	<i>N</i>	LVEF (%)	LVDs (mm)	LVDd (mm)
Administration group	1848	51.09 ± 3.52	47.56 ± 5.07	61.38 ± 6.25
Nonmedicated group	273	50.63 ± 3.14	48.27 ± 5.94	62.71 ± 6.09
<i>t</i>		2.042	2.110	3.293
<i>P</i>		0.041	0.035	0.001

TABLE 4: Comparison of glucose and lipid metabolism indicators in the medicated group.

Group	<i>N</i>	TG (mmol/L)	TC (mmol/L)	LDL-C (mmol/L)	HDL-C (mmol/L)	FBG (mmol/L)	HbA1c (%)
Administration group	1848	1.92 ± 0.21	4.79 ± 0.73	2.95 ± 0.41	1.34 ± 0.24	5.79 ± 1.12	6.08 ± 1.24
Nonmedicated group	273	2.05 ± 0.23	5.17 ± 0.69	3.11 ± 0.67	1.29 ± 0.23	6.08 ± 1.15	6.33 ± 1.36
<i>t</i>		9.427	8.084	5.462	3.230	3.980	3.070
<i>P</i>		<0.001	<0.001	<0.001	0.001	<0.001	0.002

TABLE 5: Comparison of incidence of cardiovascular adverse events in the nonmedicated group (case, %).

Group	<i>N</i>	Acute myocardial infarction	Heart failure	Cardiovascular death	Revascularization	Total occurrence
Administration group	1848	46	21	10	17	5.09 (94)
Nonmedicated group	273	11	8	3	4	9.52 (26)
X^2						8.774
<i>P</i>						0.003

physical examinations. Clinical data showed that the lipid-lowering effect of statins was closely related to drug dose [8], but relevant studies have pointed out that high-dose statins have more adverse reactions in the treatment of cardiovascular diseases, while the patient's age is too high and physical function is also weaker [9], so the dose needs to be adjusted according to the patient's age. The results of this study showed that the intensity of statin use in patients decreased with increasing age.

Statins can significantly reduce plasma cholesterol concentration, delay and inhibit the progression of atherosclerosis, and have become one of the drugs of choice for lipid-lowering therapy and antiatherosclerosis in clinical practice [10]. The results of this study showed that the TC, TG, and LDL-C levels in the medicated group were higher than those in the unmedicated group, and the HDL-C level was higher than that in the unmedicated group, indicating that statin treatment for elderly patients with cardiovascular disease can reduce the body's blood lipid level, which is mainly because statins can play a role in regulating blood lipids by competitively inhibiting enzyme secretion in hepatocytes and reducing the body's methyl dehydroabietate content [11]. In this study, we found that FBG levels were lower and HbA1c values were lower in the medicated group than in the unmedicated group, indicating that statins can improve glucose metabolism in elderly patients with cardiovascular disease, which is mainly related to the fact that statins can improve insulin resistance and glucose tolerance through their effects.

Myocardial function in patients with cardiovascular disease is affected by the amount of cholesterol in the cardiac muscle cells. Increased cholesterol levels in patients can lead to reduced cell membrane function, which in turn can affect myocardial function in patients. Statins can improve cardiac function because they reduce body cholesterol levels [12]. Relevant studies have pointed out that statins can improve glucose and lipid metabolism, reduce hyperglycemia-related sclerosing stress, and improve endothelial function [13]. It has also been reported that statins, in addition to their lipid-lowering effects, can also reduce platelet adhesiveness, prevent thrombosis, and improve endothelial function [14]. Statins can downregulate angiotensin II receptor content and reduce the degree of myocardial fibrosis, while improving myocardial function in patients [15]. The results of this study showed that the LVEF value of the medicated group was greater than that of the unmedicated group, and LVDd and LVDs were less than those of the unmedicated group, indicating that statins in the treatment of cardiovascular disease can improve the patient's cardiac function, which is mainly because statins can reduce the body cholesterol content, reduce the amount of cholesterol in the cell membrane, and then play a role in improving the patient's myocardial cell function. Some scholars have found that statins have the effect of stabilizing plaques, reducing the adhesion and aggregation of inflammatory cells and platelets in the microcirculation and preventing the activation of the coagulation system, which can improve myocardial blood perfusion in patients [16]. The results of this study showed that the total incidence of cardiovascular adverse events in

the medicated group was lower than that in the unmedicated group, indicating that statin therapy given to patients with cardiovascular disease can reduce cardiovascular adverse events. The reason for this is that statins can improve body hemodynamics and promote apoptosis and fibrosis of cardiomyocytes and interstitium by exerting selective inhibitory effects, inhibiting the activity of reductase, the rate-limiting enzyme of synthesis, and reducing intracellular cholesterol synthesis in the human body, which can reduce the incidence of cardiovascular adverse events [17]. This study has the following advantages over other previous related studies: (1) larger sample size; (2) higher proportion of elderly patients; and (3) more detailed observation indicators.

5. Conclusion

Statin use is higher in elderly patients with cardiovascular disease, and the intensity of drug use decreases with increasing age. Patients' cardiac function, glucose metabolism indicators, and prognosis are significantly improved after statin treatment.

Data Availability

The datasets used and analyzed during the current study are available from the corresponding author on reasonable request.

Conflicts of Interest

The authors declare that they have no conflict of interest.

Authors' Contributions

Chang Liu and Rui Ma contributed equally to this work.

References

- [1] A. M. Chamberlain, S. S. Cohen, J. M. Killian, K. L. Monda, S. A. Weston, and T. Okerson, "Lipid-Lowering prescription patterns in patients with diabetes mellitus or cardiovascular disease," *The American Journal of Cardiology*, vol. 124, no. 7, pp. 995–1001, 2019.
- [2] S. J. Nicholls, R. Puri, T. Anderson et al., "Effect of evolocumab on progression of coronary disease in statin-treated patients," *JAMA*, vol. 316, no. 22, pp. 2373–2384, 2016.
- [3] S. Li and C. M. Schooling, "Investigating the effects of statins on ischemic heart disease allowing for effects on body mass index: a Mendelian randomization study," *Scientific Reports*, vol. 12, no. 1, p. 3478, 2022.
- [4] X. Li, H. Xiao, C. Lin et al., "Synergistic effects of liposomes encapsulating atorvastatin calcium and curcumin and targeting dysfunctional endothelial cells in reducing atherosclerosis," *International Journal of Nanomedicine*, vol. 14, pp. 649–665, 2019.
- [5] H. Lu, O. Roux, S. Fournier et al., "Cardiologie," *Revue Médicale Suisse*, vol. 18, no. 767, pp. 144–151, 2022.
- [6] S. Opoku, Y. Gan, E. A. Yobo et al., "Awareness, treatment, control, and determinants of dyslipidemia among adults in China," *Scientific Reports*, vol. 11, no. 1, article 10056, 2021.

- [7] T. E. Strandberg, "Role of statin therapy in primary prevention of cardiovascular disease in elderly patients," *Current Atherosclerosis Reports*, vol. 21, no. 8, p. 28, 2019.
- [8] R. N. Horodinschi, A. Stanescu, O. G. Bratu, S. A. Pantea, D. G. Radavoi, and C. C. Diaconu, "Treatment with statins in elderly patients," *Medicina*, vol. 55, no. 11, p. 721, 2019.
- [9] Q. H. Zhang, R. X. Yin, W. X. Chen, X. L. Cao, and Y. M. Chen, "Association between the TIMD4-HAVCR1 variants and serum lipid levels, coronary heart disease and ischemic stroke risk and atorvastatin lipid-lowering efficacy," *Bioscience Reports*, vol. 38, no. 1, 2018.
- [10] Y. Y. Xing, J. Liu, J. Liu et al., "Statin use and low-density lipoprotein cholesterol levels in patients aged 75 years and older with acute coronary syndrome in China," *Zhonghua Xin Xue Guan Bing Za Zhi*, vol. 47, no. 5, pp. 351–359, 2019.
- [11] T. Jamialahmadi, F. Baratzadeh, Z. Reiner et al., "The effects of statin dose, lipophilicity, and combination of statins plus ezetimibe on circulating oxidized low-density lipoprotein levels: a systematic review and meta-analysis of randomized controlled trials," *Mediators of Inflammation*, vol. 2021, Article ID 9661752, 12 pages, 2021.
- [12] J. A. De La Cruz, C. G. Mihos, S. A. Horvath, and O. Santana, "The pleiotropic effects of statins in endocrine disorders," *Endocrine, Metabolic & Immune Disorders Drug Targets*, vol. 19, no. 6, pp. 787–793, 2019.
- [13] D. Tousoulis, C. Antoniades, C. Vassiliadou et al., "Effects of combined administration of low dose atorvastatin and vitamin E on inflammatory markers and endothelial function in patients with heart failure," *European Journal of Heart Failure*, vol. 7, no. 7, pp. 1126–1132, 2005.
- [14] T. Hirota, Y. Fujita, and I. Ieiri, "An updated review of pharmacokinetic drug interactions and pharmacogenetics of statins," *Expert Opinion on Drug Metabolism & Toxicology*, vol. 16, no. 9, pp. 809–822, 2020.
- [15] D. S. Kazi, J. M. Penko, and K. Bibbins-Domingo, "Statins for primary prevention of cardiovascular disease: review of evidence and recommendations for clinical practice," *The Medical Clinics of North America*, vol. 101, no. 4, pp. 689–699, 2017.
- [16] C. Xie, M. Zhu, Y. Hu, and K. Wang, "Effect of intensive and standard lipid-lowering therapy on the progression of stroke in patients with coronary artery syndromes: a meta-analysis of randomized controlled trials," *Journal of Cardiovascular Pharmacology*, vol. 75, no. 3, pp. 222–228, 2020.
- [17] M. F. van Stee, A. A. de Graaf, and A. K. Groen, "Actions of metformin and statins on lipid and glucose metabolism and possible benefit of combination therapy," *Cardiovascular Diabetology*, vol. 17, no. 1, p. 94, 2018.

Research Article

Diagnostic and Prognostic Significance of microRNA-208a in Acute Myocardial Infarction

Sheng Chen,¹ Xin Hong,¹ Yong Wu^{1,2} and Ziguo Chen¹

¹Department of Cardiology, Affiliated Nanping First Hospital, Fujian Medical University, Nanping 353000, China

²Xiamen Anxinya Biological Technology Co. Ltd., Xiamen, Fujian 361005, China

Correspondence should be addressed to Yong Wu; 280548694@qq.com and Ziguo Chen; czg8530@163.com

Received 10 March 2022; Revised 31 March 2022; Accepted 4 April 2022; Published 14 May 2022

Academic Editor: Francesco Busardò

Copyright © 2022 Sheng Chen et al. This is an open access article distributed under the Creative Commons Attribution License, which permits unrestricted use, distribution, and reproduction in any medium, provided the original work is properly cited.

Objective. To determine the prognostic and diagnostic significance of microRNA-208a (miR-208a) in acute myocardial infarction (AMI). **Methods.** Totally, 84 AMI patients hospitalized in our hospital between Jan. 2019 and Feb. 2021 were enrolled as the patient group (Pat group), and 50 healthy individuals over same time span as the control group (Con group). qRT-PCR assay was carried out to quantify serum miR-208a in the patients and receiver-operating characteristic (ROC) curves for analysing its diagnostic value in AMI patients and its predictive value in clinical efficacy and adverse events in the patients after therapy. The changes of miR-208a and clinical indexes (lactate dehydrogenase (LDH), creatine kinase (CK) as well as Creatine kinase-MB (CK-MB)) in the patients before and after therapy were evaluated. Pearson's test was adopted to analyse the associations of miR-208a with clinical indexes. Additionally, the target genes of miR-208a were forecasted. **Results.** The patient group showed a higher miR-208a level than the control group ($p < 0.05$), and the area under the curve (AUC) of miR-208a in diagnosing AMI was >0.9 . After therapy, patients presented notable decreases in serum miR-208a, LDH, CK, and CK-MB (all $p < 0.05$). Serum miR-208a presented positive associations with LDH, CK, as well as CK-MB both before and after therapy (all $p < 0.05$). Before therapy, the ineffective group presented a higher miR-208a level than the effective group ($p < 0.05$), and miR-208a had an AUC of 0.784 in forecasting efficacy. Additionally, the group with adverse events presented a higher miR-208a level than the group without them before therapy ($p < 0.05$), and miR-208a had an AUC of 0.713 in forecasting adverse events. According to enrichment analysis, the target genes of miR-208a were bound up with signal pathways of cellular senescence, MTOR and Wnt. **Conclusion.** With high expression in AMI cases, miR-208a is a promising potential biomarker for diagnosis and prognosis forecasting of AMI.

1. Introduction

Acute myocardial infarction (AMI) is a frequently seen serious cardiovascular disease with acute onset in clinical scenarios, belonging to one serious manifestation of coronary artery disease [1]. Because of the acceleration of the global aging process, the change of people's living habits, and the pollution of the surrounding environment, cardiovascular diseases present an annually growing incidence, especially AMI [2]. Statistically, approximately 1.5 million people suffer AMI each year in the United States. According to some surveys, AMI shows a growing mortality in both urban and rural population in China, with an increase of 5.6 times from 1987 to 2014, and 4%-15% of patients with it are youn-

ger than 45 years in recent years, showing that more young people is afflicted by it [3].

Clinically, AMI has no notable clinical manifestations at the initial phase, which can likely to result in missed diagnosis and misdiagnosis, so many patients come to see a doctor only when they have acute onset and thus miss the optimal therapy timing and suffer unfavourable prognosis [4]. At the current stage, the laboratory indexes frequently adopted for clinical evaluation of myocardial injury include creatine kinase isoenzyme (CK-MB), lactate dehydrogenase (LDH), and cardiac troponin (cT-nI/T), but they are limited due to their poor specificity and aberrant expression in other diseases [5]. Accordingly, the key to solving this problem lies in finding a novel diagnostic marker.

MiR is one noncoding RNA with an endogenous length between 20 and 25 nt [6]. According to one study [7], miR is able to interact with specific mRNAs by inducing the degradation of mRNAs or suppressing the translation, thus regulating the expression in diseases after transcription. An increasing number of studies have discovered the participation of miR in various basic biological processes, including proliferation, differentiation, necrosis, apoptosis, autophagy, development, and aging [8]. Reportedly, miR is abnormally expressed in diseases including cancer, cardiovascular diseases, and immunodeficiency diseases [9]. The most ideal diagnostic markers should be readily available and detectable. Interestingly, according to quite a number of reports, miR exists in serum and plasma in a consistent, stable, and repeatable way, which greatly arouses the interest of scholars in using miR in circulation as a biomarker [10].

MiR-208a, namely, miR-208a-3p, has been discovered to be with an association with the development of various cancers. For instance, Cui et al. [11] found that compared with miR-negative control (NC), miR-208a intensified the proliferation and invasion of gastric cancer cells through targeted secretion of SFRP1 and negative regulation on maternal expressed gene 3. MiR-208a acts as one oncogene in colorectal cancer via PDCD4 [12]. Moreover, reportedly, miR-208a aggravates CCl₄-induced liver injury in mice due to the lack of pathways activating cell death [13]. The association of miR-208a with AMI has been reported, but more research is needed to verify whether miR-208a can serve as a diagnostic marker of AMI.

In the present study, we analysed the diagnostic and prognostic significance of miR-208a in AMI and the potential mechanism of miR-208a in AMI to offer reference to clinical therapy and efficacy prediction.

2. Patients and Methods

2.1. Clinical Data. Totally, 84 AMI patients admitted to our hospital between January 2019 and February 2021 were enrolled into the patient group (Pat group), including 54 males and 30 females, between 48 and 80 years old, with a mean age of 63.9 ± 7.0 years, and 50 healthy individuals who underwent physical examination in our hospital during the same time span were enrolled as the control group (Con group), including 28 males and 22 females, between 43 and 78 years old, with a mean age of 60.3 ± 6.9 years. There was no significant difference exists between the two groups in gender and age ($p > 0.05$). This study was approved by the ethics committee of Affiliated Nanping First Hospital, Fujian Medical University. Signed written informed consents were obtained from all participants before the study.

2.2. Inclusion and Exclusion Criteria. The inclusion criteria are as follows: patients confirmed with acute myocardial infarction with ST-segment elevation for the first time at the first onset based on 2017 ESC Guidelines for the management of AMI in patients presenting with ST-segment elevation [14], patients who had undergone percutaneous coronary intervention (PCI), and those with detailed clinical data.

TABLE 1: Clinical efficacy evaluation.

Efficacy grading	Evaluation criteria
Markedly effective	The symptoms of heart failure disappeared; the heart rate was less than 100 beats/min; the heart function was grade I.
Effective	The symptoms of heart failure were alleviated; the heart rate was more than 100 beats/min; the heart function grade was grade II-III.
Ineffective	Electrocardiogram showed no improvement or even showed aggravation in various indexes, clinical signs, and symptoms.

The exclusion criteria are as follows: patients with comorbid tumour or immune function diseases, patients with congenital organ defects, patients who were not suitable to receive the operation, patients intolerant of the drugs applicable to this operation, and those with mental disorder.

The inclusion and exclusion criteria of the control group are as follows: healthy individuals with normal serum indexes and imaging indexes were enrolled.

2.3. Therapeutic Regimen for the Patients. All patients were given PCI. Specifically, each patient was ordered to orally take 300 mg aspirin before PCI and orally take 600 mg clopidogrel at the beginning of the surgery, and the patient was also ordered to orally take clopidogrel at 150 mg/time, once a day, and aspirin at 100 mg/time, once a day, after surgery for 7 consecutive days.

2.4. qRT-PCR. Total mRNA in tumour cells was acquired via TRIzol reagent (Invitgen, Carlsbad, CA, USA), and the extracted RNA was inversely transcribed into cDNA using SYBR PreMix Ex Taq Kit (TaKaRa Bio, Inc., Tokyo, Japan) under manual guidelines. The forward and reverse primers of miR-208a were 5'-CGCGGCATAAGACGAGCAAAAAGC-3' and reverse 5'-ACGACAGTTCAACGGCAGCACCG-3', respectively, and those of U6 were 5'-ATCGCC TTCGGCAGCACA-3' and 5'-CACGCTGCACGAATTCGCGT-3', respectively. qRT-PCR was conducted as follows: 95°C/5 min, 95°C/10 s, and 60°C/45 s, 40 cycles in total, and the expression data of miR-208a were normalized to U6 expression of the same sample. The Ct value of every target gene was normalized with that of the reference gene (Ct(miR-208a)-Ct(U6)). The relative expression was calculated using the $2^{-\Delta\Delta CT}$ method.

2.5. Detection of Clinical Indexes. Morning fasting venous blood (5 mL) was acquired from each patient via one coagulation-promoting tube, and 5 mL of it was acquired via one heparin sodium anticoagulation tube, all of which were treated by 10 min centrifugation (3,000 r/min) for separating serum/plasma. The changes of myocardial enzymes (LDH, CK, and CK-MB) were observed via one automatic biochemical analyzer (Beckman Coulter AU5800, Franklin Lakes, NJ, USA) before and after therapy.

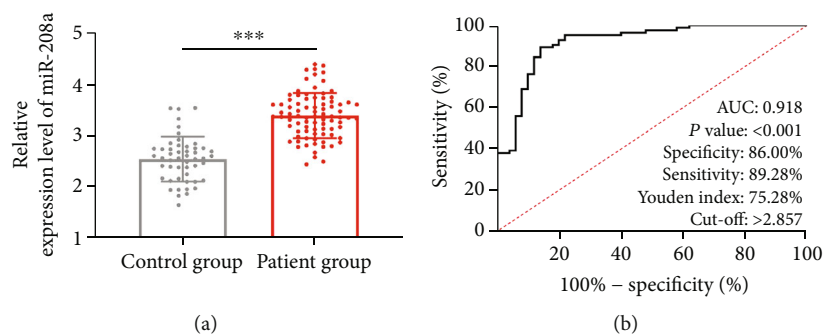


FIGURE 1: Expression and diagnostic significance of miR-208a in AMI. (a) Quantification of serum miR-208a in the control and patient groups via qRT-PCR. (b) Diagnostic value of miR-208a in AMI patients according to ROC curve. Note: *** $p < 0.001$.

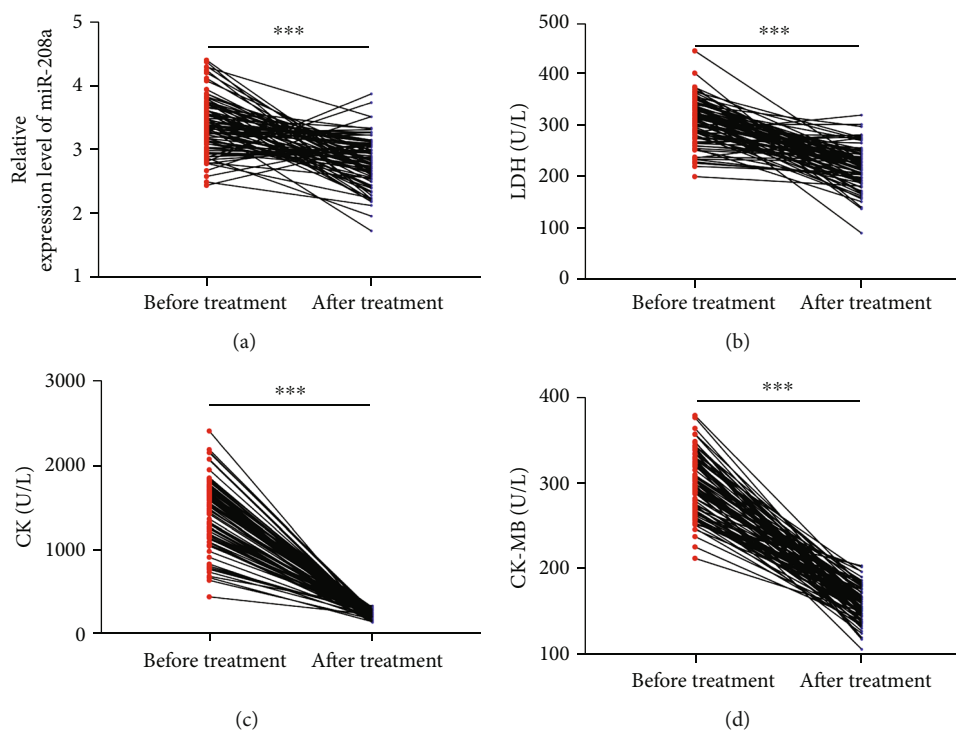


FIGURE 2: Changes of serum miR-208a, LDH, CK, and CK-MB in patients before and after therapy. (a) Changes of serum miR-208a in patients before and after therapy according to qRT-PCR assay. (b) Changes of serum LDH in patients before and after therapy according to the automatic biochemistry analyzer. (c) Changes of serum CK in patients before and after therapy according to the automatic biochemistry analyzer. (d) Changes of serum CK-MB in patients before and after therapy according to the automatic biochemistry analyzer.

2.6. Follow-Up. The patients were followed up for 6 months, once every 2 months, via telephone and reexamination of outpatient data to understand adverse cardiovascular events in them, including cardiogenic death, recurrent angina pectoris, nonfatal AMI, heart failure, and malignant arrhythmia.

2.7. Predication of Target Genes. The online databases (Targetscan, miRDB, and starBase) were utilized for forecasting the possible target genes of miR-208a, and the corresponding Wayne map was drawn.

2.8. Enrichment Analysis. GO and KEGG enrichment analyses were carried out using DAVID (6.8) online database. The former was conducted with three modules (biological pro-

cess (BP), cellular component (CC), and molecular function (MF)) for functional annotation, and the latter can display the importance of different signal pathways in protein interaction network. Finally, the bubble charts of GO and KEGG enrichment analyses were drawn and visualized. The standards of $|\text{NES}| > 1$, p value < 0.05 , and $\text{FDR} < 0.25$ were adopted.

2.9. Outcome Measures. Primary outcome measures are as follows: miR-208a in AMI patients was analysed, on which its value in diagnosing AMI was evaluated via ROC curves. The value of miR-208a in predicting clinical efficacy on patients was also analysed, and the evaluation criteria of efficacy was summarized in Table 1. The value of miR-208a in

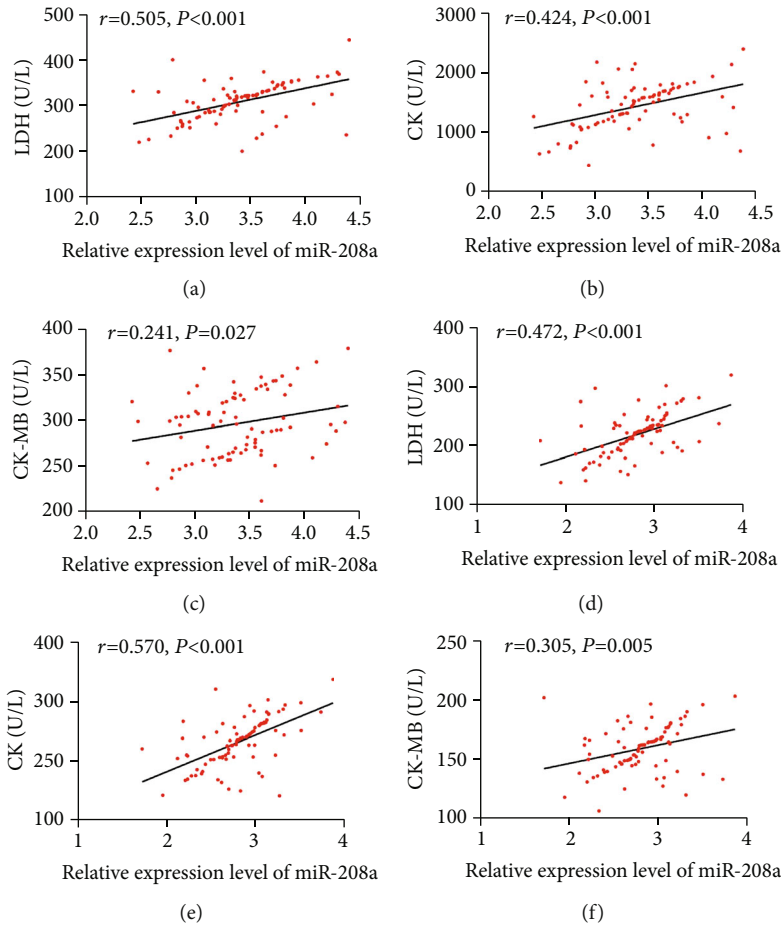


FIGURE 3: Correlation analysis of miR-208a with LDH, CK, and CK-MB before and after therapy. (a) Association of miR-208a with LDH before therapy according to the Pearson’s test. (b) Association of miR-208a with CK before therapy according to the Pearson’s test. (c) Association of miR-208a with CK-MB before therapy according to the Pearson’s test. (d) Association of miR-208a with LDH after therapy according to the Pearson’s test. (e) Association of miR-208a with CK after therapy according to the Pearson’s test. (f) Association of miR-208a with CK-MB after therapy according to the Pearson’s test.

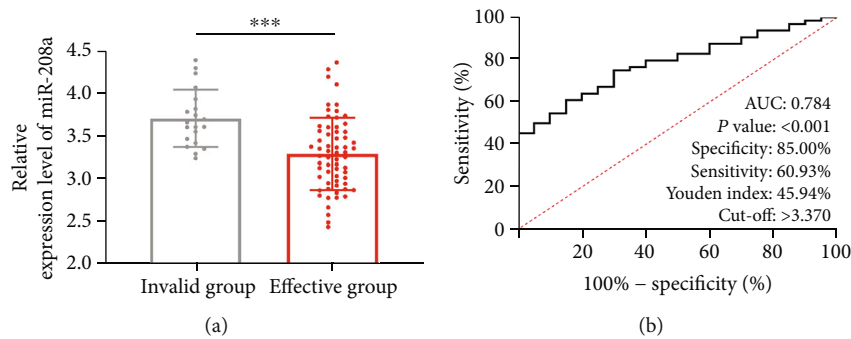


FIGURE 4: Value of miR-208a in forecasting the efficacy on AMI patients after PCI. (a) Serum miR-208a in patients with different efficacy according to qRT-PCR. (b) Predictive value of miR-208a in efficacy improvement of AMI patients after PCI based on ROC curve. Note: *** $p < 0.001$.

predicting the occurrence of adverse events after therapy was also evaluated.

Secondary observation indexes are as follows: the changes of miR-208a and clinical indexes before and after therapy were evaluated. The Pearson’s test was adopted to

analyse the associations of miR-208a with clinical indexes, and the target genes of miR-208a and bioinformatics were conducted for understanding the value of miR-208a in the diagnosis of AMI. The value of miR-208a in predicting clinical efficacy on patients was also analysed, and the evaluation

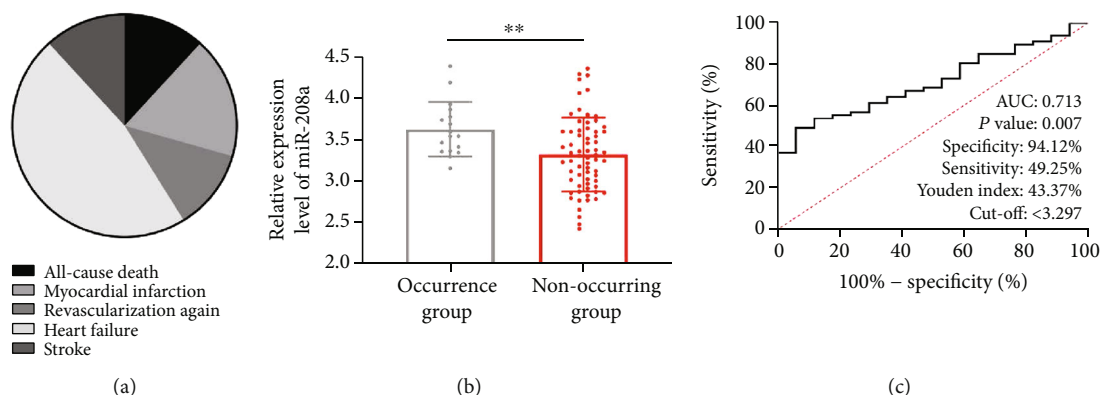


FIGURE 5: Predictive value of miR-208a in the occurrence of postoperative adverse events in patients. (a) Distribution of adverse events. (b) Serum miR-208a in patients with postoperative adverse events according to qRT-PCR. (c) Predictive value of miR-208a in AMI patients after PCI according to ROC curve. Note: $**p < 0.001$.

criteria of efficacy was summarized in Table 1. The value of miR-208a in predicting the occurrence of adverse events after therapy was also evaluated.

2.10. Statistical Analyses. Statistical Product and Service Solutions (SPSS) 21.0 (IBM, Armonk, NY, USA) for data analysis and GraphPad Prism 8.0 (La Jolla, CA, USA) for figure drawing. The counting data were analysed via the *t*-test, and their intergroup comparison and intro-group comparison were carried out using the independent-samples *t*-test and paired *t*-test, respectively. Measurement data were analysed via the chi-square test, and ROC curves were drawn to predict efficacy and the occurrence of adverse events. $p < 0.05$ implies a notable difference.

3. Results

3.1. Expression and Diagnostic Significance of miR-208a in AMI. Serum miR-208a in the patients was quantified via qRT-PCR, and comparison of it between the two groups showed that the miR-208a level in the patient group was notably higher than in the control group ($p < 0.05$, Figure 1(a)). ROC curves were adopted to analyse the clinical value of miR-208a in distinguishing healthy individuals from AMI patients, and its area under the curve (AUC) was >0.9 ($p < 0.05$, Figure 1(b)), implying its great potential to be biomarker with high clinical value.

3.2. Changes of miR-208a and Clinical Indexes in Patients before and after Therapy. For more deeply understanding the association of miR-208a with patients' condition, we analysed the changes of miR-208a before and after therapy and found a notable decrease in serum miR-208a in the patients after therapy ($p < 0.05$, Figure 2(a)). Additionally, after therapy, patients presented notable decreases in serum LDH, CK, and CK-MB (all $p < 0.05$, Figures 2(b)–2(d)).

3.3. Correlation Analysis of miR-208a with Clinical Indexes. For further analysing the associations of miR-208a with AMI development, the Pearson's Test was adopted for understanding the associations of miR-208a with LDH, CK, and CK-MB. The results revealed positive associations of miR-208a with them (all $p < 0.05$, Figure 3).

3.4. Expression and Predictive Value of miR-208a in Patients with Different Efficacy before Therapy. After therapy, we evaluated the efficacy on the patients and found 26 patients with markedly effective efficacy, 38 patients with effective efficacy, and 20 patients with ineffective efficacy. The 26 patients and 38 patients were assigned to the improvement group ($n = 64$), and the rest were assigned to the non-improvement group ($n = 20$). According to comparison of miR-208a between the two groups before therapy, the non-improvement group presented notably higher miR-208a expression than the other group ($p < 0.05$, Figure 4(a)). According to ROC curve-based analysis, the AUC of miR-208a in predicting the improvement of clinical efficacy ($p < 0.05$, Figure 4(b)), suggesting the potential of miR-208a to be a biomarker for forecasting the efficacy improvement on AMI patients after PCI.

3.5. Predictive Value of miR-208a before Therapy for Postoperative Adverse Events in Patients. We also counted adverse events within 6 months after therapy. In the past six months, 17 patients suffered adverse events, including 2 cases with all-cause death, 3 cases with myocardial infarction, 2 cases with revascularization, 8 cases with heart failure, and 2 cases with stroke. The patients were assigned to two groups in light of the occurrence of adverse events: occurrence group and nonoccurrence group (Figure 5(a)). The occurrence group presented notably higher serum miR-208a than the other before therapy ($p < 0.05$, Figure 5(b)). According to ROC curve-based analysis, miR-208a had an AUC of 0.713 in forecasting the occurrence of adverse events ($p < 0.05$, Figure 5(c)), suggesting the potential of miR-208a to be a biomarker for forecasting them in AMI patients after therapy.

3.6. MiR-208a Target Gene and Bioinformatics Analysis. We predicated the target genes of miR-208a by Targetscan, miRDB, starBase, and found 211 target genes via Targetscan, 201 via miRDB and 1963 via starBase. Through the Wayne map, we found 65 common target genes (Figure 6(a)). Then, based on DAVID online software analysis, GO enrichment revealed the primary enrichment of miR-208a target genes in the functions of MAP kinase activity, Wnt-activated receptor activity, and phosphatase activity (Figure 6(b)),

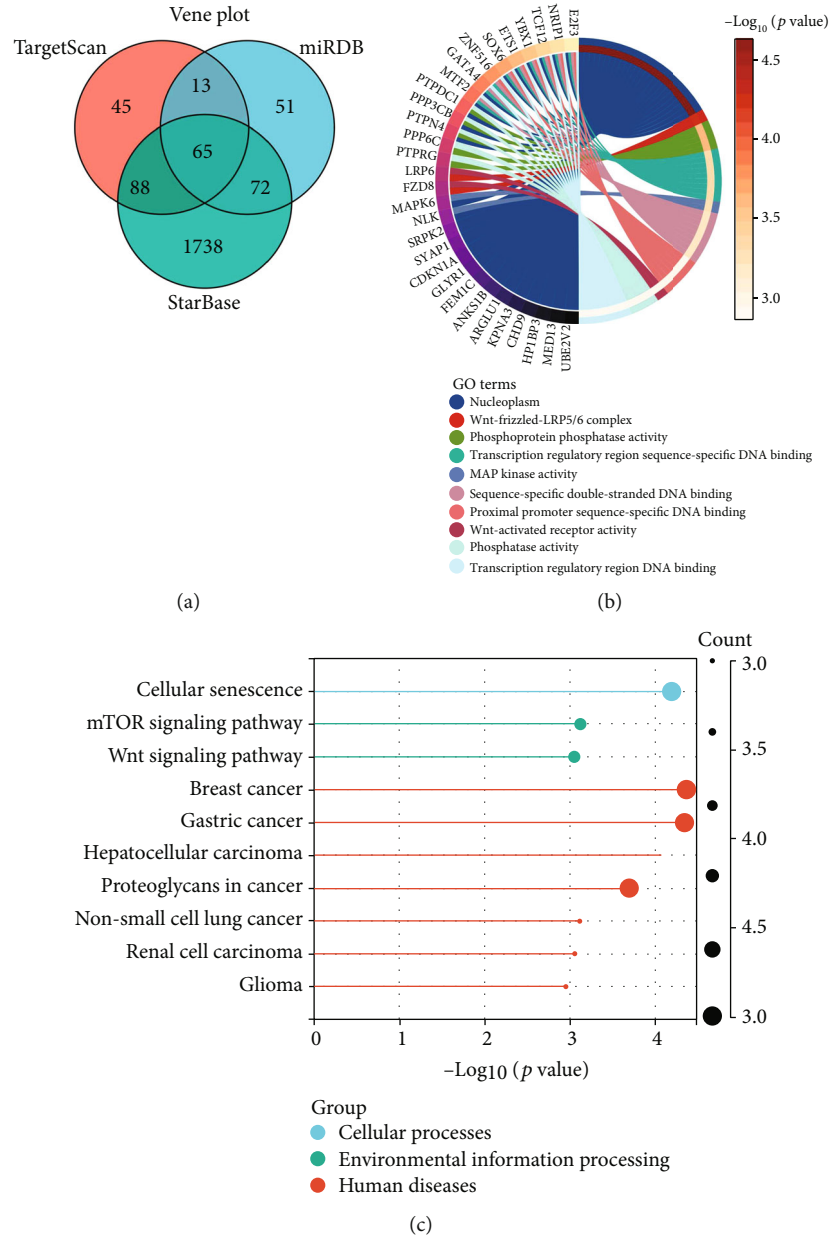


FIGURE 6: MiR-208a target gene and bioinformatics analyses. (a) Target genes of miR-208a predicted by TargetsCan, miRDB, and starBase. (b) GO enrichment analysis of the functions of 65 common target genes of miR-208a. (c) KEGG enrichment analysis of 65 target genes involved in miR-208a pathway.

and KEGG enrichment analysis revealed the associations of miR-208a target genes with cellular senescence and MTOR and Wnt signalling pathways (Figure 6(c)).

4. Discussion

The primary pathogenesis of AMI is the occurrence of thrombosis triggered by the release of many platelets due to the rupture of coronary atherosclerotic plaque [15]. The continuous expansion of infarct area gives rise to coronary artery occlusion and slow blood flow, triggering systemic microcirculation disturbance and resulting in progressive left ventricular dilatation and deterioration of heart function

[16]. Definitive diagnosis and timely guidance of clinical therapy are the key to improving the prognosis of patients with AMI.

A growing number of studies have revealed the participation of miR in the life processes of organism, its wide distribution in human body, and its expression in only specific cells and tissues [17]. MiR-208a, as one miR discovered early, is expressed in diseases including tumour and immune function diseases [18]. Feng et al. [19] have revealed the high expression of miR-208a in rat models of early myocardial infarction, suggesting that miR-208a has the potential to be a marker of AMI. In our study, serum miR-208a was quantified via qRT-PCR. The results showed its high expression

in AMI patients and its high value in distinguishing AMI patients from healthy individuals (AUC > 0.9). Similar to our study results, Oyunbileg et al. [20] have also found the high expression of miR-208a in AMI patients and its AUC > 0.9. Our research once again verified the diagnostic value of miR-208a in AMI.

Prior research has confirmed the diagnostic significance of miR-208a in AMI, but whether miR-208a changes in AMI patients after therapy has not been studied and analyzed. Over the past few years, as people have increasingly understanding of clinical research and clinical therapy of AMI, especially the application of interventional therapy, there is a new therapeutic scheme for clinical therapy of AMI [21]. With increasingly extensive application in clinical practice, PCI is regarded as one effective method to relieve myocardial necrosis and increase coronary perfusion [22]. In our study, the changes of miR-208a after PCI were analysed. According to the results, after therapy, patients presented notably downregulated miR-208a. Correlation analysis revealed positive associations of miR-208a with myocardial function indexes before and after therapy, which suggested that miR-208a could serve as one observation index for AMI patients before and after therapy. For more deeply determining the association of miR-208a with efficacy on AMI patients, the patients were grouped in light of clinical efficacy after therapy. According to the results, the non-improvement group presented a notably higher miR-208a level than the improvement group before therapy, suggesting the possible value of miR-208a in forecasting the improvement of efficacy on AMI patients. Thus, corresponding ROC curves were drawn, showing an AUC of miR-208a > 0.7 in forecasting the clinical efficacy on AMI patients, which implied the potential of miR-208a in forecasting the clinical efficacy on AMI patients.

PCI has become the primary therapy for AMI, but it can only relieve the narrow lesion, and patients still face a risk of recurrent adverse cardiac events after it because of the persistence of risk factors leading to the disease continue [23]. Our study investigated the adverse events of patients for 6 months by telephone and outpatient medical records. Among the 84 patients, 17 patients suffered adverse events after therapy, showing an incidence of 20.23%. The patients were grouped in light of the adverse events, and the comparison revealed notably higher miR-208a expression in patients with AMI than in those without it, and an AUC > 0.7, which implied the function of miR-208a in AMI patients before therapy in serving as a predictor of adverse events.

Finally, the target genes of miR-208a were forecasted. As a result, 85 potential target genes were found. GO and KEGG enrichment analyses revealed the correlations of miR-208a with MTOR and Wnt signalling pathways. Wei et al. [24] have discovered the participation of autophagy in the protection against acute myocardial infarction via 1,25-dihydroxyvitamin D₃ by PI3K/AKT/mTOR pathway. Another study has discovered the impact of miR-154 on cardiomyocyte apoptosis in rats with AMI via Wnt/ β -catenin signalling pathway [25]. The results suggest the possible involvement of miR-208a in the occurrence of AMI through many ways and also pave a way for our follow-up research.

Our study has determined the diagnostic and predictive value of miR-208a in AMI patients, but it still has some limitations. First of all, we only collected the serum of healthy individuals and AMI patients, so the existence of difference in miR-208a expression between patients with unstable angina pectoris and AMI patients needs further study. Secondly, as a clinical study, the mechanism of miR-208a in AMI has yet to confirm. We only analysed its potential mechanism through the prediction of target genes, but whether miR-208a can participate in the occurrence of AMI by regulating these functions still needs experimental verification. Therefore, we hope to carry out more experiments in the future to improve our research.

All in all, with high expression in AMI cases, miR-208a is a promising potential biomarker for diagnosis and prognosis forecasting of AMI.

Data Availability

The clinical data used to support the findings of this study are included within the article.

Conflicts of Interest

The authors declared no conflict of interest.

Authors' Contributions

Sheng Chen and Xin Hong contributed equally to this work.

References

- [1] G. W. Reed, J. E. Rossi, and C. P. Cannon, "Acute myocardial infarction," *Lancet*, vol. 389, no. 10065, pp. 197–210, 2017.
- [2] J. L. Anderson and D. A. Morrow, "Acute myocardial infarction," *The New England Journal of Medicine*, vol. 376, no. 21, pp. 2053–2064, 2017.
- [3] H. Thiele, E. M. Ohman, S. de Waha-Thiele, U. Zeymer, and S. Desch, "Management of cardiogenic shock complicating myocardial infarction: an update 2019," *European Heart Journal*, vol. 40, no. 32, pp. 2671–2683, 2019.
- [4] A. Albulushi, A. Giannopoulos, N. Kafkas, S. Dragasis, G. Pavlides, and Y. S. Chatzizisis, "Acute right ventricular myocardial infarction," *Expert Review of Cardiovascular Therapy*, vol. 16, no. 7, pp. 455–464, 2018.
- [5] S. Aydin, K. Ugur, S. Aydin, I. Sahin, and M. Yardim, "Biomarkers in acute myocardial infarction: current perspectives," *Vascular Health and Risk Management*, vol. Volume 15, pp. 1–10, 2019.
- [6] T. X. Lu and M. E. Rothenberg, "MicroRNA," *The Journal of Allergy and Clinical Immunology*, vol. 141, no. 4, pp. 1202–1207, 2018.
- [7] N. Bushati and S. M. Cohen, "MicroRNA functions," *Annual Review of Cell and Developmental Biology*, vol. 23, no. 1, pp. 175–205, 2007.
- [8] L. A. Yates, C. J. Norbury, and R. J. Gilbert, "The long and short of microRNA," *Cell*, vol. 153, no. 3, pp. 516–519, 2013.
- [9] M. Acunzo, G. Romano, D. Wernicke, and C. M. Croce, "MicroRNA and cancer—a brief overview," *Advances in Biological Regulation*, vol. 57, pp. 1–9, 2015.

- [10] M. Elaguizy, M. Sheta, N. Ibrahim, A. Eltaweel, and A. Mostafa, "Serum microRNA-18a, microRNA-21 and microRNA-92a as diagnostic markers in colorectal cancer patients," *Journal of BUON*, vol. 25, no. 3, pp. 1443–1448, 2020.
- [11] H. B. Cui, H. E. Ge, Y. S. Wang, and X. Y. Bai, "MiR-208a enhances cell proliferation and invasion of gastric cancer by targeting SFRP1 and negatively regulating MEG3," *The International Journal of Biochemistry & Cell Biology*, vol. 102, pp. 31–39, 2018.
- [12] H. Wu, L. Xu, Y. Chen, and C. Xu, "MiR-208a-3p functions as an oncogene in colorectal cancer by targeting PDCD4," *Bioscience Reports*, vol. 39, no. 4, 2019.
- [13] S. Bala, C. D. Calenda, D. Catalano et al., "Deficiency of miR-208a exacerbates CCl4-induced acute liver injury in mice by activating cell death pathways," *Hepatology Communications*, vol. 4, no. 10, pp. 1487–1501, 2020.
- [14] B. Ibanez, S. James, S. Agewall et al., "2017 ESC guidelines for the management of acute myocardial infarction in patients presenting with ST-segment elevation: the task force for the management of acute myocardial infarction in patients presenting with ST-segment elevation of the European Society of Cardiology (ESC)," *European Heart Journal*, vol. 39, no. 2, pp. 119–177, 2018.
- [15] R. Gulati, A. Behfar, J. Narula et al., "Acute myocardial infarction in young individuals," *Mayo Clinic Proceedings*, vol. 95, no. 1, pp. 136–156, 2020.
- [16] A. H. Shah, R. Puri, and A. Kalra, "Management of cardiogenic shock complicating acute myocardial infarction: a review," *Clinical Cardiology*, vol. 42, no. 4, pp. 484–493, 2019.
- [17] U. Zeymer, "Diagnosis and initial management of acute myocardial infarction," *MMW Fortschritte der Medizin*, vol. 161, no. 4, pp. 34–36, 2019.
- [18] V. Oliveira-Carvalho, V. O. Carvalho, and E. A. Bocchi, "The emerging role of miR-208a in the heart," *DNA and Cell Biology*, vol. 32, no. 1, pp. 8–12, 2013.
- [19] G. Feng, Z. Yan, C. Li, and Y. Hou, "MicroRNA-208a in an early stage myocardial infarction rat model and the effect on cAMP-PKA signaling pathway," *Molecular Medicine Reports*, vol. 14, no. 2, pp. 1631–1635, 2016.
- [20] O. Oyunbileg, G. Li, X. Wang, X. Zhao, and D. O. Cardiology, "Early diagnostic value of circulating microRNA208a, 208b in acute myocardial infarction," *Chinese Journal of Cardiovascular Medicine*, vol. 20, no. 1, pp. 13–17, 2015.
- [21] W. Silen, T. E. Machen, and J. G. Forte, "Acid-base balance in amphibian gastric mucosa," *The American Journal of Physiology*, vol. 229, no. 3, pp. 721–730, 1975.
- [22] G. Marquis-Gravel, M. Zeitouni, A. Kochar et al., "Technical consideration in acute myocardial infarction with cardiogenic shock: a review of antithrombotic and PCI therapies," *Catheterization and Cardiovascular Interventions*, vol. 95, no. 5, pp. 924–931, 2020.
- [23] W. Xia, N. Yang, and Y. Li, "Analysis of risk factors for adverse cardiovascular events in elderly patients with acute myocardial infarction and non-alcoholic fatty liver disease (NAFLD)," *Medical Science Monitor*, vol. 26, article e922913, 2020.
- [24] Y. X. Wei, S. M. Dong, Y. Y. Wang et al., "Autophagy participates in the protection role of 1,25-dihydroxyvitamin D3 in acute myocardial infarction via PI3K/AKT/mTOR pathway," *Cell Biology International*, vol. 45, no. 2, pp. 394–403, 2021.
- [25] H. Y. Sun, X. L. Wang, L. C. Ma et al., "Influence of MiR-154 on myocardial apoptosis in rats with acute myocardial infarction through Wnt/ β -catenin signaling pathway," *European Review for Medical and Pharmacological Sciences*, vol. 23, no. 2, pp. 818–825, 2019.

Research Article

The ceRNA Crosstalk between mRNAs and lncRNAs in Diabetes Myocardial Infarction

Yun Zhou , Chengjun Zhou, Lilong Wei, Chengwu Han, and Yongtong Cao 

Department of Clinical Laboratory, China-Japan Friendship Hospital, Beijing 100029, China

Correspondence should be addressed to Yongtong Cao; caoyongtong100@sina.com

Received 27 March 2022; Accepted 21 April 2022; Published 9 May 2022

Academic Editor: Francesco Busardò

Copyright © 2022 Yun Zhou et al. This is an open access article distributed under the Creative Commons Attribution License, which permits unrestricted use, distribution, and reproduction in any medium, provided the original work is properly cited.

Competitive endogenous RNA regulation suggests an intricate network of all transcriptional RNAs that have the function of repressing miRNA function and regulating mRNA expression. Today, the specific ceRNA regulatory mechanisms of lncRNA-miRNA-mRNA in patients who have diabetes mellitus (DM) and myocardial infarction (MI) are still unknown. Two data sets, GSE34198 and GSE112690, were rooted in the Gene Expression Omnibus database to search for changes of lncRNA, miRNA, and mRNA in MI patients with diabetes. Weighted gene correlation network analysis (WGCNA) was used to identify the modules related to the development of diabetes in patients with MI. Target genes of miRNAs were predicted using miRWalk, TargetScan, mirDB, RNA22, and miRanda. Then, functional and enrichment analyses were performed to build the lncRNA-miRNA-mRNA interaction network. We built ceRNA regulatory networks with three lncRNAs, two miRNAs, and nine mRNAs. Differentially expressed genes enriched in biological process, including neutrophil activation, refer to immune response and positive system of defense feedback. Besides, there is significant enrichment in molecular function of calcium toll-like receptor binding, icosanoid binding, RAGE receptor binding, and arachidonic acid binding. Kyoto Encyclopedia of Genes and Genomes (KEGG) analysis enriched differentially expressed genes (DEGs) in pathways that were well known in MI, indicating inflammation and immune response. Pathways associated with diabetes were also significantly enriched. We confirmed significantly altered lncRNA, miRNA, and mRNA in MI patients with diabetes, which might serve as biomarkers for the progress and development of diabetic cardiovascular diseases. We constructed a ceRNA regulatory network of lncRNA-miRNA-mRNA, which will enable us to understand the novel molecular mechanisms included in the initiation, progression, and interaction between DM and MI, laying the foundation for clinical diagnosis and treatment.

1. Introduction

Morbidity and mortality from cardiovascular disease (CVD) are extremely high [1, 2]. Moreover, CVD is also the leading cause of death in urban and rural areas, overshadowing cancer and other diseases in China. The incidence of CVD and mortality among Chinese patients also remains high, and more importantly, the upward trend is projected to continue into the next decade [3]. The increasing burden of CVD has become a significant public health problem. Myocardial infarction (MI) is particularly severe, resulting in progressive heart failure and cardiovascular mortality, and diabetes mel-

litus (DM) is a major risk factor for CVD [4, 5]. Patients with diabetes are twice as likely to have an MI as healthy people. Diabetes and impaired glucose tolerance are quite common among people with MI (seen in almost two-thirds of patients) and are associated with a twofold increase in mortality rate compared to those with normoglycemia [6]. In addition, there have been numerous studies proving that DM is a strong prognostic biomarker in patients with established coronary artery disease [7–9]. Follow-up studies have shown that 39.5% of patients with type 2 DM (T2DM) died within 2 years of their first MI, compared with 28.5% of non-diabetic patients with MI only [10]. However, mechanisms

that can explain the complex association between diabetes and MI remain mysterious. Therefore, to improve the poor outcome of CVDs, effort should be made toward discovering a potential pathogenesis and exploiting novel medication targets and therapeutic strategies.

Noncoding RNAs, including miRNA and lncRNA, are essential for the regulation of RNA expression [11]. miRNAs have the ability to negatively regulate the expression of target genes [12], and lncRNAs have no or little function in encoding proteins that affect many biological processes [13]. lncRNAs are important in regulating basic biological processes and may cause diseases if aberrant expression occurs [14, 15]. However, little is known about whether or how lncRNA is related to DM and MI.

lncRNAs can compete with target genes for miRNA response elements and weaken the repressive effect of miRNAs on target genes [16, 17]. Thus, they can indirectly regulate the expression of target genes and influence the onset and progression of disease [18]. Nevertheless, the association between ceRNAs and diabetic MI remains unclear. In this manuscript, we summarize the regulatory roles of lncRNAs, miRNAs, and mRNAs and discuss a regulatory network built of ceRNA.

2. Materials and Methods

2.1. Data Acquisition. miRNAs and lncRNAs in MI patients with or without DM were collected from two microarray data sets: GSE34198 (Czech Republic: 15 patients with DM and 34 controls) and GSE112690 (USA: 85 patients with DM and 244 controls), which are based on the platform of GPL6102 Illumina human-6 v2.0 expression beadchip and GPL24804 Biomark high-throughput human miRNA RT-qPCR assay (MGH, Boston, MA, USA). The GEO database is an international public repository.

2.2. Data Processing and Differential Expression Analysis. After quantile normalization to ensure differentially expressed genes (DEGs), probe identifiers of GSE34198 were transformed into gene symbols, and the single expression value of the gene was calculated. To screen related differentially expressed lncRNAs (DELncs), the probe identifiers of GSE34198 were blasted against the GENCODE (<https://www.encodegenes.org/human/>) long noncoding RNA database to be reannotated [19]. GEO series matrix files of GSE112690 were downloaded and the quantile was normalized to obtain the differentially expressed miRNAs (DEMics). Subsequently, the differential expression analysis was executed with the threshold of P value < 0.05 using Student's t -test in R software.

2.3. Gene Ontology. Gene ontology is a channel for performing gene annotation, which classifies genes into three categories [20, 21]. A gene database was used to assign genomes to specific pathway maps of molecular interactions, reactions, and relationship networks [22]. The gene ontology (GO) function annotation and enrichment analysis of DEGs were performed using the R package clusterProfiler [23], and a P value < 0.05 was considered significant.

2.4. Weighted Gene Correlation Network Analysis. We proceeded to conduct gene correlation analysis of DEGs and DELncs to verify the key genes and lncRNAs associated with diabetes in MI patients. The purpose of the WGCNA is to find coexpressed gene modules and explore any relevance between gene networks and related phenotypes. First, hierarchical cluster analysis is performed with the `hclust` function. The modules are constructed with soft thresholds filtered by the `pickSoftThreshold` function. Candidate powers (1–30) are used to test the average degree of connectivity of different patterns and their independence. If the degree of independence is > 0.8 , a suitable power value is selected. For the present study, coexpression networks were constructed [24] with the smallest module size set at 30, and each pattern was labeled with a different color. The relationship of functional modules and concerned phenotype (in our case, diabetes) was also evaluated.

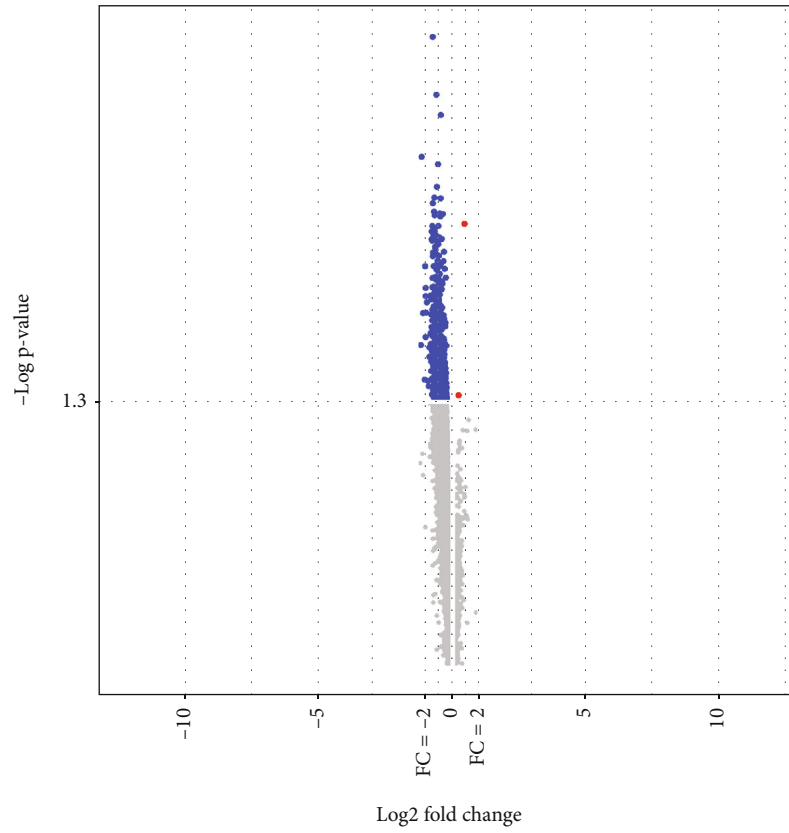
The hub genes were also described in this study as genes that were most strongly related to disease. A module that was highly related to diabetes was explored, and a regulatory network of DEGs and DELncs in the module was constructed and visualized by Cytoscape software [25], which was used because it can visualize complex networks.

2.5. miRNA Target Prediction. The construction of a ceRNA background network requires a large number of lncRNAs, miRNAs, and mRNAs, along with their interactions. Target genes of differentially expressed miRNAs found in GSE112690 were predicted with the help of the miRWalk [26], TargetScan [27], miRDB [28], RNA22 [29], and miRanda databases [30]. The predicted target genes were intersected with DEGs found in GSE34198 to be further explored.

2.6. lncRNA–miRNA–mRNA ceRNA Network. The relationship between DELncs and DEMics was calculated with the TargetScan 6.1 algorithm [31]. Then, according to ceRNA theory, gene pairs with opposite expressions were screened out based on the expression of differentially expressed miRNAs and differentially expressed lncRNAs for construction of the background network.

3. Results

3.1. Identification of DEGs, DELncs, and DEMics. To screen DEGs, lncRNAs, and miRNAs, the series matrix files of GSE34198 and GSE112690 were downloaded from the GEO database. Subsequently, Student's t -test was executed to analyze the DEGs and DELncs between controls and patients with DM in the GSE34198 data set. Meanwhile, the differential expression analysis of DEMics between controls and patients with DM was implemented with the threshold of P value < 0.05 by Student's t -test in R software. As shown in Figures 1, 499 DEGs and 23 DELncs were identified from GSE34198 microarray data using cutoff criteria of $P < 0.05$ (detailed information about the DEGs and DELncs can be found in Table S1), while four DEMics were found in GSE112690, using the same threshold (Table S2).



(a)

FIGURE 1: Continued.

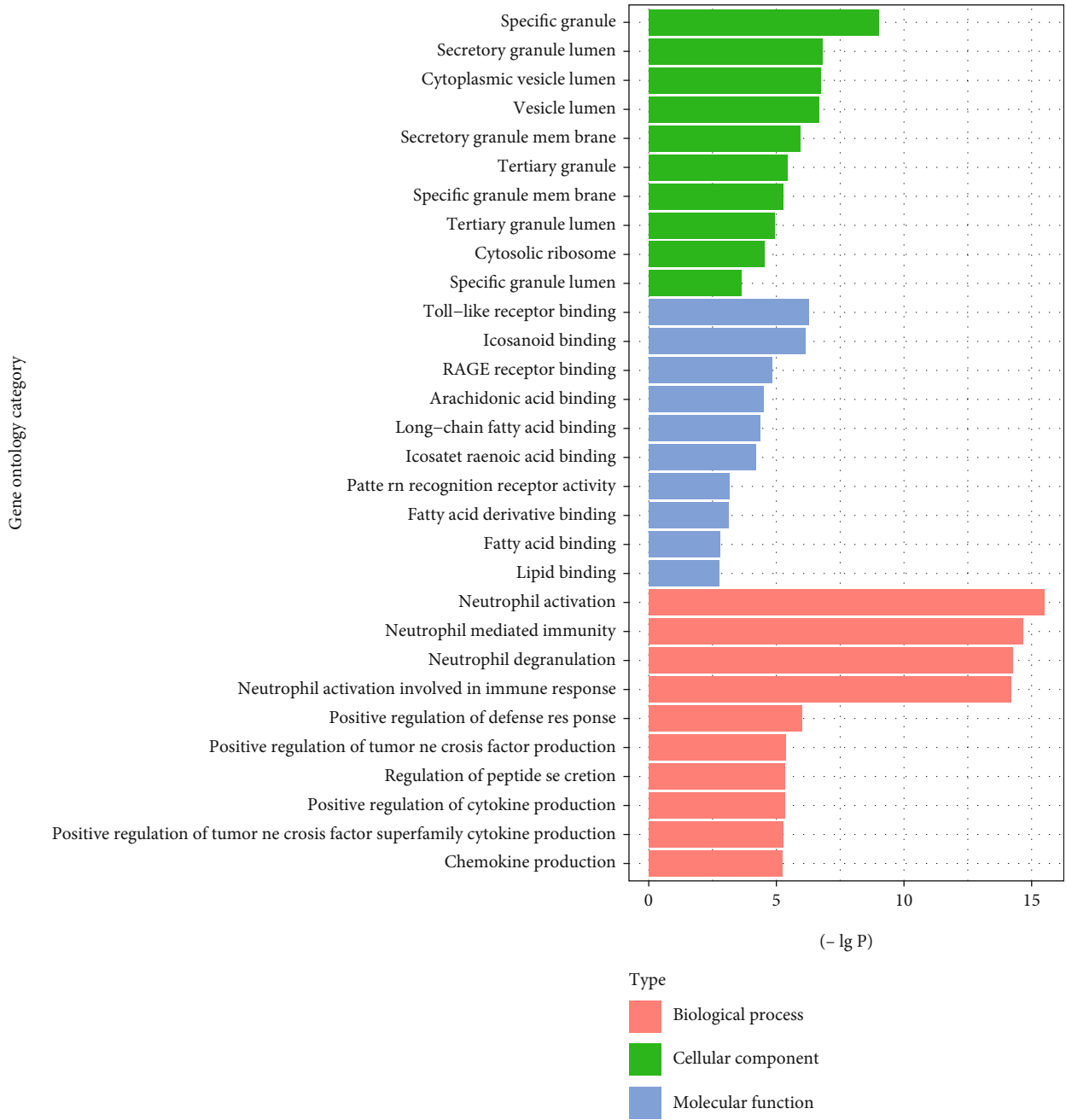


FIGURE 2: Continued.

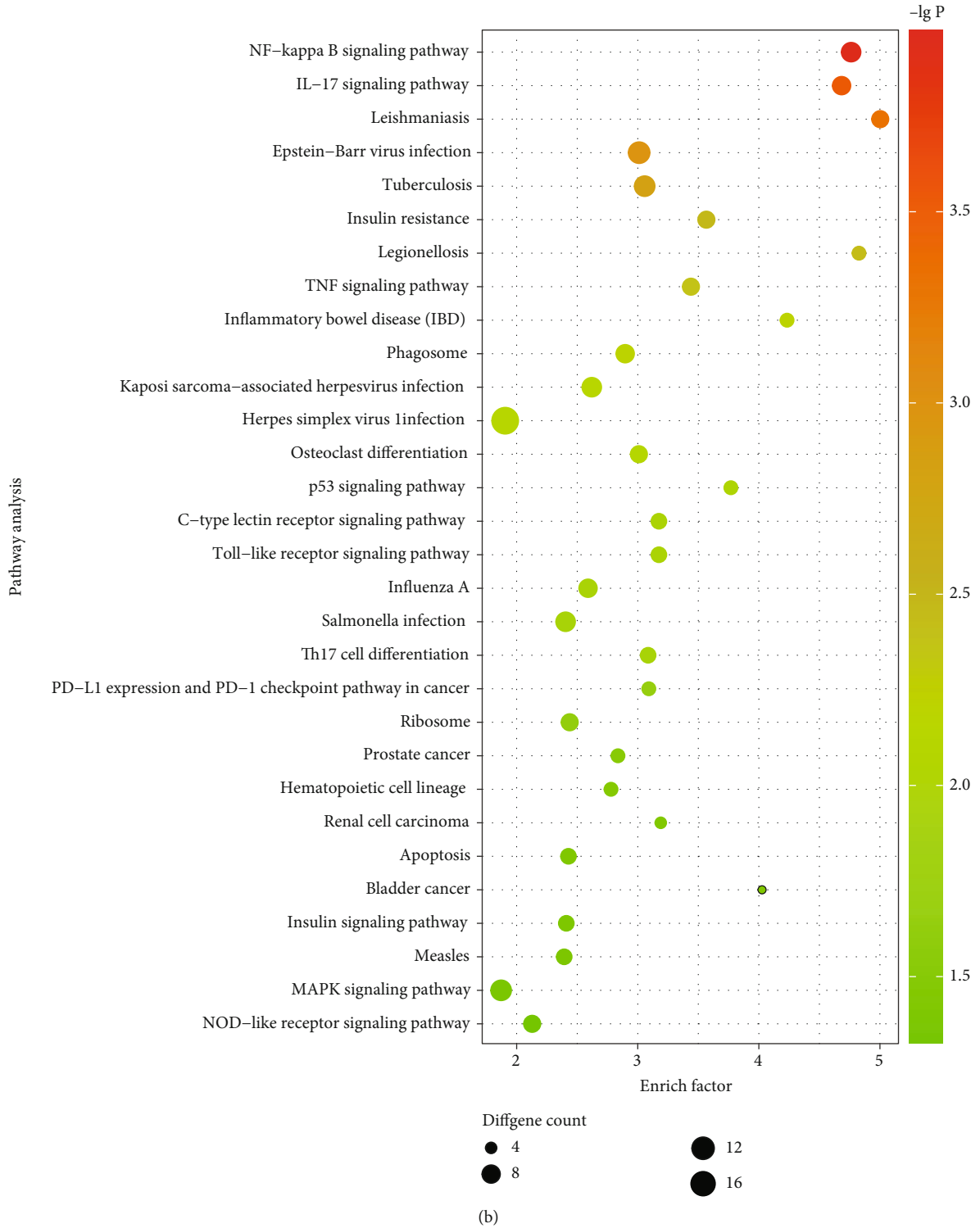


FIGURE 2: Gene ontology enrichment and KEGG pathway annotation of DEGs. (a) Bar plot showing the top 10 enriched gene ontology terms in each category. The x-axis represents the negative logarithmic of different P values, and y-axis represents GO terms. (b) x-axis representing an enriched factor, and the y-axis represents KEGG pathway terms. Sizes of the circles indicate gene counts, and the color of the circles represents different adjusted P values.

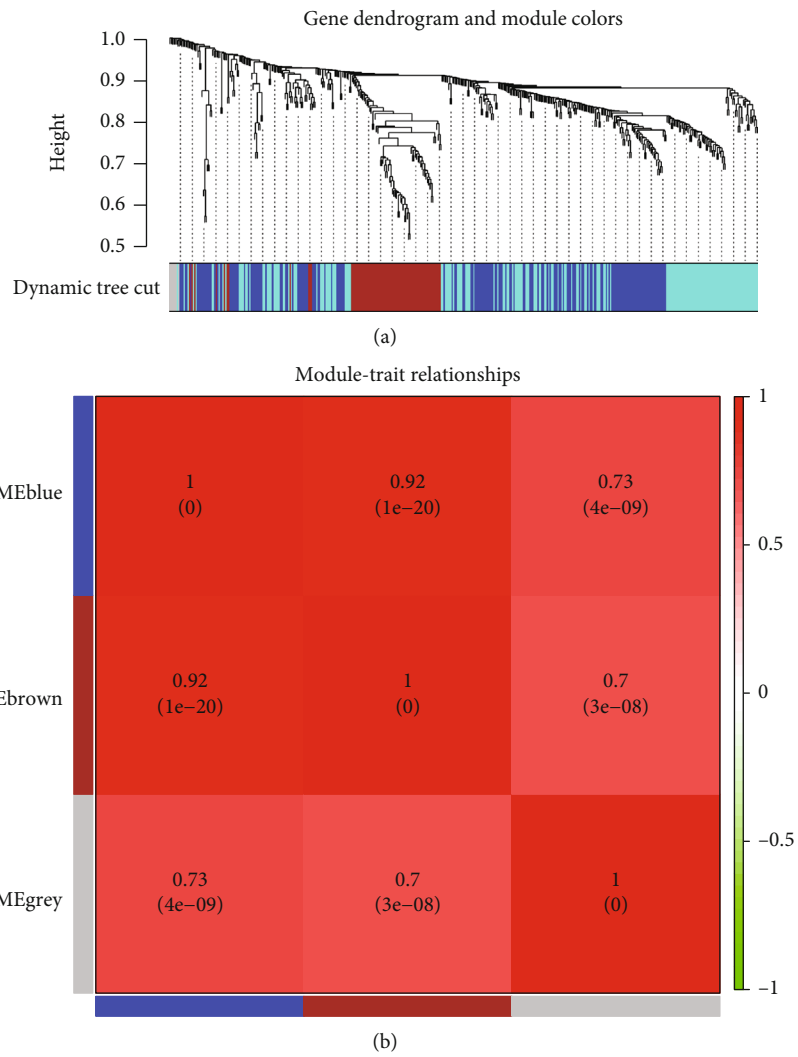


FIGURE 3: Continued.

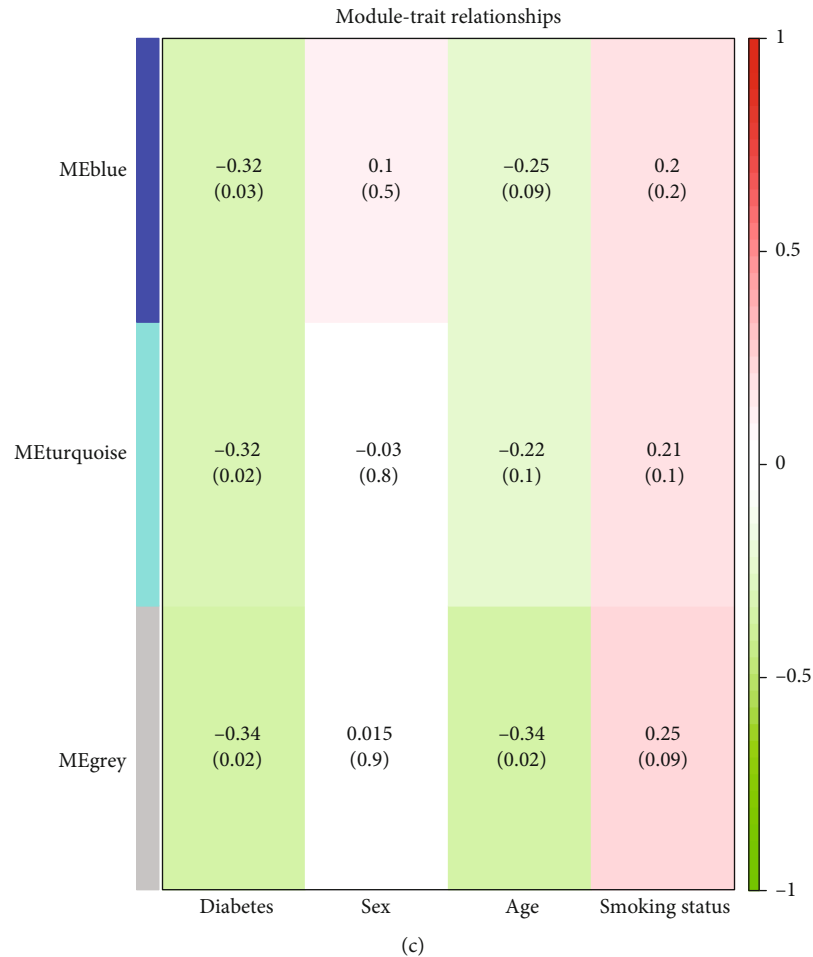


FIGURE 3: WGCNA used for the identification of key modules associated with MI patients with diabetes. (a) Dendrogram obtained by clustering the dissimilarities based on consensus topological overlap with the corresponding module colors indicated by the color row. (b) The relationships between different modules, where red indicates a positive correlation. (c) Heat map of the correlation between module eigengenes and clinical traits (diabetes, gender, age, and smoking status). Each cell contains the correlation coefficient and P value.

each other (Figure 3(c)). Hub nodes have a key role in maintaining the overall connectivity of the network. Therefore, the top 5% were selected as hubs. We chose differentially expressed genes and lncRNAs in MEturquoise to construct the correlation network (Figure 4), with 10 DEGs and 5 DELncs identified as hub genes and lncRNAs (UBE2D3, MNDA, AMN1, TMBIM4, RCSD1, CLK4, PPP1R12A, USP15, NT5C2, PCMTD1, DNAJC3-DT, LINC00921, AC108134.3, AL445524.1, and AC114980.1, Table S6).

3.4. lncRNA-miRNA-mRNA ceRNA Network. To survey the regulation of ceRNAs and identify DM-related lncRNAs in MI patients, we built a network. As shown in Figure 5, three lncRNAs, two miRNAs, and nine mRNAs were included in the network, and the red, green, and blue nodes represent lncRNAs, miRNAs, and mRNAs, respectively. The edges represent the interactions between lncRNAs, miRNAs, and mRNAs. The lncRNA acts as a natural miRNA sponge to suppress the function of miRNAs, and the expression of lncRNA-miRNA and miRNA-mRNA were negatively correlated. Notably, the key DEGs and DELncs related to MI

patients with DM that we had identified in WGCNA were also found in the ceRNA regulatory network, suggesting they also correlate with the DEMics we screened from GSE112690. In addition, based on ceRNA mechanisms, we identified LINC00921, AL445524.1, and AC114980.1 as candidate lncRNA biomarkers for diabetic MI.

4. Discussion

Salmena et al. proposed how mRNAs and lncRNAs communicate with each other [16]. lncRNAs regulate mRNA expression posttranscriptionally by competing for miRNAs [32]. Dysregulated lncRNAs and mRNAs (sequences complementary to lncRNAs) affect the expression levels of target mRNAs through interference of miRNAs, together with target mRNAs harbored by lncRNAs called miRNA response elements (MREs) [33, 34]. This endogenous RNA exchange forms a large-scale regulatory network across the transcriptome that plays a crucial role in the physiological and pathological processes of disease [35]. Next, we integrated genome-wide lncRNA, mRNA, and miRNA expression profiling data and experimentally validated miRNA-target

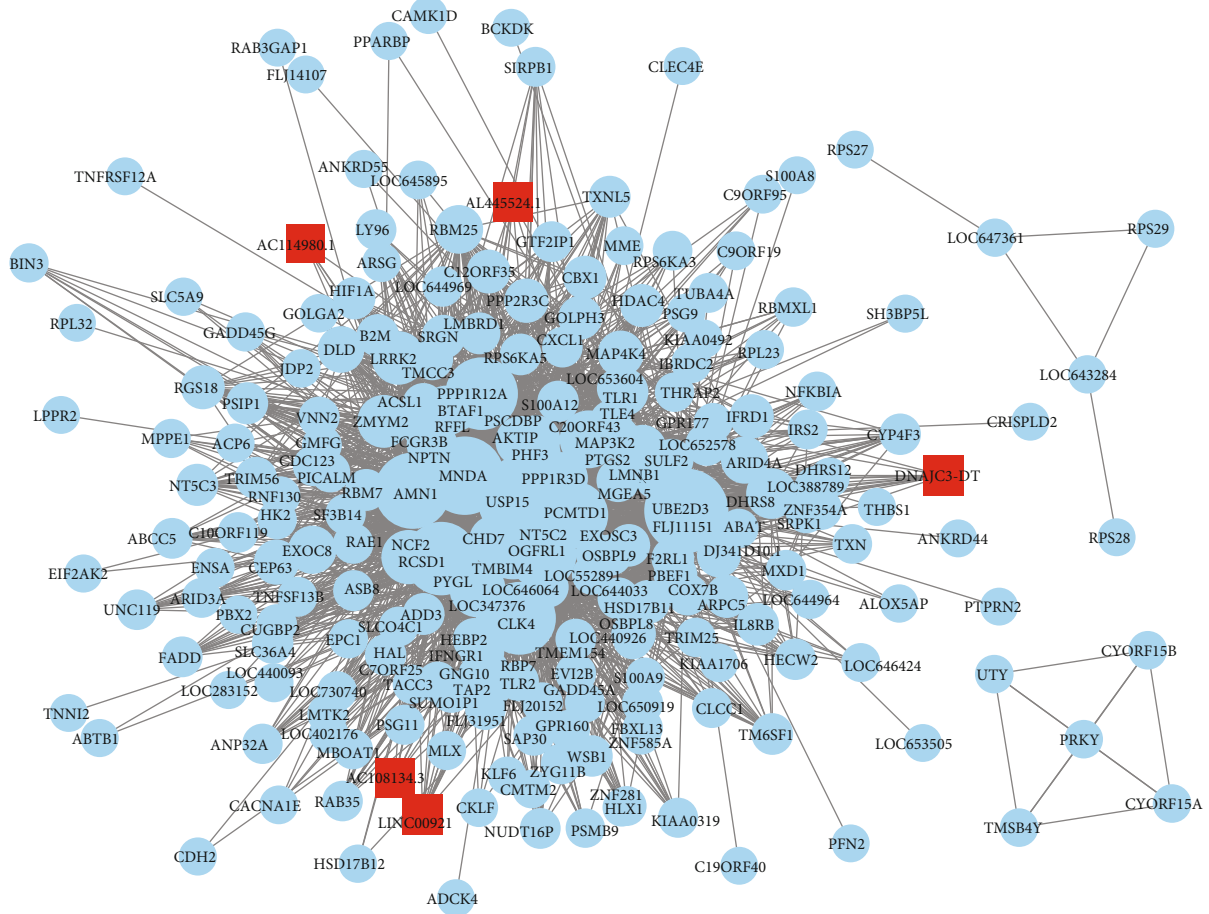


FIGURE 4: DM-related lncRNA–mRNA regulatory network. For the DM-related lncRNA–mRNA regulatory network in module MEturquoise, where the red squares stand in for hub lncRNAs, while blue circles indicate DEGs in the module.

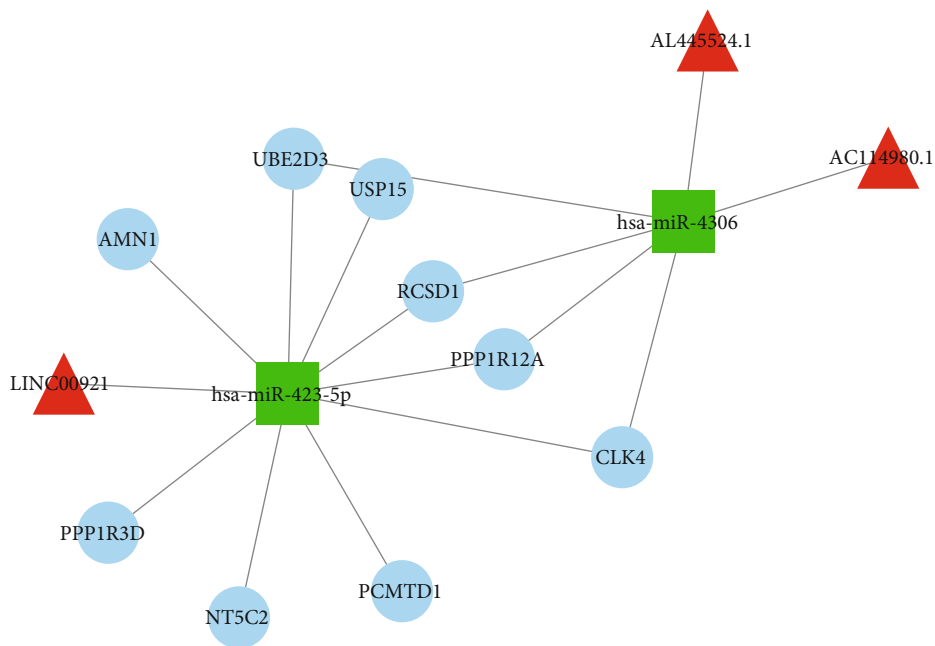


FIGURE 5: The lncRNA–miRNA–mRNA ceRNA regulatory network. Three lncRNAs, two miRNAs, and nine mRNAs were included in the network, with red triangles representing lncRNAs, green squares indicating miRNAs, and the blue nodes representing mRNAs, respectively. In addition, the edges represent the interactions between lncRNAs, miRNAs, and mRNAs.

interactions to construct a regulatory network in diabetic MI patients. Three candidate lncRNA biomarkers were identified for the comorbidity of MI and DM.

Diabetes affects the heart, including metabolic disturbances, abnormalities in subcellular components, microvascular damage, and autonomic dysfunction [36, 37]. The myocardium shows local inflammation, coronary endothelial dysfunction, necrosis, apoptosis, and autophagy [38, 39]. The hub miRNA (miR-4306) is downregulated in coronary artery disease (CAD), and miR-4306 is an independent poor prognostic factor in CAD [40].

miR-4306 noticeably inhibited the human monocyte-derived macrophages (HMDMs) in vitro and reduced the number of macrophage cells in cardiac tissue in MI mice. Another hub miRNA (miR-423-5p) was found to have significantly higher expression in the vitreous of the eyes with proliferative diabetic retinopathy (PDR) and was proved to be related to angiogenesis and fibrosis [41].

Regarding the hub genes we found in the ceRNA network, studies had proved that the ubiquitin-conjugating enzyme UBE2D3 was involved in RNA processing and splicing and was associated with increased fasting plasma glucose [42]. PPP1R3G is downregulated in the liver by fasting and increased by feeding, and it plays an important role in the control of postprandial glucose homeostasis through its regulation of hepatic gluconeogenesis during the fasting-feeding transition [43]. The 5'-nucleotidase cytosolic II (NT5C2) variants were reported to be nominally associated with coronary heart disease (CHD) susceptibility in the subgroups of males and with hypertension and diabetes [44]. Ubiquitin-specific protease 15 (USP15) was found to be a potential target of miR-26a and mediated the proautophagic and cardioprotective effects of miR-26a against ischemic injury [45]. Protein phosphatase 1 regulatory subunit 12A (PPP1R12A) was reported to be a member of the insulin-stimulated IRS1 signaling complex, and the interaction of PPP1R12A with IRS1 was dependent on Akt and mTOR/raptor activation [46]. To summarize, all the genes and miRNAs we identified in the ceRNA network were associated with either DM complication or MI side effects, indicating the analysis we conducted was solid and effective. However, no research has been found to elucidate that the lncRNA biomarkers we found are strongly related to the comorbidity of DM and MI. In the days to come, molecular biology methods, including qPCR, luciferase reporter systems, and co-immunoprecipitation assays could be helpful to substantiate our findings, thus unraveling the molecular mechanisms of the mutual effects that DM and MI bring to bear during the complex and development of certain diseases.

5. Conclusion

In conclusion, our study provides more comprehensive material for the ceRNA link between mRNAs and lncRNAs in diabetic MI by constructing competing endogenous RNA networks, and three candidate lncRNA biomarkers for the comorbidity of MI and DM were identified. The findings will improve comprehension of the molecular mechanisms underlying the pathology of MI and DM from a ceRNA per-

spective and provide potential therapeutic targets for the treatment of diabetic MI in clinical practice.

Data Availability

The data sets used and analyzed during the current study are available from the corresponding author on reasonable request.

Conflicts of Interest

The authors declare no conflicts of interest.

Authors' Contributions

Yun Zhou analyzed the data and wrote the manuscript. Chengjun Zhou and Lilong Wei participated in data interpretation and manuscript improvement. Chengwu Han and Yongtong Cao organized the final manuscript. All authors read and approved the final manuscript.

Acknowledgments

This study was supported by the National Natural Science Foundation of China (82072337 and 81400356) and Key Clinical Specialty Project of Beijing 2020.

Supplementary Materials

Supplementary 1. Table S1: the differentially expressed mRNAs and lncRNAs identified from the GEO data set.

Supplementary 2. Table S2: the differentially expressed miRNAs found in GSE112690.

Supplementary 3. Table S3: the gene ontology (GO) term enrichment for differentially expressed genes.

Supplementary 4. Table S4: the Kyoto Encyclopedia of Genes and Genomes (KEGG) pathway enrichment for differentially expressed genes.

Supplementary 5. Table S5: detailed mRNAs and lncRNAs in each WGCNA module.

Supplementary 6. Table S6: hub genes and lncRNAs in module METurquoise in the lncRNA-mRNA regulatory network.

References

- [1] Members, Writing Group, D. Mozaffarian, E. J. Benjamin et al., "Heart disease and stroke Statistics-2016 update: a report from the American Heart Association," *Circulation*, vol. 133, no. 4, pp. e38–e360, 2016.
- [2] S. S. Virani, A. Alonso, E. J. Benjamin et al., "Heart disease and stroke Statistics-2020 update: a report from the American Heart Association," *Circulation*, vol. 141, no. 9, pp. e139–e596, 2020.
- [3] L. Y. Ma, W. W. Chen, R. L. Gao et al., "China cardiovascular diseases report 2018: an updated summary," *Journal of Geriatric Cardiology*, vol. 17, no. 1, pp. 1–8, 2020.
- [4] S. M. Haffner, S. Lehto, T. Ronnema, K. Pyorala, and M. Laakso, "Mortality from coronary heart disease in subjects

- with type 2 diabetes and in nondiabetic subjects with and without prior myocardial infarction." *The New England Journal of Medicine*, vol. 339, no. 4, pp. 229–234, 1998.
- [5] A. A. Tajik, D. Dobre, D. Aguilar et al., "A history of diabetes predicts outcomes following myocardial infarction: an analysis of the 28 771 patients in the high-risk MI database," *European Journal of Heart Failure*, vol. 19, no. 5, pp. 635–642, 2017.
 - [6] L. Ryden, P. J. Grant, S. D. Anker et al., "ESC guidelines on diabetes, pre-diabetes, and cardiovascular diseases developed in collaboration with the EASD-summary," *Diabetes and Vascular Disease Research*, vol. 11, no. 3, pp. 133–173, 2014.
 - [7] N. Lamblin, M. Fertin, P. de Groote, and C. Bauters, "Cardiac remodeling and heart failure after a first anterior myocardial infarction in patients with diabetes mellitus," *Journal of Cardiovascular Medicine (Hagerstown, Md.)*, vol. 13, no. 6, pp. 353–359, 2012.
 - [8] C. Bauters, M. Deneve, O. Tricot, T. Meurice, N. Lamblin, and CORONOR Investigators, "Prognosis of patients with stable coronary artery disease (from the CORONOR Study)," *The American Journal of Cardiology*, vol. 113, no. 7, pp. 1142–1145, 2014.
 - [9] C. S. Lam, "Diabetic cardiomyopathy: an expression of stage B heart failure with preserved ejection fraction," *Diabetes & Vascular Disease Research*, vol. 12, no. 4, pp. 234–238, 2015.
 - [10] P. T. Donnan, D. I. Boyle, J. Broomhall et al., "Prognosis following first acute myocardial infarction in type 2 diabetes: a comparative population study," *Diabetic Medicine*, vol. 19, no. 6, pp. 448–455, 2002.
 - [11] M. Huarte, "The emerging role of lncRNAs in cancer," *Nature Medicine*, vol. 21, no. 11, pp. 1253–1261, 2015.
 - [12] S. Iwasaki and Y. Tomari, "Argonaute-mediated translational repression (and activation)," *Fly (Austin)*, vol. 3, no. 3, pp. 204–206, 2009.
 - [13] A. Jandura and H. M. Krause, "The new RNA world: growing evidence for long noncoding RNA functionality," *Trends in Genetics*, vol. 33, no. 10, pp. 665–676, 2017.
 - [14] W. Li, D. Notani, and M. G. Rosenfeld, "Enhancers as non-coding RNA transcription units: recent insights and future perspectives," *Nature Reviews. Genetics*, vol. 17, no. 4, pp. 207–223, 2016.
 - [15] T. Thum and G. Condorelli, "Long noncoding RNAs and microRNAs in cardiovascular pathophysiology," *Circulation Research*, vol. 116, no. 4, pp. 751–762, 2015.
 - [16] L. Salmena, L. Poliseno, Y. Tay, L. Kats, and P. P. Pandolfi, "A ceRNA hypothesis: the Rosetta Stone of a hidden RNA language?," *Cell*, vol. 146, no. 3, pp. 353–358, 2011.
 - [17] C. L. Smillie, T. Sirey, and C. P. Ponting, "Complexities of post-transcriptional regulation and the modeling of ceRNA crosstalk," *Critical Reviews in Biochemistry and Molecular Biology*, vol. 53, no. 3, pp. 231–245, 2018.
 - [18] Y. Dong, C. Liu, Y. Zhao, M. Ponnusamy, P. Li, and K. Wang, "Role of noncoding RNAs in regulation of cardiac cell death and cardiovascular diseases," *Cellular and Molecular Life Sciences*, vol. 75, no. 2, pp. 291–300, 2018.
 - [19] A. Frankish, M. Diekhans, A. M. Ferreira et al., "GENCODE reference annotation for the human and mouse genomes," *Nucleic Acids Research*, vol. 47, no. D1, pp. D766–D773, 2019.
 - [20] M. Ashburner, C. A. Ball, J. A. Blake et al., "Gene Ontology: tool for the unification of biology," *Nature Genetics*, vol. 25, no. 1, pp. 25–29, 2000.
 - [21] Gene Ontology Consortium, "The Gene Ontology Resource: 20 years and still GOing strong," *Nucleic Acids Research*, vol. 47, no. D1, pp. D330–D338, 2019.
 - [22] M. Kanehisa, M. Furumichi, M. Tanabe, Y. Sato, and K. Morishima, "KEGG: new perspectives on genomes, pathways, diseases and drugs," *Nucleic Acids Research*, vol. 45, no. D1, pp. D353–D361, 2017.
 - [23] G. Yu, L. G. Wang, Y. Han, and Q. Y. He, "clusterProfiler: an R package for comparing biological themes among gene clusters," *OMICS*, vol. 16, no. 5, pp. 284–287, 2012.
 - [24] P. Langfelder and S. Horvath, "WGCNA: an R package for weighted correlation network analysis," *BMC Bioinformatics*, vol. 9, no. 1, p. 559, 2008.
 - [25] P. Shannon, A. Markiel, O. Ozier et al., "Cytoscape: a software environment for integrated models of biomolecular interaction networks," *Genome Research*, vol. 13, no. 11, pp. 2498–2504, 2003.
 - [26] C. Sticht, C. De La Torre, A. Parveen, and N. Gretz, "miRWalk: an online resource for prediction of microRNA binding sites," *Plos One*, vol. 13, no. 10, article e206239, 2018.
 - [27] V. Agarwal, G. W. Bell, J. W. Nam, and D. P. Bartel, "Predicting effective microRNA target sites in mammalian mRNAs," *eLife*, vol. 4, article e05005, 2015.
 - [28] Y. Chen and X. Wang, "miRDB: an online database for prediction of functional microRNA targets," *Nucleic Acids Research*, vol. 48, no. D1, pp. D127–D131, 2020.
 - [29] P. Loher and I. Rigoutsos, "Interactive exploration of RNA22 microRNA target predictions," *Bioinformatics*, vol. 28, no. 24, pp. 3322–3323, 2012.
 - [30] D. Betel, A. Koppal, P. Agius, C. Sander, and C. Leslie, "Comprehensive modeling of microRNA targets predicts functional non-conserved and non-canonical sites," *Genome Biology*, vol. 11, no. 8, p. R90, 2010.
 - [31] D. M. Garcia, D. Baek, C. Shin, G. W. Bell, A. Grimson, and D. P. Bartel, "Weak seed-pairing stability and high target-site abundance decrease the proficiency of *_lsy-6_* and other microRNAs," *Nature Structural & Molecular Biology*, vol. 18, no. 10, pp. 1139–1146, 2011.
 - [32] Y. Tay, J. Rinn, and P. P. Pandolfi, "The multilayered complexity of ceRNA crosstalk and competition," *Nature*, vol. 505, no. 7483, pp. 344–352, 2014.
 - [33] D. Wang, L. Ding, L. Wang et al., "LncRNAMALAT1 enhances oncogenic activities of EZH2 in castration-resistant prostate cancer," *Oncotarget*, vol. 6, no. 38, pp. 41045–41055, 2015.
 - [34] X. Xie, B. Tang, Y. F. Xiao et al., "Long non-coding RNAs in colorectal cancer," *Oncotarget*, vol. 7, no. 5, pp. 5226–5239, 2016.
 - [35] C. Lin and L. Yang, "Long noncoding RNA in cancer: wiring signaling circuitry," *Trends in Cell Biology*, vol. 28, no. 4, pp. 287–301, 2018.
 - [36] R. A. DeFronzo, E. Ferrannini, L. Groop et al., "Type 2 diabetes mellitus," *Nature Reviews. Disease Primers*, vol. 1, no. 1, p. 15019, 2015.
 - [37] W. S. Lee and J. Kim, "Diabetic cardiomyopathy: where we are and where we are going," *The Korean Journal of Internal Medicine*, vol. 32, no. 3, pp. 404–421, 2017.
 - [38] T. Miki, S. Yuda, H. Kouzu, and T. Miura, "Diabetic cardiomyopathy: pathophysiology and clinical features," *Heart Failure Reviews*, vol. 18, no. 2, pp. 149–166, 2013.
 - [39] J. Fuentes-Antras, B. Picatoste, A. Gomez-Hernandez, J. Egido, J. Tunon, and O. Lorenzo, "Updating experimental models of

- diabetic cardiomyopathy,” *Journal Diabetes Research*, vol. 2015, article 656795, pp. 1–15, 2015.
- [40] Y. Yang, H. Luo, S. Liu et al., “Platelet microparticles-containing miR-4306 inhibits human monocyte-derived macrophages migration through VEGFA/ERK1/2/NF- κ B signaling pathways,” *Clinical and Experimental Hypertension*, vol. 41, no. 5, pp. 481–491, 2019.
- [41] K. Hirota, H. Keino, M. Inoue, H. Ishida, and A. Hirakata, “Comparisons of microRNA expression profiles in vitreous humor between eyes with macular hole and eyes with proliferative diabetic retinopathy,” *Graefe’s Archive for Clinical and Experimental Ophthalmology*, vol. 253, no. 3, pp. 335–342, 2015.
- [42] M. F. Bari, S. Ngo, C. C. Bastie, A. M. Sheppard, and M. Vatish, “Gestational diabetic transcriptomic profiling of microdissected human trophoblast,” *The Journal of Endocrinology*, vol. 229, no. 1, pp. 47–59, 2016.
- [43] X. Luo, Y. Zhang, X. Ruan et al., “Fasting-induced protein phosphatase 1 regulatory subunit contributes to postprandial blood glucose homeostasis via regulation of hepatic glycogenesis,” *Diabetes*, vol. 60, no. 5, pp. 1435–1445, 2011.
- [44] X. Chen, Z. Zhang, X. Wang, Y. Chen, and C. Wang, “*NT5C2* gene polymorphisms and the risk of coronary heart disease,” *Public Health Genomics*, vol. 23, no. 3-4, pp. 90–99, 2020.
- [45] H. Liang, X. Su, Q. Wu et al., “LncRNA2810403D21Rik/Mirf promotes ischemic myocardial injury by regulating autophagy through targeting Mir26a,” *Autophagy*, vol. 16, no. 6, pp. 1077–1091, 2020.
- [46] T. Geetha, P. Langlais, M. Caruso, and Z. Yi, “Protein phosphatase 1 regulatory subunit 12A and catalytic subunit δ , new members in the phosphatidylinositide 3 kinase insulin-signaling pathway,” *The Journal of Endocrinology*, vol. 214, no. 3, pp. 437–443, 2012.

Research Article

Targeting Circulating lncRNA ENST00000538705.1 Relieves Acute Coronary Syndrome via Modulating ALOX15

Hao Chen ¹, Shiwei Huang,¹ Fanlu Guan,¹ Sisi Han,¹ Fanhao Ye,¹ Xun Li ²,
and Liyi You ¹

¹Department of Cardiology, The Third Affiliated Hospital of Shanghai University (Wenzhou People's Hospital), Wenzhou, 325000 Zhejiang, China

²Department of Cardiology, The First Affiliated Hospital of Soochow University, Suzhou, 215006 Jiangsu, China

Correspondence should be addressed to Xun Li; lixunsuda@sina.com and Liyi You; youliyi2021@126.com

Received 19 January 2022; Revised 5 April 2022; Accepted 11 April 2022; Published 6 May 2022

Academic Editor: Simona Pichini

Copyright © 2022 Hao Chen et al. This is an open access article distributed under the Creative Commons Attribution License, which permits unrestricted use, distribution, and reproduction in any medium, provided the original work is properly cited.

Objective. Acute coronary syndrome (ACS) is the most dangerous and deadly form of coronary heart disease. Herein, we aimed to explore ACS-specific circulating lncRNAs and their regulatory mechanisms. **Methods.** This study collected serum samples from ACS patients and healthy controls for microarray analysis. Dysregulated circulating lncRNAs and mRNAs were determined with $|\log 2\text{fold} - \text{change}| > 1$ and $p < 0.05$. lncRNA-mRNA coexpression analysis was carried out. ENST00000538705.1 and ALOX15 expression was further verified in serum specimens. In human coronary artery endothelial cells (HCAECs), ENST00000538705.1 and ALOX15 were knocked out through transfecting specific siRNAs. Thereafter, proliferation and migration were investigated with CCK-8 and wound-healing assays. Myocardial infarction rat models were established and administrated with siRNAs against ENST00000538705.1 or ALOX15. Myocardial damage was investigated with H&E staining, and serum TC, LDL, and HDL levels were measured. **Results.** Microarray analysis identified 353 dysregulated circulating lncRNAs and 441 dysregulated circulating mRNAs in ACS. Coexpression analysis indicated the interaction between ENST00000538705.1 and ALOX15. RT-qPCR confirmed the remarkable upregulation of circulating ENST00000538705.1 and ALOX15 in ACS patients. In HCAECs, ENST00000538705.1 knockdown lowered the expression of ALOX15 but ALOX15 did not alter the expression of ENST00000538705.1. Silencing ENST00000538705.1 or ALOX15 weakened the proliferation and migration of HCAECs. Additionally, knockdown of ENST00000538705.1 or ALOX15 relieved myocardial damage, decreased serum TC and LDL levels, and elevated HDL levels in myocardial infarction rats. **Conclusion.** Collectively, our findings demonstrate that circulating ENST00000538705.1 facilitates ACS progression through modulating ALOX15, which provide potential targets for ACS treatment.

1. Introduction

Acute coronary syndrome (ACS), including acute myocardial infarction (AMI) and unstable angina (UA), is a highly dangerous and fatal deadly form of coronary heart disease, which is mainly triggered by ruptured atherosclerotic plaques and thrombosis [1]. In a large proportion of cases, this syndrome is the cause of acute heart failure [2]. Despite advances in treatment, ACS patients are at high risk of morbidity and mortality [3]. Approximately 20% of patients who successfully received percutaneous coronary intervention

had relapsed adverse cardiovascular events within 3 years [4]. Therefore, more effective, safer, and more affordable treatments are needed to reduce the risk of cardiovascular events and death in patients with ACS.

Genomic and transcriptomic analysis suggests that nearly 2% of the human genome is a protein-coding sequence while most of the genome is noncoding RNA (ncRNA) that is classified as small ncRNA and long ncRNA (lncRNA) [5, 6]. lncRNAs with a structure of over 200 nucleotides modulate gene expression and participate in diverse pathophysiological processes [7, 8]. On the basis of the stability of lncRNAs in

the blood and other body fluids, they are reliable biomarkers for disease diagnosis [9–11]. Emerging evidence demonstrates that several lncRNAs participate in modulating ACS initiation and progression [12]. For instance, lncRNA ANRIL triggers myocardial cell apoptosis in AMI through IL-33/ST2 signaling [13, 14]. Aging-relevant antiapoptotic lncRNA Sarrah accelerates recovery from AMI [15]. lncRNA ZFAS1 facilitates intracellular Ca^{2+} overload and contractile dysfunction in myocardial infarction (MI) mouse models [16]. Additionally, lncRNAs LNC_000226 and MALAT1 have been determined as diagnostic markers of UA [17]. Despite this, knowledge of circulating lncRNAs and their functions in ACS progression is still in its infancy. In this study, we performed microarray expression profiling to identify differences in circulating lncRNA and mRNA expression patterns between ACS patients and healthy subjects. This study was aimed at determining ACS-specific circulating lncRNAs and analyzing the potential biological functions of lncRNAs during ACS progression.

2. Materials and Methods

2.1. Patients and Samples. This study was approved by the Ethics Committee of the Third Affiliated Hospital of Shanghai University (Wenzhou People's Hospital) (KY-2017029). All patients signed written informed consent. This research was conducted in accordance with the guidelines of the Declaration of Helsinki. From June 2017 to October 2017, whole blood samples from 9 patients with ACS and 9 healthy participants were collected in the Third Affiliated Hospital of Shanghai University (Wenzhou People's Hospital). The diagnostic criteria of ACS were as follows: patients had stenosis (at least one main coronary artery $\geq 50\%$) confirmed by coronary angiography and/or met the AMI criteria (typical clinical symptoms, elevated cardiac enzyme levels, and a representative set of electrocardiography (ECG)). The inclusion criteria were as follows: (1) patients met the diagnostic criteria, (2) patients were 35–75 years old, and (3) patients provided informed consent. The exclusion criteria were as follows: (1) patients had comorbid diseases, such as cardiomyopathy, valvular heart disease, severe arrhythmia, heart failure, and other concomitant diseases; (2) patients had data collection difficulties, such as religious or language barriers; and (3) patients were pregnant or breastfeeding. Within 3–5 hours after the onset of symptoms but before angiography, venous blood samples were collected from each subject by anterior elbow venipuncture. The whole blood sample (2 ml) was directly collected into a test tube containing ethylenediaminetetraacetic acid (EDTA), and then, a red blood cell lysis buffer was added and other blood components were removed through centrifugation at 3000 g at 4°C for 5 minutes within 2 hours. Next, 1 ml of TRIzol was added, and the sample was transferred to a RNase/DNase-free tube and stored at -80°C.

2.2. Microarray Analysis. Microarray analysis was achieved by Beijing Boao Jingdian Biotechnology Co., Ltd. (China). Briefly, extracted RNA from serum samples of 4 ACS and 4 healthy subjects was reverse transcribed into complemen-

tary DNA (cDNA). Additionally, cRNA was synthesized by reverse transcription. Fluorescent labeling, microarray hybridization, microarray cleaning, and scanning were presented. GeneSpring software (version 13.0; Agilent) was adopted for analyzing lncRNA and mRNA microarray data for data aggregation, normalization, and quality control. Differentially expressed lncRNAs and mRNAs were screened in accordance with fold change ≥ 2 and Benjamini-Hochberg-corrected p value < 0.05 . Moreover, the Adjust Data function of CLUSTER 3.0 software was utilized to perform log2 conversion on the data and determine the median of lncRNAs or mRNAs. Additionally, the data were further analyzed through hierarchical clustering with average linkage. The clustering results were visualized using Java TreeView software [18]. Transcription factors of differentially expressed lncRNAs were predicted with the Match-1.0 Public transcription factor prediction tool. The binding of the 2000 bp and 500 bp regions upstream of the start site of each lncRNA with the transcription factor was predicted. On the basis of the Pearson correlation analysis between differentially expressed lncRNAs and mRNAs, a lncRNA-mRNA coexpression network was constructed in accordance with $|\text{correlation coefficient}| \geq 0.99$ and $p < 0.05$. Downstream targets of differentially expressed lncRNAs were also determined through cis-lncRNA prediction and trans-lncRNA prediction. The prediction of cis-lncRNA was carried out through close correlation with a set of expressed protein-coding genes utilizing $|\text{correlation coefficient}| \geq 0.99$ and $p < 0.05$. At the genomic locus where the lncRNA was located, the protein-coding gene and the lncRNA were within 10 kb along the genome. Therefore, “cis” referred to the regulation mechanism of the same locus, including the antisense lncRNA-mediated regulation of protein-coding genes encoded at the same locus. The complete sequence of lncRNA was compared with the 3'UTR of the coexpressed mRNA on the basis of the genome data from the UCSC website (<http://hgdownload.cse.ucsc.edu/admin/exe/>) [19]. The networks of transcription factor-lncRNA, lncRNA-mRNA, and lncRNA-downstream target were established with Cytoscape software [20]. In the network, degree centrality was defined as the number of links between one node and another node. Degree was the simplest and most important measure of gene centrality in a network of relative importance.

2.3. Real-Time Quantitative PCR (RT-qPCR). RNA extraction was conducted with the MiniBEST Universal RNA Extraction Kit (Takara, China). Total RNA was reverse transcribed into cDNA in the following reverse transcription system: 1 μl enzyme mix, 1 μl RT primer mix, 4 μl 5x PrimeScript buffer, 2.7 μg RNA, and 20 μl RNase-free H_2O . The reaction procedure included 37°C lasting 15 minutes, 85°C lasting 5 seconds, and 4°C which was held. RT-qPCR was carried out in accordance with the following reaction system: 1 μl forward primer, 1 μl reverse primer, 10 μl 2x mix, 7 μl H_2O , and 1 μl cDNA. Primer sequences were as follows: GAPDH, 5'-GCCGAGGAGGTCAACTACAT-3' (forward), 5'-GCTCAGGGTGATTGCGTAT-3' (reverse); ALOX15, 5'-CCCTGGATAAGGAAATTGAGATCC-3' (forward), 5'-

CCCTGGAGGAAATTGAGATCC-3' (reverse); ENST00000538705.1, 5'-TTGCCTTTCTTGCAAAGTTTCC-3' (forward), 5'-CACTTTCCCTTTTCTACTTGCTCG-3' (reverse); ENST00000556936.1, 5'-CTTCCTTGTTCTGCTCTGGTTG-3' (forward), 5'-ACCCTAATGAACGATGTCACCC-3' (reverse); and U6, 5'-CTCGCTTCGGCAGCACA-3' (forward), 5'-AACGCTTCACGAATTTGCGT-3' (reverse). Relative expression was determined with $2^{-\Delta\Delta C_t}$ method.

2.4. Cell Culture and Transfection. Human coronary artery endothelial cells (HCAECs) were purchased from Jiangsu Punuosheng Biotechnology Co., Ltd. (China). HCAECs were maintained in endothelial basal medium 2 (EBM-2) supplemented with 15% fetal bovine serum (FBS; HyClone, USA). All HCAECs were cultured in an incubator with a humid environment and 5% CO₂ at 37°C. siRNA sequences were as follows: siRNA negative control (si-NC): 5'-UUCUCCGAACGUGUCACGUTT-3' (forward), 5'-ACGUGACACGUUCGGAGAATT-3' (reverse); si-ALOX15#1: 5'-CGCUAUCAAAGACUCUCUAAATT-3' (forward), 5'-UUUAGAGAGUCUUUGAUAGCGTT-3' (reverse); si-ALOX15#2: 5'-AUGACUUAACCGGAUUUUCUTT-3' (forward), 5'-AGAAAUCCGGUUGAAGUCAUTT-3' (reverse); si-ALOX15#3: 5'-GUCGAUACAUCUUAUCUUAATT-3' (forward), 5'-UUGAAGAUATGGAU (reverse); si-ENST00000538705.1#1: 5'-UGCUUGUUUUUAUUAUGUUUUCUTT-3' (forward), 5'-AGAAAACAUAUAAACAAGCATT-3' (reverse); si-ENST00000538705.1#2: 5'-CACUCAAAUAAUUAUUUUG-3' (forward), 5'-AGCAAAAUAUUUAUUGAGUGTT-3' (reverse); and si-ENST00000538705.1#3: 5'-CCCCAUUUUAAUCUUUCAGUATT-3' (forward), 5'-UACUGAAAGAUUAAAUUGGGGTT-3' (reverse). The above siRNAs were transfected into HCAECs with the Lipofectamine RNAiMAX reagent (Thermo Scientific, USA). After 48 h, RT-qPCR was presented for measuring the expression of ALOX15 and ENST00000538705.1.

2.5. Western Blotting. Protein extraction was presented, and protein concentration was measured with the BCA method. Thereafter, protein was separated with SDS-PAGE electrophoresis and transferred onto the PVDF membrane. The membrane was sealed by 5% milk/TBST at room temperature for 1 h, followed by incubation with primary antibodies against ALOX15 (1:1000; 10021-1-Ig; Proteintech, China) and GAPDH (1:1500; 60004-1-Ig; Proteintech) at 4°C overnight. Thereafter, the membrane was incubated with HRP-labeled goat antirabbit secondary antibody (1:2000; SA00001-2; Proteintech) at room temperature for 1 h. Protein bands were developed with the ECL reagent and quantified with ImageJ software.

2.6. Cell Counting Kit-8 (CCK-8). HCAECs in the logarithmic phase were digested and resuspended in complete medium to a concentration of 3.5×10^4 /ml. Thereafter, HCAECs were inoculated into a 96-well plate (3500 cells/well) and incubated for 18 h for later use. HCAECs were transfected with specific siRNAs and cultured for 24 h,

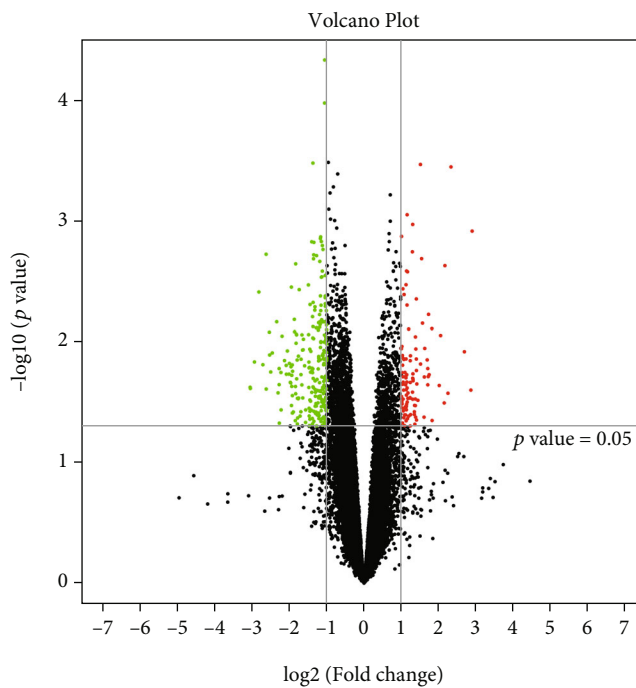
36 h, 48 h, and 72 h. 10 μ l CCK-8 solution was added to each well as well as incubated at 37°C for 4 h. After adding 10 μ l of stop solution to each well, the optical density (OD) value at 450 was measured with a microplate reader.

2.7. Wound-Healing Assay. HCAECs were plated into a 6-well plate at 3×10^5 cells/well and incubated overnight in an incubator with 5% CO₂ at 37°C. After siRNA transfection for 24 h, a 10 μ l pipette tip was utilized to make cell scratches perpendicular to the well plate. The cell culture fluid was aspirated, and the well plate was washed three times with PBS to wash away the cell debris generated by the scratch. Thereafter, the corresponding serum-free medium was added. Images were acquired at 0 h, 6 h, 24 h, and 48 h, respectively.

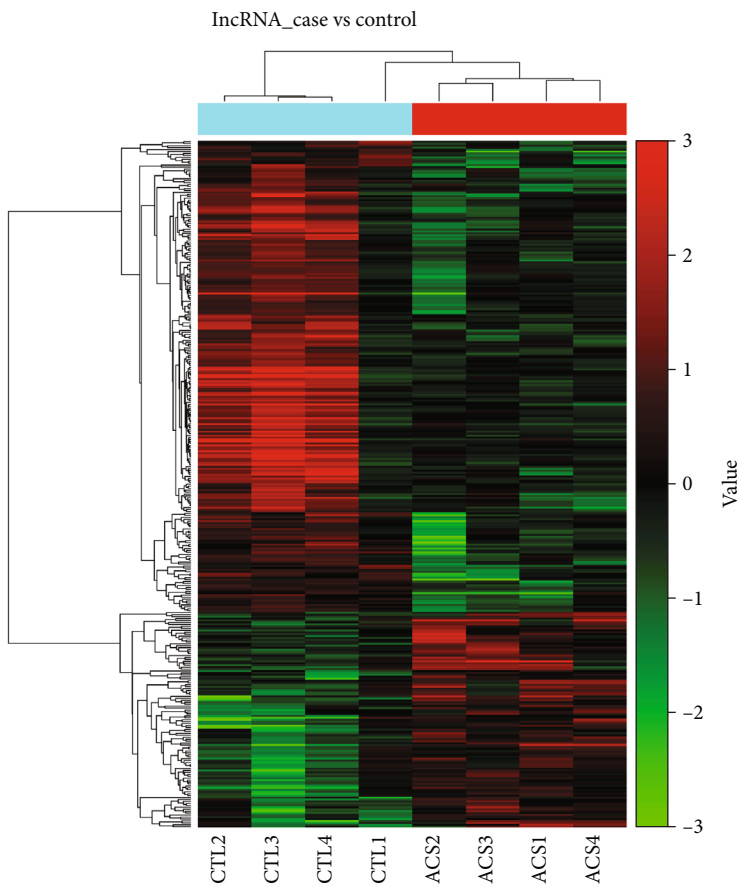
2.8. Animals. Twenty healthy adult male Sprague-Dawley rats (age 8-10 weeks; body weight 250-300 g) were purchased from the Hangzhou Scientific Cloud Biotechnology Co., Ltd. (China). According to the National Institutes of Health "Guidelines for the Care and Use of Laboratory Animals" (Bethesda, Maryland, USA), the rats were kept in the animal room at $25 \pm 1^\circ\text{C}$. All rats had a standard diet and no dietary restrictions. Our study gained the approval of the Animal Ethics Committee of the Third Affiliated Hospital of Shanghai University (Wenzhou People's Hospital) (KY-2017029).

2.9. Construction of Myocardial Infarction (MI) Rat Models. All rats were randomly divided into the sham operation group, MI+si-NC group, MI+si-ENST00000538705.1 group, and MI+si-ALOX15 group ($n = 5$ each group). The rats were anesthetized with intraperitoneal injection of pentobarbital sodium (50 mg/kg). Thereafter, their limbs were fixed, the trachea was intubated, and the electrocardiograph and respirator were connected. A 1.5 cm incision was made on the left side of the chest between the third and fourth ribs for thoracotomy. The left atrial appendage was slightly lifted with ophthalmic curved forceps. The left anterior descending artery was ligated with 5/0 surgical sutures about 1 mm below the conus artery and then sutured to close the chest. The markedly elevated ST segment in ECG lead II indicated a successful ligation. For the MI+si-NC group, the rats received a single intramyocardial injection of lentiviral therapy with a blank sequence 30 minutes before surgery. For the MI+si-ENST00000538705.1 group, the rats were treated with intramyocardial injection of 50 μ g of lentivirus with the si-ENST00000538705.1 sequence 30 minutes before surgery. For the MI+si-ALOX15 group, the rats were treated with 50 μ g lentivirus with si-ALOX15 sequence intramyocardial injection 30 minutes before surgery. For the sham operation group, the rats received only unligated surgical thread insertion. After two weeks, the rats were euthanized by intraperitoneal injection of 200 mg/kg pentobarbital sodium, and the rat hearts were excised and fixed with 4% paraformaldehyde or stored at 80°C.

2.10. Histological Analysis. Myocardial tissues were fixed in 4% paraformaldehyde for more than 24 hours, then dehydrated and embedded in paraffin. Subsequently, the paraffin-embedded tissues were cut into 4 μ m. After

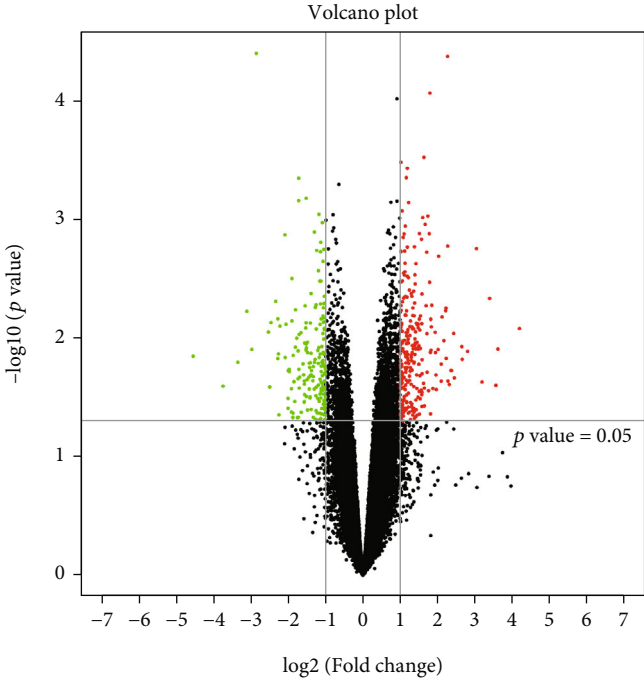


(a)

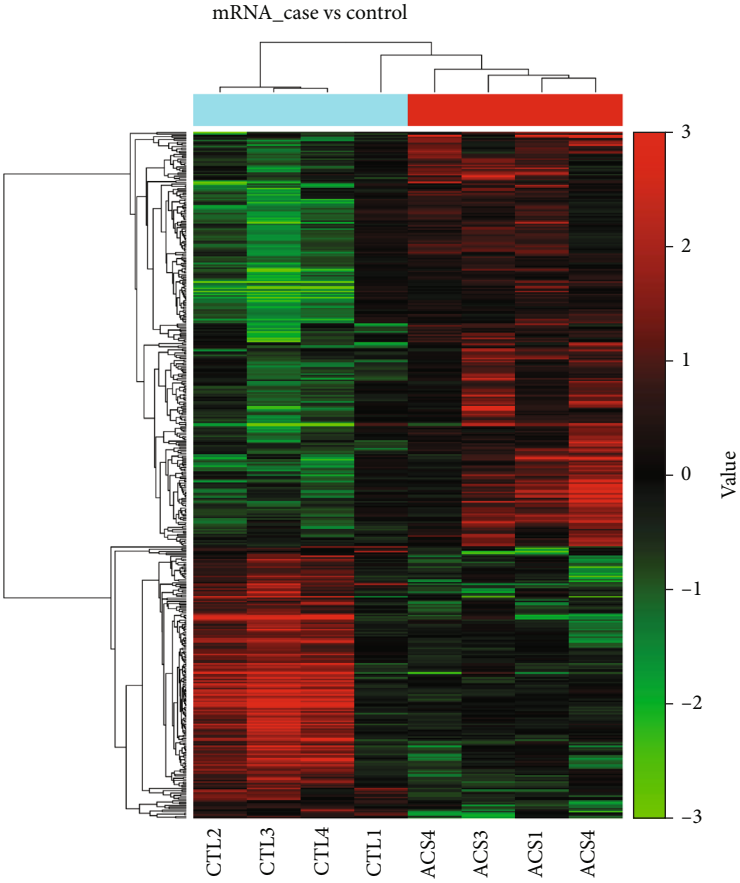


(b)

FIGURE 1: Continued.



(c)



(d)

FIGURE 1: Continued.

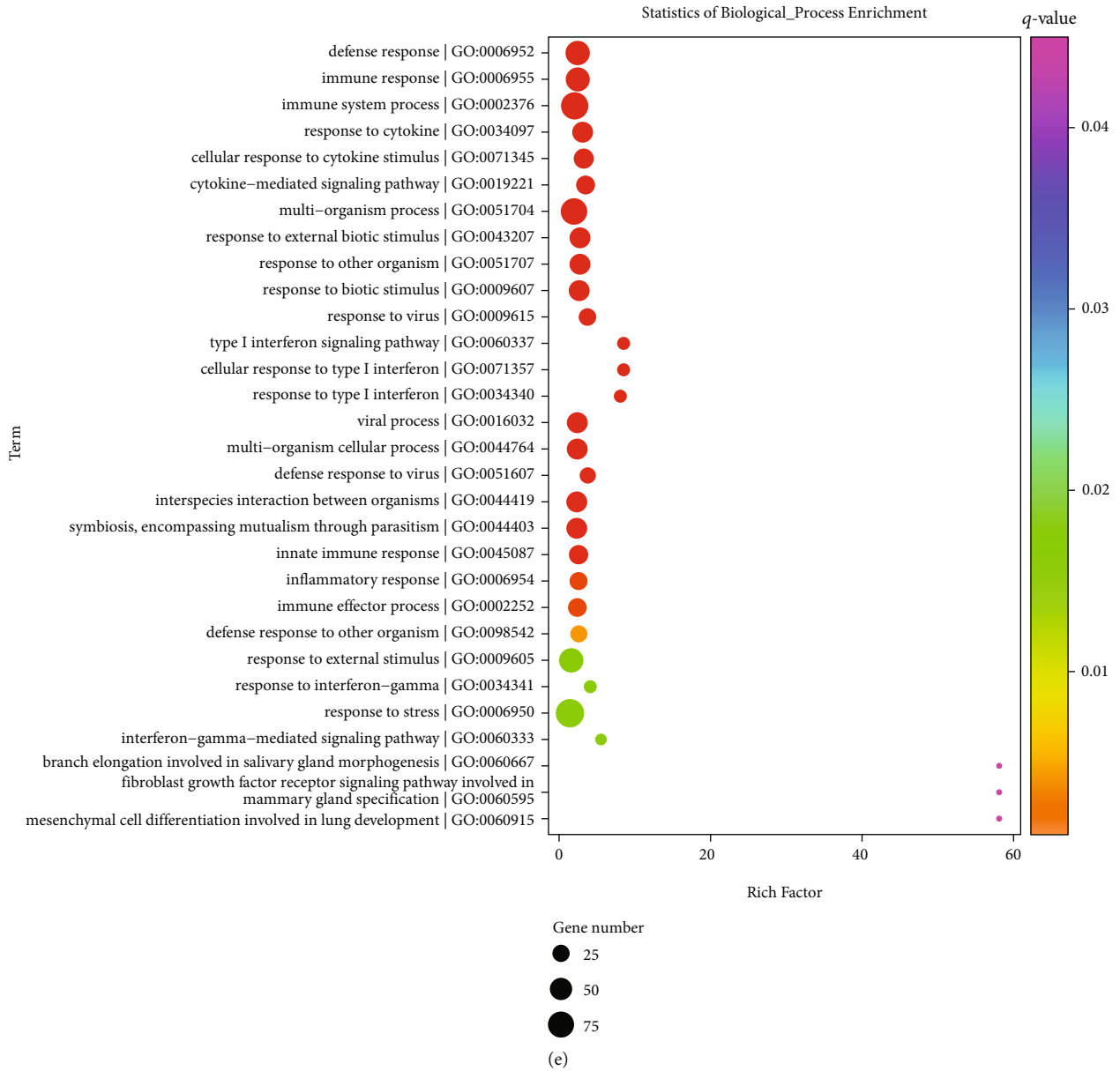


FIGURE 1: Continued.

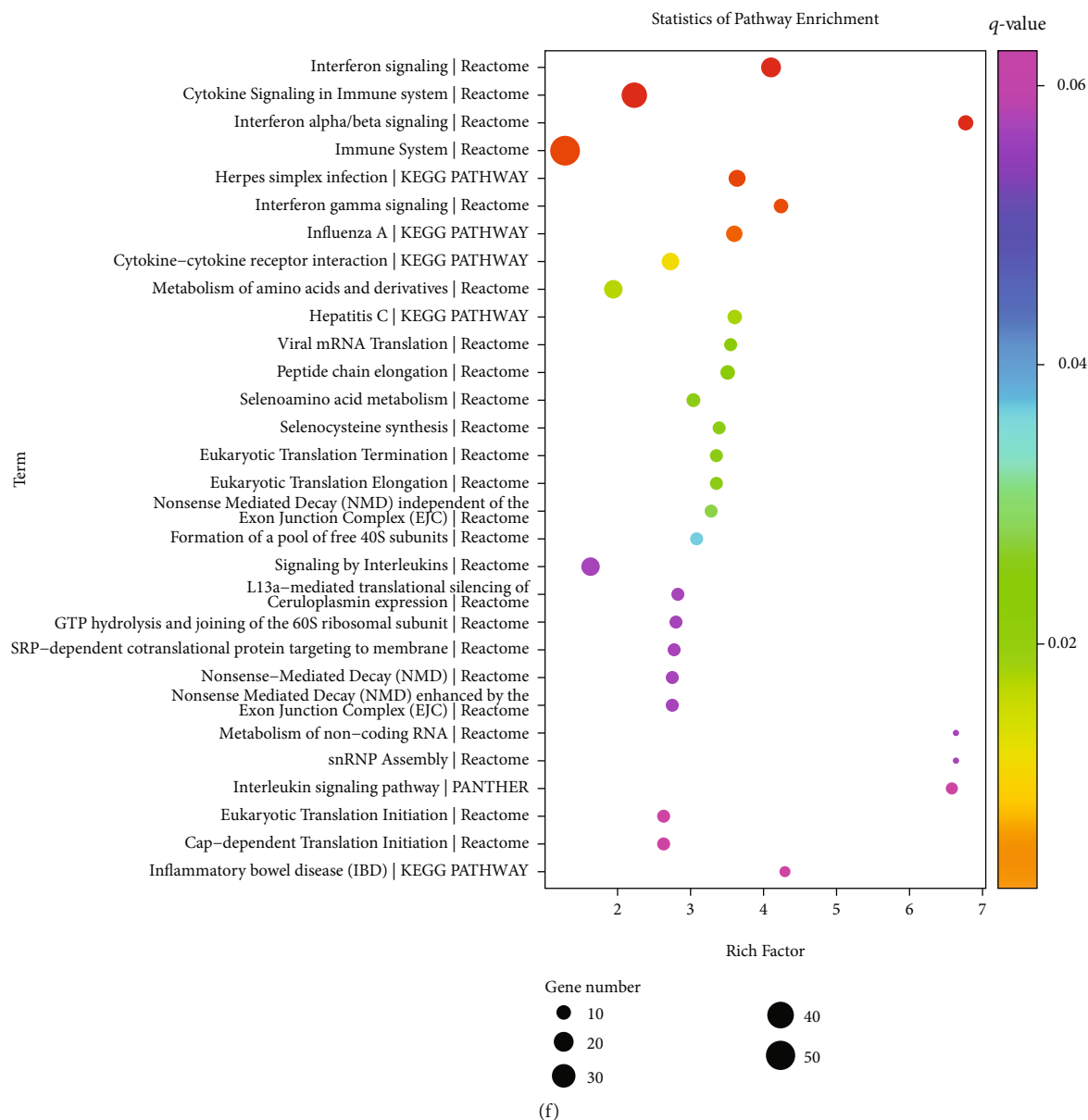


FIGURE 1: Continued.

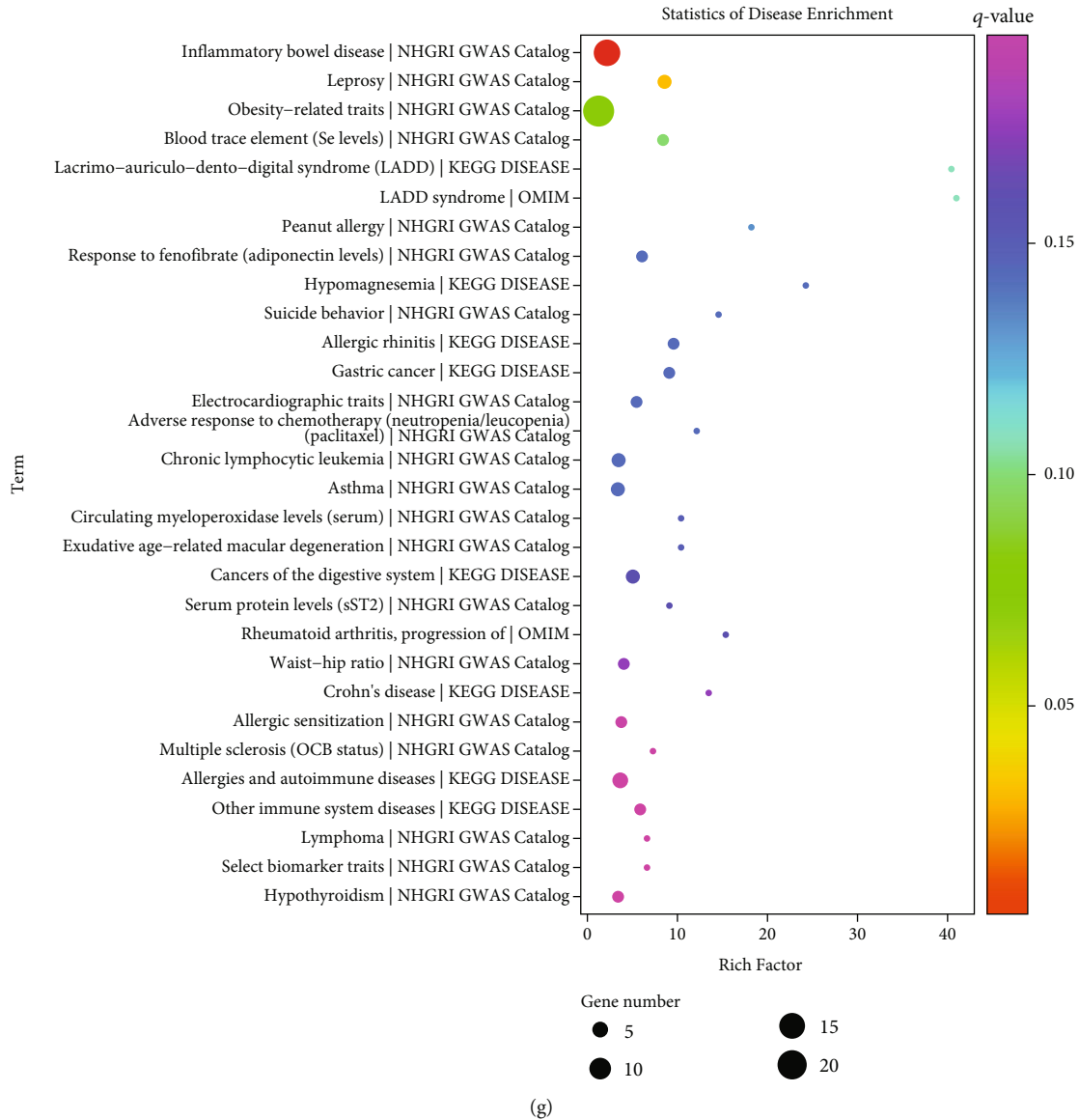
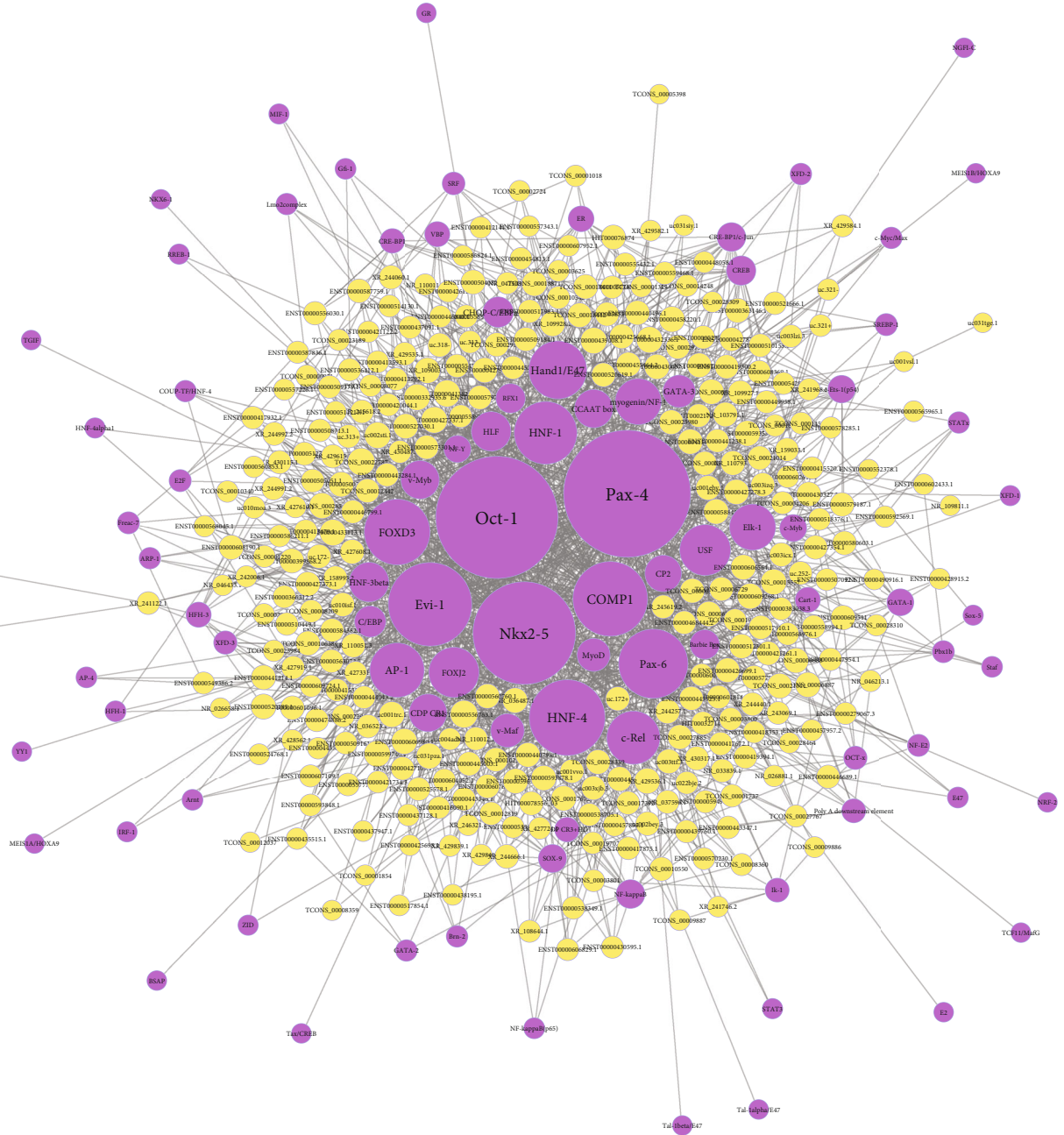


FIGURE 1: Identification of ACS-specific circulating lncRNAs and mRNAs through microarrays. (a, b) Volcano and heat map diagrams show dysregulated circulating lncRNAs in ACS patients compared with healthy subjects. (c, d) Volcano and heat map diagrams visualize dysregulated circulating mRNAs in ACS patients compared with healthy subjects. (e–g) The first 30 enrichment results of (e) biological processes, (f) KEGG pathways, and (g) diseases enriched by dysregulated circulating mRNAs. Rich factor indicates the ratio of input frequency/background frequency, the size of the bubble indicates the number of dysregulated circulating mRNAs, and the color corresponds to the *q*-value.

dewaxing into water, the sections were stained with Harris hematoxylin (Proteintech, China) for 10 minutes. After rinsing with tap water, the slices were differentiated with 1% hydrochloric acid alcohol for a few seconds. After rinsing with tap water for 10 minutes, the sections were turned blue with PBS for 5 minutes. The sections were then stained in eosin (Sigma, USA) staining solution for 3 minutes. After dehydration and mounting, microscopic examination, image acquisition, and analysis were presented.

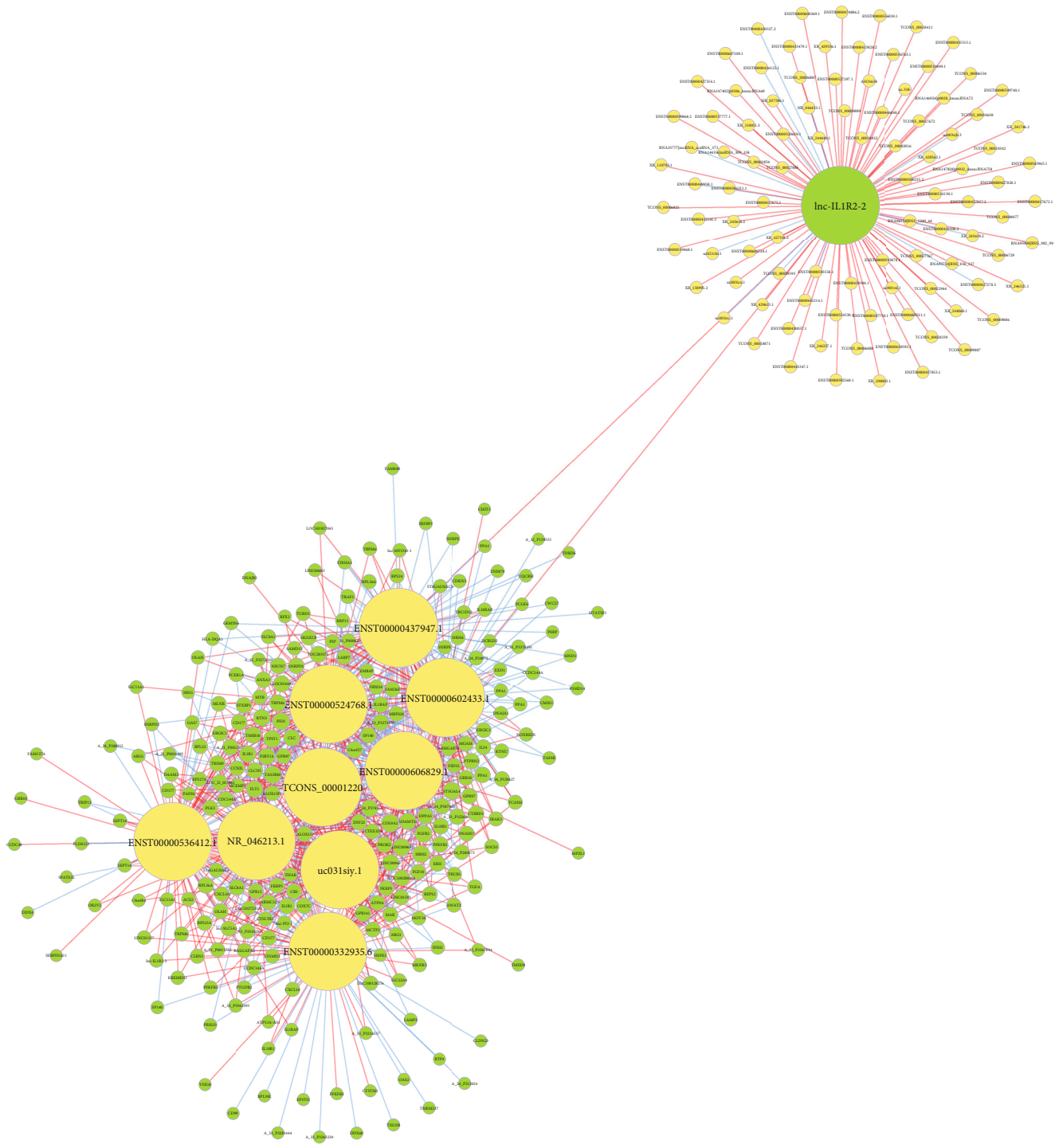
2.11. Biochemical Tests. Biochemical tests were presented strictly in accordance with the corresponding instructions of high-density lipoprotein (HDL; K076(2019005); Changchun

Huili Biotechnology Co., Ltd., China), total cholesterol (TC; C063(2019006); Changchun Huili Biotechnology Co., Ltd., China), and low-density lipoprotein (LDL; K076(2019005); Changchun Huili Biotechnology Co., Ltd., China) kits. The antigen was diluted to 0.1 ml/well with a carbonate buffer and incubated overnight at 4°C. The serum samples were washed three times the next day, and then, the diluted supernatant (0.1 ml) was added to the reaction well. The samples were then incubated at 37°C for 1 hour. Blank, negative, and positive wells were set to compare with reaction wells. A freshly diluted enzyme-labeled secondary antibody was added and incubated at 37°C for 50 minutes. Next, the holes were washed with deionized distilled water. Temporarily prepared



(a)

FIGURE 2: Continued.



(b)

FIGURE 2: Continued.

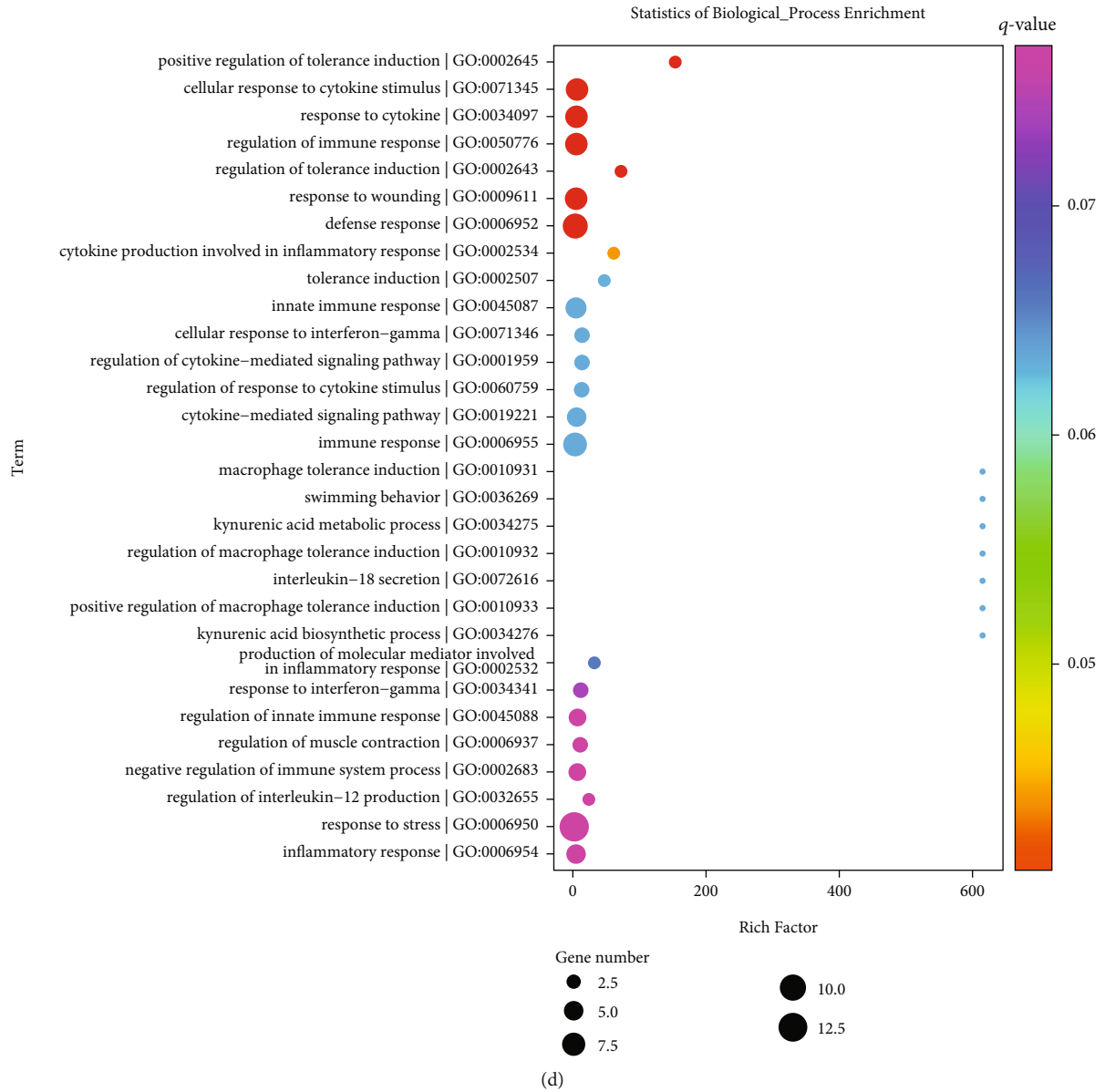


FIGURE 2: Continued.

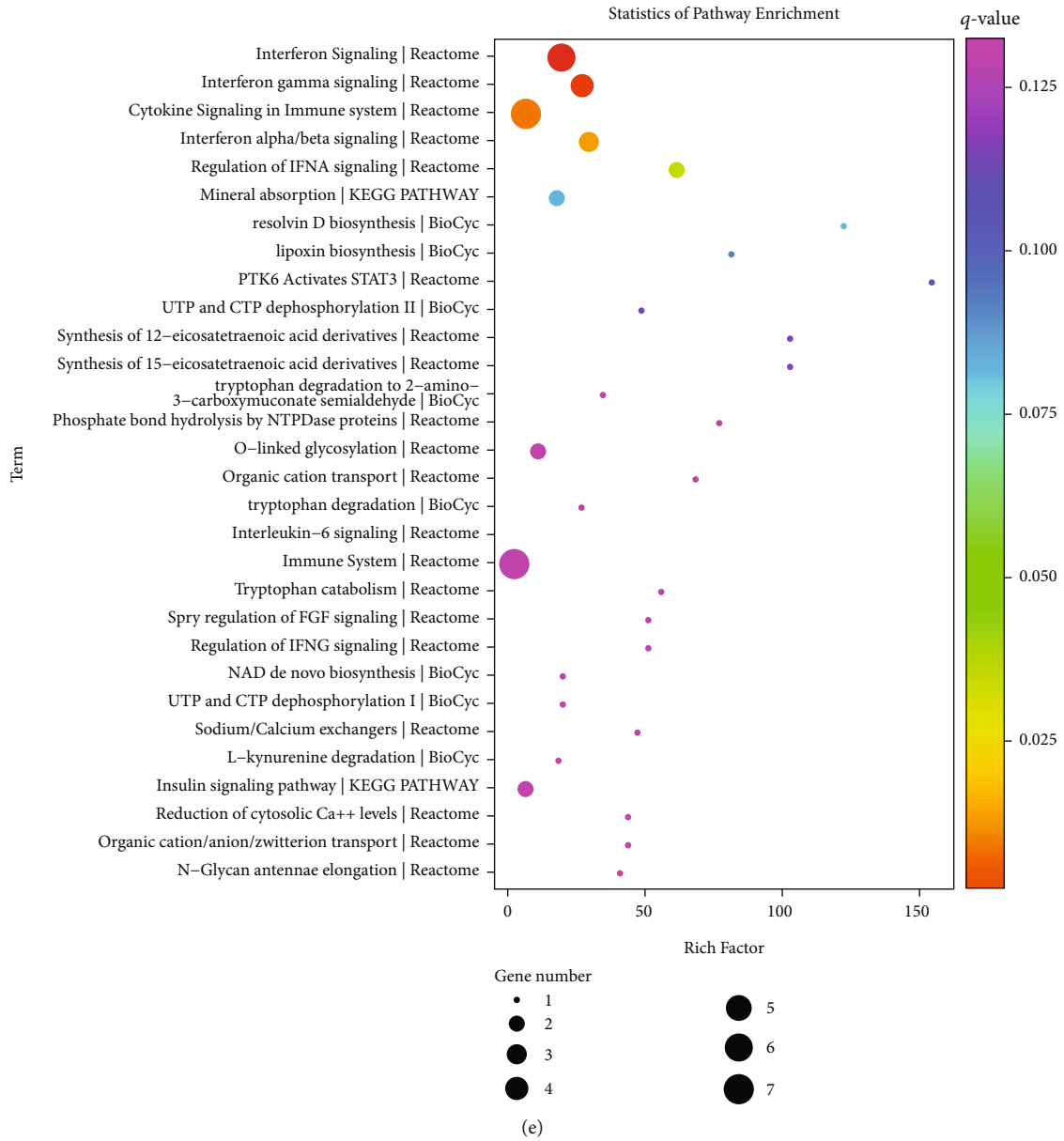


FIGURE 2: Continued.

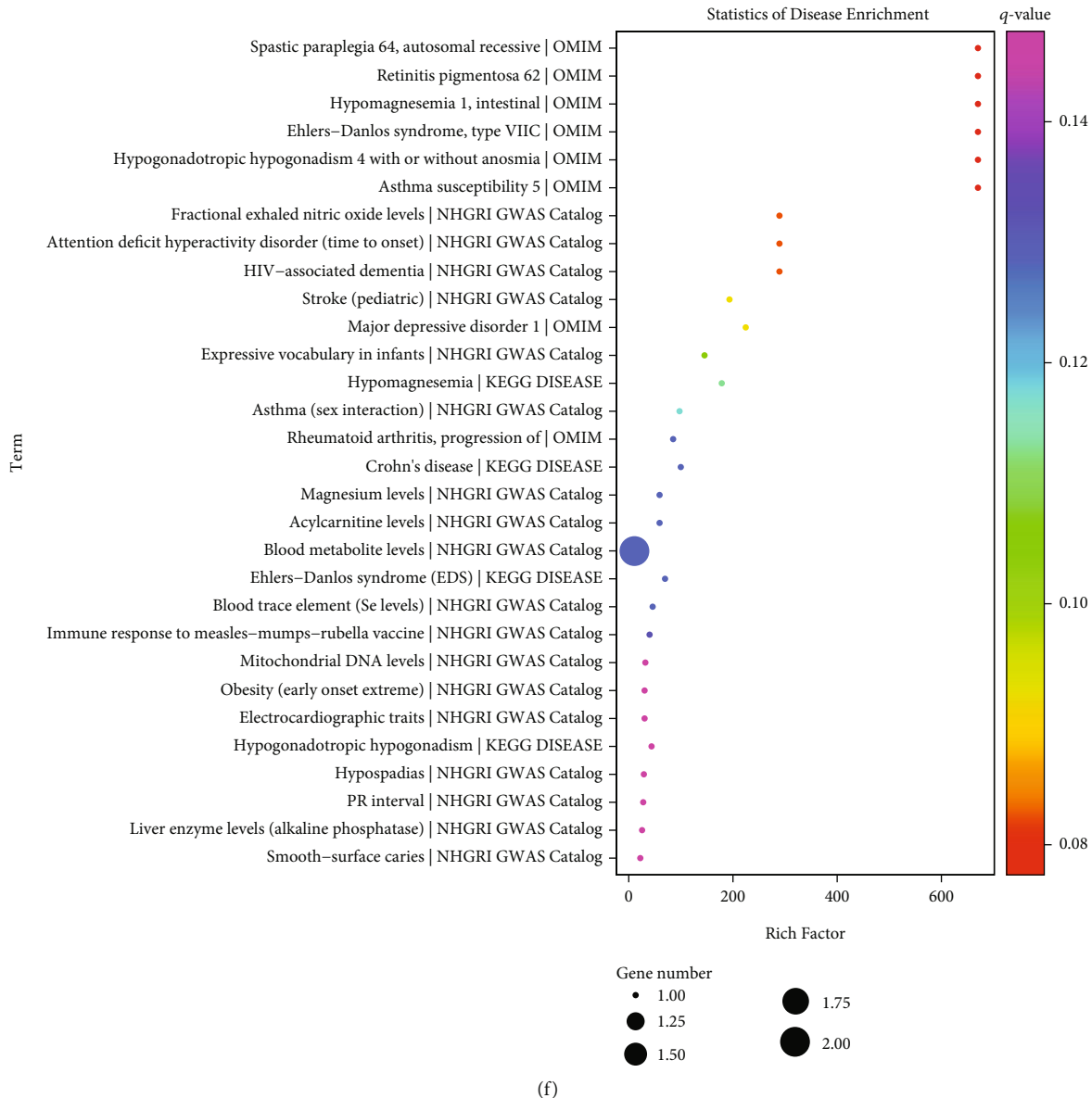


FIGURE 2: Analysis of up- and downstream factors of dysregulated lncRNAs in ACS. (a) The network of transcription factors and dysregulated lncRNAs. The yellow circle represents lncRNA, the purple circle represents transcription factor, and the size of the circle represents the degree of transcription factor or lncRNA in the network. (b) The lncRNA-mRNA coexpression network. The yellow circle represents lncRNA, the green circle represents mRNA, and the size of the circle represents the degree of lncRNA or mRNA in the network. The red line represents a positive correlation, and the blue line represents a negative correlation. (c) The network of lncRNAs and their downstream targets. The yellow circle indicates lncRNA, the green circle indicates downstream mRNA, and the size of the circle represents the degree of lncRNA or downstream target in the network. (d-f) The first 30 enrichment results of (d) biological processes, (e) KEGG pathways, and (f) diseases of downstream targets enriched by dysregulated lncRNAs. The rich factor indicates the ratio of input frequency/background frequency, the size of the bubble indicates the number of genes annotated to this function entry for downstream genes, and the color corresponds to the q -value.

tetramethylbenzidine was added to each reaction well and incubated at 37°C for 20 minutes. Stop solution (50 μ l) was added to stop the reaction. The OD value was detected at 450 nm wavelength within 20 minutes.

2.12. Statistical Analysis. All statistical analyses were conducted by the R software and GraphPad Prism 8.0 software. Each experiment was repeated at least three times. The data are expressed as mean \pm standard deviation. The differences

between different groups were analyzed by Student's t -test or one-way analysis of variance (ANOVA). $p < 0.05$ was considered statistically significant.

3. Results

3.1. Identification ACS-Specific Circulating lncRNAs and mRNAs. This study presented a microarray analysis between three pairs of serum samples from ACS patients and healthy

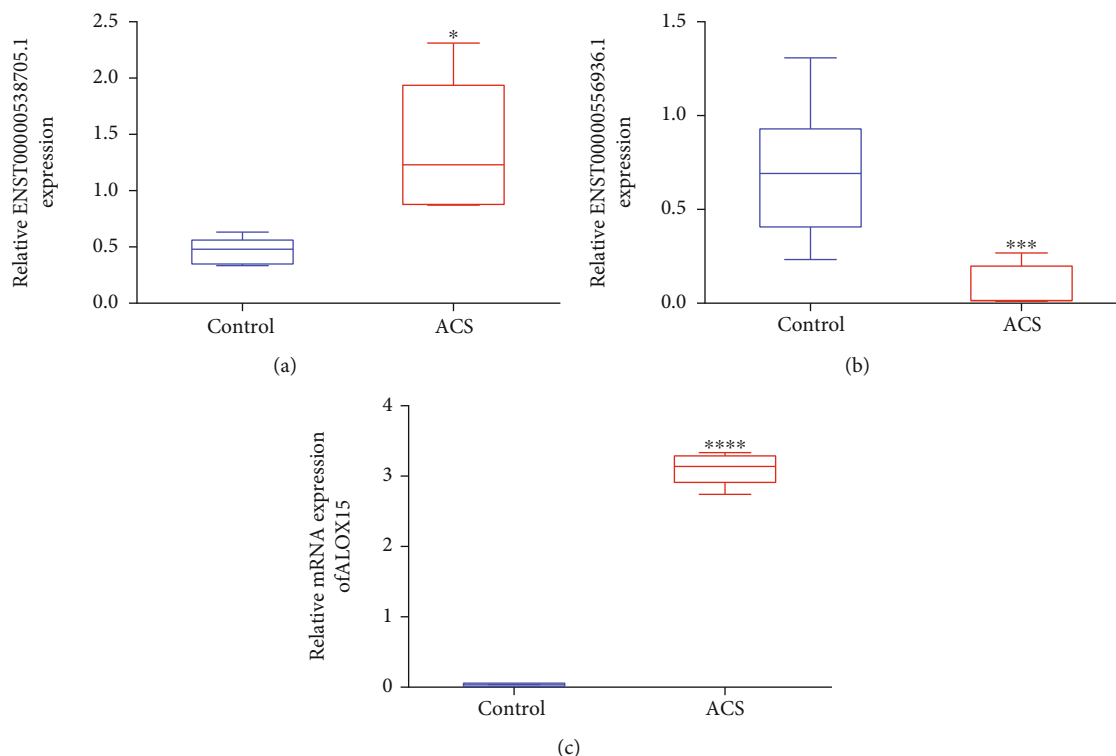


FIGURE 3: Verification of the expression of ENST00000538705.1, ENST00000556936.1, and ALOX15 in ACS patients. (a–c) RT-qPCR for measuring the expression of (a) ENST00000538705.1, (b) ENST00000556936.1, and (c) ALOX15 in serum samples of ACS patients and healthy subjects. * $p < 0.05$, *** $p < 0.001$, and **** $p < 0.0001$.

subjects. With $|\log 2\text{fold} - \text{change}| > 1$ and $p < 0.05$, we determined 111 upregulated lncRNAs and 242 downregulated lncRNAs in ACS patients compared with healthy controls (Figures 1(a) and 1(b)). Meanwhile, 266 mRNAs were upregulated, and 175 mRNAs were downregulated in ACS (Figures 1(c) and 1(d)). In Figure 1(e), we found that immune-related biological processes (immune system process, response to cytokine, cellular response to cytokine stimulus, and cytokine-mediated signaling pathway, etc.) were prominently enriched by dysregulated mRNAs. KEGG enrichment analysis demonstrated that these dysregulated mRNAs were linked to immune activation pathways such as cytokine signaling in the immune system, cytokine-cytokine receptor interaction, and interleukin signaling pathway (Figure 1(f)). Also, the above mRNAs were related to diverse diseases (Figure 1(g)).

3.2. Analysis of Up- and Downstream Factors of Dysregulated lncRNAs in ACS. Transcription factor prediction was presented utilizing the Match-1.0 Public transcription factor prediction tool. The binding of the 2000 bp upstream and 500 bp downstream region of the start site of each lncRNA to the transcription factor was predicted, and the results are shown in Figure 2(a). Coexpression analysis adopted the standardized signal value of each probe in each sample as the data source to perform pairwise correlation calculation and hypothesis verification, thereby obtaining the correlation coefficient and p value. In this study, lncRNA-mRNA coexpression pairs were determined in accordance with |

correlation coefficient| > 0.99 and p value < 0.05 , as shown in Figure 2(b). Additionally, we carried out the coexpression analysis of lncRNA and mRNA. Briefly, cis-prediction was used for exploring lncRNA-mRNA pairs within 10 kb of the genome while trans-prediction adopted the blat tool to compare the lncRNA and mRNA (3' UTR) sequences to screen lncRNA-mRNA pairs with similar sequences. Figure 2(c) depicted the interaction network of lncRNAs and their coexpressed mRNAs with $|\text{correlation coefficient}| > 0.99$ and p value < 0.05 . Biological significance of coexpressed mRNAs was further probed. In Figure 2(d), the above mRNAs were remarkably enriched in immune-relevant biological processes such as regulation of immune response, cellular response to cytokine stimulus, cytokine production involved in inflammatory response, innate immune response, cellular response to interferon-gamma, regulation of cytokine-mediated signaling pathway, macrophage tolerance induction, IL-18 secretion, and regulation of IL-12 production. Additionally, immune-relevant pathways were prominently enriched by coexpressed mRNAs, including cytokine signaling in the immune system, regulation of IFN α signaling, and IL-6 signaling (Figure 2(e)). Also, we found that these mRNAs were distinctly linked to diverse diseases (Figure 2(f)).

3.3. Verification of the Expression of ENST00000538705.1, ENST00000556936.1, and ALOX15 in ACS Patients. The expression of lncRNAs ENST00000538705.1 and ENST00000556936.1 as well as coexpressed mRNA ALOX15 was further

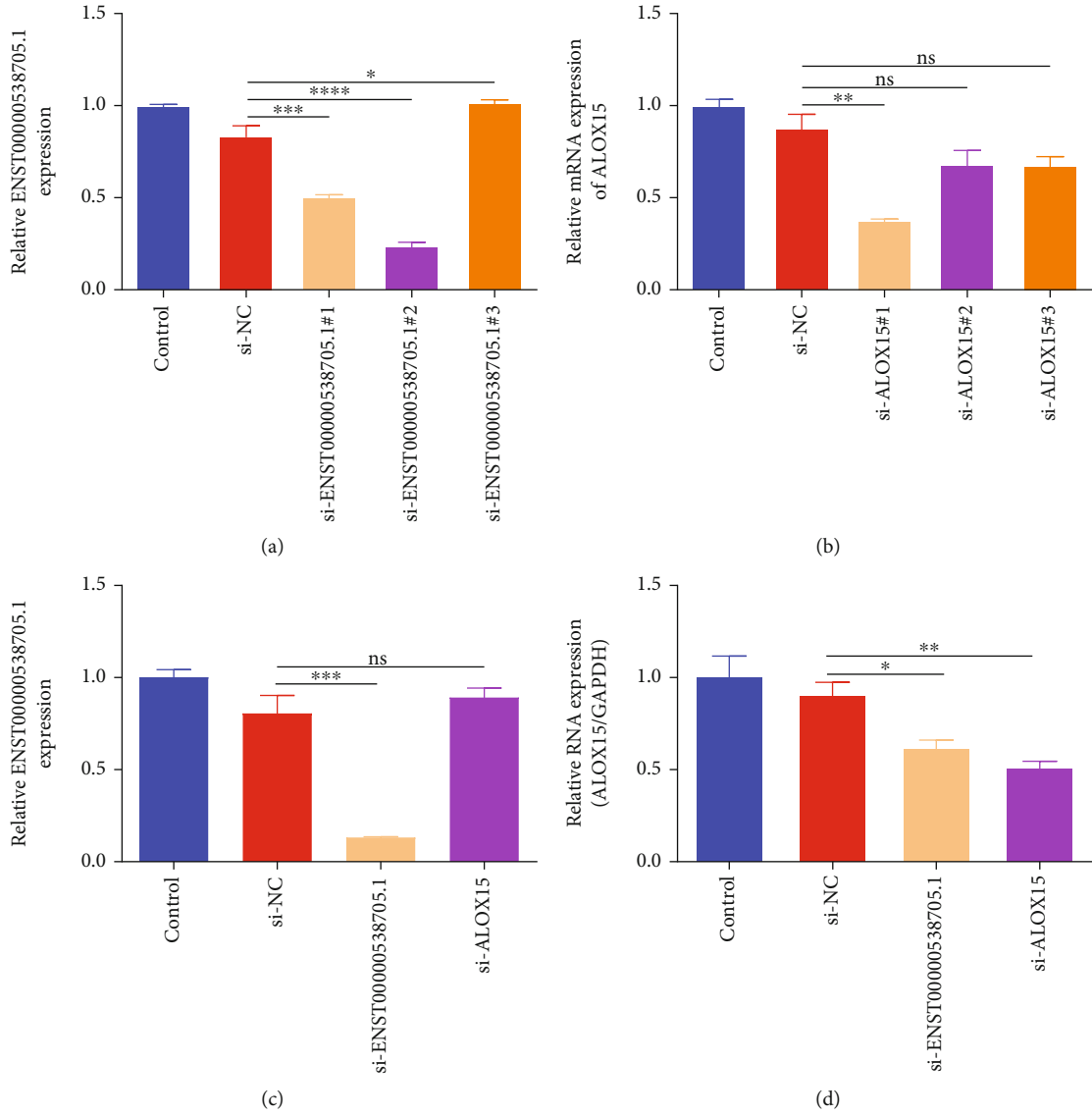


FIGURE 4: Continued.

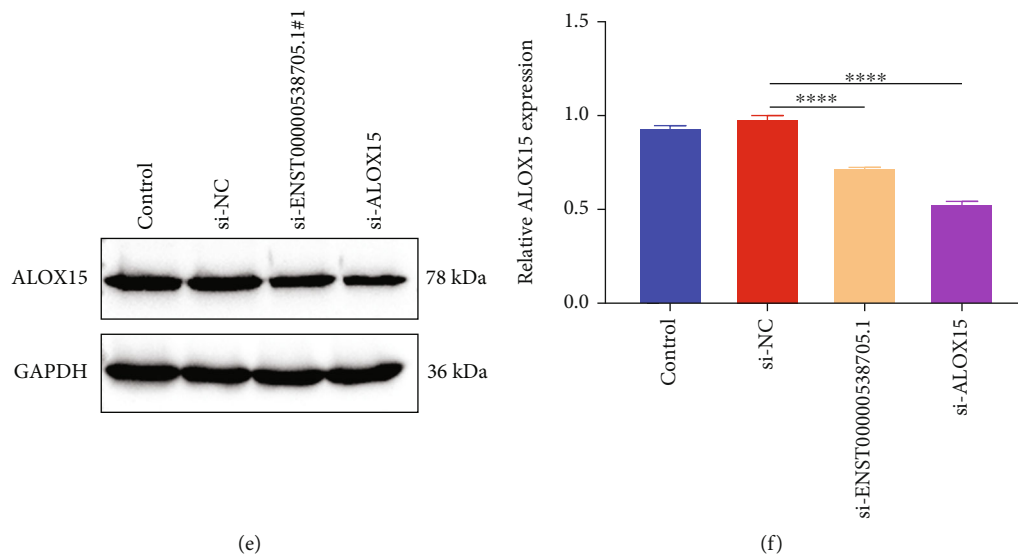


FIGURE 4: Silencing ENST00000538705.1 reduces ALOX15 expression in HCAECs. (a) RT-qPCR for evaluating the transfection effect of three specific siRNAs against ENST00000538705.1 in HCAECs. (b) The transfected effect of three specific siRNAs against ALOX15 in HCAECs via RT-qPCR. (c) RT-qPCR for measuring the expression of ENST00000538705.1 in HCAECs transfected with si-ENST00000538705.1 or si-ALOX15. (d–f) RT-qPCR and western blotting for quantifying the expression of ALOX15 in HCAECs transfected with si-ENST00000538705.1 or si-ALOX15. ns: not significant; * $p < 0.05$, ** $p < 0.01$, *** $p < 0.001$, and **** $p < 0.0001$.

verified in serum specimens of ACS patients and healthy subjects. Our data confirmed that the lncRNA ENST00000538705.1 expression was remarkably upregulated as well as the ENST00000556936.1 expression was prominently downregulated in ACS patients compared with healthy subjects (Figures 3(a) and 3(b)). Additionally, we found the prominent upregulation of ALOX15 in ACS patients (Figure 3(c)).

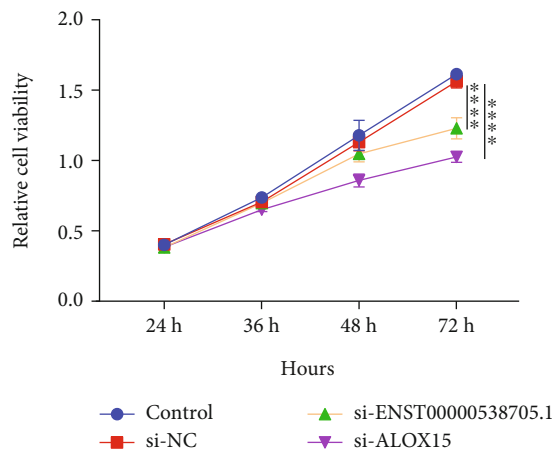
3.4. Silencing ENST00000538705.1 Reduces ALOX15 Expression in HCAECs. To investigate the interaction of ENST00000538705.1 and ALOX15 as well as their biological significance, HCAECs were separately transfected with specific siRNAs against ENST00000538705.1 and ALOX15. In Figure 4(a), si-ENST00000538705.1#2 remarkably lowered the expression of ENST00000538705.1 in HCAECs, which was adopted for further experiments. Meanwhile, we investigated the excellent knockdown effect of si-ALOX15#1 in HCAECs (Figure 4(b)). Further analysis indicated that silencing ALOX15 did not alter the ENST00000538705.1 expression in HCAECs (Figure 4(c)). However, ENST00000538705.1 knockdown remarkably reduced the expression of ALOX15 in HCAECs (Figures 4(d)–4(f)). This indicated that ALOX15 acted as a downstream target of ENST00000538705.1.

3.5. Silencing ENST00000538705.1 or ALOX15 Weakens the Proliferative and Migrated Capacities of HCAECs. CCK-8 results demonstrated that the viable HCAECs transfected with si-ENST00000538705.1 or si-ALOX15 were markedly decreased in comparison to the si-NC group (Figure 5(a)). This indicated that silencing ENST00000538705.1 or ALOX15 remarkably weakened the proliferation of HCAECs. A wound-healing assay was presented to evalu-

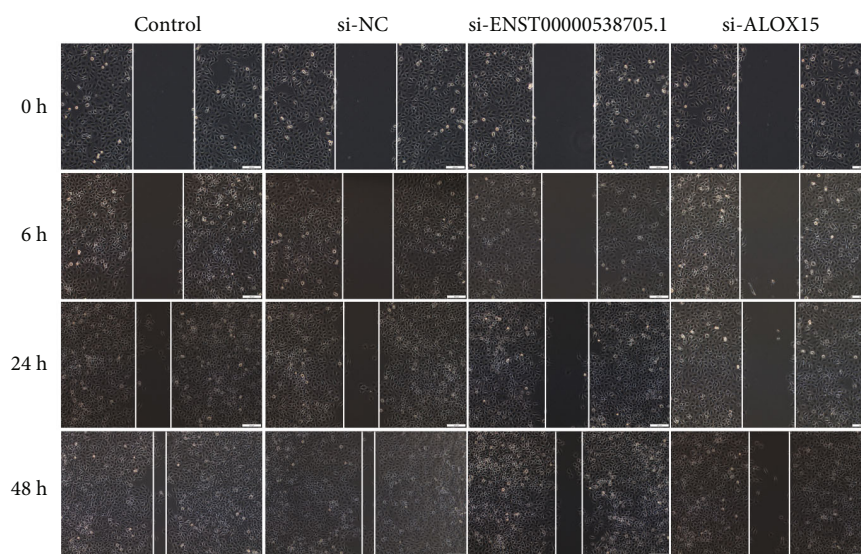
ate the migration of HCAECs. Compared with the si-NC group, the migration ability of HCAECs transfected with si-ENST00000538705.1 or si-ALOX15 was remarkably weakened (Figures 5(b) and 5(c)).

3.6. Silencing ENST00000538705.1 or ALOX15 Improves Myocardial Injury in Rats with MI. To further investigate the effects of ENST00000538705.1 and ALOX15 on ACS, we constructed MI rat models through ligating the left coronary artery. Two weeks later, the heart tissues were taken for H&E to observe the pathological condition. The cardiomyocytes of rats in the sham operation group were arranged more uniformly, without breaks and with normal cardiomyocytes (Figure 6). However, the cardiomyocytes of the MI model group were swollen and obviously thickened, with very irregular shapes and disordered arrangement. For MI rats with si-ENST00000538705.1 or si-ALOX15 treatment, cardiomyocyte hypertrophy and arrangement disorder were remarkably ameliorated.

3.7. Silencing ENST00000538705.1 or ALOX15 Reduces Blood Lipids in Rats with MI. The serum levels of TC, LDL, and HDL of rats in each group were detected separately. Compared with rats in the sham operation group, the serum levels of TC and LDL in MI rats were significantly increased (Figures 7(a) and 7(b)). Compared with rats with MI, after intervention with si-ENST00000538705.1 or si-ALOX15, the serum levels of TC and LDL of MI rats were significantly decreased. As shown in Figure 7(c), in comparison to rats in the sham operation group, the serum levels of HDL of MI rats were significantly reduced. However, the serum HDL levels of MI rats were significantly increased following treatment with si-ENST00000538705.1 or si-ALOX15.



(a)



(b)

FIGURE 5: Continued.

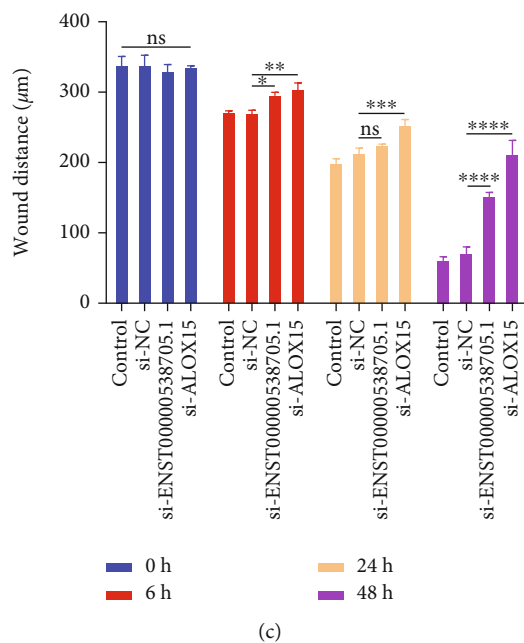


FIGURE 5: Silencing ENST00000538705.1 or ALOX15 weakens the proliferative and migrated capacities of HCAECs. (a) CCK-8 for measuring viable HCAECs transfected with si-ENST00000538705.1 or si-ALOX15 in specified time points. (b, c) Migration capacities of HCAECs transfected with si-ENST00000538705.1 or si-ALOX15 through a wound-healing assay in specified time points. Bar = 100 µm. Magnification = 200x. ns: not significant; * $p < 0.05$, ** $p < 0.01$, *** $p < 0.001$, and **** $p < 0.0001$.

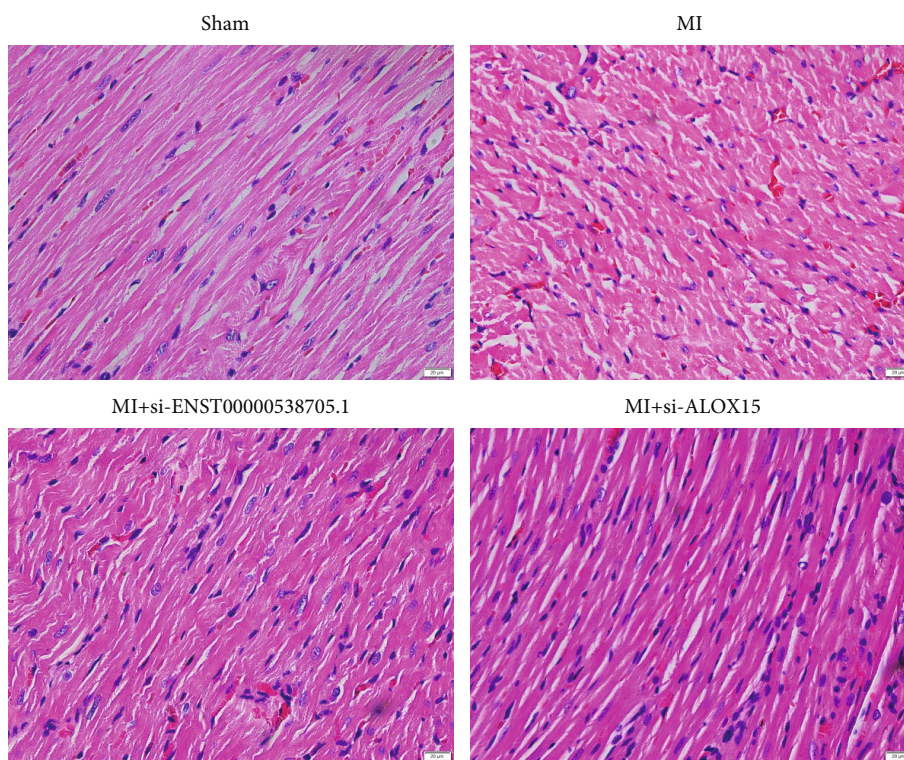


FIGURE 6: Silencing ENST00000538705.1 or ALOX15 improves myocardial injury of MI rats. H&E staining for observing the pathological condition of myocardial tissues of rats in the sham group, MI group, MI+si-ENST00000538705.1 group, and MI+ALOX15 group. Bar = 20 µm. Magnification = 200x.

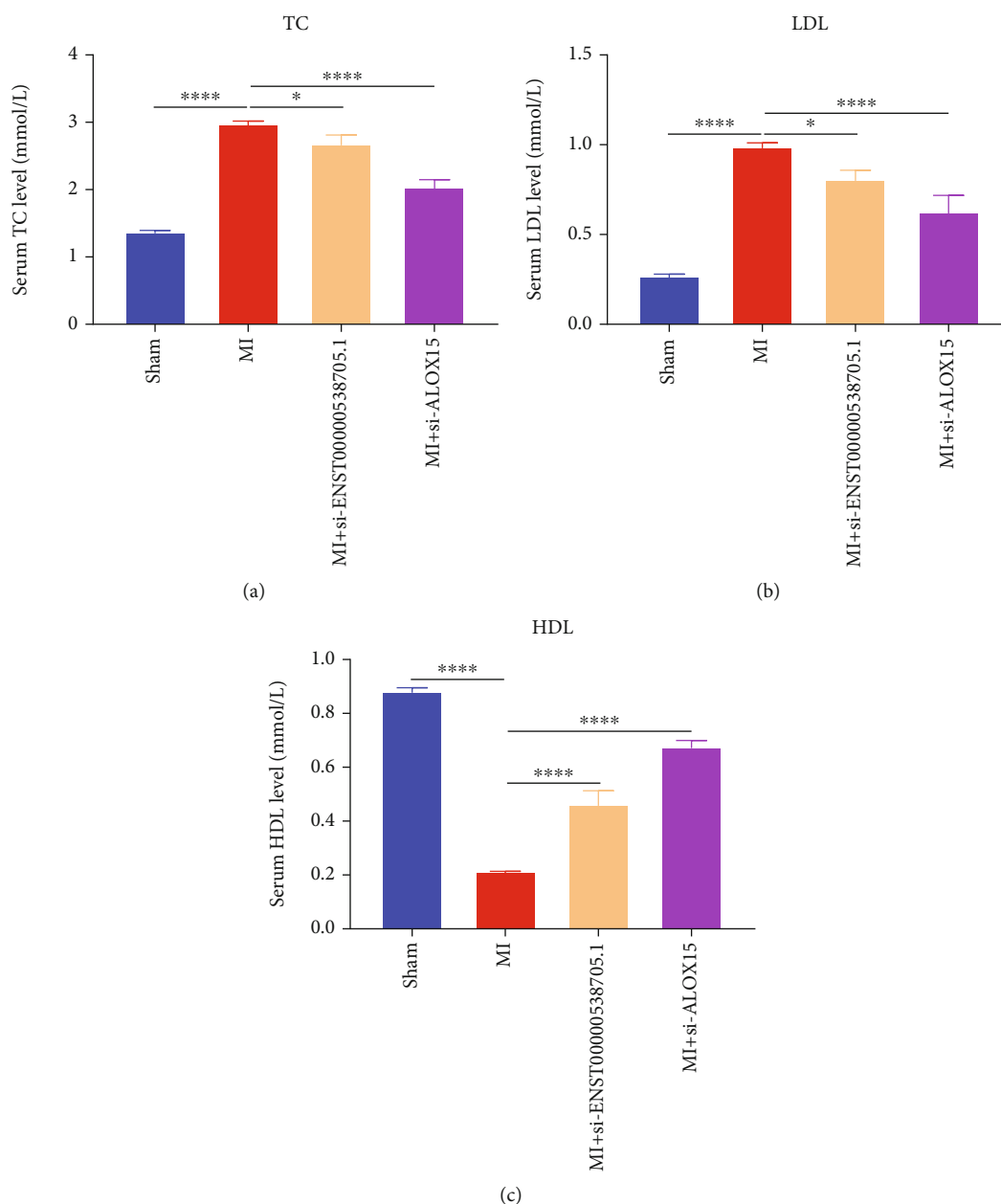


FIGURE 7: Silencing ENST00000538705.1 or ALOX15 reduces blood lipids of MI rats. (a–c) The levels of (a) TC, (b) LDL, and (c) HDL in the serum of rats in the sham group, MI group, MI+si-ENST00000538705.1 group, and MI+ALOX15 group. * $p < 0.05$ and **** $p < 0.0001$.

3.8. Silencing ENST00000538705.1 or ALOX15 Reduced their Expression Levels in the Serum of Rats with MI. The expression level of ENST00000538705.1 was further measured. The results showed that ENST00000538705.1 presented a higher expression in the serum of rats in the MI group than in the sham operation group. Nevertheless, its expression in the serum of MI rats was remarkably lowered after administration with si-ENST00000538705.1 or si-ALOX15 (Figure 8(a)). Also, ALOX15 expression was detected in serum samples. As a result, higher ALOX15 expression was investigated in the MI group in comparison to the sham group (Figures 8(b)–8(d)). But intervention with si-ENST00000538705.1 or si-ALOX15 decreased the serum levels of ALOX15 for MI rats.

4. Discussion

In the past few decades, the molecular mechanisms of ACS have been extensively studied [21–24]. Nevertheless, in-depth analysis is needed to uncover the pathogenesis of ACS. Although a few thousands of lncRNAs have been functionally characterized in ACS, their potential mechanisms in ACS remain greatly indistinct [25–27]. In our study, we adopted microarray technology to obtain the expression data of lncRNAs and mRNAs in serum specimens from 4 patients with ACS and 4 healthy controls. As a result, we determined 111 upregulated lncRNAs and 242 downregulated lncRNAs in ACS. Additionally, 266 upregulated mRNAs and 175 downregulated mRNAs were determined

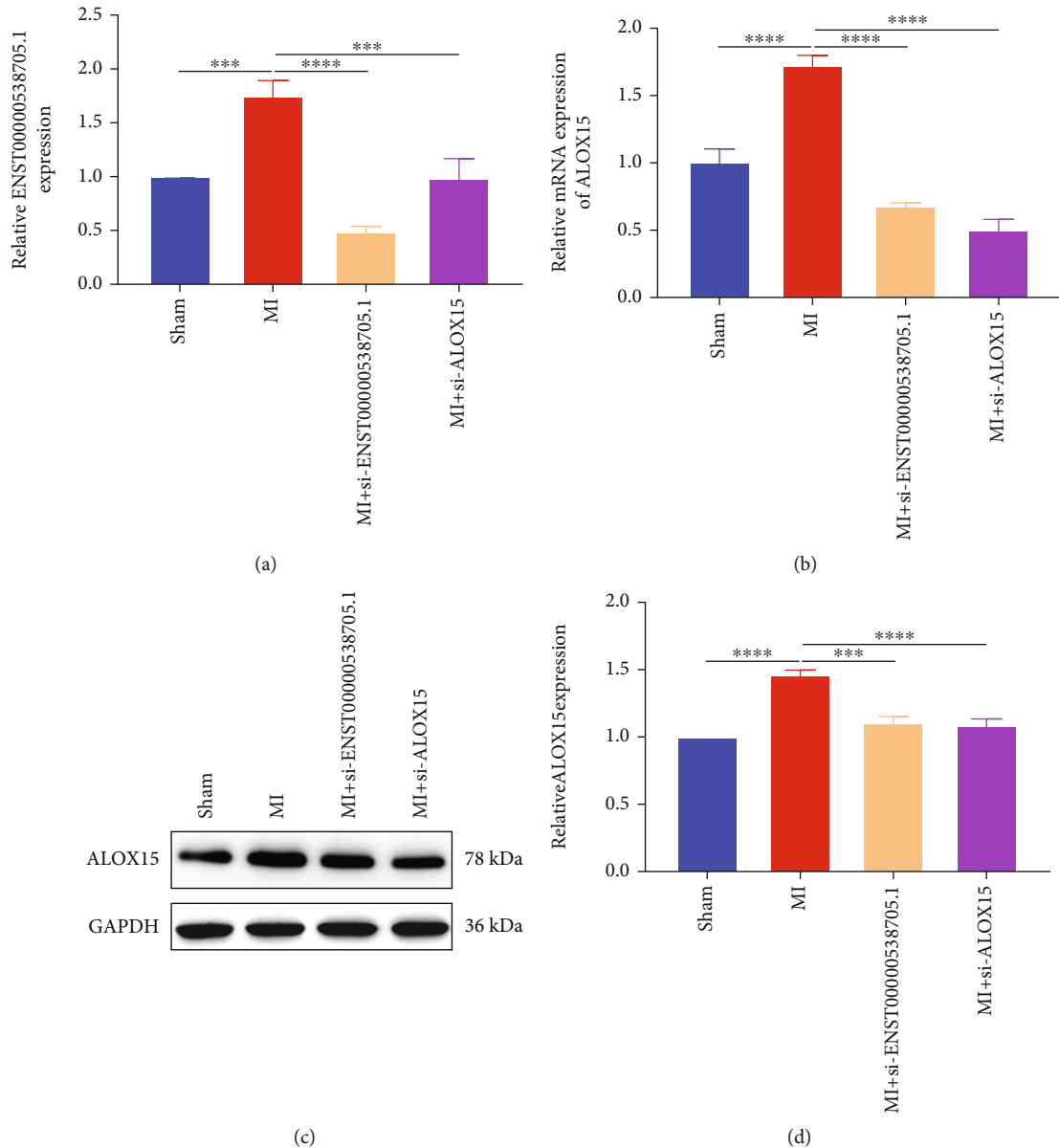


FIGURE 8: Silencing ENST00000538705.1 or ALOX15 reduces their expression levels in the serum of rats with MI. (a) ENST00000538705.1 expression in the serum of rats in the sham group, MI group, MI+si-ENST00000538705.1 group, and MI+ALOX15 group through RT-qPCR. (b–d) RT-qPCR and western blotting for measuring the expression of ALOX15 in the serum specimens from above groups. *** $p < 0.001$ and **** $p < 0.0001$.

in ACS. Immune and inflammation dysfunctions exert crucial roles in clinical manifestations and complications of ACS [3]. Our functional enrichment results showed that dysregulated circulating mRNAs were remarkably linked to immune-relevant biological processes and pathways, indicating their roles in ACS progression.

The regulatory mechanisms of these dysregulated lncRNAs were further probed out. We firstly analyzed the upstream regulatory mechanism of dysregulated lncRNAs. We identified the transcription factors of these lncRNAs, such as Nkx2-5, Pax-4, HNF-4, FOXJ2, and CHOP-C/EBPalpha. These transcription factors might be involved in modulating the expression of circulating lncRNAs in ACS. Coexpression analysis is based on correlation, looking for

lncRNA-mRNA relationship pairs with similar expression profiles from the genetic expression layer [28]. Many functionally related genes have very similar expression profiles under a set of related conditions, especially genes that are coregulated by common transcription factors, or their products form the same protein complex or participate in the same regulatory pathway [29]. In this study, our coexpression analysis and network construction based on coexpression results can help us discover the possible relationship between lncRNA and mRNA, determine the lncRNA that affects the regulation of the mRNA expression, and find the lncRNA that plays a central regulatory role in the network and discovers the possible new mechanism of action of lncRNA. It has been demonstrated that lncRNA can

regulate the expression of nearby genes through interaction with nearby genes or regulate the expression of distant genes through the indirect influence of miRNA [30–32]. Shen et al. identified key molecular markers (PDZK1IP1, PROK2, LAMP3, etc.) of ACS utilizing peripheral blood transcriptome sequencing and mRNA-lncRNA coexpression analysis [33]. Herein, we presented target gene prediction analysis on the basis of the above two mechanisms of action to predict the mRNA that lncRNA may modulate. Target gene prediction can be divided into cis-prediction and trans-prediction. For cis-prediction, we predicted the lncRNA-mRNA relationship pairs that had a certain relationship through the position alignment of lncRNA and mRNA. Meanwhile, for trans-prediction, possible lncRNA-mRNA relationship pairs were determined through sequence alignment. Overall, our analysis characterized the up- and downstream regulatory mechanisms of dysregulated lncRNAs.

Among lncRNA-mRNA relationship pairs, we focused on ENST00000538705.1 and ALOX15. After verification, circulating ENST00000538705.1 and ALOX15 were both upregulated in ACS patients. In HCAECs, we found that silencing ENST00000538705.1 remarkably decreased the expression ALOX15. Nevertheless, ALOX15 knockdown did not influence the ENST00000538705.1 expression in HCAECs. This indicated that ALOX15 might be a downstream target of ENST00000538705.1. The proliferation and migration of endothelial cells following MI are crucial for angiogenesis [34]. Previously, Liu et al. demonstrated that lncRNA ANRIL suppression enabled to promote cell proliferation and tubule formation and inhibit inflammatory activation and apoptosis of endothelial cells [35]. Du et al. reported that lncRNA HCG11 alleviated high glucose-induced vascular endothelial damage by increasing cell proliferation and tube formation [26]. Additionally, lncRNA TCONS_00024652 was identified to facilitate vascular endothelial cell proliferation and angiogenesis [36]. Herein, we found that silencing ENST00000538705.1 and ALOX15 markedly weakened the proliferation and migration of HCAECs, indicating that they might participate in ACS progression. Evidence has demonstrated that the effect of ALOX15 induces endothelial cell barrier dysfunction in high-fat-diet rats [37]. Hence, we speculated that the antisense lncRNA ENST00000538705.1 might enhance the stability of ALOX15 mRNA, thereby enhancing the proliferation and migration ability of HCAECs.

The therapeutic effects of si-ENST00000538705.1 and si-ALOX15 were also investigated in MI rat models. Our results demonstrated that silencing ENST00000538705.1 or ALOX15 remarkably relieved myocardial injury following MI. Previously, lncRNA SLC8A1-AS1 protected the myocardium from damage via weakening SLC8A1 and activating cGMP-PKG signaling in MI models [38]. Moreover, ATP2B1-AS1 knockdown protected against MI mice through blocking NF- κ B signaling [27]. Our study noted that ENST00000538705.1 or ALOX15 knockdown reduced serum TC and LDL levels as well as elevated serum HDL levels in MI rats. These results indicated that ENST00000538705.1 and ALOX15 might become potential targets for the treatment of MI.

The limitations of our study should be pointed out. First of all, the sample size used for microarray and RT-qPCR

analysis was relatively small. In our future studies, the sample size of each group will be increased for further verifying our findings. Furthermore, the molecular mechanisms underlying ENST00000538705.1 and ALOX15 in ACS progression remain to be fully elucidated, and in-depth studies are required.

5. Conclusion

In conclusion, we determined upregulated ENST00000538705.1 and ALOX15 in serum specimens of patients with ACS. Bioinformatics analysis identified the remarkable interaction between ENST00000538705.1 and ALOX15, and ENST00000538705.1 knockdown significantly inhibited ALOX15 expression in HCAECs. Silencing ENST00000538705.1 and ALOX15 both weakened the proliferation and migration of HCAECs. Additionally, their knockdown relieved myocardial damage of MI rats. Altogether, lncRNA ENST00000538705.1 and ALOX15 may become potential molecular targets for ACS therapy.

Abbreviations

ACS:	Acute coronary syndrome
AMI:	Acute myocardial infarction
MI:	Myocardial infarction
ncRNA:	Noncoding RNA
lncRNA:	Long ncRNA
RT-qPCR:	Real-time quantitative PCR
HCAECs:	Human coronary artery endothelial cells
FBS:	Fetal bovine serum
NC:	Negative control
CCK-8:	Cell counting kit-8
OD:	Optical density
HDL:	High-density lipoproteins
TC:	Total cholesterol
LDL:	Low-density lipoproteins
One-way ANOVA:	One-way analysis of variance.

Data Availability

The datasets analyzed during the current study are available from the corresponding authors on reasonable request.

Conflicts of Interest

The authors declare no conflicts of interest.

Acknowledgments

This work was funded by the Zhejiang Province Health Plan Project in 2021 (2021RC126).

References

- [1] J. P. Collet, H. Thiele, E. Barbato et al., “2020 ESC guidelines for the management of acute coronary syndromes in patients presenting without persistent ST-segment elevation,” *European Heart Journal*, vol. 42, no. 14, pp. 1289–1367, 2021.

- [2] V. P. Harjola, J. Parissis, J. Bauersachs et al., “Acute coronary syndromes and acute heart failure: a diagnostic dilemma and high-risk combination. A statement from the Acute Heart Failure Committee of the Heart Failure Association of the European Society of Cardiology,” *European Journal of Heart Failure*, vol. 22, no. 8, pp. 1298–1314, 2020.
- [3] D. C. Tong, S. Quinn, A. Nasis et al., “Colchicine in patients with acute coronary syndrome,” *Circulation*, vol. 142, no. 20, pp. 1890–1900, 2020.
- [4] A. H. McKnight, D. R. Katzenberger, and S. R. Britnell, “Colchicine in acute coronary syndrome: a systematic review,” *The Annals of Pharmacotherapy*, vol. 55, no. 2, pp. 187–197, 2021.
- [5] Y. Sun, X. Niu, G. Wang, X. Qiao, L. Chen, and M. Zhong, “A novel lncRNA ENST00000512916 facilitates cell proliferation, migration and cell cycle progression in ameloblastoma,” *Oncotargets and Therapy*, vol. Volume 13, pp. 1519–1531, 2020.
- [6] X. Qian, J. Zhao, P. Y. Yeung, Q. C. Zhang, and C. K. Kwok, “Revealing lncRNA structures and interactions by sequencing-based approaches,” *Trends in Biochemical Sciences*, vol. 44, no. 1, pp. 33–52, 2019.
- [7] X. Zhu, X. Niu, and C. Ge, “Inhibition of LINC00994 represses malignant behaviors of pancreatic cancer cells: interacting with miR-765-3p/RUNX2 axis,” *Cancer Biology & Therapy*, vol. 20, no. 6, pp. 799–811, 2019.
- [8] F. Kopp and J. T. Mendell, “Functional classification and experimental dissection of long noncoding RNAs,” *Cell*, vol. 172, no. 3, pp. 393–407, 2018.
- [9] Z. F. Liu, W. W. Hu, R. Li, Y. Gao, L. L. Yan, and N. Su, “Expression of lncRNA-ANRIL in patients with coronary heart disease before and after treatment and its short-term prognosis predictive value,” *European Review for Medical and Pharmacological Sciences*, vol. 24, no. 1, pp. 376–384, 2020.
- [10] J. Tan, S. Liu, Q. Jiang, T. Yu, and K. Huang, “LncRNA-MIAT increased in patients with coronary atherosclerotic heart disease,” *Cardiology Research and Practice*, vol. 2019, 6280195 pages, 2019.
- [11] W. Zhang, Y. Li, and P. Wang, “Long non-coding RNA-ROR aggravates myocardial ischemia/reperfusion injury,” *Brazilian Journal of Medical and Biological Research*, vol. 51, no. 6, p. e6555, 2018.
- [12] Y. Lu, X. Meng, L. Wang, and X. Wang, “Analysis of long non-coding RNA expression profiles identifies functional lncRNAs associated with the progression of acute coronary syndromes,” *Experimental and Therapeutic Medicine*, vol. 15, no. 2, pp. 1376–1384, 2018.
- [13] J. Yang, X. Huang, F. Hu, X. Fu, Z. Jiang, and K. Chen, “LncRNA ANRIL knockdown relieves myocardial cell apoptosis in acute myocardial infarction by regulating IL-33/ST2,” *Cell Cycle*, vol. 18, no. 23, pp. 3393–3403, 2019.
- [14] L. Chen, G. Wang, X. Qiao et al., “Downregulated miR-524-5p participates in the tumor microenvironment of ameloblastoma by targeting the interleukin-33 (IL-33)/suppression of tumorigenicity 2 (ST2) axis,” *Medical Science Monitor*, vol. 26, p. e921863, 2020.
- [15] D. J. Trembinski, D. I. Bink, K. Theodorou et al., “Aging-regulated anti-apoptotic long non-coding RNA *Sarrah* augments recovery from acute myocardial infarction,” *Nature Communications*, vol. 11, no. 1, p. 2039, 2020.
- [16] Y. Zhang, L. Jiao, L. Sun et al., “LncRNA ZFAS1 as a SERCA2a inhibitor to cause intracellular Ca²⁺ overload and contractile dysfunction in a mouse model of myocardial infarction,” *Circulation Research*, vol. 122, no. 10, pp. 1354–1368, 2018.
- [17] S. Liu, J. Hou, X. Gu, R. Weng, and Z. Zhong, “Characterization of lncRNA expression profile and identification of functional lncRNAs associated with unstable angina,” *Journal of Clinical Laboratory Analysis*, vol. 35, no. 11, p. e24036, 2021.
- [18] A. J. Saldanha, “Java TreeView—extensible visualization of microarray data,” *Bioinformatics*, vol. 20, no. 17, pp. 3246–3248, 2004.
- [19] M. Haeussler, A. S. Zweig, C. Tyner et al., “The UCSC genome browser database: 2019 update,” *Nucleic Acids Research*, vol. 47, no. D1, pp. D853–d858, 2019.
- [20] P. Shannon, A. Markiel, O. Ozier et al., “Cytoscape: a software environment for integrated models of biomolecular interaction networks,” *Genome Research*, vol. 13, no. 11, pp. 2498–2504, 2003.
- [21] X. Y. Cai, L. Lu, Y. N. Wang et al., “Association of increased S100B, S100A6 and S100P in serum levels with acute coronary syndrome and also with the severity of myocardial infarction in cardiac tissue of rat models with ischemia-reperfusion injury,” *Atherosclerosis*, vol. 217, no. 2, pp. 536–542, 2011.
- [22] Z. Li, J. Wu, W. Wei et al., “Association of serum miR-186-5p with the prognosis of acute coronary syndrome patients after percutaneous coronary intervention,” *Frontiers in Physiology*, vol. 10, p. 686, 2019.
- [23] S. Wu, H. Sun, and B. Sun, “MicroRNA-145 is involved in endothelial cell dysfunction and acts as a promising biomarker of acute coronary syndrome,” *European Journal of Medical Research*, vol. 25, no. 1, p. 2, 2020.
- [24] H. M. Xu, F. H. Sui, M. H. Sun, and G. L. Guo, “Retracted: downregulated microRNA-224 aggravates vulnerable atherosclerotic plaques and vascular remodeling in acute coronary syndrome through activation of the TGF- β /Smad pathway,” *Journal of Cellular Physiology*, vol. 234, no. 3, pp. 2537–2551, 2019.
- [25] S. H. A. Agwa, S. S. Elzahwy, M. S. El Meteini et al., “ABHD4-regulating RNA panel: novel biomarkers in acute coronary syndrome diagnosis,” *Cell*, vol. 10, no. 6, p. 1512, 2021.
- [26] J. Du, R. Han, Y. Li et al., “LncRNA HCG11/miR-26b-5p/QKI5 feedback loop reversed high glucose-induced proliferation and angiogenesis inhibition of HUVECs,” *Journal of Cellular and Molecular Medicine*, vol. 24, no. 24, pp. 14231–14246, 2020.
- [27] K. Y. Song, X. Z. Zhang, F. Li, and Q. R. Ji, “Silencing of ATP2B1-AS1 contributes to protection against myocardial infarction in mouse via blocking NFKBIA-mediated NF- κ B signalling pathway,” *Journal of Cellular and Molecular Medicine*, vol. 24, no. 8, pp. 4466–4479, 2020.
- [28] E. K. Robinson, S. Covarrubias, and S. Carpenter, “The how and why of lncRNA function: an innate immune perspective,” *Biochimica et Biophysica Acta (BBA)-Gene Regulatory Mechanisms*, vol. 1863, no. 4, p. 194419, 2020.
- [29] F. Ferrè, A. Colantoni, and M. Helmer-Citterich, “Revealing protein-lncRNA interaction,” *Briefings in Bioinformatics*, vol. 17, no. 1, pp. 106–116, 2016.
- [30] T. Ali and P. Grote, “Beyond the RNA-dependent function of lncRNA genes,” *eLife*, vol. 9, 2020.
- [31] Y. Wang and X. Sun, “The functions of lncRNA in the heart,” *Diabetes Research and Clinical Practice*, vol. 168, p. 108249, 2020.

- [32] Z. Yang, S. Jiang, J. Shang et al., “LncRNA: shedding light on mechanisms and opportunities in fibrosis and aging,” *Ageing Research Reviews*, vol. 52, pp. 17–31, 2019.
- [33] M. Shen, R. Gong, H. Li, Z. Yang, Y. Wang, and D. Li, “Identification of key molecular markers of acute coronary syndrome using peripheral blood transcriptome sequencing analysis and mRNA-lncRNA co-expression network construction,” *Bioengineered*, vol. 12, no. 2, pp. 12087–12106, 2021.
- [34] Q. Liao, S. Qu, L. X. Tang et al., “Irisin exerts a therapeutic effect against myocardial infarction via promoting angiogenesis,” *Acta Pharmacologica Sinica*, vol. 40, no. 10, pp. 1314–1321, 2019.
- [35] X. Liu, S. Li, Y. Yang et al., “The lncRNA ANRIL regulates endothelial dysfunction by targeting the let-7b/TGF- β R1 signalling pathway,” *Journal of Cellular Physiology*, vol. 236, no. 3, pp. 2058–2069, 2021.
- [36] M. Halimulati, B. Duman, J. Nijiati, and A. Aizezi, “Long non-coding RNA TCONS_00024652 regulates vascular endothelial cell proliferation and angiogenesis via microRNA-21,” *Experimental and Therapeutic Medicine*, vol. 16, no. 4, pp. 3309–3316, 2018.
- [37] N. K. Singh and G. N. Rao, “Emerging role of 12/15-lipoxygenase (ALOX15) in human pathologies,” *Progress in Lipid Research*, vol. 73, pp. 28–45, 2019.
- [38] G. L. Guo, L. Q. Sun, M. H. Sun, and H. M. Xu, “LncRNA SLC8A1-AS1 protects against myocardial damage through activation of cGMP-PKG signaling pathway by inhibiting SLC8A1 in mice models of myocardial infarction,” *Journal of Cellular Physiology*, vol. 234, no. 6, pp. 9019–9032, 2019.

Research Article

Knockdown of ILK Alleviates High Glucose-Induced Damage of H9C2 Cells through TLR4/MyD88/NF- κ B Pathway

Qiang Yin,^{1,2} Zhendong Li,³ and Shaoying Lu¹ 

¹Department of Vascular Surgery, The First Affiliated Hospital of Xi'an Jiaotong University, Xi'an, China

²Department of Cardiovascular Surgery, Second Affiliated Hospital, Xi'an Medical University, Xi'an, China

³Department of Vascular Surgery, Wuxi Mingci Cardiovascular Hospital, Wuxi, China

Correspondence should be addressed to Shaoying Lu; shaoying_lu@cnhospital.com.cn

Received 24 March 2022; Accepted 21 April 2022; Published 5 May 2022

Academic Editor: Francesco Busardò

Copyright © 2022 Qiang Yin et al. This is an open access article distributed under the Creative Commons Attribution License, which permits unrestricted use, distribution, and reproduction in any medium, provided the original work is properly cited.

The aim of this study was to explore the role of ILK in an in vitro model of diabetic cardiomyopathy. We used 30 mmol/L high glucose to treat H9C2 cells to construct an in vitro model, knocked down the ILK expression level of H9C2 cells by small interference technology, and detected the activity of antioxidant enzymes and inflammatory factors in the supernatant. The expression levels of SOD1 and IL-1 β were detected by immunofluorescence staining. The expression levels of the TLR4/MyD88/NF- κ B signaling pathway and its downstream factors were detected by quantitative reverse-transcription polymerase chain reaction (qRT-PCR). Compared with the control group, after high-glucose culture of H9C2 cells, the cell activity decreased, while the apoptosis rate increased, with the TLR4/MyD88/NF- κ B signaling pathway activated, thereby inducing oxidative stress and inflammation. Compared with the high-glucose group, the HG+si-ILK group increased cell activity, decreased the apoptosis rate, and inhibited the excessive activation of the TLR4/MyD88/NF- κ B signaling pathway, thereby improving oxidative stress and inflammation. Knockdown of ILK expression can protect H9C2 cells from reducing high glucose-induced inflammation, oxidative stress, and apoptosis by inhibiting the TLR4/MyD88/NF- κ B signaling pathway.

1. Introduction

With the changes in lifestyle and diet structure, the incidence of metabolic diseases, especially obesity and type 2 diabetes, has increased year by year globally. Diabetic cardiomyopathy (DCM) has become one of the most important diseases that threaten human health [1]. DCM was first proposed by Rubler in 1972 [2]. It refers to myocardial diseases that occur in diabetic patients and cannot be explained by hypertension, coronary heart disease, heart valve disease, and other heart diseases. The structural change is the main performance, which can eventually progress to heart failure (HF) [3]. Since then, research on DCM has been carried out one after another and has achieved certain results, but its pathogenesis has not yet been fully elucidated. Previous evidence showed that metabolic disorders, oxidative stress (OS), inflammatory response, and apoptosis all played crucial roles in the pathogenesis of DCM [4–6]. Diabetes is an independent risk factor for cardiovascular disease (CVD).

Patients with CVD and diabetes have worse short-term or long-term prognosis than those without diabetes. Therefore, exploring the pathogenesis of DCM is particularly important.

Integrin-linked kinase (ILK) is a serine-threonine protein kinase in the lysates of animal epithelial cells and tumor cells. As a crucial linker protein and signaling protein, integrin and growth factor receptors play a key role in mediating the interaction between cells and extracellular matrix and signal transmission inside and outside cells [7]. ILK is most abundantly distributed in the heart. Studies have found that ILK may play a role as a regulator in the cardiac hypertrophy signal transduction pathway [8]. ILK has a nonnegligible effect on the occurrence and development of cardiomyopathy. Therefore, we speculate that ILK might play a crucial role in regulating high glucose-induced cardiomyocyte apoptosis, OS, and inflammatory response.

Toll-like receptors (TLRs) are a family of receptors that mediate innate immunity. As a key transmembrane protein

that triggers inflammation, it is involved in the regulation of immune inflammation and is considered to be the main body that mediates immune and inflammation [9]. Studies have shown that TLRs not only recognize the exogenous ligand lipopolysaccharide but also the endogenous ligand expressed during diabetes injury and play a major role in the occurrence and development of diabetes and its complications [10]. TLR4 is the first TLRs found in mammals. After TLR4 on the surface of myocardial cell membrane is stimulated by the corresponding ligand, it can activate the immune inflammation of myocardial tissue [11]. TLR4 can activate MAPK and NF- κ B signaling pathways through myeloid differentiation factor 88- (MyD88-) dependent pathway cascade reactions, thus promoting the expression of related genes and initiating natural immunity [12]. NF- κ B is a crucial nuclear transcription factor, located in the pivotal position of the signaling pathway downstream of TLRs. It can complete the transmission of inflammation signals by regulating the cascade of immune and inflammation-related factors and inflammatory transmitters [13]. Therefore, the TLR4-MyD88-NF- κ B signaling pathway plays a crucial pivotal role in the regulation of immune and inflammatory responses. At present, the mechanism of TLR4-MyD88-NF- κ B signaling pathway mediating inflammatory response in diabetic nephropathy and vascular disease is relatively clear, and the specific mechanism of its regulation and control of DCM remains to be further studied.

2. Materials and Method

2.1. Cell Culture. H9C2 cells were purchased from Shanghai Institute of Life Sciences, Chinese Academy of Sciences (Cell Culture Center, Shanghai, China), and 3 to 8 passage cells were selected for experiment. H9C2 cells were cultured in Dulbecco's Modified Eagle's Medium (DMEM; Life Technology, Wuhan, China) containing 10% fetal bovine serum (FBS; Life Technology, Wuhan, China) in a 37°C normoxic cell incubator, and the fluid was changed every other day.

2.2. Cell Transfection and Treatment. H9C2 cells at log phase were planted in 6-well plates. Transfection should be performed after the cells adhere to the wall, and the confluence of the cells should be 30%-50% during transfection. Then, we transfected H9C2 cells with si-ILK and si-NC according to the instructions of Lipofectamine²⁰⁰⁰ Transfection Reagent (Thermo Fisher Scientific, Waltham, MA, USA) and observed the cell status under an optical microscope (Becton Dickinson, Heidelberg, Germany). And 24 hours after transfection, the cell culture medium was changed.

2.3. Western Blot (WB). H9C2 cells were cultured in 6-well plates and were divided into different groups as mentioned above. When the cell fusion degree is about 80%, 50 μ L of lysate (Beyotime, Nanjing, China) was used to lyse the cultured H9C2 cells. Protein concentration detection kit (Beyotime, Nanjing, China) was used to detect the concentration of the extracted protein. After boiling the protein sample, 40 μ g protein sample was added into each well for the electrophoresis at a voltage of 90 V. Then, the protein was trans-

ferred to the membrane at a constant current of 250 mA for 2 hours. Then, the polyvinylidene difluoride (PVDF, Thermo Fisher Scientific, Waltham, MA, USA) membranes were blocked with 5% skimmed milk powder, followed by being incubated with the primary antibodies (IL-1 β , Abcam, 1:1000, Cambridge, MA, USA) overnight at 4°C. After washing with phosphate-buffered saline (PBS) buffer, the secondary antibody labeled with horseradish peroxidase was added to the membranes for incubation at room temperature. After incubation for 1 hour, the membranes reacted with electrochemiluminescence (ECL, Yifei Xue Biotechnology, Nanjing, China) and were exposed in the dark room.

2.4. RNA Isolation and Quantitative Reverse-Transcription Polymerase Chain Reaction (qRT-PCR). Prechilled PBS was used to wash H9C2 cells, and then, TRIzol reagent (Thermo Fisher Scientific, Waltham, MA, USA) was used to extract total cellular RNA. The reverse transcription kit (Thermo Fisher Scientific, Waltham, MA, USA) was used to transcribe RNA into cDNA. RT-PCR was performed according to a previous report [12]. Primers used are shown in Table 1.

2.5. MTT Assay. Trypsin (Kaiji, Nanjing, China) was used to digest H9C2 cells, and then, cells were formulated into a cell suspension with a concentration of 1×10^5 /mL. Then, the cells were inoculated into 96-well plates at 1×10^4 cells/well with the total amount of medium 100 μ L per well. Then, the cells were incubated in a 37°C, 5% CO₂ incubator. Next, different stimulations were given to each experimental group. After incubating for 0, 4, 8, 12, 16, 20, and 24 hours, 20 μ L of MTT solution (Construction, Nanjing, China) was added to each well. After 4 hours, the culture was terminated and 150 μ L of dimethyl sulfoxide (Construction, Nanjing, China) was added to each well after discarding the supernatant. Finally, a microplate reader was used to measure OD570 value, and the cell survival rate was calculated according to the formula.

2.6. Tunel Staining. When the cells were nearly 80% confluent, 4% paraformaldehyde (Construction, Nanjing, China) was used for the fixation. Then, PBS was used to wash the cells to remove excess paraformaldehyde. Each group of cells was stained according to the instructions of the Tunel kit (Kaiji, Nanjing, China). 4',6-Diamidino-2-phenylindole (DAPI, Construction, Nanjing, China) was used to stain the nucleus; the positive cells were observed under a fluorescent microscope (Becton Dickinson, Heidelberg, Germany).

2.7. Enzyme-Linked Immunosorbent Assay (ELISA). After collecting the cell supernatant of each group, ELISA was performed according to the instructions of the kit (Elabscience, Wuhan, China). 100 μ L of biotinylated antibody was added to each well for incubation at 37°C. After 1 hour, 100 μ L of enzyme-binding working solution was added to each well. After the incubation was completed, the color developing agent and the terminating agent were added, and then, the OD450 value was measured with a microplate reader (Becton Dickinson, Heidelberg, Germany).

TABLE 1: Primer sequences of quantitative reverse transcription-polymerase chain reaction.

Oligo name		Sequence (5' → 3')
GPX1 (rat)	Forward	ATCATATGTGTGCTGCTCGGCTAGC
	Reverse	TACTCGAGGGCACAGCTGGGCCCTTGAG
GPX4 (rat)	Forward	GGACCTGCCGTGCTATCT
	Reverse	GGCCTCTGGACCTTCCTC
ILK (rat)	Forward	ATGGCTTCTCCCCTTTG
	Reverse	GTATCATCCCCACGATTCA
IL-1 β (rat)	Forward	GCAACTGTTTCTGAACTCAACT
	Reverse	ATCTTTTGGGGTCCGTCAACT
IL-8 (rat)	Forward	CAAGGCTGGTCCATGCTCC
	Reverse	TGCTATCACTTCCTTTCTGTTGC
MPO (rat)	Forward	CTGGCACGGAAGCTGAT
	Reverse	AATGAGGCAGGCAAGGAG
TLR4 (rat)	Forward	GACTCCATTCAAGCCCAA
	Reverse	TCTCCCAAGATCAACCGA
MyD88 (rat)	Forward	TGAGCAACCAGGACAGC
	Reverse	TAGGCATGTCAGGGGAGA
NF- κ B (rat)	Forward	ACTGCCGGGATGGCTACTAT
	Reverse	TCTGGATTTCGCTGGCTAATGG
GAPDH (rat)	Forward	CAACTCCCTCAAGATTGTCAGCAA
	Reverse	GGCATGGACTGTGGTCATGA

2.8. *Determination of Malondialdehyde (MDA) Levels, Superoxide Dismutase (SOD), Catalase (CAT), and Glutathione Peroxidase (GSH-Px) Activity in Cell Supernatants.* According to the instructions of the above kits (Construction, Nanjing, China), the cell culture supernatant or cell lysate of each group was collected after 24 hours of culture. Then, we used a microplate reader to detect the absorbance of each sample at different wavelengths and calculated according to the corresponding formula.

2.9. *Immunofluorescence Staining.* When the cells were nearly 80% confluent, 4% paraformaldehyde was used to fix the cells, then PBS was used to wash the cells to remove excess paraformaldehyde, and then, 50 ml/L goat serum was used to block for 30 minutes. After decanting excess serum, the primary antibodies SOD1 (Abcam, Cambridge, MA, USA, Rabbit, 1:1000) and IL-1 β (Abcam, Cambridge, MA, USA, Rabbit, 1:1000) were used for incubation at 4°C overnight. After washing with PBS, the secondary antibody was added dropwise and incubated at room temperature in the dark for 60 min. DAPI was used to stain the nuclei for 10 minutes. Finally, the results were observed and recorded under a fluorescent microscope.

2.10. *Statistical Analysis.* Statistical Product and Service Solutions (SPSS) 21.0 (SPSS IBM, Armonk, NY USA) statistical software was used to analyze the experimental data. Measurement data were expressed as $\bar{x} \pm s$. The *t*-test was used for comparisons between the two groups. Comparison between multiple groups was done using one-way analysis of variance (ANOVA) test followed by a post hoc test (Least

Significant Difference). The Least Significant Difference (LSD) test or Student-Newman-Keuls (SNK) test was used for pairwise comparison under the condition of homogeneity of variance. Test level $\alpha = 0.05$. All experiments were repeated 3 times.

3. Results

3.1. *High Glucose Damages H9C2 Cells.* According to reports in the literature, we selected 30mmol/L high glucose to treat H9C2 cells and tested the cell activity of each group by MTT test (Figure 1(a)). The results confirmed that high glucose can reduce the activity of H9C2 cells, and as the culture time was delayed, the lower the activity. Subsequently, we used the kit to detect the antioxidant enzyme activity in the cell supernatant of each group (Figures 1(b)–1(d)). It was found that the activities of SOD, CAT, and GSH-Px in the high-glucose group were dramatically reduced. At the same time, the MDA content also increased dramatically (Figure 1(e)). In addition, we detected the content of inflammatory factors in the supernatant of each group by ELISA method (Figures 1(f)–1(h)). The results showed that the levels of MPO, IL-1 β , and IL-8 in the high-glucose group increased dramatically. In addition, Tunel staining also found that the apoptosis rate in the high-glucose group was dramatically increased (Figure 1(i)). In summary, we verified that high glucose can induce H9C2 cells to produce OS and inflammatory responses, thereby promoting apoptosis. And RT-PCR results showed that ILK mRNA in the high-glucose group was dramatically higher than that in the control group (Figure 1(j)). Given this, we speculated that ILK

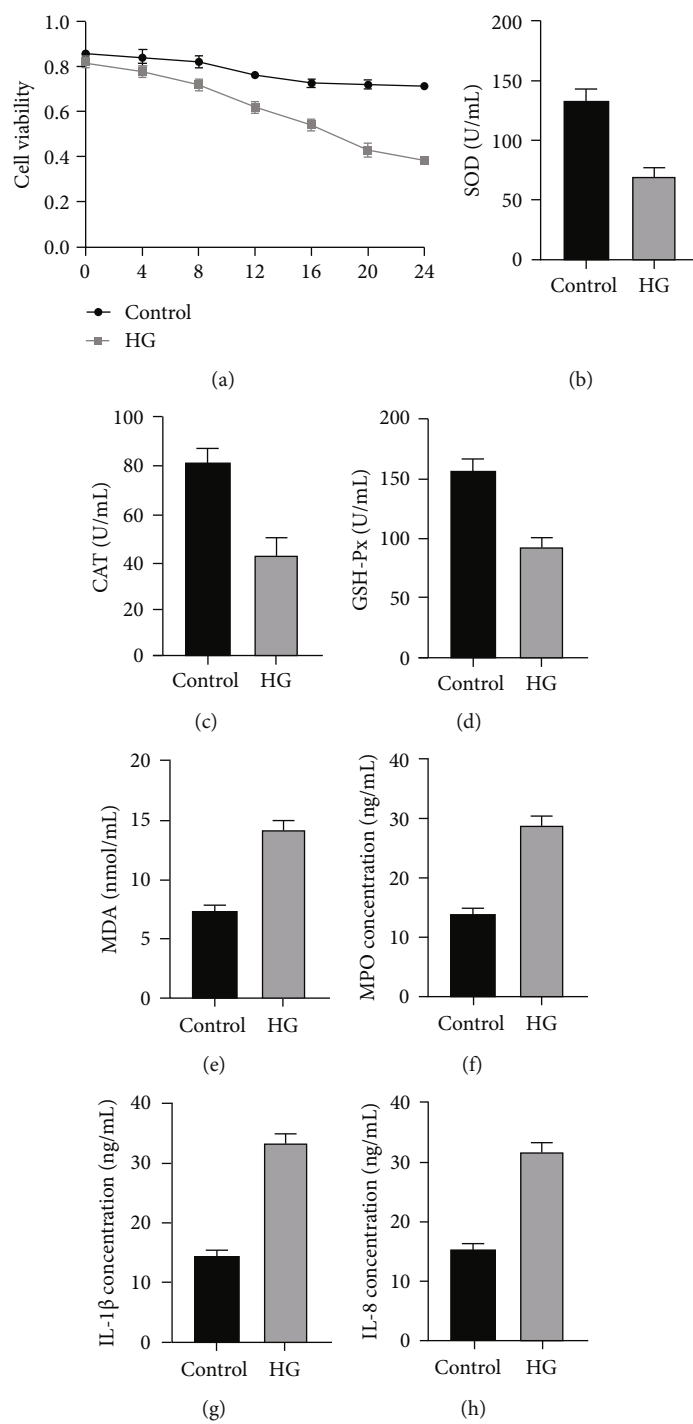


FIGURE 1: Continued.

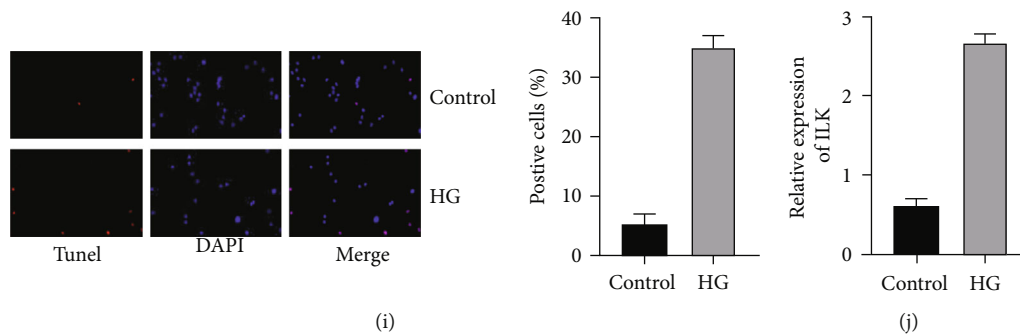


FIGURE 1: High glucose damages H9C2 cells. (a) The cell activity of H9C2 was determined by MTT assay. (b–e) The levels of SOD, CAT, GSH-Px, and MDA in the supernatant were determined by the kits. (f–h) The levels of MPO, IL-1 β , and IL-8 in the supernatant were determined by the ELISA. (i) TUNEL staining was performed to examine the apoptosis level of H9C2. (j) mRNA expression results of ILK were determined by real-time PCR. (* indicates statistical difference from the control group $P < 0.05$).

was involved in the process of high-glucose damage to H9C2 cells.

3.2. Knockdown of ILK Improves H9C2 Oxidative Stress Induced by High Glucose. Next, we used small interference technology to knock down the ILK expression level of H9C2 cells and verified our transfection efficiency by RT-PCR (Figure 2(a)). First, we detected the expression level of SOD1 in 4 groups by immunofluorescence staining and found that the expression of SOD1 in the high-glucose group was lower than that in the control group, and after knocking down the expression of ILK, the expression level of SOD1 increased dramatically (Figure 2(b)). There was no significant difference in the HG+si-NC group. Next, we detected SOD, CAT, and GSH-Px activity and MDA content in the supernatant (Figures 2(c)–2(f)). The results showed that the activities of SOD, CAT, and GSH-Px in the HG+si-ILK group were dramatically increased. At the same time, the MDA content was dramatically reduced. In addition, RT-PCR detection of GPX1 and GPX4 mRNA expression also found that the high-glucose group GPX1 and GPX4 mRNA expression levels were dramatically reduced, while in the HG+si-ILK group, GPX1 and GPX4 mRNA expression levels were increased (Figures 2(g) and 2(h)). There was no significant difference in the HG+si-NC group.

3.3. Knocking Down ILK Can Improve H9C2 Inflammatory Response Induced by High Glucose. The expression level of IL- α in the 4 groups was detected by immunofluorescence staining (Figure 3(a)). It was found that the expression of IL- α in the high-glucose group was higher than that in the control group, but after knocking down the expression of ILK, the expression level of IL- α was dramatically reduced. There was no significant difference in the HG+si-NC group. Next, WB results also found that the expression of IL-1 β protein in the high-glucose group was dramatically higher than that in the control group, while the expression of IL-1 β protein in the HG+si-ILK group was dramatically reduced, and there was no significant difference in the results of the HG+si-NC group (Figure 3(b)). Subsequently, the content of MPO, IL-1 β , and IL-8 in the supernatant was detected by the ELISA method (Figures 3(c)–3(e)). The content of the above inflammatory factors in the HG+si-ILK

group was dramatically reduced, and there was no significant difference in the results of the HG+si-NC group. At the same time, RT-PCR also obtained similar results to the former (Figures 3(f)–3(h)).

3.4. Knockdown of ILK Can Inhibit High Glucose-Induced H9C2 Apoptosis and Inhibit TLR4/MyD88/NF- κ B Pathway Activation. First, we tested the cell viability of the 4 groups by MTT method (Figure 4(a)). The results found that when we knocked down ILK expression, the activity of H9C2 cells was higher than that of the HG group. Compared with the HG group, there was no significant difference in the results of the HG+si-NC group. And TUNEL staining also found that in the HG+si-ILK group, the apoptosis rate induced by high glucose was also dramatically reduced, and there was no significant difference in the results of the HG+si-NC group (Figure 4(b)). Next, we detected TLR4, MyD88, and NF- κ B mRNA levels by RT-PCR (Figures 4(c)–4(e)). The results showed that after H9C2 cells were cultured in high glucose, TLR4, MyD88, and NF- κ B mRNA were dramatically increased, while in the HG+si-ILK group, TLR4, MyD88, and NF- κ B mRNA were dramatically inhibited. Compared with the HG group, there was no significant difference in the results of the HG+si-NC group. The above results indicated that knocking down ILK expression can dramatically inhibit high glucose-induced overactivation of the TLR4-MyD88-NF- κ B signaling pathway in H9C2 cells and inhibit H9C2 cell apoptosis.

4. Discussion

Diabetes is one of the important chronic noninfectious diseases that seriously threaten human health in today's society, and it shows a significant growth trend worldwide. DCM is an independent diabetic cardiovascular complication. It is a special form of heart disease. Its early stage is mainly diastolic dysfunction. With the extension of time, the contractile function is damaged, and the myocardium is extensively necrotic. Decreased blood fraction can eventually lead to cardiogenic shock, HF, and even death [14]. DCM is mainly due to a series of pathological changes such as inflammatory response of myocardial cells caused by diabetic metabolic dysfunction, redox imbalance, myocardial

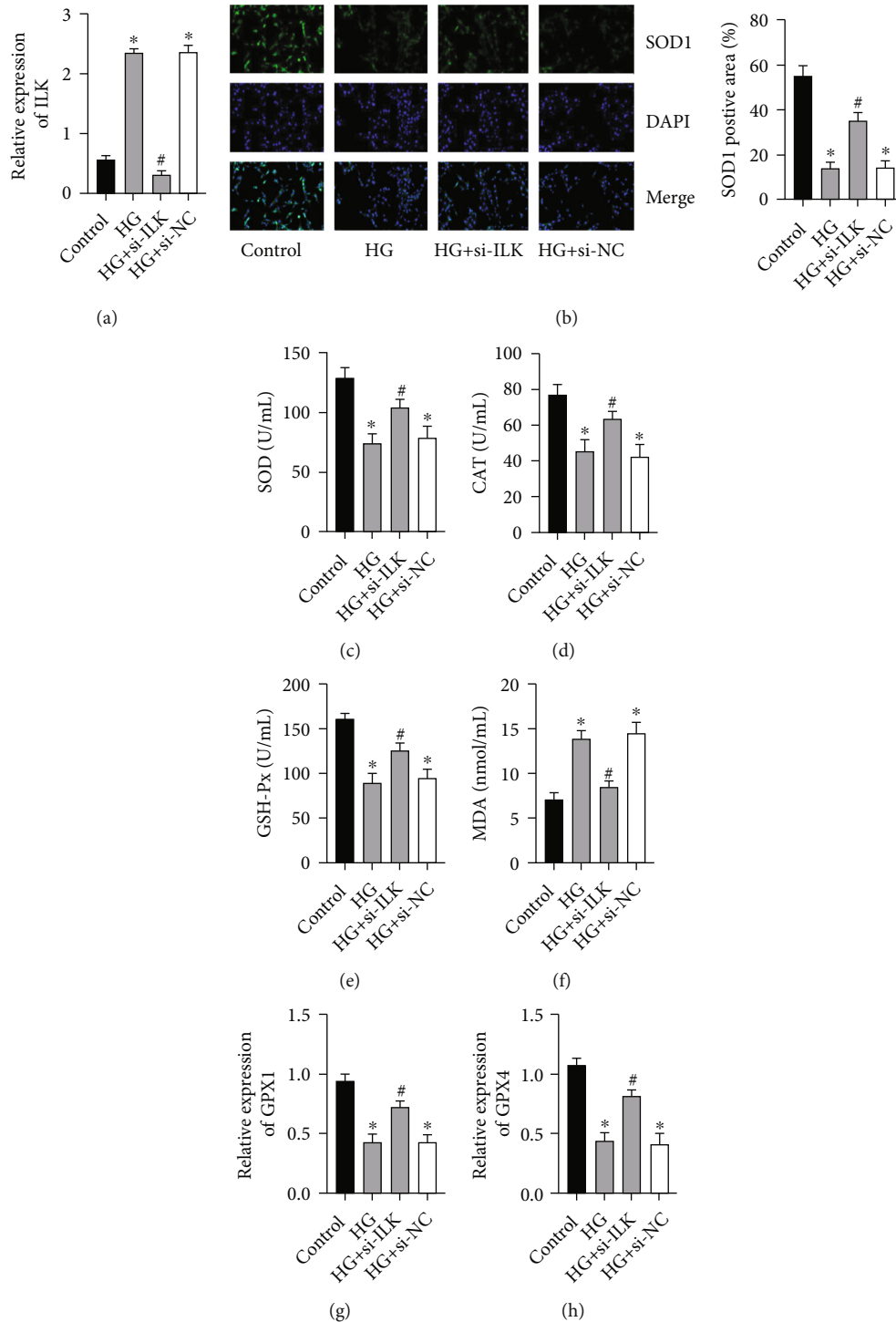


FIGURE 2: Knockdown of ILK improves H9C2 oxidative stress induced by high glucose. (a) mRNA expression results of ILK were determined by real-time PCR. (b) Immunofluorescence was performed to examine the expression of SOD1. (c–f) The levels of SOD, CAT, GSH-Px, and MDA in the supernatant were determined by the kits. (g, h) mRNA expression results of GPX1 and GPX4 were determined by real-time PCR. (“*” indicates statistical difference from the control group $P < 0.05$, and “#” indicates statistical difference from the HG group $P < 0.05$).

cell necrosis, interstitial fibrosis, and myocardial cell hypertrophy [15]. Therefore, we constructed a DCM model in vitro to explore its pathogenesis.

First, we verified the success of the construction of an in vitro model of DCM by measuring cell activity, antioxi-

dant enzyme activity, inflammatory factor expression levels, and apoptosis rates, and our results are consistent with previous studies [16]. Then, we found that in the high-glucose group, ILK expression was dramatically increased. Therefore, we speculate that ILK is involved in regulating the

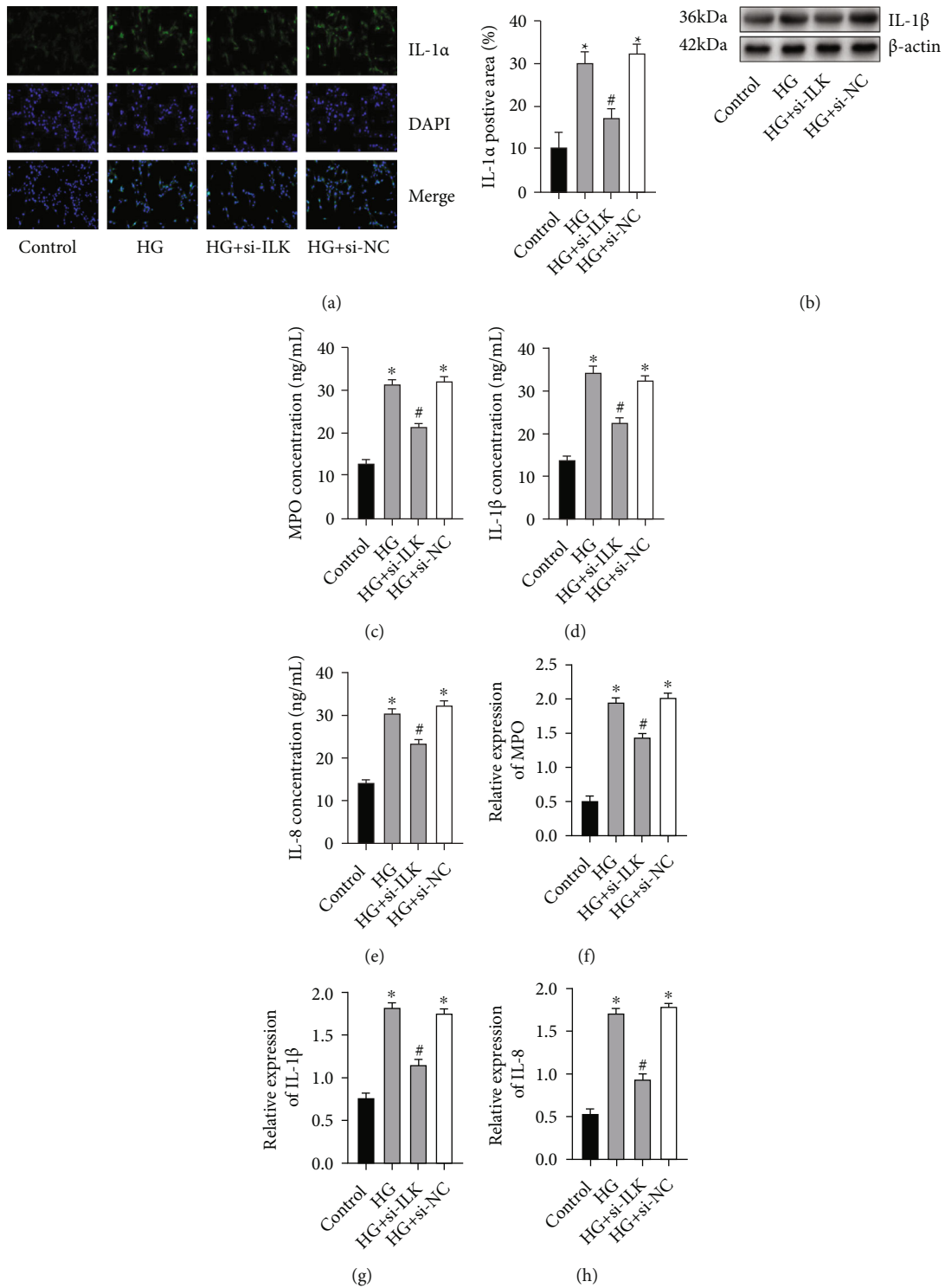


FIGURE 3: Knocking down ILK can improve H9C2 inflammatory response induced by high glucose. (a) Immunofluorescence was performed to examine the expression of IL- α . (b) Protein expression results of IL-1 β were determined by Western blotting. β -Actin was used as an internal control. (c–e) The levels of MPO, IL-1 β , and IL-8 in the supernatant were determined by the ELISA. (f–h) mRNA expression results of MPO, IL-1 β , and IL-8 were determined by real-time PCR. (“*” indicates statistical difference from the control group $P < 0.05$, and “#” indicates statistical difference from the HG group $P < 0.05$).

occurrence and development of DCM. ILK, as a key regulator of cellular response integrins and growth factor-mediated signals, is involved in the formation of cytoskeleton, cell proliferation, apoptosis, and maintenance of oxygen

balance, as well as the regulation of inflammatory factors [17–19]. From this, we speculate that ILK plays a crucial role in regulating high glucose-induced H9C2 cell OS, inflammation, and apoptosis. Immediately afterwards, we first

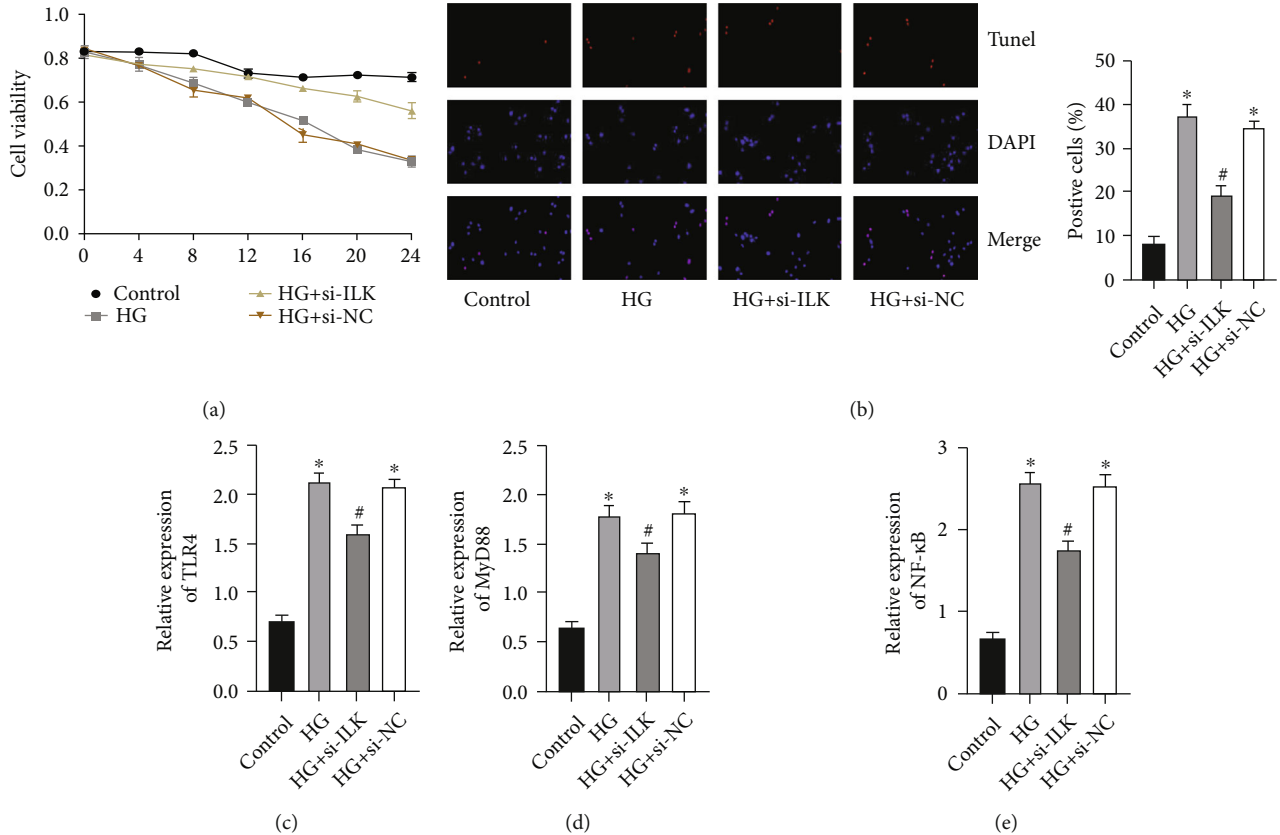


FIGURE 4: Knockdown of ILK can inhibit high glucose-induced H9C2 apoptosis and inhibit TLR4/MyD88/NF- κ B pathway activation. (a) The cell activity of H9C2 was determined by MTT assay. (b) TUNEL staining was performed to examine the apoptosis level of H9C2. (c-e) mRNA expression results of TLR4, MyD88, and NF- κ B were determined by real-time PCR. (“*” indicates statistical difference from the control group $P < 0.05$, and “#” indicates statistical difference from the HG group $P < 0.05$).

knocked down ILK expression levels through small interference techniques. By detecting the activity of antioxidant enzymes in the cell supernatant, we found that when we knocked down the expression of ILK, the activities of SOD, CAT, and GSH-Px increased dramatically, and the MDA content also decreased. MDA is one of the most important products of membrane lipid peroxidation, and its content can affect the mitochondrial respiratory chain complex and key enzyme activity in the mitochondria [20]. Therefore, we can understand the degree of OS damage in cells by detecting MDA content. In addition, high glucose reduced the expression levels of SOD1, GPX1, and GPX4. After ILK knockdown, the expression levels of SOD1, GPX1, and GPX4 increased dramatically. Based on the above results, we confirmed that knocking down ILK expression can improve high glucose-induced redox imbalance.

Inflammatory response plays a crucial regulatory role in the pathogenesis of DCM. At the same time, inflammation is a crucial part of the immune system, triggered by any stimulus that threatens tissue homeostasis. TLRs, as key transmembrane proteins that trigger inflammatory responses, participate in the regulation of immune inflammatory responses and are considered to be the main body mediating immune and inflammatory responses. After binding to specific ligands, TLRs activate the NF- κ B signaling pathway through the MyD88-dependent pathway, promote the

expression of related genes, and induce inflammatory response. Therefore, the effective intervention of inflammation in the early stage of diabetes can inhibit the expression of inflammatory factors in the blood circulation and local heart and reduce the infiltration of immune active cells into the heart muscle, thereby reducing the heart inflammation and improving cardiac dysfunction [21, 22]. Our results found that high glucose can activate the TLR4/MyD88/NF- κ B signaling pathway, thereby upregulating the expression of downstream inflammatory factors. When we knocked down ILK expression, the TLR4/MyD88/NF- κ B signaling pathway was suppressed, the downstream inflammatory factor expression level was also suppressed, and the apoptosis of H9C2 cells was also decreased. Thus, we confirmed that knocking down ILK expression can inhibit high glucose-induced TLR4/MyD88/NF- κ B signaling pathway overactivation, thereby inhibiting downstream inflammatory factor expression, and increase the H9C2 activity.

5. Conclusion

Taken above, knocking down ILK expression can improve OS and inflammation through the TLR4/MyD88/NF- κ B signaling pathway, thereby reducing the apoptosis rate of H9C2 cells. These findings may provide a new target for the treatment of DCM.

Data Availability

The datasets used and analyzed during the current study are available from the corresponding author on reasonable request.

Conflicts of Interest

The authors declare that they have no competing interests.

Authors' Contributions




Qiang Yin and Zhendong Li contributed equally to this work. QY and SL designed the study. QY and ZL conducted the experiments and analyzed the data. QY and SL prepared the manuscript. All authors approved the final version of this manuscript.

References

- [1] W. D. Strain and P. M. Paldanius, "Diabetes, cardiovascular disease and the microcirculation," *Cardiovascular Diabetology*, vol. 17, no. 1, pp. 1–10, 2018.
- [2] W. H. Dillmann, "Diabetic cardiomyopathy," *Circulation Research*, vol. 124, no. 8, pp. 1160–1162, 2019.
- [3] H. C. Kenny and E. D. Abel, "Heart failure in type 2 diabetes mellitus," *Circulation Research*, vol. 124, no. 1, pp. 121–141, 2019.
- [4] F. Giacco and M. Brownlee, "Oxidative stress and diabetic complications," *Circulation Research*, vol. 107, no. 9, pp. 1058–1070, 2010.
- [5] X. Palomer, L. Salvado, E. Barroso, and M. Vazquez-Carrera, "An overview of the crosstalk between inflammatory processes and metabolic dysregulation during diabetic cardiomyopathy," *International Journal of Cardiology*, vol. 168, no. 4, pp. 3160–3172, 2013.
- [6] X. Dong, S. Yu, Y. Wang et al., "(Pro)renin receptor-mediated myocardial injury, apoptosis, and inflammatory response in rats with diabetic cardiomyopathy," *The Journal of Biological Chemistry*, vol. 294, no. 20, pp. 8218–8226, 2019.
- [7] G. E. Hannigan, J. G. Coles, and S. Dedhar, "Integrin-linked kinase at the heart of cardiac contractility, repair, and disease," *Circulation Research*, vol. 100, no. 10, pp. 1408–1414, 2007.
- [8] S. I. Bettink, C. Werner, C. H. Chen et al., "Integrin-linked kinase is a central mediator in angiotensin II type 1- and chemokine receptor CXCR4 signaling in myocardial hypertrophy," *Biochemical and Biophysical Research Communications*, vol. 397, no. 2, pp. 208–213, 2010.
- [9] M. O. Ullah, M. J. Sweet, A. Mansell, S. Kellie, and B. Kobe, "TRIF-dependent TLR signaling, its functions in host defense and inflammation, and its potential as a therapeutic target," *Journal of Leukocyte Biology*, vol. 100, no. 1, pp. 27–45, 2016.
- [10] S. Gupta, A. Maratha, J. Siednienko et al., "Analysis of inflammatory cytokine and TLR expression levels in type 2 diabetes with complications," *Scientific Reports*, vol. 7, no. 1, p. 7633, 2017.
- [11] Y. Y. Meng, Y. Liu, Z. F. Hu et al., "Sanguinarine attenuates lipopolysaccharide-induced inflammation and apoptosis by inhibiting the TLR4/NF- κ B pathway in H9c2 cardiomyocytes," *Curr Med Sci*, vol. 38, no. 2, pp. 204–211, 2018.
- [12] L. Shang, T. Wang, D. Tong, W. Kang, Q. Liang, and S. Ge, "Prolyl hydroxylases positively regulated LPS-induced inflammation in human gingival fibroblasts via TLR4/MyD88-mediated AKT/NF- κ B and MAPK pathways," *Cell Proliferation*, vol. 51, no. 6, article e12516, 2018.
- [13] T. Liu, M. Zhang, H. Niu et al., "Astragalus polysaccharide from Astragalus Melittin ameliorates inflammation via suppressing the activation of TLR-4/NF- κ B p65 signal pathway and protects mice from CVB3-induced virus myocarditis," *International Journal of Biological Macromolecules*, vol. 126, pp. 179–186, 2019.
- [14] E. T. Kato, M. G. Silverman, O. Mosenzon et al., "Effect of dapagliflozin on heart failure and mortality in type 2 diabetes mellitus," *Circulation*, vol. 139, no. 22, pp. 2528–2536, 2019.
- [15] S. J. Nikolajevic, M. Janic, and M. Sabovic, "Molecular mechanisms responsible for diastolic dysfunction in diabetes mellitus patients," *International Journal of Molecular Sciences*, vol. 20, no. 5, article 1197, 2019.
- [16] L. Li, W. Luo, Y. Qian et al., "Luteolin protects against diabetic cardiomyopathy by inhibiting NF- κ B-mediated inflammation and activating the Nrf2-mediated antioxidant responses," *Phytomedicine*, vol. 59, article 152774, 2019.
- [17] Y. Qu, C. Hao, J. Xu, Z. Cheng, W. Wang, and H. Liu, "ILK promotes cell proliferation in breast cancer cells by activating the PI3K/Akt pathway," *Molecular Medicine Reports*, vol. 16, no. 4, pp. 5036–5042, 2017.
- [18] B. Zeng, L. Liu, S. Wang, and Z. Dai, "ILK regulates MSCs survival and angiogenesis partially through AKT and mTOR signaling pathways," *Acta Histochemica*, vol. 119, no. 4, pp. 400–406, 2017.
- [19] P. Reventun, M. Alique, I. Cuadrado et al., "iNOS-derived nitric oxide induces integrin-linked kinase endocytic lysosome-mediated degradation in the vascular endothelium," *Arteriosclerosis, Thrombosis, and Vascular Biology*, vol. 37, no. 7, pp. 1272–1281, 2017.
- [20] N. Chen, Z. Zhou, J. Li et al., "3-n-Butylphthalide exerts neuroprotective effects by enhancing anti-oxidation and attenuating mitochondrial dysfunction in an in vitro model of ischemic stroke," *Drug Design, Development and Therapy*, vol. 12, pp. 4261–4271, 2018.
- [21] M. A. de Laat, K. J. Gruntmeir, C. C. Pollitt, C. M. McGowan, M. N. Sillence, and V. A. Lacombe, "Hyperinsulinemia downregulates TLR4 expression in the mammalian heart," *Frontiers Endocrinology*, vol. 5, article 120, 2014.
- [22] Y. Zhang, S. Liu, X. Li, and J. Ye, "Protective effect of fasudil on hydrogen peroxide-induced oxidative stress injury of H9C2 cardiomyocytes," *Disease Markers*, vol. 2021, Article ID 8177705, 9 pages, 2021.

Research Article

Association between Cystatin C and Cardiac Function in Acute Myocardial Infarction Patients: A Real-World Analysis

Bowen Lou ^{1,2} **Yongbai Luo**,^{1,2} **Haoxuan Zhang**,^{3,4} **Haoyu Wu**,^{1,2} **Guliniger Tuerhong Jiang**,^{1,2} **Hui Liu**,⁵ **Kejia Kan**,⁶ **Xiang Hao**,^{1,2} **Lizhe Sun**,^{1,2} **Zuyi Yuan** ^{1,2} and **Jianqing She** ^{1,2}

¹Cardiovascular Department, First Affiliated Hospital of Xi'an Jiaotong University, 277 West Yanta Road, Xi'an 710061, China

²Key Laboratory of Environment and Genes Related to Diseases, Ministry of Education, Xi'an 710061, China

³Southwest Jiaotong University, Chengdu, 611756 Sichuan, China

⁴Biological Science, Georgia State University, GA 30303, USA

⁵Biobank, First Affiliated Hospital of Xi'an Jiaotong University, Xi'an, 710061 Shaanxi, China

⁶Department of Surgery, Universitätsmedizin Mannheim, Medical Faculty Mannheim, Heidelberg University, 68167 Mannheim, Germany

Correspondence should be addressed to Zuyi Yuan; zuyiyuan@mail.xjtu.edu.cn and Jianqing She; jianqingshe@xjtu.edu.cn

Received 15 December 2021; Revised 14 March 2022; Accepted 17 March 2022; Published 23 April 2022

Academic Editor: Francesco Busard?

Copyright © 2022 Bowen Lou et al. This is an open access article distributed under the Creative Commons Attribution License, which permits unrestricted use, distribution, and reproduction in any medium, provided the original work is properly cited.

Background. Acute myocardial infarction (AMI), as well as its long-term and short-term complications, is known to present with high morbidity and mortality. Cardiac function deterioration and ventricular remodelling after AMI are known to be correlated to worse long-term outcomes. However, the underlying mechanism remains elusive and there is a shortage of serum prediction markers. This study investigates the relationship between in-hospital Cystatin C (CysC) and cardiac function and subsequent prognosis among AMI patients. **Research Design and Methods.** We measured admission CysC and cardiac function parameters, including ejection fraction (EF) and pro-BNP value in 5956 patients diagnosed with AMI. Simple and multiregression analyses were performed to investigate the correlation between CysC and cardiac function in AMI patients. Major adverse cardiovascular events (MACE), cardiovascular, and all-cause mortality were documented, and 351 participants with high cystatin (≥ 1.09 mg/L) and 714 low cystatin (< 1.09 mg/L) were investigated for survival analysis during a 48-month follow-up. **Results.** 5956 patients with AMI were enrolled in the initial observational analysis, and 1065 patients of the whole cohort were included in the follow-up survival analysis. The admission CysC level was found to be significantly positively correlated to the pro-BNP level (R square = 0.2142, 95% CI 4758 to 5265, $p < 0.0001$) and negatively correlated to the EF value (R square = 0.0095, 95% CI -3.503 to -1.605, $p < 0.0001$). Kaplan-Meier survival analysis revealed significantly increased MACE incidence (HR = 2.293, 95% CI 1.400 to 3.755, $p < 0.0001$), cardiovascular mortality (HR = 3.016, 95% CI 1.694 to 5.371, $p = 0.0002$), and all-cause mortality (HR = 3.424, 95% CI 2.010 to 5.835, $p < 0.0001$) in high-admission CysC cohort with AMI at the end of 4-year follow-up. **Conclusions.** Admission CysC is negatively correlated with cardiac function in AMI patients and acts as a novel predictor for MACE incidence in the whole population. Further studies are needed to investigate the specific mechanism of CysC in the cardiac function deterioration among AMI patients.

1. Introduction

As one of the leading health-threatening diseases worldwide [1], acute myocardial infarction (AMI) is associated with substantial morbidity and mortality [2]. Despite advances in percutaneous coronary interventions (PCI) and their

widespread use, the mortality rate of AMI patients, together with its complications, such as heart failure, severe arrhythmia, myocardial free wall rupture (MFWR), and cardiogenic shock (CS), remain very high [3, 4]. Especially, cardiac function deterioration and ventricular remodelling after AMI are known to be correlated with increased rehospitalization rate

and worse long-term outcomes [5] and have attracted more and more attention. However, the underlying mechanism remains elusive and there is a shortage of serum prediction markers.

Cystatin C (CysC), a low-molecular-weight (13 kDa) protease inhibitor, is synthesized and released into the blood by all nucleated cells, freely filtered by kidney glomerulus and almost completely reabsorbed and metabolized by the proximal tubule, but not secreted [6]. Due to these properties, even very small changes in the glomerular filtration rate (GFR) may significantly alter serum CysC level, potentially making this basic protein a very sensitive marker of renal filtration [7]. Since it was first described in 1961 by Jorgen Clausen in human cerebrospinal fluid [8], CysC has been thoroughly investigated and is considered a promising biomarker for several diseases, including but not limited to kidney disease and nephropathy-related diabetes [9, 10], Alzheimer's disease [11], and breast cancer [12].

CysC plays pleiotropic roles in human vascular pathophysiology, particularly in regulating cathepsins S and K [13]. In vivo and in vitro studies have shown elevated levels of cathepsins and lower levels of CysC, which behaves as a potent cathepsin inhibitor—in atherosclerotic tissue [14]. Correspondingly, several studies investigated the functional role of CysC in cardiovascular disease (CVD). An observational meta-analysis showed a strong dose-dependent relation between cystatin C concentrations and CVD [14]. Rothenbacher and his team found the use of cysC based chronic kidney disease (CKD) may result in more accurate risk estimates and have better prognostic value for CVD than creatinine [15]. Additionally, in high-risk patients after ACS, CysC is a strong predictor of major adverse cardiovascular events (MACE), including death from cardiovascular causes and hospitalization for heart failure [16]. However, the evidence for the relationship between in-hospital CysC and cardiac function and subsequent long-term prognosis among AMI patients remains unclear.

In this retrospective cohort study, we investigate the relationship between admission CysC and cardiac in AMI patients. Subsequently, survival analysis was performed to investigate the effects of admission CysC levels on long-term mortality and morbidity in AMI patients.

2. Methods

2.1. Study Design and Participants. This was a single-center, retrospective cohort study. Consecutive patients admitted to the cardiology department of the First Affiliated Hospital of Xi'an Jiaotong University for AMI between January 2016 and December 2020 were enrolled. The inclusion criteria were confirmed admission diagnosis of AMI, and AMI was defined based on the universal definition criteria by the American Cardiology College [1]. The exclusion criteria were [1] severe noncardiac disease with an expected survival of less than 1 year and unwillingness to participate, [2] patients over the age of 80 years or living far away from the hospital's catchment area, and (3) extremely high CysC level (>5 mg/L). A patient could only be included once. The medical records of the patients were collected from

the Biobank of the First Affiliated Hospital of Xi'an Jiaotong University, which contains deidentified data derived from raw medical records. Information about patients' present medication, vascular risk factors, and detailed medical history were obtained via questionnaires. Follow-up information was obtained via telephone and questionnaires by the general practitioner (GP). Patients' MACE, including new-onset myocardial infarction, acute heart failure and cardiac death, and cardiovascular and all-cause mortality were documented during follow-up. Written informed consent was obtained from all study participants, with ethnic committee approval at the First Affiliated Hospital of Xi'an Jiaotong University.

2.2. Clinical Data Collection. Detailed medical histories were screened from the patients enrolled. Patient characteristics were collected, including age, sex, disease history, and physical examination. Serum CysC levels of all patients were measured within 3 h of admission, by colloidal gold particle-enhanced colorimetric immunoassay (Nescauto GC Cystatin C, Alfresa Pharma, Osaka, Japan) with a Hitachi 7600-110 automatic analyzer. Other biochemical results were evaluated immediately after the patients' admission to the hospital. They were all collected prior to PCI. Echocardiography was performed during hospital treatment.

2.3. Statistical Analysis. All statistical analyses were performed by using SPSS for Mac 22.0 (SPSS Inc., Chicago, IL) or GraphPad 9.0 Prism (GraphPad Software San Diego, CA). Data were presented as frequencies or percentages for categorical variables and mean \pm SD for continuous variables, unless otherwise indicated. Simple *t*-test was used to compare continuous variables which are in the normal distribution. Mann-Whitney *U* test was used to compare continuous variables which do not conform to the normal distribution. χ^2 test was used to compare categorical variables. One-way ANOVA was used to compare continuous variables of three or more independent (unrelated) groups. Simple linear analysis was used for calculating the correlation between CysC and cardiac function parameters. Kaplan-Meier survival curve analysis was used to represent the proportional risk of MACE, cardiovascular, and all-cause mortality for the admission CysC values in AMI patients. A Cox proportional-hazards model was performed to provide a point estimate HR (hazard ratio) and a two-sided 95% confidence interval. Receiver-operator characteristic (ROC) curve analysis and the area under the ROC curve (AUC) were used to compare the predictive value of MACE, cardiovascular, and all-cause mortality among CysC and other indexes. A value of $p < 0.05$ was considered statistically significant.

3. Results

3.1. Study Population. From January 2017 till December 2020, a total of 5973 AMI patients were enrolled in the study and 17 patients with extremely high CysC levels (>5 mg/L) were excluded. According to the universal definition criteria and Cutoff Finder, [17, 18] all populations were divided into the high-admission CysC cohort (1772 patients, CysC \geq 1.09

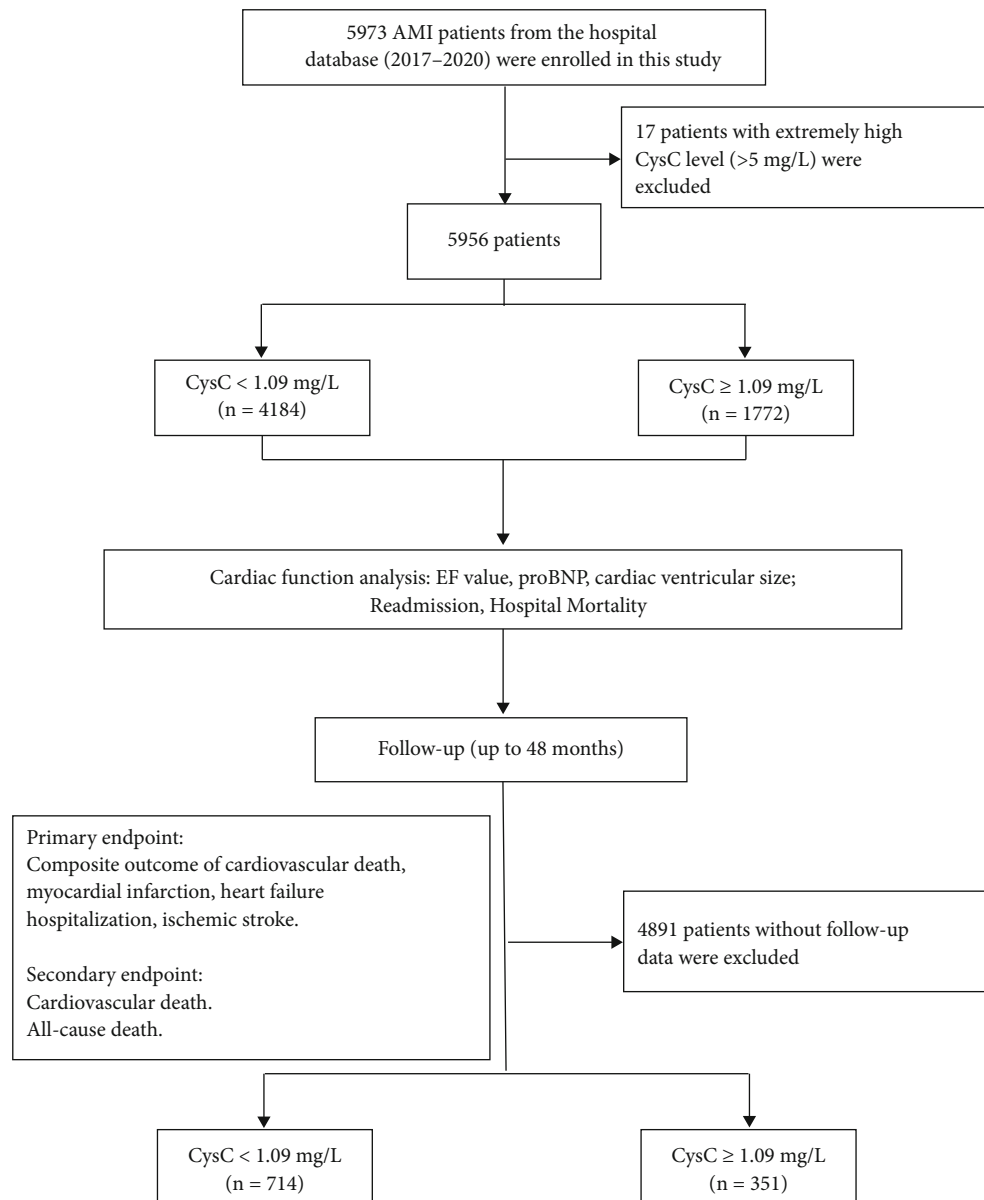


FIGURE 1: Study design, patient selection, and follow-up.

mg/L) and low-admission CysC cohort (4184 patients, CysC < 1.09 mg/L) in the initial observational analysis, while 714 low CysC patients and 351 high CysC patients were included in the follow-up survival analysis (Figure 1). Baseline patients' characteristics are shown in Table 1, and the correlation between admission CysC and other metabolomic indexes is displayed in Table 2. The mean value of CysC was 0.76 ± 0.19 mg/L in low CysC and 1.41 ± 0.47 mg/L in the high CysC cohort. The medication was started at admission. No significant difference in blood pressure/HbA1c/TG at baseline was seen in different CysC groups in AMI patients.

3.2. Association between CysC and Cardiac Function in AMI patients. To investigate the relationship between CysC and cardiac function, we utilized simple linear regression analysis. The admission CysC level was found to be significantly

positively correlated to the pro-BNP level (R square = 0.2142, 95% CI 4758 to 5265, $p < 0.0001$) (Figure 2(a)). Echocardiography analysis showed negative correlation between CysC and left ventricular ejection fraction value (EF, R square = 0.0095, 95% CI -3.503 to -1.605, $p < 0.0001$) (Figure 2(b)) and positive correlation between CysC and left ventricular size, with both increased left ventricular end-systolic dimension (LVESD, R square = 0.0184, 95% CI 1.652 to 2.904, $p < 0.0001$) and left ventricular end-diastolic dimension (LVEDD, R square = 0.0028, 95% CI 0.4422 to 2.631, $p = 0.0059$) (Figure 2(c)).

Subgroup analysis further indicated that, consistently, circulating pro-BNP and cardiac troponin T (cTnT) was higher in high-admission CysC cohort than controls (pro-BNP: 1222 vs. 577.4, $p < 0.001$; cTnT 1.340 vs. 1.644, $p < 0.001$) (Figures 2(d) and 2(e)). We also found that high-

TABLE 1: Distribution of demographic and clinical characteristics according to CysC levels.

	CysC < 1.09 mg/L (n = 4184)	CysC ≥ 1.09 mg/L (n = 1722)	p value
CysC (mg/L)	0.76 ± 0.19	1.41 ± 0.47	<0.001
Age (years)	60.67 ± 11.68	65.79 ± 12.16	<0.001
Female sex (%)	799 (19.9)	368 (20.7)	0.434
SBP (mmHg)	123.50 ± 21.64	122.62 ± 23.45	0.168
DBP (mmHg)	77.96 ± 14.83	75.90 ± 14.82	0.182
EF (%)	51.58 ± 9.67	49.31 ± 10.31	<0.001
pro-BNP (pg/mL)	577.4	1222	<0.001
HbA1c (%)	6.28 ± 1.46	6.36 ± 1.41	0.068
TG (mmol/L)	1.49	1.59	0.013
LDL (mmol/L)	2.42 ± 0.85	2.25 ± 0.82	<0.001
HDL (mmol/L)	0.95 ± 0.23	0.92 ± 0.22	<0.001
ApoA (g/L)	1.07 ± 0.19	1.03 ± 0.19	<0.001
ApoB (g/L)	0.21 ± 0.23	0.78 ± 0.22	<0.001
ApoE (mg/L)	36.30 ± 14.14	36.01 ± 14.36	0.490
Cre (μmol/L)	64.51	99.23	<0.001
UA (μmol/L)	321.33	370.06	<0.001
HomoCys (μmol/L)	23.17	26.23	<0.001
Ticagrelor (%)	2060 (51.2)	787 (44.4)	<0.001
Aspirin (%)	3934 (97.8)	1773 (96.1)	0.001
Furosemide (%)	1731 (43.0)	988 (58.8)	<0.001
Spirolactone (%)	1449 (36.2)	782 (44.2)	<0.001
Isosorbide mononitrate (%)	2340 (58.1)	1040 (58.7)	0.707
Diltiazem (%)	198 (4.9)	78 (4.4)	0.422
Nifedipine (%)	399 (9.9)	262 (14.7)	<0.001
Metoprolol (%)	3327 (82.7)	1377 (77.7)	<0.001

Data were shown in mean ± SD, median, or n (%). SBP: systolic blood pressure; DBP: diastolic blood pressure; HbA1c: hemoglobin A1c; TG: triglyceride; LDL: low-density lipoprotein; HDL: high-density lipoprotein; ApoA: apolipoprotein A; ApoB: apolipoprotein B; ApoE: apolipoprotein E; Cre: creatinine; UA: uric acid; HomoCys: homocysteine.

TABLE 2: Correlation between admission CysC and other metabolomic indexes.

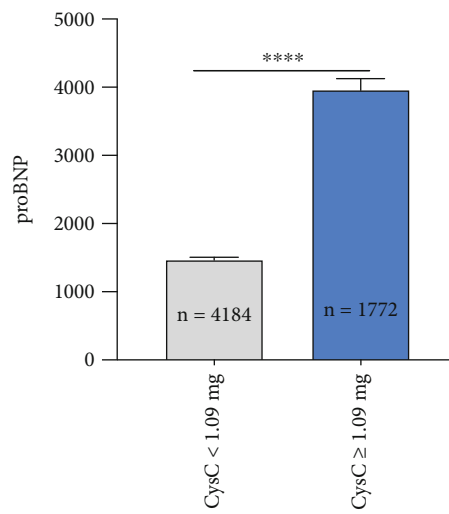
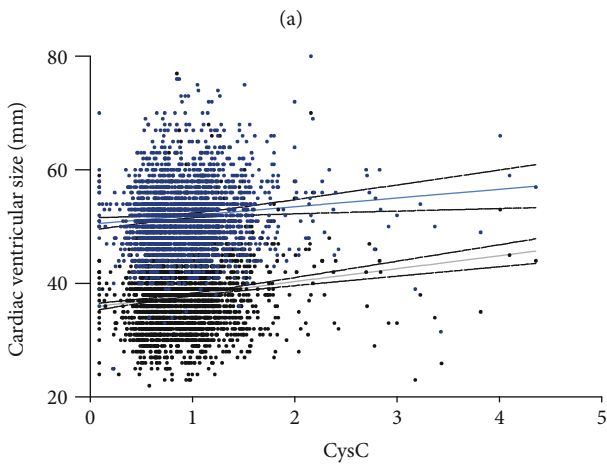
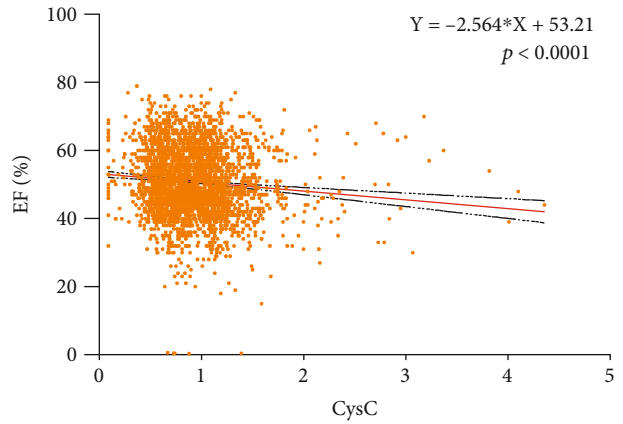
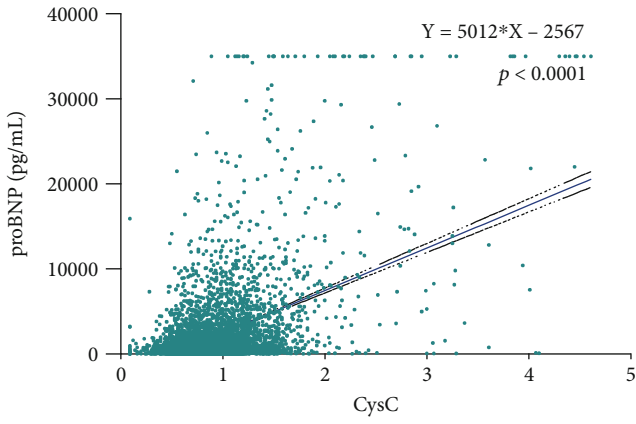
	pro-BNP	EF	HbA1c	TC	TG	LDL	HDL	Cre	UA	HomoCys
Pearson correlation coefficient	0.2142	0.0010	0.009	-0.032	-0.022	-0.027	-0.013	0.270	0.103	0.023
p value	<0.0001	<0.0001	0.515	0.017	0.097	0.049	0.350	<0.0001	<0.0001	0.128
n	5793	5787	5193	5671	5456	5455	5456	5793	5793	4451

HbA1c: hemoglobin A1c; TC: total cholesterol; TG: triglyceride; LDL: low-density lipoprotein; HDL: high-density lipoprotein; Cre: creatinine; UA: uric acid; HomoCys: homocysteine.

admission CysC cohort displayed decreased EF value (49.31 ± 10.31 vs. 51.58 ± 9.67 , $p < 0.001$) (Figure 2(f)) and increased left ventricular size evaluated by the echocardiography (Figure 2(g)).

3.3. Increased Hospital Mortality in High-Admission CysC Cohort with AMI. As the most frequently used risk assessment tools, the 'Global Registry of Acute Coronary Events' (GRACE) and the 'Can Rapid risk stratification of Unstable angina patients Suppress Adverse outcomes with Early

implementation of the American College of Cardiology/American Heart Association guidelines' (CRUSADE) scores were recommended in describing the severity and mortality risk of AMI patients and management [19]. The average GRACE and CRUSADE scores were 124.5 and 21.74 in all AMI patients, respectively. Both GRACE and CRUSADE scores were significantly positively correlated to the CysC value (Fig S1). In subgroup analysis, we found GRACE and CRUSADE scores were significantly higher in high-admission CysC cohort than controls (GRACE score 133.6



— LVEDD (mm)
— LVESD (mm)

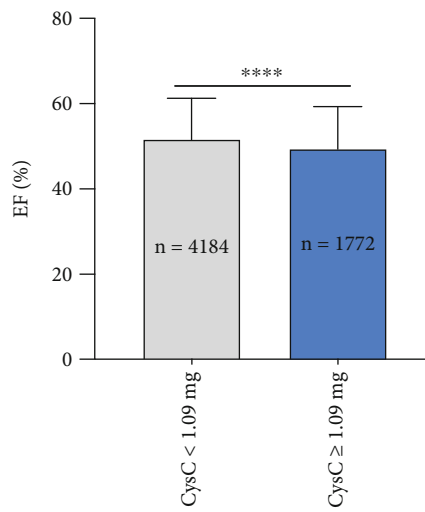
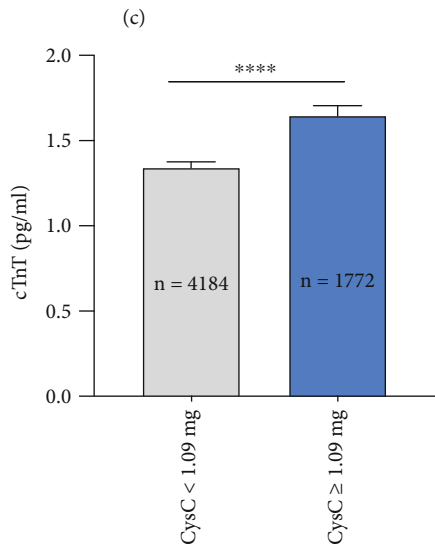


FIGURE 2: Continued.

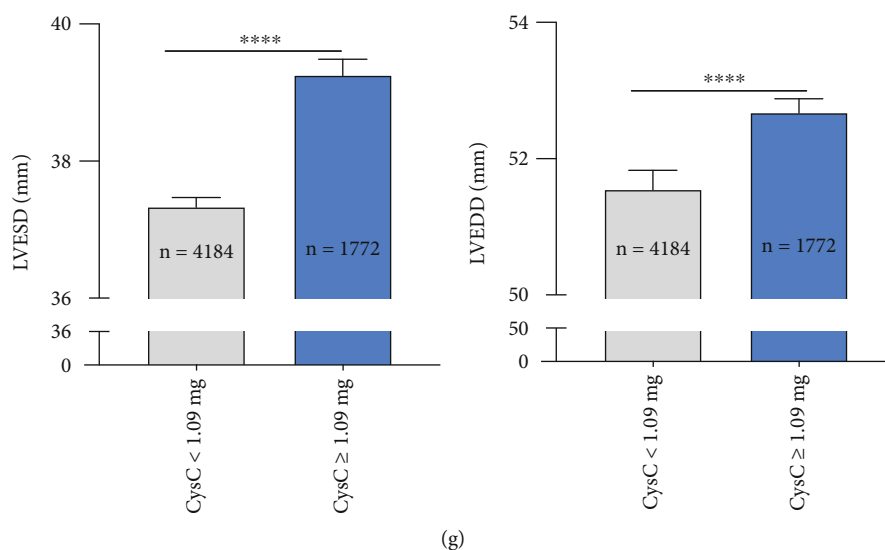


FIGURE 2: Admission CysC level was found to be significantly negatively correlated to the cardiac function in AMI patients. (a) Simple linear regression displayed a significantly positive correlation between admission CysC pro-BNP levels. (b, c) Echocardiography analysis showed a negative correlation between CysC and left ventricular EF value (b) and a positive correlation between CysC and left ventricular size, with both increased LVESD and LVEDD (c). (d–g) Subgroup analysis showed significant elevated pro-BNP value (d), elevated cTnT value (e), decreased EF value (f), and increased left ventricular size (g) in high-admission CysC cohort (CysC \geq 1.09 mg/L) than controls (CysC < 1.09 mg/L). Data were shown in mean \pm SD. For statistical analysis, Student's *t*-test was applied, **** p < 0.0001. EF: ejection fraction; LVESD: left ventricular end-systolic dimension; LVEDD: left ventricular end-diastolic dimension.

vs. 121.3, p < 0.0001; CRUSADE score 25.78 vs. 20.18, p < 0.0001) (Figure 2(a)).

5038 (84.0%) AMI patients were completely reperfused with thrombolysis in myocardial infarction (TIMI) > 2 after PCI, and 918 (16.0%) AMI patients failed to reperfusion with TIMI \leq 2 and only received medication treatment and intervention. No reflow or slow flow following PCI is independently associated with increased in-hospital mortality, malignant arrhythmias, and cardiac failure [20]. Interestingly, CysC was significantly higher in group TIMI \leq 2 compared to group TIMI > 2 (0.93 vs. 1.13, p < 0.0001).

Furthermore, the high-admission CysC cohort with AMI showed an elevated mortality rate during hospitalization and readmission rate than controls. Within the high CysC cohort, 38 (2.14%) patients died for all-cause during hospitalization and 212 (11.96%) had readmission to hospital. Within low CysC cohort, 57 (1.36%) patients died for all-cause during hospitalization and 423 (10.11%) readmission (Figures 3(a) and 3(b)). In addition, AMI patients who died during hospitalization exhibited raised admission CysC value than recovery patients (1.26 vs. 0.96, p < 0.0001), but there is no significant difference between readmission and recovery patients (0.97 vs. 0.96, p = 0.3133) (Figure 3(c)).

3.4. Increased MACE, Cardiovascular, and All-Cause Mortality Incidence in High-Admission CysC Cohort with AMI. At the end of the 48-month follow-up, within high CysC cohort, 38 (10.83%) MACE events occurred, 31 (8.83%) died for cardiac cause, and 38 (10.83%) patients for all-cause. Within low CysC cohort, 32 (4.48%) MACE events occurred, 20 (2.80%) died for cardiac cause, and 22 (3.08%) patients for all-cause.

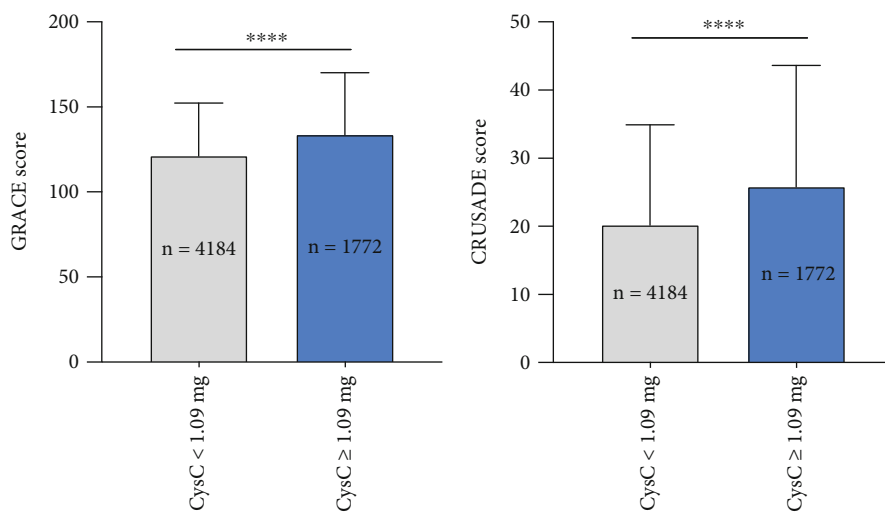
Kaplan–Meier survival analysis was utilized to evaluate the survival curve between two cohorts. Similarly, high-admission CysC cohort displayed significantly increased MACE incidence (HR = 2.293, 95% CI 1.400 to 3.755, p < 0.0001) (Figure 4), cardiovascular mortality (HR = 3.016, 95% CI 1.694 to 5.371, p = 0.0002), and all-cause mortality (HR = 3.424, 95% CI 2.010 to 5.835, p < 0.0001) as compared to controls (Figure 5).

Receiver operating characteristic curves were generated, and AUCs were calculated to estimate the predicted values of different biomarkers. The performance of CysC, pro-BNP, uric acid (UA), and creatine (Cre) in predicting MACE, cardiovascular, and all-cause mortality, and MACE was illustrated in Figure 6. CysC showed significant and similar predictive accuracy as compared to pro-BNP. Cre also exhibited a significant predicting value while UA showed no difference in MACE and mortality prediction.

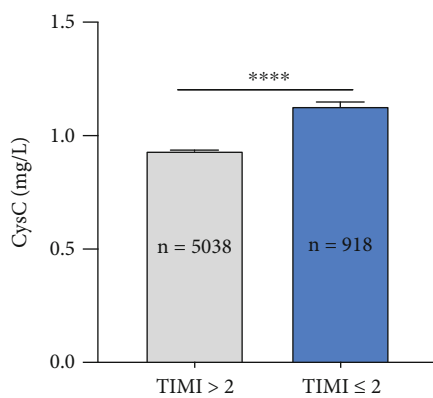
4. Discussion

In this single-center, retrospective, real-world, population-based study, we investigate the relationship between in-hospital Cystatin C (CysC) and cardiac function and subsequent prognosis among AMI patients. Serum CysC is found to be associated with cardiac function deterioration in patients with AMI. Moreover, high-admission serum CysC level exhibits high incidence of MACE as well as cardiovascular and all-cause mortality rate in AMI patients during 4-year follow-up.

The important implication of the present study is that CysC is identified as a biomarker for cardiac function in AMI patients. Several previous studies investigated the



(a)



(b)

	Recovery	Readmission	Hospital mortality	<i>p</i>
CysC < 1.09 mg/L	3704	423	57	
CysC ≥ 1.09 mg/L	1522	212	38	0.0075

(c)

FIGURE 3: Continued.

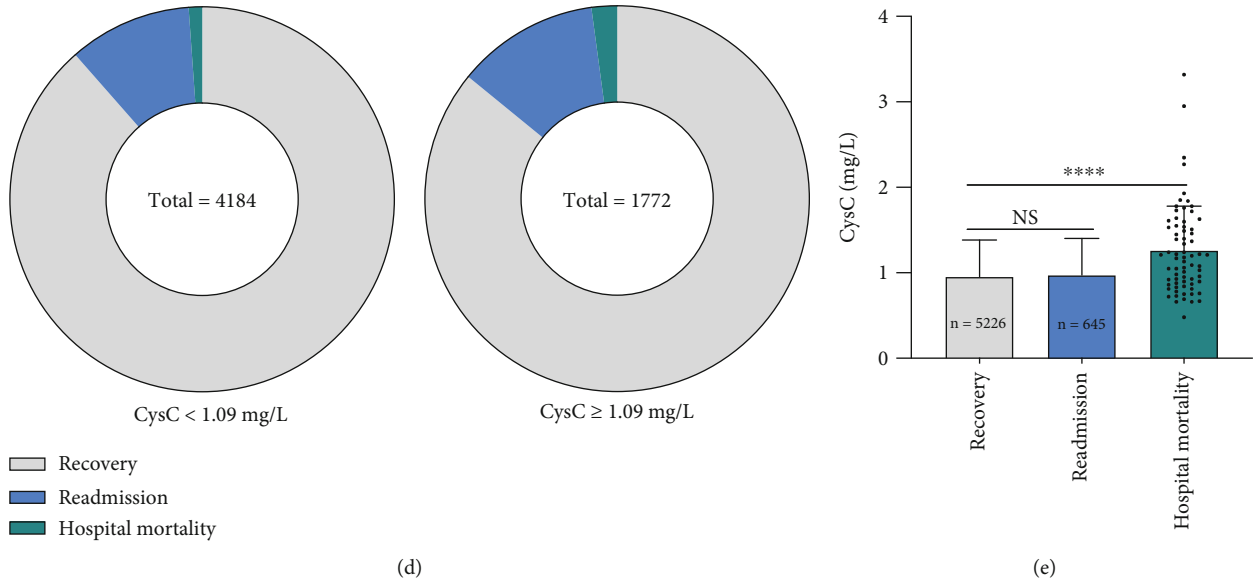


FIGURE 3: Increased hospital mortality in high-admission CysC cohort with AMI. (a) GRACE and CRUSADE score were significantly higher in high-admission CysC cohort (CysC ≥ 1.09 mg/L) than controls (CysC < 1.09 mg/L). (b) CysC was significantly higher in group TIMI ≤ 2 compared to group TIMI > 2. (c, d) High-admission CysC cohort (CysC ≥ 1.09 mg/L) showed elevated mortality rate even during hospitalization and readmission rate than controls (CysC < 1.09 mg/L). Within the high CysC cohort, 38 (2.14%) patients died for all causes during hospitalization and 212 (11.96%) for readmission. Within the low CysC cohort, 57 (1.36%) patients died for all causes during hospitalization and 423 (10.11%) for readmission. For statistical analysis, χ^2 test was performed. (e) AMI patients who died during hospitalization exhibited raised admission CysC value than recovery patients, but no significant difference between readmission and recovery patients. Data were shown in mean ± SD (a, e), mean ± SEM (Bb), or as each individual dot. For statistical analysis, one-way ANOVA followed by Sidak's multiple comparison test was applied, **** $p < 0.0001$.

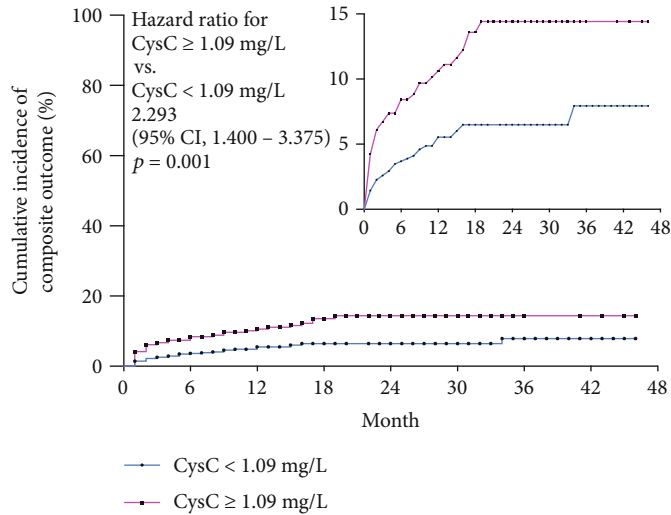


FIGURE 4: Kaplan-Meier survival analysis revealed significantly increased MACE incidence in high-admission CysC cohort with AMI at the end of 4-year follow-up. Kaplan-Meier survival analysis revealed high-admission CysC cohort (CysC ≥ 1.09 mg/L) displayed significantly increased MACE incidence (HR = 2.293, 95% CI 1.400 to 3.755, $p < 0.0001$) than controls (CysC < 1.09 mg/L).

relationship between CysC and heart failure incidents. Via 4 community-based cohorts with 12.5 years of follow-up, Navin Suthahar and their team found CysC was strongly and similarly associated with HF in both sexes [21], as these biomarkers reflect distinct pathophysiological processes [22], and the elevation may indicate cardiovascular

or systemic derangement early in the time course of HF progression [23]. Additionally, our result indicated that CysC might be eligible as a potential serum predictor for heart failure in the population after acute myocardial infarction.

Notably, the major outcomes of this study show increased MACE incidence, cardiovascular, and all-cause

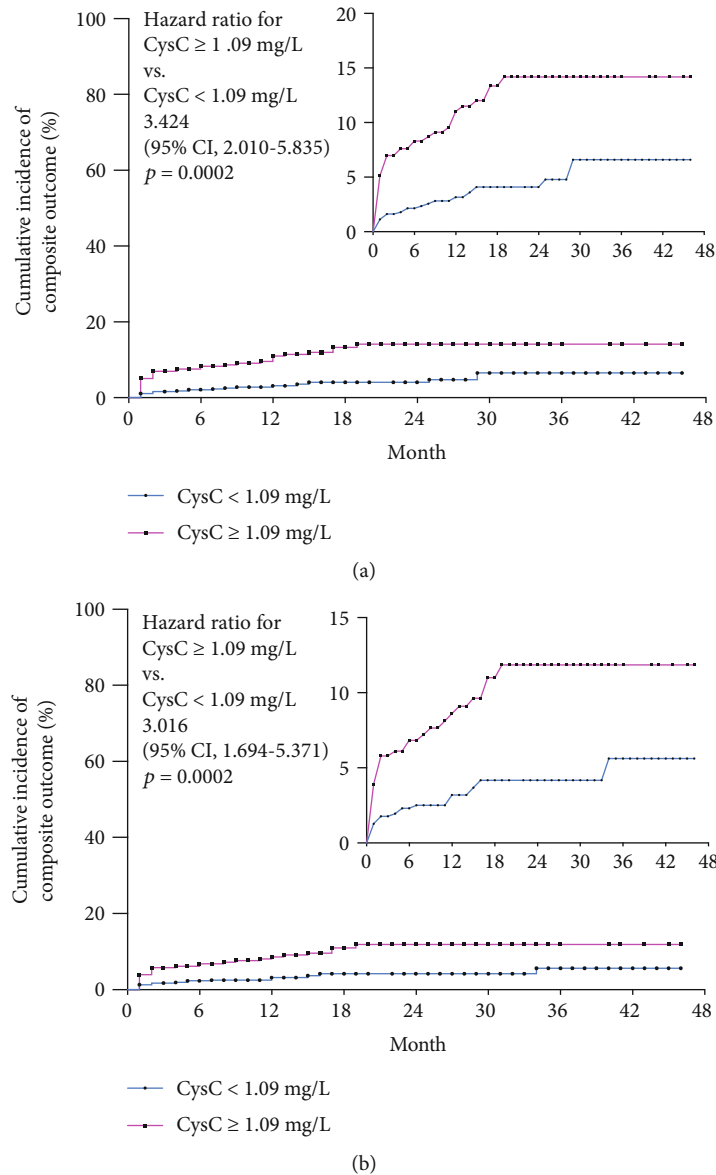
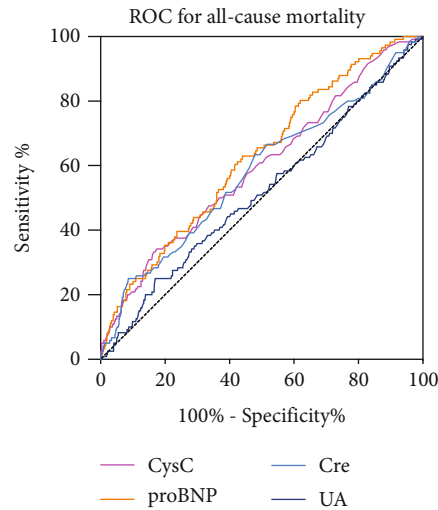
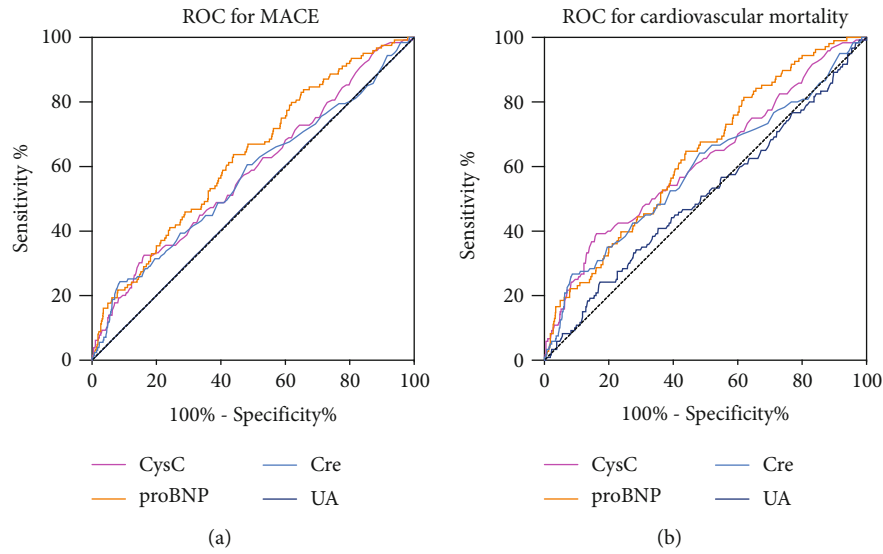


FIGURE 5: Kaplan-Meier survival analysis revealed significantly increased all/cardiovascular mortality in high-admission CysC cohort with AMI at the end of the 4-year follow-up. (a) Kaplan-Meier survival analysis revealed high-admission CysC cohort (CysC ≥ 1.09 mg/L) displayed significantly increased cardiovascular mortality (HR = 3.016, 95% CI 1.694 to 5.371, $p = 0.0002$) than controls (CysC < 1.09 mg/L). (b) Kaplan-Meier survival analysis revealed high-admission CysC cohort (CysC ≥ 1.09 mg/L) displayed significantly increased and all-cause mortality (HR = 3.424, 95% CI 2.010 to 5.835, $p < 0.0001$) than controls (CysC < 1.09 mg/L).

mortality in the high CysC cohort with AMI at the end of 4-year follow-up, indicating that CysC level is a potential independent predictor for cardiac prognosis after AMI. Increasing shreds of evidence have shown that higher CysC is associated with higher cardiovascular risk and mortality rate in patients with non-ST elevated acute coronary syndrome [24], and serum creatinine to cystatin C ratio is associated with major adverse cardiovascular events in patients with obstructive coronary artery disease [25]. In AMI patients, an increased admission CysC level was associated with a higher risk of in-hospital and 1-month death [26]. Besides, circulating cystatin C level on the 12th–14th day after hospital admission predicted the adverse cardiovascular

outcome in patients with STEMI [27]. Through a 4-year follow-up study, we further proved that CysC can be included in the risk stratification model to guide the treatment of high-risk AMI patients.

Several potential mechanisms may account for the prognostic importance of CysC in AMI patients. First, abnormal CysC value can identify early patients with renal insufficiency before circulating creatinine, which could be linked to atherosclerosis, vascular complications, and increased cardiovascular events [28]. Second, CysC may play an important role in regulating cardiac inflammatory responses [29], contributing to the development of no-reflow and the increased risk of death. Besides, CysC elevation may damage



		CysC	proBNP	Cre	UA
MACE	AUC area	0.583	0.629	0.568	0.502
	p	0.002	<0.001	0.012	0.905
Cardiovascular mortality	AUC area	0.614	0.632	0.587	0.508
	p	<0.001	<0.001	0.002	0.790
All-cause mortality	AUC area	0.600	0.624	0.578	0.516
	p	0.001	<0.001	0.005	0.581

(c)

FIGURE 6: ROC for predicting MACE, cardiovascular, and all-cause mortality among CysC, pro-BNP, Cre, and UA. Accuracies of CysC, pro-BNP, Cre, and UA for predicting MACE (a), cardiovascular mortality (b), and all-cause mortality (c) presented as areas under the receiver operating characteristic curves, individually. ROC: receiver-operator characteristic; AUC: area under the receiver operating characteristic curve.

the cardiovascular system by affecting lipid peroxidation, coagulation function, and smooth muscle cell and endothelial cell function [30], and finally, facilitate the vulnerability of atherosclerotic plaque CysC [31].

However, there are several potential limitations in the current work: first, this study is limited in its single-center, retrospective, and observational nature. A future multicenter prospective study with a larger number of patients and a

longer follow-up is required. Also, several parameters, including patient age were not balanced between the high and low CysC cohort. As age might also be a prognostic factor in AMI patients, improving risk stratification independently of age and kidney function would be considered in the further study.

In conclusion, through this retrospective cohort study, we have found that admission CysC is negatively correlated with cardiac function in AMI patients and acts as a novel predictor for MACE incidence in the whole population. Further studies are needed to investigate the specific mechanism of CysC during the cardiac function deterioration of AMI patients.

Data Availability

The authors confirm that the data supporting the findings of this study are available from the corresponding author JS upon reasonable request.

Ethical Approval

Written informed consent was obtained from all study participants, with ethnic committee approval at the First Affiliated Hospital of Xi'an Jiaotong University.

Conflicts of Interest

The authors declare that they have no conflicts of interest.

Authors' Contributions

JS, BL, and ZY participated in the design of the study. ZH, JS, BL, YL, HW, and HL collected the patients' data, did the follow-up, and finalized the revision. HW, LS, GTJ, and KK performed the statistical analysis. YL, HW, and XH finished the patients' follow-up. JS and BL drafted the manuscript. BL, HZ, and JS performed revision work. All authors have reviewed the final version of the manuscript and approve it for publication. All authors approved the final manuscript. Bowen Lou and Yongbai Luo contributed equally to this work.

Acknowledgments

The authors wish to acknowledge the assistance of Biobank from the First Affiliated Hospital of Xi'an Jiaotong University with the data extraction and preparation of the manuscript. This study was supported by the National Natural Science Foundation of China (81800390 and 82100477), Key Research and Development Program of Shaanxi (Program Nos. 2020KW-049 and 2021KWZ-25), and Clinical Research Award of the First Affiliated Hospital of Xi'an Jiaotong University, China (No. XJTU1AF-CRF-2018-025).

Supplementary Materials

Figure S1: simple linear regression displayed a significantly positive correlation between admission CysC and GRACE/CRUSADE score. (*Supplementary Materials*)

References

- [1] A. P. DeFilippis, A. R. Chapman, N. L. Mills et al., "Assessment and treatment of patients with type 2 myocardial infarction and acute nonischemic myocardial injury," *Circulation*, vol. 140, no. 20, pp. 1661–1678, 2019.
- [2] S. S. Dhruva, J. S. Ross, B. J. Mortazavi et al., "Association of use of an intravascular microaxial left ventricular assist device vs intra-aortic balloon pump with in-hospital mortality and major bleeding among patients with acute myocardial infarction complicated by cardiogenic shock," *Journal of the American Medical Association*, vol. 323, no. 8, pp. 734–745, 2020.
- [3] B. Lou, Y. Luo, X. Hao et al., "Clinical characteristics and protective factors in patients with acute myocardial infarction undergoing in-hospital myocardial free wall rupture: a single-center, retrospective analysis," *Journal of Investigative Medicine*, vol. 67, no. 8, pp. 1097–1102, 2019.
- [4] B. Schrage, K. Ibrahim, T. Loehn et al., "Impella support for acute myocardial infarction complicated by cardiogenic shock," *Circulation*, vol. 139, no. 10, pp. 1249–1258, 2019.
- [5] L. Lewicki, M. Fijalkowska, M. Karwowski et al., "The non-invasive evaluation of heart function in patients with an acute myocardial infarction: the role of impedance cardiography," *Cardiology Journal*, vol. 28, no. 1, pp. 77–85, 2021.
- [6] T. W. Ferguson, P. Komenda, and N. Tangri, "Cystatin C as a biomarker for estimating glomerular filtration rate," *Current Opinion in Nephrology and Hypertension*, vol. 24, no. 3, pp. 295–300, 2015.
- [7] S. Seronie-Vivien, P. Delanaye, L. Pieroni, C. Mariat, and M. Froissart, "Cystatin C: current position and future prospects," *Clinical Chemistry and Laboratory Medicine*, vol. 46, no. 12, pp. 1664–1686, 2008.
- [8] A. Grubb and H. Lofberg, "Human gamma-trace, a basic microprotein: amino acid sequence and presence in the adenohypophysis," *Proceedings of the National Academy of Sciences of the United States of America*, vol. 79, no. 9, pp. 3024–3027, 1982.
- [9] M. Y. Park, S. J. Choi, J. K. Kim, S. D. Hwang, and Y. W. Lee, "Urinary cystatin C levels as a diagnostic and prognostic biomarker in patients with acute kidney injury," *Nephrology*, vol. 18, no. 4, pp. 256–262, 2013.
- [10] B. A. Perkins, R. G. Nelson, B. E. Ostrander et al., "Detection of renal function decline in patients with diabetes and normal or elevated GFR by serial measurements of serum cystatin C concentration: results of a 4-year follow-up study," *Journal of the American Society of Nephrology*, vol. 16, no. 5, pp. 1404–1412, 2005.
- [11] E. Levy, M. Sastre, A. Kumar et al., "Codeposition of cystatin C with amyloid-beta protein in the brain of Alzheimer disease patients," *Journal of Neuropathology and Experimental Neurology*, vol. 60, no. 1, pp. 94–104, 2001.
- [12] G. Leto and M. V. Sepporta, "The potential of cystatin C as a predictive biomarker in breast cancer," *Expert Review of Anti-cancer Therapy*, vol. 20, no. 12, pp. 1049–1056, 2020.
- [13] G. P. Shi, G. K. Sukhova, A. Grubb et al., "Cystatin C deficiency in human atherosclerosis and aortic aneurysms," *The Journal of Clinical Investigation*, vol. 104, no. 9, pp. 1191–1197, 1999.
- [14] S. W. van der Laan, T. Fall, A. Soumare et al., "Cystatin C and cardiovascular disease: a Mendelian randomization study," *Journal of the American College of Cardiology*, vol. 68, no. 9, pp. 934–945, 2016.

- [15] D. Rothenbacher, M. Rehm, L. Iacoviello et al., "Contribution of cystatin C- and creatinine-based definitions of chronic kidney disease to cardiovascular risk assessment in 20 population-based and 3 disease cohorts: the BiomarCaRE project," *BMC Medicine*, vol. 18, no. 1, p. 300, 2020.
- [16] S. Correa, D. A. Morrow, E. Braunwald et al., "Cystatin C for risk stratification in patients after an acute coronary syndrome," *Journal of the American Heart Association*, vol. 7, no. 20, p. e009077, 2018.
- [17] M. Reinhard, E. J. Erlandsen, and E. Randers, "Biological variation of cystatin C and creatinine," *Scandinavian Journal of Clinical and Laboratory Investigation*, vol. 69, no. 8, pp. 831–836, 2009.
- [18] S. Guo, Y. Xue, Q. He et al., "Preoperative serum cystatin-C as a potential biomarker for prognosis of renal cell carcinoma," *PLoS One*, vol. 12, no. 6, p. e0178823, 2017.
- [19] K. Tscherny, C. Kienbacher, V. Fuhrmann et al., "Risk stratification in acute coronary syndrome: evaluation of the GRACE and CRUSADE scores in the setting of a tertiary care centre," *International Journal of Clinical Practice*, vol. 74, no. 2, p. e13444, 2020.
- [20] H. Ito, "No-reflow phenomenon and prognosis in patients with acute myocardial infarction," *Nature Clinical Practice. Cardiovascular Medicine*, vol. 3, no. 9, pp. 499–506, 2006.
- [21] N. Suthahar, E. S. Lau, M. J. Blaha et al., "Sex-specific associations of cardiovascular risk factors and biomarkers with incident heart failure," *Journal of the American College of Cardiology*, vol. 76, no. 12, pp. 1455–1465, 2020.
- [22] R. S. Vasan, "Biomarkers of cardiovascular Disease," *Circulation*, vol. 113, no. 19, pp. 2335–2362, 2006.
- [23] N. E. Ibrahim and J. L. Januzzi Jr., "Established and emerging roles of biomarkers in heart failure," *Circulation Research*, vol. 123, no. 5, pp. 614–629, 2018.
- [24] T. Jernberg, B. Lindahl, S. James, A. Larsson, L. O. Hansson, and L. Wallentin, "Cystatin C," *Circulation*, vol. 110, no. 16, pp. 2342–2348, 2004.
- [25] Y. W. Lu, Y. L. Tsai, R. H. Chou et al., "Serum creatinine to cystatin C ratio is associated with major adverse cardiovascular events in patients with obstructive coronary artery disease," *Nutrition, Metabolism, and Cardiovascular Diseases*, vol. 31, no. 5, pp. 1509–1515, 2021.
- [26] M. Fouad and M. Boraie, "Cystatin C as an early marker of acute kidney injury and predictor of mortality in the intensive care unit after acute myocardial infarction," *Arab Journal of Nephrology and Transplantation*, vol. 6, no. 1, pp. 21–26, 2013.
- [27] O. L. Barbarash, I. S. Bykova, V. V. Kashtalap et al., "Serum neutrophil gelatinase-associated lipocalin has an advantage over serum cystatin C and glomerular filtration rate in prediction of adverse cardiovascular outcome in patients with ST-segment elevation myocardial infarction," *BMC Cardiovascular Disorders*, vol. 17, no. 1, p. 81, 2017.
- [28] T. Machino-Ohtsuka, Y. Seo, T. Ishizu et al., "Combined assessment of carotid vulnerable plaque, renal insufficiency, eosinophilia, and hs-CRP for predicting risky aortic plaque of cholesterol crystal embolism," *Circulation Journal*, vol. 74, no. 1, pp. 51–58, 2010.
- [29] J. V. Salgado, F. L. Souza, and B. J. Salgado, "How to understand the association between cystatin C levels and cardiovascular disease: imbalance, counterbalance, or consequence?," *Journal of Cardiology*, vol. 62, no. 6, pp. 331–335, 2013.
- [30] S. H. Ballew and K. Matsushita, "Cardiovascular risk prediction in CKD," *Seminars in Nephrology*, vol. 38, no. 3, pp. 208–216, 2018.
- [31] A. P. Antoniadis, Y. S. Chatzizisis, and G. D. Giannoglou, "Pathogenetic mechanisms of coronary ectasia," *International Journal of Cardiology*, vol. 130, no. 3, pp. 335–343, 2008.

Research Article

The Relationship between Intracarotid Plaque Neovascularization and Lp (a) and Lp-PLA2 in Elderly Patients with Carotid Plaque Stenosis

Chang Sun ¹, Na Xi,² Zhijun Sun,³ Xinxin Zhang,⁴ Xiaowei Wang,⁵ Huiyang Cao,⁶ and Xiaowei Jia ¹

¹Cadre Diagnosis and Treatment Department, Eighth Medical Center of PLA General Hospital, Beijing, China

²Department of Pharmacy, Medical Supplies Center of Chinese PLA General Hospital, Beijing, China

³Department of Cardiovascular, The First Medical Center of PLA General Hospital, Beijing, China

⁴School of Foreign Languages English, Guilin University of electronic technology, Guilin, China

⁵Personnel Section, Liaoning Fuxin Center Hospital, Fuxin, China

⁶Cardiac Function Division, Liaoning Fuxin Center Hospital, Fuxin, China

Correspondence should be addressed to Xiaowei Jia; ywljxwgg@163.com

Received 14 March 2022; Accepted 11 April 2022; Published 21 April 2022

Academic Editor: Simona Pichini

Copyright © 2022 Chang Sun et al. This is an open access article distributed under the Creative Commons Attribution License, which permits unrestricted use, distribution, and reproduction in any medium, provided the original work is properly cited.

The aim of this study was to investigate the relationship between carotid plaque neovascularization and lipoprotein (a) [Lp (a)], lipoprotein-associated phospholipase A2 (Lp-PLA2) in elderly patients with carotid plaque stenosis. One hundred elderly patients with carotid plaque stenosis diagnosed in our hospital from January 2020 to January 2022 were retrospectively analyzed and divided into stable ($n = 62$) and unstable ($n = 38$) groups according to whether the plaque was stable or not. Plasma Lp (a), Lp-PLA2, apoA, and apoB levels were measured; intraplaque angiogenesis (IPN) scores were examined by contrast-enhanced ultrasound (CEUS) to assess IPN grade in patients; and Pearson correlation was used to analyze the relationship between plasma Lp (a) and Lp-PLA2 levels and plaque characteristics and angiogenesis. The maximum thickness and total thickness of carotid plaque in the unstable group were significantly greater than those in the stable group ($P < 0.05$); the IPN grade was mainly grade III and IV in the unstable group and grade II in the stable group, and the IPN score was significantly higher in the unstable group than in the stable group ($P < 0.05$); there was no significant difference in the plasma apoA and apoB levels between the two groups ($P > 0.05$), and the plasma Lp (a) and Lp-PLA2 levels were significantly higher in the unstable group than in the stable group ($P < 0.05$); the neovascular grade, plasma Lp-PLA2, and Lp (a) levels were significantly increased ($P < 0.05$); the plasma Lp (a) and Lp-PLA2 levels were positively correlated with the maximum plaque thickness, total plaque thickness, degree of stenosis, and angiogenesis ($P < 0.05$). The plasma levels of Lp (a) and Lp-PLA2 are positively correlated with intraplaque angiogenesis, and their levels can reflect the stability of carotid plaques.

1. Introduction

Carotid plaque is usually caused by lipid deposition at the bifurcation of common carotid artery, without obvious symptoms at the early stage. Severe stenosis may be accompanied by dizziness, headache, and fainting, which is a common cause of stroke and acute cerebral infarction. The incidence of carotid plaque increases with age, the intima media thickens, and carotid plaque and carotid stenosis or occlusion generally

develops in a progressive manner [1, 2]. With the development of medical imaging technology, carotid artery stenosis and plaque formation can be diagnosed and assessed clinically by CT, MRI, carotid ultrasound, and carotid angiography [3]. Current studies have found that intraplaque neovascularization (IPN) is an important predictor of plaque hemorrhage and rupture [4]. Contrast-enhanced ultrasound (CEUS) technique is a means of accurate clinical detection of IPN. After injection of contrast microbubbles, the movement direction

of contrast microbubbles into the plaque is identified. When the contrast microbubbles move from the adventitial side of the plaque or the shoulder side of the plaque to the core side of the plaque, it indicates the presence of IPN [5]. Lipoprotein (a) [lipoprotein (a), Lp (a)] is a low-density lipoprotein whose level is mainly genetically determined and consists of apolipoprotein A (apoA) covalently linked to apolipoprotein B-100 (apoB) [6]. It has been suggested that Lp (a) is involved in the development of atherosclerosis, and plasma Lp (a) levels are closely related to thrombosis and damage [7]. It has also been suggested that Lp (a) does not promote or inhibit neovascularization [8]. Whether plasma Lp (a) levels have an effect on IPN, resulting in plaque instability, remains inconclusive. Lipoprotein-associated phospholipase A2 (Lp-PLA2) is a novel vessel-specific inflammatory marker mainly secreted by macrophages and lymphocytes in atherosclerotic plaques [9]. Studies have found that intraplaque neovascularization is an important indicator of plaque stability, which can deposit a large number of inflammatory matrix in plaques, promote lymphocyte accumulation, and aggravate plaque instability [10]. The aim of this study was to analyze the relationship between carotid intraplaque angiogenesis and Lp (a) and Lp-PLA2 in elderly patients with carotid artery stenosis and to investigate the significance of plasma Lp (a) and Lp-PLA2 levels in predicting plaque stability and intraplaque angiogenesis.

2. Materials and Methods

2.1. Clinical Data. This study was approved by the Ethics Committee of Eighth Medical Center of PLA General Hospital. Signed written informed consents were obtained from all participants before the study. A total of 100 elderly patients with carotid plaque stenosis who were diagnosed in our hospital from January 2020 to January 2022 were retrospectively analyzed and divided into stable group ($n = 62$) and unstable group ($n = 38$) according to whether the plaque was stable or not. Inclusion criteria were shown as follows: (1) Carotid artery stenosis was diagnosed by carotid artery color ultrasound and other imaging examinations. (2) Patients' age was ≥ 60 years old. (3) Patients can tolerate CEUS examination. Exclusion criteria were shown as follows: (1) Patients were allergic to contrast agent. (2) Patients were neurological dysfunction or cognitive deficiency. (3) Patients were combined with severe infection. (4) Patients were combined with obvious liver, kidney, and other vital organ dysfunction.

2.2. Outcome Measures and Test Methods. The admission cases were retrospectively analyzed, and general data such as gender, age, disease history, drug treatment history, and plaque status of the patients were recorded.

2.3. Carotid CEUS Examination. All patients who underwent CEUS had signed the angiographic informed consent.

GE Vivid E95 ultrasonic diagnostic apparatus, high-frequency superficial probe, and contrast mode were used. A 1.5 mL Sono Vue microbubble suspension (Bracco, Italy) was bolus injected through the superficial vein of the elbow, followed by 2~3 mL normal saline at the same rate to observe the contrast agent development effect in the carotid

artery lumen, and DICOM format images 3 s before and 5 min after the appearance of contrast agent in the carotid artery lumen were collected and stored for real-time dynamic analysis. On CEUS examination, no microbubbles seen in the plaque were defined as an IPN score of 0; microbubbles confined to the shoulder or adventitial side of the plaque were defined as an IPN score of 1; and microbubbles seen throughout the plaque were defined as an IPN score of 2. A sum of IPN scores ≥ 2 was defined as unstable plaque, and a sum of IPN scores < 2 was defined as stable plaque.

Grading criteria for intraplaque neovascularization [11, 12] are as follows: It is divided into 4 grades according to the degree of signal enhancement in several plaques, namely, grade I, no enhancement of plaques; grade II, punctate enhancement in or around plaques; grade III, scattered punctate and linear enhancement in and around plaques; and grade IV, diffuse punctate and linear enhancement in and around plaques.

2.4. Plasma Lipoprotein and Lp-PLA2 Levels. 4 mL venous blood was collected from all patients in the morning and placed in an anticoagulant tube containing sodium citrate, mixed well, and centrifuged at 3000 r/min for 5 min at 5°C, and the plasma was separated and stored in a -20°C freezer for testing.

In determining the plasma Lp-PLA2 levels, plasma Lp-PLA2 levels were measured by immunoturbidimetric assay. The reagents were produced and provided by Wuhan Huamei Biological Engineering Co., Ltd. (Wuhan, China), and the operation was performed in strict accordance with the kit instructions.

In determining the plasma lipoprotein, the plasma levels of apolipoprotein A (apoA) and apolipoprotein B (apoB) were measured by Hitachi 7060 automatic biochemical analyzer, and the plasma Lp (a) level was measured by immunoturbidimetry. The reagents were produced and provided by Wuhan Huamei Biological Engineering Co., Ltd. (Wuhan, China). The operation process was performed in strict accordance with the instructions on the kit.

2.5. Statistical Analysis. Statistical Product and Service Solutions (SPSS) 21.0 software (IBM, Armonk, NY, USA) was used to statistically analyze the obtained data. The measurement data satisfying normal distribution were expressed as $(\bar{x} \pm s)$, and the two-sample independent t -test was used to compare the group differences between patients in the stable group and those in the unstable group; one-way ANOVA was used for the comparison between three groups and above; the count data were expressed as the number of cases (n) or rate (%); and the χ^2 test was used to compare patients in the stable group and those in the unstable group, differences between groups of patients, and Pearson correlation analysis of plasma Lp (a) and Lp-PLA2 levels in relation to plaque characteristics and revascularization; $P < 0.05$ indicates a statistically significant difference.

3. Results

3.1. Baseline Data of Patients in Stable Group. There was no significant difference in age, gender, disease history, drug treatment history, degree of carotid artery stenosis, reasons

TABLE 1: Baseline data of patients in stable group ($n, \bar{x} \pm s$).

Metrics	Stable group ($n = 62$)	Unstable group ($n = 38$)	X^2/t	P
Age (years)	70.67 \pm 8.25	71.28 \pm 8.14	0.361	0.719
Sex			0.075	0.784
Male	36	23		
Female	26	15		
Hypertension			0.214	0.643
Yes	43	28		
No	19	10		
Diabetes			1.831	0.176
Yes	15	14		
No	47	24		
Cerebral infarction			3.265	0.071
Yes	14	15		
No	48	23		
Coronary heart disease			3.552	0.059
Yes	28	10		
No	34	28		
Statin therapy			1.045	0.307
Yes	55	36		
No	7	2		
Degree of carotid artery stenosis			3.026	0.388
Mild	25	13		
Moderate	12	5		
Severe	18	11		
Occlusion	7	9		
Reason for visit			2.464	0.292
Coronary ischemia	31	25		
Cerebral artery ischemia	20	9		
Other	11	4		
Maximum thickness of carotid plaque (mm)	3.82 \pm 1.16	4.37 \pm 1.25	2.234	0.028
Total thickness of carotid plaque (mm)	6.21 \pm 2.14	7.19 \pm 2.06	2.254	0.026

for treatment, and other clinical data between the stable group and the unstable group ($P > 0.05$); the maximum thickness and total thickness of carotid plaques in the unstable group were significantly greater than those in the stable group ($P < 0.05$) (see Table 1).

3.2. IPN Score and IPN Imaging Grade in Patients with Stable and Unstable Disease. The IPN grade was mainly grade III and IV in the unstable group and grade II in the stable group ($P < 0.05$); the IPN score was significantly higher in the unstable group than in the stable group ($P < 0.05$) (see Table 2).

3.3. Plasma Lipoprotein and Lp-PLA2 Levels in Patients with Stable and Unstable Disease. There is no significant difference in plasma apoA and apoB levels between the stable and unstable groups ($P > 0.05$); plasma Lp (a) and Lp-PLA2 levels are significantly higher in the unstable group than in the stable group ($P < 0.05$), as shown in Table 3. The plasma levels of Lp-PLA2 and Lp (a) are significantly increased ($P < 0.05$), as shown in Table 4.

3.4. Correlation of Plasma Lp (a) and Lp-PLA2 Levels with Plaque Characteristics and Angiogenesis. Variable assignment was performed for the degree of plaque stenosis, mild=1, moderate=2, severe=3, and occlusion=4; Pearson correlation analysis results showed that plasma Lp (a) and Lp-PLA2 levels were positively correlated with the maximum plaque thickness, total plaque thickness, degree of stenosis, and angiogenesis, that is, plasma Lp (a) and Lp-PLA2 levels; and the more narrow the plaque thickness, the more likely it was to have plaque angiogenesis ($P < 0.05$) (see Table 5).

4. Discussion

Atherosclerosis is a common type of cardiovascular disease in the elderly population. Carotid atherosclerotic plaque is a natural part of the atherosclerosis process and tends to occur at the bifurcation of the carotid artery and at the beginning of the segment where blood flow is slower [13, 14]. The higher IPN classification suggests a greater risk of plaque instability, plaque dislodgement, or even intraplaque

TABLE 2: IPN score and IPN development grade in stable patients ($n, \bar{x} \pm s$).

Metrics	Stable group ($n = 62$)	Unstable group ($n = 38$)	X^2/t	P
Neovascularization (case)			11.963	0.008
Grade I	16	4		
Grade II	27	9		
Grade III	11	14		
Grade IV	8	11		
IPN score (points)	1.05 ± 0.33	2.17 ± 0.62	11.782	< 0.001

TABLE 3: Plasma lipoprotein and Lp-PLA2 levels in patients with stable disease ($\bar{x} \pm s$).

Metrics	Stable group ($n = 62$)	Unstable group ($n = 38$)	t	P
ApoA (mmol/L)	1.17 ± 0.15	1.13 ± 0.14	1.327	0.188
ApoB (mmol/L)	0.85 ± 0.11	0.81 ± 0.12	1.705	0.091
Lp (a) (mg/L)	162.29 ± 51.56	248.74 ± 106.31	5.453	< 0.001
Lp-PLA2 (ng/mL)	213.86 ± 78.69	297.32 ± 91.27	4.842	< 0.001

TABLE 4: Relationship between plasma Lp-PLA2 and Lp (a) levels and neovascularization grade ($\bar{x} \pm s$).

Metrics	Number of subjects	Lp (a) (mg/L)	Lp-PLA2 (ng/mL)
Neovascularization		195.14	245.57
Grade I	20	151.38 ± 45.94	199.56 ± 71.13
Grade II	36	181.91 ± 62.27	223.70 ± 79.85
Grade III	25	204.43 ± 88.17	271.71 ± 83.84
Grade IV	19	254.05 ± 109.63	301.05 ± 92.29
F		6.231	6.742
P		< 0.001	< 0.001

TABLE 5: Correlation of plasma Lp (a) and Lp-PLA2 levels with plaque characteristics and IPN.

Metrics	Lp (a)			Lp-PLA2		
	R	95% CI	P	R	95% CI	P
Maximum thickness of plaque	0.290	0.099 to 0.460	0.003	0.204	0.008 to 0.385	0.042
Total plaque thickness	0.235	0.040~0.412	0.019	0.342	0.156 to 0.505	< 0.001
Extent of stenosis	0.336	0.149 to 0.499	< 0.001	0.431	0.256~0.578	< 0.001
IPN score	0.437	0.263 to 0.584	< 0.001	0.450	0.278 to 0.594	< 0.001

hemorrhage [15]. Since the formation of atherosclerotic plaques is associated with abnormal lipid levels and their stability is related to revascularization, this study aims to establish a link between lipid levels and plaque stability by investigating the relationship between lipid-related indicators and revascularization.

The results of this study showed that the maximum and total thickness of carotid plaque was significantly greater in the plaque instability group than in the stable group and that

plaque thickness was associated with carotid stenosis, with thicker plaque thickness indicating greater stenosis in the carotid artery. The higher the plaque instability, the higher the likelihood of its detachment from the carotid artery wall, and the higher the likelihood of blockage of other vessels.

Plaque instability is high, the possibility of detachment from the carotid artery wall, and the greater the possibility of other vascular blockages. The results of CEUS examination showed that the IPN grade was mainly grade III and

IV in the unstable group and grade II in the stable group, and the IPN score was significantly higher in the unstable group than in the stable group, indicating that more intraplaque angiogenesis was observed in the unstable group. Previous studies have suggested [16, 17] that the degree of carotid artery stenosis is related to the biological characteristics of plaques, and patients in the unstable group have a high IPN grade, which may indicate the degree of carotid plaque stenosis in patients in the unstable group. Plaque stability significantly affects the occurrence of ischemic stroke and other diseases. Due to plaque instability, there is a risk of detachment and rupture at any time. When plaque ruptures and detaches, it falls off from the vessel wall and moves along the blood circulation, resulting in vascular embolism and inducing stroke [18].

The results of this study showed that plasma Lp (a) and Lp-PLA2 levels were significantly higher in the unstable group than in the stable group, and the higher the neovascular grading, the significantly higher the plasma Lp-PLA2 and Lp (a) levels. Lp (a) is a special macromolecular lipoprotein whose main physiological function is to prevent intravascular thrombolysis and pathologically promote atherogenesis, and its plasma level is mainly regulated by genes [19]. Lp (a) levels have a skewed distribution in the population with large individual differences, but the levels are basically stable in the same body and should be concerned when they show pathological increases [20]. Previous studies have shown that Lp (a) is an independent risk factor for diseases such as stroke and coronary heart disease [21]. Plasma Lp (a) levels in patients with instability indicate that high plasma Lp (a) levels indicate plaque instability, while high plaque instability also indicates more plaque angiogenesis, which may be related to the prothrombotic effect of Lp (a), and high levels of Lp (a) promote plaque instability. Previous studies have also confirmed that plaque progression and stability are closely related to IPN, because IPN increases the possibility of plaque rupture and shedding, and vessels are more likely to embolize [22]. Therefore, patients with high plasma Lp (a) levels have increased intraplaque angiogenesis, but also increase plaque instability, resulting in their rupture and shedding, ischemic stroke, and other serious events. Under physiological conditions, hemoglobin in the arterial intima provides nutrition for it. After carotid artery stenosis occurs in patients, the intima media of blood vessels thickens, resulting in local tissue hypoxia and inflammation. Under these stimuli, vascular endothelial growth factor is highly expressed, so new blood vessels are formed [23, 24]. The plasma Lp-PLA2 level can reflect the level of inflammation, which is mainly secreted by macrophages and lymphocytes in atherosclerotic plaques, and its level indicates the level of arterial plaque inflammation and increased plaque angiogenesis [25]. Plaque angiogenesis is one of the evaluation criteria for plaque stability. The degree of angiogenesis in the plaque instability group is higher than that in the stable group. Patients in the plaque instability group had a higher degree of angiogenesis classification than those in the stability group, and their plasma Lp-PLA2 levels were also higher, indicating that patients in the plaque instability group also had significantly higher levels of inflammation

than those in the instability group, establishing a link between plasma Lp-PLA2 levels, plaque stability, plaque angiogenesis, and plaque inflammation levels.

The results of Pearson correlation analysis showed that the plasma levels of Lp (a) and Lp-PLA2 were positively correlated with the maximum plaque thickness, total plaque thickness, and degree of stenosis and angiogenesis, that is, the plasma levels of Lp (a) and Lp-PLA2. The more narrow the plaque thickness, the more likely it was to appear plaque angiogenesis, indicating that the plasma levels of Lp-PLA2 and Lp (a) have certain value for predicting the occurrence of IPN and plaque progression.

In summary, plasma Lp (a) and Lp-PLA2 levels are associated with carotid plaque characteristics and angiogenesis in patients with carotid artery stenosis, and the plaque stability and the related disease progression can be assessed clinically by detecting plasma Lp (a) and Lp-PLA2 levels. The shortcomings of this study are that the limited number of samples, limited to single-center studies, may produce some statistical error on the results, and retrospective analysis cannot draw causal inferences. In addition, plasma Lp (a) levels are regulated by genes, and external factors such as lifestyle habits have little effect on them, so the effect of genetic variation on plasma Lp (a) levels should also be considered. However, this study still established a link between plasma Lp (a) and Lp-PLA2 levels and plaque angiogenesis.

Plasma Lp (a) and Lp-PLA2 levels correlated well with the characteristics of carotid plaques in patients with carotid stenosis and have been reported in several publications. Plasma Lp (a) and Lp-PLA2 can reflect the stability of plaque and may be clinically useful in the treatment and prognosis of patients.

Data Availability

The datasets used and analyzed during the current study are available from the corresponding author on reasonable request.

Conflicts of Interest

The authors declared no conflict of interest.

Authors' Contributions

Chang Sun and Na Xi contributed equally to this work. CS, NX, and XJ are for the study design. ZS, XZ, and XW collected the data. HC and XJ analyzed the data. CS and NX prepared the manuscript. All authors approved the final version of this manuscript.

References

- [1] D. Bos, B. Arshi, Q. van den Bouwhuisen et al., "Atherosclerotic carotid plaque composition and incident stroke and coronary events," *Journal of the American College of Cardiology*, vol. 77, no. 11, pp. 1426–1435, 2021.
- [2] H. Liu, Y. Hua, F. Zhou et al., "Ultrasound assessment of plaque characteristics to predict re-occlusion after surgical treatment of internal carotid artery occlusion," *Ultrasound in Medicine & Biology*, vol. 47, no. 12, pp. 3356–3363, 2021.

- [3] H. Baradaran and A. Gupta, "Carotid vessel wall imaging on CTA," *AJNR. American Journal of Neuroradiology*, vol. 41, no. 3, pp. 380–386, 2020.
- [4] L. E. Mantella, K. N. Colledanchise, M. F. Hetu, S. B. Feinstein, J. Abunassar, and A. M. Johri, "Carotid intraplaque neovascularization predicts coronary artery disease and cardiovascular events," *European Heart Journal Cardiovascular Imaging*, vol. 20, no. 11, pp. 1239–1247, 2019.
- [5] Y. Song, Y. Dang, J. Wang et al., "Carotid intraplaque neovascularization predicts ischemic stroke recurrence in patients with carotid atherosclerosis," *Gerontology*, vol. 67, no. 2, pp. 144–151, 2021.
- [6] A. Y. Jang, S. H. Han, I. S. Sohn, P. C. Oh, and K. K. Koh, "Lipoprotein(a) and cardiovascular diseases-revisited," *Circulation Journal*, vol. 84, no. 6, pp. 867–874, 2020.
- [7] E. M. Ooi, K. L. Ellis, P. Barrett et al., "Lipoprotein(a) and apolipoprotein(a) isoform size: associations with angiographic extent and severity of coronary artery disease, and carotid artery plaque," *Atherosclerosis*, vol. 275, pp. 232–238, 2018.
- [8] V. Kalaivani and A. Jaleel, "Apolipoprotein(a), an enigmatic anti-angiogenic glycoprotein in human plasma: a curse or cure?," *Pharmacological Research*, vol. 158, article 104858, 2020.
- [9] F. Huang, K. Wang, and J. Shen, "Lipoprotein-associated phospholipase A2: the story continues," *Medicinal Research Reviews*, vol. 40, no. 1, pp. 79–134, 2020.
- [10] Y. E. Park, R. Penumathy, P. P. Sun et al., "Platelet-reactive antibodies in patients after ischaemic stroke-an epiphenomenon or a natural protective mechanism," *International Journal of Molecular Sciences*, vol. 21, no. 21, 2020.
- [11] A. F. Schinkel, C. G. Krueger, A. Tellez et al., "Contrast-enhanced ultrasound for imaging vasa vasorum: comparison with histopathology in a swine model of atherosclerosis," *European Journal of Echocardiography*, vol. 11, no. 8, pp. 659–664, 2010.
- [12] Z. Aranyi, A. Csillik, K. Devay, and M. Rosero, "Ultrasonographic demonstration of intraneural neovascularization after penetrating nerve injury," *Muscle & Nerve*, vol. 57, no. 6, pp. 994–999, 2018.
- [13] P. Libby, "The changing landscape of atherosclerosis," *Nature*, vol. 592, no. 7855, pp. 524–533, 2021.
- [14] L. P. Dawson, M. Lum, N. Nerleker, S. J. Nicholls, and J. Layland, "Coronary atherosclerotic plaque regression: JACC state-of-the-art review," *Journal of the American College of Cardiology*, vol. 79, no. 1, pp. 66–82, 2022.
- [15] V. Balaya, U. Metzger, and F. Lecuru, "Ultrasonographic features in the preoperative diagnosis of primitive fallopian tube carcinoma," *Journal de Gynecologie, Obstetrique et Biologie de la Reproduction*, vol. 45, no. 1, pp. 11–20, 2016.
- [16] A. Simeone, A. Carriero, M. Armillotta et al., "Spiral CT angiography in the study of the carotid stenoses," *Journal of Neuroradiology*, vol. 24, no. 1, pp. 18–22, 1997.
- [17] J. M. Mekke, D. Egberts, F. Waissi et al., "Mast cell distribution in human carotid atherosclerotic plaque differs significantly by histological segment," *European Journal of Vascular and Endovascular Surgery*, vol. 62, no. 5, pp. 808–815, 2021.
- [18] A. Assadian, R. Rotter, O. Assadian, C. Senekowitsch, G. W. Haggmuller, and W. Hubl, "Homocysteine and early restenosis after carotid eversion endarterectomy," *European Journal of Vascular and Endovascular Surgery*, vol. 33, no. 2, pp. 144–148, 2007.
- [19] S. Xia, W. Qiu, A. Cai et al., "The association of lipoprotein(a) and intraplaque neovascularization in patients with carotid stenosis: a retrospective study," *BMC Cardiovascular Disorders*, vol. 21, no. 1, p. 285, 2021.
- [20] Y. Kaiser, M. Daghm, E. Tzolos et al., "Association of lipoprotein(a) with atherosclerotic plaque progression," *Journal of the American College of Cardiology*, vol. 79, no. 3, pp. 223–233, 2022.
- [21] L. L. Zhao, G. Su, L. X. Chen et al., "Apolipoprotein E polymorphisms are associated with ischemic stroke susceptibility in a Northwest China Han population," *Bioscience Reports*, vol. 37, no. 6, 2017.
- [22] S. Tsimikas and J. Narula, "Lipoprotein(a) and CT angiography: novel insights into high-risk plaque progression," *Journal of the American College of Cardiology*, vol. 79, no. 3, pp. 234–237, 2022.
- [23] J. Basic, S. Stojkovic, A. Assadian et al., "The relevance of vascular endothelial growth factor, hypoxia inducible factor-1 alpha, and clusterin in carotid plaque instability," *Journal of Stroke and Cerebrovascular Diseases*, vol. 28, no. 6, pp. 1540–1545, 2019.
- [24] J. Ramos-Lopes, R. Varela, R. Pascoal et al., "Phospholipase A2 and ischemic stroke etiology," *The Neurologist*, vol. 26, no. 2, pp. 32–35, 2021.
- [25] A. Bueno, J. R. March, P. Garcia, C. Canibano, A. Ferruelo, and J. L. Fernandez-Casado, "Carotid plaque inflammation assessed by (18)F-FDG PET/CT and Lp-PLA2 is higher in symptomatic patients," *Angiology*, vol. 72, no. 3, pp. 260–267, 2021.

Research Article

Paraoxonase-1 (PON-1) Arylesterase Activity Levels in Patients with Coronary Artery Disease: A Meta-Analysis

Marco Zuin ¹, Alessandro Trentini ², Judit Marsillach ³, Andrea D'Amuri ^{1,4},
Cristina Bosi ¹, Loris Roncon ⁵, Angelina Passaro ^{1,4,6}, Giovanni Zuliani ^{1,4},
Mike Mackness ⁷ and Carlo Cervellati ¹

¹Department of Translational Medicine and for Romagna, University of Ferrara, Via Luigi Borsari 46, 44121 Ferrara, Italy

²Department of Environmental and Prevention Sciences, University of Ferrara, Via Luigi Borsari 46, 44121, Italy

³Medicine (Division of Medical Genetics), University of Washington, Health Sciences Building, Seattle, WA 98195-7720, USA

⁴Medical Department, University Hospital of Ferrara Arcispedale Sant'Anna, Via Aldo Moro 8, 44124 Ferrara, Italy

⁵Department of Cardiology, Santa Maria della Misericordia Hospital, Viale Tre Martiri 140, 45100 Rovigo, Italy

⁶Research and Innovation Section, University Hospital of Ferrara Arcispedale Sant'Anna, Via Aldo Moro 8, 44124 Ferrara, Italy

⁷Avenida Principe De' Espanya, Miami Platja 43892, Tarragona, Spain

Correspondence should be addressed to Alessandro Trentini; alessandro.trentini@unife.it

Received 25 January 2022; Accepted 15 February 2022; Published 10 March 2022

Academic Editor: Simona Pichini

Copyright © 2022 Marco Zuin et al. This is an open access article distributed under the Creative Commons Attribution License, which permits unrestricted use, distribution, and reproduction in any medium, provided the original work is properly cited.

Aim. To review and compare the PON-1 arylesterase activity between coronary artery disease (CAD) and non-CAD patients. **Methods.** Data were obtained by searching MEDLINE and Scopus for all investigations published between January 1, 2000 and March 1, 2021 comparing PON-1 arylesterase activity between CAD and controls. **Results.** Twenty studies, based on 5417 patients, met the inclusion criteria and were included in the analysis. A random effect model revealed that PON-1 arylesterase activity was significantly lower in the CAD group compared to controls (SMD = -0.587, 95%CI = -0.776 to -0.339, $p < 0.0001$, $I^2 = 92.3\%$). In CAD patients, the PON-1 arylesterase activity was significantly higher among CAD patients without diabetes mellitus (DM) compared to those with diabetes (SMD: 0.235, 95% CI: 0.014 to 0.456, $p = 0.03$, $I^2 = 0\%$). **Conclusions.** PON-1 activity is significantly lower in CAD patients, and those without DM presented a significantly higher PON-1 arylesterase activity.

1. Introduction

Coronary artery disease (CAD) remains the leading cause of morbidity and mortality worldwide [1]. Over the last decades, several novel biochemical markers of oxidative stress and related genetic polymorphisms have been identified in patients with CAD [2]. Indeed, free radicals contribute to endothelial dysfunction (ED) and to the oxidation of low-density lipoproteins (LDL), which are both critical pathogenic events of atherosclerosis [3]. Furthermore, it has been widely reported that elevated concentration of several oxidative stress markers is linked with a higher incidence of cardiovascular events [4]. Paraoxonase-1 (PON-1) is an enzyme that has many enzymatic activities, such as lactonase, thiolactonase, arylesterase, and aryldialkylpho-

sphatase (commonly known as paraoxonase). The most important physiological role of PON-1 is the ability to hydrolyse oxidized LDL (ox-LDL) and thereby delay the onset of atherosclerosis [5]. PON-1 is classified as an accessory protein of high-density lipoprotein (HDL) and modulates the capacity of HDL to protect against the atherosclerosis process through antioxidant and anti-inflammatory activities [5]. Previous meta-analyses of the relationship between PON-1 and CAD have concentrated on PON-1 SNP's or PON-1 paraoxonase activity [6–8]. However, some studies have demonstrated that the arylesterase activity of PON-1 was decreased in CAD patients when compared to non-CAD subjects, thus confirming the earlier preclinical evidence [9]. However, to the best of our knowledge, these data have never been analyzed comprehensively. Therefore,

the aim of the present study is to perform a systematic review and meta-analysis comparing the serum/plasma PON-1 activity, measured as arylesterase activity between CAD and non-CAD patients.

2. Materials and Methods

2.1. Study Design and Eligibility Criteria. This study followed the Preferred Reporting Items for Systematic Reviews and Meta-analyses (PRISMA) reporting guideline (Online Resource 1) [10]. Data were obtained searching MEDLINE and Scopus for all investigations published between January 1, 2000 and March 1, 2021 comparing the PON-1 arylesterase activity between CAD and controls.

2.2. Outcomes. The primary outcome was the comparison of PON-1 arylesterase plasma/serum levels between CAD and non-CAD patients, whereas the secondary objective of the analysis was to compare the arylesterase activity in CAD patients with or without diabetes mellitus (DM). Metaregression using as moderator variables age, body mass index (BMI), and the latitude of the study site was also carried out.

2.3. Data Extraction and Quality Assessment. The selection of studies to be included in our analysis was independently conducted by 2 authors (M.Z. and C.C.) in a blinded fashion. Any discrepancies in study selection were resolved by consulting a third author (A.T.). The following MeSH terms were used for the search: “Paraoxonase -1” AND “Coronary artery disease” OR “Coronary Heart disease.” Additionally, all references cited were reviewed to identify further studies that were not included in the abovementioned electronic databases. Studies were considered eligible if they provided data regarding PON-1 activity in both CAD and controls. Conversely, they were excluded from the analysis if (1) they did not provide a comparison between PON-1 arylesterase activity between CAD patients and controls; (2) they were case reports, review articles, abstracts, editorials/letters, randomized controlled trials, and case series with less than 15 participants from the general population or (3) they were not in the English language. Data extraction was independently conducted by 2 authors (M.Z. and C.C.). Discrepancies between reviewers were resolved by consensus. For all studies reviewed, we extracted the number of patients enrolled, the mean age, male gender, mean and standard deviation (SD) of PON-1 activity levels, and prevalence of traditional cardiovascular risk factors among CAD and non-CAD subjects. Newcastle-Ottawa scale (NOS) was used to evaluate the methodology quality of eligible studies [11].

2.4. Data Synthesis and Analysis. Continuous variables were expressed as mean \pm (SD) or as median with corresponding interquartile range while categorical variables were expressed as counts and percentages. The difference of PON-1 arylesterase activity level between CAD and controls was expressed as standardized mean difference (SMD) with the corresponding 95% confidence interval (CI) using a random-effect model (DerSimonian-Laird). A $I^2 = 0$ was considered to indicate no heterogeneity while values of I^2 as <25%, 25–75%, and above 75% indicate low, moderate,

and high degrees of heterogeneity, respectively [12]. When significant publication bias was found, we used the trim-and-fill method to adjust our results. To evaluate publication bias both funnel plot and Egger’s test were computed. To further appraise the impact of potential baseline confounders, a metaregression analysis using age, body mass index (BMI), gender, HDL-C, and the latitude of the study site as moderator variables was performed. A further subanalysis was also performed to assess any difference in PON-1 arylesterase activity among Asian and European populations from the reviewed studies. The meta-analysis was conducted using Comprehensive Meta-Analysis software, version 3 (Biostat, USA).

3. Results

3.1. Search Results and Included Studies. A total of 804 articles were obtained with our search strategy. After excluding duplicates and preliminary screening, 372 full-text articles were assessed for eligibility, and 352 studies were excluded for not meeting the inclusion criteria, leaving 20 investigations fulfilling the inclusion criteria (Figure 1) [9, 13–30].

3.2. Characteristics of the Population and Quality Assessment. Overall, 5 417 patients (3 364 with CAD and 2 053 without CAD) were included in the analysis. The general characteristics of the studies included were the relative demographic, biometrical, and lipid profiles shown in Table 1. Quality assessment showed that all studies were of moderate-high quality according to the NOS scale (Online Resource 2).

3.3. PON-1 Arylesterase Activity in Patients with Coronary Artery Disease. A random effect model revealed that PON-1 arylesterase activity was significantly lower in the CAD group compared to controls (SMD = -0.587 , 95%CI = -0.776 to -0.339 , $p < 0.0001$, $I^2 = 92.3\%$) (Figure 2). Egger’s tests ($t = 4.286$, $p = 0.003$) showed evidence of potential publication bias. Therefore, a trim-and-fill analysis was performed to explore whether the publication bias influenced the stability of the results in this meta-analysis (two studies trimmed). The updated result showed a SMD = -0.881 (95% CI -1.139 to -0.624 , $p < 0.0001$). The relative funnel plot is showed in Supplementary file 3 (Panel A).

A subgroup analysis was performed in order to estimate the possible existence of a difference in PON-1 arylesterase activity in CAD patients having or not having DM; PON-1 arylesterase activity was significantly higher among CAD patients without DM compared to those with diabetes (SMD: 0.235 , 95% CI: 0.014 to 0.456 , $p = 0.03$, $I^2 = 0\%$) (Figure 3). In this case, Egger’s test revealed no evidence of publication bias ($t = 0.115$, $p = 0.927$). The relative funnel plot is presented in Online Resource 3, panel B.

3.4. PON-1 Arylesterase Activity in Patients with Coronary Artery Disease by Geographical Area. Using a random effect model, a further subanalysis revealed that PON-1 arylesterase activity remained significant lower in patients with CAD both in Asian (SMD: -0.558 , 95% CI: -0.917 to -0.200 , $p = 0.002$, $I^2 = 91\%$) and European (SMD: -0.298 ,

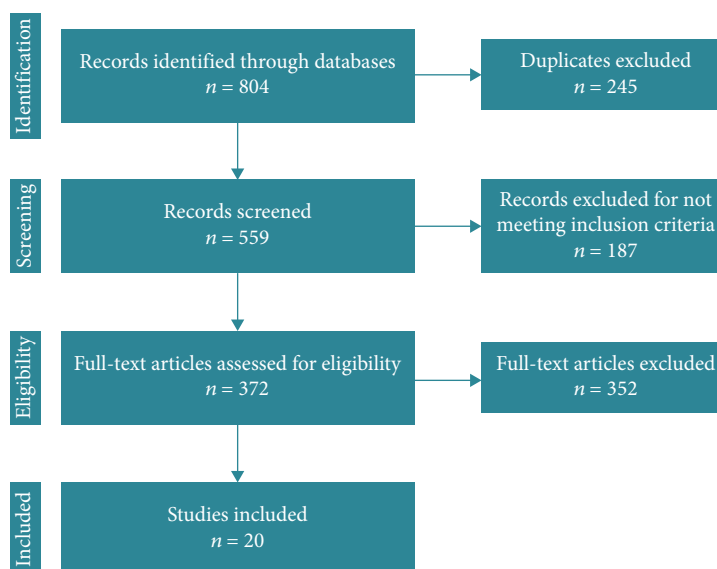


FIGURE 1: PRISMA flow chart.

95% CI: -0.497 to -0.015, $p = 0.003$, $I^2 = 90\%$) populations (forest plot shown in Online Resource 4). Although the diabetes status of patients enrolled was not systematically evaluated, from those studies that did record diabetes status, the prevalence of diabetes was higher amongst CHD patients. Notably, Asian patients with CHD were more frequently diabetic than their European counterparts (47.0% vs. 32.3%).

3.5. Metaregression. In metaregression analysis, no correlation was found between either SMD and age ($p = 0.13$), BMI ($p = 0.09$), gender ($p = 0.24$), and latitude of the study site ($p = 0.80$), while an inverse association was found using HDL-C levels ($p = 0.004$) and statin treatment ($p = 0.003$) as moderators (Table 2).

4. Discussion

The present meta-analysis revealed a significant decrease in PON-1 arylesterase activity in CAD patients compared to controls. For the first time, our results provide a comprehensive and updated evaluation of PON-1 arylesterase activity in CAD patients, reviewing all the available studies published over the last twenty years. Indeed, several investigations have been previously focused on the relationship between PON-1 single nucleotide polymorphisms (SNPs) and cardiovascular disease (CVD) [31–33], including CAD [7]. However, the results reported in these studies were highly variable, with some of them revealing either a significant or a nonsignificant association between genetic variants and disease occurrence. The most common SNPs of this HDL-associated protein (Q192R and L155M), mostly influence the so-called paraoxonase activity, are responsible for hydrolysis of certain organophosphate compounds. Indeed, the high interindividual variability of this activity is essentially due to the effect of these genetic variants. On the other hand, arylesterase, although not being the physiological activity, has been found to more properly

reflect the antiatherosclerotic properties of PON-1 [34]. This activity is by far the most frequently assessed in epidemiological-clinical studies also because of its lower interindividual variability.

Despite intense research on the topic, the biology and biochemistry of PON-1 are still poorly understood. Indeed, the physiological substrate has not been definitively ascertained; although, the most recent in vitro evidence points to endogenous lipophilic lactones such as those resulting from fatty acid oxidation (e.g., 5,6-dihydroxy-trienoic acid and 1,5-lactone). Unfortunately, at the current state of the art, a universally accepted assay to measure the (putative) native lactonase activity has not yet been validated, making a meta-analysis on this PON-1 activity unfeasible. The cause/effect relationship between PON-1 and CAD (along with other diseases) is also unclear. The enzyme structure and activity are highly susceptible of oxidative and glycation modification. Thus, the decrease in PON-1 observed in diabetic CAD patients compared to nondiabetic could be both a downstream and upstream event linked to either glycation or oxidative stresses that characterize the metabolic disease. The interest in the biological role of PON-1 was sparked by converging in vivo and in vitro evidence suggesting that this protein is able to protect lipid moiety of cell membranes and LDL from oxidation [35–37]. Mackness and colleagues were the first to demonstrate that PON-1 could prevent the accumulation of lipid peroxides in low-density lipoproteins (LDL) [38]. Afterwards, studies on transgenic mice confirmed and extended these findings. PON-1 knockout mice showed increased serum and arterial macrophage oxidative stress and an increase in atherosclerotic lesions compared to controls; moreover, the addition of PON-1 to macrophages significantly improved their redox imbalance [37].

These compelling preclinical findings provide the rationale of the cross-sectional studies included in our analysis, as well as of longitudinal studies investigating the link of

TABLE 1: General characteristics of the population enrolled.

Author	Study type	Country	CAD, N (% male)	Mean age (years)		BMI (kg/m ²)		TC mmol/L [mg/dl]		C-HDL mmol/L [mg/dl]		TG mmol/L [mg/dl]		
				CAD	Non-CAD	CAD	Non-CAD	CAD	Non-CAD	CAD	Non-CAD	CAD	Non-CAD	CAD
Sun et al. [9]	Case-control	China	130 (50)	47 (53)	67.0 ± 11.0	65.6 ± 11.0	21.3 ± 2.1	20.4 ± 14	4.54 ± 1.28	4.55 ± 0.9	1.15 ± 0.33	1.28 ± 0.31	1.45 ± 0.81	1.32 ± 0.68
Fridman et al. [13]	Case-control	Argentina	286 (37)	245 (34)	63.4 ± 1.5	60.0 ± 1.3	NR	NR	5.18 ± 0.15	5.10 ± 0.08	1.58 ± 0.03	1.65 ± 0.03*	2.00 ± 0.16	1.62 ± 0.09*
Jayakumari et al. [24]	Case-control	India	284 (100)	245 (100)	51.0 ± 6.9	44.0 ± 10.2	NR	NR	[206 ± 42]	[220 ± 44]	[33 ± 7.7]	[42 ± 9.5]	[164 ± 72]	[141 ± 68]*
Mohamed et al. [25]	Retrospective cohort	Egypt	150 (79)	50 (52)	55.5 ± 8.1	50.7 ± 9.5	NR	NR	[240.5 ± 27.4]	[185.9 ± 8.4]*	[42.1 ± 4.2]	[54.7 ± 3.2]*	[175.7 ± 13.9]	[132.0 ± 14.4]*
Shekhanawa et al. [26]	Cross-sectional	India	60 (67)	50 (58)	NR	NR	NR	NR	[222.6 ± 49.5]	[154 ± 32.7]	NR	NR	[206.157.6]	[123.0 ± 32.6]
Shen et al. [27]	Cross-sectional	China	144 (75)	69 (75)	64.8 ± 10.3	65.3 ± 9.1	25.5 ± 3.4	24.9 ± 3.1	4.3 ± 1.2	4.4 ± 1.0	1.01 ± 0.24	1.13 ± 0.22	1.82 ± 1.09	1.75 ± 0.96
Kuchta et al. [28]	Cross-sectional	Poland	105 (39)	45 (44)	65 ± 10	63 ± 10	28 ± 5	27 ± 4	[168 ± 41]	[196 ± 40]	[44 ± 11]	[52 ± 13]	107 (SD NR)	102 (SD NR)
Januszek et al. [29]	Case-control	Poland	53 (100)	53 (100)	51.3 ± 7.8	42.03 ± 4.82**	29.4 ± 4.9	29.2 ± 3.8	6.02 ± 0.81	5.81 ± 0.95*	1.29 ± 0.34	1.32 ± 0.41	2.11 ± 1.05	2.01 ± 1.42
Sun et al. [9]	Case-control	China	123 (63)	63 (44)	69.7 ± 11.3	62.7 ± 10.7*	NR	NR	4.08 ± 1.07	4.50 ± 0.99*	1.06 ± 0.32	1.14 ± 0.27*	1.56 ± 0.38	1.69 ± 1.27
Variji et al. [30]	Case-control	Iran	126 (66)	203 (52)	63.4 ± 1.5	60.0 ± 1.3	NR	NR	5.18 ± 0.15	5.10 ± 0.08	1.52 ± 0.03	1.65 ± 0.03*	2.00 ± 0.16	1.62 ± 0.09*
van Himbergen et al. [14]	Case-cohort	Netherlands	211 (NR)	1527 (NR)	61 ± 6	57 ± 5**	26.8 ± 3.9	25.8 ± 3.1**	NR	NR	1.4 ± 0.3	1.6 ± 0.4**	NR	NR
Lu et al. [15]	Case-control													
No DM cohort	-	China	88 (66)	90 (57)	55.6 ± 13.8	57.3 ± 8.6	NR	NR	4.85 ± 1.22	4.42 ± 1.21*	1.19 ± 0.29	1.41 ± 0.38*	1.90 ± 0.92	1.78 ± 1.01
IFG cohort	-	China	62 (100)	90 (57)	57.7 ± 11.4	57.3 ± 8.6	NR	NR	5.26 ± 1.25	4.42 ± 1.21*	1.15 ± 0.35	1.41 ± 0.38*	2.07 ± 0.99	1.78 ± 1.01
DM cohort	-	China	46 (57)	90 (57)	60.9 ± 11.5	57.3 ± 8.6	NR	NR	5.76 ± 2.11	4.42 ± 1.21*	1.10 ± 0.1	1.41 ± 0.38*	2.26 ± 1.23	1.78 ± 1.01
Ferrè et al. [16]	Case-control	Spain	215 (100)	215 (100)	60.6 ± 11.8	62.1 ± 16.4	27.1 ± 4.2	26.2 ± 3.5	5.74 ± 1.10*	5.27 ± 1.2*	1.11 ± 0.35	1.23 ± 0.42*	1.97 ± 1.12	1.52 ± 0.91*
Wang et al. [17]	Case-control	China	474 (100)	475 (100)	54.1 ± 8.9	53.8 ± 10.2	26.6 ± 2.9	24.2 ± 3.1	5.16 ± 1007	5.06 ± 0.94	1.06 ± 0.23	1.24 ± 0.30*	1.73 ± 1.13	1.46 ± 1.0
Kerkeni et al. [18]	Case-control	Spain	100 (74)	120 (73)	59 ± 10	54 ± 10	28 ± 5	27.6 ± 5	4.94 ± 1.11	4.20 ± 1.03**	0.73 ± 0.13	0.90 ± 0.24**	1.49 ± 1.18	1.19 ± 0.68
Rodriguez-Esparragón et al. [19]	Case-control	Spain	304 (78)	315 (74)	56 ± 10	54.5 ± 16	27.2 ± 3.7	27.3 ± 3.8	5.2 ± 1.1	6.1 ± 1.0**	0.92 ± 0.24	1.3 ± 0.32**	1.24 ± 0.67	1.52 ± 0.7*
James et al. [20]	Cross-sectional	Swiss	137 (76)	273 (64)	62.8 ± 9.6	59.0 ± 0.5**	27.5 ± 4.1	27.9 ± 4.6	6.0 ± 1.1	5.9 ± 1.1	1.18 ± 0.6	1.3 ± 0.48	1.85 ± 0.9	1.7 ± 1.1

TABLE 1: Continued.

Author	Study type	Country	CAD, N (% male)	Non CAD, N (% male)	Mean age (years)		BMI (kg/m ²)		TC mmol/L [mg/dl]		C-HDL mmol/L [mg/dl]		TG mmol/L [mg/dl]	
					CAD	Non-CAD	CAD	Non-CAD	CAD	Non-CAD	CAD	Non-CAD	CAD	Non-CAD
Itahara et al. [21]	Case-control	Japan	96 (59)	136 (52)	65 ± 11	63 ± 6	21.0 ± 3.1	22.7 ± 2.7**	[146 ± 36]	[208 ± 32]**	[**]	[60 ± 14]**	[106 ± 13]	[116 ± 64]
Rahmani et al. [22]	Cross-sectional													
DM cohort	—	Iran	89 (57)	73 (52)	56 ± 7.5	54.6 ± 7.7	27.3 ± 3.5	27.1 ± 4.3	[213 ± 38]	[196 ± 45]*	[48 ± 13]	[51 ± 13]	[209 ± 187]	[150 ± 163]
No DM cohort	—		89 (57)	73 (52)	56.7 ± 7.0	54.6 ± 7.7	25.9 ± 4.0	27.1 ± 4.3*	[205 ± 44]	[196 ± 45]	[48 ± 15]	[52 ± 13]	[173 ± 137]	[150 ± 163]
Suehiro et al. [23]	Case-control	Japan	81 (62)	103 (52)	64 ± 11	63 ± 11	21.2 ± 3.0	22.5 ± 2.0*	[149 ± 38]	[206 ± 31]*	[40 ± 13]	[58 ± 13]**	[106 ± +60]	[115 ± 67]**

CAD: coronary artery disease; BMI: body mass index; TC: total cholesterol; HDL: high-density lipoproteins; TG: triglycerides; DM: diabetes mellitus; IFG: impaired fasting glucose. The lipidic profile is presented with the measure's unit used in the original manuscript. **p* < 0.05 vs controls; ***p* < 0.0001 vs. controls.

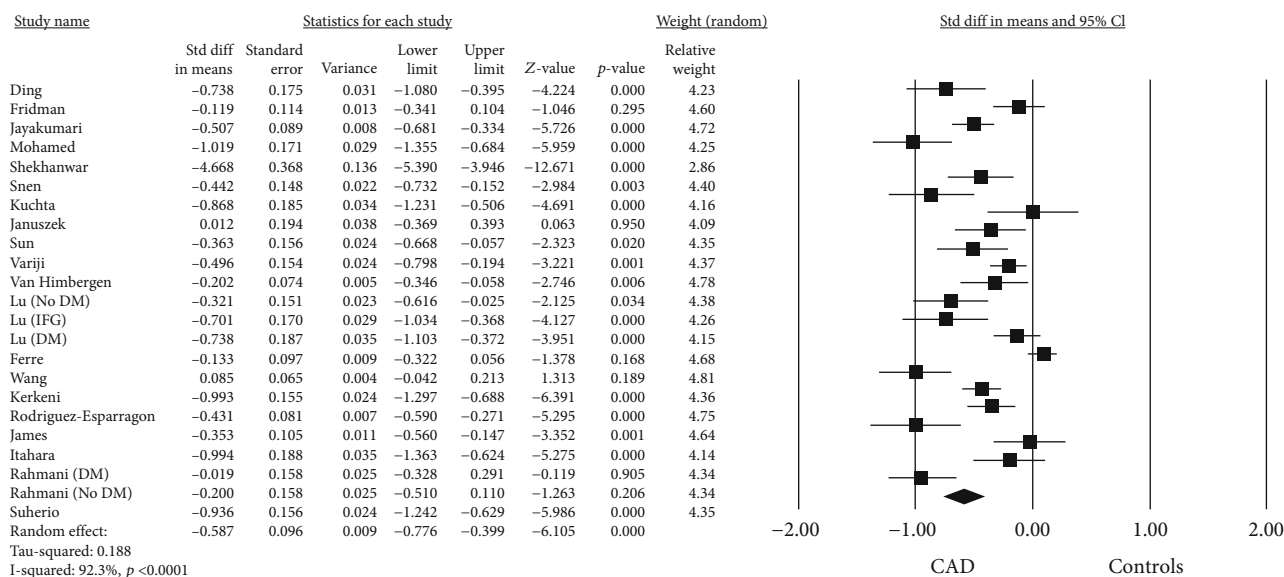


FIGURE 2: Forest plot investigating the PON-1 arylesterase activity in coronary artery disease (CAD) patients and controls.

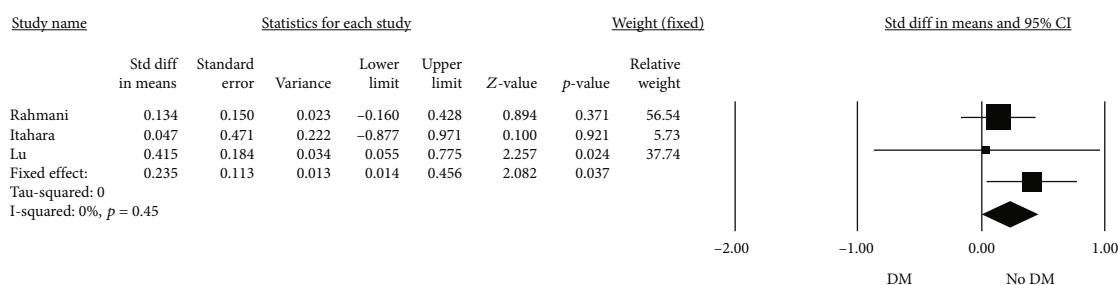


FIGURE 3: Forest plot of the PON-1 arylesterase activity in subjects with diabetes mellitus (DM) or nondiseased (no DM).

TABLE 2: Metaregression analyses.

Item	N° of interaction	β	SE	95% CI	z value	p
Age	22	-0.020	0.013	-0.047 to 0.006	-1.48	0.137
BMI	14	0.064	0.380	-0.010 to 0.139	1.68	0.092
Latitude	14	-0.003	0.012	-0.027 to 0.021	-0.25	0.805
Gender (females)	22	-0.0101	0.008	-0.271 to 0.007	-1.16	0.247
HDL-C	21	-1.913	0.670	-3.226 to -0.599	-2.85	0.004
Statin treatment	8	-1.958	0.702	-3.465 to -0.574	-2.91	0.003

β : standardized regression coefficient; SE: standard error; 95% CI: 95% confidence interval.

arylesterase and/or paraoxonase activity with CVD risk. To the best of our knowledge, the largest longitudinal study (PREVEND study, mean follow-up = 9.3 years) in this field found an approximately log-linear inverse association between the two variables, which was partly dependent on HDL-C levels [39]. This result is not surprising, since PON-1 is mostly bound to HDL particles, and PON-1 activity is strongly correlated to the level of cholesterol carried by the lipoprotein. As also confirmed by the outcome of the significant inverse association between HDL-C and PON-1 revealed by the meta-regression analysis, the level of the former marker should be always considered as potential confounding factor in all clinical studies dealing with

PON-1. The authors of PREVEND study also performed a meta-analysis, including two other studies. This further analysis showed that PON-1 arylesterase did not provide significant improvement in CVD risk assessment beyond conventional CVD risk factors [6]. However, it should be noted that the definition of CV risk encompasses several underlying acute and/or chronic conditions, which are influenced by other modifiable and nonmodifiable determinants. In this regard, our analysis specifically focused on CAD, which represents the primary cause of mortality worldwide.

Our meta-regression suggests that, besides HDL-C (or other surrogate markers of HDL concentration, such as Apo A1), statin use should also be considered in the

multivariate analysis on the link between PON-1 and CAD occurrence. This outcome agrees with a recent meta-analysis showing that statin therapy may have a positive effect in improving both PON-1 paraoxonase and arylesterase activities, either in single-arm studies or controlled trials [39]. To explain this finding, the authors hypothesized that these cholesterol lowering drugs may enhance PON-1 protein synthesis and secretion or interaction with HDL [40]. Conversely, no association with BMI, age, or gender was observed. These findings might reflect the characteristics of the subjects enrolled in the reviewed studies. Indeed, most of the patients were mid-age individuals, and BMI was not systematically reported, probably underestimating the potential effects of such variables. Indeed, to really assess the role of age in the association between PON-1 and CAD, it would be useful to include in the cohorts also younger subjects, to really assess the trend of the interaction over the decades, starting when CAD patients typically become symptomatic [41].

Serum evaluation of PON-1 may represent a useful adjunctive tool in different clinical scenarios. First, it could be used to early identify young patients with subclinical atherosclerosis, thus integrating the traditional cardiovascular risk assessment based on the lipid profile evaluation, blood pressure measurement, and intima media-thickness assessment. Second, it might be evaluated in secondary CV prevention, demonstrating the possible antioxidant effects of statins against lipid peroxidation via lipid-lowering-dependent and -independent mechanisms [42].

4.1. Limitations. Our study has several limitations related to the observational nature of the studies reviewed with all the inherited biases. In fact, the high heterogeneity observed, which probably depends on the participants' inclusion criteria as well as on the study designs, may have resulted in conclusions that are not firm. Furthermore, the presence of publication bias, despite the application of the trim-and-fill method, may have also confounded the results. In addition, most of the studies considered in the analysis lacked information regarding the use of statins and other drugs, which have been suggested to influence PON-1 expression and activity. This is an important point, since it has been shown that different types of statins may exert different effects on PON-1 expression/activity [45]. Finally, the number of studies reporting data about CAD patients with concomitant DM is limited, and this may have affected the reliability of the findings on this subtopic.

5. Conclusion

Despite the acknowledged limitations, our findings clearly suggest that patients suffering from CAD have a decreased PON-1 arylesterase. Further research efforts are required to ascertain whether change of this activity may precede and thus predict disease occurrence.

Data Availability

Data sharing is not applicable to this article as no new data were created.

Conflicts of Interest

The authors declared no potential conflicts of interest with respect to the research, authorship, and/or publication of this article.

Acknowledgments

We thank Dr. Valentina Rosta for her support in statistical analysis.

Supplementary Materials

Supplementary file 1: PRISMA statement checklist. Supplementary File 2: quality of the included studies assessed using the Newcastle-Ottawa quality assessment scale (NOS). Supplementary File 3: funnel plots for PON-1 arylesterase activity in patients with coronary artery disease (CAD) in the presence or absence of diabetes. (a) Funnel plot for subjects with/without CAD. (b) Funnel plot for subjects with CAD but with/without diabetes. Supplementary file 4: forest plot analysis for CAD patients divided by geographical area. (a) Asian subjects. (b) European subjects. (*Supplementary Materials*)

References

- [1] E. Oikonomou, G. Siasos, V. Tsigkou et al., "Coronary artery disease and endothelial dysfunction: novel diagnostic and therapeutic approaches," *Current Medicinal Chemistry*, vol. 27, no. 7, pp. 1052–1080, 2020.
- [2] M. C. Izar, F. A. H. Fonseca, S. S. M. Ihara et al., "Risk factors, biochemical markers, and genetic polymorphisms in early coronary artery disease," *Arquivos Brasileiros de Cardiologia*, vol. 80, no. 4, pp. 379–395, 2003.
- [3] C. Vassalle, L. Petrozzi, N. Botto, M. G. Andreassi, and G. C. Zucchelli, "Oxidative stress and its association with coronary artery disease and different atherogenic risk factors," *Journal of Internal Medicine*, vol. 256, no. 4, pp. 308–315, 2004.
- [4] M. K. Misra, M. Sarwat, P. Bhakuni, R. Tuteja, and N. Tuteja, "Oxidative stress and ischemic myocardial syndromes," *Medical Science Monitor : International Medical Journal of Experimental and Clinical Research*, vol. 15, no. 10, pp. - RA209–RA219, 2009.
- [5] B. Mackness, M. I. Mackness, S. Arrol, W. Turkie, and P. N. Durrington, "Effect of the human serum paraoxonase 55 and 192 genetic polymorphisms on the protection by high density lipoprotein against low density lipoprotein oxidative modification," *FEBS Letters*, vol. 423, no. 1, pp. 57–60, 1998.
- [6] S. K. Kunutsor, S. J. L. Bakker, R. W. James, and R. P. F. Dullaart, "Serum paraoxonase-1 activity and risk of incident cardiovascular disease: the PREVEND study and meta-analysis of prospective population studies," *Atherosclerosis*, vol. 245, pp. 143–154, 2016.
- [7] S. Ashiq and K. Ashiq, "The role of paraoxonase 1 (PON1) gene polymorphisms in coronary artery disease: a systematic review and meta-analysis," *Biochemical Genetics*, vol. 59, no. 4, pp. 919–939, 2021.
- [8] M. Wang, X. Lang, L. Zou, S. Huang, and Z. Xu, "Four genetic polymorphisms of paraoxonase gene and risk of coronary

- heart disease: a meta-analysis based on 88 case-control studies," *Atherosclerosis*, vol. 214, no. 2, pp. 377–385, 2011.
- [9] T. Sun, J. Hu, Z. Yin et al., "Low serum paraoxonase1 activity levels predict coronary artery disease severity," *Oncotarget*, vol. 8, no. 12, pp. 19443–19454, 2017.
 - [10] D. Moher, A. Liberati, J. Tetzlaff, D. G. Altman, and The PRISMA Group, "Preferred reporting items for systematic reviews and meta-analyses: the PRISMA Statement," *PLoS Medicine*, vol. 6, no. 7, article e1000097, 2009.
 - [11] G. Wells, B. Shea, D. O'Connell et al., *The Newcastle-Ottawa Scale (NOS) for assessing the quality of nonrandomised studies in meta-analyses*, Ottawa Hospital Research Institute, 2011, http://www.ohri.ca/programs/clinical_epidemiology/oxford.asp.
 - [12] J. P. T. Higgins, S. G. Thompson, J. J. Deeks, and D. G. Altman, "Measuring inconsistency in meta-analyses," *BMJ*, vol. 327, no. 7414, pp. 557–560, 2003.
 - [13] O. Fridman, L. Gariglio, S. Riviere, R. Porcile, A. Fuchs, and M. Potenzoni, "Paraoxonase 1 gene polymorphisms and enzyme activities in coronary artery disease and its relationship to serum lipids and glycemia," *Archivos de Cardiología de México*, vol. 86, no. 4, pp. 350–357, 2016.
 - [14] T. M. van Himbergen, Y. T. van der Schouw, H. A. M. Voorbij et al., "Paraoxonase (PON1) and the risk for coronary heart disease and myocardial infarction in a general population of Dutch women," *Atherosclerosis*, vol. 199, no. 2, pp. 408–414, 2008.
 - [15] C. Lu, Y. Gao, H. Zhou, and H. Tian, "The relationships between PON1 activity as well as oxLDL levels and coronary artery lesions in CHD patients with diabetes mellitus or impaired fasting glucose," *Coronary Artery Disease*, vol. 19, no. 8, pp. 565–573, 2008.
 - [16] N. Ferré, M. Tous, A. Paul et al., "Paraoxonase Gln-Arg(192) and Leu-Met(55) gene polymorphisms and enzyme activity in a population with a low rate of coronary heart disease," *Clinical Biochemistry*, vol. 35, no. 3, pp. 197–203, 2002.
 - [17] X. Wang, Z. Fan, J. Huang et al., "Extensive association analysis between polymorphisms of PON gene cluster with coronary heart disease in Chinese Han population," *Arteriosclerosis, Thrombosis, and Vascular Biology*, vol. 23, no. 2, pp. 328–334, 2003.
 - [18] M. Kerkeni, F. Addad, M. Chauffert et al., "Hyperhomocysteinemia, paraoxonase activity and risk of coronary artery disease," *Clinical Biochemistry*, vol. 39, no. 8, pp. 821–825, 2006.
 - [19] F. Rodríguez-Esparragón, J. C. Rodríguez-Pérez, Y. Hernández-Trujillo et al., "Allelic variants of the human scavenger receptor class B type 1 and paraoxonase 1 on coronary heart disease," *Arteriosclerosis, Thrombosis, and Vascular Biology*, vol. 25, no. 4, pp. 854–860, 2005.
 - [20] R. W. James, I. Leviev, J. Ruiz, P. Passa, P. Froguel, and M. C. Garin, "Promoter polymorphism T(-107)C of the paraoxonase PON1 gene is a risk factor for coronary heart disease in type 2 diabetic patients," *Diabetes*, vol. 49, no. 8, pp. 1390–1393, 2000.
 - [21] T. Itahara, T. Suehiro, Y. Ikeda et al., "Serum paraoxonase and arylesterase activities in hemodialysis patients," *Journal of Atherosclerosis and Thrombosis*, vol. 7, no. 3, pp. 152–158, 2000.
 - [22] M. Rahmani, F. Raiszadeh, S. Allahverdian, S. Kiaii, M. Navab, and F. Azizi, "Coronary artery disease is associated with the ratio of apolipoprotein A-I/B and serum concentration of apolipoprotein B, but not with paraoxonase enzyme activity in Iranian subjects," *Atherosclerosis*, vol. 162, no. 2, pp. 381–389, 2002.
 - [23] T. Suehiro, Y. Ikeda, T. Shiinoki et al., "Serum paraoxonase (PON1) concentration in patients undergoing hemodialysis," *Journal of Atherosclerosis and Thrombosis*, vol. 9, no. 3, pp. 133–138, 2002.
 - [24] N. Jayakumari and G. Thejaseebai, "High prevalence of low serum paraoxonase-1 in subjects with coronary artery disease," *Journal of Clinical Biochemistry and Nutrition*, vol. 45, no. 3, pp. 278–284, 2009.
 - [25] R. H. Mohamed, R. H. Mohamed, R. A. Karam, and T. A. Abd El-Aziz, "The relationship between paraoxonase1-192 polymorphism and activity with coronary artery disease," *Clinical Biochemistry*, vol. 43, no. 6, pp. 553–558, 2010.
 - [26] M. Shekhanawar, S. M. Shekhanawar, D. Krisnaswamy et al., "The role of 'Paraoxonase-1 activity' as an antioxidant in coronary artery diseases," *Journal of Clinical and Diagnostic Research*, vol. 7, no. 7, pp. 1284–1287, 2013.
 - [27] Y. Shen, F. H. Ding, J. T. Sun et al., "Association of elevated apoA-I glycation and reduced HDL-associated paraoxonase1, 3 activity, and their interaction with angiographic severity of coronary artery disease in patients with type 2 diabetes mellitus," *Cardiovascular Diabetology*, vol. 14, no. 1, p. 52, 2015.
 - [28] A. Kuchta, A. Strzelecki, A. Ćwiklińska et al., "PON-1 activity and plasma 8-isoprostane concentration in patients with angiographically proven coronary artery disease," *Oxidative Medicine and Cellular Longevity*, vol. 2016, 9 pages, 2016.
 - [29] R. Januszek, "Paraoxonase-1 and simvastatin treatment in patients with stable coronary artery disease," *International Journal of Vascular Medicine*, vol. 2016, 10 pages, 2016.
 - [30] A. Variji, Y. Shokri, S. Fallahpour et al., "The combined utility of myeloperoxidase (MPO) and paraoxonase 1 (PON1) as two important HDL-associated enzymes in coronary artery disease: which has a stronger predictive role?," *Atherosclerosis*, vol. 280, pp. 7–13, 2019.
 - [31] C. Godbole, S. Thaker, P. Kerkar, M. Nadkar, N. Gogtay, and U. Thatte, "Association of PON1 gene polymorphisms and enzymatic activity with risk of coronary artery disease," *Future Cardiology*, vol. 17, no. 1, pp. 119–126, 2021.
 - [32] N. Decharatchakul, C. Settasatian, N. Settasatian et al., "Association of combined genetic variations in SOD3, GPX3, PON1, and GSTT1 with hypertension and severity of coronary artery disease," *Heart and Vessels*, vol. 35, no. 7, pp. 918–929, 2020.
 - [33] X. Huo, Y. Guo, Y. Zhang, J. Li, X. Wen, and J. Liu, "Paraoxonase 1 gene (Q192R) polymorphism confers susceptibility to coronary artery disease in type 2 diabetes patients: evidence from case-control studies," *Drug Discoveries & Therapeutics*, vol. 13, no. 2, pp. 80–88, 2019.
 - [34] B. Mackness, G. K. Davies, W. Turkie et al., "Paraoxonase status in coronary heart disease," *Arteriosclerosis, Thrombosis, and Vascular Biology*, vol. 21, no. 9, pp. 1451–1457, 2001.
 - [35] A. Tward, Y.-R. Xia, X.-P. Wang et al., "Decreased atherosclerotic lesion formation in human serum paraoxonase transgenic mice," *Circulation*, vol. 106, no. 4, pp. 484–490, 2002.
 - [36] C. E. Furlong, J. Marsillach, G. P. Jarvik, and L. G. Costa, "Paraoxonases-1, -2 and -3: what are their functions?," *Chemico-Biological Interactions*, vol. 259, Part B, pp. 51–62, 2016.
 - [37] O. Rozenberg, M. Rosenblat, R. Coleman, D. M. Shih, and M. Aviram, "Paraoxonase (PON1) deficiency is associated with increased macrophage oxidative stress: studies in

- PON1-knockout mice,” *Free Radical Biology and Medicine*, vol. 34, no. 6, pp. 774–784, 2003.
- [38] M. I. Mackness, S. Arrol, and P. N. Durrington, “Paraoxonase prevents accumulation of lipoperoxides in low-density lipoprotein,” *FEBS Letters*, vol. 286, no. 1-2, pp. 152–154, 1991.
- [39] G. Ferretti, T. Bacchetti, and A. Sahebkar, “Effect of statin therapy on paraoxonase-1 status: a systematic review and meta-analysis of 25 clinical trials,” *Progress in Lipid Research*, vol. 60, pp. 50–73, 2015.
- [40] E. M. Tuzcu, S. R. Kapadia, E. Tutar et al., “High prevalence of coronary atherosclerosis in asymptomatic teenagers and young adults,” *Circulation*, vol. 103, no. 22, pp. 2705–2710, 2001.
- [41] G. J. Moon, S. J. Kim, Y. H. Cho, S. Ryoo, and O. Y. Bang, “Antioxidant effects of statins in patients with atherosclerotic cerebrovascular disease,” *Journal of Clinical Neurology*, vol. 10, no. 2, pp. 140–147, 2014.
- [42] H. Z. Mirdamadi, F. Sztanek, Z. Derdak, I. Seres, M. Harangi, and G. Paragh, “The human paraoxonase-1 phenotype modifies the effect of statins on paraoxonase activity and lipid parameters,” *British Journal of Clinical Pharmacology*, vol. 66, no. 3, pp. 366–374, 2008.

Research Article

Pyroptosis Patterns Are Involved in Immune Microenvironment Regulation of Dilated Cardiomyopathy

Kexin Wang ¹, Zhan Lv,¹ Chenggang Fang,¹ Chengkai Xu,¹ Zhimin Yu ¹, Liuming Gao,¹ and Yanggan Wang ^{1,2}

¹Department of Internal Medicine, Zhongnan Hospital of Wuhan University, Wuhan, China

²Medical Research Institute of Wuhan University, Wuhan, China

Correspondence should be addressed to Yanggan Wang; 1245054644@qq.com

Received 1 November 2021; Revised 28 December 2021; Accepted 18 January 2022; Published 10 March 2022

Academic Editor: Francesco Busardò

Copyright © 2022 Kexin Wang et al. This is an open access article distributed under the Creative Commons Attribution License, which permits unrestricted use, distribution, and reproduction in any medium, provided the original work is properly cited.

The importance of cell pyroptosis in immunity regulation is becoming increasingly obvious, especially in diseases of the cardiovascular system. Nevertheless, it is unknown whether the pyroptosis signalling pathway is involved in the immune microenvironment regulation of dilated cardiomyopathy (DCM). Therefore, the purpose of the study was to investigate the influence of pyroptosis on the immune environment in dilated cardiomyopathy. We found that expression of 19 pyrolysis-related genes (PRGs) in DCM samples was altered compared to healthy samples. Subsequently, based on these 12 hub pyrolysis-related genes, we developed a classifier that can distinguish between healthy samples and DCM samples. Among the hub pyrolysis-related genes, RT-PCR analyses demonstrated that five of them exhibited significant differential expression in DCM. Interestingly, we observed that immune characteristics are correlated with pyroptosis: higher expression of GSDMD is positively correlated with infiltrating activated pDCs; GSDMD is negatively correlated with Tregs; CASP1 is positively related to parainflammation; and CASP9 is negatively related to the type II IFN response. In addition, distinct pyroptosis-mediated patterns were identified, and immune characteristics under distinct patterns were revealed: pattern B mediates an active immune response, and pattern A leads to a relatively mild immune response to DCM. We also compared the biological functions between these patterns. Compared with pattern A, pattern B had more abundant pathways, such as the NOTCH signalling pathway and pentose phosphate pathway. In summary, this study proves the important influence of pyrolysis on the immune microenvironment of dilated cardiomyopathy and provides new clues for understanding the pathogenesis of dilated cardiomyopathy.

1. Introduction

Dilated cardiomyopathy (DCM) is a very common myocardial disease, and it is estimated that 1 in 250 people is affected [1, 2]. Dilated cardiomyopathy (DCM) is characterized by an enlargement in either the left or both ventricles, accompanied by myocardial hypertrophy and decreased ventricular systolic function that may also include congestive heart failure [3]. DCM progressively worsens and can easily develop into heart failure. Death can occur at any stage of DCM and is the most common indication for heart trans-

plantation. DCM portends a poor prognosis and is one of the major indications for cardiac transplantation [4]. The causes of DCM are heterogeneous and can result from idiopathic, genetic, viral, immune, or toxic aetiology [1]. DCM is caused by a combination of genetic and environmental factors in the myocardium [1, 5]. During the progression of DCM, immune function often becomes disordered, affecting both cellular immunity and humoral immunity. Inflammatory endothelial activation is often present in DCM, with lymphocyte and monocyte infiltration [6–8]. Consequently, it is important to explore the immune molecular pathways

of DCM to understand the pathological mechanisms underlying it; at the same time, these immune targets may inspire ideas for the design of therapeutic strategies in DCM.

Classically, there are three mechanisms of cell death: apoptosis, autophagic cell death, and necrosis. Recent studies have found that caspase-1 in both humans and mice, caspase-4/5 in humans, and caspase-11 in mice mediate a new type of programmed necrosis, pyroptosis [9, 10]. Under the electron microscope, before rupture of the cell plasma membrane, pyrolyzed cells can be seen forming a large number of vesicles, namely, inflammasomes. Then, pores are formed in the cell membrane, which causes subsequent rupture and release of the contents [11]. These are the morphological features of cellular pyroptosis. Pyroptosis is a form of gasdermin-mediated programmed cell necrosis [12, 13]. Pyrolysis is an important natural immune response in the body that plays a significant role in the fight against infection [12]. Recently, extensive findings have indicated that pyroptosis is involved in various diseases, especially cardiovascular diseases (CVDs) [14, 15]. For instance, in atherosclerosis, ischaemia-reperfusion injury, myocardial infarction, coronary calcification, and heart failure, related research results have led to the discovery and application of inhibitors or drugs targeting proteins involved in pyroptosis [16].

Nevertheless, few studies have focused on the mechanisms and pathways related to cell pyroptosis in dilated cardiomyopathy (DCM). Zeng et al. [17] demonstrated that in the mechanism of DCM, the NLRP3 inflammasome plays a critical role by activating caspase-1 and leading to pyroptosis. However, it is unknown whether the pyroptosis pathway is mechanistically related to the immune microenvironment in dilated cardiomyopathy.

In this study, pyroptosis patterns in DCM were systematically investigated. We found that pyroptosis-related genes could differentiate DCM samples from healthy samples. We found that the abundance of infiltrating immune cells and the immune response gene set in DCM exhibited linear pertinence, showing a strong relationship between pyroptosis-related genes and immune regulation. We analysed DCM samples based on 12 pyroptosis-related genes, and 2 distinct pyroptosis patterns were identified. Between these subtypes, we observed different characteristics in immune regulation, and biological functions were compared between these subtypes. In addition, we analysed 2142 pyroptosis-related genes and their biological functions. Our results suggest that cellular pyroptosis patterns make a critical contribution to the immune microenvironment in DCM.

2. Materials and Methods

2.1. Data Preprocessing. We downloaded the GSE141910 dataset (<http://ncbi.nlm.nih.gov/geo/query/acc.cgi?acc=GSE141910>) from the Gene Expression Omnibus (GEO) database, which included 166 healthy samples and 116 DCM samples. All data were preprocessed and obtained using the R package “GEOquery.” The GPL16791 platform file was used for annotation. Gene probes were annotated with gene symbols, and probes that did not match gene sym-

bols or that matched multiple symbols were excluded. We collected 33 PRGs from previous research [18–21].

2.2. Analysis of Changes in PRGs between DCM and Healthy Samples. To explore interactions among the 29 PRGs, we used the Search Tool for the Retrieval of Interacting Genes/Proteins (STRING) database (<http://www.string-db.org/>) to create a protein-protein interaction (PPI) network of these PRGs. We used Spearman correlation analysis to evaluate the expression relationships among 29 PRGs in all samples and specifically in DCM samples, and using the Wilcoxon test, we compared the expression differences of 29 PRGs between healthy and DCM samples. DCM-related PRGs were identified using univariate logistic regression, and the cut-off criterion was a P value < 0.05 . Then, we used least absolute shrinkage and selection operator (LASSO) to improve the accuracy of the linear regression model. We utilized multivariate logistical regression to build a PRG-related DCM classifier. To evaluate the potential performance of the signature, we used receiver operating characteristic (ROC) curve analysis.

2.3. Correlation Analysis between PRGs and Immune Characteristics. We used the “GSVA” package to conduct single-sample gene set enrichment analysis (GSEA) to estimate the scores of infiltrating immune cells and to assess the activity of immune signalling pathways. We used the Wilcoxon test to compare enrichment fractions representing immune cell abundance and immune reactivity in healthy and DCM samples. Pearson correlation analysis was utilized to determine the relevance of PRGs with respect to immune cell components and immune response activity.

2.4. Identification of Pyroptosis Patterns. Based on the expression of 29 PRGs, we chose to analyse the unsupervised clustering state to identify disparate pyroptosis patterns. At the same time, we utilized a consistent clustering algorithm for the purpose of evaluating the clustering number and robustness. During the calculation, the R package “ConsensusClusterPlus” was used to perform iterative calculations. We calculated one step at a time 1000 times to ensure the robustness of the classification [20]. Moreover, to verify the expression pattern of PRGs in various pyroptosis patterns, we chose to use PCA as an analytic method after full consideration. The Kruskal test is a method that compares the degree of expression of PRGs, the score in abundance of infiltrating immunocytes, the score of immune response, and the degree of gene expression in two pyroptosis patterns, which differ widely.

2.5. Biological Enrichment Analysis of Distinct Pyroptosis Modification Patterns. To analyse pyroptosis-related differentially expressed genes, GO (Gene Ontology) functional enrichment and KEGG (Kyoto Encyclopedia of Genes and Genomes) pathway analyses were performed using the clusterProfiler package in R. Two sets of genes, “c5.go.v7.4.-symbols” and “C2.cp.kegg.v7.4. symbols,” were used to reflect changes in biological signalling pathways. Subsequently, the expression matrix was transformed into a score matrix using the GSVA algorithm, and we used the LIMMA

TABLE 1: Primers used for RT-PCRs.

Target genes	Forward primers (5'-3')	Reverse primers (5'-3')
NLRP1	AGCAAGGGTGGAAACAGCATT	ATAGCGGGAACCAAGATAAAGAG
TNF α	CTCTTCTGTCTACTGAACCTCGGG	GGTGGTTTGTGAGTGTGAGGGT
CASP1	GGCTGACAAGATCCTGAGGG	TAGGTCCCGTGCCTTGTC
CASP9	GAGGTGAAGAACGACCTGACTG	CTCAATGGACACGGAGCATC
PRKACA	ATCGTCCTGACCTTTGAGTATCTG	ACAGCCTTGTTGTAGCCTTTGC
GAPDH	CCTCGTCCCGTAGACAAAATG	TGAGGTCAATGAAGGGGTCGT

package to compare scores of biological signalling pathways between the two groups. The threshold of difference analysis was Adj. $P < 0.05$ and $|\text{LogFC}| \geq 1$ or more.

2.6. Identification of Pyroptosis-Mediated Genes. To identify the genes regulating pyroptosis, we used the empirical Bayes method to analyse the samples with two different pyroptosis patterns to identify DEGs between different pyroptosis patterns. The threshold for determining important DEGs was an adjusted P value < 0.0001 . Using weighted gene coexpression network analysis (WGCNA), we obtained the difference between gene modules and pyroptosis pattern-related genes.

2.7. Animal Protocol. Male C57BL/6 mice at 10 weeks of age were obtained from Hubei Provincial Centres for Disease Control and Prevention. All animal studies were conducted according to the Animal Care and Use Committee Guide of Wuhan University, which obeyed the Guide for the Care and Use of Laboratory Animals of the National Institutes of Health. To induce DCM, a cumulative dose of 12 mg/kg doxorubicin (DOX) was administered via 3 weekly IP injections (4 mg/kg on days 0, 7, and 14), and follow-up analyses were conducted 6 weeks after the first injection [17].

2.8. Echocardiography. All animal studies were conducted according to the Animal Care and Use Committee Guide of Wuhan University, which obeyed the Guide for the Care and Use of Laboratory Animals of the National Institutes of Health. Mice were examined using transthoracic echocardiography. Using a Vevo 2100 imaging system equipped with a 30 MHz MS400 linear array, M-mode echocardiography was performed to obtain a short-axis view of the heart at the level of the middle papillary muscle. The left ventricular systolic inner diameter (LVIDs) and left ventricular diastolic inner diameter (LVIDd) were measured in awake mice. The left ventricular ejection fraction (LVEF) was calculated as $\%EF = [(LVIDd - LVIDs)/LVIDd] \times 100$; and fractional shortening (FS) was calculated as $\%FS = [(LVIDd - LVIDs)/LVIDd] \times 100$.

2.9. Histological Analyses. Six weeks after the first injection, the heart tissue was collected, fixed in 4% paraformaldehyde, dehydrated, and embedded in paraffin. Four-micrometre sections were collected and stained using haematoxylin and eosin (HE) and Masson's trichrome. Images were captured

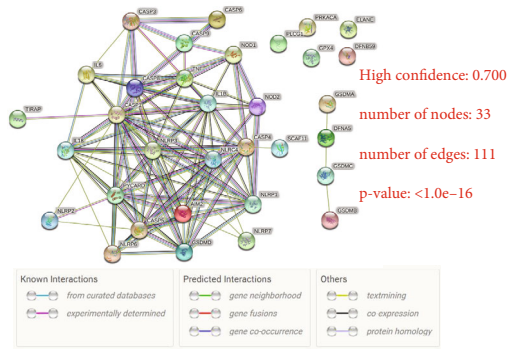
using an Aperio VERSA system (Leica Biosystems, Germany) and analysed using Image-Pro Plus 6.0.

2.10. Real-Time PCR. Total RNA was extracted from apical tissue using TRIzol and reverse transcribed into cDNA, and real-time quantitative PCR was performed. All data are normalized to the GAPDH mRNA level as an internal reference, and the relative quantification of apical tissue mRNA expression was determined using the $2^{-\Delta\Delta CT}$ method. The primers used are shown in Table 1.

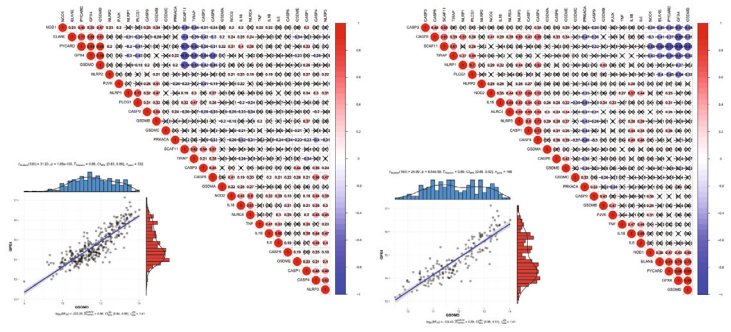
3. Results

3.1. Expression Alterations of PRG in DCM Compared to Healthy Samples. The expression interactions of PRGs are shown in a protein-protein network (Figure 1(a)) with 111 edges and 33 nodes as determined using the STRING database. We observed that with a confidence level of 0.700, apart from PLCG1, GPX4, PRKACA, ELANE, and DFNB89, the rest of the PRGs were very closely connected. In addition, the transcriptome relationship was investigated, and we found that GSDMD and GPX4 were the most relevant PRG regulators in all samples ($r = 0.86$) and in DCM samples ($r = 0.89$), which may indicate that they work together (Figure 1(b)). At the same time, differential expression analysis identified 19 PRGs with altered expression (Figures 1(c) and 1(d)). Among them, compared to normal myocardial tissue, the fold change in TNF was the largest and most significant (Figure 1(e)).

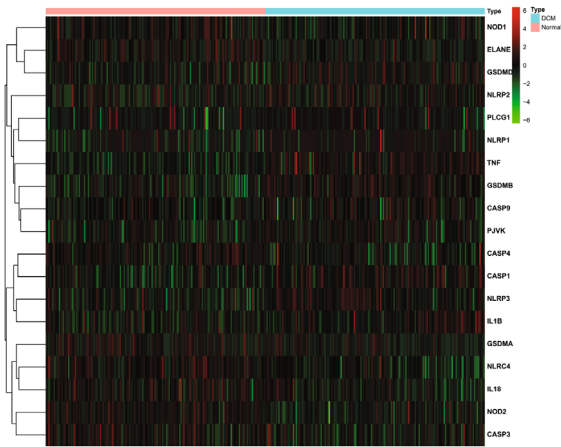
3.2. PRGs Participate in the Process of DCM Generation. To determine the role of PRGs in the DCM pathogenesis, we used several common bioinformatics algorithms. To identify DCM-related PRGs, we used univariate logistic regression, which showed that 21 PRGs were most closely related to DCM (Figure 2(a)). Subsequently, LASSO regression was performed on 21 DCM-related PRGs for feature selection and dimensionality reduction to exclude unimportant regulators (Figures 2(b) and 2(c)), which ultimately identified 12 hub PRGs. We used multivariate logistic regression for a classifier to distinguish between normal and DCM samples (Figure 2(d)). The classifier is composed of hub PRGs, which can well classify both normal and DCM samples based on the risk scores. The risk score of DCM was much higher than that of the normal samples (Figure 2(e)). Moreover, the ROC curve showed that the 12 PRGs could distinguish



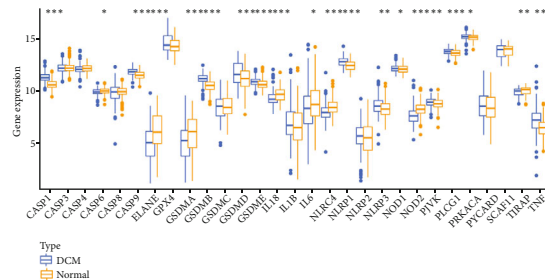
(a)



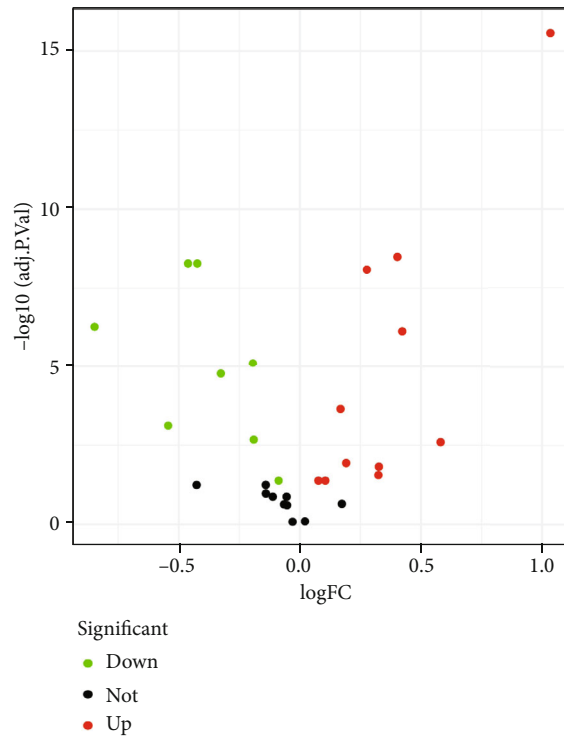
(b)



(c)



(d)



(e)

FIGURE 1: Expression landscape of PRGs in DCM. (a) The protein-protein interactions among PRGs. (b) Interrelationships of the expression of PRGs for all samples (left) and DCM samples (right). The two most interrelated PRGs shown in the two scatter plots: GSDMD and GPX4. (c) The box plot shows the expression of 19 PRGs in DCM compared to healthy samples. (d) The heatmap shows the expression status of 19 PRGs in DCM compared to healthy samples. (e) The volcano plot visually shows the expression of PRGs between healthy and DCM samples.

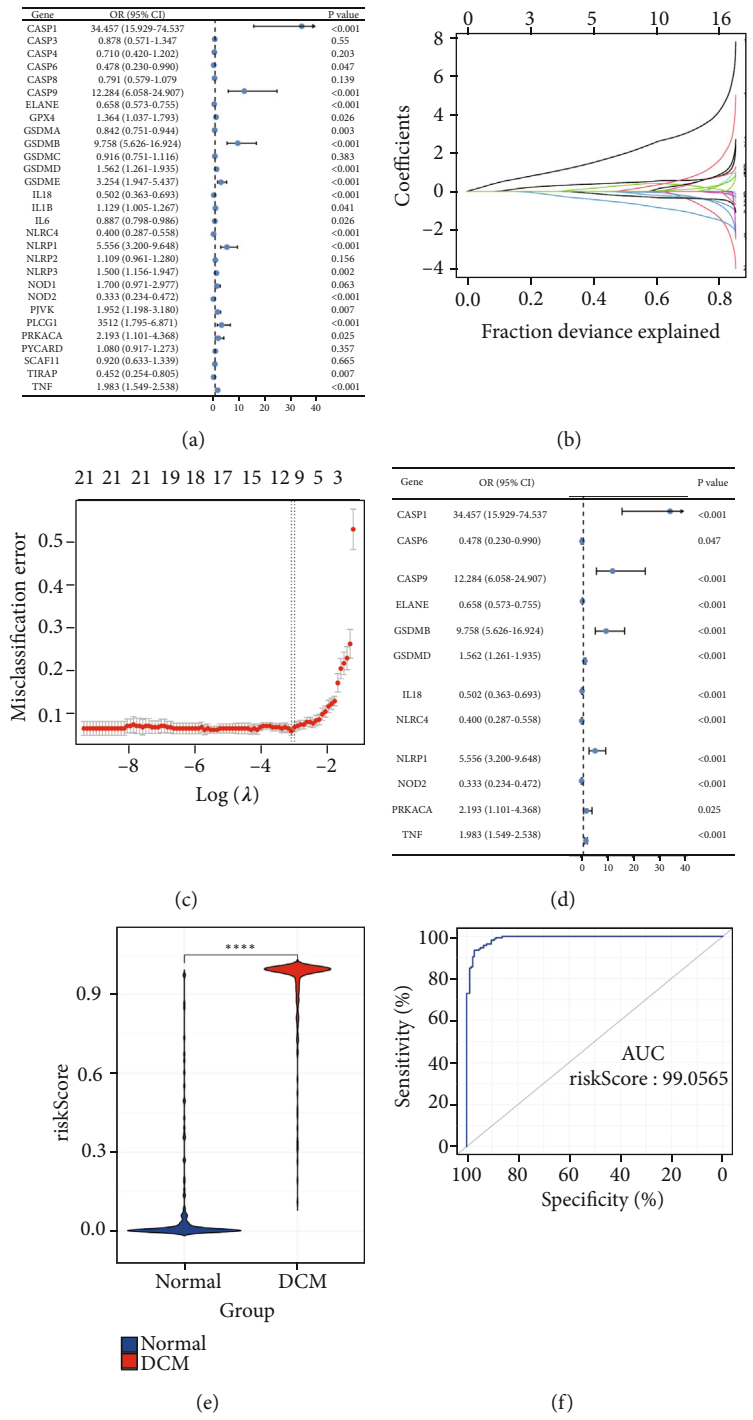


FIGURE 2: PRGs can be used to classify normal and DCM samples. (a) Univariate logistic regression was used to study the correlation between PRGs and DCM ($P < 0.05$) and uncovered 21 DCM-related PRGs. (b) LASSO coefficient distribution of 21 DCM-related PRGs. (c) In LASSO regression, 10-fold cross-validation was used to fine-tune parameter selection. λ is the adjustment parameter, and the partial likelihood deviance is plotted according to $\log(\lambda)$. (d) Through multivariate logistic regression, a distinguishing feature with 12 PRGs was developed, and the risk scores of DCM and healthy samples were estimated. (e) The risk profile between DCM and healthy samples illustrates that the risk score of DCM was higher than that of healthy samples. (f) ROC curves were used to analyse the ability of 12 PRGs to distinguish between healthy and DCM samples, and the AUC value was used to evaluate the distinction ability.

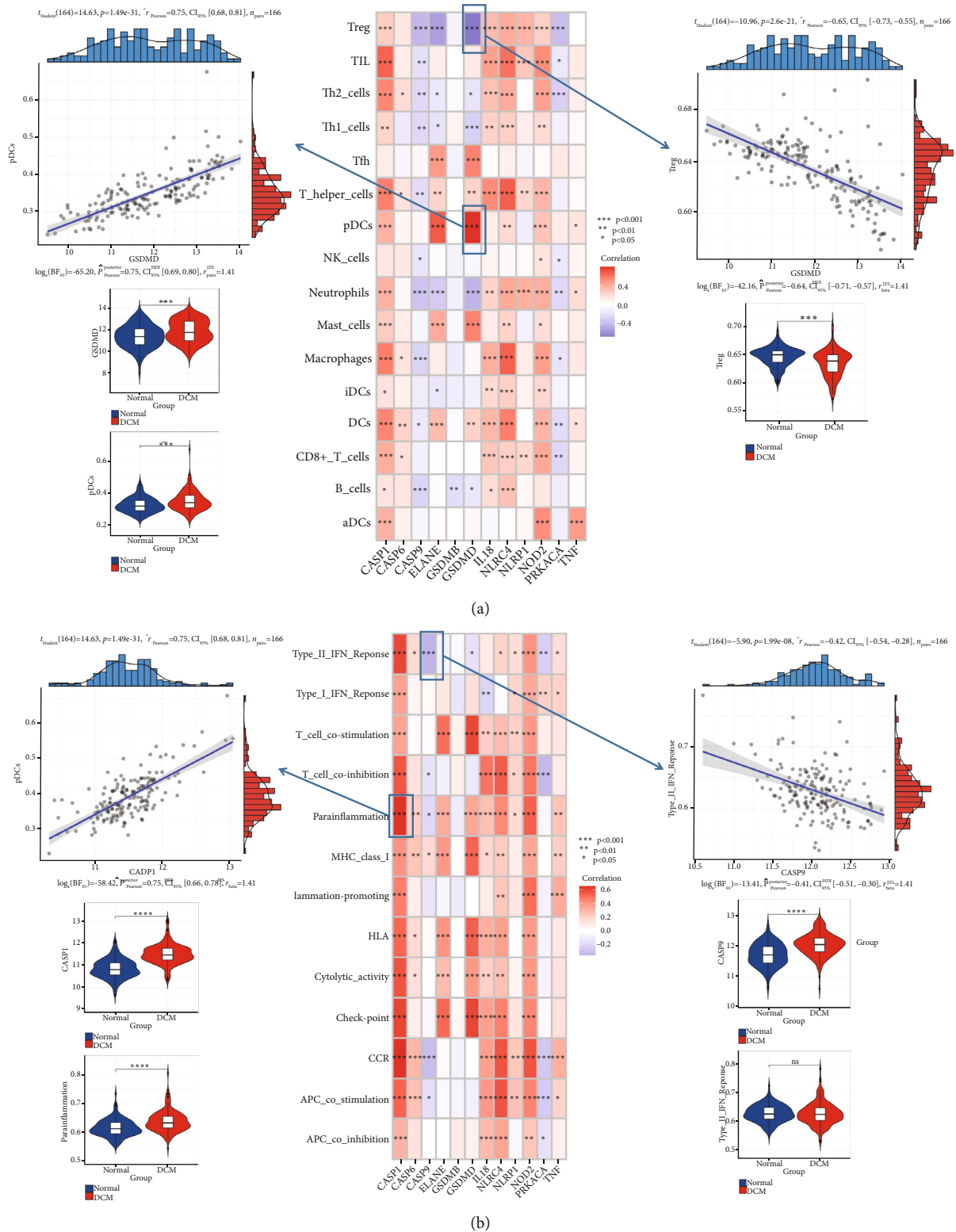


FIGURE 3: Association of PRGs with immune cells and immune response pathways. (a) The dot plot shows the correlation between each infiltrating cell and each hub PRG in the dysregulated immune microenvironment. The most positive interrelated immune cell-hub PRG pair was GSDMD-pDCs, and the violin plot on the right shows the expression or fraction status. The most negatively correlated immune cell-hub PRG pair was GSDMD-Tregs, and the violin plot on the left shows the expression or fraction status. (b) The dot plot shows the association between each gene set of the immune dysregulation response and the 12 hub PRGs. The most positively correlated pair was CASP1-parainflammation, and the violin plot in the right shows the expression or activity. The most negative interrelated pair was CASP9-type_II_IFN_response, and the violin plot on the right shows the expression or activity.

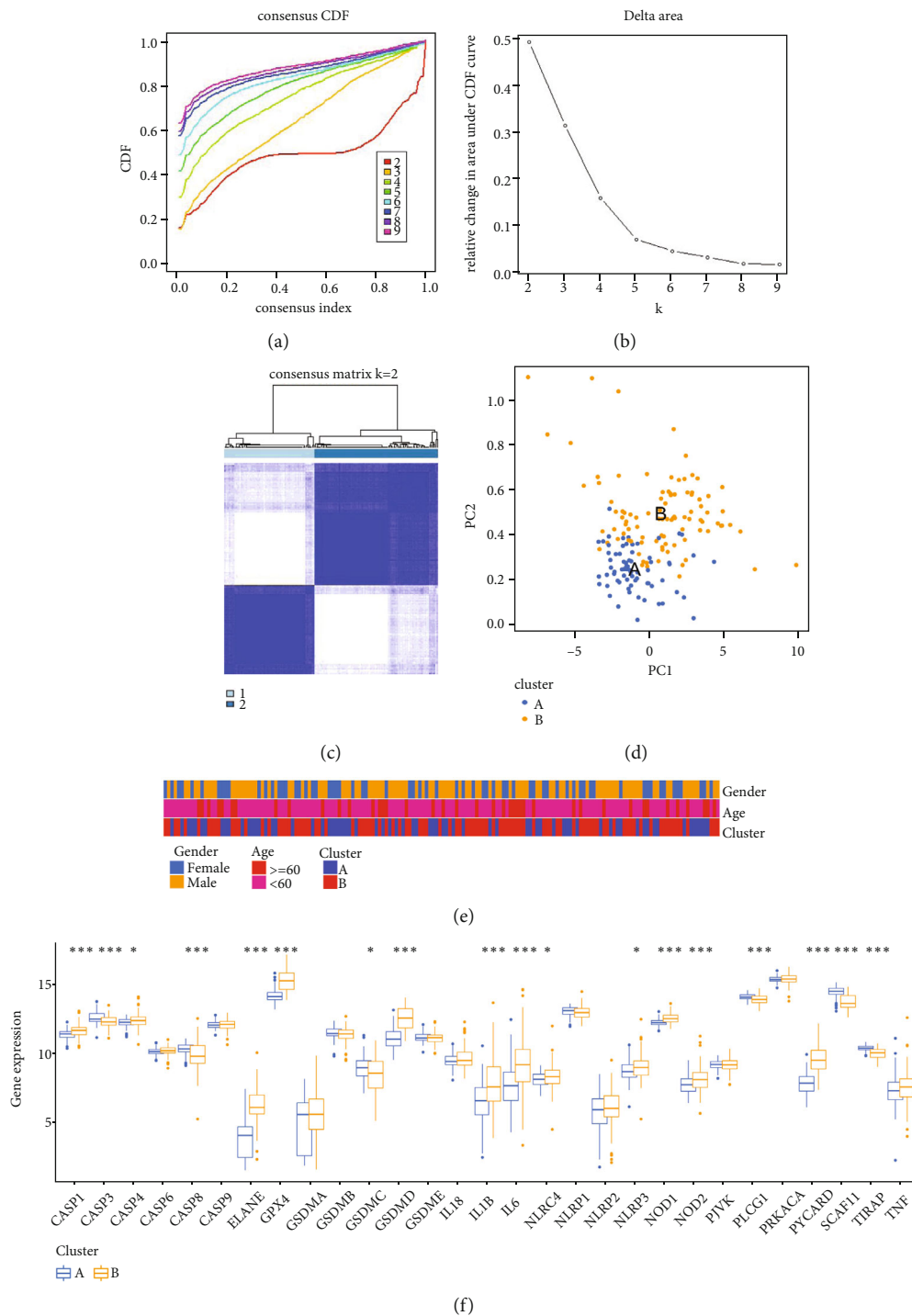


FIGURE 4: Continued.

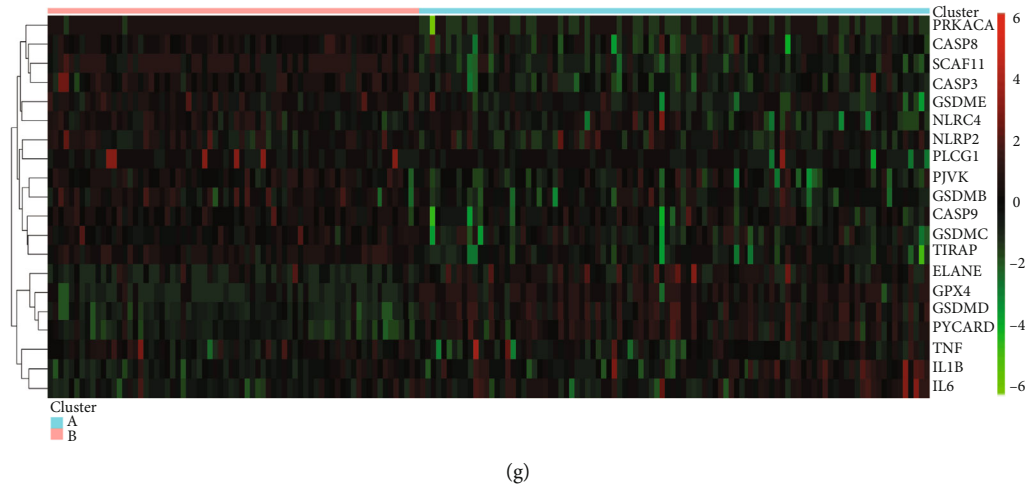


FIGURE 4: Identification two different subtypes of pyroptosis patterns in DCM. (a) A consensus clustering cumulative distribution function (CDF) with $k = 2 - 7$ is shown. (b) The relative change in the area under the CDF curve for $k = 2 - 7$ is shown. (c) Heat map of the matrix of cooccurrence proportions for DCM samples. (d) Principal component analysis (PCA) of the transcriptome profiles of the two pyroptosis patterns, indicating that there were significant differences in the transcriptome between the two pyroptosis patterns. (e) Comparison of age and sex between the two pyroptosis patterns. The correlation of different clinical features between the 2 patterns is shown by the heat map. (f) Box plot of the expression status of PRGs in two pyroptosis patterns. (g) Heat map of the expression status of PRGs in the two pyroptosis patterns.

between normal and DCM samples (AUC = 0.99, Figure 2(f)). These results show that PRGs play a crucial role in the development of DCM.

3.3. PRGs Are Related to Immune Characteristics in DCM Tissue. To investigate the biological behaviours between PRGs and the immune microenvironment, we analysed expression of the 12 hub PRGs, infiltrating immunocytes, and immune-related signalling pathways. Statistical analysis revealed differences in the abundance of infiltrating immunocytes between healthy and DCM samples (Figure S1A). Compared to healthy myocardial tissue, most infiltrating immune cells were altered in DCM. Correlation analysis revealed that 12 hub PRGs were closely associated with most immune cells (Figure 3(a)). For example, GSDMD had the strongest positive correlation with pDC abundance ($r = 0.75$) and the strongest negative correlation with Treg abundance ($r = -0.65$), which was related to the expression status of GSDMD, pDCs, and Tregs. The box plot shows differences in the activity of each immune response pathway between healthy and DCM samples (Figure S1B). In addition, we found that CASP1 was positively correlated with parainflammation ($r = 0.73$) and that CASP9 was negatively correlated with the type II IFN response ($r = -0.42$) (Figure 3(b)). This indicates that CASP1 and CASP9 play important roles in parainflammation or type II IFN response in DCM.

3.4. PRG-Mediated Pyroptosis Patterns in DCM. Based on the expression of 29 PRGs, we performed unsupervised consensus clustering analysis for DCM samples to investigate pyroptosis patterns in DCM (Figures 4(a)–4(c)). Two distinct DCM subtypes were identified. PCA showed that expression of PRGs was qualitatively different between the subtypes, including 70 samples in subtype A and 96 samples

in subtype B (Figure 4(d)). In addition, correlation analysis indicated no significant difference in clinical characteristics between the different patterns (Figure 4(e)). Except for CASP6, CASP9, GSDMA, GSDMB, GSDME, IL18, NLRP1, NLRP2, PJVK, PRKACA, and TNF, expression of the remaining 19 PRGs in different pyroptosis patterns exhibited obvious differences (Figures 4(f) and 4(g)). Multiple pyroptosis patterns were verified in DCM.

3.5. Characteristics of the Immune Microenvironment in Different Pyroptosis Patterns. To identify differences in immune microenvironmental characteristics between these different pyroptosis patterns, we evaluated immune cells, immune response gene sets, and human leukocyte antigen (HLA) gene expression. Many immune cells were different between the two patterns (Figure 5(a)). Compared to pattern B, pattern A had relatively few infiltrated immunocytes. Pattern B displayed higher levels of aDCs, DCs, macrophages, mast cells, NK cells, T helper cells, Tfh, and TILs. Of note, only Treg cells were more enriched in pattern A. In addition, in terms of immune response, the immune response of pattern B was more active. For instance, the immune response of MHC class I and HLA was very active in pattern B (Figure 5(b)). At the same time, we observed a similar trend in the gene expression of HLA (Figure 5(c)). These results indicated that pyroptosis pattern B mediates a more active immune response, while the pyroptosis pattern A-mediated immune response is relatively mild. These results once again strongly demonstrated that pyroptosis has an important regulatory effect on the formation of different immune microenvironments of DCM

3.6. Biological Characteristics of Pyroptosis Patterns. To investigate the biological response of the pyroptosis patterns,

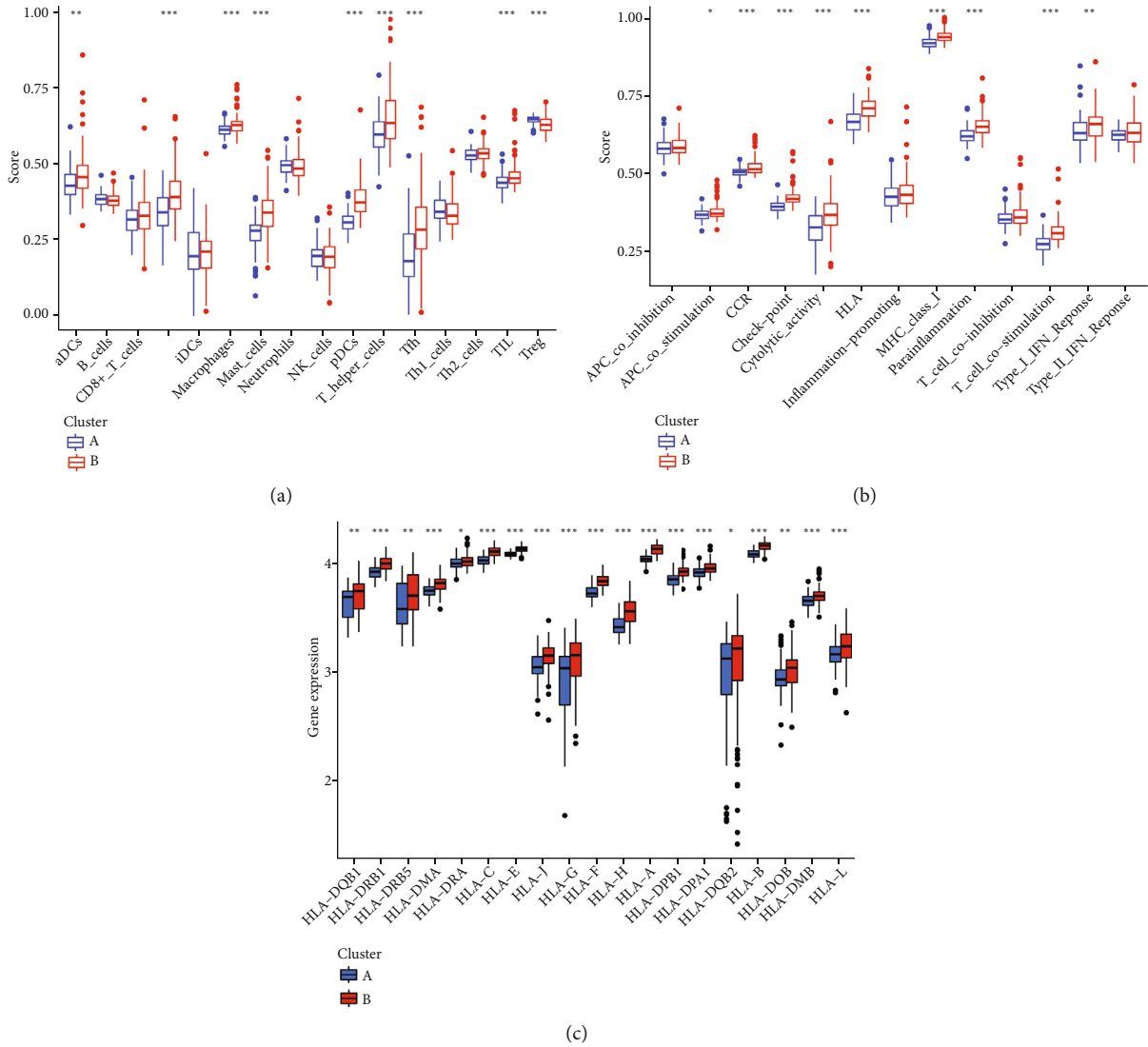
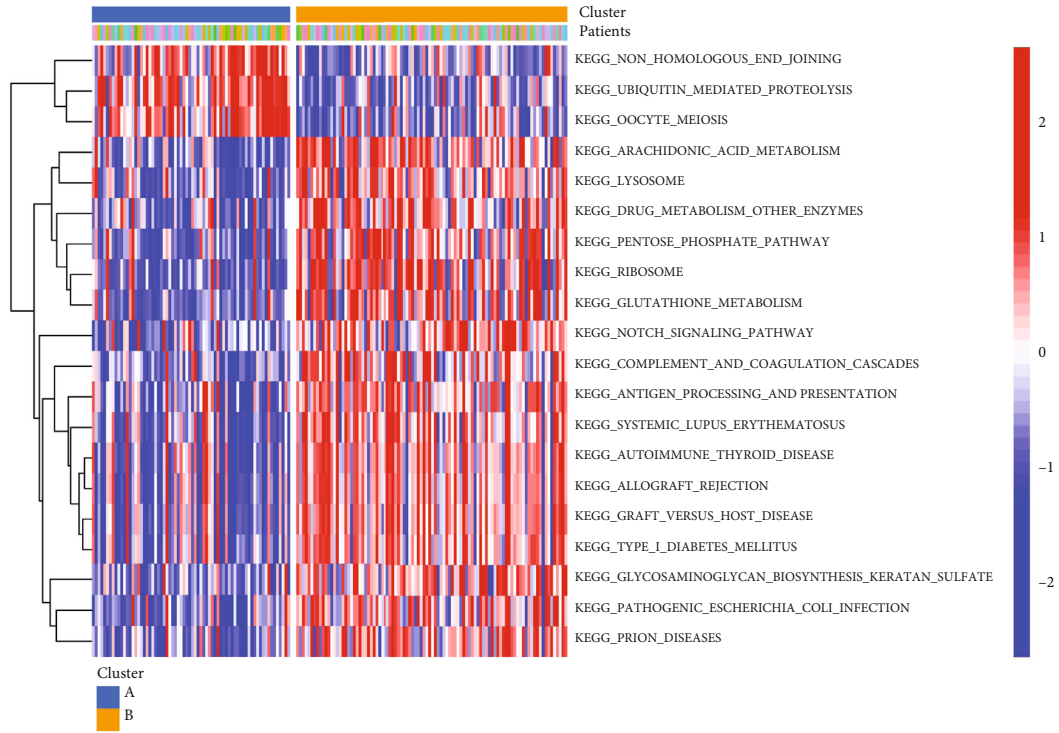


FIGURE 5: Differences in immune microenvironmental features in different pyroptosis patterns. (a) The abundance difference of infiltrating immunocytes in each immune microenvironment in pyroptosis patterns. (b) Activity differences in each immune response gene set in pyroptosis patterns. (c) Expression differences in each HLA gene in the pyroptosis patterns.

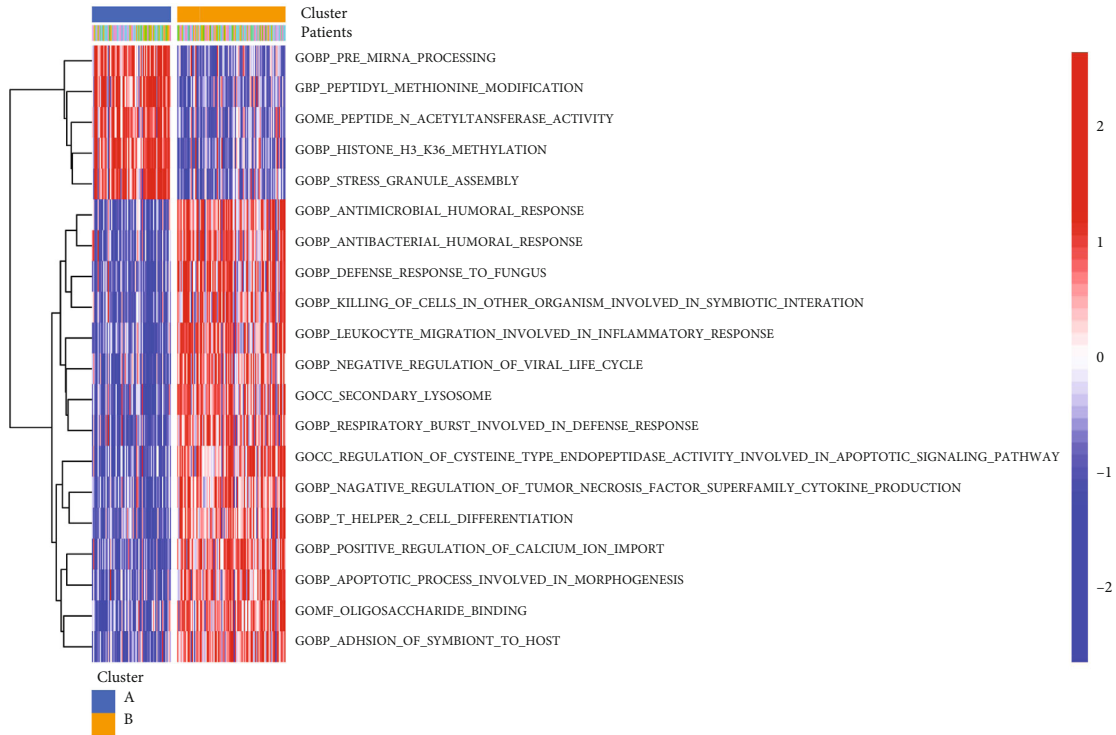
GO analysis and KEGG analysis were performed. We applied GSVA enrichment analysis to estimate the activity of the biological pathways that were assessed. In the KEGG pathway analysis, compared to pattern A, pattern B had more abundant pathways, such as the NOTCH signalling pathway and pentose phosphate pathway (Figure 6(a), Supplementary File 1). In GO pathway analysis, compared to pattern A, pattern B also had more abundant pathways, such as antimicrobial humoral response and other biological processes (Figure 6(b), Supplementary File 2). To investigate the mechanism of genes related to PRG-mediated regulation, we identified DEGs related to the pyroptosis phenotype. A total of 2142 common genes were considered to be related to the pyroptosis phenotype (Figure 7(a)), and GO enrichment analysis showed that they were primarily involved in immune processes such as neutrophil activation in the immune response (Figure 7(b)). In addition, in the KEGG analysis, the selected biological process of DEG enrichment

was significantly related to biological processes such as cytokine–cytokine receptor interaction (Figure 7(c)). In addition, we used WGCNA to identify gene–gene modules related to different modifications (Figures 7(d)–7(f)). We identified three gene modules where different pyroptosis patterns matched their related genes (Figure 7(g)); for example, pyroptosis pattern A was closely related to genes in the magenta module (Figure 7(h)). The above results could clarify that pyroptosis patterns mediate the related gene expression regulation network.

3.7. Validation of the Expression Levels of Five Core PRGs in DCM. According to the bioinformatics results, we further validated expression of the five core PRGs (NLRP1, TNF α , CASP1, CASP9, and PRKACA) in healthy mouse myocardial tissue and Dox-induced DCM myocardial tissue (Figures 8(a) and 8(b)). The RT–PCR results showed that the mRNA expression of NLRP1, TNF α , CASP1, CASP9,



(a)



(b)

FIGURE 6: Diversity of potential biological function characteristics between the two pyroptosis patterns. (a) Differences in KEGG pathway enrichment scores between the two pyroptosis patterns. (b) Differences in GO pathway enrichment scores between the two pyroptosis patterns.

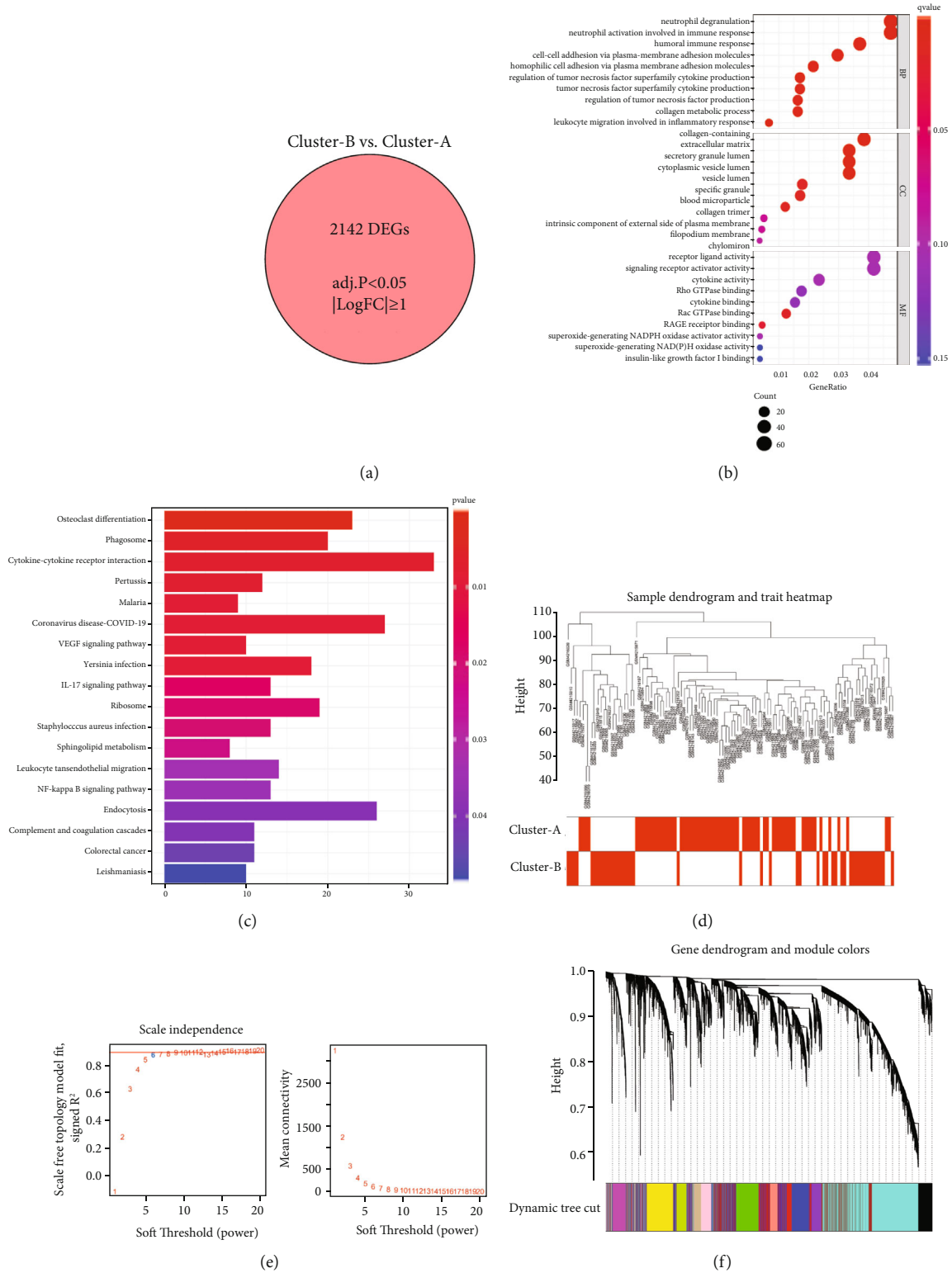


FIGURE 7: Continued.

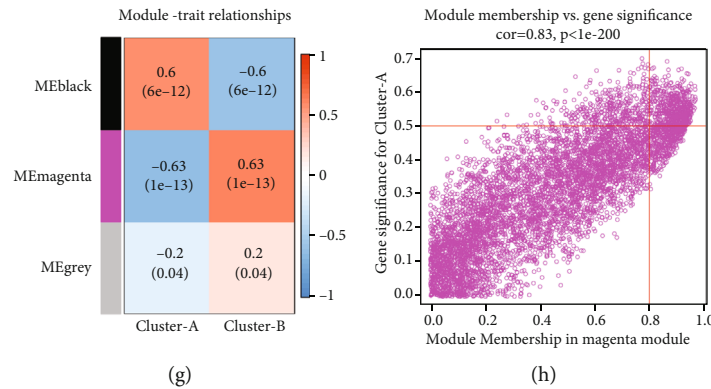


FIGURE 7: Identification and functional analysis of genes involved in the pyroptosis phenotype in DCM. (a) 2142 genes were related to the pyroptosis phenotype. (b) GO-BP functional enrichment analysis showed the biological features of genes involved in the pyroptosis phenotype. (c) GO enrichment analysis of genes related to the pyroptosis phenotype revealed the correlation between PRGs and immune mechanisms. (d) Sample clustering was performed on the strength of the expression information of all samples. All differentially expressed genes with $P < 0.05$ were used for WGCNA. (e) Analysis of the scale-free fit index and analysis of the mean connectivity for various soft-thresholding powers. (f) Gene tree diagram. The coloured line below the tree diagram shows the modules determined using dynamic tree cutting. (g) Heat map of the relevance between the characteristic genes of the module and the pyrolysis pattern. (h) Gene significance (GS) scatter plot of pyrolysis pattern A and module member (MM) in the magenta module.

and PRKACA in DCM myocardial tissues was significantly higher than that in normal myocardial tissues ($P < 0.05$), consistent with the results of bioinformatics analysis (Figure 8(c)).

4. Discussion

Dilated cardiomyopathy (DCM) is considered the final common reaction of the myocardium due to a combination of genetic and environmental factors. Pyroptosis was initially found to be a key mechanism for fighting against infection [22–24]. Recently, extensive findings have indicated that pyroptosis is involved in various cardiovascular diseases (CVDs) [15, 25, 26]. However, it is unknown whether the pyroptosis signalling pathway is involved in the immune microenvironment regulation of dilated cardiomyopathy. In this study, pyroptosis patterns were found in the immune response of DCM. To understand how PRG mediates the immune response and the alteration of immune cells in DCM, we used multiple bioinformatics analyses to obtain these results. First, our results identified 19 PRGs with altered expression between healthy and DCM samples, indicating that PRGs do indeed participate in the development of DCM. Based on hub DCM-related PRGs, we developed a classifier to differentiate between normal samples from DCM samples. The classifier performed well in distinguishing between healthy and DCM samples, revealing that PRGs do indeed play a critical role in the development of DCM. The mRNA expression levels of core PRGs, which are upregulated in DCM tissues, were indeed higher than that of healthy tissues. This was verified using qRT-PCR analysis in mouse myocardial tissue. In addition, our findings revealed that differences in the abundance of immune cells do indeed exist in the immune microenvironment between healthy and DCM samples. CASP1 was positively related to parainflammation, and CASP9 was negatively related to the type II IFN response. This indicates that CASP1 and

CASP9 play important roles in parainflammation or the type II IFN response in DCM. In addition, we found that gasdermin D (GSDMD) was strongly positively correlated with pDC abundance. GSDMD was recently identified as the factor responsible for the inflammatory form of lytic pyroptotic cell death, a critical antibacterial innate immune defence mechanism [27–29]. GSDMD is pleiotropic, exerting both pro- and anti-inflammatory effects, which make it a potential target for antibacterial and anti-inflammatory therapies [27, 30]. These findings may indicate the existence of a PRG immune regulatory mechanism in DCM. To investigate pyroptosis patterns in DCM, unsupervised consensus clustering analysis was conducted for DCM samples based on the expression of 29 PRGs. Two distinct DCM subtypes were identified. In addition, correlation analysis showed that there was no significant difference in clinical characteristics between different pyroptosis patterns. Expression of most PRGs in different pyroptosis patterns displayed obvious differences. It was verified that there were multiple pyroptosis patterns in DCM. Compared to pattern B, pattern A exhibited relatively few infiltrated immunocytes. Pattern B presented higher levels of aDCs, DCs, macrophages, mast cells, NK cells, T helper cells, Tfh, and TILs, while Tregs were more highly enriched in pattern A. In addition, the immune response of pattern B was more active. For instance, the immune response of MHC class I and HLA is active in pattern B. We identified a similar trend in HLA gene expression. These results indicated that pyroptosis pattern B is characterized by a more active immune response, while pyroptosis pattern A features are relatively mild immune response. These results once again strongly demonstrate that cell pyroptosis exerts an important regulatory effect on the formation of different immune microenvironments of DCM. Moreover, compared to pattern A, pattern B contained more abundant pathways, such as the NOTCH signalling pathway, pentose phosphate pathway, antimicrobial humoral response, and other biological processes. These

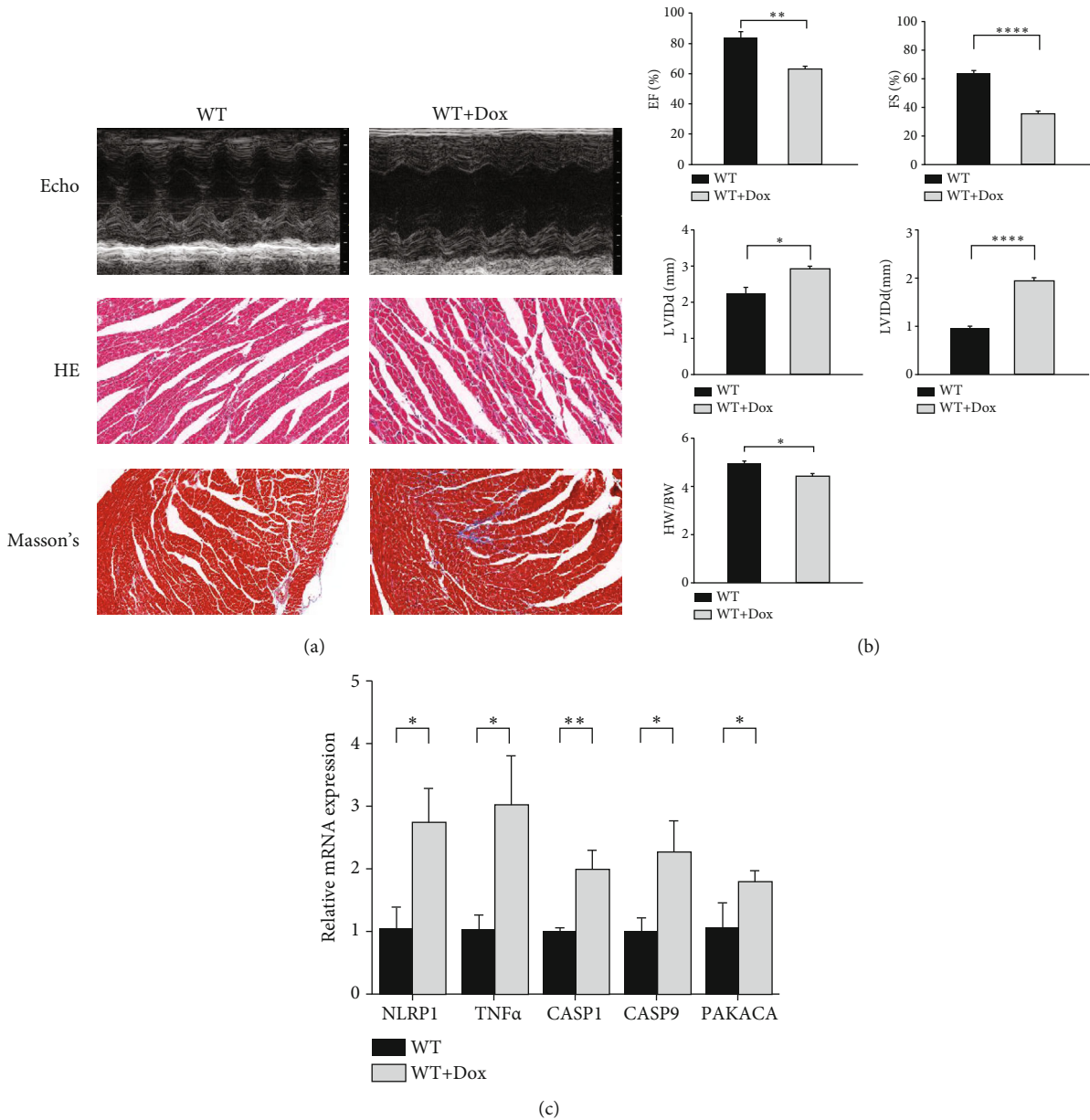


FIGURE 8: Validation of the expression levels of NLRP1, TNFα, CASP1, CASP9, and PRKACA in healthy and Dox-induced DCM mouse myocardial tissues. (a) Representative echocardiographic (echo), HE, and Masson's trichrome staining images. (b) Cardiac function index ($n = 6$). (c) Expression levels of NLRP1, TNFα, CASP1, CASP9, and PRKACA were quantified using qRT-PCR analysis in myocardial tissue. * $P < 0.05$, ** $P < 0.01$, *** $P < 0.001$, and **** $P < 0.0001$.

results regarding biological response clarify the gene expression regulation network mediated by pyroptosis patterns. This study provides some important findings for the exploration of cell pyroptosis in DCM to facilitate characterization of pyroptosis mechanisms and immune characteristics in DCM by other investigators.

Abundant results were generated that will promote our understanding of immune mechanisms with respect to pyroptosis in DCM. In addition, we identified two different patterns of pyroptosis, and they can help us deepen our comprehension of pyroptosis in DCM to understand how it mediates the immune response. According to our infer-

ences, the correlation between cell pyroptosis and the immune microenvironment is strong and significant.

However, our study still has some limitations that need to be considered. First, the number of samples included in this study was limited, so further experiments are needed to confirm the results of this study. Second, all data in this study are based on the expression values of mRNA and do not directly reflect protein expression levels, which may result in poor performance in the evaluation of immune signal pathways based on protein expression. For instance, inconsistency between the molecular pathways is directly related to cellular activities. Although such limitations should not be ignored,

our results suggest that pyroptosis has a significant influence on the immune microenvironment in DCM and deepens our understanding of the potential pathogenesis of DCM.

Our findings systematically revealed the potential association between cell pyroptosis and the immune microenvironment in DCM. Through our research, it was confirmed that pyroptosis is closely related to DCM and that pyroptosis has a regulatory effect on the immune microenvironment in DCM. The findings could provide ideas for other researchers in the field to further investigate the mechanisms of pyroptosis in DCM. We screened out genes that are closely related to pyroptosis in DCM. By regulating these genes to inhibit pyroptosis, these genes are likely to become potential targets for new therapeutic interventions and play a role in relieving or treating DCM. In addition, the mechanism of DCM is very complicated, and it is not yet fully understood. Through studying the relationship between pyroptosis and the immune environment, we can gain a deeper understanding of the immune mechanism of DCM. Through studying the molecular pathways of pyroptosis in DCM, these results may offer clues for new therapeutic strategies for DCM. We believe that the investigation of pyroptosis in the immune microenvironment in DCM may be meaningful in the future.

5. Conclusions

In summary, pyroptosis plays a critical role in the immune regulation of dilated cardiomyopathy. The study demonstrated that pyroptosis has an important regulatory effect on the formation of different immune microenvironments by impacting infiltrating immunocytes. This study offers novel ideas for understanding the pathogenesis of dilated cardiomyopathy, which will be very significant in the future.

Data Availability

<https://www.ncbi.nlm.nih.gov/geo/query/acc.cgi?acc=GSE141910>.

Conflicts of Interest

The authors confirm that there are no conflicts of interest.

Acknowledgments

This work was supported by grants awarded to YW from the National Natural Science Foundation of China (NSFC, Grant Nos. 81270304, 81873507, and 81420108004).

Supplementary Materials

Figure S1: differential expression of infiltrating immune cells and immune response pathways. (*Supplementary Materials*)

References

- [1] R. G. Weintraub, C. Semsarian, and P. Macdonald, "Dilated cardiomyopathy," *Lancet*, vol. 390, no. 10092, pp. 400–414, 2017.
- [2] R. E. Hershberger, D. J. Hedges, and A. Morales, "Dilated cardiomyopathy: the complexity of a diverse genetic architecture," *Nature Reviews. Cardiology*, vol. 10, no. 9, pp. 531–547, 2013.
- [3] P. Elliott, "Cardiomyopathy. Diagnosis and management of dilated cardiomyopathy," *Heart*, vol. 84, no. 1, pp. 106–112, 2000.
- [4] M. Merlo, A. Pivetta, B. Pinamonti et al., "Long-term prognostic impact of therapeutic strategies in patients with idiopathic dilated cardiomyopathy: changing mortality over the last 30 years," *European Journal of Heart Failure*, vol. 16, no. 3, pp. 317–324, 2014.
- [5] W. J. McKenna, B. J. Maron, and G. Thiene, "Classification, epidemiology, and global burden of cardiomyopathies," *Circulation Research*, vol. 121, no. 7, pp. 722–730, 2017.
- [6] U. Kühn, M. Noutsias, and H. P. Schultheiss, "Immunohistochemistry in dilated cardiomyopathy," *European heart journal*, vol. 16, Suppl O, pp. 100–106, 1995.
- [7] M. Noutsias, B. Seeberg, H. P. Schultheiss, and U. Kühn, "Expression of cell adhesion molecules in dilated cardiomyopathy," *Circulation*, vol. 99, no. 16, pp. 2124–2131, 1999.
- [8] R. Wojnicz, E. Nowalany-Kozielska, J. Wodniecki et al., "Immunohistological diagnosis of myocarditis. Potential role of sarcolemmal induction of the MHC and ICAM-1 in the detection of autoimmune mediated myocyte injury," *European Heart Journal*, vol. 19, no. 10, pp. 1564–1572, 1998.
- [9] N. Kayagaki, S. Warming, M. Lamkanfi et al., "Non-canonical inflammasome activation targets caspase-11," *Nature*, vol. 479, no. 7371, pp. 117–121, 2011.
- [10] J. Shi, Y. Zhao, Y. Wang et al., "Inflammatory caspases are innate immune receptors for intracellular LPS," *Nature*, vol. 514, no. 7521, pp. 187–192, 2014.
- [11] X. Liu, Z. Zhang, J. Ruan et al., "Inflammasome-activated gasdermin D causes pyroptosis by forming membrane pores," *Nature*, vol. 535, no. 7610, pp. 153–158, 2016.
- [12] P. Broz, P. Pelegrín, and F. Shao, "The gasdermins, a protein family executing cell death and inflammation," *Nature Reviews Immunology*, vol. 20, no. 3, pp. 143–157, 2020.
- [13] J. Ding, K. Wang, W. Liu et al., "Pore-forming activity and structural autoinhibition of the gasdermin family," *Nature*, vol. 535, no. 7610, pp. 111–116, 2016.
- [14] X. Li, N. Du, Q. Zhang et al., "MicroRNA-30d regulates cardiomyocyte pyroptosis by directly targeting foxo3a in diabetic cardiomyopathy," *Cell death & disease*, vol. 5, no. 10, article e1479, 2014.
- [15] P. Duwell, H. Kono, K. J. Rayner et al., "NLRP3 inflammasomes are required for atherogenesis and activated by cholesterol crystals," *Nature*, vol. 464, no. 7293, pp. 1357–1361, 2010.
- [16] R. Li, K. Lu, Y. Wang et al., "Triptolide attenuates pressure overload-induced myocardial remodeling in mice via the inhibition of NLRP3 inflammasome expression," *Biochemical and Biophysical Research Communications*, vol. 485, no. 1, pp. 69–75, 2017.
- [17] C. Zeng, F. Duan, J. Hu et al., "NLRP3 inflammasome-mediated pyroptosis contributes to the pathogenesis of non-ischemic dilated cardiomyopathy," *Redox Biology*, vol. 34, article 101523, 2020.
- [18] R. Karki and T. Kanneganti, "Diverging inflammasome signals in tumorigenesis and potential targeting," *Nature Reviews. Cancer*, vol. 19, no. 4, pp. 197–214, 2019.

- [19] X. Xia, X. Wang, Z. Cheng et al., "The role of pyroptosis in cancer: pro-cancer or pro-"host"?", *Cell Death & Disease*, vol. 10, no. 9, p. 650, 2019.
- [20] B. Wang and Q. Yin, "AIM2 inflammasome activation and regulation: a structural perspective," *Journal of Structural Biology*, vol. 200, no. 3, pp. 279–282, 2017.
- [21] S. Man and T. Kanneganti, "Regulation of inflammasome activation," *Immunological Reviews*, vol. 265, no. 1, pp. 6–21, 2015.
- [22] B. J. Maron, J. A. Towbin, G. Thiene et al., "Contemporary definitions and classification of the cardiomyopathies: an American Heart Association scientific statement from the Council on Clinical Cardiology, Heart Failure and Transplantation Committee; Quality of Care and Outcomes Research and Functional Genomics and Translational Biology Interdisciplinary Working Groups; and Council on Epidemiology and Prevention," *Circulation*, vol. 113, no. 14, pp. 1807–1816, 2006.
- [23] Y. Wang, B. Gao, and S. Xiong, "Involvement of NLRP3 inflammasome in CVB3-induced viral myocarditis," *American Journal of Physiology. Heart and Circulatory Physiology*, vol. 307, no. 10, pp. H1438–H1447, 2014.
- [24] F. Martinon, K. Burns, and J. Tschopp, "The inflammasome: a molecular platform triggering activation of inflammatory caspases and processing of proIL- β ," *Molecular Cell*, vol. 10, no. 2, pp. 417–426, 2002.
- [25] N. A. Bracey, P. L. Beck, D. A. Muruve et al., "The Nlrp3 inflammasome promotes myocardial dysfunction in structural cardiomyopathy through interleukin-1 β ," *Experimental Physiology*, vol. 98, no. 2, pp. 462–472, 2013.
- [26] M. Kawaguchi, M. Takahashi, T. Hata et al., "Inflammasome activation of cardiac fibroblasts is essential for myocardial ischemia/reperfusion injury," *Circulation*, vol. 123, no. 6, pp. 594–604, 2011.
- [27] N. Kayagaki, I. B. Stowe, B. L. Lee et al., "Caspase-11 cleaves gasdermin D for non-canonical inflammasome signalling," *Nature*, vol. 526, no. 7575, pp. 666–671, 2015.
- [28] J. Shi, Y. Zhao, K. Wang et al., "Cleavage of GSDMD by inflammatory caspases determines pyroptotic cell death," *Nature*, vol. 526, no. 7575, pp. 660–665, 2015.
- [29] W. T. He, H. Wan, L. Hu et al., "Gasdermin D is an executor of pyroptosis and required for interleukin-1 β secretion," *Cell Research*, vol. 25, no. 12, pp. 1285–1298, 2015.
- [30] M. Tamura, S. Tanaka, T. Fujii et al., "Members of a novel gene family, *_Gsdm_* are expressed exclusively in the epithelium of the skin and gastrointestinal tract in a highly tissue-specific manner," *Genomics*, vol. 89, no. 5, pp. 618–629, 2007.

Research Article

Ferroptosis-Specific Inhibitor Ferrostatin-1 Relieves H₂O₂-Induced Redox Imbalance in Primary Cardiomyocytes through the Nrf2/ARE Pathway

Chaofeng Sun,¹ Fang Peng,² Jianfei Li,² Xudong Cui,² Xin Qiao,² and Wangliang Zhu ¹

¹The First Affiliated Hospital of Xi'an Jiaotong University, Xi'an, China

²Inner Mongolia Autonomous Region People's Hospital, Hohhot, China

Correspondence should be addressed to Wangliang Zhu; 18647991940@163.com

Received 9 January 2022; Accepted 27 January 2022; Published 22 February 2022

Academic Editor: Francesco Busard?

Copyright © 2022 Chaofeng Sun et al. This is an open access article distributed under the Creative Commons Attribution License, which permits unrestricted use, distribution, and reproduction in any medium, provided the original work is properly cited.

Objective. Ischemic heart disease (IHD) has always been the focus of attention of many researchers in cardiovascular disease, and its pathogenesis is also very complicated. Ferroptosis may be involved in the occurrence and development of IHD. **Methods.** First, primary cardiomyocytes were treated with H₂O₂ to simulate the IHD in vitro model. After pretreatment with different concentrations of ferrostatin-1, cell survival rate was detected by MTT method, cell apoptosis was detected by TUNEL staining and flow cytometry, and the expression of oxidative stress, ferroptosis, and related molecules of Nrf2/ARE pathway was detected by Western blotting (WB) and quantitative real-time polymerase chain reaction (qRT-PCR). **Results.** The mortality of primary cardiomyocytes in the H₂O₂ group was obviously increased. Ferrostatin-1 treatment can effectively inhibit cell death, improve antioxidant enzyme activity, inhibit the expression of ferroptosis-related molecules, and activate Nrf2/ARE pathway expression. **Conclusion.** Ferroptosis-specific inhibitor ferrostatin-1 relieves H₂O₂-induced redox imbalance in primary cardiomyocytes through the Nrf2/ARE pathway, inhibits ferroptosis, and thereby slows cardiomyocyte death.

1. Introduction

Ischemic heart disease (IHD) is the most common cause of health problems and heart failure in the world. As a common chronic disease, IHD can often cause myocardial ischemia, hypoxia, and even necrosis, posing a serious threat to human health [1]. An important pathophysiological mechanism of IHD is oxidative stress (OS) injury. In the process of OS injury, it will not only cause cell apoptosis and autophagy but also cause changes in cell energy metabolism [2–4]. In the occurrence of IHD, cardiomyocytes produce a large number of oxygen free radicals, and at the same time, the activity of antioxidant enzymes in the cells is reduced, resulting in lipid peroxidation on the cell membrane, the change of membrane permeability, and the destruction of cell function and structure and inducing the occurrence of cell death [5]. With the increase of the global aging population, IHD has become one of today's serious social problems. Therefore, the

research on the pathogenesis, prevention, and treatment of IHD has profound significance.

In 2012, DixOri discovered a new nonapoptotic cell death form, ferroptosis, while studying the small molecule Erastin to kill cancer cells containing the RAS mutation of the oncogene [6]. Ferroptosis is an iron-dependent unique form of cell death that involves a complex array of biochemical reactions, gene expression, and signaling. At present, the study found ferroptosis in morphology, biochemistry, etc., is different from apoptosis, autophagy, necrosis, etc., the process does not depend on the classic apoptosis pathway, at the same time, it is also not affected by other cell death inhibitor, its performance of the typical morphological features of mitochondria in cells becomes smaller, but the double membrane density increases, and its metabolism process involves the increase of cytoplasmic ROS and lipid ROS [7, 8]. At present, the discovery and research of ferroptosis are mainly related to tumor cell death, but it is not clear how it relates to noncancerous cells.

Ferostatin-1 (Fer-1) is a synthetic antioxidant. It inhibits iron death more effectively than phenolic antioxidants. Fer-1 is the first ferroptosis inhibitor and is widely used in vitro and in vivo experiments [9]. The anti-ferroptosis function of Fer-1 mainly depends on the inhibition of lipid peroxidation.

Recent studies have shown that healthy cells are also affected by a similar “iron death” mechanism, and the key to this process is the glutathione peroxidase 4 (GPX4) protein [10]. GPX4 is the only known enzyme that can effectively reduce lipid peroxidation in biofilms. Studies have shown that silencing or overexpressing the GPX4 gene can obviously change the sensitivity of cells to ferroptosis inducer FINS (Erastin, etc.). By inhibiting System xc- blocking cystine uptake and depleting cell glutathione (GSH), Erastin leads to the inactivation of GPX4, resulting in an increase in cytoplasmic ROS and lipid ROS, which ultimately triggers ferroptosis [11]. Therefore, the occurrence of ferroptosis has a similar mechanism to the increase of oxygen radicals and the decrease of antioxidant enzyme activity in the known pathogenesis of IHD, both of which are related to ROS.

There are few researches of ferroptosis in IHD. We hypothesized that ferroptosis could be regulated to inhibit cardiomyocyte damage during the occurrence of IHD.

2. Materials and Methods

2.1. Primary Cardiomyocyte Extraction. Newborn specific pathogen free (SPF) grade Sprague Dawley (SD) rats, 1 to 3 days, male and female, with a body weight of about 5 to 6 g, were provided by Henan Animal Experiment Center. The apex of the suckling mouse was removed under aseptic conditions, it was washed with phosphate-buffered saline (PBS, Jia May, Shanghai, China) at 4°C for three times, and then, it was cut into a tissue block of about 1 mm³ in size and mixed with 0.08% trypsin-containing cardiomyocyte digestion solution (Jia May, Shanghai, China). Then, the tissue was transferred to a glass bottle and incubated in a 37°C water bath for 6 min. It was precipitated naturally, and the supernatant was discarded. The digestion was repeated about 7-8 times in the same way until the tissue block became white and translucent. The supernatant after each natural precipitation was mixed with an equal volume of Dulbecco's Modified Eagle Medium (DMEM; Life Technology, Wuhan, China) medium containing 20% fetal bovine serum (FBS; Life Technology, Wuhan, China) and centrifuged at 1000 r/min for 5 min. Then the supernatant was discarded, and the cells were cultured with DMEM containing 10% FBS in a 37°C, 5% CO₂ incubator for differential adherent culture. After 90 min, we drew the cell suspension, and the cells were centrifuged at 1000 r/min for 5 min. Then, the supernatant was discarded, and the cells were mixed with the complete medium to make a cell suspension. The cell concentration was adjusted to 4 × 10⁵/mL with complete medium and added to 0.1 mmol/L Brdu solution (Life Technology, Wuhan, China) to inhibit the proliferation of fibroblasts. After 48 hours of culture, the supernatant was

discarded. DMEM medium was cultured simultaneously for 24 h.

2.2. Cell Grouping and Processing. The primary cardiomyocytes were seeded in 6-well plates, and the cells were divided into 4 groups: control, H₂O₂ (Jia May, Shanghai, China) treatment, 3 μM ferostatin-1+200 μM H₂O₂ treatment, and 12 μM ferostatin-1+200 μM H₂O₂ treatment. Ferostatin-1 powder (Med Chem Express, Shanghai, China) was dissolved in dimethyl sulfoxide (DMSO) (Jia May, Shanghai, China) and formulated into a solution with a concentration of 50 mM and stored at -80°C until use. When the experiment was used, the medium was diluted to the required working concentration.

2.3. MTT (3-(4,5-Dimethylthiazol-2-yl)-2,5-Diphenyl Tetrazolium Bromide). The primary cardiomyocytes were seeded in 96-well plates at approximately 2 × 10⁴ cells per well. The experiment was set up with 6 multiple wells, and a normal control group and a blank control group were set. After cells were incubated in a 37°C, 5% CO₂ incubator overnight, the original culture solution was discarded. The normal control group was replaced with complete medium. The blank control group was added with equal volume of phosphate-buffered saline (PBS). The H₂O₂ group was added with 200 μM H₂O₂. The ferostatin-1 group was added with different concentrations (3, 6, and 12 μM) of ferostatin-1 before adding H₂O₂. After 12 hours of cocultivation, 5 mg/mL of 20 μL MTT solution (Jian Cheng, Nanjing, China) was added to each well. Four hours later, the supernatant was discarded, 150 μL DMSO was added to each well, and it was shaken steadily for 10 min. It was placed on the enzyme-linked immunoassay detector (Rongjin, Shenzhen, China), the optical density value (OD value) of each well was detected at a wavelength of 490 nm, and the experiment was repeated 3 times.

2.4. Lactic Dehydrogenase (LDH) Kit Detection. According to the experimental grouping, the supernatant solution of each group was collected, and the configured working solution (Thermo Fisher Scientific, Waltham, MA, USA) was added and was reacted in the water bath at 37°C for 15 minutes each time. Finally, 0.4 mol/L NaOH solution was added, and the absorbance of each group was determined by enzyme-linked immunoassay detector with the wavelength of 450 nm after oscillating and mixing.

2.5. Superoxide Dismutase (SOD) Kit Detection. According to the experimental grouping, we collected the supernatant solution of each group, added the configured working solution (Thermo Fisher Scientific, Waltham, MA, USA), and reacted in the water bath at 37°C for 20 minutes. After oscillating and mixing, the absorbance of each group was determined by enzyme-linked immunoassay detector at a wavelength of 450 nm.

2.6. GSH Kit Detection. We collected the cells and suck up the supernatant. The protein removal reagent S solution (Thermo Fisher Scientific, Waltham, MA, USA) was added and vortexed fully and evenly. Then, the samples were

freeze-thawed rapidly twice by liquid nitrogen and 37°C water baths. Next, the samples were centrifuged at 4°C at 10000 r/min for 10 min. The supernatant was used for the determination of total GSH, and the contents of each group were compared.

2.7. Intracellular MDC Levels Were Detected by Flow Cytometry. The primary cardiomyocytes were inoculated with 2×10^5 per well in a 6-well plate, and the cells were cultured in an incubator at 37°C for 24 hours. After the cells were treated as above, 1 ml of MDC dye solution (Jian Cheng, Nanjing, China) with final concentration of 50 μ M was added to each cell, and the cells were incubated in an incubator in dark for 30 minutes. After washing with PBS for 3 times, flow cytometry (Becton Dickinson, Heidelberg, Germany) was used for detection.

2.8. GPX Kit Detection. The experiment was divided into control group, H₂O₂ group, and 12 μ M ferrostatin-1 group. The test buffer, cell sample, and GPX test fluid (Thermo Fisher Scientific, Waltham, MA, USA) were added to the 96-well plate according to the requirements of the kit. After the oscillation mixing, the absorbance of each group was measured by enzyme-linked immunoassay detector at the wavelength of 340 nm, and then, the absorbance of each group was detected again every 2 min to calculate the GPX activity.

2.9. Intracellular ROS Levels Were Detected by Flow Cytometry. The cells were inoculated on a 6-well culture plate. After 24 hours of dosing and culture, the cells were digested with trypsin and centrifuged at 1500 r/min for 5 minutes, and cells of each group were collected. The cells were resuspended in DCFH-DA (Jian Cheng, Nanjing, China) serum-free medium with a final concentration of 10 μ M, mixed by pipetting, and incubated for 20 minutes. The cells were washed 3 times with fresh medium to fully remove the DCFH-DA. The flow cytometer detects fluorescence intensity at an excitation wavelength of 488 nm and an emission wavelength of 525 nm.

2.10. Immunofluorescence Staining. Cells in the logarithmic growth stage were inoculated in 6-well plates with 2×10^5 cells per well, and 2 mL fresh medium was added to each well for overnight culture. After culture for 24 hours, the medium was discarded and washed twice with precooled PBS at 4°C. 1 mL of 2% paraformaldehyde was gently added to each well for fixation. After 15 minutes, the paraformaldehyde solution was discarded, 1 mL PBS was added into each well to wash the cells, and then, the diluted primary anti-SOD1 (Abcam, Cambridge, MA, USA, Rabbit, 1:500) was added, and it was incubated overnight at 4°C. The next day, 1 mL PBS was added to each hole and washed twice. Second antibody was added and incubated at room temperature for 1 hour. Finally, 4',6-diamidino-2-phenylindole (DAPI) dye solution (Thermo Fisher Scientific, Waltham, MA, USA) of 1 mL/well was added, and the cells were kept out of light for 10 minutes at room temperature. Then, the cells were lightly washed with precooled PBS and observed

under an inverted fluorescence microscope (Thermo Fisher Scientific, Waltham, MA, USA).

2.11. TUNEL Staining. 2×10^5 cells of log phase-proliferated primary cardiac myocytes were inoculated into 24-well plates and cultured for 12 hours in an incubator. Then, the cells of different treatment groups were stained with TUNEL kit (Elabscience, Wuhan, China) in the dark. After DAPI staining, the results were observed under a fluorescence microscope (Sunny Optical, Zhejiang, China) and recorded.

2.12. Western Blot Test. The cell protein was collected by radioimmunoprecipitation assay (RIPA) protein lysate (Jia May, Shanghai, China) and centrifuged at 4°C for 10 min at 12,000 r/min. The supernatant was taken. After the protein concentration of each group was determined by bicinchoninic acid (BCA) method (Jia May, Shanghai, China), an appropriate amount of 4 \times protein buffer was added and boiled at 100°C for 5 min. The denatured proteins were subjected to sodium dodecyl sulphate-polyacrylamide gel electrophoresis (SDS-PAGE), film transferred, and blocked with 5% skimmed milk at room temperature for 2 hours; then, the corresponding primary antibody (SOD1, Abcam, Cambridge, MA, USA, Rabbit, 1:2000; SOD2, Abcam, Cambridge, MA, USA, Rabbit, 1:2000; FP1, Abcam, Cambridge, MA, USA, Mouse, 1:3000; Ptg2, Abcam, Cambridge, MA, USA, Mouse, 1:2000; Nrf2, Abcam, Cambridge, MA, USA, Rabbit, 1:1000; HO-1, Abcam, Cambridge, MA, USA, Rabbit, 1:2000; GPX4, Abcam, Cambridge, MA, USA, Mouse, 1:1000; and GAPDH, Proteintech, Rosemont, IL, USA, 1:5000) was added and incubated overnight at 4°C. Then, the corresponding secondary antibody (1:1000 dilution, Yifei Xue Biotechnology, Nanjing, China) was added and incubated at room temperature for 2 h. After incubation with enhanced chemiluminescence (ECL, Elabscience, Wuhan, China) solution, it was developed on the chemiluminescence imaging system.

2.13. Total RNA Extraction and Quantitative Real-Time Polymerase Chain Reaction (qRT-PCR). The total RNA of each group of cells was extracted according to the instructions of the RNA rapid extraction kit (Thermo Fisher Scientific, Waltham, MA, USA). The ultraviolet spectrophotometer (Becton Dickinson, Heidelberg, Germany) was used to determine the purity and concentration of RNA. The primer sequence of the target gene after reverse transcription is shown in Table 1.

2.14. Statistical Analysis. Statistical analysis was performed using the Prism 8.0 (GraphPad software, La Jolla, CA, USA) software. Each experiment was repeated 3 times. The experimental data was expressed as mean \pm standard deviation (mean \pm SD). The comparison of the two groups of data was performed by independent sample *t* test. Analysis of variance was used for comparison among multiple groups. $P < 0.05$ was considered statistically significant, and $P < 0.01$ was considered statistically significant.

TABLE 1: qRT-PCR primers.

Gene name	Forward (5'>3')	Reverse (5'>3')
FP1	CAACCCGCTCCATAAG	GGCAAACAACAACAGCAA
Ptgs2	TTCAACACACTCTATCACTGGC	AGAAGCGTTTTCGGTACTCAT
GPX4	TTCTCAGCCAAGGACATCG	CACTCAGCATATCGGGCAT
Nrf2	GATGGACTTGGAGTTGCC	CCTTCTGGAGTTGCTCTTG
HO-1	ACAGCCCCACCAAGTTC	GGCGGTCTTAGCCTCTTC
SOD1	GGTGAACCAGTTGTGTTGTC	CCGTCCTTTCCAGCAGTC
SOD2	CAGACCTGCCTTACGACTATGG	CTCGGTGGCGTTGAGATTGTT
GAPDH	ACAACCTTGGTATCGTGGAAGG	GCCATCACGCCACAGTTTC

qRT-PCR: quantitative reverse-transcription polymerase chain reaction.

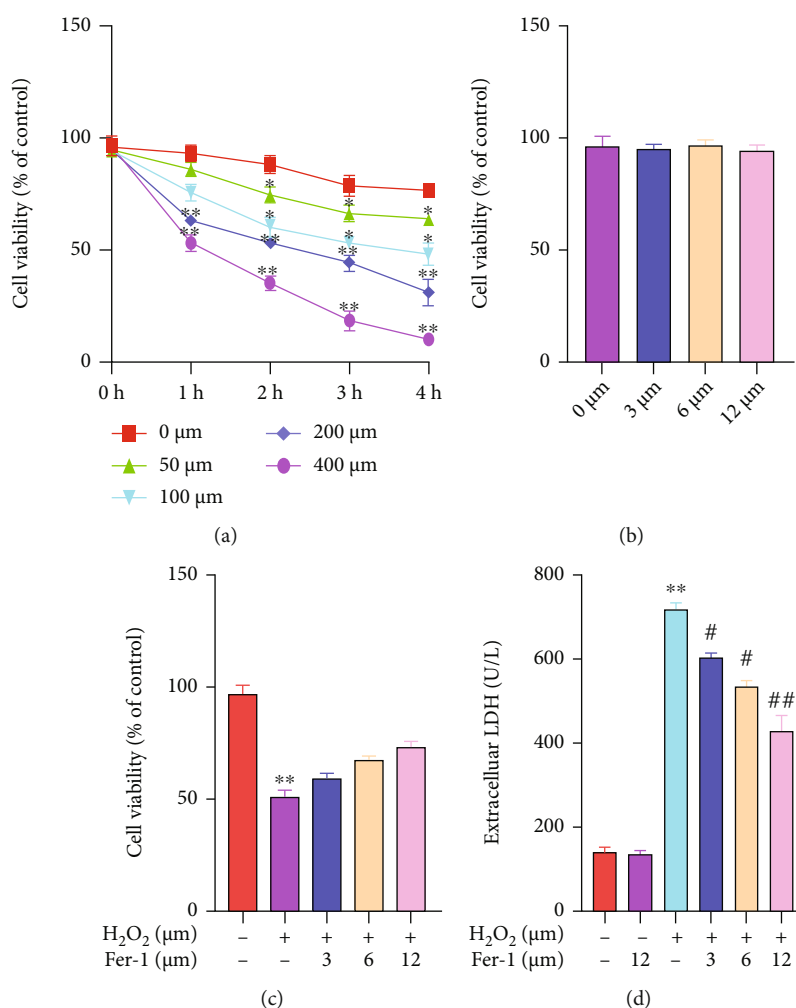


FIGURE 1: Effects of H₂O₂ and ferrostatin-1 on the survival rate of primary cardiomyocytes. (a) The effect of H₂O₂ on cell viability was detected by MTT (“*” indicates statistical difference from the 0 μM H₂O₂ group, $P < 0.05$; “**” indicates statistical difference from the 0 μM H₂O₂ group, $P < 0.01$). (b) The effect of ferrostatin-1 on cell viability was detected by MTT. (c) The effect of ferrostatin-1 on H₂O₂-induced cell viability was detected by MTT. (d) LDH activity was detected by kit (“**” indicates statistical difference from the control group, $P < 0.01$; “#” indicates statistical difference from the H₂O₂ group, $P < 0.05$; “##” indicates statistical difference from the H₂O₂ group, $P < 0.05$).

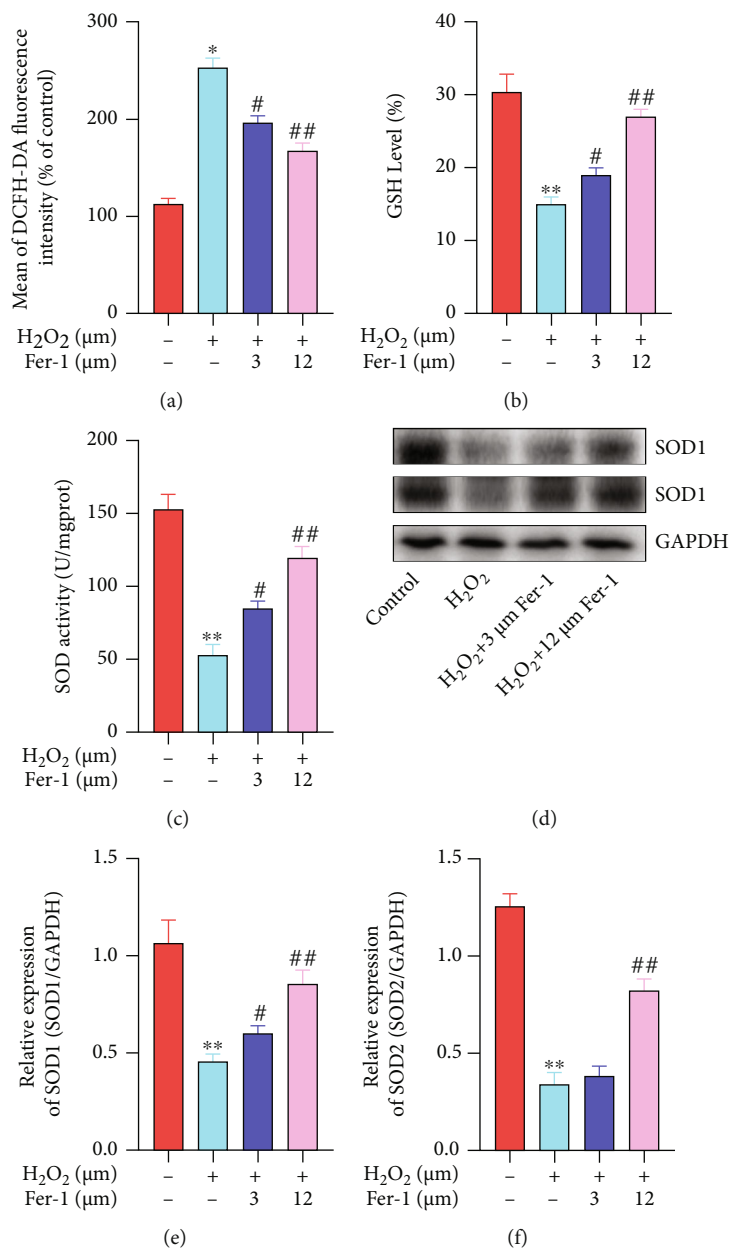


FIGURE 2: Continued.

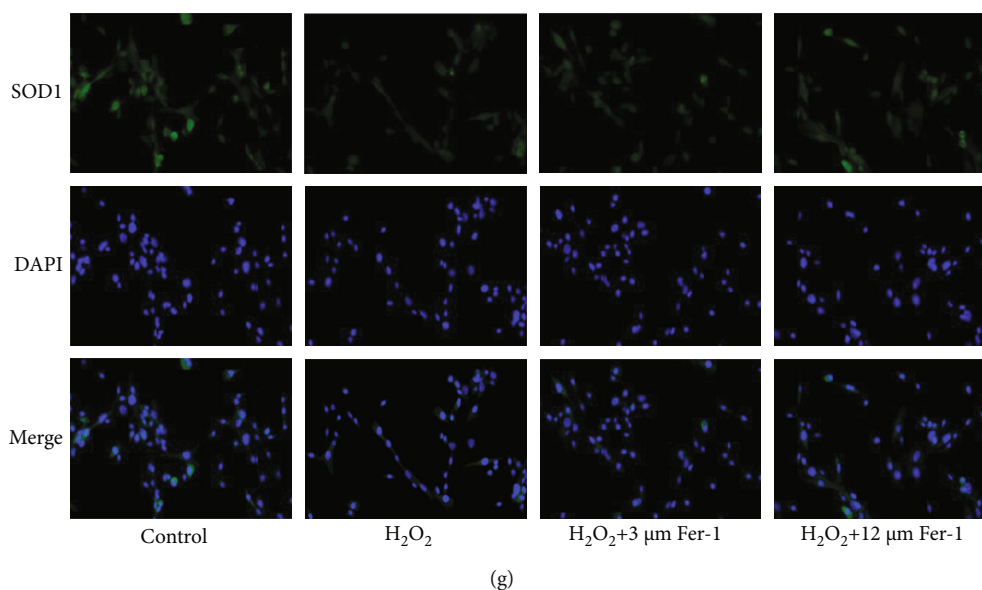


FIGURE 2: Ferrostatin-1 inhibited H_2O_2 -induced oxidative stress in primary cardiomyocytes. (a) Intracellular ROS levels were detected by flow cytometry. (b) GSH activity was detected by kit. (c) SOD activity was detected by kit. (d) SOD1 and SOD2 protein level was detected by WB. (e) SOD1 mRNA level was detected by qRT-PCR. (f) SOD2 mRNA level was detected by qRT-PCR. (g) The expression of SOD1 was detected by immunofluorescence staining (“*” indicates statistical difference from the control group, $P < 0.05$; “**” indicates statistical difference from the control group, $P < 0.01$; “#” indicates statistical difference from the H_2O_2 group, $P < 0.05$; “##” indicates statistical difference from the H_2O_2 group, $P < 0.05$).

3. Results

3.1. Effects of H_2O_2 and Ferrostatin-1 on the Survival Rate of Primary Cardiomyocytes. In order to establish the H_2O_2 concentration suitable for the OS injury model of primary myocardial cells, H_2O_2 concentration was divided into 5 groups (0 $\mu\text{mol/L}$, 50 $\mu\text{mol/L}$, 100 $\mu\text{mol/L}$, 200 $\mu\text{mol/L}$, and 400 $\mu\text{mol/L}$). After 4 hours of H_2O_2 treatment, the survival rate of each group was detected by MTT kit (Figure 1(a)). The results showed that compared with the control group, with the increase of H_2O_2 concentration, the cell survival rate gradually decreased. At the same time, we examined the effect of different ferrostatin-1 concentrations on the survival rate of primary cardiomyocytes using the MTT kit (Figure 1(b)). The results showed that after ferrostatin-1 was applied to primary cardiomyocytes at a concentration range of 3 μM –12 μM for 12 hours, there was no significant change in cell survival compared with the normal group, indicating that ferrostatin-1 had no significant effect on the growth of primary cardiomyocytes at this dose range. Next, we pretreated the cells with ferrostatin-1 for 12 hours, then added 200 $\mu\text{mol/L}$ H_2O_2 for 2 hours, and tested the cell survival rate with the MTT kit (Figure 1(c)). The results show that 3–12 μM ferrostatin-1 has a protective effect on primary cardiomyocytes injured by H_2O_2 , and its protective effect was concentration-dependent. Among them, 12 μM ferrostatin-1 can obviously inhibit H_2O_2 -induced cell death. At the same time, in order to detect the damage degree of H_2O_2 to cells and cell membrane, we detected the LDH activity in the cell supernatant and found that the LDH activity in the cell supernatant after the treatment of 12 μM

ferrostatin-1 alone had no significant change compared with the control group (Figure 1(d)). After the injury of 200 $\mu\text{mol/L}$ H_2O_2 , the LDH activity in the cell supernatant obviously increased. On the contrary, the LDH activity in the supernatant of the ferrostatin-1 group was lower than that of the H_2O_2 group, and there was a significant difference between the H_2O_2 group and the ferrostatin-1 group at the dose of 12 μM , indicating that ferrostatin-1 could obviously inhibit the LDH leakage of H_2O_2 -damaged primary cardiomyocytes.

3.2. Ferrostatin-1 Inhibited H_2O_2 -Induced OS in Primary Cardiomyocytes. In order to detect the degree of redox imbalance in primary cardiomyocytes, we detected intracellular ROS levels and found that the ROS level in the 200 μM H_2O_2 group increased, while in the 3 μM and 12 μM ferrostatin-1 groups, ROS level decreased obviously and was dose-dependent (Figure 2(a)). At the same time, we detected the activity of GSH and SOD in the cell supernatant and found that 3 μM and 12 μM ferrostatin-1 can inhibit the decrease of GSH and SOD activity caused by H_2O_2 (Figures 2(b) and 2(c)). Next, we detected the expression of SOD1 and SOD2 by WB and PCR (Figures 2(d)–2(f)). As a result, it was found that the expression of SOD1 and SOD2 in the H_2O_2 group was obviously reduced, while ferrostatin-1 can effectively promote the increase of SOD1 and SOD2 expression, and the 12 μM ferrostatin-1 group was more significant. Then, we detected the expression of SOD1 in primary cardiomyocytes by immunofluorescence staining, and the results obtained were similar to the former (Figure 2(g)).

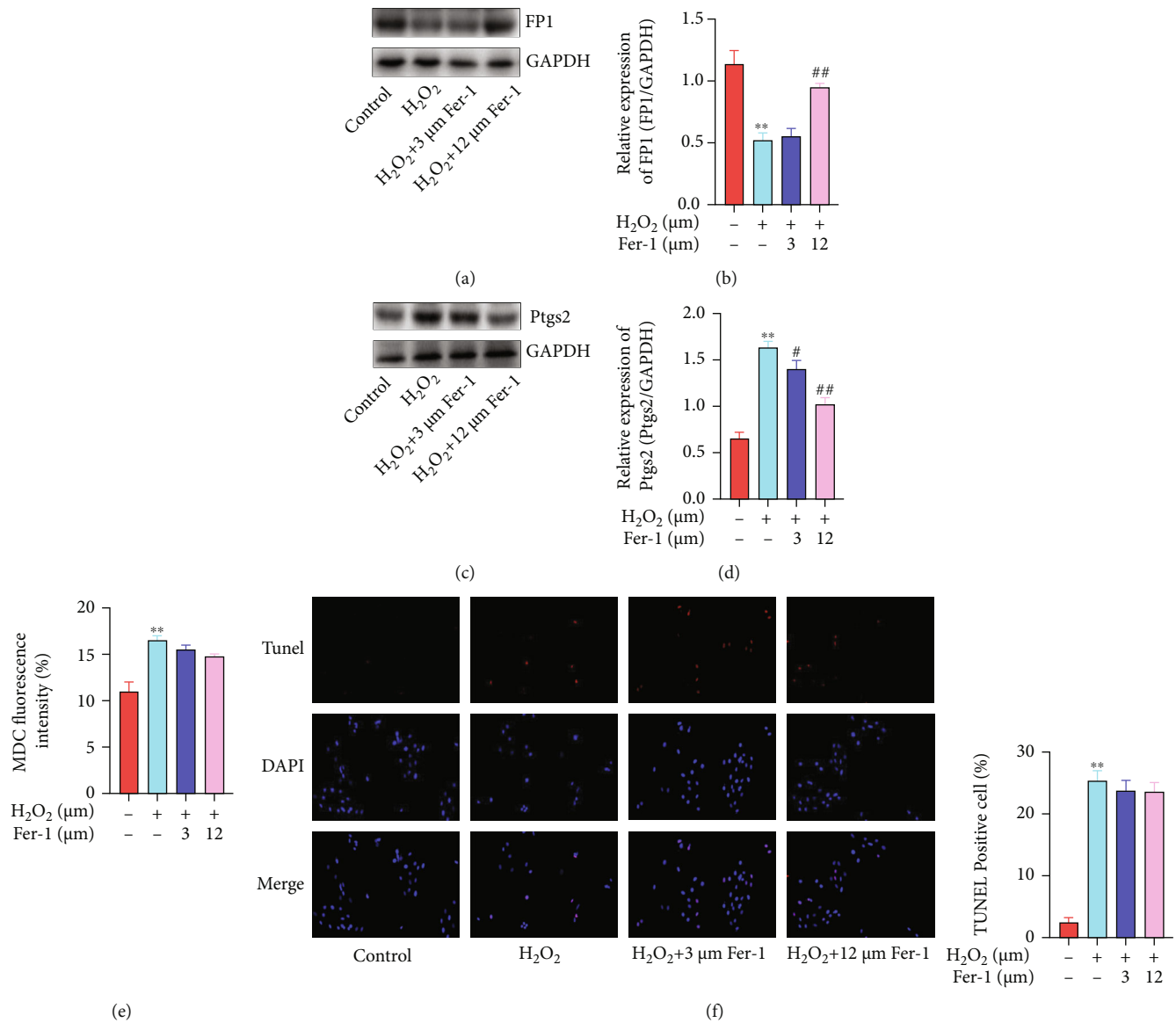


FIGURE 3: Ferrostatin-1 inhibited H₂O₂-induced ferroptosis in primary cardiomyocytes. (a) FP1 protein level was detected by WB. (b) FP1 mRNA level was detected by qRT-PCR. (c) Ptg2 protein level was detected by WB. (d) Ptg2 mRNA level was detected by qRT-PCR. (e) MDC fluorescence intensity was detected by flow cytometry. (f) The cell apoptosis was detected by TUNEL staining (“**” indicates statistical difference from the control group, $P < 0.01$; “#” indicates statistical difference from the H₂O₂ group, $P < 0.05$; “##” indicates statistical difference from the H₂O₂ group, $P < 0.05$).

3.3. Ferrostatin-1 Inhibited H₂O₂-Induced Ferroptosis in Primary Cardiomyocytes. Studies have confirmed that ferroportin1 (FP1) plays an important role in the process of cellular iron circulation [12]. WB results showed that compared with the control group, FP1 protein expression in the H₂O₂ group obviously decreased, while compared with the H₂O₂ group, FP1 protein expression in the 12 μM ferrostatin-1 group was obviously upregulated, showing a significant difference, while in the 3 μM ferrostatin-1 group, there was no significant difference (Figure 3(a)). Similar results were obtained by qRT-PCR (Figure 3(b)). In order to further prove the occurrence and situation of ferroptosis in the primary cardiomyocyte model of H₂O₂ injury, we detected the level of prostaglandin peroxidase 2 (Ptgs2) pro-

tein (Figure 3(c)). Compared with the control group, the expression of Ptg2 in the H₂O₂ group was obviously increased and there was a significant difference; after pretreatment with ferrostatin-1, the expression of Ptg2 protein could be obviously reduced. At the same time, we also detected the expression of Ptg2 mRNA (Figure 3(d)). The expression of Ptg2 mRNA in the H₂O₂ group was higher than that in the control group, and the difference was statistically significant; compared with the H₂O₂ group, with the increase in the concentration of ferrostatin-1, the expression level of Ptg2 mRNA decreased. This result was consistent with the results of protein level experiments, suggesting that ferrostatin-1 can inhibit the occurrence of ferroptosis induced by H₂O₂ in primary cardiomyocytes. At the same

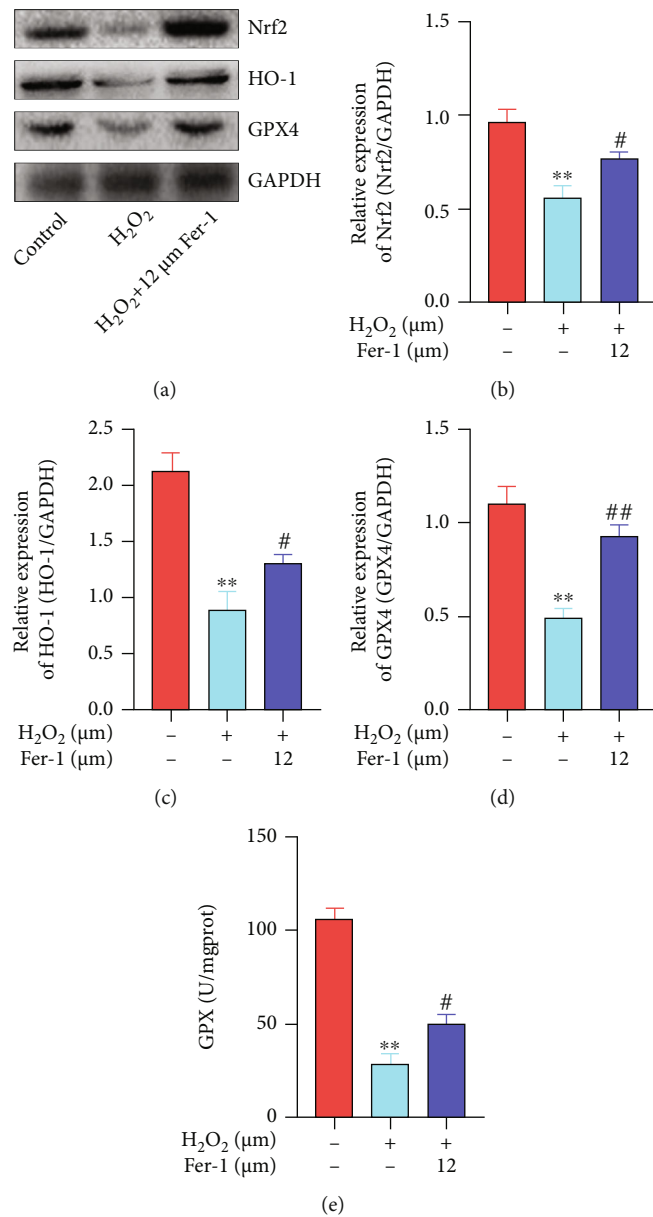


FIGURE 4: Nrf2/ARE pathway was involved in H₂O₂-induced ferroptosis of primary cardiomyocytes. (a) Nrf2, HO-1, and GPX4 protein level was detected by WB. (b) Nrf2 mRNA level was detected by qRT-PCR. (c) HO-1 mRNA level was detected by qRT-PCR. (d) GPX4 mRNA level was detected by qRT-PCR. (e) GPX activity was detected by kit (“**” indicates statistical difference from the control group, $P < 0.01$; “#” indicates statistical difference from the H₂O₂ group, $P < 0.05$; “##” indicates statistical difference from the H₂O₂ group, $P < 0.05$).

time, in order to quantitatively analyze the level of cell autophagy, we used flow cytometry to detect monodansylcadaverine (MDC) fluorescence intensity (Figure 3(e)). Studies confirm that MDC is commonly considered a specific marker for detecting autophagosome formation [13]. And our results showed that compared with the control group, the fluorescence intensity of the H₂O₂ group increased, suggesting that the model cells do exist autophagy; adding different doses of inhibitor ferrostatin-1, compared with the H₂O₂ group, the average fluorescence intensity did not obviously weaken. It suggests that there may be weak autophagy in the cell, but ferrostatin-1 was not a protective effect by inhibiting autophagy. In addition, observation of TUNEL

staining by fluorescence microscopy showed that the number of positive cells in the H₂O₂ group was significantly higher than that in the control group, while in the ferrostatin-1 group, the inhibitory effect of different concentrations of ferrostatin-1 on the number of positive cells was not obvious (Figure 3(f)).

3.4. Nrf2/ARE Pathway Was Involved in H₂O₂-Induced Ferroptosis of Primary Cardiomyocytes. The Nrf2/ARE pathway is currently widely regarded as a defensive molecular pathway for the body to resist oxidative and chemical stimuli in the internal and external environment [14]. Nrf2 can regulate the oxidation and anti-inflammatory proteins of many

endogenous genes in cells [15, 16], such as HO-1 and GPX4. WB results showed that compared with the control group, the levels of Nrf2, HO-1, and GPX4 protein in the H₂O₂ group were decreased, and there was a significant difference (Figure 4(a)). After pretreatment with 12 μ M ferrostatin-1, it can obviously promote the upregulation of Nrf2, HO-1, and GPX4 protein expression. At the same time, qRT-PCR also obtained similar results (Figures 4(b)–4(d)). Next, we tested the activity of GPX in the cell supernatant, and the results showed that the GPX level of the H₂O₂ group cells was obviously reduced compared to the control group (Figure 4(e)). The results indicated that H₂O₂ induced cell ferroptosis by reducing the level of GPX. Compared with the H₂O₂ group, the 12 μ M ferrostatin-1 group had obviously higher GPX levels. The above results suggest that ferrostatin-1 can reduce the damage of H₂O₂ on primary cardiomyocytes, and its mechanism may be related to the upregulation of Nrf2, HO-1, and GPX4 expression and improvement of cell antioxidant capacity.

4. Discussion

Ferroptosis is a cell death method discovered when the small molecule substance elastin kills cancer cells containing the RAS mutation of the oncogene [17]. At present, the research of ferroptosis is only in the initial stage, mainly involving in the research of antitumor. The study found that the use of antitumor drugs such as sorafenib to induce ferroptosis in cancer cells suggests that ferroptosis can be used as a new target for antitumor therapy [18]. However, whether this type of cell death is involved in other diseases besides tumors and whether there is an accurate detection method to confirm its existence, these series of problems need to be studied and confirmed.

In this study, in order to study the relationship between the primary cardiomyocyte death caused by H₂O₂ and ferroptosis, first, we found that ferroptosis-specific inhibitor ferrostatin-1 can obviously improve the primary cardiomyocyte status and reduce cell death. Cell death is a complicated process, in which different forms of death such as autophagy and apoptosis coexist [19]. In this experiment, by detecting different indicators such as MDC and TUNEL, it was confirmed that the form of cell death can coexist in the process of primary myocardial cell injury. In this experiment, compared with the model group, the fluorescence intensity of MDC in the ferrostatin-1 group did not increase and the number of TUNEL positive cells did not increase in the ferrostatin-1 group, but the cell viability was obviously improved, indicating that ferrostatin-1 did not inhibit apoptosis, autophagy, etc.

Therefore, we speculate that H₂O₂ induces iron-related death in primary cardiomyocytes. Cell iron load is an important factor affecting ferroptosis. Studies have shown that FP1 is a transmembrane iron export protein present on the cell membrane. FP1 is an important protein that maintains the balance of iron concentration in the cell, and it plays an important role in the transfer and export of iron. The results of this experiment found that after primary cardiomyocytes treated with 200 μ M H₂O₂, the expression level of FP1 pro-

tein in the cells decreased compared with the control group, indicating that the induction of H₂O₂ affected the iron homeostasis of the cells. This also confirms that the cell damage caused by H₂O₂ is related to iron-related death. In addition, Ptg2 is a key enzyme in the prostaglandin synthesis process. It can increase the peroxidase activity through prostaglandin and other metabolites, leading to the generation of free radicals and affecting the oxidation balance of the body. Therefore, the upregulation of Ptg2 protein is believed to be a ferroptosis occurring in marker [20]. In view of this, we detected the Ptg2 protein and mRNA levels, and the results showed that the Ptg2 protein and mRNA levels of the model group were upregulated simultaneously.

The results of this series further confirmed that H₂O₂ induced primary cardiomyocyte death mainly due to the occurrence of ferroptosis. Therefore, further in-depth study of ferroptosis exploring the mechanism of its occurrence in myocardial cell injury model is needed. The detection of ferroptosis presence of accurate indicators and methods will have important significance for the treatment of IHD.

5. Conclusion

Ferroptosis-specific inhibitor ferrostatin-1 alleviates H₂O₂-induced redox imbalance in primary cardiomyocytes through the Nrf2/ARE pathway, inhibits ferroptosis, and thus slows cardiomyocyte death. This provides a new basis for clinical treatment of IHD.

Data Availability

The datasets used and analyzed during the current study are available from the corresponding author on reasonable request.

Conflicts of Interest

The authors declare that they have no competing interests.

References

- [1] A. Henderson, "Coronary heart disease: overview," *The Lancet*, vol. 348, Supplement 1, pp. s1–s4, 1996.
- [2] E. Teringova and P. Tousek, "Apoptosis in ischemic heart disease," *Journal of Translational Medicine*, vol. 15, no. 1, p. 87, 2017.
- [3] D. Wang, W. Yu, Y. Liu et al., "Roles of autophagy in ischemic heart diseases and the modulatory effects of Chinese herbal medicine," *The American Journal of Chinese Medicine*, vol. 45, no. 7, pp. 1401–1419, 2017.
- [4] B. L. Maximilian, "Mitochondria in ischemic heart disease," *Advances in Experimental Medicine and Biology*, vol. 982, pp. 127–140, 2017.
- [5] D. R. Janero, "Ischemic heart disease and antioxidants: mechanistic aspects of oxidative injury and its prevention," *Critical Reviews in Food Science and Nutrition*, vol. 35, no. 1–2, pp. 65–81, 1995.
- [6] S. J. Dixon, K. M. Lemberg, M. R. Lamprecht et al., "Ferroptosis: an iron-dependent form of nonapoptotic cell death," *Cell*, vol. 149, no. 5, pp. 1060–1072, 2012.

- [7] T. Hirschhorn and B. R. Stockwell, "The development of the concept of ferroptosis," *Free Radical Biology & Medicine*, vol. 133, pp. 130–143, 2019.
- [8] K. Kazan and S. Kalaipandian, "Ferroptosis: yet another way to die," *Trends in Plant Science*, vol. 24, no. 6, pp. 479–481, 2019.
- [9] A. Degtarev and A. Linkermann, "Generation of small molecules to interfere with regulated necrosis," *Cellular and Molecular Life Sciences*, vol. 73, pp. 2251–2267, 2016.
- [10] H. Imai, M. Matsuoka, T. Kumagai, T. Sakamoto, and T. Koumura, "Lipid peroxidation-dependent cell death regulated by GPx4 and ferroptosis," *Current Topics in Microbiology and Immunology*, vol. 403, pp. 143–170, 2017.
- [11] M. M. Gaschler, A. A. Andia, H. Liu et al., "FINO₂ initiates ferroptosis through GPX4 inactivation and iron oxidation," *Nature Chemical Biology*, vol. 14, no. 5, pp. 507–515, 2018.
- [12] N. T. Le and D. R. Richardson, "Ferroportin1: a new iron export molecule?," *The International Journal of Biochemistry & Cell Biology*, vol. 34, no. 2, pp. 103–108, 2002.
- [13] S. Liang, G. Figtree, M. Aiqun, and Z. Ping, "GAPDH-knockdown reduce rotenone-induced H9C2 cells death via autophagy and anti-oxidative stress pathway," *Toxicology Letters*, vol. 234, no. 3, pp. 162–171, 2015.
- [14] L. Li, T. Liu, L. Liu et al., "Effect of hydrogen-rich water on the Nrf2/ARE signaling pathway in rats with myocardial ischemia-reperfusion injury," *Journal of Bioenergetics and Biomembranes*, vol. 51, no. 6, pp. 393–402, 2019.
- [15] Y. Zhang, K. A. Ahmad, F. U. Khan, S. Yan, A. U. Ihsan, and Q. Ding, "Chitosan oligosaccharides prevent doxorubicin-induced oxidative stress and cardiac apoptosis through activating p38 and JNK MAPK mediated Nrf2/ARE pathway," *Chemico-Biological Interactions*, vol. 305, pp. 54–65, 2019.
- [16] M. Zhang, J. Zhang, Y. Xiong, J. Peng, and X. Wu, "Pyrroloquinoline quinone inhibits oxidative stress in rats with diabetic nephropathy," *Medical Science Monitor*, vol. 26, article e924372, 2020.
- [17] Y. Xie, W. Hou, X. Song et al., "Ferroptosis: process and function," *Cell Death and Differentiation*, vol. 23, no. 3, pp. 369–379, 2016.
- [18] X. Sun, X. Niu, R. Chen et al., "Metallothionein-1G facilitates sorafenib resistance through inhibition of ferroptosis," *Hepatology*, vol. 64, no. 2, pp. 488–500, 2016.
- [19] M. S. D'Arcy, "Cell death: a review of the major forms of apoptosis, necrosis and autophagy," *Cell Biology International*, vol. 43, no. 6, pp. 582–592, 2019.
- [20] W. S. Yang, R. SriRamaratnam, M. E. Welsch et al., "Regulation of ferroptotic cancer cell death by GPX4," *Cell*, vol. 156, no. 1-2, pp. 317–331, 2014.

Research Article

LINC00460 Stimulates the Proliferation of Vascular Endothelial Cells by Downregulating miRNA-24-3p

Ruofei Jia,¹ Xingxing Yuan,² Chengzhi Yang,¹ Jing Han,¹ Xiaojing Cao,¹ Zheng Qin,¹ Jing Nan,¹ and Zening Jin¹ 

¹Department of Cardiology, Beijing Tiantan Hospital, Capital Medical University, Beijing, China

²Department of Clinical Laboratory Center, Beijing Youan Hospital, Capital Medical University, Beijing, China

Correspondence should be addressed to Zening Jin; jin_zening@163.com

Received 3 November 2021; Accepted 23 December 2021; Published 18 February 2022

Academic Editor: Francesco Busardò

Copyright © 2022 Ruofei Jia et al. This is an open access article distributed under the Creative Commons Attribution License, which permits unrestricted use, distribution, and reproduction in any medium, provided the original work is properly cited.

Objective. To clarify the effect of LINC00460 on mediating the proliferative ability of vascular endothelial cells (ECs) by targeting microRNA-24-3p (miRNA-24-3p), thus influencing the progression of atherosclerotic diseases. **Methods.** Relative levels of LINC00460 and miRNA-24-3p in ECs induced with different doses of ox-LDL (oxidized low density lipoprotein) for different time points were determined by quantitative real-time polymerase chain reaction (qRT-PCR). Influences of LINC00460 and miRNA-24-3p on the viability of ECs were assessed by Cell Counting Kit-8 (CCK-8) and 5-ethynyl-2'-deoxyuridine (EdU) assay. Through dual-luciferase reporter gene assay, the binding between LINC00460 and miRNA-24-3p was evaluated. At last, rescue experiments were performed to identify the function of the LINC00460/miRNA-24-3p axis in regulating the proliferative ability of ECs. **Results.** LINC00460 was upregulated after ox-LDL treatment in a dose- and time-dependent manner. Viability of ECs gradually increased with the prolongation of ox-LDL treatment and the treatment of increased dose. The overexpression of LINC00460 enhanced the viability and EdU-positive rate in ECs treated with ox-LDL. miRNA-24-3p was the direct target of LINC00460, which was negatively regulated by LINC00460. miRNA-24-3p was downregulated with the prolongation of ox-LDL treatment. The overexpression of miRNA-24-3p could reverse the effect of LINC00460 on regulating the proliferative ability of ECs. **Conclusions.** LINC00460 regulates the proliferative ability of ECs and thus the occurrence and development of coronary atherosclerotic diseases by targeting miRNA-24-3p.

1. Introduction

Cardiovascular and cerebrovascular diseases are resulted from hyperlipidemia, blood viscosity, atherosclerosis, and hypertension, leading to the ischemic or hemorrhagic lesions in the heart, brain, and whole body [1]. The causes of cardiovascular and cerebrovascular diseases mainly include atherosclerosis, hypertension, hyperlipidemia, diabetes, leukemia, thrombocytosis, and other factors [2]. Cardiovascular and cerebrovascular diseases seriously threaten the human health, especially middle-aged and elder people over 50 years. They are characterized by high prevalence, disability, and mortality. There are 15 million people die of cardiovascular and cerebrovascular diseases every year, ranking the first in disease mortality [3]. Taking aspirin to prevent vascular embolism, changing lifestyles, and controlling blood

pressure and blood lipids are considered to effectively prevent the cardiovascular and cerebrovascular diseases [4].

Endothelial cells exert a crucial role in the progression of cardiovascular diseases, such as coronary heart disease, stroke, and atherosclerosis [5]. Abnormal migration and proliferation of ECs owing to epigenetic changes are identified to participate in the pathogenesis of cardiovascular diseases [6]. Nevertheless, specific mechanisms underlying the abnormal cellular behaviors of ECs remain unclear.

Long noncoding RNAs (lncRNAs) are noncoding RNAs with over 200 nucleotides long [7, 8]. Numerous studies have shown the important role of noncoding RNAs in the epigenetic regulation [9]. lncRNAs could able to affect a variety of cellular processes [10]. Dysregulated lncRNAs are involved in many diseases, such as tumors, diabetes, and cardiovascular diseases [11]. Recent studies have found that LINC00460

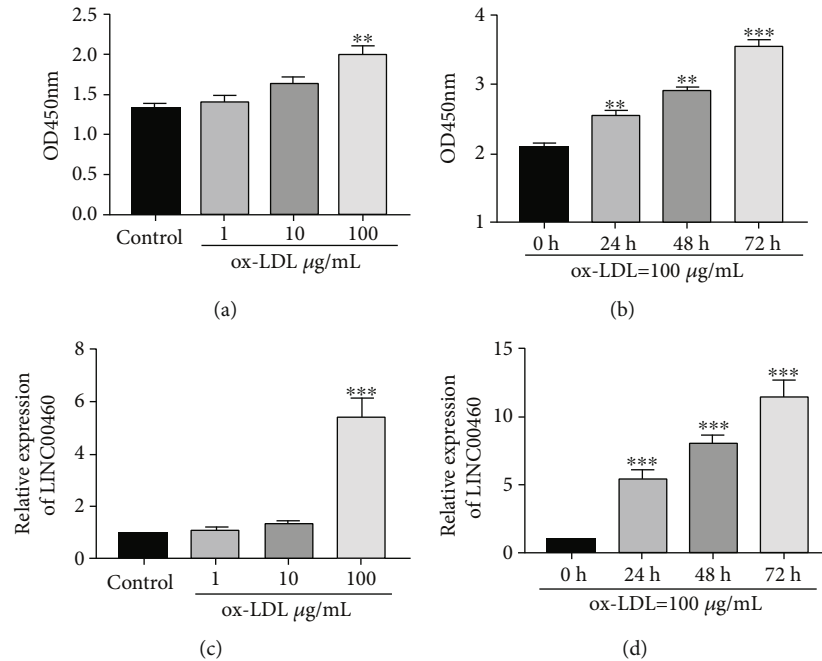


FIGURE 1: LINC00460 was upregulated after ox-LDL treatment. (a) CCK-8 assay showed the viability in ECs treated with 0, 1, 10, and 100 $\mu\text{g}/\text{mL}$ ox-LDL for 24 h. (b) CCK-8 assay showed the viability in ECs treated with 100 $\mu\text{g}/\text{mL}$ ox-LDL for 0, 24, 48, and 72 h. (c) Relative level of LINC00460 in ECs treated with 0, 1, 10, and 100 $\mu\text{g}/\text{mL}$ ox-LDL for 24 h. (d) Relative level of LINC00460 in ECs treated with 100 $\mu\text{g}/\text{mL}$ ox-LDL for 0, 24, 48, and 72 h.

promotes the development of nasopharyngeal carcinoma by absorbing microRNA-149-5p (miR-149-5p) to upregulate IL-6 [12]. LINC00460 regulates KDM2A by targeting miR-342-3p in gastric cancer and thereafter promotes proliferative and migratory abilities of cancer cells [13]. Upregulation of LINC00460 inhibits colorectal cancer to proliferate [14]. LINC00460 accelerates the progression of epithelial ovarian cancer by modulating miRNA-338-3p [15]. LINC00460 stimulates the malignant growth of lung adenocarcinoma by targeting the miR-302c-5p/FOXA1 axis [16]. The role of LINC00460 in the development of cardiovascular diseases, however, is poorly understood.

2. Materials and Methods

2.1. Cell Culture. ECs were provided by American Type Culture Collection (ATCC) (Manassas, VA, USA) and cultured in Dulbecco's Modified Eagle Medium (DMEM) (Gibco, Rockville, MD, USA) containing 10% fetal bovine serum (FBS) (Gibco, Rockville, MD, USA), 100 $\mu\text{g}/\text{mL}$ penicillin, and 0.1 mg/mL streptomycin, in a 37°C and 5% CO₂ incubator. ECs were treated with 100 $\mu\text{g}/\text{mL}$ ox-LDL to mimic the high-fat environment.

2.2. RNA Extraction and Quantitative Real-Time Polymerase Chain Reaction (qRT-PCR). Cells were digested in TRIzol Reagent (Invitrogen, Carlsbad, CA, USA) to isolate total RNAs. RNAs were then reversely transcribed into complementary deoxyribose nucleic acid (cDNA) and subjected to PCR using the SYBR Green method (TaKaRa, Tokyo, Japan) for 5 min at 94°C and 40 cycles for 30 s at 94°C, 30 s at 55°C, and 90 s at 72°C. The primers are as follows, LINC00460,

F:5'-AGAAATCCTCCAGCCCTGTT-3', R:5'-GGGTGACTCTTAGCCGAGAA-3'; GAPDH, F:5'-GAAGAGAGAGACCCTCACGCTG-3', R:5'-ACTGTGAGGAGGGGAGATTCAGT-3'.

2.3. Dual-Luciferase Reporter Gene Assay. ECs were cotransfected with miRNA-24-3p mimic/negative control and LINC00460-WT/LINC00460-MT, respectively. After transfection of 48 h, cells were lysed for determining relative luciferase activity.

2.4. Cell Counting Kit-8 (CCK-8). ECs were seeded in the 96-well plate at 5×10^3 cells per well and cultured overnight. Absorbance (A) at 450 nm was recorded at the appointed time points using the CCK-8 kit (Dojindo Laboratories, Kumamoto, Japan) for depicting the viability curves.

2.5. Construction of Overexpression Vectors and Transfection. After constructing the pcDNA3.0-LINC00460 vector based on amplification with specific primers, the cDNA of LINC00460 was cloned into the mammalian expression vector pcDNA3.0 (Invitrogen, Carlsbad, CA, USA). ECs were cultured until 60% of confluence and subjected to transfection using Lipofactamine 2000 (Invitrogen, Carlsbad, CA, USA). 6 hours later, complete medium was replaced. Transfected cells for 24-48 h were harvested for in vitro experiments.

2.6. 5-Ethynyl-2'-Deoxyuridine (EdU) Assay. ECs were seeded in the 96-well plate with 300 cells per well. ECs were labeled with 50 $\mu\text{mol}/\text{L}$ EdU (Guangzhou RiboBio Co., Ltd., Guangzhou, China) at 37°C for 2 h. After 30-min fixation in

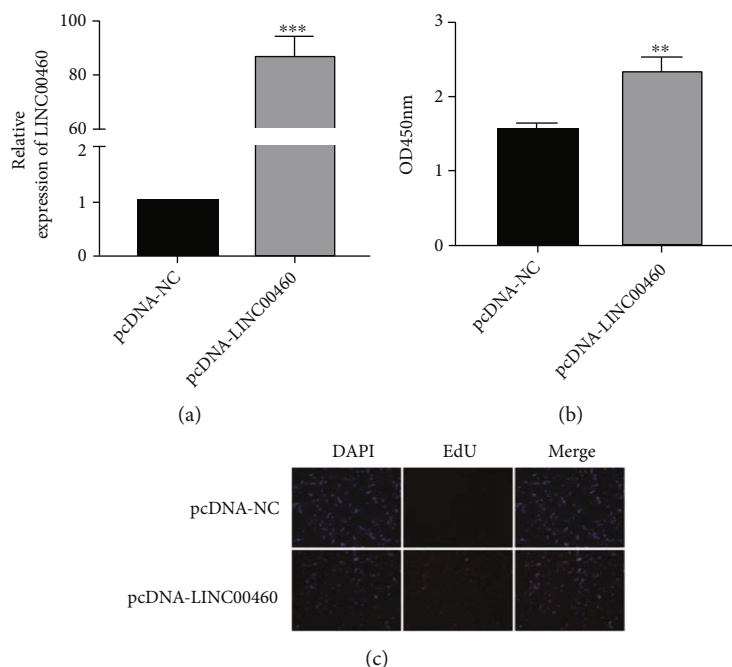


FIGURE 2: The overexpression of LINC00460 accelerated the proliferative ability of ECs. (a) Transfection efficacy of pcDNA-LINC00460 in ECs. (b) CCK-8 assay showed the viability in ECs transfected with pcDNA-NC or pcDNA-LINC00460. (c) DAPI-labeled, EdU-labeled, and merged images of ECs transfected with pcDNA-NC or pcDNA-LINC00460.

4% paraformaldehyde, cells were incubated with phosphate buffered saline (PBS) containing 0.5% Triton-100 for 20 min. After washing with PBS containing 3% bovine serum albumin (BSA), cells were incubated in 100 μ L of dying solution in dark for 1 h and counterstained with 100 μ L of 4',6-diamidino-2-phenylindole (DAPI) (5 μ g/mL) for 30 min. EdU-positive cells, DAPI-labeled nucleus, and merged images were captured under a microscope (magnification \times 100).

2.7. Statistical Analysis. Statistical Product and Service Solutions (SPSS) 18.0 (SPSS Inc., Chicago, IL, USA) was used for data analyses. GraphPad Prism 6.0 (La Jolla, CA, USA) was applied for depicting figures. Data were expressed as mean \pm standard deviation. Differences between two groups were compared by the *t*-test. Differences among multigroups were compared by ANOVA analysis. $P < 0.05$ is considered statistically significant.

3. Results

3.1. LINC00460 Was Upregulated after Ox-LDL Treatment. Hyperlipidemia and abnormal lipid metabolism are important causes of atherosclerosis. The treatment of ox-LDL (oxidized low density lipoprotein) can aggravate atherosclerosis by stimulating the formation of foam cells, platelet adhesion and thrombosis, and EC injury. It is generally believed that ox-LDL is the important induction factor for atherosclerosis and in vitro EC injury. The viability of ECs was gradually enhanced with the treatment of increased dose of ox-LDL (Figure 1(a)). In addition, the viability increased with the

prolongation of ox-LDL treatment (Figure 1(b)). QRT-PCR data showed that LINC00460 was greatly upregulated after 100 μ g/mL ox-LDL treatment for 24 h (Figure 1(c)). Its level gradually increased after 100 μ g/mL ox-LDL treatment for 24, 48, and 72 h (Figure 1(d)).

3.2. The overexpression of LINC00460 Accelerated the Proliferative Ability of ECs. pcDNA-LINC00460 was constructed, and its transfection efficacy was tested. As qRT-PCR data revealed, transfection of pcDNA-LINC00460 remarkably upregulated LINC00460 level in ECs (Figure 2(a)). After transfection of pcDNA-LINC00460, the viability and EdU-labeled cells were enhanced, indicating the promoted proliferative ability of ECs (Figures 2(b) and 2(c)).

3.3. LINC00460 Bound to miRNA-24-3p. Several potential miRNAs binding to LINC00460 were searched from online bioinformatic websites, including miRNA-24-3p, miRNA-485-5p, miRNA-149-5p, miRNA-662, and miRNA-671-5p. Transfection of pcDNA-LINC00460 downregulated miRNA-24-3p, but upregulated miRNA-662 and miRNA-671-5p (Figure 3(a)). After 100 μ g/mL ox-LDL treatment for 0, 24, 48, and 72 h, relative level of miRNA-24-3p gradually decreased (Figure 3(b)). Potential binding sequences between LINC00460 and miRNA-24-3p were identified in Figure 3(c). Subsequently, a remarkable decline in luciferase activity was observed after cotransfection of LINC00460-WT and miRNA-24-3p mimics, verifying the binding between LINC00460 and miRNA-24-3p (Figure 3(d)). To further uncover the biological function of miRNA-24-3p,

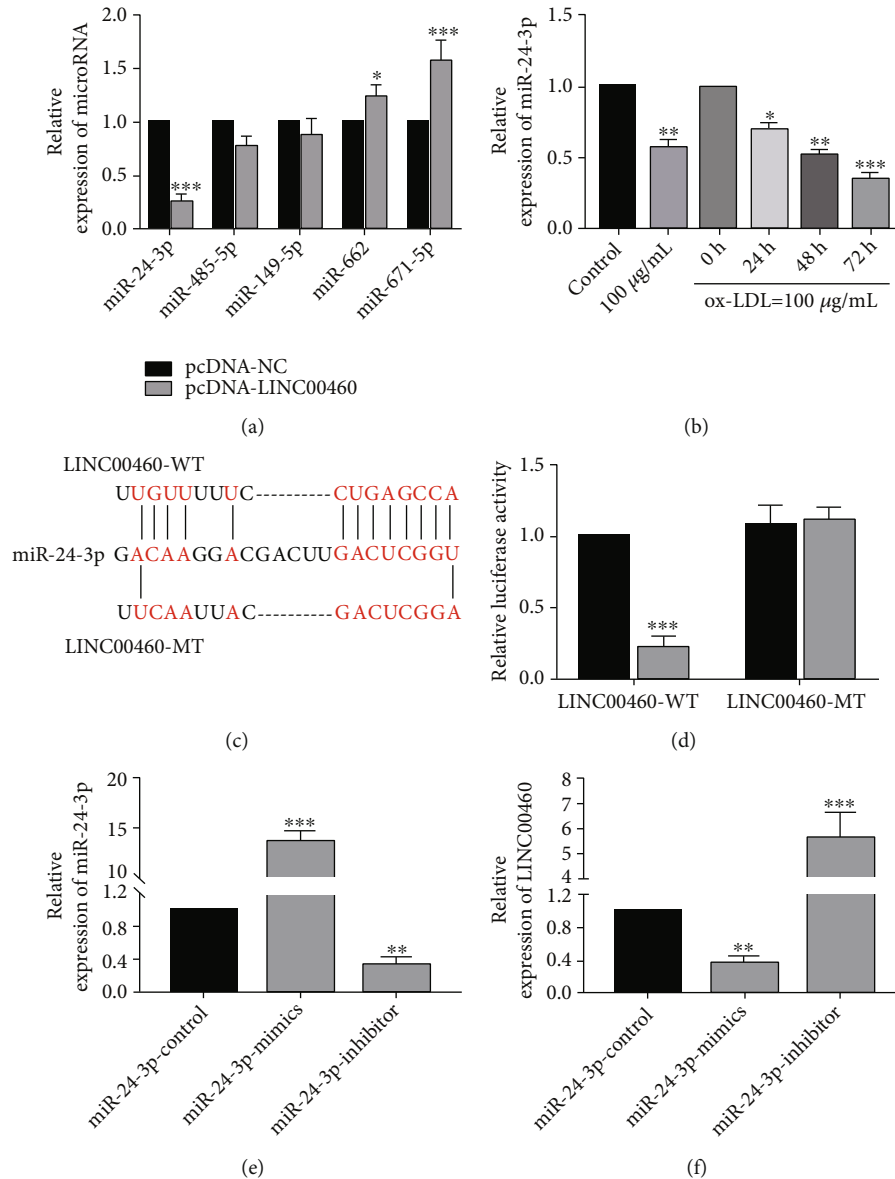


FIGURE 3: LINC00460 bound to miR-24-3p. (a) Relative levels of miRNA-24-3p, miRNA-485-5p, miRNA-149-5p, miRNA-662, and miRNA-671-5p in ECs transfected with pcDNA-NC or pcDNA-LINC00460. (b) MiR-24-3p level in ECs treated with 100 µg/mL ox-LDL for 0, 24, 48, and 72 h. (c) Binding sites in promoter regions of LINC00460 and miR-24-3p. (d) Luciferase activity in ECs after cotransfection with miR-24-3p mimic/negative control and LINC00460-WT/LINC00460-MT, respectively. (e) Transfection efficacies of miR-24-3p mimics and miR-24-3p inhibitor. (f) LINC00460 level in ECs transfected with NC, miR-24-3p mimics, or miR-24-3p inhibitor.

we constructed miRNA-24-3p mimics and miRNA-24-3p inhibitor (Figure 3(e)). LINC00460 level was found to be negatively regulated by miRNA-24-3p (Figure 3(f)).

3.4. The Overexpression of miRNA-24-3p Reversed the Role of LINC00460 on EC Proliferation. We further focused on the potential role of the LINC00460/miRNA-24-3p axis in influencing the proliferative ability of ECs. The elevated viability in EC overexpressing LINC00460 was reduced after cotransfection of miRNA-24-3p mimics (Figure 4(a)). Similarly, the number of EdU-positive cells was reduced after cotransfection of pcDNA-LINC00460 and miRNA-24-3p mimics compared with those overexpressing LINC00460

(Figure 4(b)). It is concluded that the miRNA-24-3p overexpression reversed the promotive effect of LINC00460 on the proliferative rate of ECs.

4. Discussion

Cardiovascular and cerebrovascular diseases are the leading causes of death in developed countries. Atherosclerosis is the main cause of coronary heart disease, cerebral infarction, and peripheral vascular disease [17]. Lipid metabolism disorder is the basis of atherosclerosis, which eventually leads to thickening and hardening of the arterial wall and narrowing of the vascular lumen [18]. Atherosclerosis is named

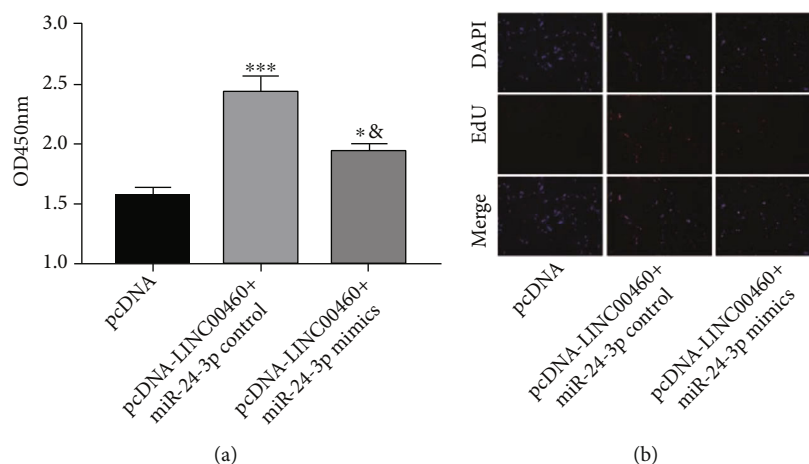


FIGURE 4: The overexpression of miR-24-3p reversed the role of LINC00460 on EC proliferation. ECs were transfected with pcDNA-NC, pcDNA-LINC00460 + miR-24-3p control, or pcDNA-LINC00460 + miR-24-3p mimics. (a) CCK-8 assay showed the viability. (b) DAPI-labeled, EdU-labeled, and merged images of ECs.

because of the yellow atheroma appearance of deposited lipids in the intima [19]. The main risk factors for atherosclerosis include hypertension, hyperlipidemia, heavy smoking, obesity, and genetic factors. Symptoms of atherosclerosis mainly depend on the vascular lesions and the ischemic degree of the affected organs [20]. Severe complications of coronary atherosclerosis include angina pectoris, myocardial infarction, and even sudden death. Cerebral atherosclerosis may cause cerebral ischemia, brain atrophy, or cerebral vascular rupture [21]. Good living habits and discontinuing the habit of smoking and drinking could prevent the occurrence of atherosclerosis [22].

MiRNAs are a class of noncoding, single-stranded RNAs encoded by endogenous genes. They are approximately 22 nucleotides in length and involved in the posttranscriptional regulation in plants and animals [23]. One miRNA regulates expressions of multiple genes, and several miRNAs could regulate the expression of a single gene. It is speculated that miRNAs are able to regulate one-third of human genes [24]. MiRNAs are capable of degrading mRNAs of the target genes through complementary base pairing in a complete way. Meanwhile, miRNAs inhibit the translation of target genes in an incomplete way without affecting the stability of the mRNAs [25]. Cellular behaviors could be mediated by miRNAs [26]. Abnormalities in miRNA expressions are involved in the disease development. For example, miRNA-210 induces the apoptosis of ECs by targeting PDK1 and thus aggravates atherosclerosis [27]. Exosomal-mediated miR-155 transfers it from smooth muscle cells to ECs and thereafter induces the occurrence of atherosclerosis [28]. Upregulated miRNA-876 induces the apoptosis of ECs by inhibiting Bcl-X1 [29]. This study mainly investigated the biological role of miRNAs in promoting proliferative ability of ECs.

Accumulating evidences have reported that lncRNAs act as miRNA sponges and eliminate the inhibitory effects of miRNAs on their target genes. For example, melatonin prevents the apoptosis of ECs by modulating the lncRNA MEG3/miR-223/NLRP3 axis [30]. The interaction of miR-

193a-3p with HMGB1 suppresses ECs to proliferate and migrate [31]. LncRNA PVT1 activates CTGF/ANGPT2 by targeting miR-26b, thus promoting angiogenesis in vascular ECs [32]. SNHG15 affects the viability of glioma microvascular ECs through negatively mediating miR-153 level [33]. In this paper, we investigated the interaction between LINC00460 and miRNA-24-3p in influencing the proliferative ability of ECs.

The treatment of ox-LDL mimics the effects of atherosclerotic hyperlipidemia on ECs. LINC00460 was time-dependently and dose-dependently upregulated after ox-LDL treatment. The overexpression of LINC00460 enhanced the viability and EdU-positive rate in ECs treated with ox-LDL. Subsequently, dual-luciferase reporter gene assay verified the binding between LINC00460 and miRNA-24-3p. miRNA-24-3p was downregulated with the prolongation of ox-LDL treatment. Notably, the overexpression of miRNA-24-3p could reverse the regulatory role of LINC00460 on the proliferative ability of ECs. In this present study, we slightly uncover the role of LINC00460 in vascular endothelial cells by *in vitro* assay. However, the mechanism should be explored more deeply in the future research.

5. Conclusions

LINC00460 regulates the proliferative ability of ECs and thus the occurrence and development of coronary atherosclerotic diseases by targeting miRNA-24-3p.

Data Availability

The datasets used and analyzed during the current study are available from the corresponding author on reasonable request.

Conflicts of Interest

The authors declared no conflict of interest.

Authors' Contributions

Study conception and design were contributed by RJ and ZJ. Data collection was contributed by CY, JH, and XC. Analysis and interpretation of results were contributed by XY, CY, ZQ, and JN. Draft manuscript preparation was contributed by RJ and ZJ. Manuscript revision and language editing were contributed by RJ and XY. All authors reviewed the results and approved the final version of the manuscript.

References

- [1] D. P. Leong, P. G. Joseph, M. McKee et al., "Reducing the global burden of cardiovascular disease, part 2: prevention and treatment of cardiovascular disease," *Circulation Research*, vol. 121, no. 6, pp. 695–710, 2017.
- [2] E. Jokinen, "Obesity and cardiovascular disease," *Minerva Pediatrica*, vol. 67, no. 1, pp. 25–32, 2015.
- [3] M. Aggarwal, B. Aggarwal, and J. Rao, "Integrative medicine for cardiovascular disease and prevention," *The Medical Clinics of North America*, vol. 101, no. 5, pp. 895–923, 2017.
- [4] E. Berinstein and A. Levy, "Recent developments and future directions for the use of pharmacogenomics in cardiovascular disease treatments," *Expert Opinion on Drug Metabolism & Toxicology*, vol. 13, no. 9, pp. 973–983, 2017.
- [5] K. Yamagata, "Docosahexaenoic acid regulates vascular endothelial cell function and prevents cardiovascular disease," *Lipids in Health and Disease*, vol. 16, no. 1, p. 118, 2017.
- [6] L. Chen, W. Yang, Y. Guo et al., "Exosomal lncRNA GAS5 regulates the apoptosis of macrophages and vascular endothelial cells in atherosclerosis," *PLoS One*, vol. 12, no. 9, p. e185406, 2017.
- [7] M. Zhou, W. J. Ding, Y. W. Chen et al., "Expression changes of long noncoding RNA in the process of endothelial cell activation," *Cellular Physiology and Biochemistry*, vol. 41, no. 1, pp. 115–123, 2017.
- [8] S. Shen, H. Jiang, Y. Bei, J. Xiao, and X. Li, "Long non-coding RNAs in cardiac remodeling," *Cellular Physiology and Biochemistry*, vol. 41, no. 5, pp. 1830–1837, 2017.
- [9] S. Uchida and S. Dimmeler, "Long noncoding RNAs in cardiovascular diseases," *Circulation Research*, vol. 116, no. 4, pp. 737–750, 2015.
- [10] M. S. Leisegang, C. Fork, I. Josipovic et al., "Long noncoding RNA MANTIS facilitates endothelial angiogenic function," *Circulation*, vol. 136, no. 1, pp. 65–79, 2017.
- [11] J. M. Lorenzen and T. Thum, "Long noncoding RNAs in kidney and cardiovascular diseases," *Nature Reviews. Nephrology*, vol. 12, no. 6, pp. 360–373, 2016.
- [12] Y. G. Kong, M. Cui, S. M. Chen, Y. Xu, Y. Xu, and Z. Z. Tao, "LncRNA-LINC00460 facilitates nasopharyngeal carcinoma tumorigenesis through sponging miR-149-5p to up-regulate IL6," *Gene*, vol. 639, pp. 77–84, 2018.
- [13] F. Wang, S. Liang, X. Liu, L. Han, J. Wang, and Q. Du, "LINC00460 modulates KDM2A to promote cell proliferation and migration by targeting miR-342-3p in gastric cancer," *Oncotargets and Therapy*, vol. 11, pp. 6383–6394, 2018.
- [14] X. Wang, F. M. Mo, H. Bo et al., "Upregulated expression of long non-coding RNA, LINC00460, suppresses proliferation of colorectal cancer," *Journal of Cancer*, vol. 9, no. 16, pp. 2834–2843, 2018.
- [15] X. Liu, J. Wen, H. Wang, and Y. Wang, "Long non-coding RNA LINC00460 promotes epithelial ovarian cancer progression by regulating microRNA-338-3p," *Biomedicine & Pharmacotherapy*, vol. 108, pp. 1022–1028, 2018.
- [16] J. J. Ye, Y. L. Cheng, J. J. Deng, W. P. Tao, and L. Wu, "LncRNA LINC00460 promotes tumor growth of human lung adenocarcinoma by targeting miR-302c-5p/FOXA1 axis," *Gene*, vol. 685, pp. 76–84, 2019.
- [17] B. Li, W. Li, X. Li, and H. Zhou, "Inflammation: a novel therapeutic target/direction in atherosclerosis," *Current Pharmaceutical Design*, vol. 23, no. 8, pp. 1216–1227, 2017.
- [18] P. Libby, K. E. Bornfeldt, and A. R. Tall, "Atherosclerosis: successes, surprises, and future challenges," *Circulation Research*, vol. 118, no. 4, pp. 531–534, 2016.
- [19] E. Matsuura, F. Atzeni, P. Sarzi-Puttini, M. Turiel, L. R. Lopez, and M. T. Nurmohamed, "Is atherosclerosis an autoimmune disease?," *BMC Medicine*, vol. 12, no. 1, pp. 1–5, 2014.
- [20] A. C. Foks and I. Bot, "Preface: pathology and pharmacology of atherosclerosis," *European Journal of Pharmacology*, vol. 816, pp. 1-2, 2017.
- [21] J. Frostegard, "Immunity, atherosclerosis and cardiovascular disease," *BMC Medicine*, vol. 11, p. 117, 2013.
- [22] W. Herrington, B. Lacey, P. Sherliker, J. Armitage, and S. Lewington, "Epidemiology of atherosclerosis and the potential to reduce the global burden of atherothrombotic disease," *Circulation Research*, vol. 118, no. 4, pp. 535–546, 2016.
- [23] P. Hartmann, Z. Zhou, L. Natarelli et al., "Endothelial dicer promotes atherosclerosis and vascular inflammation by miRNA-103-mediated suppression of KLF4," *Nature Communications*, vol. 7, p. 10521, 2016.
- [24] X. Loyer, Z. Mallat, C. M. Boulanger, and A. Tedgui, "MicroRNAs as therapeutic targets in atherosclerosis," *Expert Opinion on Therapeutic Targets*, vol. 19, no. 4, pp. 489–496, 2015.
- [25] M. W. Feinberg and K. J. Moore, "MicroRNA regulation of atherosclerosis," *Circulation Research*, vol. 118, no. 4, pp. 703–720, 2016.
- [26] X. Lu and V. Kakkar, "The roles of microRNAs in atherosclerosis," *Current Medicinal Chemistry*, vol. 21, no. 13, pp. 1531–1543, 2014.
- [27] Y. Li, C. Yang, L. Zhang, and P. Yang, "MicroRNA-210 induces endothelial cell apoptosis by directly targeting PDK1 in the setting of atherosclerosis," *Cellular & Molecular Biology Letters*, vol. 22, p. 3, 2017.
- [28] B. Zheng, W. N. Yin, T. Suzuki et al., "Exosome-mediated miR-155 transfer from smooth muscle cells to endothelial cells induces endothelial injury and promotes atherosclerosis," *Molecular Therapy*, vol. 25, no. 6, pp. 1279–1294, 2017.
- [29] K. Xu, P. Liu, and Y. Zhao, "Upregulation of microRNA-876 induces endothelial cell apoptosis by suppressing Bcl-xl in development of atherosclerosis," *Cellular Physiology and Biochemistry*, vol. 42, no. 4, pp. 1540–1549, 2017.
- [30] Y. Zhang, X. Liu, X. Bai et al., "Melatonin prevents endothelial cell pyroptosis via regulation of long noncoding RNA MEG3/miR-223/NLRP3 axis," *Journal of Pineal Research*, vol. 64, no. 2, p. e12449, 2018.
- [31] C. P. Khoo, M. G. Roubelakis, J. B. Schrader et al., "MiR-193a-3p interaction with HMGB1 downregulates human endothelial cell proliferation and migration," *Scientific Reports*, vol. 7, p. 44137, 2017.

- [32] J. Zheng, L. Hu, J. Cheng et al., “LncRNA PVT1 promotes the angiogenesis of vascular endothelial cell by targeting miR-26b to activate CTGF/ANGPT2,” *International Journal of Molecular Medicine*, vol. 42, no. 1, pp. 489–496, 2018.
- [33] Y. Ma, Y. Xue, X. Liu et al., “SNHG15 affects the growth of glioma microvascular endothelial cells by negatively regulating miR-153,” *Oncology Reports*, vol. 38, no. 5, pp. 3265–3277, 2017.

Research Article

Effects of Escin on Oxidative Stress and Apoptosis of H9c2 Cells Induced by H₂O₂

Peng Qiao,¹ Baokun Zhang,² Xueni Liu ,³ Jie Xu,⁴ and Xuehan Li ⁵

¹Department of Traditional Chinese Medicine, Yantai Hospital, Yantai, China

²Public Health, The University of Sheffield, UK

³Critical Care Medicine, PLA Rocket Force Characteristic Medical Center, Beijing, China

⁴Department of Medical Security Center, PLA Rocket Force Characteristic Medical Center, Beijing, China

⁵Department of Geriatric, Liaocheng People's Hospital, Liaocheng, China

Correspondence should be addressed to Xueni Liu; 317959274@qq.com

Received 20 October 2021; Accepted 14 December 2021; Published 27 January 2022

Academic Editor: Simona Pichini

Copyright © 2022 Peng Qiao et al. This is an open access article distributed under the Creative Commons Attribution License, which permits unrestricted use, distribution, and reproduction in any medium, provided the original work is properly cited.

Objective. Myocardial infarction (MI) is a serious heart health problem in the world with a high mortality rate. Our study is mainly aimed at validating the antioxidative stress and antiapoptotic effects of escin in a H₂O₂-induced cardiomyocyte injury model. **Methods.** H9c2 cells were divided into control group, H₂O₂ treatment group, and H₂O₂+escin group. We studied the effect of escin on H9c2 cells and its mechanism by flow cytometry, real-time PCR, CCK-8 assay and Western blot. Cell morphology was observed by cell staining and optical microscopy. **Results.** We found that the level of reactive oxygen species (ROS) in the H₂O₂ treatment group was significantly elevated, while the high level of ROS was significantly reversed after treatment with escin. The protein levels of SOD1, SOD2, Bcl-2, and IκB-α in the H₂O₂ treatment group were significantly decreased compared with the H₂O₂+escin group, and the Bax, TNF-α, IL-1β, p65, and IκKα protein expressions were greatly higher than those in the H₂O₂+escin group. And the results of PCR were also consistent with those. TUNEL-positive cells also decreased significantly when treated with escin. Flow cytometry showed that the percentage of apoptotic cells decreased greatly after treatment of escin. Through IL-1β immunofluorescence, the fluorescence intensity of the H₂O₂ treatment group was greatly higher compared with that of the control group, but escin reversed this effect. **Conclusions.** These results indicated that escin inhibits H₂O₂-induced H9c2 cell apoptosis, oxidative stress, and inflammatory responses via the NF-κB signaling pathway.

1. Introduction

Myocardial infarction is a serious cardiovascular disease in the world. It is mainly due to coronary atherosclerosis which leads to narrowing of the lumen and causes damage to the myocardium innervated by blocked blood vessels [1]. Due to ischemia and hypoxia, myocardial infarction produces excessive ROS, which destroys surrounding myocardial tissue and further causes apoptosis of cardiomyocytes [2]. It is well known that cardiomyocytes are nonrenewable, and oxidative stress and apoptosis of the myocardium can lead to the death of some myocardium, eventually leading to deterioration of heart function and even death. The existing treatments are mainly to achieve

recanalization of blood vessels but cannot reverse the apoptosis of cardiomyocytes, and myocardial ischemia and reperfusion may aggravate oxidative stress [3]. Therefore, new treatments are urgently needed to inhibit myocardial oxidative stress and apoptosis in the early stages of myocardial infarction.

Escin is a pentacyclic triterpenoid saponin extracted from the dried mature seeds of the horse chestnut [4]. At present, there are many studies describing the role of escin in various histopathophysiology, including ovary, nervous system, and skin. Many people have also studied its role in tumors. Selvakumar et al. [5] believed that escin plays an antiapoptotic and antioxidative stress in Parkinson's disease and can improve the motor function of

patients. Wang et al. [6] believed that escin can play an antioxidative stress on retinal pigment epithelial cells. Cheng et al. [7] suggested that escin can regulate apoptosis in ovarian cancer. However, the effect of escin on cardiomyocytes has not been studied.

In this study, H₂O₂-induced myocardial cell injury model was adopted to investigate whether escin can play an antioxidative, antiapoptotic, and anti-inflammatory role and its potential mechanism of action. Our results showed that escin may provide a potential new treatment for MI.

2. Materials and Methods

2.1. Cell Culture. Dulbecco's Modified Eagle's Medium (MCE, Nanjing, China) complemented with 10% fetal bovine serum (FBS) (MCE, Nanjing, China) was used to culture H9c2 cells in 37 degrees Celsius incubator under 5% CO₂. When the cells grew to about 80% confluence, they began to be plated and treated with H₂O₂ (100 μM) for 4 hours and escin (10 μM) for 24 hours.

2.2. Drug Preparation. Escin was purchased from Tianpu Biochemical Pharmaceutical in Guangdong (Guangzhou, China). The stock solution was stored in a refrigerator at -20 degrees Celsius.

2.3. RNA Extraction and Real-Time Polymerase Chain Reaction (PCR). TRIzol reagent (MCE, Nanjing, China) was utilized to extract the total RNA of H9c2 cells. 0.5 ml of TRIzol was added into each well of a 24-well plates, and the liquid was transferred to the EP tube after grinding. Then, chloroform was added in 1/5 times of the amount of TRIzol. We let the eppendorf (EP) tubes shake, and let it stand for 5 minutes. After that, the EP tubes were centrifuged with a centrifugal force of 12000 × g for about 20 minutes at 4°C. We aspirated the upper aqueous phase of the mixture obtained by centrifugation and added an equal amount of isopropanol, mixed it, and placed it at 4°C for 15 minutes. Then, we centrifuged the mixture at 4°C for 15 minutes with a centrifugal force of 12000 × g, after which the supernatant was discarded and 1 mL of a 75% ethanol solution was added. The solution was centrifuged at 4°C for 5-10 minutes with a centrifugal force of 7500 × g, after which the supernatant was discarded and dried at room temperature, and 20 μL of ribonuclease free water was added. Finally, we used NanoDrop™ 8000 to measure RNA concentration.

Reverse transcription was performed using reverse transcriptase kit (MCE, Nanjing, China). Real-time PCR was performed by using Prism 7900 System. We used a 10 μL reaction system in accordance with the protocol. GAPDH (MCE, Nanjing, China) was used to standardize the data. All the primers are listed in Table 1.

2.4. Western Blot. The total protein of the cells placed in a 6-well plate was extracted by a protein extraction kit [8]. The protein concentration was measured by the bicinchoninic acid (BCA) method (Pierce, Rockford, IL, USA). Then, the loading buffer was added to the total protein and boiled the mixture for 7 minutes. After that, we took the same

amount of total protein and performed electrophoresis with 10% sodium dodecyl sulphate-polyacrylamide gel electrophoresis (SDS-PAGE). Then, we transferred the electrophoresed protein to the polyvinylidene fluoride (PVDF, EpiZyme, Shanghai, China) membrane. 5% concentration of skim milk was prepared with Tween-20 (TBST) to block the nonspecific antigens of the protein bands. After 2 hours, the primary antibodies were used to incubate the bands overnight (SOD1, Abcam, Cambridge, MA, USA, Rabbit, 1:2000; SOD2, Abcam, Cambridge, MA, USA, Rabbit, 1:2000; Bcl-2, Abcam, Cambridge, MA, USA, Mouse, 1:1000; Bax, Abcam, Cambridge, MA, USA, Mouse, 1:1000; TNF-α, Abcam, Cambridge, MA, USA, Rabbit, 1:1000; IL-1β, Abcam, Cambridge, MA, USA, Rabbit, 1:5000; p65, Abcam, Cambridge, MA, USA, Rabbit, 1:1000; IκKα, Abcam, Cambridge, MA, USA, Rabbit, 1:2000; IκB-α, Abcam, Cambridge, MA, USA, Rabbit, 1:2000; and GAPDH, Proteintech, Rosemont, IL, USA, 1:3000), followed by incubation with secondary antibodies for 1.5 hours. After the bands were washed 3 times for 30 minutes, the protein bands were exposed by the Image Lab™ Software.

2.5. ROS Quantification. Quantification of ROS was performed using the DHR-ROS test kit (KeyGen, Shanghai, China) in accordance with the manufacturer's protocol.

2.6. Superoxide Dismutase (SOD) Activity Assay. We lysed the H9c2 cells with lysate and collected and centrifuged to remove the supernatant. Detection of SOD levels in cells was performed by the SOD assay kit (KeyGen, Shanghai, China) in accordance with the protocol.

2.7. TUNEL Staining. TUNEL kit (Roche, Basel, Switzerland) was used as instructed by the manufacturer to detect the apoptotic cells. Briefly, the H9c2 cells were fixed with 4% paraformaldehyde for 20 minutes at room temperature and then treated with Triton X-100 for another 20 minutes. After that, the cells were treated with 150 μl TUNEL reaction solution at 37°C for 60 minutes. And the nucleus was stained with DAPI (Beyotime Biotechnology, Shanghai, China). TUNEL staining was shown by a Confocal Laser Scanning Microscope (CLSM).

2.8. Cell Counting Kit-8 (CCK-8) Assay. We placed H9c2 cells in a 96-well plate. After H₂O₂ and escin treatment, the viability of different groups of cells was examined by CCK-8 assay (Dojindo, Kumamoto, Japan) to explore the effect of escin on H9c2 cells. The absorbance at 450 nm was detected using a microplate reader.

2.9. Flow Cytometry. H9c2 cells were treated with H₂O₂ and escin as described above. The supernatant was then collected, and adherent cells were collected after digestion with trypsin. We centrifuged the cell suspension with a centrifugal force of 200 × g for 5 minutes, discarded the supernatant, washed with PBS, and centrifuged again in the same manner, repeating twice. Then, we resuspended the cells with 100 μL of binding buffer after discarding the supernatant. After that, we added 5 μL of Annexin V-FITC (KeyGen,

TABLE 1: Real-time PCR primers.

Gene name	Forward (5'>3')	Reverse (5'>3')
Bax	CAGTTGAAGTTGCCATCAGC	CAGTTGAAGTTACCATCAGC
Bcl-2	GACTGAGTACCTGAACCGGCATC	CTGAGCAGCGTCTTCAGAGACA
SOD1	GGTGAACCAGTTGTGTTGTC	CCGTCCTTTCCAGCAGTC
SOD2	CAGACCTGCCTTACGACTATGG	CTCGGTGGCGTTGAGATTGTT
IL-1 β	GCAACTGTTCTGAACTCAACT	ATCTTTTGGGGTCCGTCAACT
TNF- α	CCTCTCTCTAATCAGCCCTCTG	GAGGACCTGGGAGTAGATGAG
I κ K α	GTCAGGACCGTGTCTCAAGG	GCTTCTTTGATGTTACTGAGGGC
I κ B- α	GGATCTAGCAGCTACGTACG	TTAGGACCTGACGTAACACG
p65	ACTGCCGGGATGGCTACTAT	TCTGGATTTCGCTGGCTAATGG
GAPDH	ACAACCTTTGGTATCGTGGAAGG	GCCATCACGCCACAGTTTC

RT-PCR: quantitative reverse-transcription polymerase chain reaction.

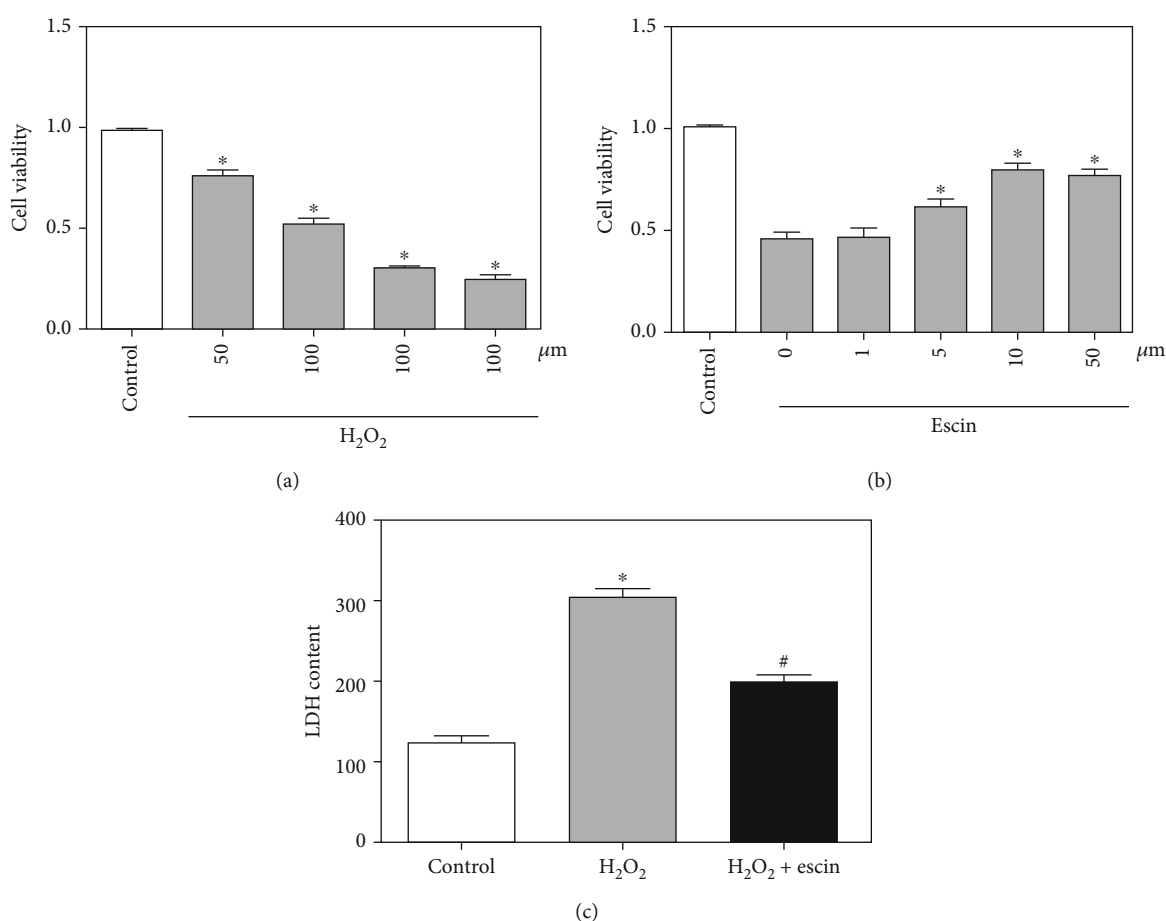


FIGURE 1: Escin protected H9c2 cells from damage. (a) CCK-8 assay showed viability of H9c2 cells at different concentrations of H₂O₂ (* $p < 0.05$ vs. control, $n = 3$). (b) CCK-8 assay showed cell viability after addition of different concentrations of escin in H₂O₂-treated H9c2 cells (* $p < 0.05$ vs. 0 μ M, $n = 3$). (c) The LDH content increased significantly in the H₂O₂ treatment group and decreased significantly in the H₂O₂+escin group (* $p < 0.05$ vs. control; # $p < 0.05$ vs. H₂O₂, $n = 3$).

Shanghai, China) and 5 μ L of propidium iodide (KeyGen, Shanghai, China) in per tube in the dark. Finally, the apoptotic H9c2 cells were detected using flow cytometry.

2.10. IL-1 β Immunofluorescence. H9c2 cells were placed in a 24-well plate, fixed with 4% paraformaldehyde after the

above treatment, then added goat serum, and incubated for 1 hour. After that, an appropriate amount of primary antibody IL-1 β was added and incubated overnight at 4 degrees Celsius. On the second day, we added the corresponding fluorescent secondary antibody and incubated them in the dark for 1 hour. 4',6-Diamidino-2-phenylindole (DAPI)

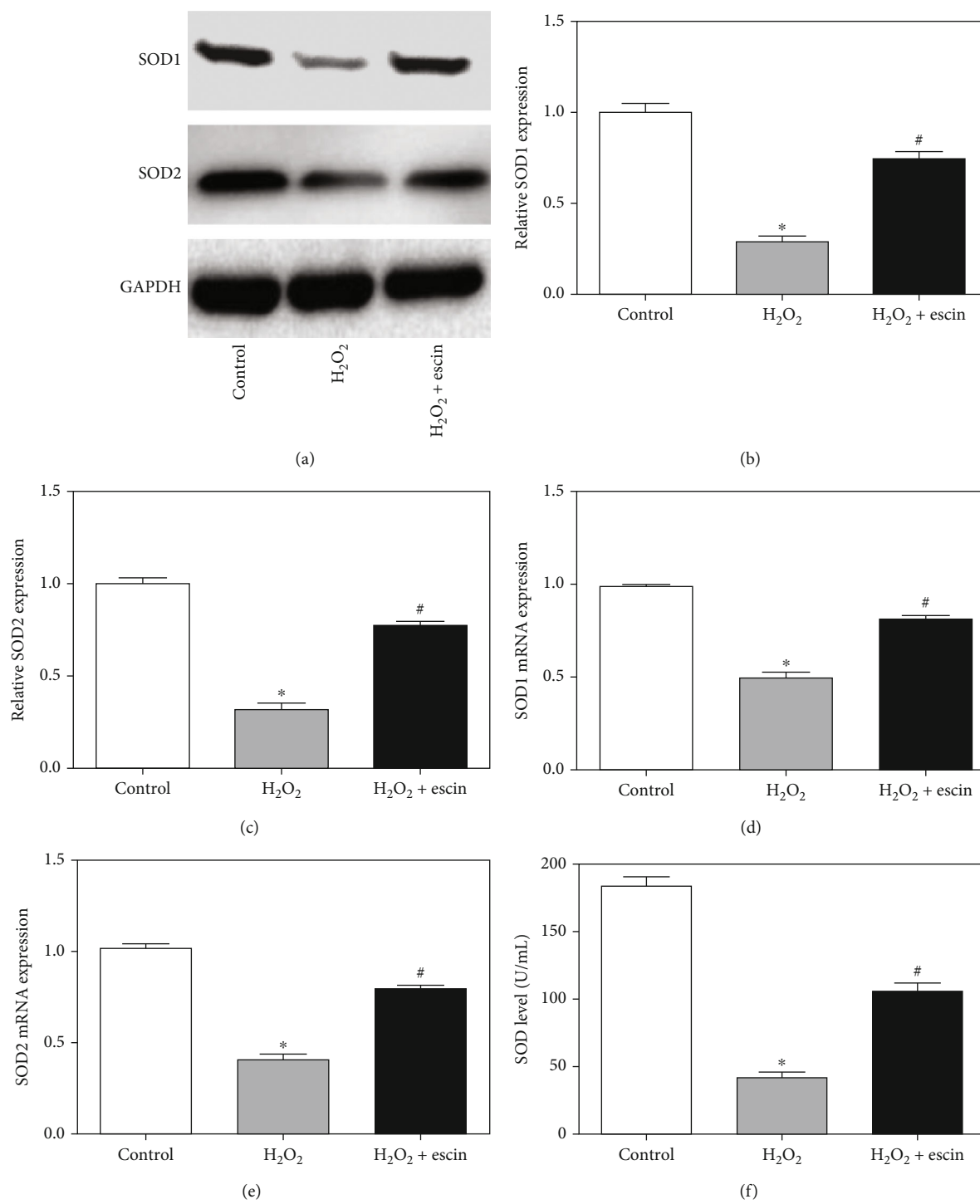


FIGURE 2: Continued.

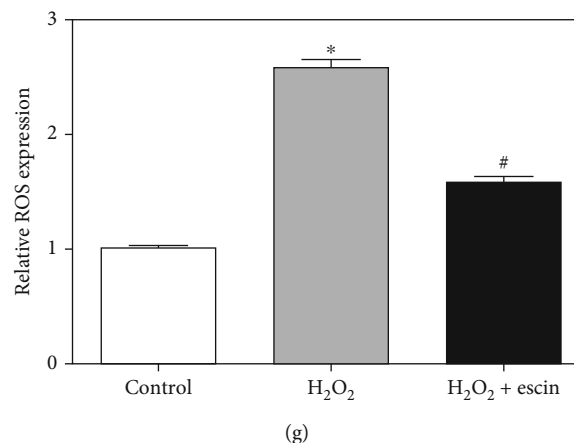


FIGURE 2: Escin inhibited oxidative stress in H9c2 cells. (a) The expression of SOD1 and SOD2 in the H₂O₂ treatment group decreased significantly, and the expression of SOD1 and SOD2 increased in the H₂O₂+escin group. (b) Statistical results of protein level of SOD1 (* $p < 0.05$ vs. control; # $p < 0.05$ vs. H₂O₂, $n = 3$). (c) Statistical results of protein level of SOD2 (* $p < 0.05$ vs. control; # $p < 0.05$ vs. H₂O₂, $n = 3$). (d) The expression of SOD1 mRNA in the H₂O₂ treatment group decreased significantly, and the expression increased in the H₂O₂+escin group (* $p < 0.05$ vs. control; # $p < 0.05$ vs. H₂O₂, $n = 3$). (e) The expression of SOD2 mRNA in the H₂O₂ treatment group decreased significantly, and the expression increased in the H₂O₂+escin group (* $p < 0.05$ vs. control; # $p < 0.05$ vs. H₂O₂, $n = 3$). (f) SOD activity assay showed that H₂O₂ can significantly reduce SOD levels, while escin can reverse SOD levels (* $p < 0.05$ vs. control; # $p < 0.05$ vs. H₂O₂, $n = 3$). (g) The expression of ROS increased in the H₂O₂ treatment group but decreased significantly in the H₂O₂+escin group (* $p < 0.05$ vs. control; # $p < 0.05$ vs. H₂O₂, $n = 3$).

was also added to stain the nucleus. Finally, it was observed by a Confocal Laser Scanning Microscope (CLSM).

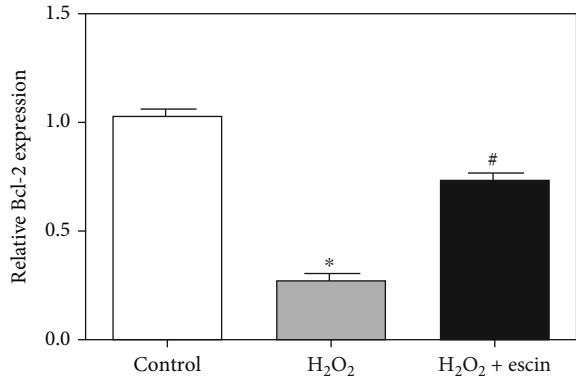
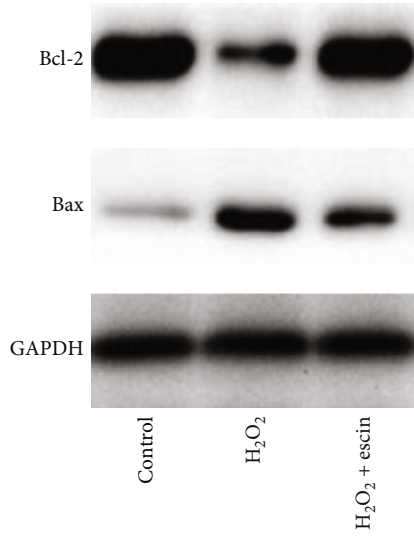
2.11. Statistics Analysis. Measurement data is expressed as $\bar{x} \pm s$. Differences between two groups were analyzed by using the Student *t*-test. Comparison between multiple groups was done using one-way ANOVA test followed by post hoc test (Least Significant Difference). Least Significant Difference (LSD) test or Student-Newman-Keuls (SNK) test was used for pairwise comparison under the condition of homogeneity of variance. Test level $\alpha = 0.05$. All experiments were repeated 3 times.

3. Results

3.1. Escin Protected H₂O₂-Induced H9c2 Cell Injury. To measure the appropriate H₂O₂ concentration for H9c2 cells, H9c2 cells were treated with different concentrations of H₂O₂ for 4 hours. As shown in Figure 1(a), when H9c2 cells were treated with 100 μ M of H₂O₂, cell viability was suppressed by about 50% by CCK-8 assay, so we selected 100 μ M of H₂O₂ for subsequent studies. Next, in order to determine the optimal dosing concentration, we treated H₂O₂-treated H9c2 cells with different concentrations of escin for 24 hours. We measured cell viability using CCK-8 assay, and the highest cell viability was obtained when H9c2 cells were treated with 10 μ M of escin (Figure 1(b)). After that, we collected the supernatant of H9c2 cells and detected them with the LDH kit. The results showed that escin significantly inhibited H₂O₂-mediated LDH elevation (Figure 1(c)). These results indicated that escin can act directly on H9c2 cells and reduced the damage caused by H₂O₂.

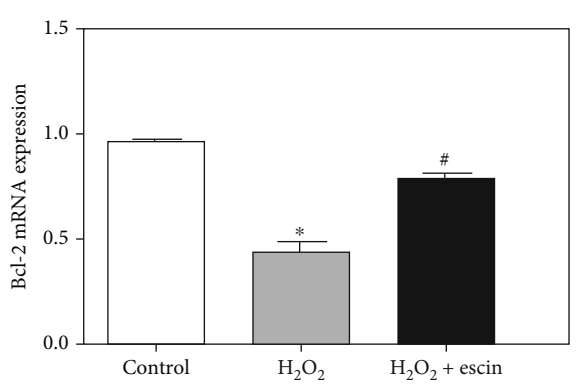
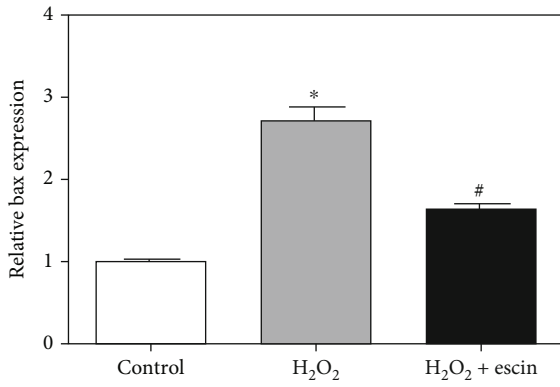
3.2. Escin Inhibited H₂O₂-Induced Oxidative Stress in H9c2 Cells. We used Western blot to detect the expression levels of SOD1 protein and SOD2 protein (Figure 2(a)). In the H₂O₂ treatment group, the expression levels of SOD1 and SOD2 were greatly decreased compared to the control group, while the treatment with escin greatly increased the expression levels of SOD1 and SOD2 (Figures 2(b) and 2(c)). Then, we used real-time PCR to detect the expression levels of SOD1 mRNA and SOD2 mRNA, which were consistent with the results of Western blot (Figures 2(d) and 2(e)). At the same time, the SOD activity assay was used to detect the level of SOD. The results showed that the addition of escin can significantly reverse the decrease of H₂O₂-mediated SOD levels (Figure 2(f)). Finally, we tested the level of ROS production by DHR dye assay. We can see from Figure 2(g) that the treatment of H₂O₂ increased the level of ROS production, while in the H₂O₂+escin group, the level of ROS production decreased significantly. These results demonstrated that escin can inhibit oxidative stress in H9c2 cells treated with H₂O₂.

3.3. Escin Inhibited H₂O₂-Induced Apoptosis in H9c2 Cells. First, we examined the expression of Bcl-2 and Bax proteins by Western blot (Figure 3(a)). It can be seen that the expression of Bcl-2 in the H₂O₂ treatment group was greatly decreased compared with the control group, while the level of Bax was greatly increased. After using escin, the level of Bcl-2 was increased and the level of Bax was decreased (Figures 3(b) and 3(c)). Similarly, we detected the levels of Bcl-2 and Bax mRNA using real-time PCR, which was consistent with the results of Western blot (Figures 3(d) and 3(e)). To further demonstrate the antiapoptotic effect of escin, we used TUNEL staining to detect the level of TUNEL-positive cells. It can be seen that the TUNEL-



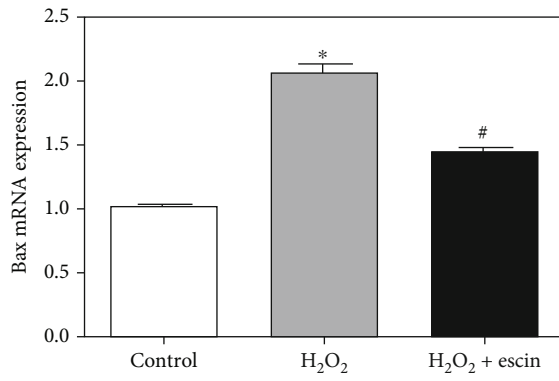
(a)

(b)



(c)

(d)



(e)

FIGURE 3: Continued.

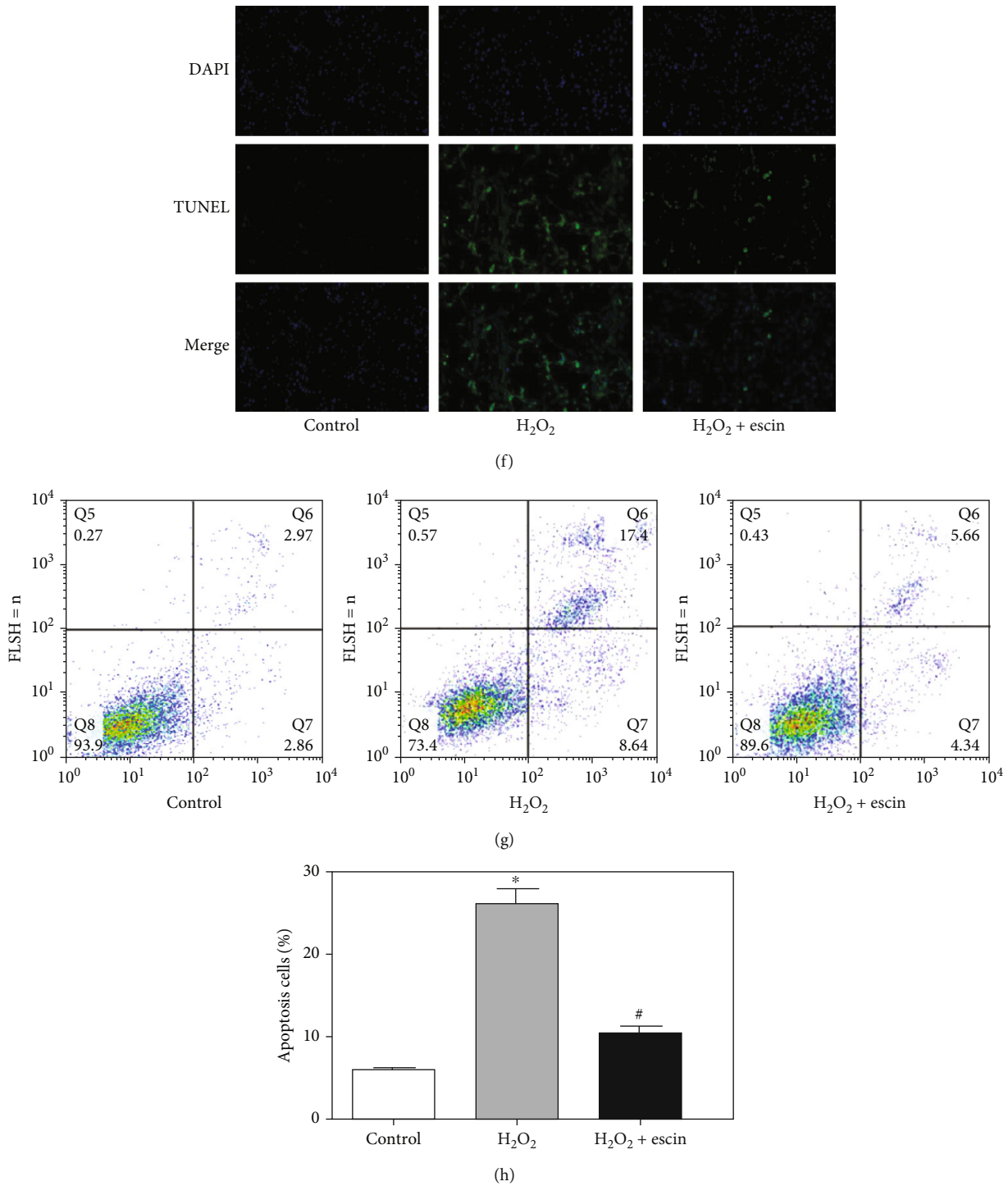


FIGURE 3: Eschin inhibited apoptosis of H9c2 cells. (a) The expression of Bcl-2 in the H₂O₂ treatment group decreased significantly but increased in the H₂O₂+escin group. Bax expression was opposite to Bcl-2. (b) Statistical results of protein level of Bcl-2 (**p* < 0.05 vs. control; #*p* < 0.05 vs. H₂O₂, *n* = 3). (c) Statistical results of expression of Bax (**p* < 0.05 vs. control; #*p* < 0.05 vs. H₂O₂, *n* = 3). (d) The expression of Bcl-2 mRNA was consistent with the Bcl-2 protein (**p* < 0.05 vs. control; #*p* < 0.05 vs. H₂O₂, *n* = 3). (e) The expression of Bax mRNA was consistent with the Bax protein (**p* < 0.05 vs. control; #*p* < 0.05 vs. H₂O₂, *n* = 3). (f) TUNEL staining showed that eschin can obviously reduce the increase of H9c2 cell apoptosis caused by H₂O₂ (magnification: ×400). (g) The apoptotic rate of the H₂O₂ treatment group increased and decreased in the H₂O₂+escin group. (h) Statistical results of apoptotic rate of H9c2 cells (**p* < 0.05 vs. control; #*p* < 0.05 vs. H₂O₂, *n* = 3).

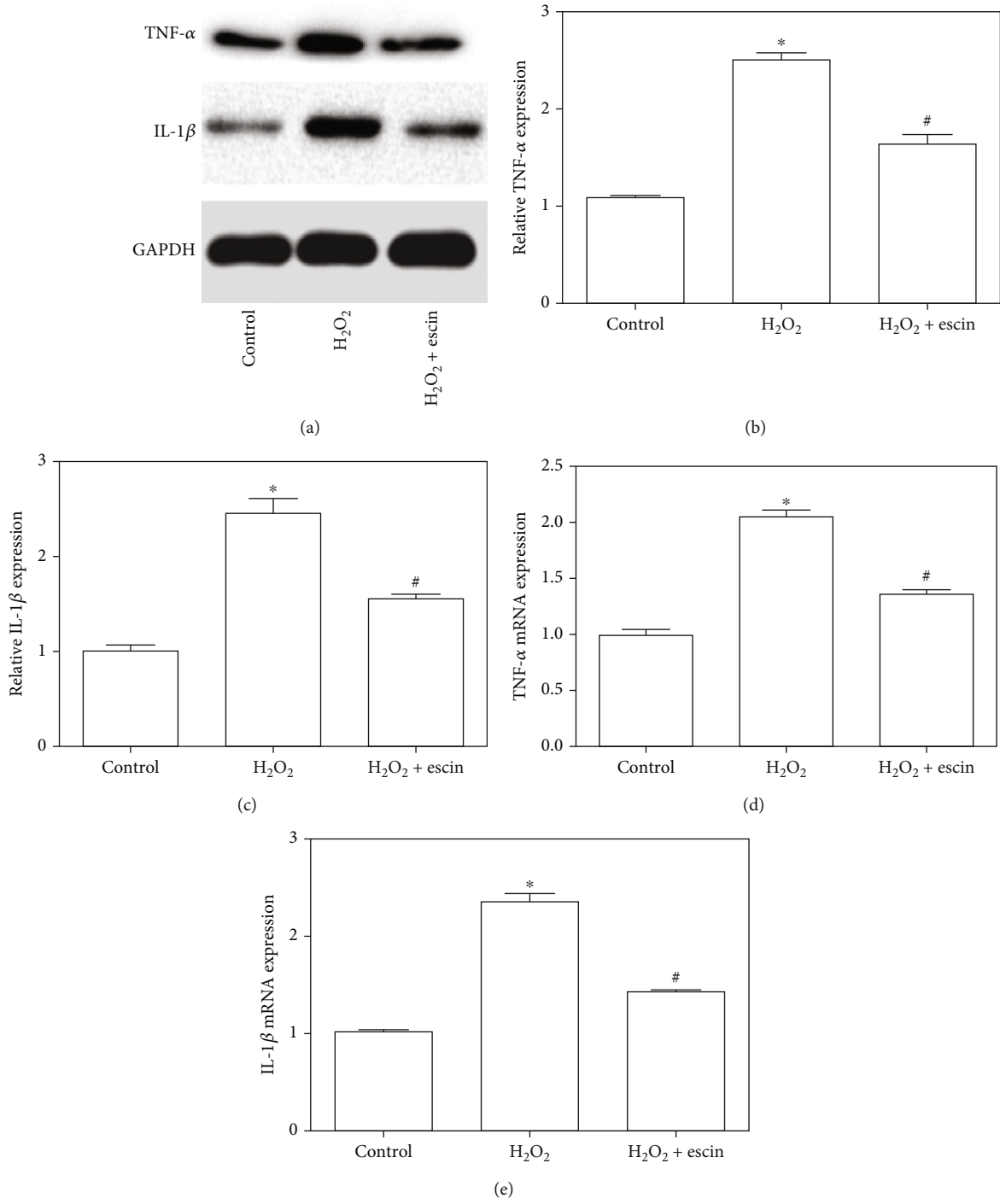


FIGURE 4: Continued.

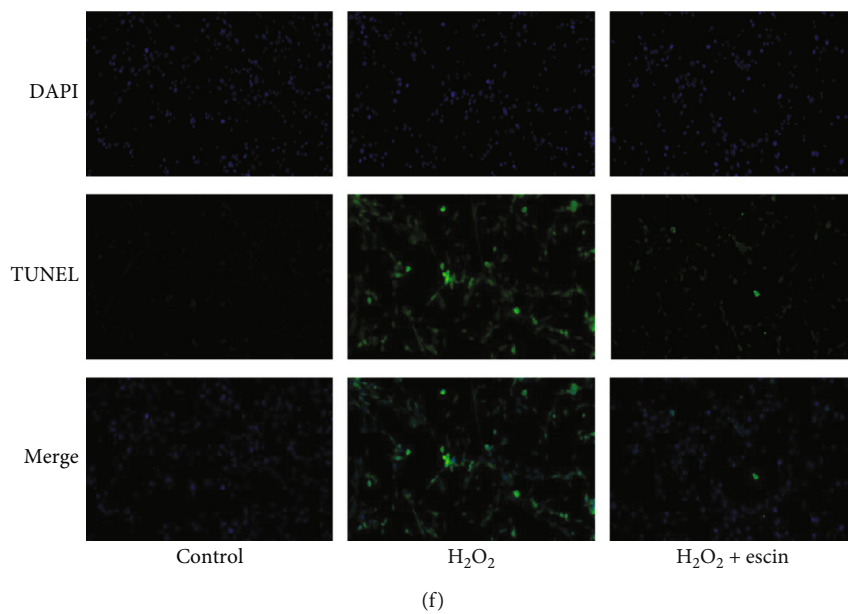


FIGURE 4: Escin inhibited inflammation of H9c2 cells. (a) The expression of IL-1 β and TNF- α in the H₂O₂ treatment group increased significantly but decreased in the H₂O₂+escin group. (b) Statistical results of expression of TNF- α (* p < 0.05 vs. control; # p < 0.05 vs. H₂O₂, n = 3). (c) Statistical results of expression of IL-1 β (* p < 0.05 vs. control; # p < 0.05 vs. H₂O₂, n = 3). (d) TNF- α mRNA expression was similar to the results of Western blot (* p < 0.05 vs. control; # p < 0.05 vs. H₂O₂, n = 3). (e) IL-1 β mRNA expression was also similar to the results of Western blot (* p < 0.05 vs. control; # p < 0.05 vs. H₂O₂, n = 3). (f) Immunofluorescence showed that escin significantly reduced H₂O₂-mediated elevation of IL-1 β (magnification: \times 400).

positive cells in the H₂O₂+escin group were greatly reduced compared to the H₂O₂ treatment group (Figure 3(f)). We also used flow cytometry to detect the effect of escin on H9c2 cells treated with H₂O₂. We can see that escin can significantly reduce the apoptotic rate of H₂O₂-treated H9c2 cells (Figures 3(g) and 3(h)). These results indicated that escin can inhibit H₂O₂-mediated apoptosis of H9c2 cells.

3.4. Escin Inhibited H₂O₂-Induced Inflammation of H9c2 Cells. The expression of IL-1 β and TNF- α was examined by Western blotting (Figure 4(a)). We can see that H₂O₂ significantly induced the increase of IL-1 β and TNF- α , while the escin inhibited their increase (Figures 4(b) and 4(c)). Similar results were obtained for mRNA levels (Figures 4(d) and 4(e)). Immunofluorescence showed that IL-1 β expression in the H₂O₂+escin group was significantly decreased compared with the H₂O₂ treatment group (Figure 4(f)). These results showed that escin can inhibit the inflammation of H9c2 cells induced by H₂O₂.

3.5. Escin Inhibited the NF- κ B Pathway. The NF- κ B pathway plays a very important role in regulating apoptosis and oxidative stress, so we examined the NF- κ B pathway in different treatment groups by Western blot (Figure 5(a)). We can see from Figures 5(b)–5(d) that the expression of p65 and I κ B kinase α (I κ B α) in the H₂O₂ treatment group was significantly increased, while the expression of inflammatory inhibitor NF- κ B α (I κ B- α) was greatly decreased, compared with the control group. After treatment with escin, the expression of p65 and I κ B α was decreased, while the expression level of I κ B- α increased

compared to the H₂O₂ treatment group. And the results of the real-time PCR matched the results of the Western blot (Figures 5(e)–5(g)). These results suggested that escin can inhibit the NF- κ B pathway.

4. Discussion

In this present study, we revealed for the first time the role of escin in MI. H₂O₂ treatment successfully induced oxidative stress, inflammation, and apoptosis of H9c2 cardiomyocytes. However, escin can reverse the damage of H9c2 cells caused by H₂O₂. This protective effect was achieved at least in part by targeting the NF- κ B pathway.

AMI is a serious health problem in the world with a high mortality rate [9]. Current treatments can reconstitute the blood supply to the ischemic areas [10]. However, these treatments do not fully restore the apoptosis and oxidative stress of some cardiomyocytes. Previous studies have shown that in AMI, the myocardial ischemia site produces a large amount of ROS due to oxidative stress, which causes damage to the myocardial cell membrane, and at the same time produces a large number of inflammatory factors, causing apoptosis of cardiomyocytes [11]. Therefore, in addition to rebuilding the blood supply in the ischemic areas, treatments such as antioxidative stress, antiapoptosis, and anti-inflammatory are also essential.

Many studies have previously reported antioxidative, antiapoptotic, and anti-inflammatory effects of escin in other diseases. So, we want to verify whether escin has a similar effect in MI. We first tested the cell viability of

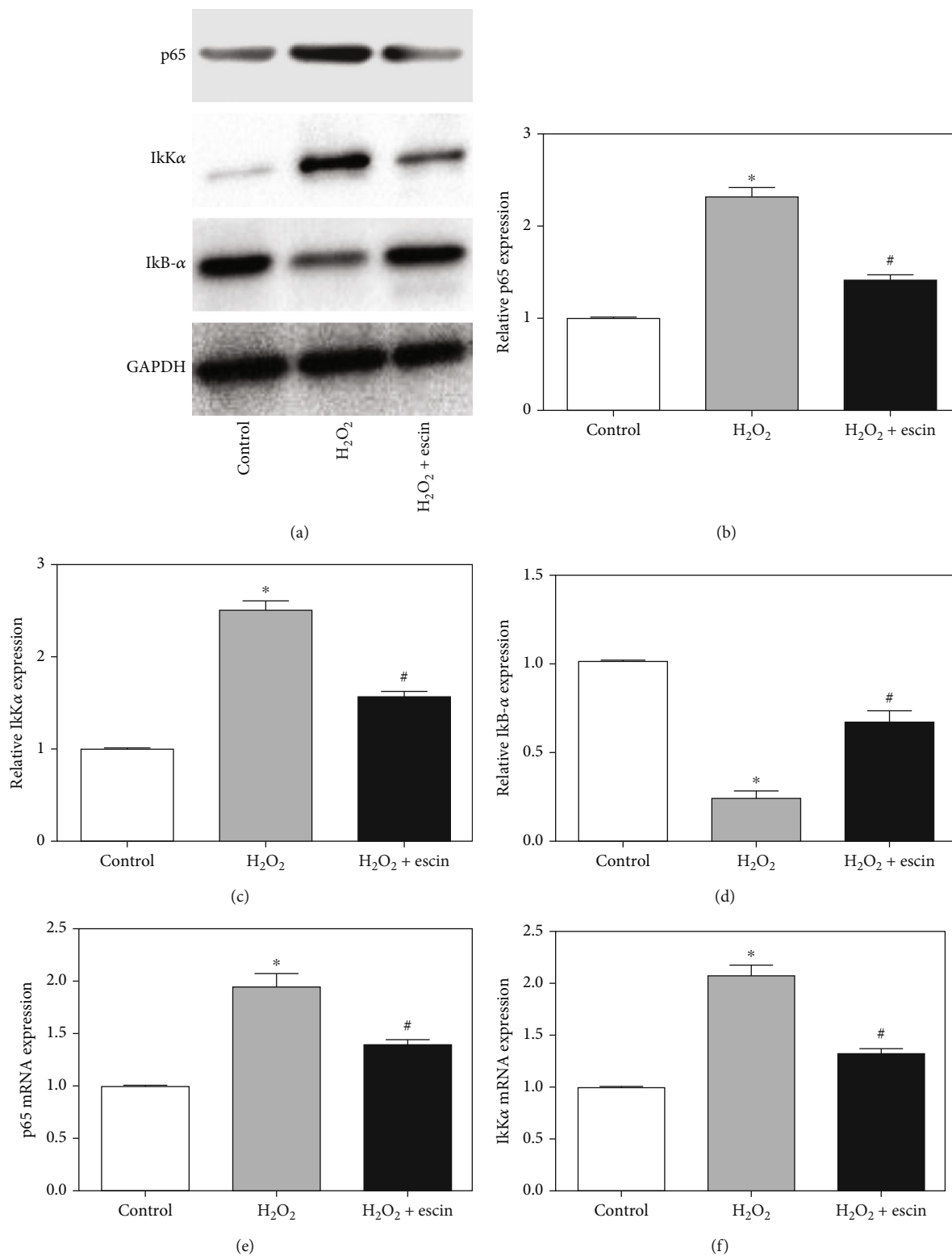


FIGURE 5: Continued.

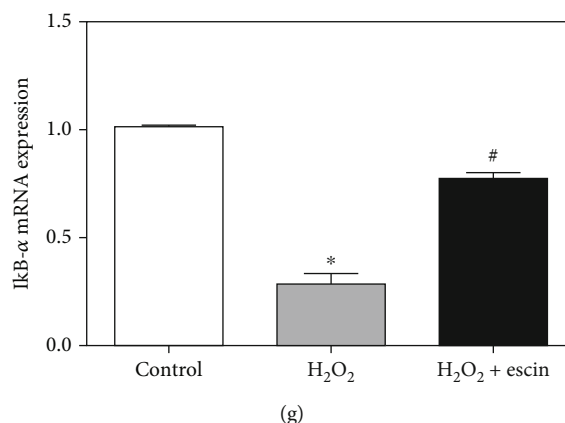


FIGURE 5: Escin inhibited the NF- κ B pathway. (a) In the H₂O₂ treatment group, the expression of p65 and I κ K α increased, and the expression of I κ B- α decreased. In the H₂O₂+escin group, the expression of p65 and I κ K α decreased, and the expression of I κ B- α increased. (b) Statistical results of protein level of p65 (* p < 0.05 vs. control; # p < 0.05 vs. H₂O₂, n = 3). (c) Statistical results of protein level of I κ K α (* p < 0.05 vs. control; # p < 0.05 vs. H₂O₂, n = 3). (d) Statistical results of protein level of I κ B- α (* p < 0.05 vs. control; # p < 0.05 vs. H₂O₂, n = 3). (e) Expression of p65 mRNA in three groups (* p < 0.05 vs. control; # p < 0.05 vs. H₂O₂, n = 3). (f) Expression of I κ K α mRNA in three groups (* p < 0.05 vs. control; # p < 0.05 vs. H₂O₂, n = 3). (g) Expression of I κ B- α mRNA was consistent with the results of Western blot (* p < 0.05 vs. control; # p < 0.05 vs. H₂O₂, n = 3).

H9c2 cells treated with H₂O₂ and found that escin did increase the cell viability. Then, we examined the expression of oxidative stress-related proteins, apoptosis-related proteins, and some inflammatory factors and also detected the corresponding mRNA expression. The final result confirmed our hypothesis that escin can inhibit oxidative stress, apoptosis, and inflammation in H9c2 cells, thereby increasing cell viability. This also provided a potential treatment for MI.

Studies have shown that MI involves multiple signaling pathways such as Rho/ROCK pathway, MAPK pathway, and NF- κ B pathway [12]. Among them, NF- κ B pathway is a classical signaling pathway that has an important influence on inflammation, apoptosis, and oxidative stress. Xiong et al. [13] believed that quercetin acts to treat periodontitis through NF- κ B signaling pathway. Yi et al. [14] suggested that inhibition of NF- κ B signaling pathway promoted autophagy and inhibited apoptosis and inflammation in nucleus pulposus cells. By detecting the expression of p65, I κ K α , I κ B- α protein, and mRNA in different treatment groups, our study also confirmed that escin can inhibit cardiomyocyte apoptosis, inflammation, and oxidative stress through the NF- κ B pathway.

In summary, our study suggests that the effect of escin on MI is primarily due to the inhibition of the NF- κ B signaling pathway. This finding is of great help to the clinical treatment of MI.

5. Conclusions

Escin inhibits the NF- κ B pathway and thus inhibits oxidative stress, apoptosis, and inflammation induced by H₂O₂ in H9c2 cells. Therefore, escin may provide a new treatment for MI.

Data Availability

The datasets used and analyzed during the current study are available from the corresponding author on reasonable request.

Conflicts of Interest

The authors declared no conflict of interest.


References

- [1] K. Thygesen, J. S. Alpert, A. S. Jaffe, M. L. Simoons, B. R. Chaitman, and H. D. White, "Third Universal Definition of Myocardial Infarction," *Global Heart*, vol. 7, no. 4, pp. 275–295, 2012.
- [2] M. Chiong, Z. V. Wang, Z. Pedrozo et al., "Cardiomyocyte death: mechanisms and translational implications," *Cell Death & Disease*, vol. 2, no. 12, 2011.
- [3] E. G. Nabel and E. Braunwald, "A Tale of Coronary Artery Disease and Myocardial Infarction," *The New England Journal of Medicine*, vol. 366, no. 1, pp. 54–63, 2012.
- [4] D. Cheong, F. Arfuso, G. Sethi et al., "Molecular targets and anti-cancer potential of escin," *Cancer Letters*, vol. 422, pp. 1–8, 2018.
- [5] G. P. Selvakumar, T. Manivasagam, K. R. Rekha, R. L. Jayaraj, and N. Elangovan, "Escin, a novel triterpene, mitigates chronic MPTP/p-induced dopaminergic toxicity by attenuating mitochondrial dysfunction, oxidative stress, and apoptosis," *Journal of Molecular Neuroscience*, vol. 55, no. 1, pp. 184–197, 2015.
- [6] K. Wang, Y. Jiang, W. Wang, J. Ma, and M. Chen, "Escin activates AKT-Nrf2 signaling to protect retinal pigment epithelium cells from oxidative stress," *Biochemical and Biophysical Research Communications*, vol. 468, no. 4, pp. 541–547, 2015.
- [7] C. L. Cheng, W. T. Chao, Y. H. Li et al., "Escin induces apoptosis in human bladder cancer cells: An *in vitro* and *in vivo* study," *European Journal of Pharmacology*, vol. 840, pp. 79–88, 2018.

- [8] D. L. Dong, C. Chen, R. Huo et al., "Reciprocal repression between microRNA-133 and calcineurin regulates cardiac hypertrophy," *Hypertension*, vol. 55, no. 4, pp. 946–952, 2010.
- [9] J. Pöss, J. Köster, G. Fuernau et al., "Risk stratification for patients in cardiogenic shock after acute myocardial infarction," *Journal of the American College of Cardiology*, vol. 69, no. 15, pp. 1913–1920, 2017.
- [10] M. Myojo, J. Ando, M. Uehara, M. Daimon, M. Watanabe, and I. Komuro, "Feasibility of extracorporeal shock wave myocardial revascularization therapy for post-acute myocardial infarction patients and refractory angina pectoris patients," *International Heart Journal*, vol. 58, no. 2, pp. 185–190, 2017.
- [11] M. Neri, V. Fineschi, M. Di Paolo et al., "Cardiac oxidative stress and inflammatory cytokines response after myocardial infarction," *Current Vascular Pharmacology*, vol. 13, no. 1, pp. 26–36, 2015.
- [12] Y. Wang, P. Lu, D. Zhao, and J. Sheng, "Targeting the hedgehog signaling pathway for cardiac repair and regeneration," *Herz*, vol. 42, no. 7, pp. 662–668, 2017.
- [13] G. Xiong, W. Ji, F. Wang et al., "Quercetin inhibits inflammatory response induced by LPS from *Porphyromonas gingivalis* in human gingival fibroblasts via suppressing NF-kappaB signaling pathway," *BioMed Research International*, vol. 2019, Article ID 6282635, 10 pages, 2019.
- [14] W. Yi, Y. Wen, F. Tan et al., "Impact of NF- κ B pathway on the apoptosis-inflammation-autophagy crosstalk in human degenerative nucleus pulposus cells," *Aging*, vol. 11, no. 17, pp. 7294–7306, 2019.

Research Article

lncRNA ROR and miR-125b Predict the Prognosis in Heart Failure Combined Acute Renal Failure

Qianlong Xue,¹ Lipeng Yang,¹ Jia Wang,¹ Linlin Li,¹ Hui Wang,¹ and Ying He ²

¹Department of Emergency Medicine, The First Affiliated Hospital of Hebei North University, Zhangjiakou, China

²Department of Gynecology, The First Affiliated Hospital of Hebei North University, Zhangjiakou, China

Correspondence should be addressed to Ying He; heyings@bjtu.edu.cn

Received 15 October 2021; Accepted 20 December 2021; Published 20 January 2022

Academic Editor: Francesco Busardò

Copyright © 2022 Qianlong Xue et al. This is an open access article distributed under the Creative Commons Attribution License, which permits unrestricted use, distribution, and reproduction in any medium, provided the original work is properly cited.

Objective. To elucidate the correlation between expression levels of long noncoding RNA (lncRNA) ROR and microRNA-125b (miR-125b) with the prognosis in heart failure (HF) patients combined acute renal failure (ARF). **Methods.** HF patients combined ARF ($n = 90$) and healthy controls ($n = 90$) in the same period were included in our hospital from April 2016 to December 2018. Every subject was followed up for 24 months. Serum levels of lncRNA ROR and miR-125b were detected, and their expression correlation was analyzed by Pearson correlation test. Receiver operating characteristic (ROC) curves were depicted for assessing the sensitivity and specificity of lncRNA ROR and miR-125b in diagnosing HF combined ARF. **Results.** lncRNA ROR was upregulated in serum of HF patients combined ARF, and its level was positively correlated to NYHA classification. miR-125b displayed an opposite trend. In serum samples of HF combined ARF, expression level of lncRNA ROR was negatively related to that of miR-125b. Diagnostic potentials of lncRNA ROR and miR-125b in HF combined ARF were confirmed by ROC curve analyses (lncRNA ROR: AUC = 0.9199, cutoff value = 5.595, sensitivity = 92.22%, and specificity = 73.33%; miR-125b: AUC = 0.8509, cutoff value = 2.290, sensitivity = 81.11%, and specificity = 74.44%). After 2-year follow-up, 16 cases were dead. Higher incidences of death and rehospitalization were observed in HF combined ARF cases expressing higher serum level of lncRNA ROR or lower level of miR-125b. **Conclusions.** Serum level of lncRNA ROR is upregulated, and miR-125b is downregulated in HF patients combined ARF. Their levels are linked to NYHA classification, which can be utilized as prognostic biomarkers in HF combined ARF.

1. Introduction

Heart failure (HF) is caused by increased cardiac load and dyscirculatory syndrome owing to systolic and diastolic dysfunctions. As the heart disease worsens, insufficient blood perfusion and renal blood stasis impairs renal function [1]. Acute renal failure (ARF) is a clinical syndrome of rapid decline of glomerular filtration function, imbalance of water and electrolyte, and accumulation of nitrogen wastes in the body in a short period of time [2]. Clinically, HF patients are prone to develop ARF. ARF-induced water retention seriously continues to aggravate HF, thus increasing treatment difficulty [3].

Long noncoding RNAs (lncRNAs) are functional RNAs with over 200 nt long. They are generally transcribed in eukaryotes and unable to encode proteins [4]. Initially,

lncRNAs were considered as byproducts of RNA polymerase II transcription without biological functions. Later, accumulating evidences have proven the vital functions in genomic imprinting, chromatin modification, transcriptional activation, and nuclear transportation at multiple levels [5]. In recent years, lncRNAs are reported as important regulators in HF [6]. Further, lncRNA ZNF593-AS alleviates contractile dysfunction in dilated cardiomyopathy [7]. And lncRNA H19 alleviates muscular dystrophy by stabilizing dystrophin [8]. lncRNA ROR locates on human chromosome 18q21.31 containing 4 exons [9]. Numerous previous studies have demonstrated the vital role of ROR in cardiovascular diseases. It is reported that lncRNA ROR is upregulated in *in vitro* cultured hypertrophic cardiomyocytes, which deteriorates myocardial hypertrophy into cardiac hypertrophy and even HF [10]. Further, the ROR/miR-124-3p/TRAF6 axis

regulated the ischemia reperfusion injury-induced inflammatory response in human cardiomyocytes [11]. Besides, overexpressed ROR promotes the biological characteristics of ox-LDL-induced HUVECs let-7b-5p/HOXA1 axis in atherosclerosis [12]. However, the importance of ROR in HF patients was unknown.

MicroRNAs (miRNAs) are endogenous, single-strand RNAs containing 22 nucleotides. Through complementary base pairing, miRNAs posttranscriptionally regulate target gene expressions [13]. miRNAs are extensively involved in cardiac pathophysiological process, including cardiac development, cardiac hypertrophy, myocardial ischemia, and HF [14–16]. The miR-125 family is highly conserved in mammals and participates in embryogenesis, immune response, tumorigenesis, and ischemia reperfusion injury [17, 18].

miR-125b is transcribed on chromosome 11q23 (has-miR-125b-1) and 21q21 (has-miR-125b-2) [19]. Busk and Cirera [20] suggested that miR-125b is downregulated in HF patients. Further, miR-125b is critical for fibroblast-to-myofibroblast transition and cardiac fibrosis [21]. In addition, hypoxia-elicited mesenchymal stem cell-derived exosomes facilitate cardiac repair through miR-125b-mediated prevention of cell death in myocardial infarction [22]. However, the role of miR-125b in heart failure was unclear. In this paper, we aim to uncover the prognostic potentials of lncRNA ROR and miR-125b in HF patients combined ARF.

2. Patients and Methods

2.1. Baseline Characteristics. A total of 90 HF patients combined ARF treated in our hospital from April 2016 to December 2018 were included. Based on the New York Heart Association (NYHA) functional classification, there were 0 case in class I, 30 in class II, 32 in class III, and 28 in class IV. NYHA is classified into four categories according to limited levels of physical activities. Class I: physical activity is not limited. Class II: physical activity in patients with heart diseases is slightly limited with fatigue, palpitation, and dyspnea. Class III: physical activity is markedly limited and comfortable at rest. Class IV: unable to carry out normal physical activity.

A total of 90 healthy subjects undergoing physical examination in our hospital during the same period were included as controls. Subjects with (1) no urine; (2) endocrine diseases, skeletal muscle diseases, immune diseases, and malignancies; and (3) mental disorders were excluded. This study was approved by the Ethics Committee of the First Affiliated Hospital of Hebei North University. Signed written informed consents were obtained from all participants before the study.

2.2. Sample Collection. 5 mL of venous blood was extracted in each subject under the fasting state in the morning. Blood was centrifuged at 3000 r/min for 10 min, and the serum was collected and stored at -80°C .

2.3. Quantitative Real-Time Polymerase Chain Reaction (qRT-PCR). TRIzol method (Invitrogen, Carlsbad, CA, USA) was applied for isolating RNAs from serum samples. Through

TABLE 1: Baseline characteristics of subjects.

Variable	Control	HF combined ARF	<i>p</i>
Age	62.13 ± 6.75	60.93 ± 5.85	0.204
Sex (male/female)	45/45	45/45	N.S.
BMI (kg/m ²)	22.62 ± 3.11	22.73 ± 3.51	0.824

HF: heart failure; ARF: acute renal failure; BMI: body mass index; N.S.: no significant difference.

reverse transcription of RNA, the extracted complementary deoxyribonucleic acid (cDNA) was used for PCR detection by SYBR Green method (TaKaRa, Tokyo, Japan). Primer sequences were listed as follows: lncRNA ROR, F: 5'-CGAA CGAGAGGACCGAAG-3', R: 5'-GCCAAGTTCTAGATAA GC-3'; GAPDH, F: 5'-ACGGCAAGTTCAACGGCACAG-3', R: 5'-GACGCCAGTAGACTCCACGACA-3'; miR-125b, F: 5'-GATCTGCAGCTCTCCCAGGGGCTGGCTTCAG-3', R: 5'-GATCATATGGAGGCAGAAAGGATGGAG-3'; U6, F: 5'-CTCGCTTCGGCAGCACATATACT-3', R: 5'-ACGC TTCACGAATTTGCGTGTC-3'.

2.4. Follow-Up. All patients were followed up through telephone, outpatient review, hospitalized investigation, or other methods for 24 months with 6 months interval. Disease onset, rehospitalization, and death were recorded.

2.5. Statistical Analysis. Statistical Product and Service Solutions (SPSS) 20.0 (IBM, Armonk, NY, USA) was used for all statistical analysis. Data were expressed as mean ± SD (standard deviation). Differences between two groups were analyzed by using the Student *t*-test. Comparison between multiple groups was done using one-way ANOVA test followed by post hoc test (least significant difference). Pearson correlation test was applied for assessing the relationship between serum levels of lncRNA ROR and miR-125b. Diagnostic potentials were assessed by depicting receiver operating characteristic (ROC) curves. $p < 0.05$ indicated the significant difference.

3. Results

3.1. Baseline Characteristics of Subjects. Through analyzing clinical data of subjects, no significant differences were found in age, sex, and BMI between healthy subjects and HF patients combined ARF (Table 1). Baseline characteristics of them were comparable.

3.2. Serum Levels of lncRNA ROR and miR-125b. Compared with healthy subjects, serum level of lncRNA ROR was upregulated in HF patients combined ARF (Figure 1(a)), while miR-125b level was downregulated (Figure 1(b)).

3.3. Correlation between Serum Levels of lncRNA ROR and miR-125b with NYHA. There were 0 case in NYHA class I, 30 in class II, 32 in class III, and 28 in class IV included in this trial. Interestingly, serum level of lncRNA ROR gradually increased with NYHA worsening in HF patients combined ARF (Figure 2(a)). Conversely, miR-125b level

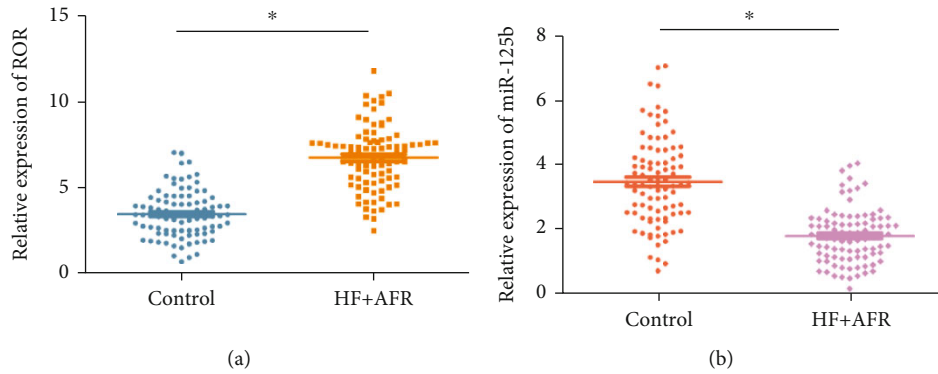


FIGURE 1: Serum levels of lncRNA ROR and miR-125b. Serum levels of (a) lncRNA ROR and (b) miR-125b in healthy subjects and heart failure patients combined acute renal failure.

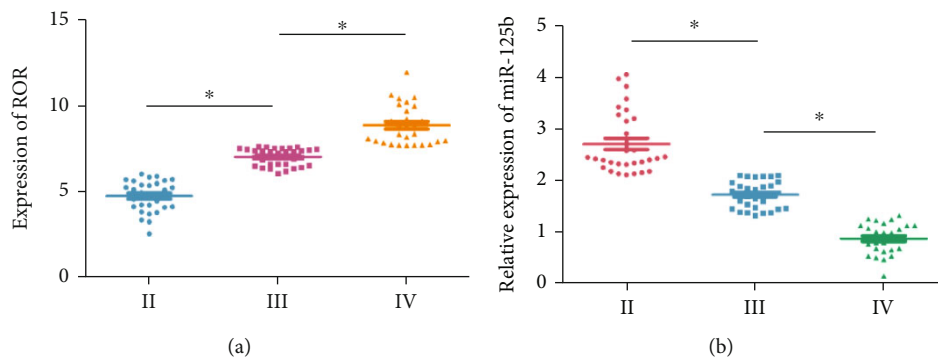


FIGURE 2: Correlation between serum levels of lncRNA ROR and miR-125b with NYHA. Serum levels of (a) lncRNA ROR and (b) miR-125b in heart failure patients combined acute renal failure with NYHA classes II, III, and IV.

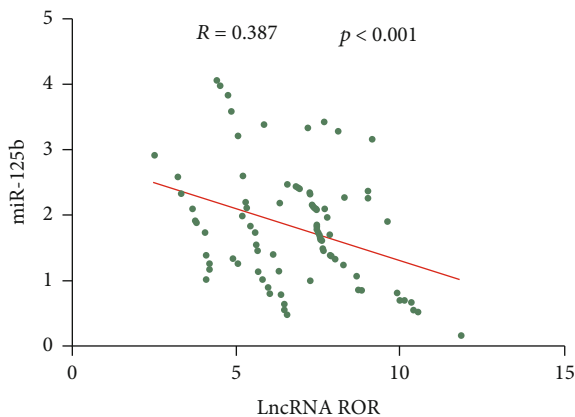


FIGURE 3: Correlation between serum levels of lncRNA ROR and miR-125b. A negative link between serum levels of lncRNA ROR and miR-125b in heart failure patients combined acute renal failure.

showed the opposite trend (Figure 2(b)). It is believed that high level of lncRNA ROR and low level of miR-125b aggravated the development of HF.

3.4. Correlation between Serum Levels of lncRNA ROR and miR-125b. Pearson correlation test uncovered a negative link between serum levels of lncRNA ROR and miR-125b in HF patients combined ARF (Figure 3).

3.5. Diagnostic Potentials of lncRNA ROR and miR-125b in HF Combined ARF. ROC curves were depicted for assessing the potentials of lncRNA ROR and miR-125b as diagnostic biomarkers in HF combined ARF. As the data revealed, lncRNA ROR and miR-125b were qualified in diagnosing HF combined ARF (lncRNA ROR: AUC = 0.9199, cutoff value = 5.595, sensitivity = 92.22%, and specificity = 73.33% ; miR-125b: AUC = 0.8509, cutoff value = 2.290, sensitivity = 81.11%, and specificity = 74.44%) (Figures 4(a) and 4(b)).

3.6. Correlation between Serum Levels of lncRNA ROR and miR-125b with Prognosis in HF Combined ARF. Based on the mentioned cutoff value of lncRNA ROR, included patients were assigned into two groups. After 2-year follow-up, 16 cases were dead. Higher incidences of death and rehospitalization were observed in HF combined ARF cases expressing higher serum level of lncRNA ROR. In a similar way, patients were assigned into two groups according to the cutoff value of miR-125b. HF patients combined ARF expressing lower level of miR-125b had higher incidences of death and rehospitalization (Table 2).

4. Discussion

Renal insufficiency secondary to HF is commonly seen and its mortality is high [23]. ARF is a key factor in determining the progression and prognosis of HF [24]. Recently, biomarkers of impaired renal function have been identified as

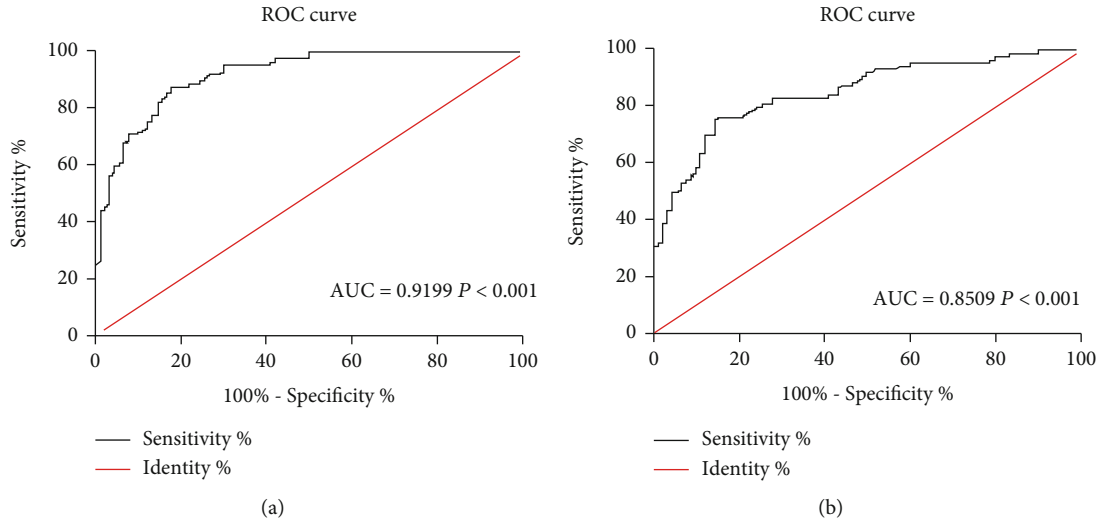


FIGURE 4: Diagnostic potentials of lncRNA ROR and miR-125b in heart failure combined ARF. (a) Diagnostic potential of lncRNA ROR in heart failure patients combined acute renal failure (AUC = 0.9199, cutoff value = 5.595, sensitivity = 92.22%, and specificity = 73.33%). (b) Diagnostic potential of miR-125b in heart failure patients combined acute renal failure (AUC = 0.8509, cutoff value = 2.290, sensitivity = 81.11%, and specificity = 74.44%).

TABLE 2: Correlation between serum levels of lncRNA ROR and miR-125b with prognosis in heart failure combined ARF.

Variable	Death	Rehospitalization	Nonhospitalized
lncRNA ROR			
Low level ($n = 36$)	4	12	20
High level ($n = 54$)	12	33	9
χ^2		55.573	
p		<0.001	
miR-125b			
Low level ($n = 58$)	13	34	11
High level ($n = 32$)	3	11	18
χ^2		52.874	
p		<0.001	

risk factors for HF, displaying a predictive value for poor, long-term prognosis [25].

Critical functions of lncRNAs have been highlighted [26, 27]. Yang et al. [28] discovered differentially expressed lncRNAs between ischemic HF patients and nonischemic HF ones by RNA-seq. It is reported that lncRNA Mhrt 779 antagonizes the development of cardiac hypertrophy and HF in mice induced by aortic contraction [29]. miRNAs are highly conserved in different species and tissue-specific. Primary transcripts are cleaved into pre-miRNAs and then translocate into nuclei to form mature miRNAs [30, 31]. About 30% of human genomes can be regulated by miRNAs [9]. Scrutinio et al. [32] found downregulated miR-150-5p in advanced HF patients, which is linked to cardiac remodeling, disease severity, and prognosis. To uncover the role of ROR and miR-125b, compared to previous research, we found that lncRNA ROR was upregulated in serum of HF patients combined ARF; however, miR-125b was found to be downregulated in serum of HF combined ARF. Further,

ROR increased as disease stage advanced while miR-125b showed an opposite phenotype. The previous findings indicated the potential relation between ROR and miR-125b in HF combined ARF. lncRNA-miRNA interaction contributes to cell phenotype regulations [33]. Through absorbing miRNAs as ceRNAs, lncRNAs inhibit miRNA expressions [34]. Besides, lncRNAs are precursors of miRNAs through intracellular cleavage [35]. GAS5 is downregulated in fibrotic cardiac tissues, which alleviates HF by negatively regulating miR-21 [36]. Upregulated HOTAIR may be a biomarker of HF [37]. HOTAIR regulates phosphatase and tensin homologue expressions in HF by competing with miR-19 [38]. Through Pearson correlation test, we found that lncRNA ROR was negatively linked to miR-125b in serum of HF patients combined ARF.

Circulating lncRNA could act as a prognostic factor for disease. In previous study, NEAT1 was reported as an unfavorable prognostic factor in chronic heart failure patients by log-rank test and ROC analysis [39]. Further, Chen et al. also found that NEAT1 was an unfavorable factor in acute ST-segment elevation myocardial infarction by ROC analysis [40]. In our research, we found that ROR and miR-125b were prognostic factors by ROC analysis.

However, there are still limitations in our research. This research only detected the level of ROR and miR-125b in clinical samples; thus, the in vivo and in vitro assays should be conducted to further explore the relationship of ROR and miR-125b and HF. Moreover, their diagnostic and prognostic potentials in HF combined ARF were identified as well.

5. Conclusions

Serum level of lncRNA ROR is upregulated, and miR-125b is downregulated in HF patients combined ARF. Their levels are linked to NYHA classification, which can be utilized as prognostic biomarkers in HF combined ARF.

Data Availability

The datasets used and analyzed during the current study are available from the corresponding author on reasonable request.

Conflicts of Interest

The authors declared no conflict of interest.

References

- [1] Z. F. Zhu, J. J. Li, J. Liu et al., "Circulating Th17 cells are not elevated in patients with chronic heart failure," *Scandinavian Cardiovascular Journal*, vol. 46, no. 5, pp. 295–300, 2012.
- [2] S. Shrivastava, N. Srivastava, and M. Alfanzo-Jaume, "Acute renal failure with cocaine and SGLT-2 inhibitor," *American Journal of Therapeutics*, vol. 26, no. 6, pp. e762–e763, 2019.
- [3] O. Kawarada, S. Yasuda, T. Noguchi, T. Anzai, and H. Ogawa, "Renovascular heart failure: heart failure in patients with atherosclerotic renal artery disease," *Cardiovascular Intervention and Therapeutics*, vol. 31, no. 3, pp. 171–182, 2016.
- [4] Y. B. Meng, X. He, Y. F. Huang, Q. N. Wu, Y. C. Zhou, and D. J. Hao, "Long noncoding RNA CRNDE promotes multiple myeloma cell growth by suppressing miR-451," *Oncology Research*, vol. 25, no. 7, pp. 1207–1214, 2017.
- [5] M. Sun and W. L. Kraus, "From discovery to function: the expanding roles of long noncoding RNAs in physiology and disease," *Endocrine Reviews*, vol. 36, no. 1, pp. 25–64, 2015.
- [6] R. Kumarswamy, C. Bauters, I. Volkmann et al., "Circulating long noncoding RNA, LIPCAR, predicts survival in patients with heart failure," *Circulation Research*, vol. 114, no. 10, pp. 1569–1575, 2014.
- [7] J. Fan, H. Li, R. Xie et al., "LncRNA ZNF593-AS alleviates contractile dysfunction in dilated cardiomyopathy," *Circulation Research*, vol. 128, no. 11, pp. 1708–1723, 2021.
- [8] Y. Zhang, Y. Li, Q. Hu et al., "The lncRNA H19 alleviates muscular dystrophy by stabilizing dystrophin," *Nature Cell Biology*, vol. 22, no. 11, pp. 1332–1345, 2020.
- [9] H. Chen and X. Li, "LncRNA ROR is involved in cerebral hypoxia/reoxygenation-induced injury in PC12 cells via regulating miR-135a-5p/ROCK1/2," *American Journal of Translational Research*, vol. 11, no. 9, pp. 6145–6158, 2019.
- [10] F. Gorzin, A. A. Amirzargar, M. J. Mahmoudi et al., "FOXP3, ROR γ t and IL-10 cytokine profile in chronic heart failure," *Bratislavské Lekárske Listy*, vol. 118, no. 10, pp. 637–641, 2017.
- [11] Y. P. Liang, Q. Liu, G. H. Xu et al., "The lncRNA ROR/miR-124-3p/TRAF6 axis regulated the ischaemia reperfusion injury-induced inflammatory response in human cardiac myocytes," *Journal of Bioenergetics and Biomembranes*, vol. 51, no. 6, pp. 381–392, 2019.
- [12] C. Yu, B. Wu, J. Jiang, G. Yang, C. Weng, and F. Cai, "Overexpressed lncRNA ROR promotes the biological characteristics of ox-LDL-induced HUVECs via the let-7b-5p/HOXA1 axis in atherosclerosis," *Frontiers in Cardiovascular Medicine*, vol. 8, article 659769, 2021.
- [13] J. Krol, I. Loedige, and W. Filipowicz, "The widespread regulation of microRNA biogenesis, function and decay," *Nature Reviews Genetics*, vol. 11, no. 9, pp. 597–610, 2010.
- [14] J. X. Wang, X. J. Zhang, Q. Li et al., "MicroRNA-103/107 regulate programmed necrosis and myocardial ischemia/reperfusion injury through targeting FADD," *Circulation Research*, vol. 117, no. 4, pp. 352–363, 2015.
- [15] Q. Su, L. Li, J. Zhao, Y. Sun, and H. Yang, "MiRNA expression profile of the myocardial tissue of pigs with coronary micro-embolization," *Cellular Physiology and Biochemistry*, vol. 43, no. 3, pp. 1012–1024, 2017.
- [16] J. S. Lee, D. K. Yang, J. H. Park et al., "MicroRNA-101b attenuates cardiomyocyte hypertrophy by inhibiting protein kinase C epsilon signaling," *FEBS Letters*, vol. 591, no. 1, pp. 16–27, 2017.
- [17] K. H. Kim, Y. M. Seo, E. Y. Kim et al., "The miR-125 family is an important regulator of the expression and maintenance of maternal effect genes during preimplantational embryo development," *Open Biology*, vol. 6, no. 11, article 160181, 2016.
- [18] X. Wang, T. Ha, J. Zou et al., "MicroRNA-125b protects against myocardial ischaemia/reperfusion injury via targeting p53-mediated apoptotic signalling and TRAF6," *Cardiovascular Research*, vol. 102, no. 3, pp. 385–395, 2014.
- [19] A. Rodriguez, S. Griffiths-Jones, J. L. Ashurst, and A. Bradley, "Identification of mammalian microRNA host genes and transcription units," *Genome Research*, vol. 14, no. 10A, pp. 1902–1910, 2004.
- [20] P. K. Busk and S. Cirera, "MicroRNA profiling in early hypertrophic growth of the left ventricle in rats," *Biochemical and Biophysical Research Communications*, vol. 396, no. 4, pp. 989–993, 2010.
- [21] V. Nagpal, R. Rai, A. T. Place et al., "MiR-125b is critical for fibroblast-to-myofibroblast transition and cardiac fibrosis," *Circulation*, vol. 133, no. 3, pp. 291–301, 2016.
- [22] L. P. Zhu, T. Tian, J. Y. Wang et al., "Hypoxia-elicited mesenchymal stem cell-derived exosomes facilitates cardiac repair through miR-125b-mediated prevention of cell death in myocardial infarction," *Theranostics*, vol. 8, no. 22, pp. 6163–6177, 2018.
- [23] M. Metra, G. Cotter, M. Gheorghide, C. L. Dei, and A. A. Voors, "The role of the kidney in heart failure," *European Heart Journal*, vol. 33, no. 17, pp. 2135–2142, 2012.
- [24] S. Ather, W. Chan, B. Bozkurt et al., "Impact of noncardiac comorbidities on morbidity and mortality in a predominantly male population with heart failure and preserved versus reduced ejection fraction," *Journal of the American College of Cardiology*, vol. 59, no. 11, pp. 998–1005, 2012.
- [25] D. L. Dries, D. V. Exner, M. J. Domanski, B. Greenberg, and L. W. Stevenson, "The prognostic implications of renal insufficiency in asymptomatic and symptomatic patients with left ventricular systolic dysfunction," *Journal of the American College of Cardiology*, vol. 35, no. 3, pp. 681–689, 2000.
- [26] R. B. Lanz, N. J. McKenna, S. A. Onate et al., "A steroid receptor coactivator, SRA, functions as an RNA and is present in an SRC-1 complex," *Cell*, vol. 97, no. 1, pp. 17–27, 1999.
- [27] C. A. Klattenhoff, J. C. Scheuermann, L. E. Surface et al., "Braveheart, a long noncoding RNA required for cardiovascular lineage commitment," *Cell*, vol. 152, no. 3, pp. 570–583, 2013.
- [28] K. C. Yang, K. A. Yamada, A. Y. Patel et al., "Deep RNA sequencing reveals dynamic regulation of myocardial noncoding RNAs in failing human heart and remodeling with mechanical circulatory support," *Circulation*, vol. 129, no. 9, pp. 1009–1021, 2014.
- [29] C. Wu and P. Arora, "Long noncodingMhrRNA," *Circulation. Cardiovascular Genetics*, vol. 8, no. 1, pp. 213–215, 2015.

- [30] A. E. Pasquinelli, B. J. Reinhart, F. Slack et al., "Conservation of the sequence and temporal expression of *let-7* heterochronic regulatory RNA," *Nature*, vol. 408, no. 6808, pp. 86–89, 2000.
- [31] D. P. Bartel, "MicroRNAs: genomics, biogenesis, mechanism, and function," *Cell*, vol. 116, no. 2, pp. 281–297, 2004.
- [32] D. Scrutinio, F. Conserva, A. Passantino, M. Iacoviello, R. Lagioia, and L. Gesualdo, "Circulating microRNA-150-5p as a novel biomarker for advanced heart failure: a genome-wide prospective study," *The Journal of Heart and Lung Transplantation*, vol. 36, no. 6, pp. 616–624, 2017.
- [33] Y. Huang, "The novel regulatory role of lncRNA-miRNA-mRNA axis in cardiovascular diseases," *Journal of Cellular and Molecular Medicine*, vol. 22, no. 12, pp. 5768–5775, 2018.
- [34] Q. Zhou, Q. Yu, Y. Gong et al., "Construction of a lncRNA-miRNA-mRNA network to determine the regulatory roles of lncRNAs in psoriasis," *Experimental and Therapeutic Medicine*, vol. 18, no. 5, pp. 4011–4021, 2019.
- [35] L. He, Y. Chen, S. Hao, and J. Qian, "Uncovering novel landscape of cardiovascular diseases and therapeutic targets for cardioprotection via long noncoding RNA-miRNA-mRNA axes," *Epigenomics-Uk*, vol. 10, no. 5, pp. 661–671, 2018.
- [36] H. Tao, J. G. Zhang, R. H. Qin et al., "LncRNA GAS5 controls cardiac fibroblast activation and fibrosis by targeting miR-21 via PTEN/MMP-2 signaling pathway," *Toxicology*, vol. 386, pp. 11–18, 2017.
- [37] S. Greco, G. Zaccagnini, A. Perfetti et al., "Long noncoding RNA dysregulation in ischemic heart failure," *Journal of Translational Medicine*, vol. 14, no. 1, p. 183, 2016.
- [38] Y. Lai, S. He, L. Ma et al., "HOTAIR functions as a competing endogenous RNA to regulate PTEN expression by inhibiting miR-19 in cardiac hypertrophy," *Molecular and Cellular Biochemistry*, vol. 432, no. 1-2, pp. 179–187, 2017.
- [39] H. Zhang, N. Zhang, W. Jiang, and X. Lun, "Clinical significance of the long non-coding RNA NEAT1/miR-129-5p axis in the diagnosis and prognosis for patients with chronic heart failure," *Experimental and Therapeutic Medicine*, vol. 21, no. 5, p. 512, 2021.
- [40] Z. Chen, Y. Yan, J. Wu, C. Qi, J. Liu, and J. Wang, "Expression level and diagnostic value of exosomalNEAT1/miR-204/MMP-9 in acuteST-segment elevation myocardial infarction," *IUBMB Life*, vol. 72, no. 11, pp. 2499–2507, 2020.

Research Article

Death-Associated Protein Kinase 1 (DAPK1) Protects against Myocardial Injury Induced by Myocardial Infarction in Rats via Inhibition of Inflammation and Oxidative Stress

Jun Zhang , Jing Zhang, Bo Zhou, Xiaojing Jiang, Yanrong Tang, and Zhenzhen Zhang

Department of Cardiology, Chengdu First People's Hospital, Chengdu, China

Correspondence should be addressed to Jun Zhang; zhang2008wuhan@hotmail.com

Received 17 November 2021; Accepted 15 December 2021; Published 17 January 2022

Academic Editor: Simona Pichini

Copyright © 2022 Jun Zhang et al. This is an open access article distributed under the Creative Commons Attribution License, which permits unrestricted use, distribution, and reproduction in any medium, provided the original work is properly cited.

Objective. Heart failure and ventricular remodeling after acute myocardial infarction (AMI) are important factors affecting the prognosis of patients. Therefore, we expected to explore the therapeutic target of AMI by studying the effect of death-associated protein kinase 1 (DAPK1) on AMI rat model. **Materials and Methods.** We used male Sprague-Dawley rats to make AMI model, and after 1, 3, 7, and 14 d, we detect the success rate of modeling and the expression change of DAPK1 through 2, 3, 5-triphenyl tetrazolium chloride staining, myocardial injury markers detection, echocardiographic detection, and histological experiment. In addition, we determined the effect of DAPK1 on AMI by subcutaneous injection of the DAPK1 inhibitor (TC-DAPK 6). The effect of DAPK1 on cardiomyocytes has also been verified in cell experiments on H9c2 cells. **Results.** The expression of DAPK1 in AMI rats was significantly higher than that in sham group, and it increased with time. The expression of inflammatory factors (interleukin- (IL-) 1 β , IL-6, and tumor necrosis factor- α) in AMI rats treated by TC-DAPK 6 was reduced. In addition, TC-DAPK 6 also reduced the activity of malonaldehyde and increased the activities of superoxide dismutase, glutathione, and catalase. The expression of antioxidant molecules such as peroxiredoxin1/4 and glutathione peroxidase1/3 was also promoted by TC-DAPK 6. In H9c2 cells, TC-DAPK 6 also reduced its oxidative stress level. **Conclusions.** The increase of DAPK1 may be related to the pathogenesis of AMI. DAPK1 inhibitors protect cardiomyocytes from AMI-induced myocardial injury by reducing levels of inflammation and oxidative stress in myocardial tissue and cells.

1. Introduction

Acute myocardial infarction (AMI) is a cardiovascular disease with high morbidity and high mortality [1]. Current treatment methods include drug thrombolysis, coronary intervention, and coronary artery bypass grafting. Although these treatments have benefited more and more patients, and the mortality rate has decreased significantly, the heart cannot be repaired by the regeneration of myocardial cells due to the poor regeneration of myocardial cells after infarction [2]. The loss of myocardial cells after AMI and the subsequent ventricular remodeling are the main causes of a series of complications after AMI, especially heart failure, which affects the prognosis of patients [3]. How to promote the repair and functional reconstruction of myocardial cells in the necrotic area after AMI and prevent ventricular

remodeling has become the key to improving the prognosis of MI patients.

Death-associated protein kinase 1 (DAPK1) was discovered by Deiss in 1995 using gene cloning analysis technology in HeLa cell apoptosis induced by interferon- γ [4]. Recent studies have found that DAPK1 is an important serine/threonine kinase and is involved in a variety of cell-to-cell interactions, such as apoptosis, autophagy, cellular blebbing, tumor metastasis, and inflammation [5, 6]. A study found that the inhibition of DAPK1 can reduce the inflammatory factors in lung tissue and inhibit the level of oxidative stress by regulating the activity of p38MAPK/NF- κ B signaling pathway, thereby alleviating lung injury [7]. In addition, DAPK1 was also found to be regulated by resveratrol and affect autophagy in human skin fibroblasts [8]. DAPK1 has also been found to affect apoptosis and autophagy in various

tumor cells [6]. In the process of myocardial infarction, myocardial cell ischemia and hypoxia lead to myocardial cell necrosis and apoptosis. In addition, local inflammation and oxidative damage are also important reasons for aggravating myocardial damage [2]. In view of the above-mentioned physiological functions of DAPK1, we speculated that DAPK1 may play a role in AMI. However, there are few studies on the effect of DAPK1 on AMI. Therefore, in this study, we made the rat AMI model to detect DAPK1 expression changes and used DAPK1 inhibitors to detect their effect on AMI rats and cardiomyocytes.

2. Materials and Methods

2.1. Animals. 80 male Sprague-Dawley (SD) rats (200-250 g) were used in this study. SD rats were housed in the Chengdu First People's Hospital Experimental Animal Center. We use standard sterile rodent feed to feed rats. The rats were in the environment with room temperature of 18-22°C, relative humidity of 45-65% and routine lighting. The experimental environment complies with the standards set by the International Animal Protection Association. The animal experiments in this study have been approved by the Animal Ethics Committee of Chengdu First People's Hospital.

2.2. AMI Model. We weighed the rats and used electric clipper to dehair the rats. Then, we used 10 g/L pentobarbital sodium (50 mg/kg) to anesthetize rats by intraperitoneal injection. After the rat lost consciousness, we fixed the rat on the operating table in a supine position. Then, we used an 18G venous indwelling needle for tracheal intubation and connected it to a small animal ventilator (CWE SAR-830, Orange, CA, USA). The small animal ventilator was set to tidal volume of 5-7 mL and frequency of 75 times/min. We used iodophor to disinfect the chest and abdomen of the mouse and then used scissors to cut the skin of the left chest and cut the third and fourth ribs. Then, we used forceps to carefully tear the envelope. Under the cold light spotlight, we carefully identified the left anterior descending coronary artery. The left anterior coronary artery descends to the root of the left atrial appendage. We ligated the coronary arteries with nylon thread and recorded the electrocardiogram of the rat using an electrocardiograph. The elevation of the ST segment of the electrocardiogram indicated that the coronary artery was successfully blocked. We then closed the rat thoracic cavity layer by layer and sutured the surgical incision. The rats were placed on a 37°C water bath. After the rats regained consciousness and mobility, we put the rats back into the rat cage. The rats in the sham group only opened the chest cavity, but the coronary arteries were not ligated. For the treatment group, we used TC-DAPK 6 (1 mg/kg, 2 mg/kg) (MCE, Monmouth Junction, NJ, USA), an inhibitor of DAPK1, to subcutaneously inject AMI rats daily from the first day of modeling. For the non-treatment group, we injected the same amount of normal saline every day.

2.3. 2, 3, 5-Triphenyl Tetrazolium Chloride (TTC) Staining. After collecting the rat heart, we used phosphate-buffered

saline (PBS) to wash away excess blood from the heart. Then, we put the rat heart in the -20°C refrigerator for refrigeration. After 30 min, we took the rat heart and confirmed whether the heart was completely frozen. Then, we cut the heart into 2 mm slices perpendicular to the longitudinal axis. Heart slices were placed in 2% TTC staining solution (Sigma-Aldrich, St. Louis, MO, USA) and incubated in the dark for 15 min. Normal myocardial tissue appears red, while infarcted myocardium appears pale. We used the percentage of infarcted myocardium to represent the extent of myocardial infarction.

2.4. Echocardiography for Detecting Cardiac Function in Rats. 1, 3, 7, and 14 d after making the AMI model, we examined the cardiac function of rats by echocardiography. After anesthetizing the rat with 10 g/L pentobarbital sodium (50 mg/kg), we fixed the rat in a supine position and performed cardiac ultrasound using a Vevo high-resolution ultrasound system (VisualSonics, Toronto, Canada). The left ventricular end-systolic diameter and left ventricular end-diastolic diameter were recorded. Left ventricular ejection fraction (LVEF) and left ventricular fractional shortening (LVFS) are automatically calculated by an echocardiogram computer.

2.5. Lactic Dehydrogenase (LDH) and Creatine Kinase (CK) Levels in Serum. We collected rat blood and left it at room temperature for 15 min. Then, we obtained the serum by centrifugation (3000 rpm, 15 min, 4°C). LDH activity detection kit (Sigma-Aldrich, St. Louis, MO, USA) and CK activity detection kit (Sigma-Aldrich, St. Louis, MO, USA) were used to detect the level of LDH and CK in serum. We used purified rat LDH antibody coating plate to make solid phase antibody. Then, we added unknown concentration of LDH test sample and known concentration of LDH standards to the monoclonal antibody. After incubating for 15 min, we added biotin-labeled anti-IgG antibody. The IgG antibody then binds to streptavidin-HRP to form an immune complex. Then, we added substrate TMB for color development. The color depth is positively correlated with the LDH in the sample. Finally, we used a microplate reader to measure the absorbance (OD value) at a wavelength of 450 nm and calculated the concentration of rat LDH in the sample through the standard curve. The same principle was also used to detect the level of CK.

2.6. Enzyme-Linked Immunosorbent Assay (ELISA). After obtaining rat serum, we used interleukin- (IL-) 1 β , IL-6, and tumor necrosis factor- (TNF-) α ELISA kits (Sigma-Aldrich, St. Louis, MO, USA) to detect the levels of inflammatory factors in serum. The standards in the ELISA kit were used to make a standard curve. Then, we calculated the concentration of the sample based on the absorbance of the sample and the standard curve.

2.7. Activity Detection of Malonaldehyde (MDA), Glutathione (GSH), Superoxide Dismutase (SOD), and Catalase (CAT) in Myocardium and Cell Supernatant. We collected 2 mg of rat myocardial tissue and added 9 times the volumes of normal saline. Then, we used scissors to

shred the tissue and add 3 small steel balls to each EP tube. Then, we put the EP tube into the homogenizer for homogenization (10000 r/min) 3 times, 1 min each time. Then, we took the supernatant in the EP tube by centrifugation (12000 rpm, 15 min, 4°C). MDA, GSH, SOD, and CAT activity detection kits (Sigma-Aldrich, St. Louis, MO, USA) were used to detect the levels of MDA, GSH, SOD, and CAT in serum. The detection of MDA, GSH, SOD, and CAT in the cell supernatant was similar to that of myocardial tissue.

2.8. Histology and Hematoxylin-Eosin (HE) Staining. After collecting the rat heart, we used PBS to wash away excess blood from the heart. Then, we used 4% paraformaldehyde to fix myocardial tissue for 24h. The fixed tissue can be stored in PBS for a long time. We put myocardial tissue into gradient alcohol in order to dehydrate. Then, we put myocardial tissue in xylene and paraffin solution to make paraffin blocks. The microtome is used to make paraffin sections with the thickness of 5 μ m. We put paraffin sections in a 37°C incubator for 3 d. Then, we put the paraffin sections in xylene solution and gradient alcohol sequentially. After washing the sections with running water, we stained the cell nucleus with hematoxylin stain (Beyotime, Shanghai, China). Then, we put the sections in 1% hydrochloric acid alcohol for 3 s and quickly rinsed the sections with running water. Then, we put the sections in eosin stain (Beyotime, Shanghai, China) and gradient alcohol in turn for 3 min each time. Finally, we use neutral gum for mounting and observe the staining results using an optical microscope.

2.9. Immunohistochemical (IHC) Staining. After dewaxing and hydration using xylene and gradient alcohol, we rinsed the sections in running water for 3 min. We put the sections in citrate buffer. The buffer just barely goes through the sections. Then, we heated the citrate buffer slowly to 95°C in a water bath for 20 min. After it naturally cooled to room temperature, we took out the sections and washed it with PBS three times for 3 min each time. Then, we put the sections in a wet box and incubate them for 30 min with 3% hydrogen peroxide on myocardial tissue. Then, we blocked the nonspecific antigen with 10% goat serum and incubated them at 4°C overnight with primary antibody dilution (DAPK1, ab200549; peroxiredoxin (Prdx)1, ab15571; Prdx4, ab59542; Abcam, Cambridge, MA, USA). After washing the sections with PBS, we incubated them with secondary antibody dilution (GeneTech, Shanghai, China) for 1 h and used DAB for color development. Hematoxylin is used in the cell nucleus. Finally, we used an optical microscope to observe the results.

2.10. Cell Culture. The rat cardiomyocyte cell line, H9c2 cells, was used in this study. DMEM medium containing 10% fetal bovine serum (FBS) (Gibco, Rockville, MD, USA) and 1% double antibody (Gibco, Rockville, MD, USA) was used to culture H9c2 cells. IL-1 β (100 ng/mL) (Invitrogen, Carlsbad, CA, USA) was used to stimulate cell injury.

2.11. RNA Isolation and Quantitative Real-Time Reverse Transcription-Polymerase Chain Reaction (RT-PCR). The TRIzol (Sigma-Aldrich, St. Louis, MO, USA) method was

TABLE 1: Primer sequences for RT-PCR.

Name	Sense/antisense	Sequences (5'-3')
DAPK1	Sense	CACCTCACTCCCTTCCC
	Antisense	TCACCCACAGACGGATG
Prdx1	Sense	TTCTGTCATCTGGCATGG
	Antisense	CCCAATCCTCCTTGTCTTCT
Prdx4	Sense	CCAGCACCTTATTGGGAA
	Antisense	GCGATGATTTTCAGTTGGAC
GPX1	Sense	TGAGAAGTGCGAGGTGAA
	Antisense	TCCGCAGGAAGGTAAAGAG
GPX3	Sense	CGGGGAGAAAGAGCAGAA
	Antisense	CAAAGTTCCAGCGGATGTC
GAPDH	Sense	ATGGCTACAGCAACAGGGT
	Antisense	TTATGGGGTCTGGGATGG

used to extract total RNA from myocardial tissue and H9c2 cells. Then, we used a spectrophotometer to detect RNA concentration and A260/A280. Samples with A260/A280 around 2.0 can be used for subsequent experiments. We took 0.5 μ g total RNA (5 μ L) for reverse transcription. The 10 μ L reverse transcription system is 5 + 3 μ L RNase-free H₂O+2 μ L 5x HiScript II Q RT SuperMix (Vazyme, Nanjing, Jiangsu, China). The PCR instrument was set to 50°C for 15 min, 85°C for 5 s, and 4°C for 30 min. SYBR Green Master Mix (Vazyme, Nanjing, Jiangsu, China) was used for real-time RT-PCR. The reaction system is 5 μ L SYBR Green Master Mix +0.4 μ L Primer forward/reverse +1 μ L cDNA template +3.6 μ L ddH₂O. Reaction temperature and time refer to primer company's instructions. The endogenous GAPDH expression was used as a reference. The relative expression of RNA is expressed as $2^{-\Delta\Delta Ct}$. The primer sequences are shown in Table 1.

2.12. Flow Cytometry Analyses. Flow cytometry was used to detect reactive oxygen species (ROS) levels. Pancreatin was used to prepare single-cell suspensions. Then, we took 1 mL of single-cell suspension and added 5 μ L of 2', 7'-dichlorodihydrofluorescein diethyl ester (DCF-DA) (Sigma-Aldrich, St. Louis, MO, USA) for 30 min. Then, we put it in a centrifuge (1500 rpm, 5 min) and discard the supernatant. Then, we added 10% fetal bovine serum and incubated it at 37°C for 20 min. After centrifuging it again in a centrifuge (1500 rpm, 5 min), we discarded the supernatant and added cold PBS. Then, we used flow cytometry (Thermo Fisher Scientific, Waltham, MA, USA) to detect the average fluorescence intensity of the fluorescent probes in the cells. The relative fluorescence intensity value is the ratio of the fluorescence intensity value of the experimental group to that of the control group.

2.13. Cell Counting Kit-8 (CCK8). CCK8 (Dojindo Molecular Technologies, Kumamoto, Japan) was used to detect the proliferation ability of H9c2 cells. We used 96-well plates to culture H9c2 cells. 10 μ L of CCK8 reagent was added to each well of a 96-well plate. The 96-well plate was placed in a 37°C incubator for 2 h in the dark. Then, we used a

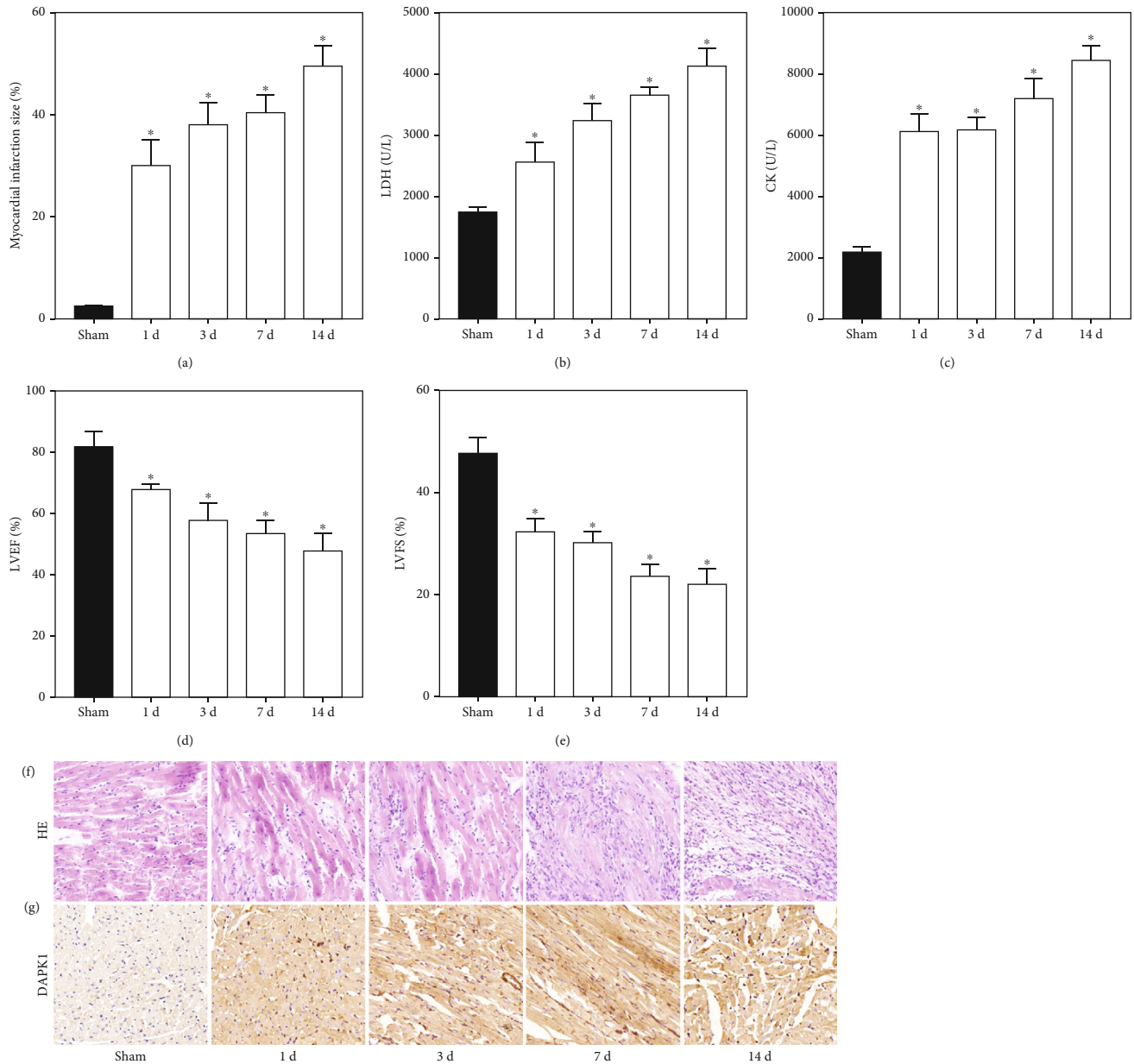


FIGURE 1: High expression of DAPK1 in myocardium of AMI rats. After 1, 3, 7, and 14 d of coronary artery occlusion, the myocardial infarction size (a), myocardial injury markers (b, c), and cardiac function (d, e) were detected to confirm modeling efficiency. HE staining (f) also demonstrated the destruction of myocardial structure due to coronary artery occlusion (magnification: 200x). IHC staining (g) showed that DAPK1 expression increased in AMI rats (magnification: 200x) (“*” means $P < 0.05$ vs. sham group).

microplate reader to detect the absorbance (OD value) of each well at 450 nm. There was only the medium and no cells in the blank wells, and there were medium and noninterfering cells in control wells. Cell viability = (OD intervention – OD blank)/(OD control – OD blank).

2.14. Statistical Analysis. Statistical Product and Service Solutions (SPSS) 20.0 statistical software (IBM, Armonk, NY, USA) was used for the statistical analysis of this study. Graphpad prism 7.0 software (La Jolla, CA, USA) was used for graphing in this study. We use the mean \pm standard deviation to represent the study data. Differences between two groups were analyzed by using Student’s *t*-test. Compar-

ison between multiple groups was done using one-way ANOVA test followed by post hoc test (least significant difference). $P < 0.05$ was considered statistically significant.

3. Results

3.1. High Expression of DAPK1 in Myocardium of AMI Rats. After 1, 3, 7, and 14 d of blocking the rat coronary arteries, we took rat myocardial tissue for TTC staining (Figure 1(a)). We found that the scope of myocardial infarction gradually increased with time. The concentrations of myocardial infarction markers LDH (Figure 1(b)) and CK (Figure 1(c)) also increased with the time of myocardial

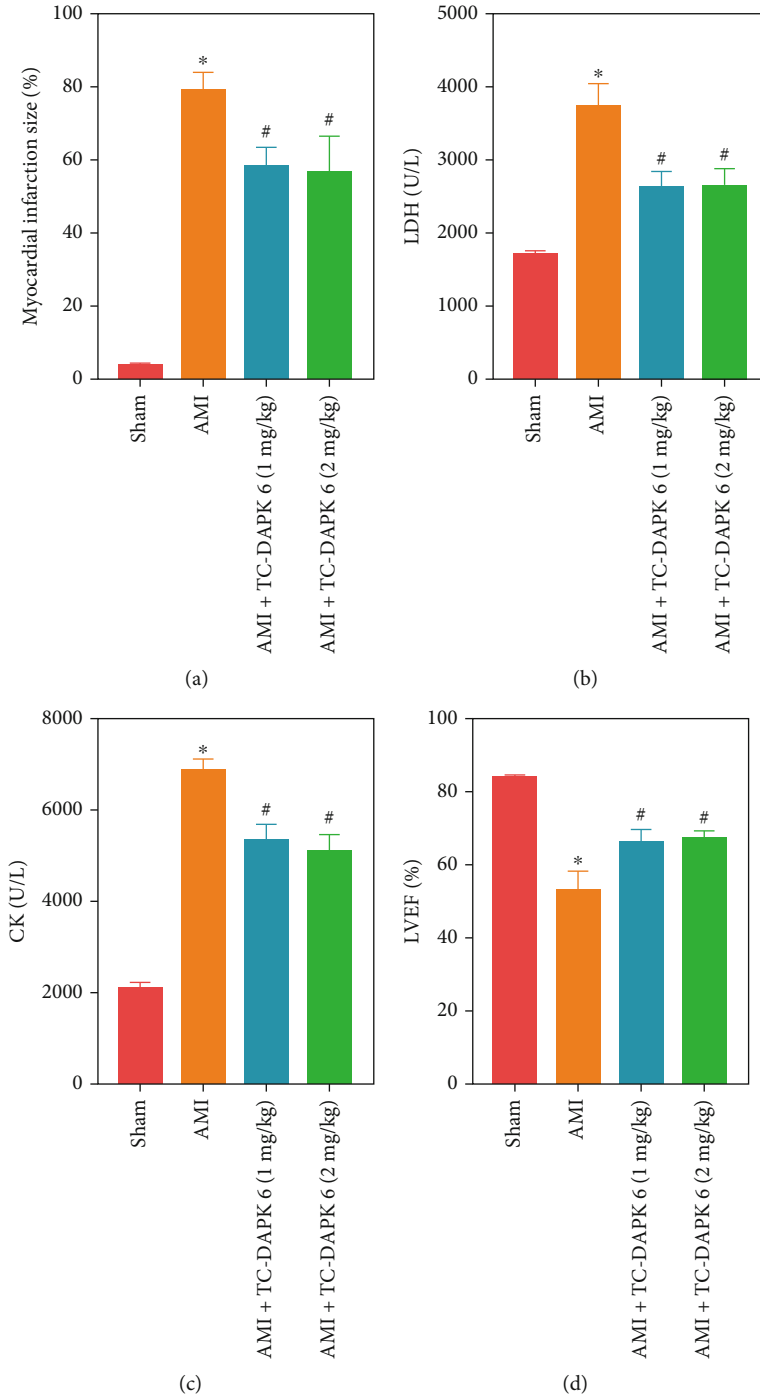


FIGURE 2: Continued.

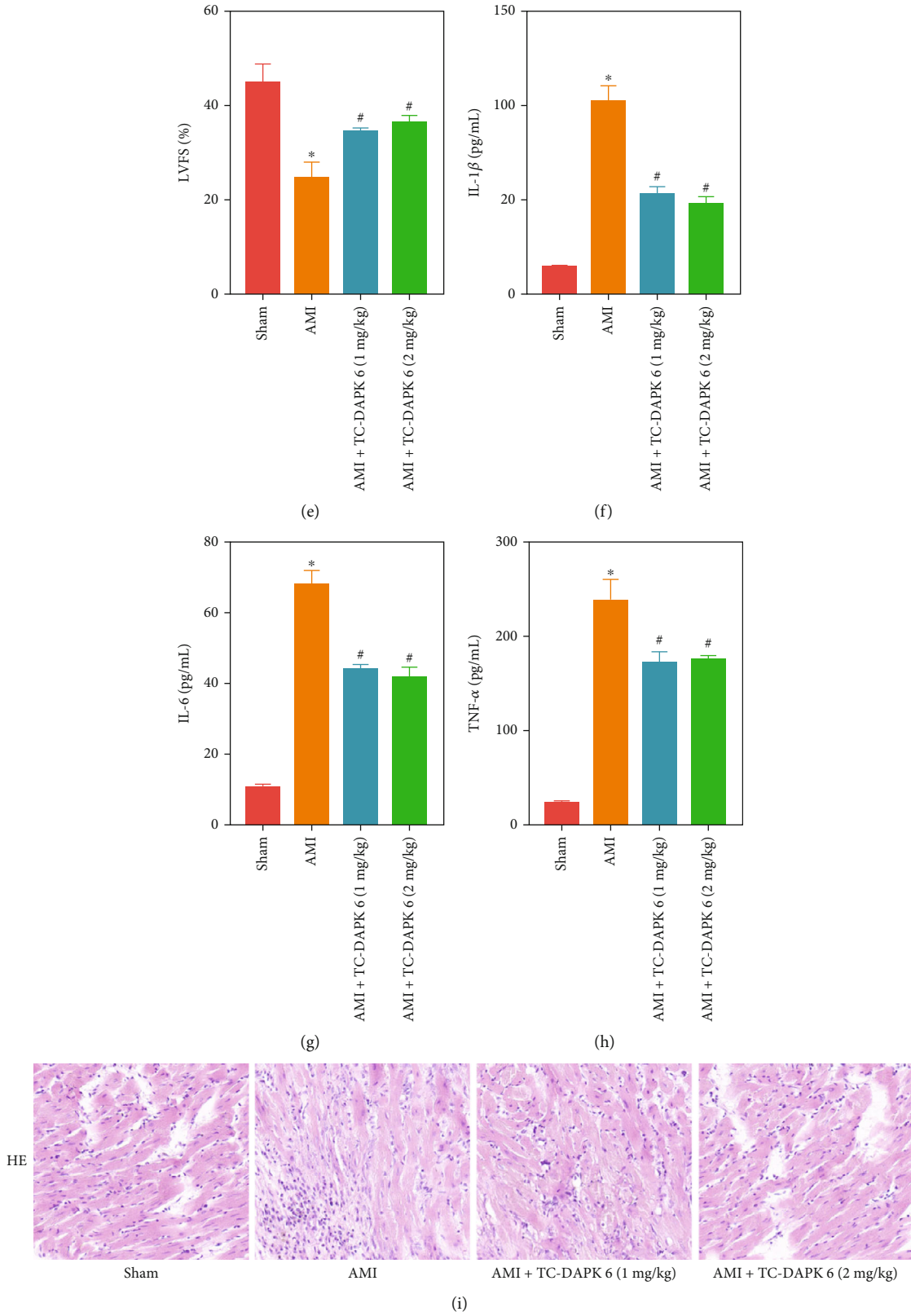


FIGURE 2: Inhibition of DAPK1 alleviates cardiac dysfunction and inflammation in AMI rats. TC-DAPK 6 was used to treat AMI rats and to detect changes in myocardial infarction size (a), myocardial injury markers (b, c), and cardiac function (d, e) in AMI rats. The expression of inflammatory cytokines (IL-1 β , IL-6, and TNF- α) in rat serum was detected by ELISA (f-h). HE staining (i) was used to detect the structural changes of rat myocardial tissue (magnification: 200x) (“*” means $P < 0.05$ vs. sham group, and “#” means $P < 0.05$ vs. AMI group).

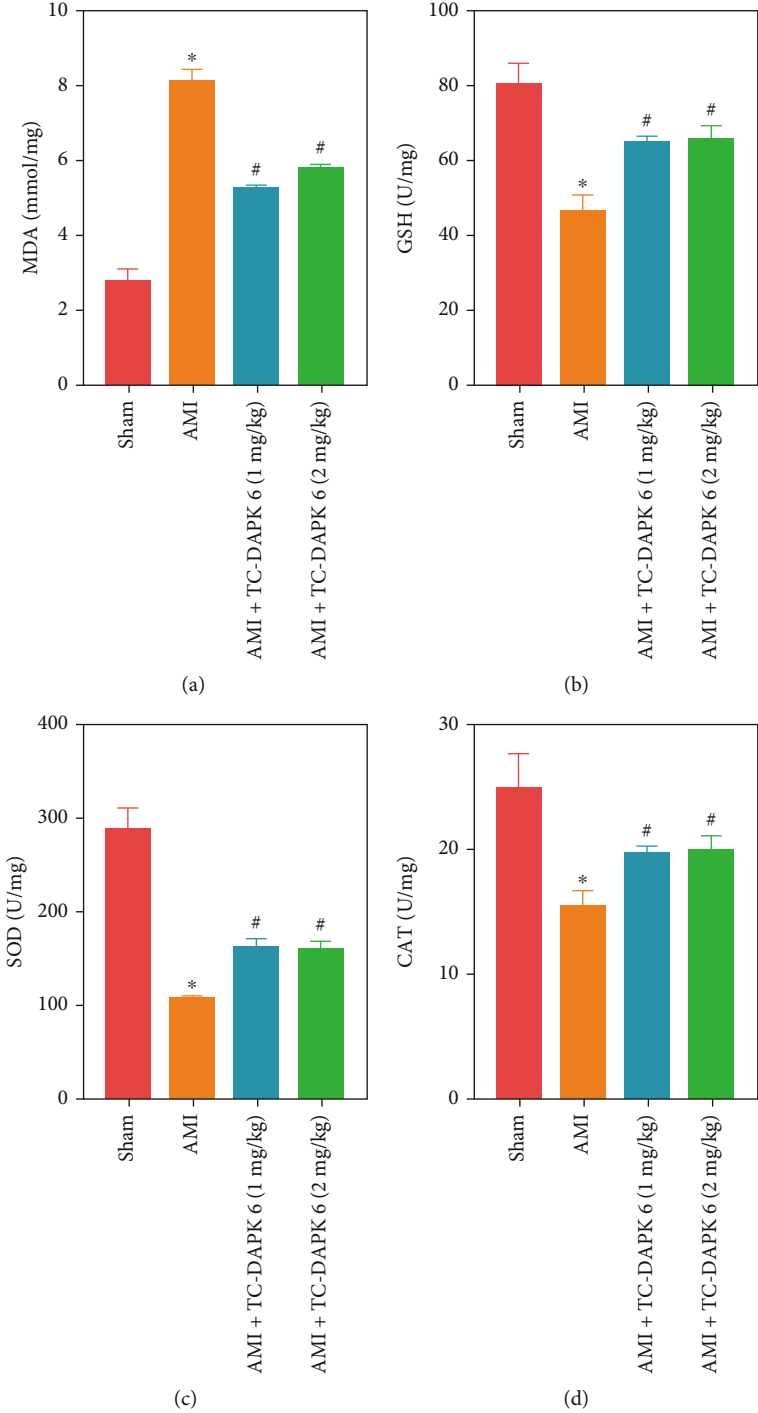


FIGURE 3: Continued.

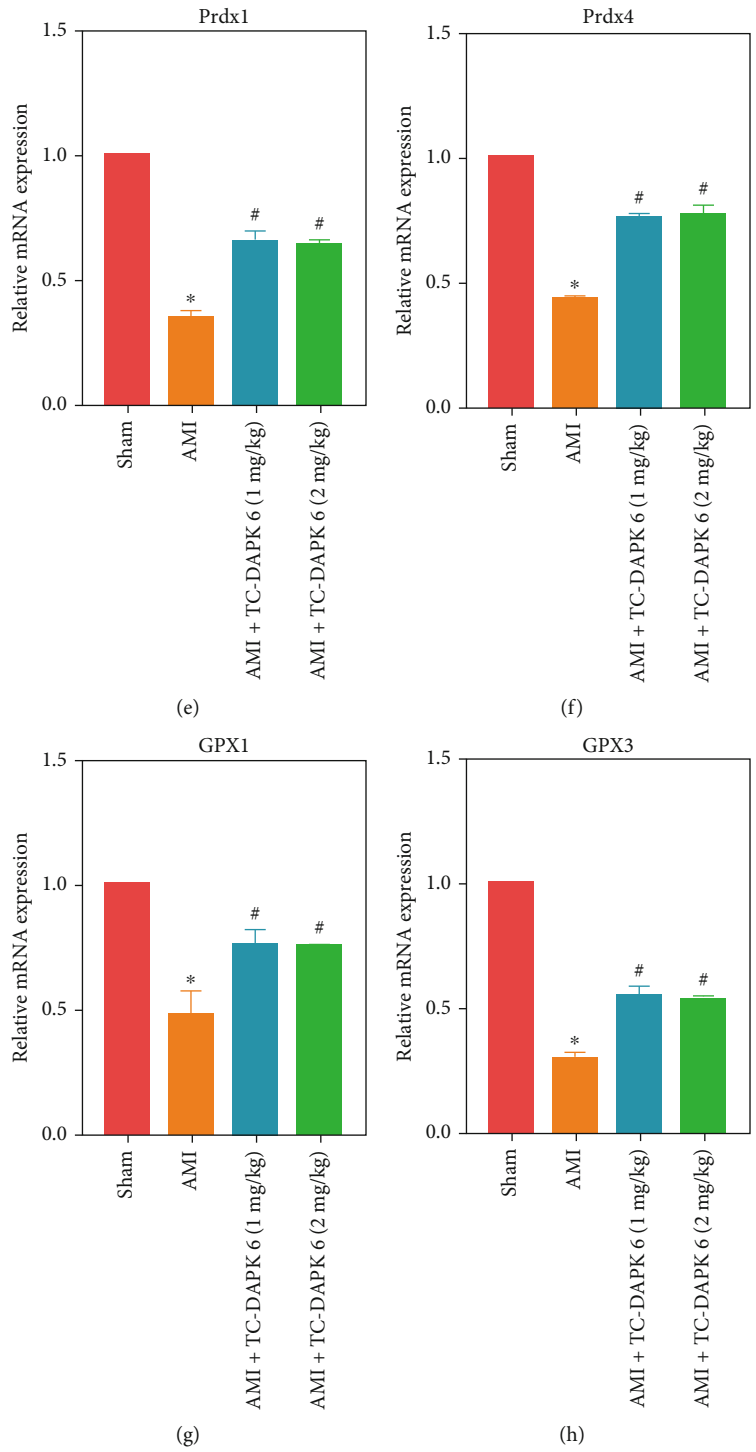


FIGURE 3: Continued.

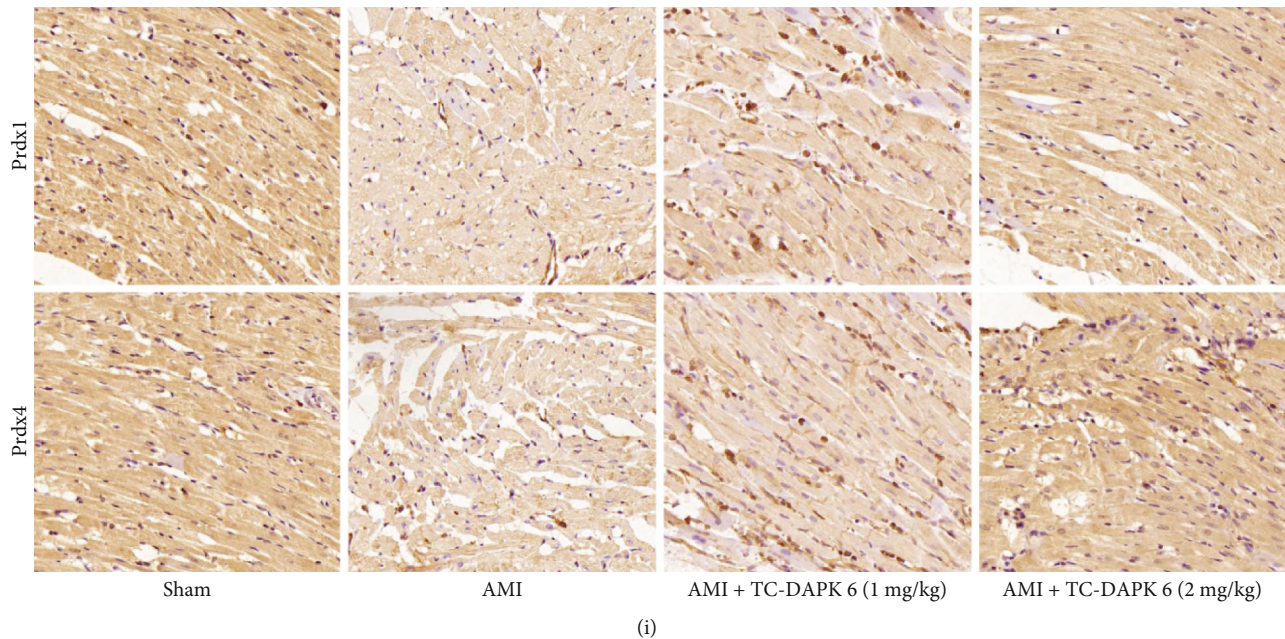


FIGURE 3: Inhibition of DAPK1 alleviates AMI-induced oxidative injury. The activities of MDA (a), GSH (b), SOD (c), and CAT (d) were measured to determine the level of oxidative stress in rat myocardial tissue. The mRNA expression of Prdx1 (e), Prdx4 (f), GPX1 (g), and GPX3 (h) was detected by RT-PCR. The protein expression of Prdx1 and Prdx4 was detected by IHC staining (magnification: 200x) (i) (“**” means $P < 0.05$ vs. sham group, and “#” means $P < 0.05$ vs. AMI group).

infarction. In addition, we detected the cardiac function of rats by echocardiography. The LVEF (Figure 1(d)) and LVFS (Figure 1(e)) of AMI rats were significantly lower than that of the sham group and decreased with time. HE staining (Figure 1(f)) detected the structure of rat myocardial tissue. The arrangement of myocardial cells in AMI rats was disordered, and the morphology of myocardial cells also changed. The myocardial injury in AMI rats was most obvious after 14d and was accompanied by the infiltration of inflammatory cells. IHC staining (Figure 1(g)) detected the expression of DAPK1 in rat myocardium. We found that with the increase of myocardial infarction time, the expression of DAPK1 in myocardial tissue gradually increased.

3.2. Inhibition of DAPK1 Alleviates Cardiac Dysfunction and Inflammation in AMI Rats. Considering the myocardial injury of the 14d AMI rats was too severe, we chose 7d AMI rats for subsequent experiment. We divided the rats into sham, AMI, AMI + TC-DAPK 6 (1 mg/kg), and AMI + TC-DAPK 6 (2 mg/kg) groups. The results of TTC staining (Figure 2(a)) showed that after inhibition of DAPK1, the range of myocardial infarction in rats was reduced. Myocardial infarction markers LDH (Figure 2(b)) and CK (Figure 2(c)) also decreased with the inhibition of DAPK1. The inhibition of DAPK1 also improved the cardiac function of rats, which was manifested by the increase of LVEF (Figure 2(d)) and LVFS (Figure 2(e)). In addition, we detected changes in inflammatory factors by ELISA. After TC-DAPK 6 was used to treat AMI rats, the expressions of IL-1 β (Figure 2(f)), IL-6 (Figure 2(g)), and TNF- α (Figure 2(h)) in rat serum were all reduced. HE staining (Figure 2(i)) results also prove that TC-DAPK 6 improved

the structure of myocardial tissue. However, there was no significant difference between the AMI + TC-DAPK 6 (1 mg/kg) and AMI + TC-DAPK 6 (2 mg/kg) groups.

3.3. Inhibition of DAPK1 Alleviates AMI-Induced Oxidative Injury. The effect of DAPK1 on oxidative stress of myocardial tissue has also been studied. We detected the activities of MDA (Figure 3(a)), GSH (Figure 3(b)), SOD (Figure 3(c)), and CAT (Figure 3(d)) in rat myocardium. MDA activity of AMI rats was significantly higher than that of sham group, while GSH, SOD, and CAT activities of AMI group were lower than that of sham group. Inhibition of DAPK1 was found to attenuate the AMI-induced changes. RT-PCR detected the expression of Prdx1 (Figure 3(e)), Prdx4 (Figure 3(f)), GPX1 (Figure 3(g)), and GPX3 (Figure 3(h)). Their expression decreased in myocardial tissue of AMI rats, and the inhibition of DAPK1 increased the expression of these indicators. IHC staining (Figure 3(i)) also proved the promoting effect of TC-DAPK 6 on Prdx1 and Prdx4. However, there was no significant difference between the AMI + TC-DAPK 6 (1 mg/kg) and AMI + TC-DAPK 6 (2 mg/kg) groups.

3.4. Inhibition of DAPK1 Alleviates IL-1 β -Induced H9c2 Cell Injury. We verified the effect of DAPK1 on cardiomyocytes in H9c2 cells. IL-1 β is used to induce H9c2 cell injury. We found by IF staining (Figure 4(a)) and RT-PCR (Figure 4(b)) that after IL-1 β stimulated H9c2 cells for 1d and 3d, the expression of DAPK1 mRNA and protein gradually increased. We used 1, 5, 10, 20, and 50 μ M TC-DAPK 6 to stimulate H9c2 cells and detect cell viability by CCK8 (Figure 4(c)). 20 μ M was found to be the optimal

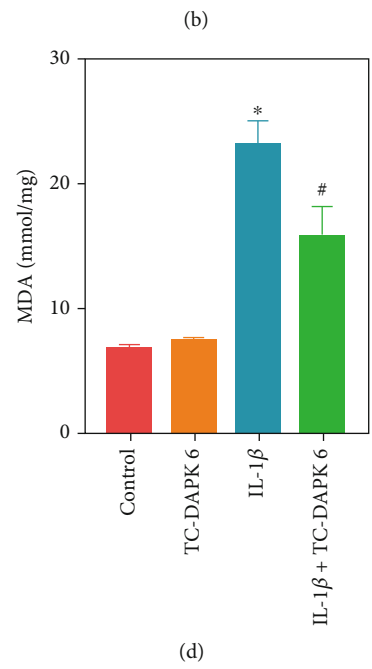
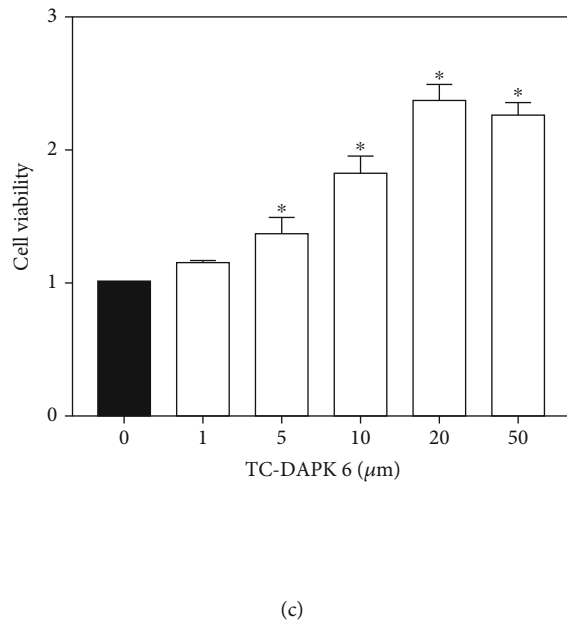
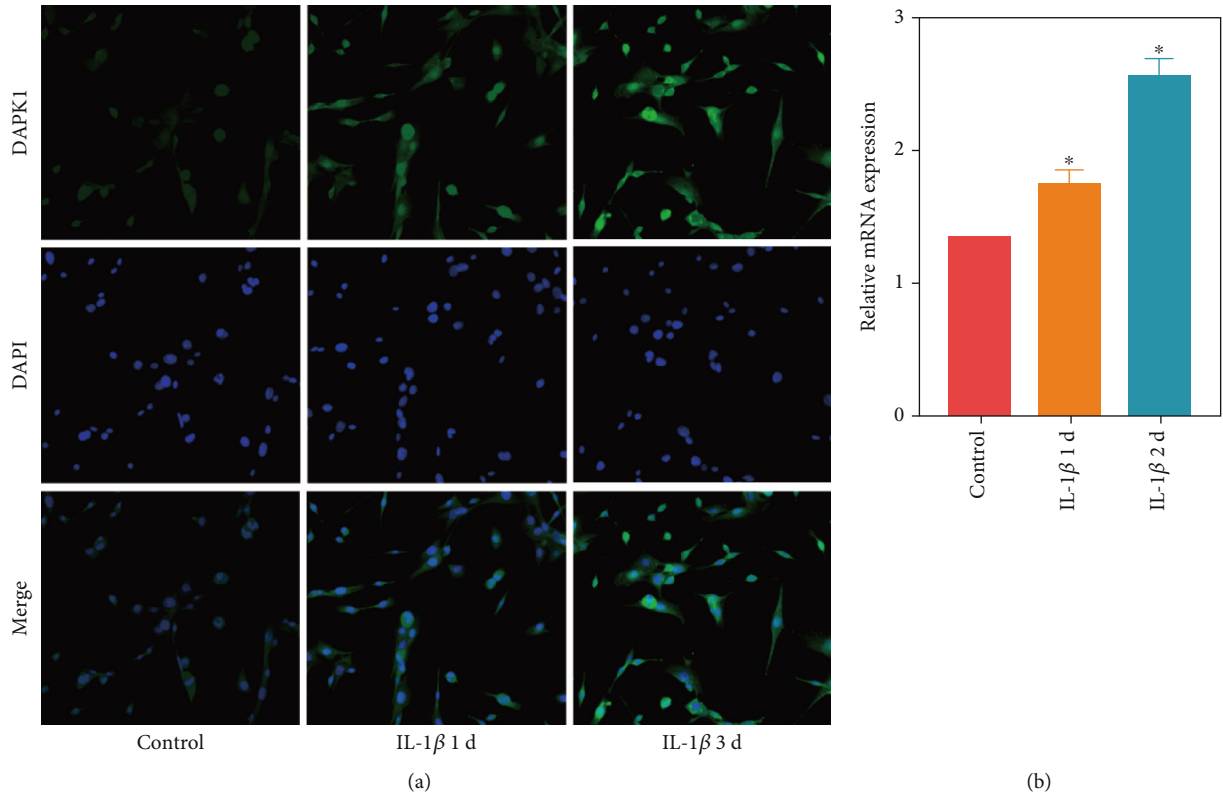


FIGURE 4: Continued.

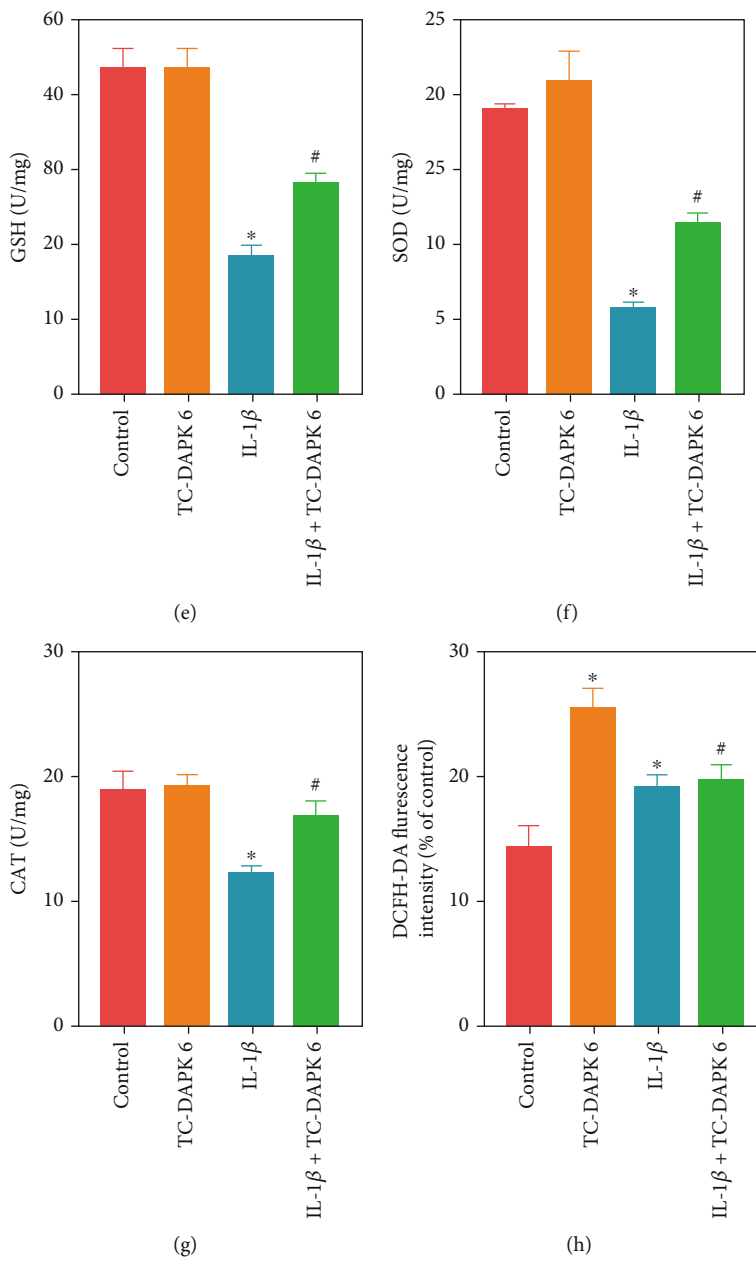


FIGURE 4: Continued.

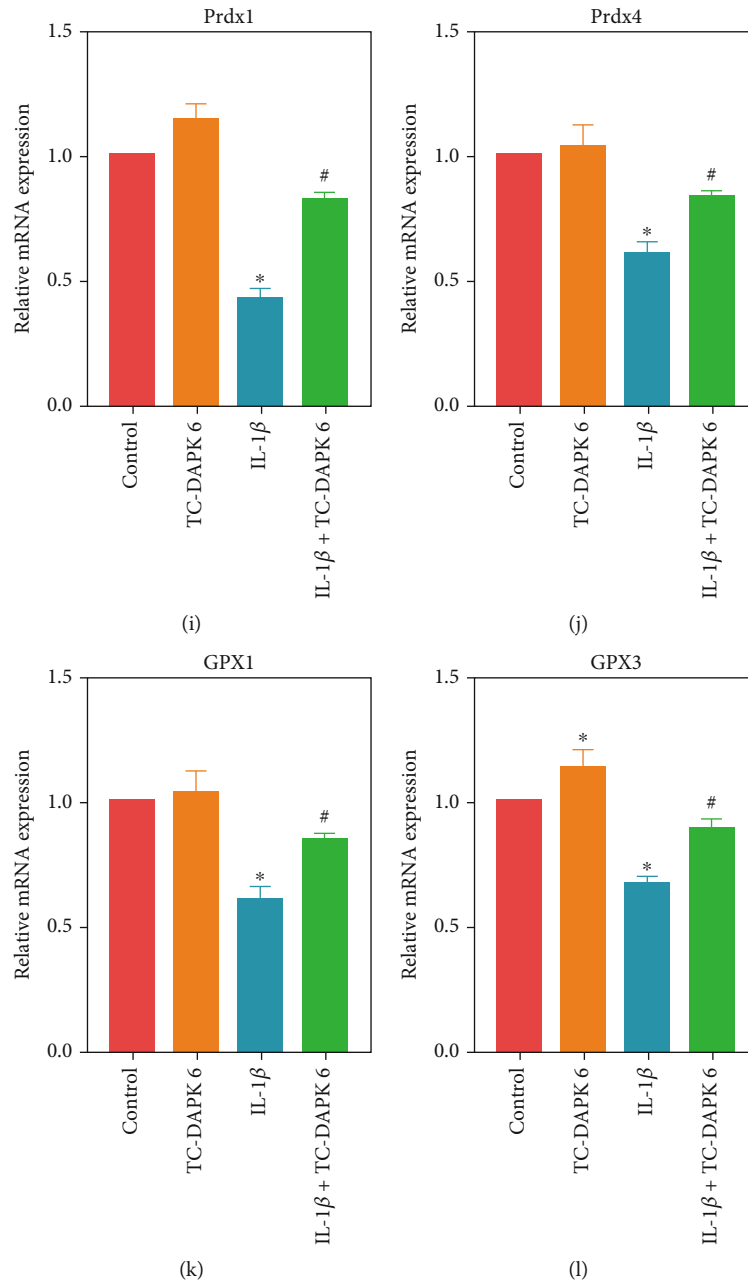


FIGURE 4: Inhibition of DAPK1 alleviates IL-1 β -induced H9c2 cell injury. Expression of DAPK1 in H9c2 cells was detected by IF staining (magnification: 200x) (a) and RT-PCR (b). CCK8 (c) detected the effect of 1, 5, 10, 20, and 50 μ M TC DAPK 6 on H9c2 cells viability. The activities of MDA (d), GSH (e), SOD (f), and CAT (g) were measured to determine the level of oxidative stress in H9c2 cells. ROS level in H9c2 cells was detected by flow cytometry (h). The mRNA expression of Prdx1 (i), Prdx4 (j), GPX1 (k), and GPX3 (l) was detected by RT-PCR (“*” means $P < 0.05$ vs. control group, and “#” means $P < 0.05$ vs. IL-1 β group).

concentration for TC-DAPK 6 to stimulate H9c2 cells, so we used 20 μ M TC-DAPK 6 for subsequent experiments. We divided H9c2 cells into control, TC-DAPK 6, IL-1 β , and IL-1 β + TC-DAPK 6 groups. The activities of MDA (Figure 4(d)), GSH (Figure 4(e)), SOD (Figure 4(f)), and CAT (Figure 4(g)) were detected, and we found that IL-1 β increased the level of oxidative stress, while TC-DAPK 6 can attenuate oxidative stress injury induced by IL-1 β . Flow cytometry (Figure 4(h)) detected ROS levels, and the results showed that TC-DAPK 6 can also reduce ROS levels in H9c2

cells. RT-PCR results also indicated that TC-DAPK 6 can promote the expression of antioxidant molecules Prdx1 (Figure 4(i)), Prdx4 (Figure 4(j)), GPX1 (Figure 4(k)), and GPX3 (Figure 4(l)).

4. Discussion

With the formation of fibrous scar tissue and ventricular remodeling after AMI, myocardial contractility gradually decreases and eventually leads to heart failure and even

death [9]. At present, DAPK1 is expected to become a new target for AMI treatment. We found high expression of DAPK1 in AMI rats. The use of DAPK1 inhibitors significantly improved the cardiac function and myocardial injury in rats and alleviated the H9c2 cell injury induced by IL-1 β . Therefore, DAPK1 inhibitors are expected to become new drugs for clinical treatment of AMI.

Coronary artery occlusion is the main cause of AMI, and the most intuitive manifestation of AMI is the increase in the extent of myocardial infarction [10]. A study investigated the effect of melatonin receptor agonist, ramelteon, on myocardial protection through the model of myocardial ischemia-reperfusion. They found that after coronary artery occlusion and recanalization, the infarct size of the rat heart increased significantly [11]. We made the AMI model by occluding coronary arteries and observed the changes of myocardial infarction size in rats by TTC staining. LDH and CK are important indicators for judging myocardial injury, and their expression in normal myocardial tissue is low. When the body is subjected to a stress response or cardiac ischemia, LDH and CK in the blood increase significantly [12]. Therefore, in order to determine the success rate of modeling, we also detected the activity of LDH and CK in the serum of AMI rats. The range of myocardial infarction, the activity of LDH and CK, and the detection of rat cardiac function proved that the AMI rat model was successfully made. However, considering the myocardial injury of the 14-day-old model rats was very serious, we chose 7 d as the optimal time for modeling, in order to prevent obscuring the therapeutic effect of the intervention.

The inflammation triggered after AMI plays a vital role in determining the extent of myocardial infarction and subsequent ventricular remodeling [13, 14]. After the occurrence of AMI, a large number of myocardial cells rupture due to ischemia, hypoxia, and necrosis, inducing the activation of nonspecific immune responses [15, 16]. Therefore, a large number of inflammatory cytokines are released and enter the blood circulation, such as IL-6, IL-1 β , and TNF- α . The inflammatory factors promote the activation of inflammatory cells such as neutrophils, macrophages, and natural killer cells. These cells are chemoattracted to damaged myocardium and participate in tissue repair and ventricular remodeling [17]. A study on the relationship among inflammation, autophagy, and apoptosis in myocardial infarction found that inflammation, autophagy, and apoptosis have a common role in the course of myocardial infarction [18]. In addition, data from a clinical study also revealed that inflammation affects the hospitalization and prognosis of elderly AMI patients [19]. We also found similar results in this study. Inflammatory factors (IL-1 β , IL-6, and TNF- α) in serum of AMI rats were significantly increased, but the application of DAPK1 inhibitors reduced the myocardial inflammation.

When AMI occurs, it will destroy the balance of the oxidative and antioxidative systems in the myocardial tissue, resulting in the generation of large amounts of oxygen free radicals. At the same time, the activity of SOD and GSH will decrease, leading to the accumulation of oxygen free radicals in the body [20]. Oxygen free radicals can act on lipids to

peroxidation to produce MDA, causing the cross-linking polymerization of proteins, nucleic acids, and other life macromolecules, so oxygen free radicals are also cytotoxic [21]. The sum of the results of four large cohort studies from Europe found that oxidative stress injury has a clear association with AMI. They found that the imbalance of the redox system was involved in the pathogenesis of AMI [22]. In another study, oxidative stress injury was restricted by interfering with the Akt signaling pathway in cardiomyocytes; therefore, cardiomyocyte death caused by AMI was reduced [23]. Wang et al. found a decrease in SOD and GSH and an increase in MDA in a mouse model of septic heart dysfunction, suggesting a decrease in the antioxidant capacity of sepsis mice, while dexmedetomidine can reverse these changes and alleviate heart dysfunction in mice [24]. Therefore, we also detected the oxidative stress level of rat myocardial tissue and H9c2 cells. The decrease of MDA activity and the increase of GSH, SOD, and CAT activities suggested the antioxidation effect of DAPK1 inhibitors. Prdx1/4 and GPX1/3 are important antioxidant molecules, and the inhibition of DAPK1 also promotes their expression in cardiomyocytes.

Therefore, DAPK1 plays an important role in the occurrence and development of AMI. The DAPK1 inhibitors may have potential application prospects for the treatment of AMI. We hope that this study can provide new targets for clinical treatment of AMI.

5. Conclusions

DAPK1 was highly expressed in the myocardium of AMI rats and affects the occurrence and development of AMI. DAPK1 inhibitors reduce the levels of inflammation and oxidative stress in myocardial tissues and cells, thereby improving the structure and function of the rat heart. Therefore, DAPK1 inhibitors have potential application prospects for the treatment of AMI.

Data Availability

The datasets used and analyzed during the current study are available from the corresponding author on reasonable request.

Conflicts of Interest

The authors declared no conflict of interest.

Acknowledgments

This study was supported by the National Natural Science Foundation of China (no. 81270220).

References

- [1] M. Bally, N. Dendukuri, B. Rich et al., "Risk of acute myocardial infarction with NSAIDs in real world use: Bayesian meta-analysis of individual patient data," *BMJ*, vol. 357, p. j1909, 2017.

- [2] R. A. Kloner, W. Dai, S. L. Hale, and J. Shi, "Approaches to improving cardiac structure and function during and after an acute myocardial infarction," *Journal of Cardiovascular Pharmacology and Therapeutics*, vol. 21, no. 4, pp. 363–367, 2016.
- [3] S. Safi, N. J. Sethi, E. E. Nielsen, J. Feinberg, J. C. Jakobsen, and C. Gluud, "Beta-blockers for suspected or diagnosed acute myocardial infarction," *Cochrane Database of Systematic Reviews*, vol. 12, p. D12484, 2019.
- [4] M. Feng, X. Zhu, and C. Zhuo, "H19/miR-130a-3p/DAPK1 axis regulates the pathophysiology of neonatal hypoxic-ischemia encephalopathy," *Neuroscience Research*, vol. 163, pp. 52–62, 2021.
- [5] C. Xu, Z. Zhou, C. Liu et al., "Generation of a DAPK1 knock-out first (conditional ready) human embryonic stem cell line (ZSSYe001-A) by CRISPR-Cas9 technology," *Stem Cell Research*, vol. 43, 2020.
- [6] O. R. Buonarati, S. G. Cook, D. J. Goodell et al., "CaMKII versus DAPK1 binding to GluN2B in ischemic neuronal cell death after resuscitation from cardiac arrest," *Cell Reports*, vol. 30, 2020.
- [7] T. Li, Y. N. Wu, H. Wang, J. Y. Ma, S. S. Zhai, and J. Duan, "_Dapk1_ improves inflammation, oxidative stress and autophagy in LPS-induced acute lung injury via p38MAPK/NF- κ B signaling pathway," *Molecular Immunology*, vol. 120, pp. 13–22, 2020.
- [8] M. S. Choi, Y. Kim, J. Y. Jung, S. H. Yang, T. R. Lee, and D. W. Shin, "Resveratrol induces autophagy through death-associated protein kinase 1 (DAPK1) in human dermal fibroblasts under normal culture conditions," *Experimental Dermatology*, vol. 22, no. 7, pp. 491–494, 2013.
- [9] M. C. Kontos and J. S. Turlington, "High-sensitivity troponins in cardiovascular disease," *Current Cardiology Reports*, vol. 22, no. 5, p. 30, 2020.
- [10] K. Semiczuk-Kaczmarek, A. E. Platek, A. Rys-Czaporowska, F. M. Szymanski, and K. J. Filipiak, "Acute myocardial infarction due to antiphospholipid syndrome - case report and review of the literature," *Current Problems in Cardiology*, vol. 46, no. 3, 2021.
- [11] M. Stroethoff, L. Goetze, C. Torregroza et al., "The melatonin receptor agonist ramelteon induces cardioprotection that requires MT2 receptor activation and release of reactive oxygen species," *Cardiovascular Drugs and Therapy*, vol. 34, no. 3, pp. 303–310, 2020.
- [12] Q. Lai, G. Yuan, H. Wang et al., "Metabolomic profiling of metoprolol-induced cardioprotection in a murine model of acute myocardial ischemia," *Biomedicine & Pharmacotherapy*, vol. 124, 2020.
- [13] Z. Ren, K. Yang, M. Zhao et al., "Calcium-sensing receptor on neutrophil promotes myocardial apoptosis and fibrosis after acute myocardial infarction via NLRP3 inflammasome activation," *The Canadian Journal of Cardiology*, vol. 36, no. 6, pp. 893–905, 2020.
- [14] V. Biemmi, G. Milano, A. Ciullo et al., "Inflammatory extracellular vesicles prompt heart dysfunction via TRL4-dependent NF- κ B activation," *Theranostics*, vol. 10, no. 6, pp. 2773–2790, 2020.
- [15] P. R. Lawler, D. L. Bhatt, L. C. Godoy et al., "Targeting cardiovascular inflammation: next steps in clinical translation," *European Heart Journal*, vol. 42, no. 1, pp. 113–131, 2021.
- [16] T. Borchert, A. Hess, M. Lukacevic, T. L. Ross, F. M. Bengel, and J. T. Thackeray, "Angiotensin-converting enzyme inhibitor treatment early after myocardial infarction attenuates acute cardiac and neuroinflammation without effect on chronic neuroinflammation," *European Journal of Nuclear Medicine and Molecular Imaging*, vol. 47, no. 7, pp. 1757–1768, 2020.
- [17] M. Frydland, J. E. Møller, M. G. Lindholm et al., "Biomarkers predictive of late cardiogenic shock development in patients with suspected ST-elevation myocardial infarction," *European Heart Journal Acute Cardiovascular Care*, vol. 9, no. 6, pp. 557–566, 2020.
- [18] X. Wang, Z. Guo, Z. Ding, and J. L. Mehta, "Inflammation, autophagy, and apoptosis after myocardial infarction," *Journal of the American Heart Association*, vol. 7, no. 9, 2018.
- [19] H. W. Wang, M. Ahmad, R. Jadayel, F. Najjar, D. Lagace, and F. Leenen, "Inhibition of inflammation by minocycline improves heart failure and depression-like behaviour in rats after myocardial infarction," *PLoS One*, vol. 14, no. 6, 2019.
- [20] S. Roumeliotis, A. Roumeliotis, X. Gorny, and P. Mertens, "Could antioxidant supplementation delay progression of cardiovascular disease in end-stage renal disease patients?," *Current Vascular Pharmacology*, vol. 19, no. 1, pp. 41–54, 2020.
- [21] H. Bugger and K. Pfeil, "Mitochondrial ROS in myocardial ischemia reperfusion and remodeling," *Biochimica et Biophysica Acta - Molecular Basis of Disease*, vol. 1866, no. 7, 2020.
- [22] Y. Xuan, M. Bobak, A. Anusriti et al., "Association of serum markers of oxidative stress with myocardial infarction and stroke: pooled results from four large European cohort studies," *European Journal of Epidemiology*, vol. 34, no. 5, pp. 471–481, 2019.
- [23] B. A. Kerr, L. Ma, X. Z. West et al., "Interference with akt signaling protects against myocardial infarction and death by limiting the consequences of oxidative stress," *Science Signaling*, vol. 6, no. 287, article a67, 2013.
- [24] C. Wang, W. Yuan, A. Hu et al., "Dexmedetomidine alleviated sepsis-induced myocardial ferroptosis and septic heart injury," *Molecular Medicine Reports*, vol. 22, no. 1, pp. 175–184, 2020.

Research Article

Genetic Polymorphism of Matrix Metalloproteinase-9 and Susceptibility to Myocardial Infarction: A Meta-Analysis

Beili Feng^{1,2} and Hengdong Li^{1,2} 

¹Department of Cardiology, HwaMei Hospital, University of Chinese Academy of Sciences, Ningbo, Zhejiang, China

²Ningbo Institute of Life and Health Industry, University of Chinese Academy of Sciences, Ningbo, Zhejiang, China

Correspondence should be addressed to Hengdong Li; lhdhldhdd@163.com

Received 13 October 2021; Accepted 10 December 2021; Published 15 January 2022

Academic Editor: Simona Pichini

Copyright © 2022 Beili Feng and Hengdong Li. This is an open access article distributed under the Creative Commons Attribution License, which permits unrestricted use, distribution, and reproduction in any medium, provided the original work is properly cited.

Objective. Current findings on the association between MMP-9 rs3918242 and susceptibility to myocardial infarction (MI) are inconsistent, and their definite relationship is discussed in this meta-analysis. **Methods.** Eligible literatures reporting MMP-9 rs3918242 and susceptibility to MI were searched in PubMed, Cochrane Library, CNRI, and VIP using keywords such as “MMP-9”, “matrix metalloproteinase-9” and “myocardial infarction”, “acute myocardial infarction”, “AMI”, and “polymorphism”. Data from eligible literatures were extracted for calculating OR and corresponding 95% CI using RevMan 5.3 and STATA12.0. **Results.** Ten independent literatures reporting MMP-9 rs3918242 and susceptibility to MI were enrolled. Compared with subjects carrying CT&TT genotype of MMP-9 rs3918242, susceptibility to MI was lower in those carrying CC genotype (OR = 1.49, 95%CI = 1.19 – 1.86, $P = 0.0004$). Such a significance was observed in the overdominant (OR = 1.27, 95% CI = 1.14 – 1.41, $P < 0.0001$) and allele genetic models (OR = 1.43, 95%CI = 1.17 – 1.74, $P = 0.0005$) as well. This finding was also valid in the Asian population. **Conclusions.** Mutation on MMP-9 rs3918242 has a potential relevance with susceptibility to MI.

1. Introduction

Acute myocardial infarction (AMI) manifests as myocardial necrosis which resulted from acute, persistent ischemia and hypoxia in the coronary arteries. In the United States, there are 5 million people that visit the emergency department because of acute chest pain. More than 800,000 AMI cases each year are newly onset, and 27% of them die before arriving at the hospital [1]. In recent years, the incidence of AMI has an obvious rise. There are at least 500,000 newly onsets and 2 million present illness cases of AMI. Risk factors for MI include three major categories: unchangeable factors (age, gender, and family history), variable factors (smoking, alcohol, lack of exercise, poor diet, high blood pressure, diabetes, dyslipidemia, and metabolism syndrome), and emerging factors (abnormal levels of CRP, fibrinogen, CAC, homocysteine, lipoprotein (a), and LDL) [2, 3]. Current researches have defined that interactions between various environmental factors and certain genetic polymorphisms may lead to AMI [4, 5]. In recent studies, SNP

genetic variants were closely related to AMI. Williams et al. found that a SNP in CRP (rs2592902) was closely linked to ischemic and recurrent stroke [6]. Further, myocardial infarction-associated SNP at 6p24 interferes with MEF2 binding and associates with PHACTR1 expression levels in human coronary arteries [7]. In short, it is necessary to find new SNP site which was closely related to AMI.

The matrix metalloproteinase (MMP) family is composed of 20 secretory or ectocellular enzymes that degrade extracellular matrix proteins, coagulation factors, lipoproteins, latent growth factors, chemokines, and cell adhesion molecules [8, 9]. MMP levels are mainly mediated by transcriptional regulation. Meanwhile, MMP activities are linked with the activation of MMP zymogen and TIMPs (tissue inhibitors of MMPs) [8, 9]. MMP levels in blood vessels and heart tissues are closely related to many cardiovascular diseases, including atherosclerosis, aneurysms, restenosis after angioplasty, and heart failure [10, 11]. MMP-9 is an important enzyme that degrades the main component of vascular basement membrane (type IV collagen) and is

closely related to the occurrence and development of atherosclerosis [10, 12]. The promoter region of MMP-9 C-1562T (rs3918242) is believed to be linked with MI. So far, a considerable number of studies have been conducted to analyze the MMP-9 rs3918242 and MI, whereas their conclusions are controversial. This study is aimed at uncovering a precise involvement of MMP-9 rs3918242 in MI.

2. Materials and Methods

2.1. Literature Screening. Eligible literatures reporting MMP-9 rs3918242 and susceptibility to MI published before May 2019 were searched in PubMed, Cochrane Library, CNRI, and VIP. Keywords searched were as follows: “MMP-9”, “matrix metalloproteinase-9” and “myocardial infarction”, “acute myocardial infarction”, “AMI”, and “polymorphism”. Citations in the selected literatures were manually examined.

Full text of each literature was reviewed and its eligibility determined using the following inclusive criteria: (1) independent case-control studies analyzing hospital-based or population-based subjects without any language limitations, (2) adequate data provided to obtain genotype frequencies, (3) literatures reporting MMP-9 rs3918242 and susceptibility to MI; (4) genotype distribution in the controls in accordance to HWE (Hardy-Weinberg equilibrium), and (5) no repeated published data.

Exclusive criteria included the following: (1) reviews, comments, animal experiments, mechanism researches, and case reports; (2) repeatedly published articles; and (3) studies with inadequate data. The flow diagram of the publication selection is depicted in Figure 1.

2.2. Data Extraction. Data were independently extracted and analyzed by two researchers. Any disagreement was solved by the third researcher. Extracted data included first author, year of publication, country of publication, genotype number and distribution, and case number.

2.3. Statistical Processing. Heterogeneity test was conducted by calculating OR and the corresponding 95% CI with the I^2 test and the Q test. The pooled OR in studies lacking the heterogeneity was calculated by the fixed-effects model; otherwise, a random-effects model was used. Sensitivity analysis was conducted by removing one study each time and analyzing the remaining in a combination way. The HWE of control genotype distribution was evaluated using the χ^2 test, and $P < 0.05$ considered as inequivalent. Publication bias was evaluated by depicting funnel plots and quantified by Egger's test. Data analyses were conducted using RevMan 5.3 and STATA12.0 (London, UK).

3. Results

3.1. Baseline Characteristics of Eligible Literatures. At first, 556 relevant literatures were searched from online databases. 276 repeated literatures and 241 irrelevant ones were excluded after reviewing the titles and abstracts. The remaining 39 literatures were assessed in details. 12 literatures with irrelevant findings, 5 abstracts/meta-analyses, 4 nonpolymorphism researches, and 8 literatures lacking adequate

data or full text were excluded. At last, 10 eligible literatures published from 2005 to 2017 were enrolled [11–20]. Baseline characteristics of them and HWE results of the controls were detailed (Table 1). A total of 3087 MI patients and 5019 healthy controls were involved. Serum samples were detected by PCR/PCR-RFLP/TaqMan.

3.2. Meta-Analysis Results. MMP-9 rs3918242 polymorphism and susceptibility to MI were analyzed using different genetic models. Heterogeneity existed in the dominant ($I^2 = 53\%$, $P = 0.02$) and allele genetic models ($I^2 = 52\%$, $P = 0.03$), rather than recessive ($I^2 = 13\%$, $P = 0.33$) and overdominant genetic models ($I^2 = 46\%$, $P = 0.06$). Pooled OR was calculated according to the heterogeneity results. Compared with subjects carrying CT&TT genotype of MMP-9 rs3918242, susceptibility to MI was lower in those carrying CC genotype (OR = 1.49, 95%CI = 1.19 – 1.86, $P = 0.0004$). In addition, subjects carrying TT genotype had higher susceptibility to MI than those carrying CT&CC genotype (OR = 1.54, 95%CI = 1.08 – 2.20, $P = 0.02$). Such a significance was observed in the overdominant (OR = 1.27, 95%CI = 1.14 – 1.41, $P < 0.0001$) and allele genetic models (OR = 1.43, 95%CI = 1.17 – 1.74, $P = 0.0005$) as well (Figure 2).

Subgroup analyses were conducted based on ethnicity. A significant association between MMP-9 rs3918242 polymorphism and susceptibility to MI in Asian population was identified in dominant (OR = 1.61, 95%CI = 1.26 – 2.06, $P = 0.0001$), recessive (OR = 3.34, 95%CI = 1.29 – 8.67, $P = 0.01$), overdominant (OR = 1.50, 95%CI = 1.16 – 1.92, $P = 0.002$), and allele genetic models (OR = 1.58, 95%CI = 1.26 – 1.99, $P < 0.0001$). Such an association in Caucasian population was only uncovered in dominant (OR = 1.20, 95%CI = 1.06 – 1.36, $P = 0.003$), overdominant (OR = 1.17, 95%CI = 1.03 – 1.33, $P = 0.01$), and allele genetic models (OR = 1.55, 95%CI = 1.07 – 2.24, $P = 0.02$), rather than recessive model (OR = 1.39, 95%CI = 0.03 – 3.28, $P = 0.10$) (Figures 3–6).

3.3. Sensitivity Analysis. No significant changes in pooled P and OR were observed after removing one single article for each time, demonstrating the robust results of our analysis.

3.4. Publication Bias. Funnel plots depicted a symmetrical shape in the four genetic models (Figure 7). Egger's test clarified no significant difference in publication bias in allele ($t = 1.44$, $P = 0.188$), overdominant ($t = 1.70$, $P = 0.128$), recessive ($t = 0.68$, $P = 0.528$), and dominant genetic models ($t = 1.67$, $P = 0.134$), as well as subgroup analyses (data not shown).

4. Discussion

MMPs are a family of Zn^{2+} -dependent neutral proteases that degrade and reshape extracellular matrices, maintain the homeostasis of extracellular matrices, and participate in pathological and physiological processes in humans. MMP-9 is the active enzyme in MMP family with the largest molecule size of all members. It mediates the formation,

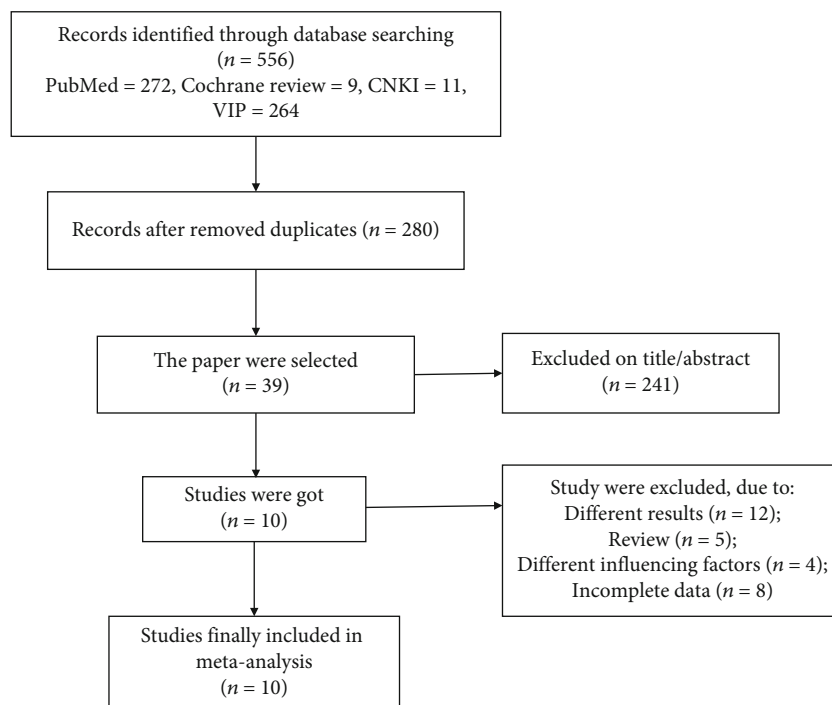


FIGURE 1: Flow diagram of the publication selection process.

TABLE 1: Baseline characteristics of eligible literatures.

Author	Year	Country	Journal name/ publication origin	Genotyping methods	SNP loci (P_{HWE})	Sample size	Control	Sample
Chen	2005	China	Chin J Arterioscler	PCR-RFLP	rs3918242 ($P_{HWE} = 0.17$)	78 (male = 57, female = 21)	81 (male = 58, female = 23)	Blood
Meng	2006	China	Tianjin Med J	PCR	rs3918242 ($P_{HWE} = 0.99$)	59 (male = 19, female = 40)	99 (male = 32, female = 67)	Blood
Nuzzo	2006	Sicily	Ann N Y Acad Sci	PCR	rs3918242 ($P_{HWE} = 0.18$)	115 (male = 109, female = 6)	123 (male = 100, female = 23)	Blood
Wang	2007	China	Journal of Clinical Hematology	PCR-RFLP	rs3918242 ($P_{HWE} = 0.27$)	37 (male = 29, female = 8)	84 (male = 52, female = 32)	Blood
Horne	2007	America	Am Heart J.	TaqMan	rs3918242 ($P_{HWE} = 0.34$)	1693	3455	Blood
Koh	2008	South Korea	International Journal of Cardiology	PCR-RFLP	rs3918242 ($P_{HWE} = 0.20$)	206	173	Blood
Ma	2010	China	Chin J Hypertens	PCR-SphI	rs3918242 ($P_{HWE} = 0.70$)	362 (male = 249, female = 113)	419 (male = 292, female = 127)	Blood
J.M.	2016	Mexico	Genetics and Molecular Research	PCR-RFLP	rs3918242 ($P_{HWE} = 0.67$)	236 (male = 194, female = 42)	285 (male = 134, female = 151)	Blood
EI-Aziz	2017	Egypt	International Journal of Cardiology	PCR-RFLP	rs3918242 ($P_{HWE} = 0.69$)	184 (male = 150, female = 34)	180 (male = 155, female = 25)	Whole blood
Abdolreza Daraei	2017	Iran	Genetic Testing and Molecular Biomarkers	PCR-RFLP	rs3918242 ($P_{HWE} = 0.53$)	117 (male = 72, female = 45)	120 (male = 68, female = 52)	Whole blood

SNP = single nucleotide polymorphism; HWE = Hardy-Weinberg equilibrium; P_{HWE} = P value of Hardy-Weinberg equilibrium test in controls for each locus; PCR = polymerase chain reaction.

development, and rupture of atherosclerotic plaques by mediating metastasis, viability, apoptosis, and extracellular matrix remodeling of vascular smooth muscle cells [21, 22]. Studies have found that elevated levels of MMPs are

closely associated with the development of unstable angina and AMI [23, 24]. Zouridakis et al. [25] analyzed the data from 124 patients with stable angina and demonstrated that MMP-9 is an independent predictor of atherosclerosis

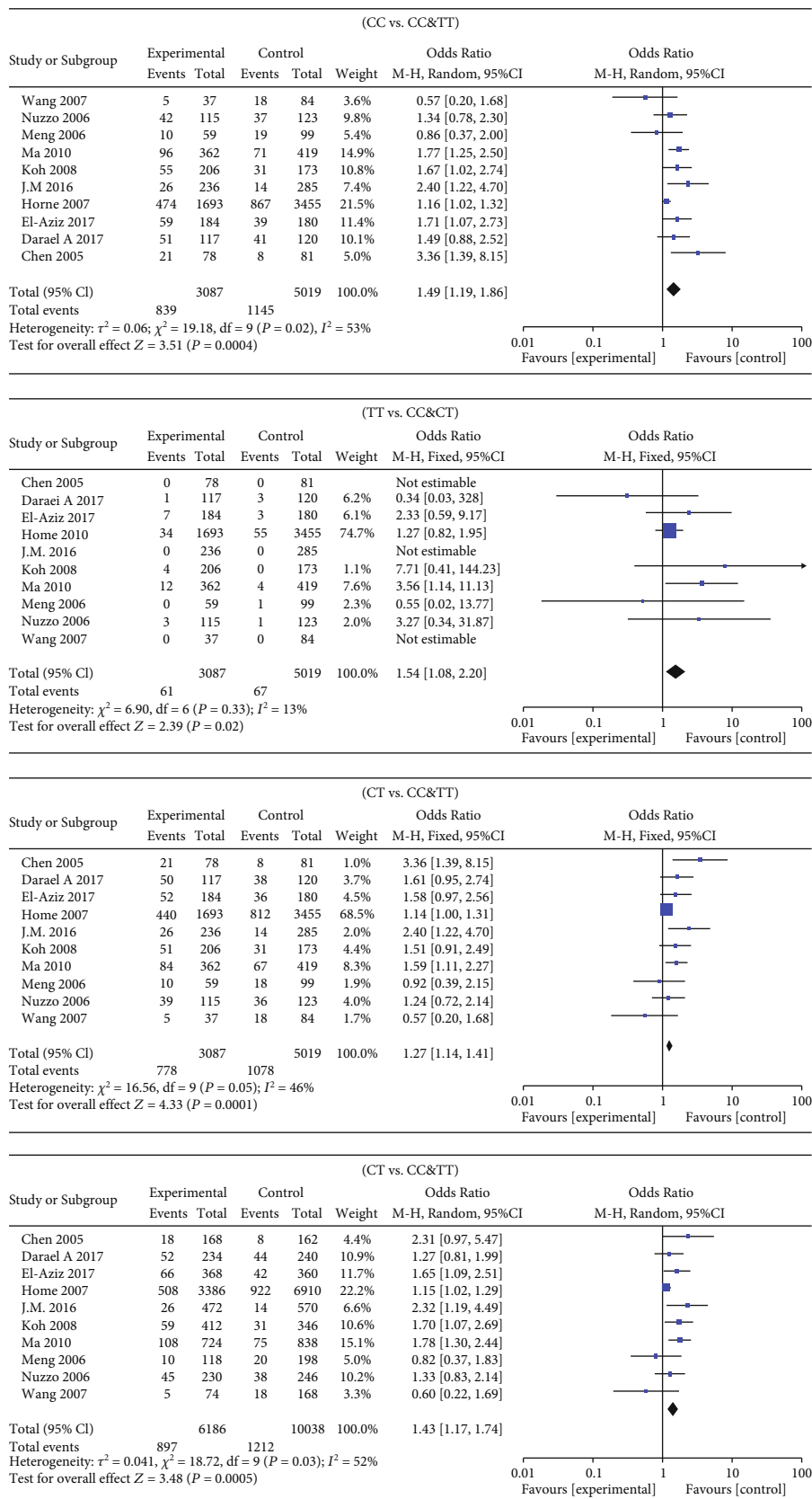


FIGURE 2: Forest plots demonstrating the association between MMP-9 polymorphism and susceptibility to myocardial infarction.

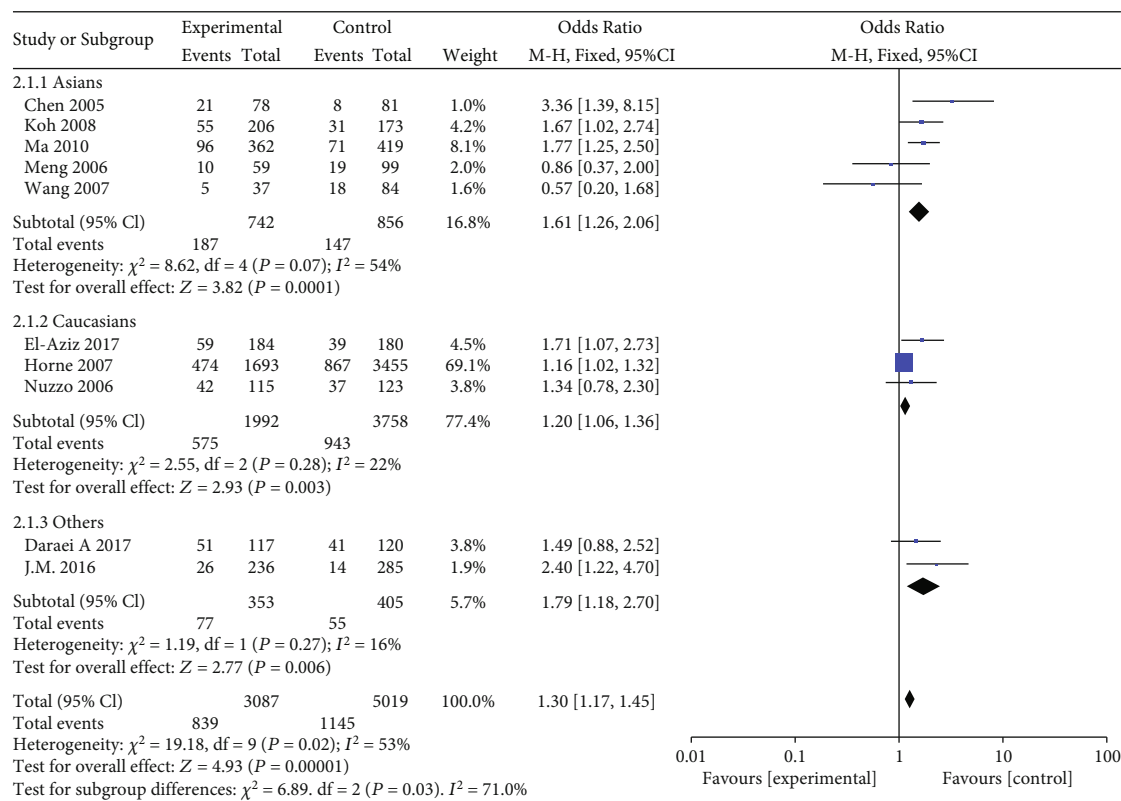


FIGURE 3: Forest plot of the meta-analysis of the association between MMP-9 C-1562T (rs3918242) and susceptibility to myocardial infarction in different ethnic subgroups using a dominant genetic model.

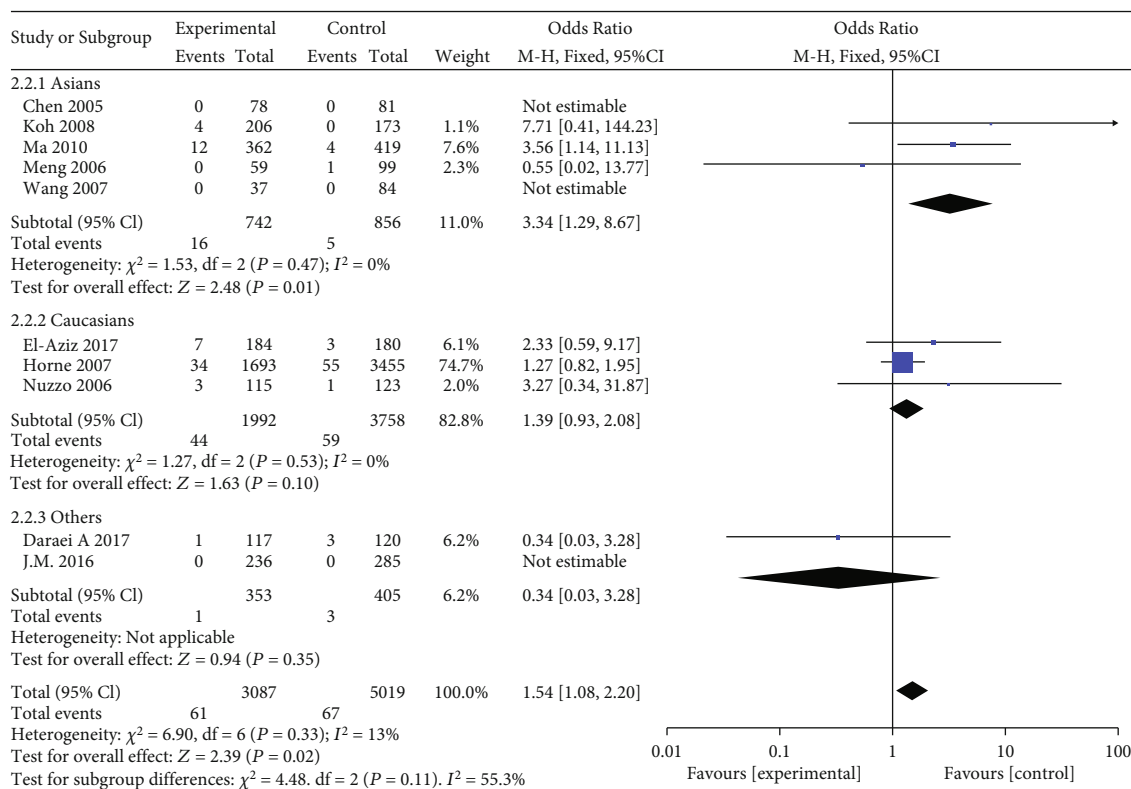


FIGURE 4: Forest plot of the meta-analysis of the association between MMP-9 C-1562T (rs3918242) and susceptibility to myocardial infarction in different ethnic subgroups using a recessive genetic model.

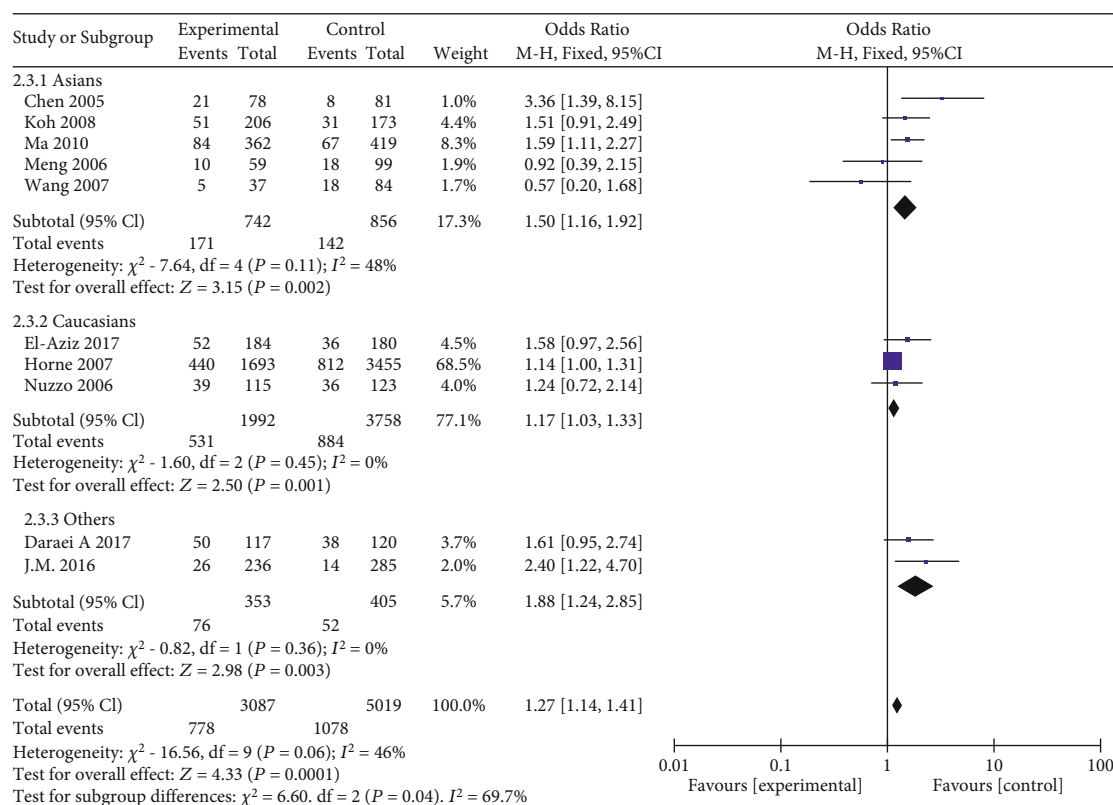


FIGURE 5: Forest plot of the meta-analysis of the association between MMP-9 C-1562T (rs3918242) and susceptibility to myocardial infarction in different ethnic subgroups using an overdominant genetic model.

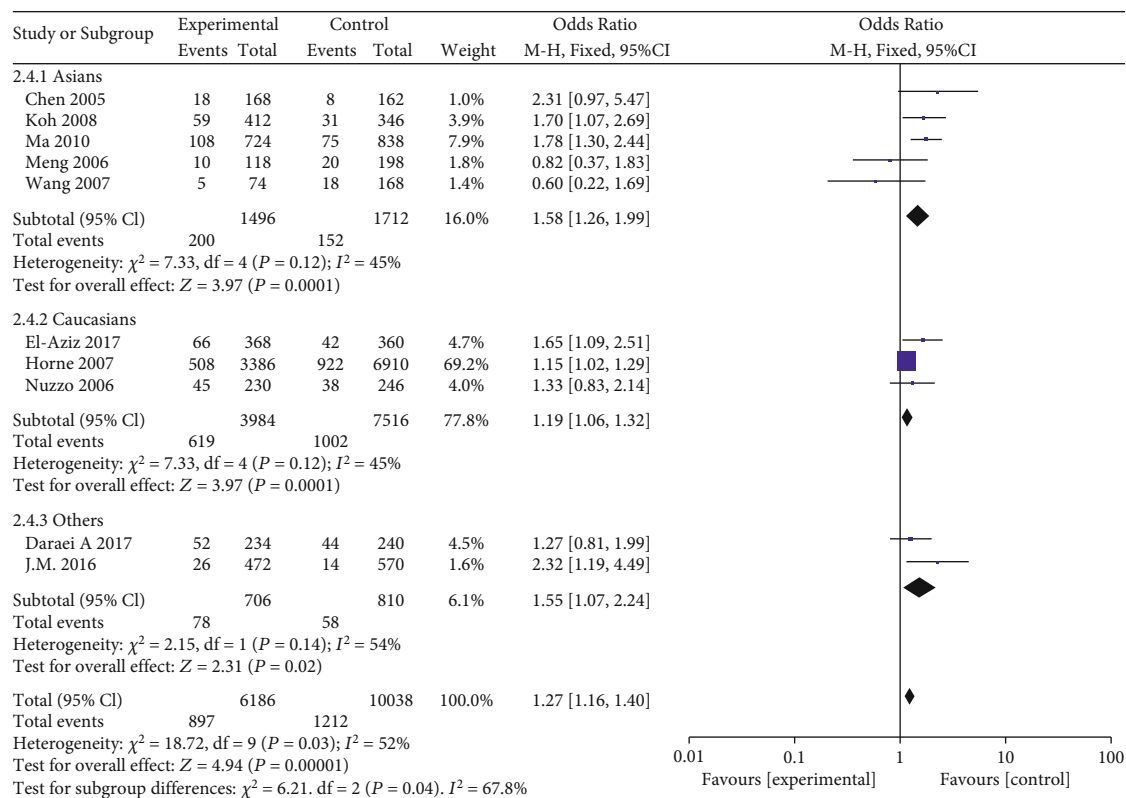


FIGURE 6: Forest plot of the meta-analysis of the association between MMP-9 C-1562T (rs3918242) and susceptibility to myocardial infarction in different ethnic subgroups using an allele genetic model.

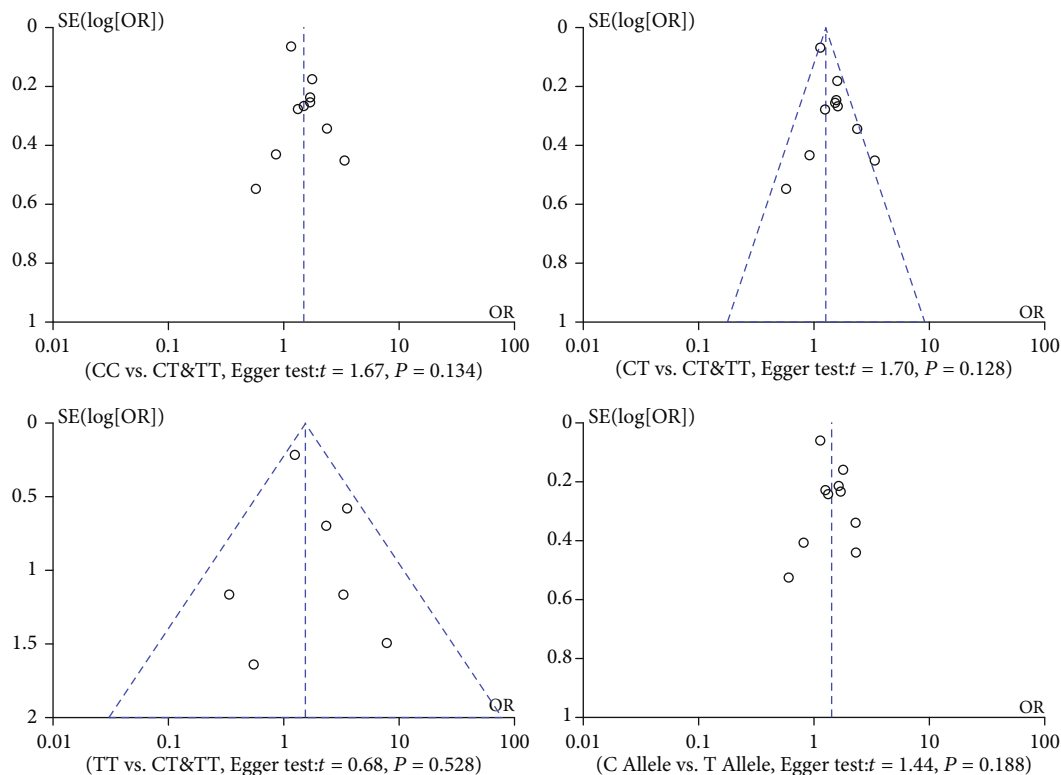


FIGURE 7: Publication bias on polymorphisms of MMP-9 rs3918242 and susceptibility to myocardial infarction.

progression. Another study found that MMP-9 is one of the key factors affecting plaque stability and rupture [26].

MMP-9 contains 13 exons and 12 introns. The substitution of C in the promoter region -1562 of MMP-9 by T can change its activity. Morgan et al. [27] reported that the affinity of the MMP-9 gene nucleoprotein of the -1562T allele carrier is markedly higher than that of the C allele carrier. Promoter activity is higher in the population carrying MMP-9 -1562T relative to those carrying MMP-9 -1562C, indicating the influence of MMP-9-1562C>T polymorphism on the onset of MI.

Our findings illustrated higher frequency of MMP-9 T-base mutation in MI patients than that in healthy controls no matter in the whole population or different ethnicities. Higher susceptibility to MI was uncovered in people carrying T allele of MMP-9 (TC+CC) compared with those carrying CC genotype in both Asian and Caucasian population. Consistently, Wang et al. [28] analyzed 7 articles published from 1999 to 2010, involving 4473 MI patients and 3343 healthy controls. They pointed out the involvement of MMP-9 polymorphism in MI risk. Another meta-analysis demonstrated that MMP-9 C-1562T is only associated with MI onset in East Asian population rather than Western population [29]. Here, three enrolled articles were conducted in Caucasian population. Such an association in Caucasian population was only uncovered in dominant (TT & CT vs. CC), overdominant (CT vs. CC & TT), and allele genetic models (C allele vs. T allele).

Some limitations were present in this paper. Firstly, MMP-9 polymorphism may be interacted with unknown or well-known risk factors of MI, such as hypertension, dia-

betes, dyslipidemia, and previous coronary artery disease. Secondly, genotype distribution of MMP-9 failed to be calculated owing to a small sample size. Thirdly, literatures published in other languages were excluded. Fourthly, gender and other factors in MI patients should be taken into consideration. In summary, there was a lot of work that need to be done to confirm that the SNP in MMP-9 was a very key factor for AMI.

5. Conclusions

Collectively, MMP-9 rs3918242 had a potential relevance with susceptibility to MI. Our findings required to be validated in a multicenter hospital with larger sample size.

Data Availability

The datasets used and analyzed during the current study are available from the corresponding author on reasonable request.

Conflicts of Interest

The authors declared no conflict of interest.

Acknowledgments

This study was supported by the Ningbo Health Branding Subject Fund (PPXK2018-01) and the Medical Scientific Research Foundation of Zhejiang Province, China (2020KY846).

References

- [1] S. Boateng and T. Sanborn, "Acute myocardial infarction," *Disease-a-Month*, vol. 59, no. 3, pp. 83–96, 2013.
- [2] E. M. Antman, M. Cohen, P. J. Bernink et al., "The TIMI risk score for unstable angina/non-ST elevation MI," *JAMA*, vol. 284, no. 7, pp. 835–842, 2000.
- [3] AHA, ACC, National Heart, Lung, and Blood Institute et al., "AHA/ACC Guidelines for Secondary Prevention for Patients With Coronary and Other Atherosclerotic Vascular Disease: 2006 Update: Endorsed by the National Heart, Lung, and Blood Institute," *Journal of the American College of Cardiology*, vol. 47, no. 10, pp. 2130–2139, 2006.
- [4] M. E. Marenberg, N. Risch, L. F. Berkman, B. Floderus, and U. de Faire, "Genetic susceptibility to death from coronary heart disease in a study of twins," *The New England Journal of Medicine*, vol. 330, no. 15, pp. 1041–1046, 1994.
- [5] M. A. Hlatky, T. Quertermous, D. B. Boothroyd et al., "Polymorphisms in hypoxia inducible factor 1 and the initial clinical presentation of coronary disease," *American Heart Journal*, vol. 154, no. 6, pp. 1035–1042, 2007.
- [6] S. R. Williams, F. C. Hsu, K. L. Keene et al., "Shared genetic susceptibility of vascular-related biomarkers with ischemic and recurrent stroke," *Neurology*, vol. 86, no. 4, pp. 351–359, 2016.
- [7] M. Beaudoin, R. M. Gupta, H. H. Won et al., "Myocardial infarction-associated SNP at 6p24 interferes with MEF2 binding and associates with PHACTR1 expression levels in human coronary arteries," *Arteriosclerosis, Thrombosis, and Vascular Biology*, vol. 35, no. 6, pp. 1472–1479, 2015.
- [8] C. E. Brinckerhoff and L. M. Matrisian, "Matrix metalloproteinases: a tail of a frog that became a prince," *Nature Reviews. Molecular Cell Biology*, vol. 3, no. 3, pp. 207–214, 2002.
- [9] M. D. Sternlicht and Z. Werb, "How matrix metalloproteinases regulate cell behavior," *Annual Review of Cell and Developmental Biology*, vol. 17, no. 1, pp. 463–516, 2001.
- [10] A. C. Newby, "Dual role of matrix metalloproteinases (matrixins) in intimal thickening and atherosclerotic plaque rupture," *Physiological Reviews*, vol. 85, no. 1, pp. 1–31, 2005.
- [11] Z. S. Galis and J. J. Khatri, "Matrix metalloproteinases in vascular remodeling and Atherogenesis," *Circulation Research*, vol. 90, no. 3, pp. 251–262, 2002.
- [12] D. L. Brown, M. S. Hibbs, M. Kearney, C. Loushin, and J. M. Isner, "Identification of 92-kD gelatinase in human coronary atherosclerotic lesions. Association of active enzyme synthesis with unstable angina," *Circulation*, vol. 91, no. 8, pp. 2125–2131, 1995.
- [13] X. F. Chen, L. J. Tang, M. Zhu, J. J. Jiang, W. F. Shen, and Y. Q. Du, "Matrix metalloproteinase-9 polymorphism (C1562T) and the susceptibility to myocardial infarction in Han population of China," *Chinese Journal of Arteriosclerosis*, vol. 13, pp. 775–778, 2005.
- [14] D. M. Meng, Y. M. Mao, Q. Chen et al., "Relationship between polymorphisms of matrix metalloproteinase and coronary heart disease," *Tianjin Medical Journal*, vol. 34, pp. 295–298, 2006.
- [15] D. Nuzzo, S. Vasto, C. R. Balistreri et al., "Role of proinflammatory alleles in longevity and atherosclerosis: results of studies performed on -1562C/T MMP-9 in centenarians and myocardial infarction patients from Sicily," *Annals of the New York Academy of Sciences*, vol. 1089, no. 1, pp. 496–501, 2006.
- [16] M. F. Wang, C. S. Xiao, S. W. Gong, R. Y. Wang, X. E. Liu, and L. H. Hou, "Relationships study about polymorphism of matrix metalloproteinase-9 with coronary heart disease," *Journal of Clinical Hematology*, vol. 20, pp. 28–30, 2007.
- [17] B. D. Horne, N. J. Camp, J. F. Carlquist et al., "Multiple-polymorphism associations of 7 matrix metalloproteinase and tissue inhibitor metalloproteinase genes with myocardial infarction and angiographic coronary artery disease," *American Heart Journal*, vol. 154, no. 4, pp. 751–758, 2007.
- [18] Y. S. Koh, K. Chang, P. J. Kim et al., "A close relationship between functional polymorphism in the promoter region of matrix metalloproteinase-9 and acute myocardial infarction," *International Journal of Cardiology*, vol. 127, no. 3, pp. 430–432, 2008.
- [19] Y. Ma, L. Wang, X. Xie et al., "Interactions between matrix metalloproteinase-9 polymorphism and hypertension in relation to myocardial infarction in a Chinese population," *Chinese Journal of Hypertension*, vol. 18, pp. 1167–1172, 2010.
- [20] J. M. Rodríguez-Pérez, G. Vargas-Alarcón, R. Posadas-Sánchez et al., "rs3918242 MMP9 gene polymorphism is associated with myocardial infarction in Mexican patients," *Genetics and Molecular Research*, vol. 15, no. 1, article 15017776, 2016.
- [21] T. El-Aziz and R. H. Mohamed, "Matrix metalloproteinase -9 polymorphism and outcome after acute myocardial infarction," *International Journal of Cardiology*, vol. 227, pp. 524–528, 2017.
- [22] A. Daraei, Y. Mansoori, Z. Zendeabad et al., "Influences of IL-1b-3953 C>T and MMP-9-1562C >T gene variants on myocardial infarction susceptibility in a subset of the Iranian population," *Genetic Testing and Molecular Biomarkers*, vol. 21, no. 1, pp. 33–38, 2017.
- [23] A. K. Chow, J. Cena, and R. Schulz, "Acute actions and novel targets of matrix metalloproteinases in the heart and vasculature," *British Journal of Pharmacology*, vol. 152, no. 2, pp. 189–205, 2007.
- [24] Y. Kuge, N. Takai, S. Ishino, T. Temma, M. Shiomi, and H. Saji, "Distribution profiles of membrane type-1 matrix metalloproteinase (MT1-MMP), matrix metalloproteinase-2 (MMP-2) and cyclooxygenase-2 (COX-2) in rabbit atherosclerosis: comparison with plaque instability analysis," *Biological & Pharmaceutical Bulletin*, vol. 30, no. 9, pp. 1634–1640, 2007.
- [25] E. Zouridakis, P. Avanzas, R. Arroyo-Espliguero, S. Fredericks, and J. C. Kaski, "Markers of inflammation and rapid coronary artery disease progression in patients with stable angina pectoris," *Circulation*, vol. 110, no. 13, pp. 1747–1753, 2004.
- [26] J. Johnson, R. Fritschedanielson, M. Behrendt et al., "Effect of broad-spectrum matrix metalloproteinase inhibition on atherosclerotic plaque stability," *Cardiovascular Research*, vol. 71, no. 3, pp. 586–595, 2006.
- [27] A. R. Morgan, B. Zhang, W. Tapper, A. Collins, and S. Ye, "Haplotype analysis of the MMP-9 gene in relation to coronary artery disease," *Journal of Molecular Medicine (Berlin, Germany)*, vol. 81, no. 5, pp. 321–326, 2003.
- [28] J. Wang, D. Xu, X. Wu et al., "Polymorphisms of matrix metalloproteinases in myocardial infarction: a meta-analysis," *Heart*, vol. 97, no. 19, pp. 1542–1546, 2011.
- [29] X. Wang and L. Z. Shi, "Association of matrix metalloproteinase-9 C1562T polymorphism and coronary artery disease: a meta-analysis," *Journal of Zhejiang University. Science. B*, vol. 15, no. 3, pp. 256–263, 2014.

Research Article

Simvastatin Improves Myocardial Ischemia Reperfusion Injury through KLF-Regulated Alleviation of Inflammation

Tingju Wei, Jun Li, Guowei Fu, Hui Zhao, Chen Huang, Xiaohua Zhu, Gongcheng Huang, and Jing Xu 

Department of Cardiovascular Surgery, The First Affiliated Hospital of Zhengzhou University, Zhengzhou, China

Correspondence should be addressed to Jing Xu; fccxuj@zzu.edu.cn

Received 15 October 2021; Revised 26 November 2021; Accepted 8 December 2021; Published 11 January 2022

Academic Editor: Francesco Busardò

Copyright © 2022 Tingju Wei et al. This is an open access article distributed under the Creative Commons Attribution License, which permits unrestricted use, distribution, and reproduction in any medium, provided the original work is properly cited.

Objective. To clarify the protective effect of simvastatin on myocardial ischemia reperfusion injury (MIRI) and the underlying mechanism. **Materials and Methods.** The MIRI model in rats was firstly constructed. Twenty-four male rats were randomly assigned into the sham group, ischemia-reperfusion (I/R) group, and simvastatin group, with 8 rats in each group. Contents of superoxide dismutase (SOD) and malondialdehyde (MDA), as well as serum levels of CK and inflammatory factors, in rats were determined by the enzyme-linked immunosorbent assay (ELISA). Lactate dehydrogenase (LDH) activity in the three groups was examined. Through flow cytometry and Cell Counting Kit-8 (CCK-8) assay, apoptosis and viability in each group were detected, respectively. Relative levels of HMGB1, Kruppel-like factor 2 (KLF2), eNOS, and thrombomodulin (TM) were finally determined. **Results.** Simvastatin treatment markedly enhanced SOD activity and reduced contents of MDA, LDH, and creatine kinase (CK) in MIRI rats. The increased apoptosis and decreased viability following MIRI were partially reversed by simvastatin treatment. Besides, MIRI resulted in the upregulation of inflammatory factors and chemokines. Their elevations were abolished by simvastatin. In MIRI rats, simvastatin upregulated KLF2 and p-eNOS. **Conclusions.** Simvastatin protects inflammatory response at post-MIRI through upregulating KLF2, thus improving cardiac function.

1. Introduction

Myocardial ischemia reperfusion injury (MIRI) is a cardiovascular disease manifested as acute angina owing to stenosis of the coronary artery and myocardial blood supply disorder [1]. MIRI occurs following reperfusion in thrombolytic therapy, coronary angioplasty, organ transplantation, aortic occlusion, or cardiopulmonary bypass [2]. Currently, it is believed that oxidative stress, intracellular calcium overload and hypercontraction, endothelial cell activation, microvascular dysfunction, and myocardial metabolic changes are major pathogenic factors of MIRI [3]. Eventually, cardiomyocytes are necrotic because of ischemia in myocardial tissues. Researches on alleviating MIRI have been well concerned.

Statins (HMG-CoA reductase inhibitors) are a class of cholesterol-lowering drugs used for preventing and treating

cardiovascular diseases [4]. In addition, statins also exert cardioprotective properties through alleviating inflammatory responses [5, 6] and improving endothelial functions [7, 8]. Because of the low cost, statins are extensively applied for the treatment of coronary heart diseases.

Kruppel-like factor 2 (KLF2) is a transcription factor induced by laminar flow in vascular endothelial cells, which is a vital regulator in vascular endothelial functions [9–11]. KLF2 participates in the regulation of inflammation, angiogenesis, barrier integrity, vascular reactivity, and cell phenotypes of the endothelium [12]. Through downregulating eNOS, thrombomodulin (TM), HO-1, and adhesion molecules, KLF2 protects the stability and function of the vascular endothelium from external stimuli [13, 14]. In liver ischemia-reperfusion (I/R) injury, statins inhibit oxidative stress and inflammatory response by upregulating KLF2 [15]. In this paper, we first constructed the MIRI model in

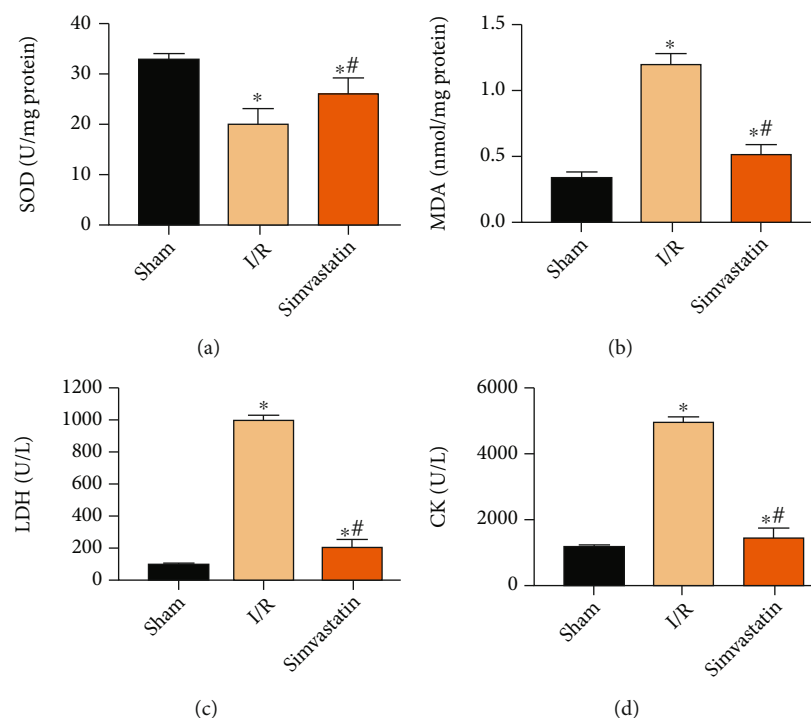


FIGURE 1: Simvastatin alleviated oxidative stress at post-MIRI. Rats were assigned into the sham group, I/R group, and simvastatin group. Relative levels of SOD (a), MDA (b), LDH (c), and CK (d) in each group. * $p < 0.05$ vs. sham group; # $p < 0.05$ vs. I/R group.

rats. The protective role of simvastatin in MIRI was specifically explored.

2. Materials and Methods

2.1. Experimental Animals. A total of 24 male Wistar rats (250-300 g) were habituated in a standard environment with free access to food and water. Animal procedures were conducted after 12 h food fasting. Rats were sacrificed at 6 and 24 h after reperfusion. This experiment was approved by the Ethic Committee of Zhengzhou University.

2.2. MIRI Construction. 24 male rats were randomly assigned into the sham group, I/R group, and simvastatin group, with 8 in each. Mechanical ventilation was conducted initially with 5 mL of tidal volume and 50 beats/min of respiratory rate. The rat heart was exposed through left thoracotomy at the third rib space. A 6.0 silk nontraumatic suture was passed through the epicardial layer around the main branch of the left coronary artery, with approximately 2 mm from its starting point. A plastic button with a diameter of about 5 mm was passed through the ligature and in contact with the heart. Both ends of the suture were passed through an exposed small vinyl tube. This method was convenient for generating MIRI in advanced preconditioning (24 hours postoperatively and acute pretreatment). ECG was performed during the whole process of model construction for monitoring cardiac function. Rats in the sham group were subjected to 150 min continuous perfusion. Rats in the I/R and simvastatin groups underwent 30 min ischemia, followed by 120 min reperfusion. Rats in the simvastatin group and I/R group were administrated with 1 mg/kg sim-

vastatin (MedChemExpress, Monmouth Junction, NJ, USA) or 0.1% dimethyl sulfoxide (DMSO) 0.5 h prior to reperfusion, respectively. At 24 h following MIRI, rats were anesthetized for reocclusion of the coronary artery at the initial occluded location, and the heart was collected.

2.3. Lactate Dehydrogenase (LDH) Activity Determination. Myocardial tissues were extracted after MIRI, homogenized, and cultured. The culture medium was collected for LDH activity determination using the commercial kit (Jiancheng, Nanjing, China). Values at 450 nm were recorded using a microplate reader.

2.4. Enzyme-Linked Immunosorbent Assay (ELISA). Heart tissues were homogenized in phosphate-buffered saline (PBS) (1:10 w/v) containing 1% Triton X-100 and protease inhibitor [16]. Samples were centrifuged at 4°C and 14000 rpm for 20 min [17]. The supernatant was collected for measuring corresponding indicators using the ELISA kit (Signosis, Santa Clara, CA, USA).

2.5. Flow Cytometry. Homogenized tissues were centrifuged at 1000 rpm for 5 min, and the precipitant was harvested and centrifuged again. Cells were resuspended in 100 μ L of marker buffer for 15 min. Subsequently, cells were incubated with SA-FLOUS and incubated in dark, at 4°C for 20 min. Absorbances at 488 nm (excitation wavelength), 515 nm (FITC wavelength), and 560 nm (PI wavelength) were recorded for calculating the apoptotic rate.

2.6. Cell Counting Kit-8 (CCK-8). Cells were inoculated in a 96-well plate with 3000 cells per well. At the appointed time points, absorbance value at 450 nm of each sample was

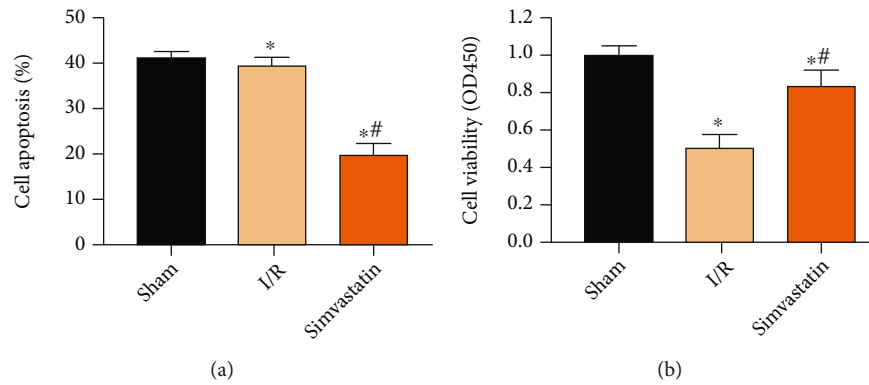


FIGURE 2: Simvastatin alleviated apoptosis at post-MIRI. Rats were assigned into the sham group, I/R group, and simvastatin group. Cell apoptosis (a) and viability (b) in each group. * $p < 0.05$ vs. sham group; ** $p < 0.05$ vs. I/R group.

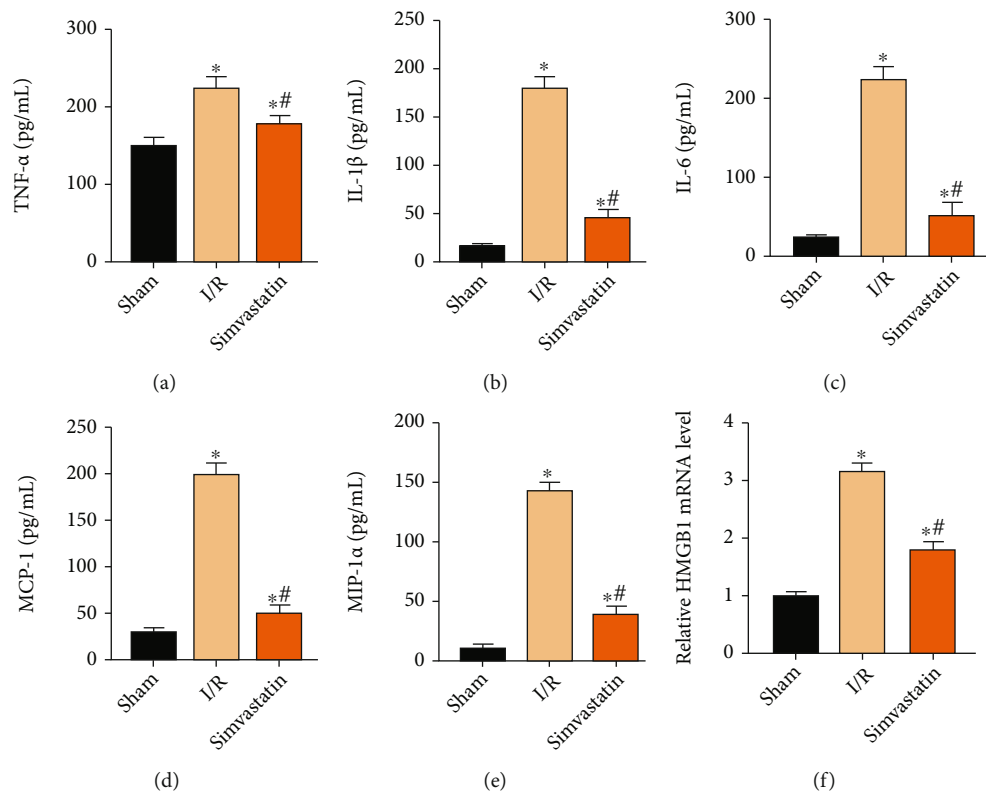


FIGURE 3: Simvastatin alleviated inflammation at post-MIRI. Rats were assigned into the sham group, I/R group, and simvastatin group. Relative levels of TNF- α (a), IL-1 β (b), IL-6 (c), MCP-1 (d), MIP-1 α (e), and HMGB1 (f) in each group. * $p < 0.05$ vs. sham group; ** $p < 0.05$ vs. I/R group.

recorded using the CCK-8 kit (Dojindo Laboratories, Kumamoto, Japan) for plotting the viability curves.

2.7. Quantitative Real-Time Polymerase Chain Reaction (RT-qPCR). RNAs were extracted from rat myocardial tissues using TRIzol (Invitrogen, Carlsbad, CA, USA) and reversely transcribed into complementary deoxyribose nucleic acids (cDNAs) (Thermo Scientific, Waltham, MA, USA). QRT-PCR was conducted by the SYBR Green method with β -actin as the internal reference. Primer sequences were as follows: HMGB1: 5'-TATGGCAAAGCGGACAAGG-3' (F) and 5'-CTTCGCAACATACCAATGGA-3' (R); KLF2: 5'

-GAGCCTATCTTGCCGTCCTT-3' (F) and 5'-AGCAGCTGTTTAGGTCCTC-3' (R); eNOS: 5'-CAACTGGAAAAAGGCAGCCC-3' (F) and 5'-AAGAGCCTCTAGCTCC TGCT-3' (R); TM: 5'-CCTTTGTCTTTCCGGGCTCT-3' (F) and 5'-TCAAGTCCTCCCTACCCTCG-3' (R); and β -actin: 5'-TGCTATGTTGCCCTAGACTTCG-3' (F) and 5'-GTTGGCATAGGTCCTTACGG-3' (R).

2.8. Western Blot. Tissues were homogenized for extracting proteins. After concentration determination, protein samples were loaded on polyvinylidene fluoride (PVDF) membranes (Roche, Basel, Switzerland). Subsequently,

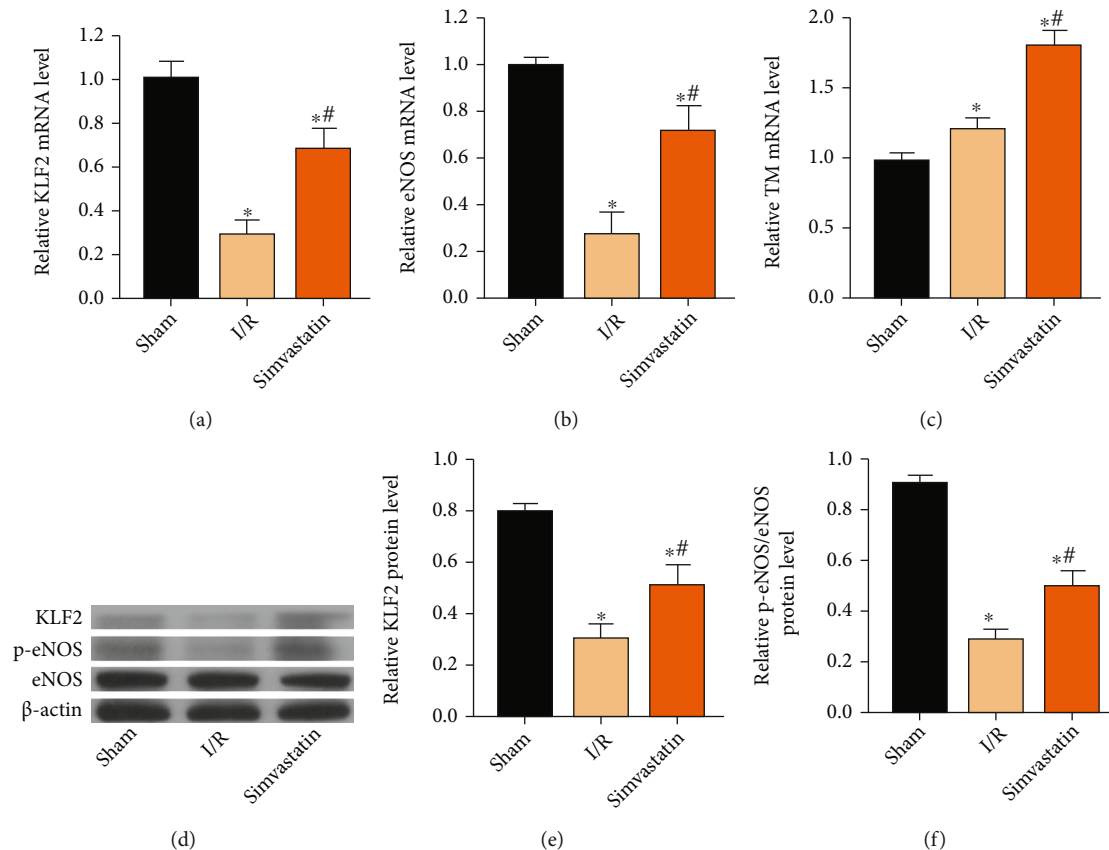


FIGURE 4: Simvastatin upregulated KLF2 and p-eNOS. Rats were assigned into the sham group, I/R group, and simvastatin group. (a–c) Relative levels of KLF2 (a), eNOS (b), and TM (c) in each group. (d) Western blot analyses on KLF2, p-eNOS, and eNOS in each group. (e, f) Protein levels of KLF2 (e) and p-eNOS/eNOS (f) in each group. * $p < 0.05$ vs. sham group; # $p < 0.05$ vs. I/R group.

nonspecific antigens were blocked with 5% skim milk for 2 h. Membranes were then incubated with primary and secondary antibodies. Band exposure and grey value analysis were finally conducted.

2.9. Statistical Analyses. Statistical Product and Service Solutions (SPSS) 22.0 (IBM, Armonk, NY, USA) was used for all statistical analyses. Data were expressed as mean \pm SD (standard deviation). Comparison between multiple groups was done using the one-way ANOVA test followed by the post hoc test (least significant difference). $p < 0.05$ indicated the significant difference.

3. Results

3.1. Simvastatin Alleviated Oxidative Stress at Post-MIRI. Compared with the sham group, superoxide dismutase (SOD) activity declined and malondialdehyde (MDA) level was elevated in the I/R group. The above changes were markedly reversed by simvastatin treatment (Figures 1(a) and 1(b)). Subsequently, serum levels of LDH and CK were determined in each group. Their elevated levels following MIRI were markedly reduced by simvastatin (Figures 1(c) and 1(d)).

3.2. Simvastatin Alleviated Apoptosis at Post-MIRI. Cell apoptosis is a key event during cardiomyocyte loss and cardiac

insufficiency following MIRI. Our findings uncovered that increased apoptotic rate (Figure 2(a)) and decreased viability (Figure 2(b)) were improved by applying simvastatin.

3.3. Simvastatin Alleviated Inflammation at Post-MIRI. Hypoxia triggers the deterioration of inflammatory response [18, 19]. Accumulation of activated inflammatory factors would result in adhesion of neutrophils, further aggravating tissue and organ damage resulted by MIRI [20–22]. Here, increased contents of TNF- α (Figure 3(a)), IL-1 β (Figure 3(b)), and IL-6 (Figure 3(c)) were inhibited by simvastatin. In addition, lower levels of MCP-1 (Figure 3(d)) and MIP-1 α (Figure 3(e)) were observed in the simvastatin group than in the I/R group. HMGB1 level was also reduced after simvastatin treatment (Figure 3(f)).

3.4. Simvastatin Upregulated KLF2 and p-eNOS. A previous study has shown that simvastatin protects against liver I/R injury through upregulating KLF2 [23]. Here, both mRNA and protein levels of KLF2 were upregulated by simvastatin, which were initially downregulated following MIRI (Figures 4(a), 4(d), and 4(e)). Besides, relative levels of p-eNOS and TM were also upregulated by simvastatin (Figures 4(b), 4(c), and 4(f)).

4. Discussion

MIRI is a pathological state with initial limitation on myocardial blood supply and subsequently reperfusion of blood flow [18]. Although reperfusion is the most effective approach for rescuing the ischemic myocardium, it may paradoxically aggravate or cause additional myocardial injury. During the process of MIRI, a series of inflammatory response, oxidative stress, and cytokine activation occur [24]. ROS would be abundantly produced and accumulated in the initial phase of MIRI [25]. Our findings consistently found decreased SOD level and increased MDA level in the I/R group compared to the sham group, suggesting the severe oxidative stress. Notably, simvastatin treatment markedly improved oxidative stress indicators. Changes in hemodynamic parameters support MIRI injury [26]. Herein, relative levels of LDH and CK were determined. Simvastatin markedly reduced their elevated levels following MIRI.

Cell apoptosis is a determinant event for MIRI-induced myocardial infarction [27]. It is reported that inhibition of myocardial apoptosis could reduce 50-70% infarcted size in the myocardium, thus improving cardiac function [28]. In this paper, the apoptotic rate markedly increased, while viability decreased at post-MIRI, and the above trends were abolished by simvastatin.

Inflammatory response following MIRI is of significance in aggravating its secondary injury. MIRI may lead to local aseptic inflammation and production of multiple inflammatory factors [29]. HMGB1 is a vital proinflammatory mediator during the initiation and cascade of inflammation [30]. Simvastatin is demonstrated to prevent inflammation through inactivating inflammatory chemokines [31]. In our analysis, simvastatin markedly downregulated inflammatory factors, chemokines, and proinflammatory mediator in MIRI rats. In addition, KLF2 was downregulated in MIRI rats, and the reduced trend was alleviated by simvastatin treatment. As previously reported, KLF2 is closely linked to the eNOS pathway [23]. In a recent study, it was shown that increased VEGF synthesis in astrocytes is driven by endothelial nitric oxide (NO) generated as a consequence of KLF2- and KLF4-dependent elevation of eNOS in the CCM endothelium [32]. Further, betulinic acid induces eNOS expression via the AMPK-dependent KLF2 signaling pathway [33]. Our results revealed that simvastatin protected the downregulated p-eNOS in MIRI rats. Collectively, we believed that simvastatin protected MIRI through upregulating KLF2. However, the mechanism was very simple; we will further explore the deep mechanism in our next research.

5. Conclusions

Simvastatin protects inflammatory response at post-MIRI through upregulating KLF2, thus improving cardiac function.

Data Availability

The datasets used and analyzed during the current study are available from the corresponding author on reasonable request.

Conflicts of Interest

The authors declared no conflict of interest.

Acknowledgments

This study was supported by the National Natural Science Foundation of China for Young Scientists (81901571).


References

- [1] J. Hao, H. Du, W. W. Li et al., "Effects of atorvastatin combined with trimetazidine on myocardial injury and inflammatory mediator in unstable angina patients during perioperative of percutaneous coronary intervention," *European Review for Medical and Pharmacological Sciences*, vol. 19, no. 23, pp. 4642–4646, 2015.
- [2] H. K. Eltzschig and C. D. Collard, "Vascular ischaemia and reperfusion injury," *British Medical Bulletin*, vol. 70, no. 1, pp. 71–86, 2004.
- [3] A. Anselmi, A. Abbate, F. Girola et al., "Myocardial ischemia, stunning, inflammation, and apoptosis during cardiac surgery: a review of evidence," *European Journal of Cardio-Thoracic Surgery*, vol. 25, no. 3, pp. 304–311, 2004.
- [4] C. Y. Wang, P. Y. Liu, and J. K. Liao, "Pleiotropic effects of statin therapy: molecular mechanisms and clinical results," *Trends in Molecular Medicine*, vol. 14, no. 1, pp. 37–44, 2008.
- [5] C. Weber, W. Erl, K. S. Weber, and P. C. Weber, "HMG-CoA reductase inhibitors decrease CD11b expression and CD11b-dependent adhesion of monocytes to endothelium and reduce increased adhesiveness of monocytes isolated from patients with hypercholesterolemia," *Journal of the American College of Cardiology*, vol. 30, no. 5, pp. 1212–1217, 1997.
- [6] C. Klufft, M. P. de Maat, L. J. Gevers, V. L. B. Potter, and M. F. Mohrschladt, "Statins and C-reactive protein," *Lancet*, vol. 353, no. 9160, p. 1274, 1999.
- [7] E. S. Stroes, H. A. Koomans, T. J. Rabelink, and T. W. A. de Bruin, "Vascular function in the forearm of hypercholesterolaemic patients off and on lipid-lowering medication," *The Lancet*, vol. 346, no. 8973, pp. 467–471, 1995.
- [8] J. Dupuis, J. C. Tardif, P. Cernacek, and P. Theroux, "Cholesterol reduction rapidly improves endothelial function after acute coronary Syndromes," *Circulation*, vol. 99, no. 25, pp. 3227–3233, 1999.
- [9] G. B. Atkins and M. K. Jain, "Role of Krüppel-Like transcription factors in endothelial biology," *Circulation Research*, vol. 100, no. 12, pp. 1686–1695, 2007.
- [10] L. Nayak, Z. Lin, and M. K. Jain, "'Go with the flow': how Krüppel-Like factor 2 regulates the vasoprotective effects of shear stress," *Antioxidants & Redox Signaling*, vol. 15, no. 5, pp. 1449–1461, 2011.
- [11] C. Collins and E. Tzima, "Hemodynamic forces in endothelial dysfunction and vascular aging," *Experimental Gerontology*, vol. 46, no. 2-3, pp. 185–188, 2011.
- [12] S. SenBanerjee, Z. Lin, G. B. Atkins et al., "KLF2 is a novel transcriptional regulator of endothelial proinflammatory activation," *The Journal of Experimental Medicine*, vol. 199, no. 10, pp. 1305–1315, 2004.
- [13] Z. Lin, A. Kumar, S. SenBanerjee et al., "Kruppel-like factor 2 (KLF2) regulates endothelial thrombotic function," *Circulation Research*, vol. 96, no. 5, pp. e48–e57, 2005.

- [14] K. M. Parmar, H. B. Larman, G. Dai et al., "Integration of flow-dependent endothelial phenotypes by Kruppel-like factor 2," *The Journal of Clinical Investigation*, vol. 116, no. 1, pp. 49–58, 2005.
- [15] Z. Liu, C. H. Lai, X. Zhang et al., "Simvastatin ameliorates total liver ischemia/reperfusion injury via KLF2-mediated mechanism in rats," *Clinics and Research in Hepatology and Gastroenterology*, vol. 43, no. 2, pp. 171–178, 2019.
- [16] M. Zhang, Y. J. Xu, H. K. Saini, B. Turan, P. P. Liu, and N. S. Dhalla, "Pentoxifylline attenuates cardiac dysfunction and reduces TNF- α level in ischemic-reperfused heart," *American Journal of Physiology. Heart and Circulatory Physiology*, vol. 289, no. 2, pp. H832–H839, 2005.
- [17] M. Granado, N. Fernández, L. Monge et al., "Effects of coronary ischemia-reperfusion in a rat model of early overnutrition. Role of angiotensin receptors," *PLoS One*, vol. 8, no. 2, article e54984, 2013.
- [18] H. K. Eltzschig and T. Eckle, "Ischemia and reperfusion—from mechanism to translation," *Nature Medicine*, vol. 17, no. 11, pp. 1391–1401, 2011.
- [19] C. T. Taylor and S. P. Colgan, "Regulation of immunity and inflammation by hypoxia in immunological niches," *Nature Reviews. Immunology*, vol. 17, no. 12, pp. 774–785, 2017.
- [20] B. C. Perry, D. Soltys, A. H. Toledo, and L. H. Toledo-Pereyra, "Tumor necrosis Factor- α in liver ischemia/reperfusion injury," *Journal of Investigative Surgery*, vol. 24, no. 4, pp. 178–188, 2011.
- [21] C. A. Dinarello, "Immunological and inflammatory functions of the interleukin-1 family," *Annual Review of Immunology*, vol. 27, no. 1, pp. 519–550, 2009.
- [22] M. Rincon, "Interleukin-6: from an inflammatory marker to a target for inflammatory diseases," *Trends in Immunology*, vol. 33, no. 11, pp. 571–577, 2012.
- [23] Z. Liu, X. Zhang, Q. Xiao et al., "Pretreatment donors after circulatory death with simvastatin alleviates liver ischemia reperfusion injury through a KLF2-dependent mechanism in rat," *Oxidative Medicine and Cellular Longevity*, vol. 2017, Article ID 3861914, 10 pages, 2017.
- [24] A. Prasad, G. W. Stone, D. R. Holmes, and B. Gersh, "Reperfusion injury, microvascular dysfunction, and Cardioprotection," *Circulation*, vol. 120, no. 21, pp. 2105–2112, 2009.
- [25] L. Zhang, J. Ma, and H. Liu, "Protective effect of ischemic post-conditioning against ischemia reperfusion-induced myocardium oxidative injury in IR rats," *Molecules*, vol. 17, no. 4, pp. 3805–3817, 2012.
- [26] J. Z. Li, M. Q. Xie, D. Mo et al., "Picoside II protects myocardium from ischemia/reperfusion-induced injury through inhibition of the inflammatory response," *Experimental and Therapeutic Medicine*, vol. 12, no. 6, pp. 3507–3514, 2016.
- [27] A. Saraste, K. Pulkki, M. Kallajoki, K. Henriksen, M. Parvinen, and L. M. Voipio-Pulkki, "Apoptosis in human acute myocardial infarction," *Circulation*, vol. 95, no. 2, pp. 320–323, 1997.
- [28] P. Lee, M. Sata, D. J. Lefer, S. M. Factor, K. Walsh, and R. N. Kitsis, "Fas pathway is a critical mediator of cardiac myocyte death and MI during ischemia-reperfusion in vivo," *American Journal of Physiology. Heart and Circulatory Physiology*, vol. 284, no. 2, pp. H456–H463, 2003.
- [29] Z. Liang, L. F. Liu, T. M. Yao, Y. Huo, and Y. L. Han, "Cardio-protective effects of Guanxinshutong (GXST) against myocardial ischemia/reperfusion injury in rats," *Journal of Geriatric Cardiology*, vol. 9, no. 2, pp. 130–136, 2012.
- [30] A. Tsung, S. Tohme, and T. R. Billiar, "High-mobility group box-1 in sterile inflammation," *Journal of Internal Medicine*, vol. 276, no. 5, pp. 425–443, 2014.
- [31] N. R. Veillard, V. Brauersreuther, C. Arnaud et al., "Simvastatin modulates chemokine and chemokine receptor expression by geranylgeranyl isoprenoid pathway in human endothelial cells and macrophages," *Atherosclerosis*, vol. 188, no. 1, pp. 51–58, 2006.
- [32] M. A. Lopez-Ramirez, C. C. Lai, S. I. Soliman et al., "Astrocytes propel neurovascular dysfunction during cerebral cavernous malformation lesion formation," *The Journal of Clinical Investigation*, vol. 131, no. 13, 2021.
- [33] G. H. Lee, J. S. Park, S. W. Jin et al., "Betulinic acid induces eNOS expression via the AMPK-dependent KLF2 signaling pathway," *Journal of Agricultural and Food Chemistry*, vol. 68, no. 49, pp. 14523–14530, 2020.

Research Article

Valsartan Regulates PI3K/AKT Pathways through lncRNA GASL1 to Improve Isoproterenol-Induced Heart Failure

Jian Zhou,¹ Xiujuan Duan,² Jibing Wang,² Yunhong Feng,³ and Jiangyong Yuan^{1,4} 

¹Department of Cardiovascular Medicine, Shanghai East Hospital, Tongji University School of Medicine, Shanghai, China

²The Second Department of Cardiology, The Eighth People's Hospital of Hengshui City, Hengshui, China

³Cardiopulmonary Function Room, People's Hospital of Rugao City, Rugao, China

⁴The Second Department of Cardiology Affiliated to Hebei University of Engineering, Handan, China

Correspondence should be addressed to Jiangyong Yuan; hebeuyjy@163.com

Received 2 November 2021; Revised 8 December 2021; Accepted 14 December 2021; Published 6 January 2022

Academic Editor: Francesco Busardò

Copyright © 2022 Jian Zhou et al. This is an open access article distributed under the Creative Commons Attribution License, which permits unrestricted use, distribution, and reproduction in any medium, provided the original work is properly cited.

Objective. This study is aimed at determining the expression and function of the GASL1 and PI3K/AKT pathways in isoproterenol- (ISO-) induced heart failure (HF). To determine the moderating effect of valsartan (VAL) on the progression of ISO-induced HF and to elucidate the related mechanism. **Materials and Methods.** First, in *in vivo* experiment, we examined the effect of VAL on cardiac function in rats with ISO-induced HF. Similarly, quantitative real-time polymerase chain reaction (qRT-PCR) and Western blot were used to detect the effect of VAL on ISO-treated rat primary cardiomyocytes. Then, si-GASL1-transfected primary cardiomyocytes were constructed and Ad-si-GASL1 was injected through rat tail vein to achieve the effect of lowering GASL1 expression, so as to investigate the role of GASL1 in VAL's treatment of ISO-induced HF. **Results.** In ISO-induced HF rat models, the GASL1 decreased while PI3K and p-AKT expressions were abnormally elevated and cardiac function deteriorated, and VAL was able to reverse these changes. In primary cardiomyocytes, ISO induces apoptosis of cardiomyocytes, and expression of GASL1 decreased while PI3K and p-AKT were abnormally elevated, which can be reversed by VAL. The transfection of primary cardiomyocytes with si-GASL1 confirmed that GASL1 affected the expression of PI3K, p-AKT, and the apoptosis of primary cardiomyocytes. Rat myocardium injected with Ad-si-GASL1 was found to aggravate the cardiac function improved by VAL. **Conclusions.** This study was the first to confirm that VAL improves ISO-induced HF by regulating the PI3K/AKT pathway through GASL1. And this study demonstrated a significant correlation between HF, VAL, GASL1, and the PI3K/AKT pathway.

1. Introduction

Heart failure (HF) is a clinical syndrome of fluid retention, dyspnea, and fatigue caused by impaired ventricular filling and bleeding capacity caused by various functional or structural heart diseases [1]. The cardiovascular disease report released by China provides data that shows that China has 290 million cardiovascular patients and 4.5 million patients with HF [2]. The cardiovascular mortality rate still ranks first, higher than that of tumors and other diseases. The total number of HF patients worldwide is over 26 million, and the incidence of HF continues to rise with the extension of human life [3]. HF

has become a chronic disease endangering public health and economic interests. The pathogenesis and effective treatment of HF have also become important contents of scientific research and clinical work. Isoproterenol (ISO) is a major adrenergic receptor agonist. Large doses can damage the heart muscle and cause diastolic and systolic dysfunction, and ISO is widely used in the manufacture of models of HF [4].

The human genome is only about 2% of the total genome, while the remaining 98% can be transcribed into many non-coding or weakly coding RNA molecules of varying lengths, known as noncoding RNAs (ncRNAs) [5]. According to length, ncRNAs are divided into microRNA (miRNA) and

long noncoding RNA (lncRNA). ncRNAs larger than 200 nt are called long noncoding RNAs. In the early stage, lncRNA was considered to have no biological function due to poor technical means. With the development of high-throughput technology and the deepening of scientific research, more and more long noncoding RNAs have been discovered, named, and studied. With the deepening of research, the biological functions of lncRNA were gradually disclosed. lncRNA can regulate target genes at various levels, participate in chromosomal dose compensation [6] and genomic imprinting [7], regulate cell cycle [8] and cytoplasmic transmission [9], and regulate cell differentiation and maintenance of stem cells [10]. Many lncRNAs have been proved to have a regulatory effect on various physiological and pathological processes such as the heart and kidney. A new lncRNA was recently discovered, named GASL1 (growth-arrest-associated lncRNA 1). GASL1 can regulate the cell cycle and participate in cell proliferation and colony formation [11, 12]. Other studies have found that the expression of lncRNA GASL1 is downregulated in chronic HF and correlated with cell apoptosis [13]. In this study, GASL1 was selected as one of the research objects to explore its role in isoproterenol cardiac failure.

Phospholipid inositol (PI3K) is a cytoplasmic lipid kinase, and AKT is a key kinase (serine/threonine kinase) in the PI3K pathway. AKT activation requires membrane interaction and phosphorylation of serine 473 (AKT-Ser473) and threonine 308 (AKT-Thr308). After multiple stimuli, the PH domain interacts with phosphatidylinositol 3,4,5-triphosphate (PIP3) produced by PI3K to allow cytoplasmic AKT to enter the plasma membrane [14]. Then, AKT-PIP3 interaction, through the interdomain conformational change-induced AKT for open conformer, exposes Thr308 and Ser473 subsequent phosphorylation of phosphoinositide-dependent protein kinase, and phosphorylation of Thr308 and Ser473 fully activated AKT, which through the phosphorylation of the downstream kinases, participate in a variety of regulating cell proliferation and growth, and it also has played an important role in many fields such as cancer [15], angiogenesis [16], and osteoporosis [17].

Valsartan (VAL) was originally an antihypertensive drug but was later used in the treatment of symptomatic HF patients and played a huge role in the development of HF [18]. As early as 2005, Majani confirmed that VAL can also dramatically reduce the decline in the quality of life of patients with HF [19]. In addition, the Maggioni equivalent year study found that adding VAL to prescribed treatments can reduce the incidence of atrial fibrillation [20]. There are many clinical studies on VAL in the treatment of HF, but guidelines often refer to VAL as an intolerable alternative to angiotensin-converting enzyme inhibitors (ACEI). VAL provides an effective means for the treatment of HF. It is widely used in clinical practice and is well known for its cardioprotective effect.

The aim of this study was to determine the function of GASL1 and PI3K-AKT in myocardial tissue and myocardial cells in patients with ISO-induced HF. And explore the effectiveness and related mechanisms of VAL in the treatment of ISO-induced HF.

2. Materials and Method

2.1. Animal Experiment. 24 male SPF 8-week-old healthy male rats (Shanghai East hospital, Tongji University School of Medicine Animal Center, Shanghai, China) weighing 240-260 g were used. They were reared at 25°C and 50% humidity and freely fed. Rats were randomly divided into 3 groups: the sham group, ISO-induced HF model group, and ISO-induced HF+VAL treatment group. We prepared a rat model of HF by giving ISO (Tianpu Biochemical Pharmaceutical, Guangzhou, China) 2 times of doses of 170 mg/kg at 24 h intervals. Rats in the sham group were injected with an equal volume of sterile saline, and rats in the ISO+VAL treatment group were treated with ISO and treated with VAL (Tianpu Biochemical Pharmaceutical, Guangzhou, China) at 30 mg/kg/d for 4 weeks. All rats were housed in cages of appropriate size. Rat myocardial tissues were excised and immediately stored at -80°C for further experiments. This study was approved by the Animal Ethics Committee of Shanghai East hospital, Tongji University School of Medicine Animal Center.

2.2. Heart Function Test in Rats. After disinfecting the abdomen of rats, the rats were anesthetized with 0.1% pentobarbital by intraperitoneal injection. The anesthetized rats fixed their limbs and head on the operation platform. Heparin (2 mg/ml, Shanghai East hospital, Tongji University School of Medicine Animal Center, Weihui, China) was injected through the tail vein. After heparinization, we prepared the skin and sterilized the surgical area, took a midline incision of the neck to cut the skin, bluntly separated the layers of tissue, exposed and freed the right common carotid artery, and ligated the distal end of the carotid artery with a surgical line. A rat artery clamp was used to clamp the proximal heart of the carotid artery, and a gap was cut along the common carotid artery at a 30° angle with microscissors under a microscope, and the PV catheter (Nuohai Life Science, Shanghai, China) with an electrode at the front end was inserted into the rat aorta through the cut gap and extended to the left ventricle. Continuously, the pressure-volume data was recorded for 10 min. Hemodynamic data was analyzed using pressure-volume analysis software to obtain the maximal rate of the increase of left ventricular pressure dP/dt_{max} and the maximal rate of the decrease of left ventricular pressure, dP/dt_{min}, and the left ventricular systolic pressure (LVSP), and the left ventricular end-diastolic pressure (LVEDP).

2.3. Primary Cardiomyocyte Isolation and Cell Culture. The heart was removed using elbow forceps and placed in sterile prechilled D-Hank's solution (Camilo Biological, Nanjing, China). Ophthalmic scissors were used to cut the myocardium into small pieces. The prechilled D-Hank's solution was used to wash the cut myocardial tissue 3-4 times and then transferred to a sterile conical flask containing 10 ml of prechilled trypsin (Camilo Biological, Nanjing, China) and sealed in a 4°C refrigerator overnight. After 12-16 h, we added precooled 10 ml Dulbecco's modified Eagle's medium (DMEM) (Life Technology, Wuhan, China) (complete medium) containing 10% fetal bovine serum

(FBS) (Life Technology, Wuhan, China) and penicillin-streptomycin (Life Technology, Wuhan, China) for 10 min and then incubated for 30 min in a 37°C, 5% CO₂ incubator. We aspirated the supernatant and added 10 ml of type II collagenase (Camilo Biological, Nanjing, China) to digest myocardial tissue and then placed it in a 37°C water bath for 15 min and transferred the supernatant to a sterilized centrifuge tube and added complete medium. 10 ml of type II collagenase was added to the remaining myocardial tissue to redigest the myocardial tissue. The cell suspension obtained by two digestions was centrifuged. Then, we discard the supernatant and resuspend the cell pellet by adding prewarmed complete medium at 37°C. Cell suspensions were seeded into cell culture dishes, and 5×10^5 cells were inoculated in each culture dish. Then, we cultured in an incubator for 1 h and waited for the fibroblasts to adhere to the wall; then, we aspirated the supernatant and washed them again with complete medium to collect the cardiomyocytes attached to the surface of the fibroblasts. The adherence screening process above was repeated once. The screened cells were collected, and the concentration of neonatal rat cardiomyocytes was adjusted to 5×10^5 /ml with 37°C prewarmed complete culture medium. BrdU (Camilo Biological, Nanjing, China) was added to the suspension of neonatal rat cardiomyocytes to inhibit the proliferation of fibroblasts. Then, we inoculated it into a culture dish and placed it in an incubator for 48 h. It was washed once with DMEM and then changed the complete medium. The medium was changed once a day and adhered to the culture for 72 h. When the cell fusion appears as a whole beat, we switched to serum-free medium culture. The concentration of $2 \mu\text{mol/l}$ was used for the construction of ISO-induced HF model. And concentration of $10 \mu\text{mol/l}$ was used for the construction of VAL.

2.4. Cell Transfection. Cells were harvested 48 h after transfection for further analysis. To silence GASL1, a GASL1 siRNA or a control siRNA was transfected by using RNAiMax (Invitrogen) following the manufacturer's manuscript. Cells were harvested 72 h after transfection for further analysis.

2.5. RNA Isolation and Quantitative Real-Time Polymerase Chain Reaction (qRT-PCR). The total RNA extraction kit (Thermo Fisher Scientific, Waltham, MA, USA) was used to extract the RNA of the rat's heart tissue and cellular RNA and then reversed transcribed into cDNA for later use. We found the glyceraldehyde 3-phosphate dehydrogenase (GAPDH), Inc-GASL1 sequence on the NCBI website. The cDNA was amplified by a two-step method using an RT-PCR instrument. The reaction system was $20 \mu\text{l}$. The amplification conditions were as follows: first denaturation at 95°C for 10 min; then denaturation at 95°C for 15 s, and annealing at 60°C for 1 min, and this step was repeated 40 times. The GAPDH housekeeping gene was used as an internal reference control, and the target gene transcription level was calculated by formula $2^{-\Delta\Delta C_t}$. Primers used were shown in Table 1.

2.6. Western Blot. Cut myocardial tissue into small pieces or added lysate (Camilo Biological, Nanjing, China) to cells in a 6-well plate, homogenized until completely lysed, centrifuged at 40°C, 12000 g for 15 min, took the supernatant for protein quantification, and performed polyacrylamide gel electrophoresis (PAGE) and transferred film, 5% skim milk powder blocked for 1 h. Diluted primary antibody (PI3K 1:1000 Abcam, AKT 1:1000 Abcam, p-AKT 1:1000 Abcam, cleaved-caspase-3 1:2000 Abcam, GAPDH 1:2000 Abcam, Cambridge, MA, USA) incubated with the membrane for 6 h. It was washed with TBST 3 times and diluted the HRP-labeled secondary antibody (Yifei Xue Biotechnology, Nanjing, China) 1:1000; then, it was incubated with membrane 37°C for 1 h. The TBST was washed 3 times; the electrochemiluminescence (ECL) luminescent solution (Thermo Fisher Scientific, Waltham, MA, USA) was developed, and the scanning analysis was performed with a Tanon-5200 imaging system (Bio, Hercules, CA, USA).

2.7. Statistical Analysis. All data are expressed as the mean \pm standard deviation (mean \pm SD). Differences between two groups were analyzed by using Student's *t*-test. Comparison between multiple groups was done using one-way ANOVA test followed by post hoc test (least significant difference). Statistical analysis was performed using Statistical Product and Service Solutions (SPSS) 22.0 software (IBM, Armonk, NY, USA). When $p < 0.05$, the differences between the groups were statistically significant.

3. Results

3.1. Effect of VAL on Cardiac Function in Rats with ISO-Induced HF. We divided the rats into three groups, namely, the sham group, ISO group, and ISO+VAL group. Compared with the sham group, the ISO group showed decreased LVSP, increased LVEDP, and decreased \pm dp/dtmax. In contrast, when VAL was used to treat ISO-induced HF, the cardiac function indicators above alleviated (Figures 1(a)–1(d)). In addition, the expression of GASL1 in the heart decreased dramatically after ISO treatment and increased after VAL treatment (Figure 1(e)). Meanwhile, we found that the expression of PI3K and p-AKT in the ISO group was dramatically increased, while the expression of PI3K and p-AKT in the heart tissues of the model group was decreased (Figure 1(f)) after VAL treatment, while the expression of AKT was not different among the three groups. At the same time, we examined the apoptosis-related molecules and found that cleaved-caspase-3 expression increased in the heart tissue of rats treated with ISO but decreased in the ISO+VAL group (Figure 1(g)). In ISO-induced HF rats, expression of GASL1 decreased, expression of PI3K, p-AKT, and cleaved-caspase-3 was abnormally elevated, and VAL reversed these changes. VAL has been shown to be effective in the treatment of ISO-induced HF and may be associated with GASL1, PI3K/AKT, and cleaved-caspase-3.

3.2. Effect of VAL on ISO-Treated Rat Cardiomyocytes. The results of GASL1 expression detection in primary

TABLE 1: Real time PCR primers.

Gene name	Forward (5'>3')	Reverse (5'>3')
lnc GASL1	CTGAGGCCAAAGTTTCCAAC	CAGCCTGACTTTCCT CTCT
GAPDH	ACAACCTTGGTATCGTGGAAGG	GCCATCACGCCACAGTTTC

qRT-PCR: quantitative real-time polymerase chain reaction.

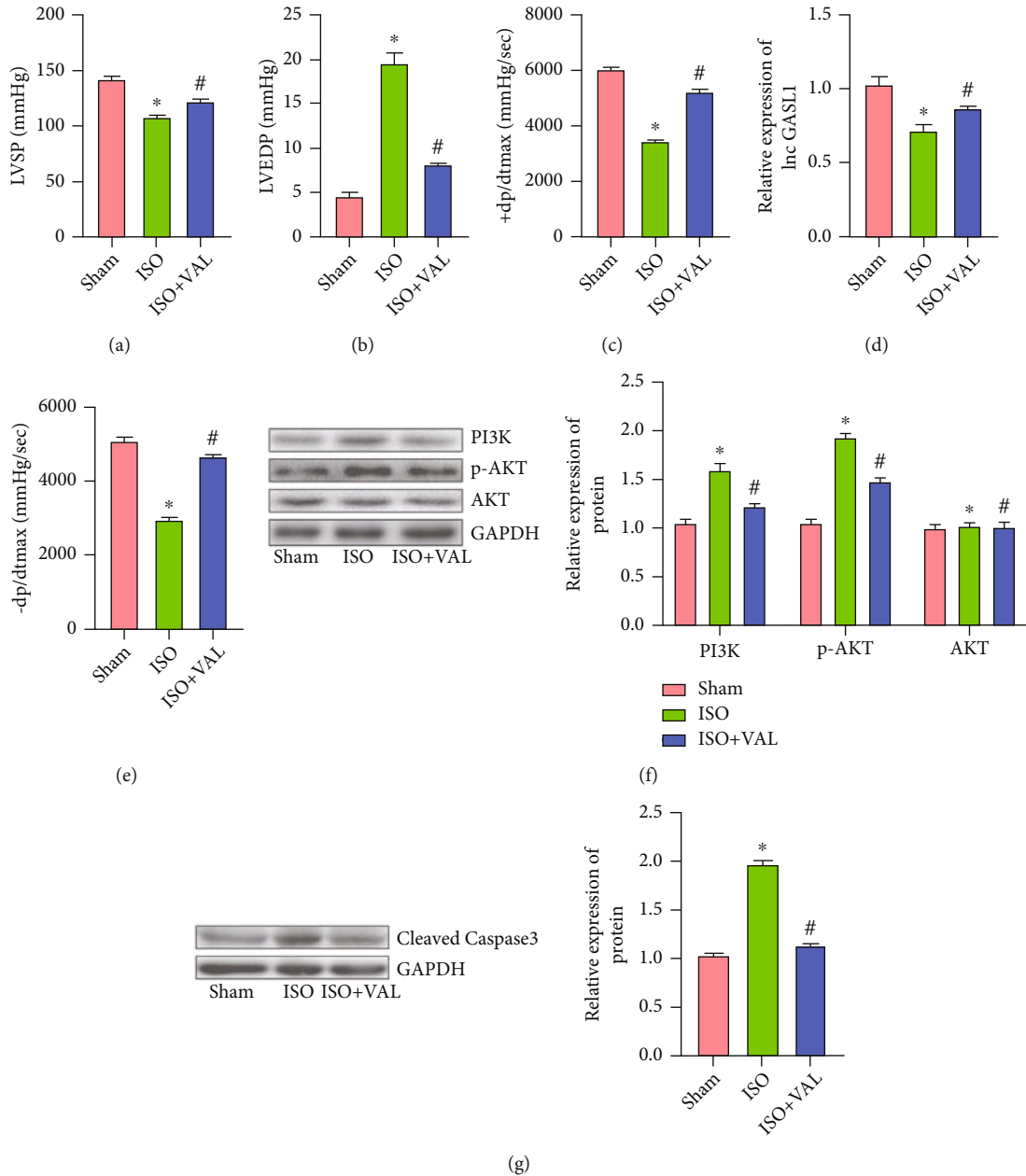


FIGURE 1: Effect of VAL on cardiac function in rats with ISO-induced HF. (a-d) Results of cardiac function (LVSP, LVEDP, +dP/dtmax, and -dP/dtmax) of rats in different treatment groups (“*” indicates that compared with the sham group, “#” indicates that compared with the ISO group $p < 0.05$). (e) The expression levels of lnc GASL1 in rat heart tissues (“*” indicates that compared with the sham group, “#” indicates that compared with the ISO group $p < 0.05$). (f) Western blot bands and gray value analysis of PI3K, AKT, and p-AKT (“*” indicates that compared with the sham group, “#” indicates that compared with the ISO group $p < 0.05$). (g) Western blot bands and gray value analysis of cleaved-caspase-3 (“*” indicates that compared with the sham group, “#” indicates that compared with the ISO group $p < 0.05$).

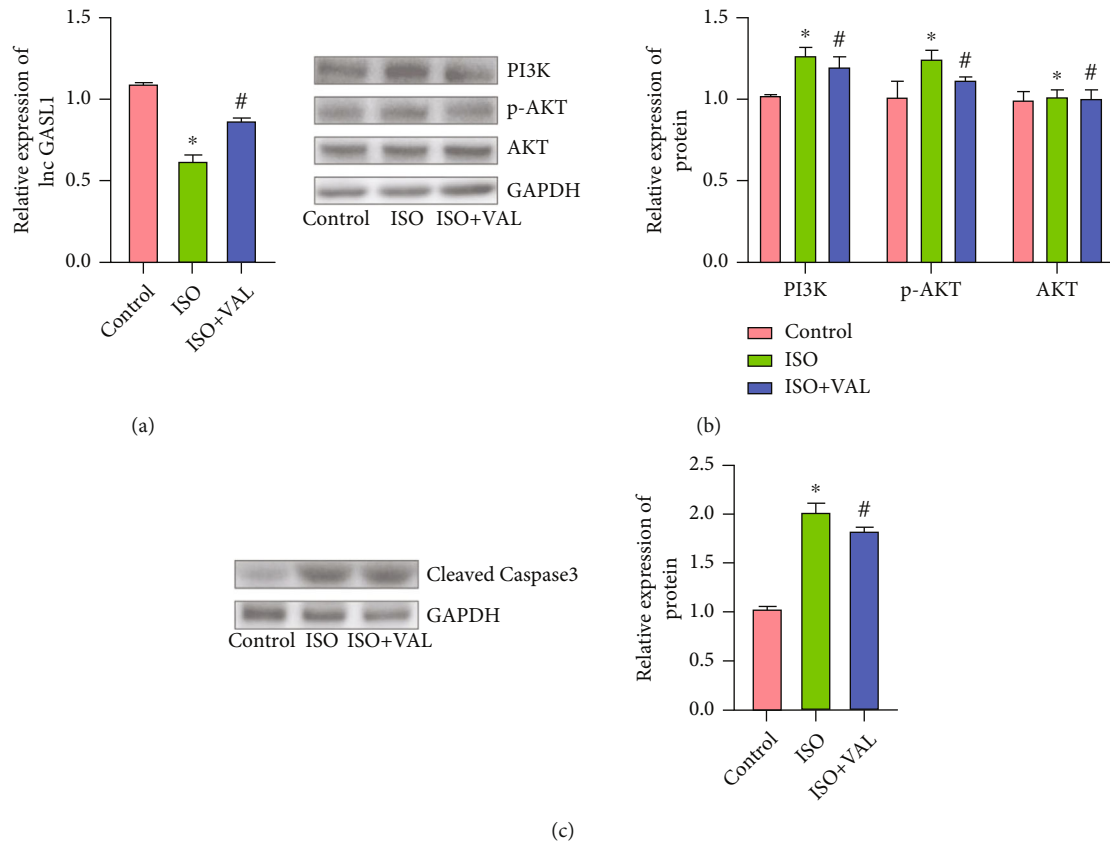


FIGURE 2: Effect of VAL on ISO-treated rat cardiomyocytes. (a) The expression levels of lnc GASL1 in cardiomyocytes (“*” indicates that compared with the control group, “#” indicates that compared with the ISO group $p < 0.05$). (b) Western blot bands and gray value analysis of PI3K, AKT, and p-AKT (“*” indicates that compared with the control group, “#” indicates that compared with the ISO group $p < 0.05$). (c) Western blot bands and gray value analysis of cleaved-caspase-3 (“*” indicates that compared with the control group, “#” indicates that compared with the ISO group $p < 0.05$).

cardiomyocytes of three groups are shown in Figure 2(a): after ISO treatment of primary cardiomyocytes, GASL1 expression decreased, but the decrease of GASL1 can be inhibited by VAL (Figure 2(a)). At the same time, we examined the expression of PI3K and p-AKT in the three groups of primary cardiomyocytes. The results are shown in Figure 2(b) below: PI3K and p-AKT expression increased after ISO treatment, while VAL inhibited the ISO-induced increase in PI3K and p-AKT expressions in the primary cardiomyocytes, while the expression of AKT showed no difference among the three groups (Figure 2(b)). In addition, cleaved-caspase-3 expression in the three groups was dramatically increased after ISO treatment, while cleaved-caspase-3 expression was dramatically inhibited after intervention with VAL (Figure 2(c)). At the cellular level, it was confirmed that VAL can improve myocardial cell damage caused by ISO. The corresponding changes in the expressions of GASL1, PI3K, and p-AKT were also observed in the experiment, which suggested that GASL1, PI3K/AKT might be involved in the process of the effects of VAL and ISO in cardiomyocytes.

3.3. The Effects of GASL1 on VAL in ISO-Treated Primary Rat Cardiomyocytes. We divided primary cardiomyocytes into 4 groups: control, ISO, ISO+si-NC, and ISO+si-GASL1.

The results showed that the expression of GASL1 in ISO-treated rat cardiomyocytes was dramatically decreased. The primary cardiomyocytes of the ISO-treated group were transfected with si-NC, and the expression of GASL1 was not dramatically different from that of the ISO group. However, the expression of GASL1 in rat cardiomyocytes transfected with si-GASL1 dramatically decreased compared with the control group (Figure 3(a)). Transfection of ISO-treated rat cardiomyocytes with si-GASL1 interferes with GASL1 expression and observes the expression of PI3K and P-AKT. The results show that in the ISO-treated rat cardiomyocytes, the PI3K and P-AKT expressions were dramatically increased. And in the ISO+si-NC group, the expression of PI3K and P-AKT had no dramatical difference from that of the ISO group. However, PI3K and P-AKT expression levels in rat cardiomyocytes transfected with si-GASL1 were dramatically higher than that in the ISO group (Figure 3(b)). Similarly, the results showed that cleaved-caspase-3 expression level in ISO-treated rat cardiomyocytes was dramatically increased. And cleaved-caspase-3 expression level in the ISO+si-GASL1 group was dramatically higher than that in the ISO group (Figure 3(c)). It was observed in the experiment that as the expression of GASL1 decreased, the expression of PI3K and P-AKT also changed correspondingly, and accompanied by the change in the

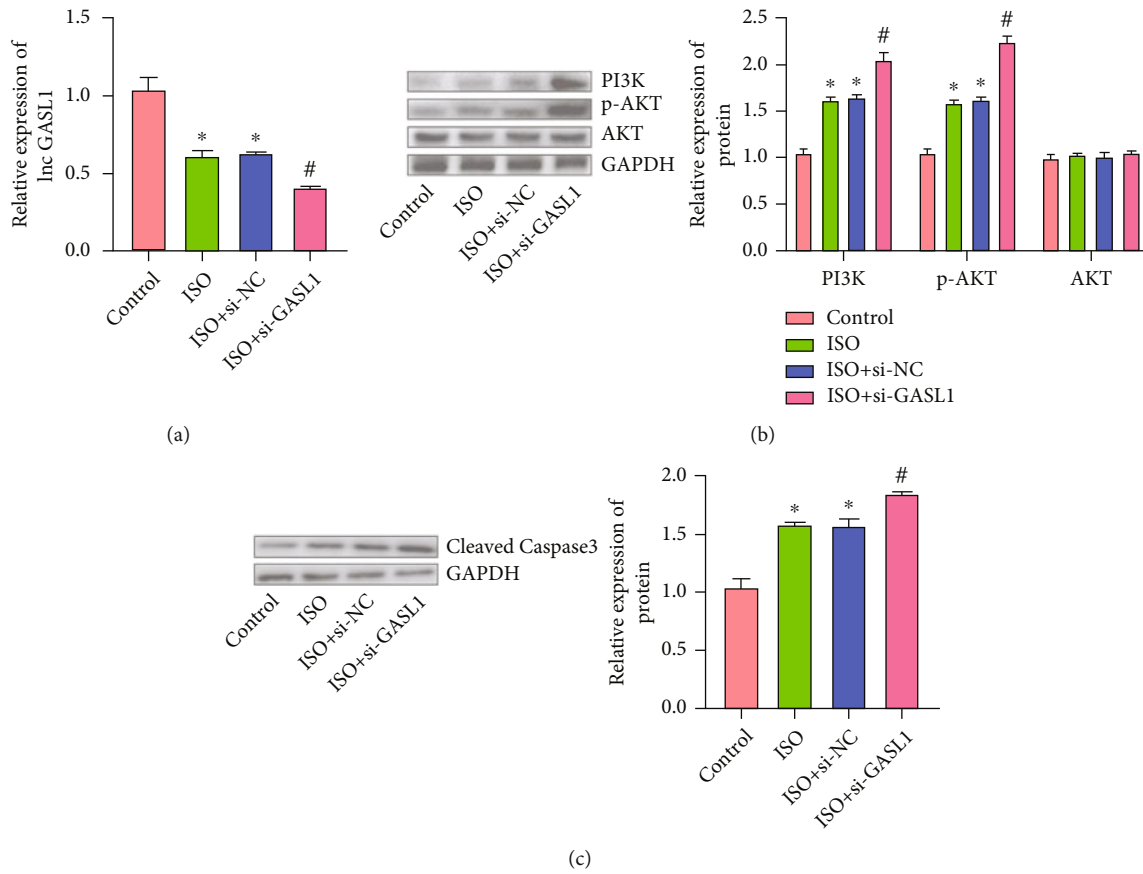


FIGURE 3: The effects of GASL1 on VAL in ISO-treated primary rat cardiomyocytes. (a) The expression levels of lnc GASL1 in cardiomyocytes (“*” indicates that compared with the control group, “#” indicates that compared with the ISO group $p < 0.05$). (b) Western blot bands and gray value analysis of PI3K, AKT, and p-AKT (“*” indicates that compared with the control group, “#” indicates that compared with the ISO group $p < 0.05$). (c) Western blot bands and gray value analysis of cleaved-caspase-3 (“*” indicates that compared with the control group, “#” indicates that compared with the ISO group $p < 0.05$).

degree of cardiomyocyte apoptosis, which confirmed that during the process of ISO-induced cardiomyocyte injury, PI3K/AKT participates as the downstream signaling part of GASL1.

3.4. The Effects of VAL and GASL1 on Heart Function in ISO-Induced HF Rats. The ISO-induced HF model rats were given VAL or VAL combined with myocardium injection of recombinant adenovirus (Ad-NC or Ad-si-GASL1) to compare the cardiac function results of rats in different treatment groups. Compared with ISO-induced HF model group, rats in the ISO+VAL group had higher level of LVSP, +dP/dtmax, and -dP/dtmax, and with LVEDP decreased. LVSP, +dP/dtmax, and -dP/dtmax were lower than that in the ISO+VAL+Ad-si-GASL1 group compared with ISO+VAL group. However, LVEDP showed the different result (Figures 4(a)–4(d)). We attenuated the myocardial protective effect of VAL by artificially lowering the expression of GASL1 and clinically confirmed the improvement of ISO-induced HF by VAL via GASL1.

4. Discussion

VAL is a drug that has been clearly demonstrated to improve myocardial remodeling, and it is not clear whether it is effective

in ISO-induced heart HF. Long noncoding RNA is a research hotspot in the cardiovascular field in recent years [21, 22], among which, growth-arrest associated 1 lncRNA (GASL1) has been proved to be related to HF, but other related studies are poor. In this study, animal models and cell (rat primary cardiomyocytes) models of ISO-induced HF were successfully established, and VAL was used for drug intervention to confirm the improvement effect of VAL on ISO-induced HF.

The plasmid si-GASL1 was successfully constructed to transfect the cells, and the upstream and downstream target proteins of the signal transduction pathway were determined, which confirmed that the signal transduction pathways of VAL to improve ISO induced HF were GASL1 and PI3K/AKT. Ad-si-GASL1, an adenovirus vector of GASL1, was successfully constructed and injected into the myocardium of ISO-induced rats to verify the effect of GASL1 on the myocardial protection of VAL. This study is the first to confirm that VAL modulates the PI3K/AKT signaling pathway through GASL1 in ISO-induced HF. GASL1 is a new entry point for the treatment of ISO-induced HF.

Although the significant correlation between HF, VAL, GASL1, and the PI3K/AKT pathway had been confirmed in the experiment, the specific transcription genes and

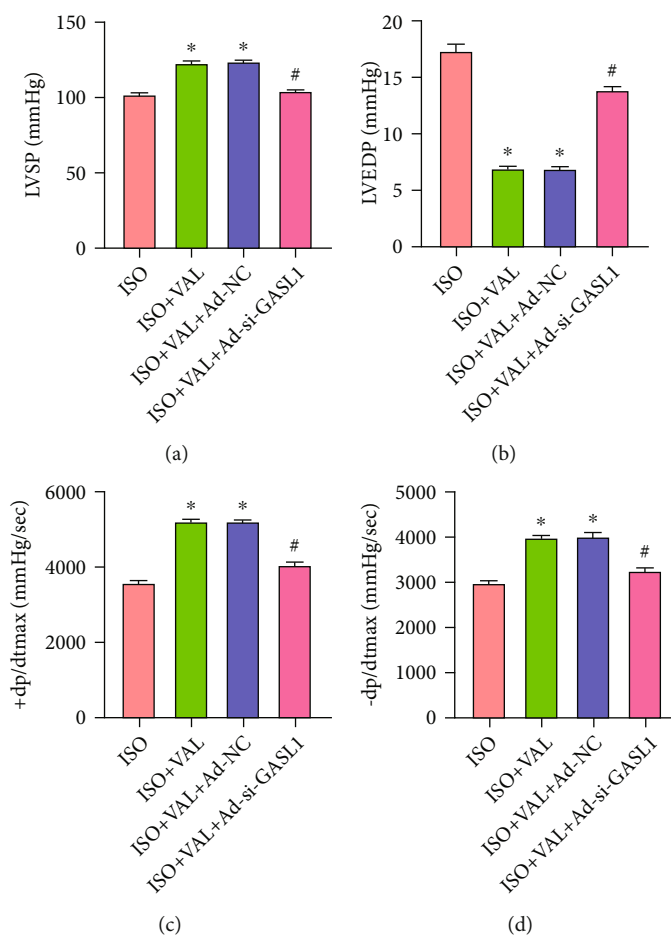


FIGURE 4: The effects of VAL and GASL1 on heart function in ISO-induced HF rats. (a–d) Results of cardiac function (LVSP, LVEDP, +dP/dtmax, and -dP/dtmax) of rats in different treatment groups (“*” indicates that compared with the ISO group, “#” indicates that compared with the ISO+VAL+Ad-NC group $p < 0.05$).

cytokines involved in the signaling process still need to be further clarified. VAL has been shown to interfere with ISO-induced HF; however, other possible mechanisms for VAL in the treatment of HF remain to be developed. GASL1 has been shown to have a protective role in the process of ISO-induced HF, which provides a new entry point for treatment, but specific effective intervention methods need to be developed.

5. Conclusion

This study was the first time to confirm that VAL improves ISO-induced HF by regulating the PI3K/AKT pathway through GASL1. And this study demonstrated a significant correlation between HF, VAL, GASL1, and the PI3K/AKT pathway.

Data Availability

The datasets used and analyzed during the current study are available from the corresponding author on reasonable request.

Conflicts of Interest

The authors declared no conflict of interest.

References

- [1] B. Davison and G. Cotter, “Why is heart failure so important in the 21st century?,” *European journal of heart failure Supplements*, vol. 17, no. 2, pp. 122–124, 2015.
- [2] G. Dai, “Heart failure in China: review and prospect,” *Zhonghua Xin Xue Guan Bing Za Zhi*, vol. 43, no. 2, pp. 104–107, 2015.
- [3] Y.-M. Kang, Q. Yang, X.-J. Yu et al., “Hypothalamic paraventricular nucleus activation contributes to neurohumoral excitation in rats with heart failure,” *Regenerative Medicine Research*, vol. 2, no. 1, 2014.
- [4] J. J. Wang, C. Rau, R. Avetisyan et al., “Genetic Dissection of Cardiac Remodeling in an Isoproterenol-Induced Heart Failure Mouse Model,” *PLoS Genetics*, vol. 12, no. 7, article e1006038, 2016.
- [5] M. Esteller, “Non-coding RNAs in human disease,” *Nature Reviews. Genetics*, vol. 12, no. 12, pp. 861–874, 2011.

- [6] D. U. Menon and V. H. Meller, "Identification of the *Drosophila* X chromosome: The long and short of it," *RNA Biology*, vol. 12, no. 10, pp. 1088–1093, 2015.
- [7] H. Liu, X. Shang, and H. Zhu, "LncRNA/DNA binding analysis reveals losses and gains and lineage specificity of genomic imprinting in mammals," *Bioinformatics*, vol. 33, no. 10, pp. 1431–1436, 2017.
- [8] Y. W. Hu, C. M. Kang, J. J. Zhao et al., "LncRNA PLAC2 down-regulates RPL36 expression and blocks cell cycle progression in glioma through a mechanism involving STAT1," *Journal Of Medicine And Biochemistry*, vol. 22, no. 1, pp. 497–510, 2018.
- [9] Z. Wu, L. Wang, J. Li, L. Wang, Z. Wu, and X. Sun, "Extracellular vesicle-mediated communication within host-parasite interactions," *Frontiers in Immunology*, vol. 9, p. 3066, 2018.
- [10] K. Katsushima, A. Natsume, F. Ohka et al., "Targeting the Notch-regulated non-coding RNA TUG1 for glioma treatment," *Nature Communications*, vol. 7, no. 1, 2016.
- [11] W. Z. Su and X. Yuan, "LncRNA GASL1 inhibits tumor growth of non-small cell lung cancer by inactivating TGF- β pathway," *European Review for Medical and Pharmacological Sciences*, vol. 22, no. 21, pp. 7282–7288, 2018.
- [12] C. Peng, X. Li, Y. Yu, and J. Chen, "LncRNA GASL1 inhibits tumor growth in gastric carcinoma by inactivating the Wnt/ β -catenin signaling pathway," *Experimental and Therapeutic Medicine*, vol. 17, no. 5, pp. 4039–4045, 2019.
- [13] H. Deng, W. Ouyang, L. Zhang, X. Xiao, Z. Huang, and W. Zhu, "LncRNA GASL1 is downregulated in chronic heart failure and regulates cardiomyocyte apoptosis," *Cellular & Molecular Biology Letters*, vol. 24, no. 1, p. 41, 2019.
- [14] I. Yudushkin, "Getting the Akt together: guiding intracellular Akt activity by PI3K," *Biomolecules*, vol. 9, no. 2, 2019.
- [15] Q. Lin, Y. B. Ling, J. W. Chen et al., "Circular RNA circCDK13 suppresses cell proliferation, migration and invasion by modulating the JAK/STAT and PI3K/AKT pathways in liver cancer," *International Journal of Oncology*, vol. 53, no. 1, pp. 246–256, 2018.
- [16] Y. Yang, M. Gao, Z. Lin et al., "DEK promoted EMT and angiogenesis through regulating PI3K/AKT/mTOR pathway in triple-negative breast cancer," *Oncotarget*, vol. 8, no. 58, pp. 98708–98722, 2017.
- [17] J. Xi, Q. Li, X. Luo et al., "Celestrol inhibits glucocorticoid-induced osteoporosis in rat via the PI3K/AKT and Wnt signaling pathways," *Molecular Medicine Reports*, vol. 18, no. 5, pp. 4753–4759, 2018.
- [18] E. J. Velazquez, D. A. Morrow, A. D. DeVore et al., "Rationale and design of the com Par I son O f sacubitril/valsarta N versus E nalapril on E ffect on nt-p R o-bnp in patients stabilized from an acute Heart Failure episode (PIONEER-HF) trial," *American Heart Journal*, vol. 198, pp. 145–151, 2018.
- [19] G. Majani, A. Giardini, C. Opasich et al., "Effect of Valsartan on Quality of Life When Added to Usual Therapy for Heart Failure: Results From The Valsartan Heart Failure Trial," *Journal of Cardiac Failure*, vol. 11, no. 4, pp. 253–259, 2005.
- [20] A. P. Maggioni, R. Latini, P. E. Carson et al., "Valsartan reduces the incidence of atrial fibrillation in patients with heart failure: Results from the Valsartan Heart Failure Trial (Val-HeFT)," *American Heart Journal*, vol. 149, no. 3, pp. 548–557, 2005.
- [21] C. Y. Liu, Y. H. Zhang, R. B. Li et al., "LncRNA CAIF inhibits autophagy and attenuates myocardial infarction by blocking p53-mediated myocardin transcription," *Nature Communications*, vol. 9, no. 1, p. 29, 2018.
- [22] J. X. Pan, "LncRNA H19 promotes atherosclerosis by regulating MAPK and NF- κ B signaling pathway," *European Review for Medical and Pharmacological Sciences*, vol. 21, no. 2, pp. 322–328, 2017.

Research Article

Potential Effects of Metformin on the Vitality, Invasion, and Migration of Human Vascular Smooth Muscle Cells via Downregulating lncRNA-ATB

Wei Jia,¹ Yue Zhou,² Lina Sun,³ Jianlong Liu,¹ Zhiyuan Cheng,¹ and Shuofang Zhao ⁴

¹Department of Vascular Surgery, Beijing Jishuitan Hospital, Beijing, China

²Department of Neurological Rehabilitation, Weifang Yidu Central Hospital, Weifang, China

³Emergency Center, Qingdao Central Hospital Affiliated to Qingdao University, Qingdao, China

⁴Guangdong Academy of Medical Sciences and Guangdong Provincial People's Hospital, Guangzhou, China

Correspondence should be addressed to Shuofang Zhao; shuofang9@163.com

Received 2 November 2021; Revised 7 December 2021; Accepted 10 December 2021; Published 4 January 2022

Academic Editor: Francesco Busardò

Copyright © 2022 Wei Jia et al. This is an open access article distributed under the Creative Commons Attribution License, which permits unrestricted use, distribution, and reproduction in any medium, provided the original work is properly cited.

Objective. To elucidate the role of metformin in influencing VSMCs via the involvement of lncRNA-ATB. **Methods.** qRT-PCR was conducted to detect serum levels of lncRNA-ATB and p53 in CHD patients ($n = 50$) and healthy subjects ($n = 50$). Correlation in serum levels of lncRNA-ATB and p53 in CHD patients was assessed by Pearson correlation test. ROC curves were depicted for analyzing the predictive potential of lncRNA-ATB in the occurrence of CHD. After metformin induction in VSMCs overexpressing lncRNA-ATB, relative levels of lncRNA-ATB and p53 were detected. Meanwhile, proliferative, migratory, and invasive abilities in VSMCs were, respectively, examined by CCK-8 and transwell assay. The interaction between lncRNA-ATB and p53 was tested by RIP. In addition, the coregulation of lncRNA-ATB and p53 in cell functions of VSMCs was finally determined. **Results.** Increased serum level of lncRNA-ATB and decreased p53 level were detected in CHD patients than those of healthy subjects. lncRNA-ATB could interact with p53 and negatively regulate its level. In addition, lncRNA-ATB could serve as a potential biomarker for predicting the occurrence of CHD. The overexpression of lncRNA-ATB triggered viability, migratory, and invasive abilities in VSMCs, and the above trends were abolished by metformin induction. The overexpression of p53 partially abolished the promotive effects of lncRNA-ATB on proliferative, migratory, and invasive abilities in VSMCs. **Conclusions.** Metformin induction inhibits proliferative, migratory, and invasive abilities in VSMCs by downregulating lncRNA-ATB, which may be related to p53 activation.

1. Introduction

Vascular smooth muscle cells (VSMCs) are the main cell types of vascular wall components. They are mainly located in the vascular mesothelium for maintaining blood vessel tension and regulating blood pressure [1]. Abnormal proliferation and migration of VSMCs are the fundamental pathological basis for atherosclerosis, hypertension, and restenosis after coronary artery intervention and other vascular proliferative diseases [2].

Metformin is a widely applied drug for type 2 diabetes mellitus. In addition, it is useful in preventing against atherosclerosis. A clinical trial involving 3,234 prodromal dia-

betes subjects showed that compared with the placebo group, the incidence and severity of coronary artery calcification remarkably decrease in those treated by metformin [3]. It is suggested that metformin can prevent diabetes-induced atherosclerosis. Sainio et al. [4] also suggested the long-term protection of metformin on blood vessels.

LncRNAs are transcripts containing more than 200 nucleotides and they cannot be transcribed into proteins [5]. They are involved in the regulation of atherosclerosis progression [6]. lncRNA-ATB is the first lncRNA that can be activated by TGF- β , which is located on chromosome 14 [7]. It is vital regulator involved in phenotype transformation of human peritoneal mesothelial cells, hepatitis C-

related cirrhosis, and preeclampsia [8–10]. Yue et al. [11] demonstrated that the upregulated lncRNA-ATB is an oncogene involved in the progression of colorectal cancer. Shi et al. [12] uncovered that lncRNA-ATB drives trastuzumab resistance and invasion-metastasis cascade. Currently, the potential influences of lncRNA-ATB on cell functions of VSMCs and progression of vascular diseases remain unclear.

A previous study has elucidated the biological function of metformin in regulating bladder cancer cell proliferation and glycolysis [13]. In addition, metformin is reported to inhibit proliferative and migratory potentials in human primary VSMCs [14]. However, whether lncRNA-ATB is involved in metformin-induced VSMCs behaviors is unknown, which is specifically explored in this paper.

2. Patients and Methods

2.1. Case Collection. CHD (coronary heart disease) patients ($n = 50$) pathologically confirmed by coronary angiography in Beijing Jishuitan Hospital were recruited. During the same period, 50 healthy subjects undergoing physical examinations were recruited in the control group. Inclusion criteria of CHD patients were as follows: stable angina patients with at least one main coronary artery stenosis $> 80\%$. Exclusion criteria is as follows: (i) unstable angina or myocardial infarction patients; (ii) combined with other organic heart diseases; and (iii) combined with severe liver and kidney diseases, familial hypercholesterolemia, malignant tumors, or inflammatory diseases. 3 mL of venous blood was extracted from each subject. Sample collection was reviewed and approved by the hospital ethics committee, and every subject signed written informed consent.

2.2. Cell Culture of VSMCs. Human VSMCs were purchased from the National Infrastructure of Cell Line Resource. Cells were quickly taken out from liquid nitrogen tank and subjected to water bath at 37°C . Cells were suspended in 5–10 times the volume of Roswell Park Memorial Institute 1640 (RPMI 1640) (HyClone, South Logan, UT, USA) and centrifuged at $160 \times g$ for 5 min. The precipitant was resuspended in 1 mL of RPMI-1640 containing 10% fetal bovine serum (FBS) (Gibco, Rockville, MD, USA) for cell culture in a $5\% \text{CO}_2$ incubator at 37°C . VSMCs were induced with 10 mmol/L metformin for 24 h.

2.3. Cell Transfection. Overexpression plasmids and siRNAs were, respectively, provided by Genomeditech (Shanghai, China) and Ribobio (Guangzhou, China). 2×10^5 cells per well were inoculated in 6-well plates and cultured to 80% confluence. Subsequently, 1,750 μL of serum-free medium was replaced per well. Transfection plasmids (2 μg) and Lipofectamine 3000 (5 μL) (Invitrogen, Carlsbad, CA, USA) were, respectively, diluted in 125 μL of serum-free medium and let stand at room temperature for 5 min, followed by mixture of two solutions. The mixture was applied in each well. Fresh medium containing 10% FBS was replaced at 5 h.

2.4. Quantitative Real-Time Polymerase Chain Reaction (qRT-PCR). RNA extraction kit (ABI, Foster City, CA,

USA) was used for extracting total RNAs from tissues or cells, and their concentration and purity were measured by an ultraviolet spectrophotometer (Thermo Fisher, Waltham, MA, USA). Reverse transcription in a 20 μL system was conducted to obtain complementary deoxyribose nucleic acid (cDNA), which was subjected to qRT-PCR at 95°C predenaturation for 1 min, 40 cycles at 95°C for 15 s, and 60°C for 1 min. Relative levels of lncRNA-ATB, p53, and glyceraldehyde 3-phosphate dehydrogenase (GAPDH) were calculated by $2^{-\Delta\Delta\text{Ct}}$. GAPDH was the internal reference. Primer sequences were as follows: lncRNA-ATB forward, 5'-CTTCACCAGCACCCAGAGA-3' and reverse, 5'-AAGACAGAAAAACAGTTCCGAGTC-3'; p53 forward, 5'-TCAGTCTACCTCCCGCCATA-3' and reverse, 5'-TTACATCTCCCAAACATCCCT-3'; GAPDH forward, 5'-GGTGAAGGTCGGAGTCAACG-3' and reverse, 5'-CAAAGTTGTCATGGATGHACC-3'.

2.5. Cell Counting Kit-8 (CCK-8). Cells were inoculated in the 96-well plates at the density of 3×10^3 cells/well. Six replicates were prepared in each group. At day 0, 1, 2, and 3, 10 μL of CCK-8 solution (Dojindo, Kumamoto, Japan) was used for 1 h incubation, and optical density at 450 nm was measured.

2.6. Transwell Assay. Transwell chambers (8 μm) containing 200 μL of serum-free suspension (2×10^4 cells) were inserted in the 24-well plate where 600 μL of medium containing 10% FBS was applied in each well. After 24 h cell culture, transwell chambers were taken out. Cells in the bottom were subjected to methanol fixation for 15 min and crystal violet staining for 20 min. Migratory cells were counted in 5 randomly selected fields per sample. Transwell invasion assay was conducted using chambers that were precoated with 50 μL of diluted Matrigel (dilution in serum-free medium at 1:7).

2.7. RNA Binding Protein Immunoprecipitation Assay (RIP). EZMagna RIP kit (Millipore, Billerica, MA, USA) was used. Cells were lysed in RIPA and incubated at 4°C for 6 hours with magnetic beads conjugated with anti-Ago2 or anti-IgG. Subsequently, magnetic beads were washed and incubated with Protease K for removing proteins. The purified RNA was subjected to qRT-PCR.

2.8. Statistical Analysis. Statistical Product and Service Solutions (SPSS) 20.0 (IBM, Armonk, NY, USA) was adopted for statistical processing. Correlation in serum levels of lncRNA-ATB and p53 in CHD patients was assessed by Pearson correlation test. ROC curves were depicted for analyzing the potential of lncRNA-ATB in predicting the occurrence of CHD. Differences between groups were analyzed by the Student's t -test. A significant difference was set at $p < 0.05$.

3. Results

3.1. Serum Level of lncRNA-ATB Increases in CHD Patients. Compared with healthy subjects, serum level of lncRNA-

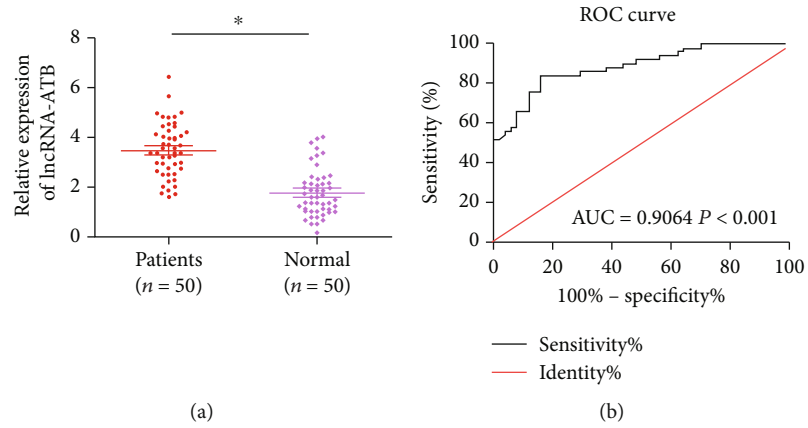


FIGURE 1: Serum level of lncRNA-ATB increases in CHD patients. (a) Serum level of lncRNA-ATB was higher in CHD patients than healthy subjects. (b) lncRNA-ATB could be used as a potential biomarker for predicting the occurrence of CHD.

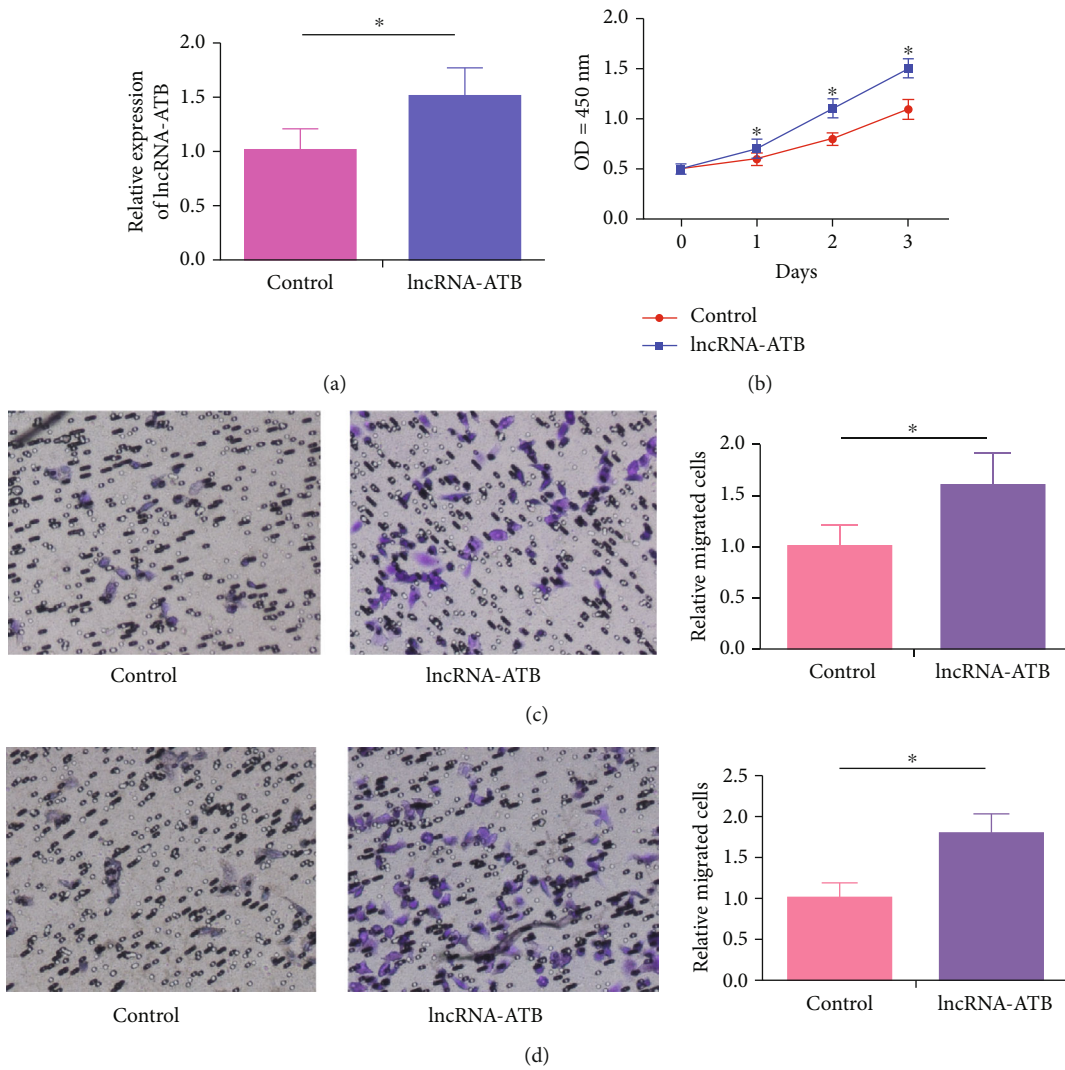


FIGURE 2: lncRNA-ATB triggers viability, migratory, and invasive abilities in VSMCs. (a) Transfection of pcDNA-lncRNA-ATB effectively upregulated lncRNA-ATB in VSMCs. (b) CCK-8 assay showed dose-dependently increased viability in VSMC overexpressing lncRNA-ATB. (c) Transwell assay showed enhanced migration in VSMC overexpressing lncRNA-ATB. (d) Transwell assay showed enhanced invasion in VSMC overexpressing lncRNA-ATB.

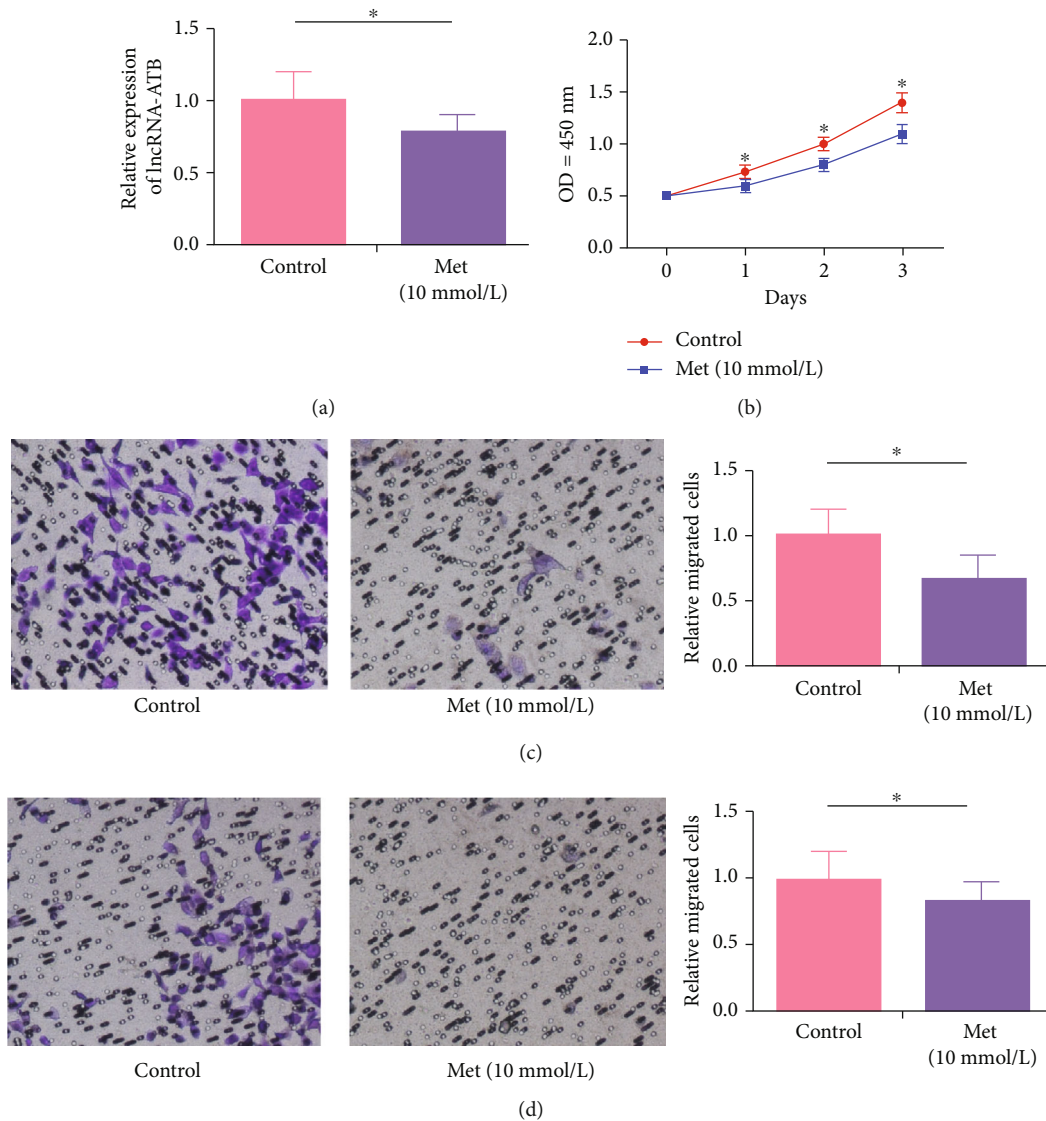


FIGURE 3: Metformin inhibits viability, migratory, and invasive abilities in VSMCs. (a) lncRNA-ATB was downregulated by metformin induction in VSMCs. (b) CCK-8 assay showed dose-dependently increased viability in metformin-induced VSMCs. (c) Transwell assay showed enhanced migration in metformin-induced VSMCs. (d) Transwell assay showed enhanced invasion in metformin-induced VSMCs.

ATB was higher in CHD patients (Figure 1(a)). To ascertain the potential of lncRNA-ATB as a biomarker for predicting the occurrence of CHD, ROC curves were depicted. The AUC was 0.9064, indicating that lncRNA-ATB exerted a certain diagnostic potential in CHD ($p < 0.001$, Figure 1(b)).

3.2. lncRNA-ATB Triggers Viability, Migratory, and Invasive Abilities in VSMCs. In vitro experiments were conducted in VSMCs to elucidate the potential role of lncRNA-ATB in the progression of CHD. Transfection of pcDNA-lncRNA-ATB remarkably upregulated lncRNA-ATB in VSMCs, verifying the pronounced transfection outcome (Figure 2(a)). The overexpression of lncRNA-ATB time-dependently enhanced cell viability in VSMCs (Figure 2(b)). Moreover, transwell assay showed that the overexpression of lncRNA-ATB increased the rates of migratory and invasive cells in

VSMCs, indicating the stimulated metastasis ability (Figures 2(c) and 2(d)).

3.3. Metformin Inhibits Viability, Migratory, and Invasive Abilities in VSMCs. We subsequently explored the potential influence of metformin on cell functions of VSMCs. After 10 mmol/L metformin induction for 24h, lncRNA-ATB was markedly downregulated in VSMCs (Figure 3(a)). Besides, metformin induction reduced viability and the rates of migratory and invasive cells in VSMCs (Figures 3(b) and 3(d)).

3.4. lncRNA-ATB Inhibits p53 Level. RIP assay showed that lncRNA-ATB was mainly enriched in anti-p53, indicating the interaction between lncRNA-ATB and p53 (Figure 4(a)). Compared with healthy subjects, serum level of p53 was lower in CHD patients (Figure 4(b)). Moreover,

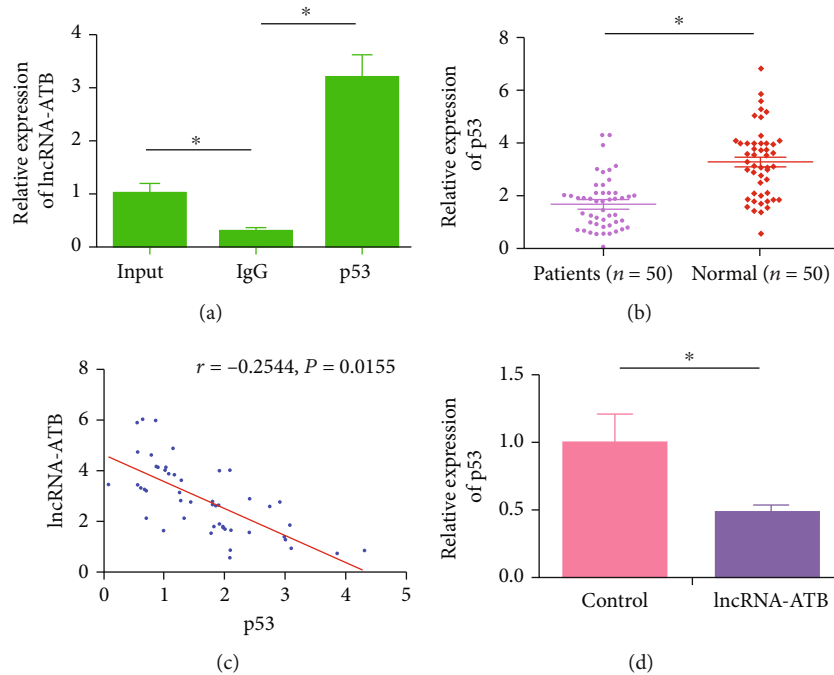


FIGURE 4: LncRNA-ATB inhibits p53 level. (a) RIP assay showed that lncRNA-ATB interacted with p53. (b) Serum level of p53 was lower in CHD patients than healthy subjects. (c) Pearson correlation analysis showed a negative correlation between serum levels of lncRNA-ATB and p53 in CHD patients. (d) Overexpression of lncRNA-ATB downregulated p53 in VSMCs.

serum level of lncRNA-ATB was negatively correlated to that of p53 in CHD patients ($r = -0.2544, p = 0.0155$, Figure 4(c)). As expected, the overexpression of lncRNA-ATB could downregulate p53 in VSMCs, further supporting their negative interaction (Figure 4(d)). The above data demonstrated that lncRNA-ATB was negatively interacted with p53, and they were both involved in CHD progression.

3.5. Regulatory Effects of lncRNA-ATB on VSMCs Require the Interaction with p53. To further verify that both lncRNA-ATB and p53 were involved in the regulatory mechanism of metformin on VSMCs, p53 level in metformin-induced VSMCs was detected by qRT-PCR, which was remarkably upregulated (Figure 5(a)). It is suggested that metformin could stimulate p53 activation. CCK-8 assay uncovered that the overexpression of p53 in VSMCs could reverse the effect of lncRNA-ATB on stimulating VSMC proliferation (Figure 5(b)). Identically, p53 also abolished the promotive effects of highly expressed lncRNA-ATB on VSMC metastasis (Figures 5(c) and 5(d)). To sum up, metformin activated the p53 expression by downregulating lncRNA-ATB, thereafter inhibiting proliferative, migratory, and invasive abilities in VSMCs.

4. Discussion

VSMCs are responsible for regulating blood flow, balancing vessel wall elasticity, and tension [15, 16]. Under the normal circumstance, VSMCs lack the abilities to proliferate and migrate. Once vascular endothelium damages, VSMCs rapidly acquire the capacities of proliferation, metastasis, and

release of extracellular matrix under the stimuli of multiple molecules [17]. Marx et al. [18] and Uemura et al. [19] uncovered that the main component of angiogenesis intima is the migrated VSMCs from the tunica media, and they will continue to proliferate in the neointima. Overproliferated VSMCs will develop to vessel wall thickening and lumen stenosis. Excessive proliferated and migrated VSMCs are almost involved in every process of intimal neoplasia, atherosclerosis, and restenosis [20, 21]. Therefore, inhibition of overproliferated VSMCs contributes to alleviate the progression of atherosclerosis.

A growing number of studies have reported that lncRNAs are able to regulate cell functions of VSMCs. lncRNA TUG1 induces hypertension progression via mediating proliferative and migratory abilities in VSMCs [22]. lncRNA-ATB is activated by TGF- β , with the transcription length of 2.4 kb [23]. In renal cell carcinoma (RCC) samples, lncRNA-ATB is upregulated, especially metastatic ones. Silence of lncRNA-ATB by siRNA transfection remarkably blocks EMT and induces apoptosis [24]. Furthermore, high level of lncRNA-ATB predicts poor prognosis in RCC patients as an independent prognostic factor [25]. Consistently, our analysis showed higher serum level of lncRNA-ATB in CHD patients, and lncRNA-ATB may become a potential diagnostic factor for CHD. In vitro experiments subsequently proved that lncRNA-ATB was able to stimulate VSMCs to proliferate and metastasize. Meanwhile, metformin induction time-dependently decreased viability in VSMCs overexpressing lncRNA-ATB. We believed that metformin inhibited VSMC viability by downregulating lncRNA-ATB.

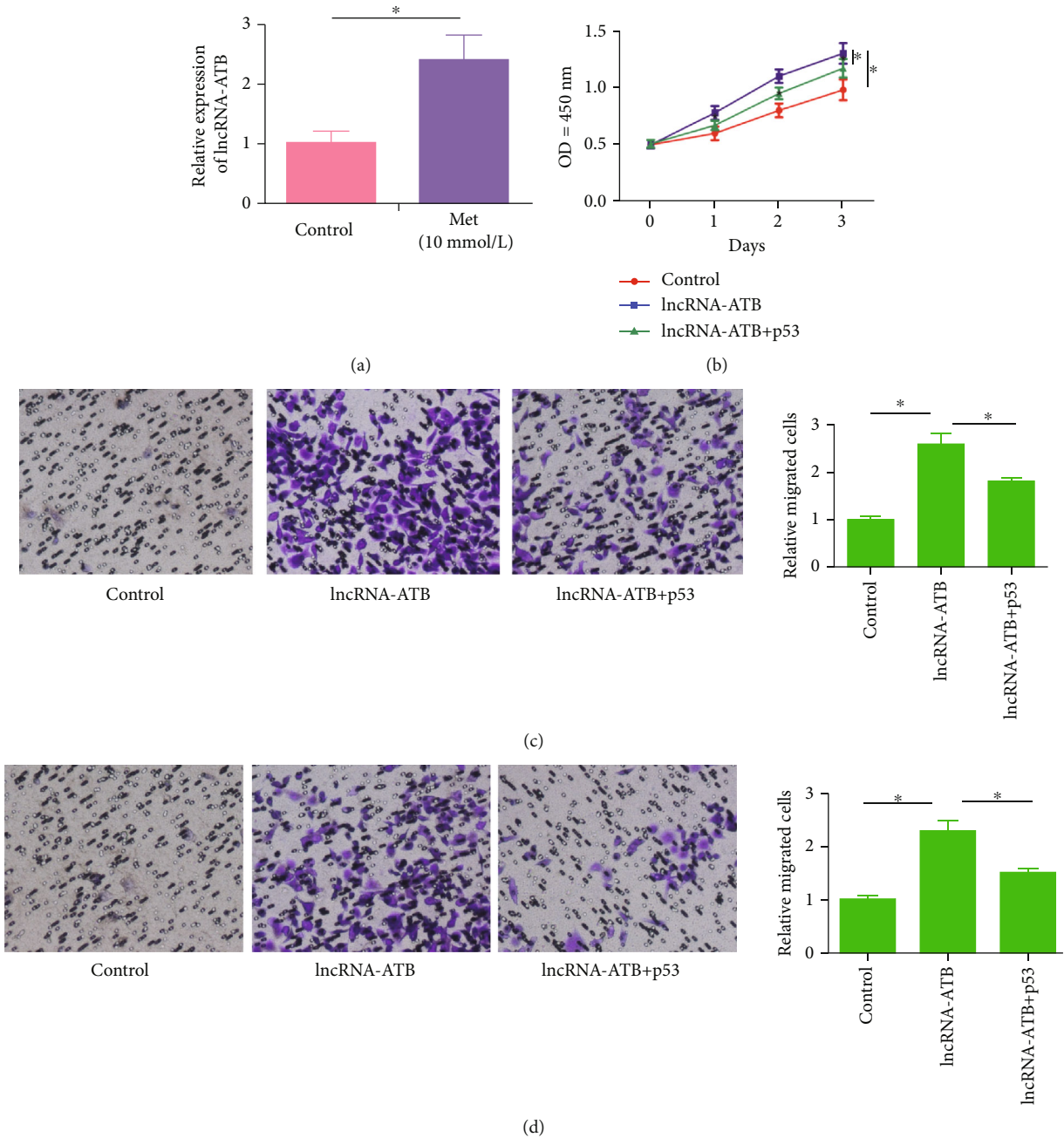


FIGURE 5: Regulatory effects of lncRNA-ATB on VSMCs require the interaction with p53. (a) P53 was upregulated by metformin induction in VSMCs. (b) Overexpression of p53 abolished the role of lncRNA-ATB in promoting VSMC proliferation. (c) Overexpression of p53 abolished the role of lncRNA-ATB in promoting VSMCs migration. (d) Overexpression of p53 abolished the role of lncRNA-ATB in promoting VSMC invasion.

P53 is a widely analyzed transcription factor, which is capable of regulating cell cycle progression, cell apoptosis, autophagy, and other cell functions [26, 27]. Tripathi et al. [28] found out that p53 activity is weakened by silencing MALAT1 in HeLa, U2OS, and WI-38-VA13 cancer cell lines, suggesting that p53 is the downstream target of MALAT1. Our findings revealed a decline in p53 level by the overexpression of lncRNA-ATB in VSMCs. In previous studies, lncRNA usually bind to the RNA binding protein thus to regulate the expression level of target

genes. In our research, we find that ATB could directly bind to p53 and thus regulate the expression level. In a recent study, LINC01554 maintained the high G3BP2 expression in ESCC by protecting G3BP2 from degradation through ubiquitination also edified us the mechanism that lncRNA could bind to target gene and regulate that [29]. In addition, metformin induction remarkably upregulated p53 in VSMCs. Based the above results, it is speculated that metformin activated p53 by downregulating lncRNA-ATB, thereby exerting its inhibitory effects on

proliferative, migratory and invasive abilities in VSMCs. In summary, this research slightly uncovers the interaction of metformin, ATB, and p53 by in vitro assay. However, the in vivo assay should be done to deeply explore the role of ATB in CHD.

5. Conclusion

Metformin induction inhibits proliferative, migratory, and invasive abilities in VSMCs by downregulating lncRNA-ATB, which may be related to p53 activation. This study provides innovative insights into the treatment of vascular diseases.

Data Availability

The datasets used and analyzed during the current study are available from the corresponding author on reasonable request.

Conflicts of Interest

The authors declared no conflict of interest.

References

- [1] M. Huarte, M. Guttman, D. Feldser et al., "A large intergenic noncoding RNA induced by p53 mediates global gene repression in the p53 response," *Cell*, vol. 142, no. 3, pp. 409–419, 2010.
- [2] M. R. Bennett, S. Sinha, and G. K. Owens, "Vascular smooth muscle cells in atherosclerosis," *Circulation Research*, vol. 118, no. 4, pp. 692–702, 2016.
- [3] Y. Lu, Y. Wang, T. Weng et al., "Association between metformin use and coronary artery calcification in type 2 diabetic patients," *Journal Diabetes Research*, vol. 2019, article 9484717, 8 pages, 2019.
- [4] A. Sainio, P. Takabe, S. Oikari et al., "Metformin decreases hyaluronan synthesis by vascular smooth muscle cells," *Journal of Investigative Medicine*, vol. 68, no. 2, pp. 383–391, 2020.
- [5] I. Martianov, A. Ramadass, B. A. Serra, N. Chow, and A. Akoulitchev, "Repression of the human dihydrofolate reductase gene by a non-coding interfering transcript," *Nature*, vol. 445, no. 7128, pp. 666–670, 2007.
- [6] F. X. Guo, Q. Wu, P. Li et al., "The role of the lncRNA-FA2H-2-MLKL pathway in atherosclerosis by regulation of autophagy flux and inflammation through mTOR-dependent signaling," *Cell Death and Differentiation*, vol. 26, no. 9, pp. 1670–1687, 2019.
- [7] N. Fu, S. X. Zhao, L. B. Kong et al., "lncRNA-ATB/microRNA-200a/beta-catenin regulatory axis involved in the progression of HCV-related hepatic fibrosis," *Gene*, vol. 618, pp. 1–7, 2017.
- [8] X. Liu, H. Chen, W. Kong et al., "Down-regulated long non-coding RNA-ATB in preeclampsia and its effect on suppressing migration, proliferation, and tube formation of trophoblast cells," *Placenta*, vol. 49, pp. 80–87, 2017.
- [9] Y. Liu, Y. Li, Q. Xu et al., "Long non-coding RNA-ATB promotes EMT during silica-induced pulmonary fibrosis by competitively binding miR-200c," *Biochimica et Biophysica Acta - Molecular Basis of Disease*, vol. 1864, no. 2, pp. 420–431, 2018.
- [10] J. Qiu, Y. Chen, G. Huang, Z. Zhang, L. Chen, and N. Na, "Transforming growth factor-beta activated long non-coding RNA ATB plays an important role in acute rejection of renal allografts and may impact the postoperative pharmaceutical immunosuppression therapy," *Nephrology (Carlton)*, vol. 22, no. 10, pp. 796–803, 2017.
- [11] B. Yue, S. Qiu, S. Zhao et al., "lncRNA-ATB mediated E-cadherin repression promotes the progression of colon cancer and predicts poor prognosis," *Journal of Gastroenterology and Hepatology*, vol. 31, no. 3, pp. 595–603, 2016.
- [12] S. J. Shi, L. J. Wang, B. Yu, Y. H. Li, Y. Jin, and X. Z. Bai, "lncRNA-ATB promotes trastuzumab resistance and invasion-metastasis cascade in breast cancer," *Oncotarget*, vol. 6, no. 13, pp. 11652–11663, 2015.
- [13] T. Li, X. Sun, and X. Jiang, "UCA1 involved in the metformin-regulated bladder cancer cell proliferation and glycolysis," *Tumour Biology*, vol. 39, no. 6, 2017.
- [14] B. Hao, Y. Xiao, F. Song et al., "Metformin-induced activation of AMPK inhibits the proliferation and migration of human aortic smooth muscle cells through upregulation of p53 and IFI16," *International Journal of Molecular Medicine*, vol. 41, no. 3, pp. 1365–1376, 2018.
- [15] S. M. Schwartz, M. B. Stemerman, and E. P. Benditt, "The aortic intima. II. Repair of the aortic lining after mechanical denudation," *The American Journal of Pathology*, vol. 81, no. 1, pp. 15–42, 1975.
- [16] J. A. Vita, C. B. Treasure, E. G. Nabel et al., "Coronary vasomotor response to acetylcholine relates to risk factors for coronary artery disease," *Circulation*, vol. 81, no. 2, pp. 491–497, 1990.
- [17] V. Schachinger, M. B. Britten, M. Elsner, D. H. Walter, I. Scharrer, and A. M. Zeiher, "A positive family history of premature coronary artery disease is associated with impaired endothelium-dependent coronary blood flow regulation," *Circulation*, vol. 100, no. 14, pp. 1502–1508, 1999.
- [18] S. O. Marx, H. Totary-Jain, and A. R. Marks, "Vascular smooth muscle cell proliferation in restenosis," *Circulation. Cardiovascular Interventions*, vol. 4, no. 1, pp. 104–111, 2011.
- [19] Y. Uemura, R. Shibata, K. Ohashi et al., "Adipose-derived factor CTRP9 attenuates vascular smooth muscle cell proliferation and neointimal formation," *The FASEB Journal*, vol. 27, no. 1, pp. 25–33, 2013.
- [20] E. Caglayan, M. Vantler, O. Leppänen et al., "Disruption of Platelet-Derived Growth Factor-Dependent Phosphatidylinositol 3-Kinase and Phospholipase C γ 1 Activity Abolishes Vascular Smooth Muscle Cell Proliferation and Migration and Attenuates Neointima Formation In Vivo," *Journal of the American College of Cardiology*, vol. 57, no. 25, pp. 2527–2538, 2011.
- [21] J. D. Stone, A. W. Holt, J. R. Vuncannon, J. J. Brault, and D. A. Tulis, "AMP-activated protein kinase inhibits transforming growth factor-beta-mediated vascular smooth muscle cell growth: implications for a Smad-3-dependent mechanism," *American Journal of Physiology. Heart and Circulatory Physiology*, vol. 309, no. 8, pp. H1251–H1259, 2015.
- [22] L. Shi, C. Tian, L. Sun, F. Cao, and Z. Meng, "The lncRNA TUG1/miR-145-5p/FGF10 regulates proliferation and migration in VSMCs of hypertension," *Biochemical and Biophysical Research Communications*, vol. 501, no. 3, pp. 688–695, 2018.
- [23] T. Saito, J. Kurashige, S. Nambara et al., "A long non-coding RNA activated by transforming growth factor- β is an independent prognostic marker of gastric cancer," *Annals of Surgical Oncology*, vol. 22, Supplement 3, pp. 915–S922, 2015.

- [24] J. Xiong, Y. Liu, L. Jiang, Y. Zeng, and W. Tang, "High expression of long non-coding RNA lncRNA-ATB is correlated with metastases and promotes cell migration and invasion in renal cell carcinoma," *Japanese Journal of Clinical Oncology*, vol. 46, no. 4, pp. 378–384, 2016.
- [25] J. J. Qi, Y. X. Liu, and L. Lin, "High expression of long non-coding RNA ATB is associated with poor prognosis in patients with renal cell carcinoma," *European Review for Medical and Pharmacological Sciences*, vol. 21, no. 12, pp. 2835–2839, 2017.
- [26] T. Riley, E. Sontag, P. Chen, and A. Levine, "Transcriptional control of human p53-regulated genes," *Nature Reviews. Molecular Cell Biology*, vol. 9, no. 5, pp. 402–412, 2008.
- [27] K. T. Bieging and L. D. Attardi, "Deconstructing p53 transcriptional networks in tumor suppression," *Trends in Cell Biology*, vol. 22, no. 2, pp. 97–106, 2012.
- [28] V. Tripathi, Z. Shen, A. Chakraborty et al., "Long noncoding RNA MALAT1 controls cell cycle progression by regulating the expression of oncogenic transcription factor B-MYB," *PLoS Genetics*, vol. 9, no. 3, 2013.
- [29] Y. Zheng, J. Wu, R. Deng et al., "G3BP2 regulated by the lncRNA LINC01554 facilitates esophageal squamous cell carcinoma metastasis through stabilizing HDGF transcript," *Oncogene*, 2021.

Research Article

MiR-218 Promotes Adriamycin-Induced H9C2 Apoptosis by Inhibiting Stress-Associated Endoplasmic Reticulum Protein 1

Qinghua Chen,¹ Gang Chen,² and Shuofang Zhao ³

¹Department of Cardiology, People's Hospital of Danzhou City, Danzhou, China

²Department of Gynecology and Obstetrics, The Public Health Clinical Center of Chengdu, Chengdu, China

³Guangdong Academy of Medical Sciences and Guangdong Provincial People's Hospital, Guangzhou, China

Correspondence should be addressed to Shuofang Zhao; shuofang9@163.com

Received 2 November 2021; Accepted 11 December 2021; Published 4 January 2022

Academic Editor: Simona Pichini

Copyright © 2022 Qinghua Chen et al. This is an open access article distributed under the Creative Commons Attribution License, which permits unrestricted use, distribution, and reproduction in any medium, provided the original work is properly cited.

Objective. Adriamycin is a clinically important chemotherapeutic drug, but its use is restricted due to its myocardial toxicity. Therefore, it is especially important to explore the toxicity mechanism of Adriamycin (ADR) to cardiomyocytes. **Methods.** The myocardial toxicity model of ADR was constructed in vitro, and the effect of miR-218 inhibitor and sh-Serp1 on the activity of H9C2 cells induced by ADR was detected by MTT method. Also, flow cytometry, real-time polymerase chain reaction (RT-PCR), and TUNEL staining were used to detect the cell apoptosis. The activity of LDH was detected by colorimetry, and the interaction of miR-218 with Serp1 was detected by double-luciferase reporter gene assay. Western blotting technique was used to detect the expression level of caspase3 and p38 MAPK signal pathway. **Results.** miR-218 inhibitor can obviously inhibit ADR-induced decrease in cell activity of H9C2 cells, inhibit cell apoptosis, and inhibit p38 MAPK signaling pathway activation. Conversely, sh-Serp1 aggravated the decrease in H9C2 cell activity and promoted cell apoptosis. **Conclusion.** Upregulation of miR-218 expression will promote ADR-induced apoptosis of H9C2 cells. At the same time, we confirmed that the mechanism by which miR-218 promotes myocardial apoptosis was through the Serp1/p38 MAPK/caspase-3 signaling pathway.

1. Introduction

The discovery of malignant tumor chemotherapy drugs—"anthracycline antibiotics"—is a major success in the history of cancer treatment, especially for the treatment of pediatric tumors. More than 50% of the survivors who had suffered from cancer in childhood had been treated with onion ring antibiotics. And with the use of this type of chemotherapy drugs, the 5-year survival rate of pediatric tumors has increased from about 30% in the sixties to the current 70%-80% [1, 2]. However, the clinical use of ADR is limited by the cardiac toxic side effects it can cause, mainly manifested as congestive cardiomyopathy [3]. At the end of the 1970s, the first retrospective clinical study confirmed that cardiac dysfunction can be directly attributed to the repeated accumulation of ADR. The changes in heart function caused by ADR are similar to dilated cardiomyopathy, and once the disease progresses, the prognosis is usually very

poor, often lethal, and the current treatment methods seem to improve the prognosis. Although there is already a lot of evidence to give hypotheses about the mechanism of ADR's cardiac toxic side effects from different aspects, people still do not fully understand its precise cause. The cell death mechanism is considered to be an important mechanism for ADR-induced cardiomyopathy. Many in vivo and external experiments over the past decades have shown that the cardiac toxicity caused by ADR is related to the apoptosis or necrosis of myocardial cells [4, 5].

In recent years, miRNA has been a hot spot in medical research. miRNA is a single-stranded noncoding small RNA composed of 21-25 nucleotides, which mainly mediates the posttranscriptional degradation of target genes or inhibits their translation, thereby affecting a variety of pathophysiological processes including development, differentiation, proliferation, and apoptosis in the course of life [6, 7]. miRNAs are widely distributed in the genomes of animals

and plants, and their expression is highly conservative, time-series, and tissue-specific. It can regulate about 30% of human protein-related genes. Therefore, changes in miRNA expression levels directly participate in important pathophysiological processes that regulate the occurrence and development of many cardiovascular diseases (CVD), such as myocardial hypertrophy, angiogenesis, arrhythmia, myocardial ischemia, myocardial apoptosis, and myocardial fibrosis [8, 9]. At present, multiple miRNAs have been confirmed to be involved in the process of myocardial apoptosis. Some studies have found that miR-1 expression is increased in ischemic cardiomyocytes and plays a key role in apoptosis. Its expression level is proportional to the degree of heart injury [10]. Another study showed that miR-1 and miR-133 can regulate oxidative stress-induced apoptosis in rat cardiomyocytes, miR-1 promotes apoptosis, and miR-133 inhibits apoptosis [11]. However, we still do not know the specific role of miRNA regulation in cardiovascular disease. We need to further study the disease-associated miRNAs and the target genes, so as to clarify the effects of miRNAs on CVD. Whether these miRNAs are upregulated or downregulated, they may become new molecular targets for the treatment of CVD.

Serp1, as one of the important chaperone proteins of unfolded protein response that can alleviate endoplasmic reticulum stress damage, has been shown to play a crucial role in alleviating tissue apoptosis caused by endoplasmic reticulum stress [12]. However, the role and mechanism of Serp1 in CVD are still unclear. Therefore, in this study, we will explore its role in ADR-induced apoptosis of cardiomyocytes.

MAPKs are key apoptosis regulating proteins that can transduce various extracellular signals into intracellular pathophysiological processes. There are three main enzymes in the MAPK family, including extracellular signal-regulated kinase (ERK), c-Jun NH2-terminal kinase, and p38 MAPK. p38 MAPK, a serine/threonine enzyme, can be activated by various environmental stimuli. A large number of studies have confirmed that p38 MAPK activation may be related to cardiomyocyte apoptosis [13]. Therefore, inhibiting the activation of p38 MAPK has a good therapeutic effect on cardiovascular disease and can reduce myocardial cell necrosis and apoptosis, inhibit downstream caspase-3 activation, and improve heart function. Caspases are an important member of the aspartate-specific cysteine protease family and are widely expressed in various mammalian cells. Caspase-3, as a basic agonist of apoptosis and a crucial effector, plays a key role in performing the intrinsic apoptotic protease cascade and the external apoptotic pathway [14]. This indicates that p38 MAPK plays a crucial role in cardiomyocyte apoptosis. Therefore, we speculate that p38 MAPKs also have a similar regulatory effect on ADR-induced cardiomyocyte apoptosis.

2. Materials and Methods

2.1. Cell Culture. Rat H9C2 cells were purchased from the American type culture collection (ATCC, Manassas, VA, USA). The cell culture medium was Dulbecco's modified

eagle medium (DMEM, Life Technology, Wuhan, China) containing 10% fetal bovine serum (FBS, Life Technology, Wuhan, China) and 1% penicillin (Life Technology, Wuhan, China). The cells will be passaged 1-2 times before transfection to ensure the cells grow vigorously. Approximately 12 hours before transfection, cells were passaged from culture flasks at 80% density and plated into culture dishes (Life Technology, Wuhan, China).

2.2. Transfection and Cell Processing. The design and synthesis of miR-218 inhibitor, inhibitor NC, shRNA Serp1, and shRNA-NC were completed by Shanghai Gene Pharma. H9C2 cells were plated in 12-well plates at a density of $3-5 \times 10^5$ /mL and transfected after 48 hours of culture. Before transfection, the cell culture medium was replaced with 900 μ L of complete DMEM medium (without antibiotics). Next, we transfected cells according to the Lipofectamine²⁰⁰⁰ instructions (Gene Pharma, Shanghai, China). After the transfection, the cells were transferred to a 37°C, 5% CO₂ incubator for 8 hours, and then, the culture medium was replaced with fresh complete DMEM culture medium and placed in the incubator for 48 hours. According to literature reports, we selected 1 μ M ADR treatment model group. The control group used phosphate-buffered saline (PBS) for treatment.

2.3. MTT (3-(4,5-Dimethylthiazol-2-Yl)-2,5-Diphenyl Tetrazolium Bromide) Experiment. The cultured H9C2 cells were seeded in 96-well culture plates, and after transfection and 1 μ M ADR treatment, MTT solution (R&D Systems, Minneapolis, MN, USA) was added to each well. The cells continued to incubate for 4 hours in the incubator, then the supernatant of the 96-well plate was carefully discarded. 150 μ L dimethyl sulfoxide (DMSO) (R&D Systems, Minneapolis, MN, USA) was added to each well and shaken for 10 minutes to fully melt the crystals. The activity of myocardial cells was detected, and the absorbance value of each well was measured by enzyme-linked immunoassay (Thermo Fisher Scientific, Waltham, MA, USA).

2.4. Lactate Dehydrogenase (LDH) Activity. After centrifugation, the supernatant was transferred to the new EP tube. 25 μ L matrix buffer and 5 μ L coenzyme I solution were added to the EP tube. After mixing, the supernatant was bathed at 37°C for 15 minutes, then 25 μ L 2, 4-dinitrobenzene hydrazine was added, 37°C water bath for 15 minutes after blending. 25 μ L, 0.4 mol/L sodium hydroxide solution was blended and placed 5 minutes at room temperature and 450 nm wavelength determination of optical density (OD) value. The LDH activity was calculated according to the formula (Jian Cheng, Nanjing, China).

2.5. Western Blotting (WB) Technology. H9C2 cells were lysed by radioimmunoprecipitation assay (RIPA) lysate (Camilo Biological, Nanjing, China) containing phenylmethylsulfonyl fluoride (PMSF) to extract proteins. 30 μ g protein in each group was separated by 10% sodium dodecyl sulphate-polyacrylamide gel electrophoresis (SDS-PAGE). Then, a polyvinylidene difluoride (PVDF; Thermo Fisher Scientific, Waltham, MA, USA) membrane was used to

TABLE 1: RT-PCR primers.

Gene name	Forward (5' > 3')	Reverse (5' > 3')
MiR-218	AGGGTTGTGCTTGATCTAA	GTTGTGGTTGGTTGGTTTGT
Serp1	CCCTGGTTATTGGCTCTCT	ACTTCACATGCCCATCCT
Bax	GAGGTCTTCTCCGTGTGG	GATCAGCTCGGGCACTTT
Bcl-2	GTCGCTACCGTCGTGACTTC	CAGACATGCACCTACCCAGC
Caspase3	ATGGAGAACAACAAAACCTCAGT	TTGCTCCCATGTATGGTCTTTAC
Caspase9	TCCTGGTACATCGAGACCTTG	AAGTCCCTTTCGCAGAAACAG
GAPDH	ACAACCTTTGGTATCGTGAAGG	GCCATCACGCCACAGTTTC

RT-PCR, quantitative reverse-transcription polymerase chain reaction.

transfer the separated protein, then, blocked with 5% skim milk, incubated the primary antibody (Caspase3, Abcam, Cambridge, MA, USA, Rabbit, 1:1000; Serp1, Abcam, Cambridge, MA, USA, Mouse, 1:2000; p38, Abcam, Cambridge, MA, USA, Rabbit, 1:1000; P-p38, Abcam, Cambridge, MA, USA, Mouse, 1:2000; GAPDH, Abcam, Cambridge, MA, USA, Mouse, 1:5000) at 4°C overnight; the next day, added with secondary antibodies (goat anti-rabbit IgG antibody, Yifei Xue Biotechnology, Nanjing, China, 1:2000) and incubated at room temperature for 1 hour. The enhanced chemiluminescence (ECL) technology (Thermo Fisher Scientific, Waltham, MA, USA) was used to develop immunoblots, and GAPDH was used as an internal reference.

2.6. RNA Isolation and Real-Time Polymerase Chain Reaction (RT-PCR). After corresponding treatment, the H9C2 cells were washed twice with phosphate-buffered saline (PBS), 500 μ L TRIzol reagent (Thermo Fisher Scientific, Waltham, MA, USA) was added to each well of the 12-well plate, and total RNA was extracted according to the kit instructions, measured the RNA concentration by ultraviolet absorption method, and read the absorbance at 260 nm and 280 nm of the spectrophotometer. If the A260/280 ratio of the RNA solution was in the range of 1.6-2.0, the extracted RNA can be reverse transcribed. The reaction conditions were as follows: 25°C, 10 minutes, 37°C, 120 minutes, 85°C, 5 minutes. Next, we used the steps of Applied Biosystems' SYBR Green PCR Master Mix kit (R&D Systems, Minneapolis, MN, USA) for polymerase chain reaction. GAPDH was considered as an internal reference for mRNA. The analysis of experimental results uses the $2^{-\Delta\Delta Ct}$ method. Primer sequence is shown in Table 1.

2.7. TUNEL Staining. Place the sterile slides in a 24-well plate, and H9C2 cells were seeded onto the coverslip of the 24-well plate according to the culture method described above and placed in a cell culture box for cultivation. After the H9C2 cells received the corresponding treatment, the cell slides were washed three times with prechilled PBS for 5 minutes each time. 200 μ L of 4% paraformaldehyde (Jian Cheng, Nanjing, China) was added to each well to fix the cardiomyocytes on the slide and fixed at room temperature for 10 minutes. Then, the H9C2 cells were washed twice with PBS for 5 minutes each time and treated the slides with Proteinase K working solution (R&D Systems, Minneapolis, MN, USA) for another 20

minutes. After washing the H9C2 cells twice with PBS, the TUNEL reaction mixture (R&D Systems, Minneapolis, MN, USA) was added dropwise to the slide and incubated for 1 hour at room temperature. Then, it was washed twice with PBS, and the nuclei were stained with DAPI reagent (Elabscience, Wuhan, China) in the dark room for 10 minutes, finally, observed under a fluorescence microscope (R&D Systems, Minneapolis, MN, USA).

2.8. Double-Luciferase Reporter Gene Assay. Luciferase plasmids (R&D Systems, Minneapolis, MN, USA) containing wild-type and mutant Serp1 mRNA 3'UTR were cotransfected with miR-218 mimics and miR-218 NC into 293 T cells (ATCC, Manassas, VA, USA), respectively. After transfection for 48 hours, 293 T cells were lysed, and the firefly luciferase activity and Renilla luciferase activity were detected, respectively.

2.9. Annexin V-FITC/PI Double-Staining Flow Cytometry to Detect Apoptosis Rate. After the H9C2 cells were treated according to the experimental design, the cells were digested with trypsin (Sinopharm Chemical Reagent, Shanghai, China) without EDTA (ethylenediaminetetraacetic acid). After centrifugation, the cells were washed twice with prechilled PBS. After centrifugation again, the supernatant was discarded, and 500 μ L of 1 \times binding buffer (Sinopharm Chemical Reagent, Shanghai, China) was added to resuspend the cells. After adding 5 μ L fluorescein 5-isothiocyanate (FITC) and mixed well, such was incubated at room temperature in the dark for 15 minutes. Then, 3 μ L propidium iodide (PI) was added to mix and incubate for 5 minutes in the dark. Finally, the cells were transferred to a sample tube for instrumental analysis.

2.10. Statistical Analysis. GraphPad Prism21.0 (La Jolla, CA, USA) was used to perform statistical analysis on the data. The experimental data was expressed as mean \pm standard deviation (mean \pm SD). The comparison of the two groups of data was performed by independent sample *t*-test. Analysis of variance was used for comparison among multiple groups. Take $p < 0.05$ as the standard of significant difference.

3. Results

3.1. ADR Induces Apoptosis of H9C2 Cells. According to previous reports in the literature, excessive ADR in the human

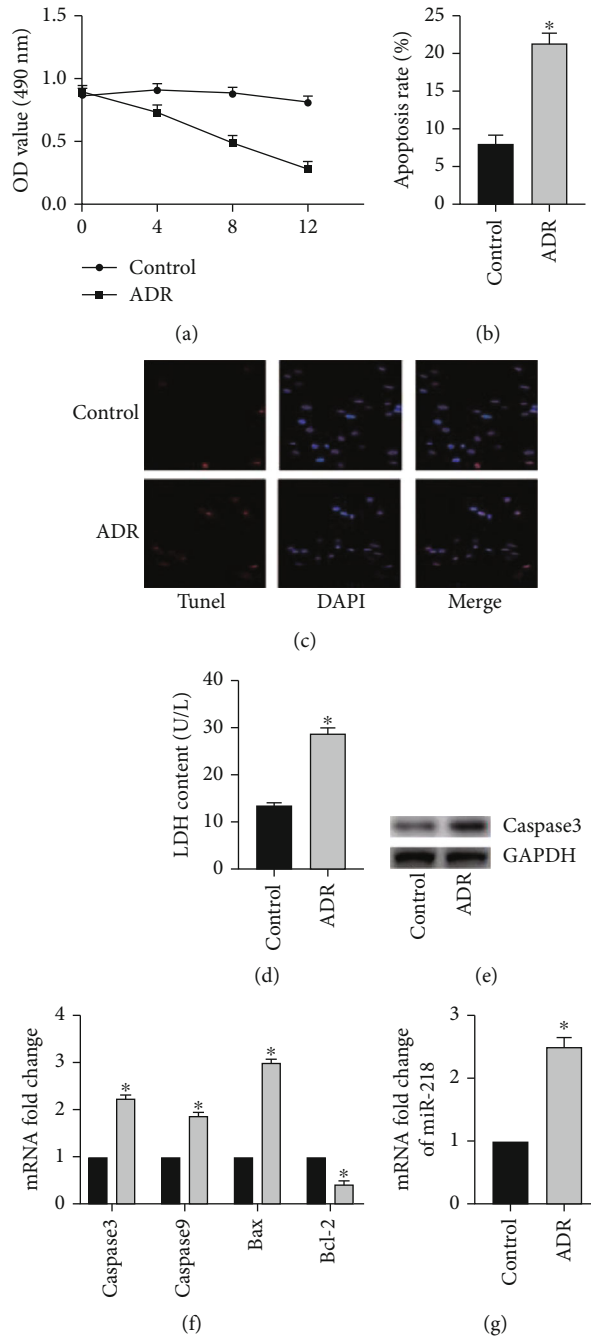


FIGURE 1: ADR induces apoptosis of H9C2 cells. (a) The cell activity was detected by MTT method, $n = 6$. (b) The apoptosis level of cell was detected by flow cytometry, $n = 3$. (c) TUNEL staining, $n = 3$. (d) The activity of LDH detected by the colorimetry method, $n = 3$. (e) The protein expression of caspase3 was detected by Western blot, $n = 3$. (f) The mRNA level of caspase3, caspase9, Bax, and Bcl-2 was detected by RT-PCR, $n = 3$. (g) The mRNA level of miR-218 was detected by RT-PCR, $n = 3$ (“*” versus the control group, $p < 0.05$).

body activates exogenous and endogenous apoptosis pathways, thereby inducing cardiomyocyte apoptosis. In order to test the success of the in vitro model, we first measured the cell activity of two groups by MTT (Figure 1(a)). As a result, it was found that after treatment of H9C2 cells with $1 \mu\text{M}$ ADR, the cell activity decreased obviously with the incubation time. Immediately, we used Annexin V for FITC labeling and flow cytometry to detect the apoptosis rate (Figure 1(b)). The test results found that compared with the control group, the percentage of Annexin V-FITC-

positive cells in H9C2 cells after 12 hours of ADR treatment increased obviously. At the same time, TUNEL staining also obtained similar results (Figure 1(c)). Subsequently, we found that after ADR treatment of H9C2 cells, the LDH content in the cell supernatant was obviously increased, confirming that ADR treatment of H9C2 cells would induce increased cytotoxicity (Figure 1(d)). Next, we examined the key molecule caspase3 in the apoptosis pathway and found that the expression of caspase3 protein in the ADR group was obviously increased (Figure 1(e)). At the same time,

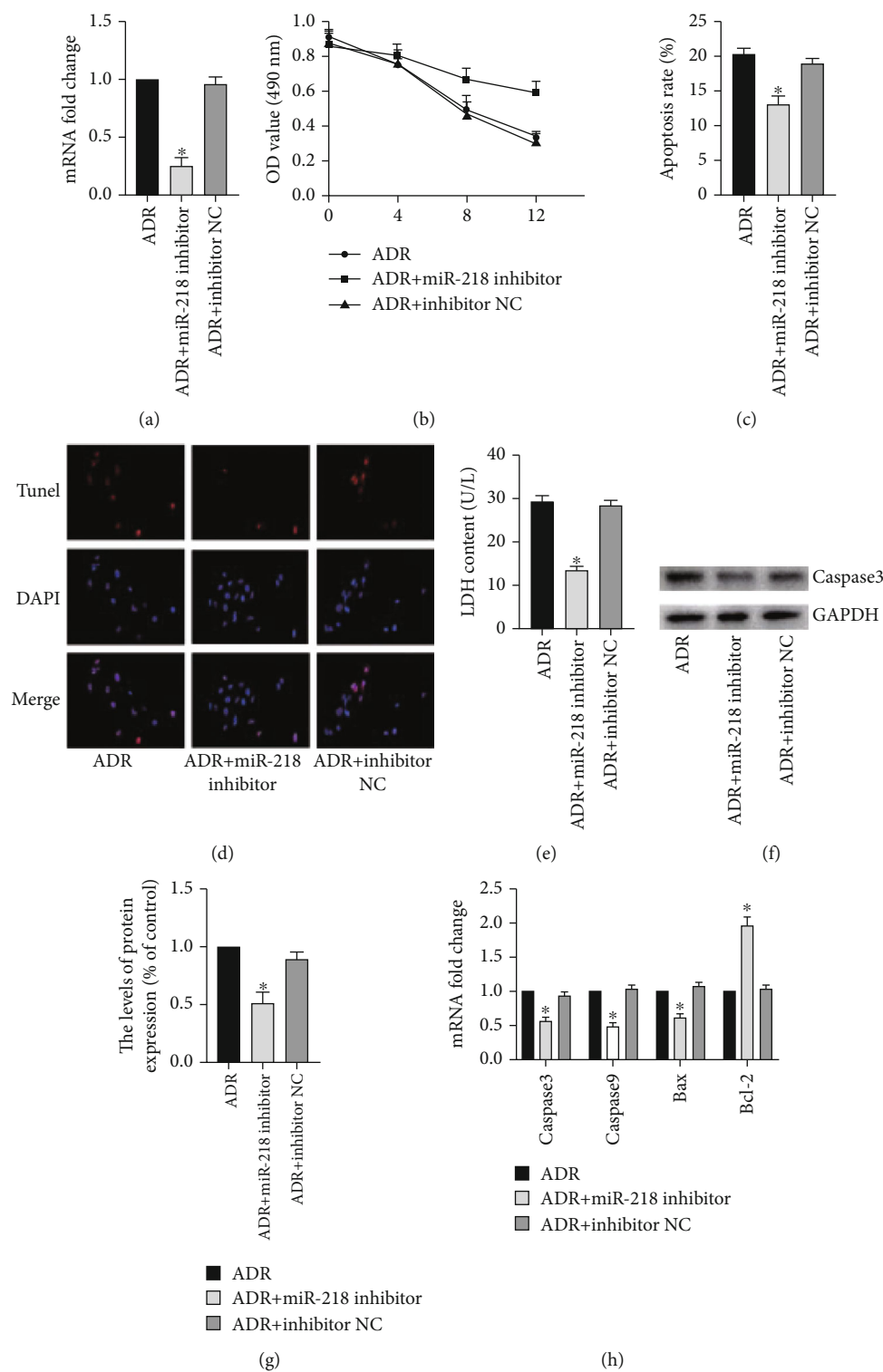


FIGURE 2: Knocking down miR-218 expression can alleviate ADR-induced apoptosis in H9C2 cells. (a) The mRNA level of miR-218 was detected by RT-PCR. (b) The cell activity was detected by MTT method, $n = 6$. (c) The apoptosis level of cell was detected by flow cytometry, $n = 3$. (d) TUNEL staining, $n = 3$. (e) the activity of LDH detected by the colorimetry method, $n = 3$. (f) The protein expression of caspase3 was detected by Western blot. (g) Gray value analysis of protein strips, $n = 3$. (h). The mRNA level of caspase3, caspase9, Bax, and Bcl-2 was detected by RT-PCR, $n = 3$ (“*” versus the ADR group, $p < 0.05$).

RT-PCR results also found that the ADR group caspase3, caspase9, and Bax also increased obviously at the transcription level, while the expression of antiapoptotic molecule

Bcl-2 was obviously reduced (Figure 1(f)). In summary, our preliminary results are consistent with previous studies. In addition, we also found that miR-218 expression was

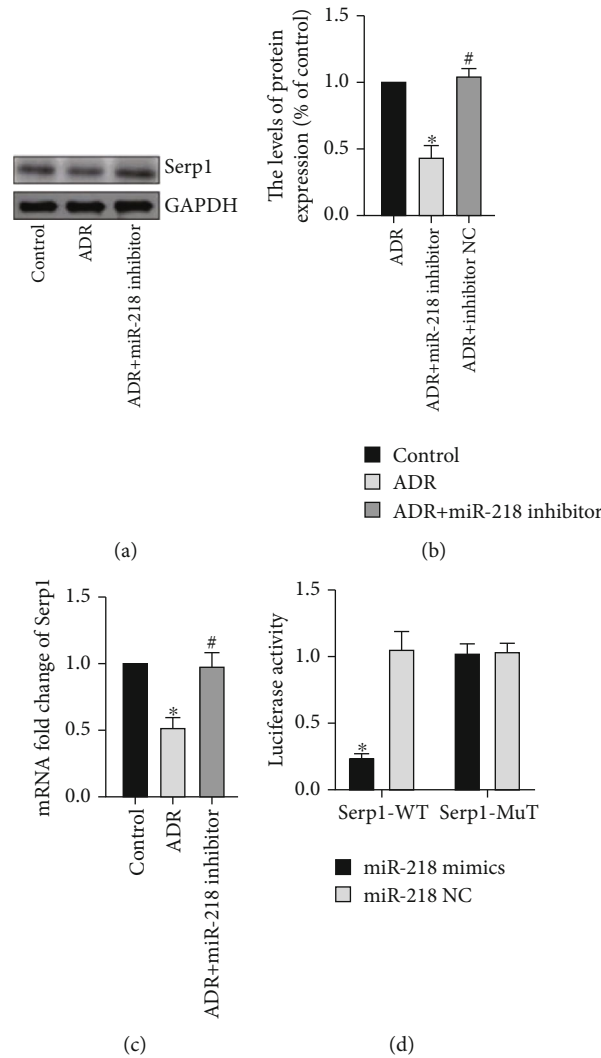


FIGURE 3: Interaction of miR-218 and Serp1. (a) The protein expression of Serp1 was detected by Western blot. (b) Gray value analysis of protein strips, $n = 3$. (c) The mRNA level of Serp1 was detected by RT-PCR, $n = 3$. (d) luciferase gene report experiment, $n = 3$ (“*”) versus the control group, $p < 0.05$; (“#”) versus the ADR group, $p < 0.05$.

obviously increased in the ADR group, suggesting that miR-218 may be involved in the process of apoptosis (Figure 1(g)).

3.2. Knocking down miR-218 Expression Can Alleviate ADR-Induced Apoptosis in H9C2 Cells. In order to examine the effect of miR-218 on apoptosis of H9C2 cells, based on the above results, we first transfected H9C2 cells with miR-218 inhibitor to downregulate the expression of endogenous miR-218 and verified the transfection efficiency by RT-PCR (Figure 2(a)). Then, MTT detected the cell activity of each group and found that the cell activity of the ADR + miR-218 inhibitor group was higher than that of the ADR and ADR + inhibitor NC groups (Figure 2(b)). At the same time, the results of flow cytometry and TUNEL staining found that the apoptosis rate of the ADR + miR-218 inhibitor group was obviously lower than that of the other two groups (Figures 2(c) and 2(d)). Next, we used colorimetry to detect cytotoxicity. The results showed that the cytotoxic-

ity of the ADR + miR-218 inhibitor group was obviously reduced (Figure 2(e)). Then, we used WB and RT-PCR to detect apoptosis-related molecules to observe the effect of miR-218 on cell apoptosis (Figures 2(f)–2(h)). The results showed that compared with the ADR and ADR + inhibitor NC groups, the expression of caspase3 protein in the ADR + miR-218 inhibitor group was reduced. At the same time, the transcription levels of caspase3, caspase9, and Bax were also obviously reduced, while the expression of antiapoptotic molecule Bcl-2 was obviously increased.

3.3. Interaction of miR-218 and Serp1. First, we predicted through the targets can website that miR-218 and Serp1 have binding sites. Next, we detected by WB and RT-PCR that Serp1 expression in the ADR group was obviously reduced, while in the ADR + miR-218 inhibitor group, the Serp1 expression was higher than the ADR group (Figures 3(a)–3(c)). At the same time, the results of the luciferase gene report experiment also confirmed our speculation that the

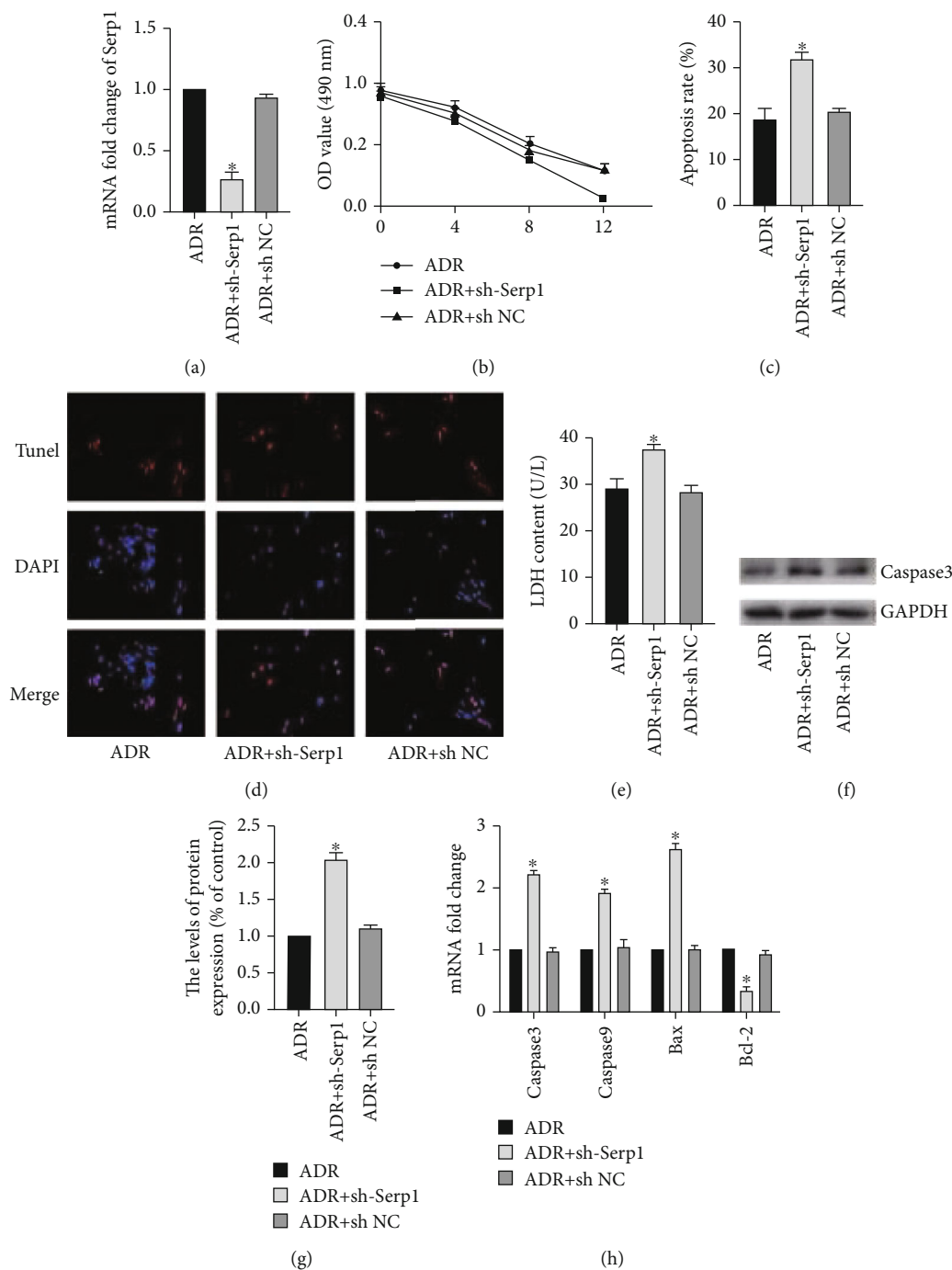


FIGURE 4: Inhibiting Serp1 promotes ADR-induced apoptosis of H9C2 cells. (a) The mRNA level of Serp1 was detected by RT-PCR, $n = 3$. (b) The cell activity was detected by MTT method, $n = 6$. (c) The apoptosis level of cell was detected by flow cytometry, $n = 3$. (d) TUNEL staining, $n = 3$. (e) The activity of LDH detected by the colorimetry method, $n = 3$. (f) The protein expression of caspase3 was detected by Western blot. (g) Gray value analysis of protein strips, $n = 3$. (h) The mRNA level of caspase3, caspase9, Bax, and Bcl-2 was detected by RT-PCR, $n = 3$ (“*” versus the ADR group, $p < 0.05$).

fluorescence activity was the lowest in the miR-218 mimics + Serp1-WT group (Figure 3(d)).

3.4. Inhibiting Serp1 Promotes ADR-Induced Apoptosis of H9C2 Cells. Based on the above results, we first transfected H9C2 cells with sh-Serp1 and sh-NC and then incubated H9C2 cells with $1 \mu\text{M}$ ADR for 12 hours. And the transfection efficiency was detected by RT-PCR (Figure 4(a)). Next, MTT found that interfering with Serp1 expression accelerated ADR-induced decrease in H9C2 cell activity (Figure 4(b)). At the same time, flow cytometry and TUNEL staining to detect the apoptosis rate also found that interference with Serp1 expression increased the ADR-induced apoptosis of H9C2 cells (Figures 4(c) and 4(d)). In addition, the

tion efficiency was detected by RT-PCR (Figure 4(a)). Next, MTT found that interfering with Serp1 expression accelerated ADR-induced decrease in H9C2 cell activity (Figure 4(b)). At the same time, flow cytometry and TUNEL staining to detect the apoptosis rate also found that interference with Serp1 expression increased the ADR-induced apoptosis of H9C2 cells (Figures 4(c) and 4(d)). In addition, the

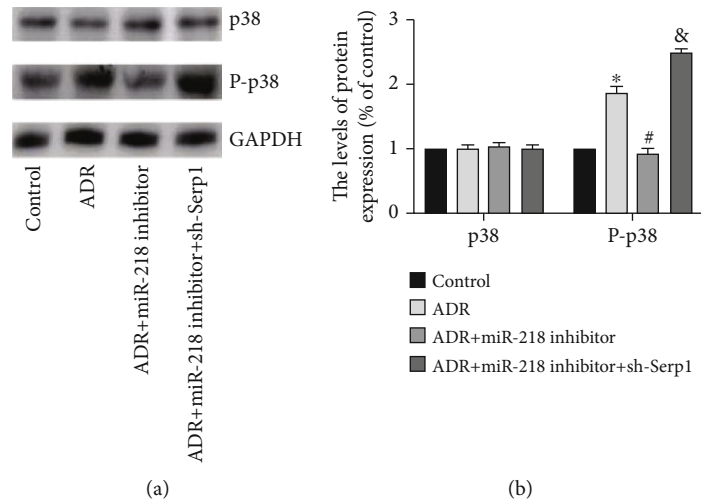


FIGURE 5: Effect of miR-218 on p38 MAPK pathway. (a) The protein expression of p38 and P-p38 was detected by Western blot. (b) Gray value analysis of protein strips, $n = 3$ (“*” versus the control group, $p < 0.05$; “#” versus the ADR group, $p < 0.05$; “&” versus the ADR+miR-218 inhibitor group, $p < 0.05$).

cytotoxicity of the ADR + sh Serp1 group also increased obviously (Figure 4(e)). Next, in order to detect the effect of interference with Serp1 on apoptosis, we detected apoptosis-related molecules by WB and RT-PCR (Figures 4(f)–4(h)). The results showed that the caspase3 protein in the ADR + sh Serp1 group was obviously increased. At the same time, the transcription levels of caspase3, caspase9, and Bax were also obviously increased, while the expression of Bcl-2 was obviously reduced.

3.5. Effect of miR-218 on p38 MAPK Pathway. The activation of p38 MAPK will lead to cardiomyocyte apoptosis. Therefore, we detected the expression of p-38 and P-p38 protein in H9C2 cells of each group (Figures 5(a) and 5(b)). WB results showed that there was no significant difference in the total p38 of each group. Compared with the control group, the P-p38 protein expression in the ADR group was obviously increased. When we inhibited miR-218 expression, the ADR-induced P-p38 protein expression was obviously reduced, and after interfering with Serp1 expression, P-p38 protein expression was higher than that in the ADR + miR-218 inhibitor group. In summary, the mechanism by which miR-218 promotes H9C2 cells apoptosis was targeted inhibition of Serp1, thereby activating p38 MAPK signaling pathway.

4. Discussion

ADR is an antitumor chemotherapy drug. However, due to its toxic effect on the heart, it has been clinically restricted. At present, the mechanism of ADR’s cardiotoxicity is roughly divided into (1) ion and free radical hypothesis. The hypothesis believes that the enhancement of oxidative stress and the lack of antioxidants may play a crucial role in the occurrence of cardiomyopathy and heart failure; (2) metabolic mechanism; (3) apoptosis mechanism. Many CVD including ADR-induced cardiomyopathy have reported apoptosis and reduction of cardiomyocytes [3, 15]. Moreover, the above-

mentioned intracellular changes will lead to apoptosis of cardiomyocytes, and apoptosis is currently considered to be one of the important mechanisms of ADR-induced cardiomyopathy. Cardiomyocytes are terminally differentiated cells, and the reduction of cardiomyocytes caused by cell necrosis or apoptosis caused by antitumor drugs may cause insufficient cardiac contractility. This may be another reason why the heart is more sensitive to ADR than other tissues [16]. In addition, apoptosis is a highly conservative, strictly regulated, energy-dependent active cell death process, which is essential for normal tissue development and homeostasis [17]. Typical morphological changes of apoptosis include cell and chromatin condensation, DNA fragmentation, and formation of apoptotic bodies. At present, it is believed that there are two classic pathways, including exogenous and endogenous pathways to mediate the transmission of apoptosis signals. Both of these pathways will eventually activate the downstream executor caspases 3. Under different cell types and death stimulation signals, the precise molecular regulation mechanism of caspases will be different. Therefore, the apoptosis of cardiomyocytes caused by ADR is also different from that of tumor cells [18].

miRNA is a type of small noncoding RNA that can mediate gene silencing at the posttranscriptional level. Therefore, miRNA plays a key regulatory role in biological processes such as cell proliferation, differentiation, apoptosis, and stress response [19]. For example, miR-19b and miR-499 inhibited hydrogen peroxide-induced cardiomyocyte apoptosis through their respective target genes [20]. MiR-24 can inhibit the apoptosis of myocardial cells during myocardial infarction and reduce the infarct size [21]. In this study, it was found that miR-218 is upregulated in myocardial cells incubated with ADR, and ADR can cause obvious apoptosis of H9C2 cells. We proposed the hypothesis that miR-218 participates in the regulation of cardiomyocyte apoptosis. To further explore this issue, we used transfected miR-218 inhibitor to achieve downregulation of miR-218 in H9C2 cells. After 12 hours of ADR treatment, flow

cytometry and TUNEL staining were used to detect cardiomyocyte apoptosis. Both results found that after miR-218 expression was downregulated, H9C2 cells showed less apoptosis after ADR treatment. Next, we predicted through the tagscan website that Serp1 and miR-218 have binding sites, and Serp1 has a role in regulating apoptosis. From this, we speculate that miR-218 may regulate apoptosis by regulating Serp1. Therefore, after transfecting sh-Serp1, we continue to explore its mechanism of action. The results showed that when we interfered with Serp1 expression, it increased the H9C2 cell apoptosis induced by ADR. Combined with the above results, we demonstrated that miR-218 negatively regulates Serp1, thereby promoting apoptosis of H9C2 cells.

A large number of studies have proved that the activation of p38 MAPK phosphorylation plays a crucial role in ischemia-induced cardiomyocyte apoptosis. Recent studies have found that miR-146a directly inhibits the activation of p38MAPK by directly targeting TRAF6, thereby inhibiting cardiomyocyte apoptosis induced by ischemia and hypoxia [22]. Whether miR-218 promotes ADR-induced cardiomyocyte apoptosis via the p38 MAPK pathway has not been reported. Therefore, we conducted research on this. Our results found that we found that after treatment of H9C2 cells with ADR, miR-218 expression increased, and Serp1 expression decreased, thereby promoting the increase in apoptosis rate. When we inhibited miR-218 expression, the apoptosis rate decreased, and the p38 MAPK pathway was suppressed. Conversely, when we interfere with Serp1 expression, the apoptosis rate increases, and the p38 MAPK pathway was activated.

5. Conclusion

This study clarifies that upregulation of miR-218 expression will promote ADR-induced cardiomyocyte apoptosis. Furthermore, we confirmed that the mechanism by which miR-218 promotes myocardial apoptosis is through the Serp1/p38 MAPK/caspase-3 signaling pathway. Therefore, our research will provide a new treatment strategy for the treatment of ADR toxic cardiomyopathy.

Data Availability

The datasets used and analyzed during the current study are available from the corresponding author on reasonable request.

Conflicts of Interest

The authors declare that they have no competing interests.


References

- [1] D. Coughlan, M. Gianferante, C. F. Lynch, J. L. Stevens, and L. C. Harlan, "Treatment and survival of childhood neuroblastoma: evidence from a population-based study in the United States," *Pediatric Hematology and Oncology*, vol. 34, no. 5, pp. 320–330, 2017.
- [2] "Adriamycin," *Report on Carcinogens*, vol. 12, pp. 31–32, 2011.
- [3] K. Renu, V. G. Abilash, T. P. PB, and S. Arunachalam, "Molecular mechanism of doxorubicin-induced cardiomyopathy - an update," *European Journal of Pharmacology*, vol. 818, pp. 241–253, 2018.
- [4] Y. Ma, L. Yang, J. Ma et al., "Rutin attenuates doxorubicin-induced cardiotoxicity via regulating autophagy and apoptosis," *Biochimica et Biophysica Acta - Molecular Basis of Disease*, vol. 1863, no. 8, pp. 1904–1911, 2017.
- [5] L. Zhao and B. Zhang, "Doxorubicin induces cardiotoxicity through upregulation of death receptors mediated apoptosis in cardiomyocytes," *Scientific Reports*, vol. 7, no. 1, p. 44735, 2017.
- [6] Y. Tian, Y. Liu, T. Wang et al., "A microRNA-hippo pathway that promotes cardiomyocyte proliferation and cardiac regeneration in mice," *Science Translational Medicine*, vol. 7, no. 279, pp. 238r–279r, 2015.
- [7] X. Xiao, Z. Lu, V. Lin et al., "MicroRNA miR-24-3p reduces apoptosis and regulates Keap1-Nrf2 pathway in mouse cardiomyocytes responding to ischemia/reperfusion injury," *Oxidative Medicine and Cellular Longevity*, vol. 2018, 2018.
- [8] R. Verjans, T. Peters, F. J. Beaumont et al., "MicroRNA-221/222 family counteracts myocardial fibrosis in pressure overload-induced heart failure," *Hypertension*, vol. 71, no. 2, pp. 280–288, 2018.
- [9] A. Wojciechowska, A. Braniewska, and K. Kozar-Kaminska, "MicroRNA in cardiovascular biology and disease," *Advances in Clinical and Experimental Medicine*, vol. 26, no. 5, pp. 865–874, 2017.
- [10] B. He, J. Xiao, A. J. Ren et al., "Role of miR-1 and miR-133a in myocardial ischemic postconditioning," *Journal of Biomedical Science*, vol. 18, no. 1, p. 22, 2011.
- [11] "The muscle-specific microRNAs miR-1 and miR-133 produce opposing effects on apoptosis by targeting HSP60, HSP70 and caspase-9 in cardiomyocytes," *Journal of Cell Science*, vol. 124, no. 18, p. 3187, 2011.
- [12] L. Shang, P. Dong, L. Du, X. Yang, H. Wang, and S. Li, "SERP1 prevents hypoxia-reoxygenation-induced H9c2 apoptosis through activating JAK2/STAT3 pathway-dependent attenuation of endoplasmic reticulum stress," *Biochemical and Biophysical Research Communications*, vol. 508, no. 1, pp. 256–262, 2019.
- [13] T. Liu, Y. Zhou, Y. C. Liu et al., "Coronary microembolization induces cardiomyocyte apoptosis through the LOX-1-dependent endoplasmic reticulum stress pathway involving JNK/P38 MAPK," *The Canadian Journal of Cardiology*, vol. 31, no. 10, pp. 1272–1281, 2015.
- [14] D. R. McIlwain, T. Berger, and T. W. Mak, "Caspase functions in cell death and disease," *Cold Spring Harbor Perspectives in Biology*, vol. 5, no. 4, article a8656, 2013.
- [15] H. Tang, A. Tao, J. Song, Q. Liu, H. Wang, and T. Rui, "Doxorubicin-induced cardiomyocyte apoptosis: role of mitofusin 2," *The International Journal of Biochemistry & Cell Biology*, vol. 88, pp. 55–59, 2017.
- [16] P. W. Burrridge, Y. F. Li, E. Matsa et al., "Human induced pluripotent stem cell-derived cardiomyocytes recapitulate the predilection of breast cancer patients to doxorubicin-induced cardiotoxicity," *Nature Medicine*, vol. 22, no. 5, pp. 547–556, 2016.
- [17] M. S. D'Arcy, "Cell death: a review of the major forms of apoptosis, necrosis and autophagy," *Cell Biology International*, vol. 43, no. 6, pp. 582–592, 2019.

- [18] M. Brentnall, L. Rodriguez-Menocal, R. L. De Guevara, E. Cepero, and L. H. Boise, "Caspase-9, caspase-3 and caspase-7 have distinct roles during intrinsic apoptosis," *BMC Cell Biology*, vol. 14, no. 1, p. 32, 2013.
- [19] R. W. Zealy, S. P. Wrenn, S. Davila, K. W. Min, and J. H. Yoon, "microRNA-binding proteins: specificity and function," *Wiley Interdiscip Rev RNA*, vol. 8, no. 5, article e1414, 2017.
- [20] S. Costantino, F. Paneni, T. F. Luscher, and F. Cosentino, "MicroRNA profiling unveils hyperglycaemic memory in the diabetic heart," *European Heart Journal*, vol. 37, no. 6, pp. 572–576, 2016.
- [21] L. J. Pan, X. Wang, Y. Ling, and H. Gong, "MiR-24 alleviates cardiomyocyte apoptosis after myocardial infarction via targeting BIM," *European Review for Medical and Pharmacological Sciences*, vol. 21, no. 13, pp. 3088–3097, 2017.
- [22] G. Zuo, X. Ren, X. Qian et al., "Inhibition of JNK and p38 MAPK-mediated inflammation and apoptosis by ivabradine improves cardiac function in streptozotocin-induced diabetic cardiomyopathy," *Journal of Cellular Physiology*, vol. 234, no. 2, pp. 1925–1936, 2019.

Research Article

Relationship between Expression of Plasma lncRNA-HEIH and Prognosis in Patients with Coronary Artery Disease

Zhenying Zhang,¹ Sushuang Nan,² Xiujuan Duan,² Lizhong Wang,¹ Xiaojing Sun,¹ and Haiying Zheng ³

¹Cardiac Rehabilitation Center, Beijing Rehabilitation Hospital, Capital Medical University, Beijing, China

²Department of Cardiology, The Eighth People's Hospital of Hengshui City, Hengshui, China

³Department of Cardiovascular, Affiliated Hospital of Inner Mongolia Medical University, Hohhot, China

Correspondence should be addressed to Haiying Zheng; 20150134@stu.nun.edu.cn

Received 11 October 2021; Revised 12 December 2021; Accepted 14 December 2021; Published 31 December 2021

Academic Editor: Simona Pichini

Copyright © 2021 Zhenying Zhang et al. This is an open access article distributed under the Creative Commons Attribution License, which permits unrestricted use, distribution, and reproduction in any medium, provided the original work is properly cited.

Objective. We aimed to investigate the expression of long noncoding RNA- (lncRNA-) HEIH in patients with coronary artery disease (CAD) and its impact on patients' prognosis. **Patients and Methods.** From July 2015 to December 2018, 250 patients who underwent coronary angiography, including 50 in the control group and 150 in the CAD group, were collected for detection of the expression of lncRNA-HEIH by real-time quantitative polymerase chain reaction (qPCR). The severity of CAD was evaluated through SYNTAX scoring system. In addition, these patients with CAD were followed up for 3 years, and the major cardiac adverse events such as myocardial infarction and revascularization were recorded. **Results.** The expression of lncRNA-HEIH in plasma of patients with CAD was remarkably higher than that in the control subjects and was verified to be relevant to the severity of CAD. Meanwhile, it was found that CAD patients with high expression of lncRNA-HEIH had higher rates of dyslipidemia as well as CAD family history and higher overall incidence of major cardiac adverse events than those with low expression of lncRNA-HEIH. **Conclusions.** lncRNA-HEIH expression is upregulated in the plasma of CAD patients, which is capable of affecting the prognosis of patients.

1. Introduction

Coronary artery disease (CAD) is one of the main causes of death in the world at present [1]. About 5% of Asians over the age of 18 suffer from CAD; what is more, its prevalence is still increasing [2]. Despite the rapid development of cardiovascular interventional techniques, a significant proportion of patients with coronary heart disease have not been accurately diagnosed at an early stage and cannot be effectively treated during the onset of myocardial infarction, causing severe damage to myocardial cells and ultimately leading to myocardial cell necrosis, apoptosis, hypertrophy, or fibrosis [3, 4].

Long noncoding RNA (lncRNA) refers to a nonproteinized nucleotide with a length greater than 200, which can regulate the expression level of genes in the form of RNA at various levels, so it has a lot of complex secondary structures

[5]. It can be involved in a variety of important regulatory processes such as intracellular transport, transcriptional activation and interference, and chromosome silencing, through multiple mechanisms such as cell differentiation regulation, gene imprinting, splicing regulation, degradation, chromatin remodeling, and mRNA translation regulation [6, 7].

It has been confirmed that lncRNA plays a pivotal role in a number of biological processes, including fat metabolism, atherosclerosis formation, embryonic development, and tumor occurrence [8]. Recent studies have demonstrated that lncRNAs have high tissue specificity in myocardial tissue. Moreover, a genome-wide analysis of cardiac transcription following myocardial infarction revealed that a large number of cardiac-specific lncRNAs have unique regulatory and functional properties for pathophysiological processes such as myocardial remodeling and myocardial regeneration. This finding means that cardiac-specific

lncRNA may serve as a targeting molecule and biomarker for heart development and disease [9]. lncRNA-HEIH is a newly discovered long-chain noncoding RNA with high expression level in liver cancer tissues, which was confirmed to be correlated with high recurrence rate of liver cancer patients and thus can be used as one of the predictors of survival after treatment [10]. Even many reports demonstrated that lncRNA-HEIH plays an important role in the prognosis of patients in different kinds of cancers. However, there is no evidence showing the association between lncRNA-HEIH and nontumor diseases. We attempted to detect the expression level of lncRNA-HEIH in the serum of CAD patients and tried to explore the potential association with the prognosis. Therefore, in this study, we detected serum lncRNA-HEIH level of CAD patients and explored its relationship with the occurrence of major clinical adverse events, which may provide a basis for risk prediction of CAD events.

2. Patients and Methods

2.1. Research Object. Patients who underwent coronary angiography in Beijing Rehabilitation Hospital, Capital Medical University, were randomly selected from July 2015 to December 2018 including 50 patients in the control group (negative control (NC)) and 150 patients in the CAD group. Diagnostic criteria are as follows. Patients in the control group were admitted to the hospital with precordial discomfort, and no obvious stenosis in the coronary arteries was found by coronary angiography. For patients with CAD, results of coronary angiography were analyzed by computerized quantitative software, and the degree of stenosis was calculated using the diameter method. According to the American College of Cardiology coronary vascular scoring criteria, one or more branches, including the left anterior descending artery, the left coronary artery trunk, the circumflex artery, and the right coronary artery, occurred \geq he circumflex can be diagnosed as CAD. This study was approved by the Ethics Committee of the hospital.

2.2. Plasma Collection. Fasting blood samples of each subject were collected before coronary angiography and anticoagulated with ethylenediaminetetraacetic acid (EDTA) dipotassium salt in the morning. After centrifugation at 3000 r/min at 4°C for 15 min, plasma was collected and stored at -80°C until assayed.

2.3. RNA Extraction. Total RNA in serum was extracted by TRIzol method (Invitrogen, Carlsbad, CA, USA) and then reverse transcribed into complementary deoxyribonucleic acid (cDNA). RT-PCR was performed according to the TaqMan RNA Reverse Transcript Kit protocol. The reaction system volume was in total 25 μ l, predenaturation at 95° for 5 min, denaturation at 95° for 30 sec, annealing at 60° for 45 sec, extension at 72° for 3 min, with 35 cycles, and then extension at 72° for 5 min. PCR products were stored at 4°. Quantitative analysis was carried out using the ABI 7500 fluorescence PCR amplification instrument (Applied Biosystems; Thermo Fisher Scientific, Inc.). lncRNA-HEIH primer sequence: forward: 5'-CCTCTTGCCCTTTCT-3',

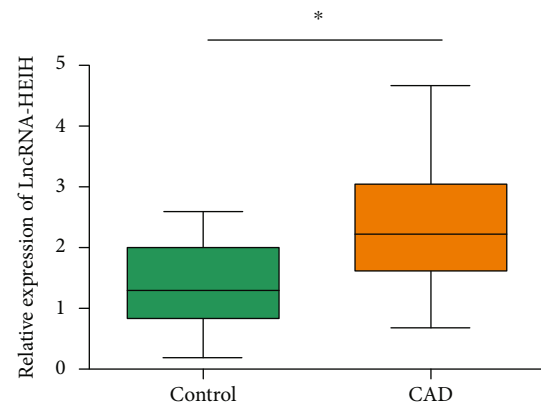


FIGURE 1: High expression of lncRNA-HEIH in plasma of CAD patients. The expression of lncRNA-HEIH in plasma of patients with CAD was remarkably higher than that in plasma of control subjects.

reverse: 5'-AGGTCTCATGGCTTCTCG-3'; internal reference glyceraldehyde 3-phosphate dehydrogenase (GAPDH) upstream primer forward: 5'-TGTTGCCATCAATGAC CCCTT-3', downstream primer reverse: 5'-CTCCACGAC GTACTCAGCG-3'.

2.4. SYNTAX Score. The angiographic results of each patient were scored using the SYNTAX webpage (<http://www.syntaxscore.com/>), and CAD patients were subdivided into three groups.

2.5. Follow-Up Information. After discharge, major adverse cardiac events (nonfatal myocardial infarction, death, revascularization, etc.) in all patients were recorded by telephone or outpatient follow-up at least once a month. Determination of myocardial infarction: chest pain lasting more than 20 minutes or new abnormal changes in electrocardiogram accompanied by abnormal increase of troponin. Determination of revascularization: retreatment of the blood vessel after surgery or intervention or the treatment of new stenosis of the blood vessel. The follow-up period lasted for 3 years.

2.6. Statistical Analysis. Analysis was performed using Statistical Product and Service Solutions (SPSS) 20.0 statistical software (IBM, Armonk, NY, USA). The measurement data were expressed as mean \pm standard deviation, the independent sample *t*-test was used for comparison between the two groups, and the variance analysis was used for comparison of multiple groups. The count data was compared by the χ^2 test; **p* < 0.05.

3. Results

3.1. High Expression of lncRNA-HEIH in Plasma of CAD Patients. To determine the role of lncRNA-HEIH in CAD, we examined its expression in plasma by qRT-PCR, and lncRNA-HEIH was found to be remarkably increased in plasma of CAD patients compared with that in the control

TABLE 1: Plasma lncRNA-HEIH levels in CAD patients.

Variable	<i>n</i>	High level (<i>n</i> = 103)	Low level (<i>n</i> = 47)	χ^2	<i>p</i>
Sex					
Male	27	22	5	2.513	0.168
Female	123	81	42		
Age					
<60	56	37	19	0.280	0.716
≥60	94	66	28		
BMI (kg/m ²)					
<24	61	42	19	0.002	1.000
≥24	89	61	28		
Smoking					
No	72	45	27	2.447	0.158
Yes	78	58	20		
Family history of hypertension					
No	38	28	10	0.596	0.545
Yes	112	75	37		
Family history of CAD					
No	32	29	3	9.116	0.002*
Yes	118	74	44		
Dyslipidemia					
No	58	34	24	4.436	0.047*
Yes	92	69	23		

BMI: body mass index; **p* < 0.05.

group (Figure 1), indicating that lncRNA-HEIH may affect the development of CAD.

3.2. Comparison of Plasma lncRNA-HEIH Levels in CAD Patients. Based on the average expression level of lncRNA-HEIH in all CAD patients, we divided CAD patients into the lncRNA-HEIH high-expression group (*n* = 103) and the low-expression group (*n* = 47). The χ^2 test of the clinical parameters of CAD patients revealed that the rate of CAD family history and dyslipidemia was closely relevant to lncRNA-HEIH expression in the serum of CAD patients, but no significant relevance was found between its level and some other indicators, such as gender, age, BMI, smoking, and hypertension history (Table 1). The above observations confirmed that lncRNA-HEIH expression is associated with a family history of CAD and dyslipidemia incidence.

3.3. Correlation between Plasma lncRNA-HEIH Levels and Severity of CAD. To further clarify the impact of lncRNA-HEIH on CAD, according to the SYNTAX score, we divided CAD patients into the low-risk group (SYNTAX score < 23; *n* = 29), the intermediate-risk group (SYNTAX score 23-32; *n* = 52), and the high-risk group (SYNTAX score > 32; *n* = 96) and then verified through qPCR assay that patients in the high-risk group contained the highest expression of lncRNA-HEIH (Figure 2), further demonstrating that lncRNA-HEIH is able to affect the severity of CAD patients.

3.4. Effect of lncRNA-HEIH on the Occurrence of Major Clinical Adverse Events in CAD Patients. To investigate the

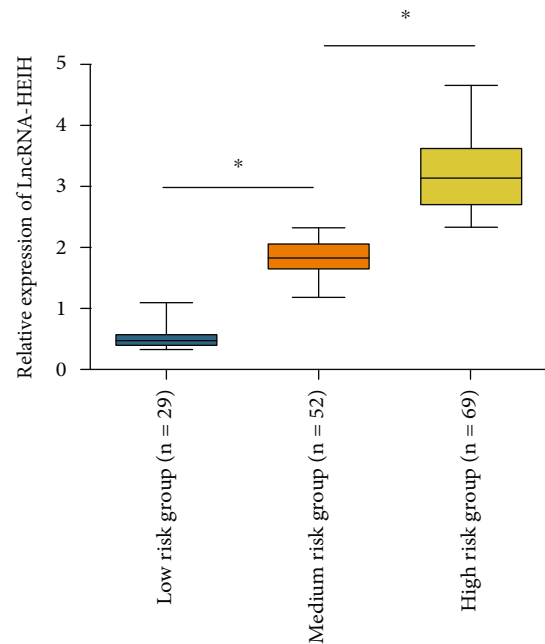


FIGURE 2: Analysis of correlation between plasma lncRNA-HEIH levels with severity of CAD. CAD patients were divided into the low-risk group (SYNTAX score < 23; *n* = 29), the intermediate-risk group (SYNTAX score 23-32; *n* = 52), and the high-risk group (SYNTAX score > 32; *n* = 96) according to SYNTAX score. The level of lncRNA-HEIH in plasma was detected by qRT-PCR. The lncRNA-HEIH in the middle-risk group was remarkably higher than that in the low-risk group. The lncRNA-HEIH in the high-risk group was also remarkably higher than that in the middle-risk group.

TABLE 2: Effect of lncRNA-HEIH on major clinical adverse events of CAD patients [n (%)].

Variable	High level ($n = 103$)	Low level ($n = 47$)	χ^2	p
Cardiac adverse event ($n = 42$)	37 (35.92%)	5 (10.64%)	10.23	0.001*
Death ($n = 15$)	14 (13.59%)	1 (2.13%)	4.713	0.038*
Nonfatal myocardial infarction ($n = 17$)	11 (10.68%)	6 (12.77%)	0.14	0.783
Vascular reconstruction ($n = 23$)	18 (17.48%)	5 (10.64%)	1.162	0.336
Restenosis ($n = 19$)	11 (10.68%)	8 (17.02%)	1.173	0.297
First stenosis ($n = 6$)	4 (3.88%)	2 (4.26%)	0.012	1.000

* $p < 0.05$.

impact of lncRNA-HEIH on the prognosis of patients with CAD, we performed 3 years of follow-up and found that patients with high expression of lncRNA-HEIH had a higher overall incidence of major adverse cardiac events and a higher death rate ($p < 0.05$, Table 2), suggesting that highly expressed lncRNA-HEIH is not conducive to the prognosis of CAD patients.

4. Discussion

Coronary artery disease is one of the major diseases threatening health. The occurrence of CAD can be induced by the deposition of cholesterol and fat in the artery, which narrows the channel of blood into the heart and leads to thrombosis. Insufficient coronary artery blood supply can easily lead to angina pectoris and myocardial infarction [11]. Although percutaneous coronary intervention (PCI) and coronary artery bypass grafting (CABG) have been confirmed to be effective heart artery reconstruction methods for clinical CAD treatment, some studies [12–14] have suggested that the limited effect of CABG and PCI on improving the survival and the high cost limit their use in clinical practice. Since early clinical intervention on CAD patients can remarkably prolong the survival of patients, finding a less invasive examination method with higher accuracy has become the focus of clinical attention [15].

Research findings in the last decade indicate that, driven by the rapid emergence of genomics and proteomics, circular lncRNAs have become the most attractive and promising biomarkers in cardiovascular diseases. In a study published by Li et al. [16] on microarray of mouse model, they analyzed the expression level of lncRNAs in different body fluids (mainly whole blood and plasma) and found a more abundant gene expression profile compared with specific heart tissue lncRNAs. For example, ANRIL [9] and CDKN2A/B [17] are closely associated with atherosclerosis (especially coronary arteries), while MIAT [18] and LIPCAR [19] play an irreplaceable role in myocardial infarction and heart failure.

lncRNA-HEIH is a long-chain noncoding RNA specifically expressed in liver cancer tissues, which has certain reference value for recurrence and prognosis of liver cancer [20]. The main novelty of this research is that we investigated for the first time the expression of lncRNA-HEIH in patients with coronary artery disease (CAD) and its impact on patients' prognosis. In our research, lncRNA-HEIH levels were found to be markedly elevated in CAD

patients compared to control subjects, and this increase was positively correlated with the severity of CAD. In addition, statistical analysis revealed that patients with a family history of CAD and dyslipidemia had higher expression levels of lncRNA-HEIH. The 3-year follow-up results also suggested that highly expressed lncRNA-HEIH induced a higher incidence of major adverse cardiac events, which indicates a poor prognosis. This study may provide further evidence for CAD diagnosis and prognosis assessment. There are still some limitations in this present study. The sample was not big and the follow-up was not long enough to conduct the further analysis. Also, we did not perform the molecular cellular experiments to explore the potential mechanism. In our future study, we plan to conduct the in vitro and in vivo assays for the further verification.

5. Conclusions

lncRNA-HEIH is highly expressed in serum of CAD patients, which is not conducive to the prognosis of patients.

Data Availability

The datasets used and analyzed during the current study are available from the corresponding author on reasonable request.

Conflicts of Interest

The authors declared no conflict of interest.

References

- [1] X. Dai, S. Wiernek, J. P. Evans, and M. S. Runge, "Genetics of coronary artery disease and myocardial infarction," *World Journal of Cardiology*, vol. 8, no. 1, pp. 1–23, 2016.
- [2] Y. Nakagawa, "Role of statins in coronary artery disease," *Nihon Rinsho*, vol. 74, Supplement 4 Part 1, pp. 400–404, 2016.
- [3] K. Aihara and H. Daida, "The impact of disaster-induced stress on coronary artery disease," *Nihon Rinsho*, vol. 74, Supplement 4 Part 1, pp. 193–198, 2016.
- [4] N. Cheung, S. Rogers, T. H. Mosley, R. Klein, D. Couper, and T. Y. Wong, "Vital exhaustion and retinal microvascular changes in cardiovascular disease: atherosclerosis risk in communities study," *Psychosomatic Medicine*, vol. 71, no. 3, pp. 308–312, 2009.
- [5] Y. Hu and J. Hu, "Diagnostic value of circulating lncRNA ANRIL and its correlation with coronary artery disease

- parameters,” *Brazilian Journal of Medical and Biological Research*, vol. 52, no. 8, article e8309, 2019.
- [6] Y. Xiao, J. Xu, and W. Yin, “Aberrant epigenetic modifications of non-coding RNAs in human disease,” *Advances in Experimental Medicine and Biology*, vol. 1094, pp. 65–75, 2018.
- [7] O. M. Rogoyski, J. I. Pueyo, J. P. Couso, and S. F. Newbury, “Functions of long non-coding RNAs in human disease and their conservation in *Drosophila* development,” *Biochemical Society Transactions*, vol. 45, no. 4, pp. 895–904, 2017.
- [8] A. Cardona-Monzonís, J. L. García-Giménez, S. Mena-Mollá et al., “Non-coding RNAs and coronary artery disease,” *Advances in Experimental Medicine and Biology*, vol. 1229, pp. 273–285, 2020.
- [9] L. Li, L. Wang, H. Li et al., “Characterization of LncRNA expression profile and identification of novel LncRNA biomarkers to diagnose coronary artery disease,” *Atherosclerosis*, vol. 275, pp. 359–367, 2018.
- [10] C. Zhang, X. Yang, Q. Qi, Y. Gao, Q. Wei, and S. Han, “lncRNA-HEIH in serum and exosomes as a potential biomarker in the HCV-related hepatocellular carcinoma,” *Cancer Biomarkers*, vol. 21, no. 3, pp. 651–659, 2018.
- [11] R. Lozano, M. Naghavi, K. Foreman et al., “Global and regional mortality from 235 causes of death for 20 age groups in 1990 and 2010: a systematic analysis for the Global Burden of Disease Study 2010,” *Lancet*, vol. 380, no. 9859, pp. 2095–2128, 2012.
- [12] M. Otsuka, M. Zheng, M. Hayashi et al., “Impaired microRNA processing causes corpus luteum insufficiency and infertility in mice,” *The Journal of Clinical Investigation*, vol. 118, no. 5, pp. 1944–1954, 2008.
- [13] K. V. Voudris and C. J. Kavinsky, “Advances in management of stable coronary artery disease: the role of revascularization?,” *Current Treatment Options in Cardiovascular Medicine*, vol. 21, no. 3, p. 15, 2019.
- [14] M. L. Simoons and S. Windecker, “Chronic stable coronary artery disease: drugs vs. revascularization,” *European Heart Journal*, vol. 31, no. 5, pp. 530–541, 2010.
- [15] “CT coronary angiography in patients with suspected angina due to coronary heart disease (SCOT-HEART): an open-label, parallel-group, multicentre trial,” *Lancet*, vol. 385, no. 9985, pp. 2383–2391, 2015.
- [16] D. Li, G. Chen, J. Yang et al., “Transcriptome analysis reveals distinct patterns of long noncoding RNAs in heart and plasma of mice with heart failure,” *PLoS One*, vol. 8, no. 10, article e77938, 2013.
- [17] R. McPherson, A. Pertsemlidis, N. Kavaslar et al., “A common allele on chromosome 9 associated with coronary heart disease,” *Science*, vol. 316, no. 5830, pp. 1488–1491, 2007.
- [18] P. M. Visscher, M. A. Brown, M. I. McCarthy, and J. Yang, “Five years of GWAS discovery,” *American Journal of Human Genetics*, vol. 90, no. 1, pp. 7–24, 2012.
- [19] R. Kumarswamy, C. Bauters, I. Volkmann et al., “Circulating long noncoding RNA, LIPCAR, predicts survival in patients with heart failure,” *Circulation Research*, vol. 114, no. 10, pp. 1569–1575, 2014.
- [20] Y. Ma, G. Cao, J. Li, X. L. Hu, and J. Liu, “Retracted: Silence of lncRNA HEIH suppressed liver cancer cell growth and metastasis through miR-199a-3p/mTOR axis,” *Journal of Cellular Biochemistry*, vol. 120, no. 10, pp. 17757–17766, 2019.

Research Article

Effects of Long Noncoding RNA HOTAIR Targeting miR-138 on Inflammatory Response and Oxidative Stress in Rat Cardiomyocytes Induced by Hypoxia and Reoxygenation

Guofeng Wang¹,¹ Qi Wang,¹ and Weixue Xu²

¹Department of Cardiology, The Fourth Affiliated Hospital of China Medical University, Shenyang, China

²Department of General Surgery, Shengjing Hospital of China Medical University, Shenyang, China

Correspondence should be addressed to Guofeng Wang; mercury4587@163.com

Received 14 October 2021; Accepted 12 November 2021; Published 21 December 2021

Academic Editor: Simona Pichini

Copyright © 2021 Guofeng Wang et al. This is an open access article distributed under the Creative Commons Attribution License, which permits unrestricted use, distribution, and reproduction in any medium, provided the original work is properly cited.

Objective. To investigate the effects of HOX transcript antisense RNA (HOTAIR) and miR-138 on inflammatory response and oxidative stress (OS) induced by IRI in rat cardiomyocytes. **Methods.** H9C2 cells were divided into the control group, H/R group, H/R+siRNA NC group, H/R+si-HOTAIR group, and H/R+si-HOTAIR+inhibitor group. Expression levels of HOTAIR, miR-138, and inflammatory factors were detected by quantitative reverse-transcription polymerase chain reaction (qRT-PCR). The double luciferase reporter gene assay was used to detect the targeting relationship between HOTAIR and miR-138. **Results.** Compared with the control group, the level of miR-138 and SOD in the H/R group was obviously reduced, while the expression levels of the HOTAIR, MDA, and NF- κ B pathway were obviously increased. Compared with the H/R group, the level of miR-138 and SOD in the H/R+si-HOTAIR group was obviously increased, and the expression levels of the HOTAIR, MDA, and NF- κ B pathway were obviously decreased. Compared with the H/R+si-HOTAIR group, the level of SOD in the H/R+si-HOTAIR+inhibitor group decreased; MDA content and the NF- κ B pathway expression level increased. In the double luciferase reporter gene assay, compared with the HOTAIR wt+NC group, the luciferase activity of the HOTAIR wt+miR-138 mimic group was obviously decreased. **Conclusions.** Silent HOTAIR can promote the expression of miR-138 and inhibit H/R-induced inflammatory response and OS by regulating the NF- κ B pathway, thus protecting cardiomyocytes.

1. Introduction

Acute myocardial infarction (AMI) is the acute manifestation of coronary heart disease and the main cause of death. Its basic pathological changes are the rupture of coronary artery plaques, thrombosis, significant reduction, or even interruption of blood supply, which eventually leads to severe ischemic and hypoxic lesions in some myocardial tissues [1]. If blood flow to the occluded vessels does not return, myocardial tissue in the infarct-related area will die. Timely reperfusion strategies, such as drug thrombolysis, percutaneous coronary intervention, and coronary artery bypass grafting, are conducive to the early opening of occluded blood vessels, effectively saving ischemic myocar-

dial tissue, reducing infarction area, and improving cardiac function, and have greatly improved the prognosis of patients [2]. However, as the study of myocardial ischemia reperfusion proceeds further, the researchers found that although the reperfusion therapy can make the ischemia heart regain the blood perfusion in a short period of time to limit infarct area expansion, and many other benefits, it also leads to myocardial ischemia reperfusion treatment itself after more serious dysfunction and structural damage; this phenomenon is called myocardial ischemia reperfusion injury (MIRI) [3, 4]. Moreover, in 1960, Jennings et al. first proposed the MIRI hypothesis and named the description [5]. MIRI can cause the destruction of myocardial cell membrane and then change the myocardial ultrastructure; the

scope of infarction is further expanded. Myocardial reversible or irreversible injury results in decreased systolic function of myocardium, and decreased ventricular threshold is accompanied by obvious refractory period shortening, which can be manifested as malignant arrhythmia, cardiac dysfunction, or even broken death [6]. In addition, MIRI can cause up to 50% of patients with successful PCI to have microcirculation disorder, which seriously affects the treatment effect and the prognosis of patients [7]. Therefore, how to reduce MIRI has become the focus and hot topic of research in the field of coronary heart disease.

The mechanism of the occurrence of MIRI has not been fully clarified. Currently, the mechanisms with more evidence include oxidative stress (OS), intracellular calcium overload, vascular endothelial injury, endoplasmic reticulum stress, and inflammatory response [8, 9]. Studies have shown that OS is one of the main causes leading to cardiac systolic dysfunction and myocardial reperfusion after ischemia; although the blood supply was restored, the increase in the number of generated oxygen free radicals (OFRs) in cells during ischemia and partly due to the overload of calcium ion will launch the apoptosis of myocardial cells, resulting in the structure and function of the myocardial cell injury [10]. Moreover, inflammatory reaction was also involved in the process of MIRI; the ischemia injury area has a variety of cytokines, including the interleukin family (IL-1, IL-6, IL-8, etc.), tumor necrosis factor (TNF- α), and NF- κ B; in addition to direct effect, inflammatory cytokines can also activate neutrophils and endothelial cells and cause OFRs, microcirculation thrombosis, and vascular endothelial cell dysfunction [11]. Therefore, the intervention of OS and inflammatory response is also an important way to reduce MIRI.

The results of the human genome research project confirmed that 2/3 of the gene sequences of more than 3 billion base pairs of humans have been transcribed, while less than 2% of nucleic acid sequences are used to encode proteins. The remaining 98% of DNA is mostly transcribed into RNA instead of being further translated into proteins. This type of RNA molecule is called the noncoding RNA (ncRNA) [12]. They regulate coding RNA and proteins at the transcriptional level and posttranscriptional level and play a complex and precise regulatory function in the process of biological evolution and disease occurrence and development. Among them, the long noncoding RNA (lncRNA) is a kind of ncRNA with a length greater than 200 nt, which is another endogenous RNA molecule after microRNA (miRNA) [13]. Many studies have shown that lncRNA plays an important role in the pathological process of I/R in many vital organs such as the heart, brain, liver, and kidney. In particular, some lncRNAs have been shown to be biomarkers in cardiac I/R studies, which provide potential therapeutic targets for the clinical prevention of MIRI. Through the establishment of the mouse cardiomyocyte model, the researchers found that lncRNA-MDRL could downregulate miRNA 361-miRNA 484 and reduce mitochondrial division and apoptosis, which ultimately protected MIRI [14]. lncRNA-HOTAIR was found to promote TNF- α protein expression in cardiomyocytes of LPS-induced sepsis

mice by activating the NF- κ B pathway [15]. However, the role of lncRNA-HOTAIR in MIRI has not been reported. Through the NONCODE database (<http://www.noncode.org>), lncRNA HOTAIR was found to be widely conserved among species including humans and rats.

The nuclear transcription factor is a class of proteins, which has the function of binding to fixed nucleotide sequences in certain promoter regions to initiate gene transcription. NF- κ B is an important group of proteins, which can be seen in a variety of cells, such as vascular endothelial cells, vascular smooth muscle cells, and cardiomyocytes, and is involved in the gene regulation of a variety of physiological and pathological processes such as inflammation, immunity, cell proliferation, and apoptosis [16, 17].

In this study, rat myocardial cell line H9C2 was transfected into cells to silence lncRNA-HOTAIR, and then, anoxic reoxygenation was performed to simulate cardiac I/R for *in vitro* experiments to further investigate the role of lncRNA-HOTAIR in cardiac ischemia-reperfusion injury in rats.

2. Materials and Methods

2.1. Cell Culture. Rat myocardial cell line H9C2 (American Type Culture Collection, Manassas, VA, USA) was cultured in Dulbecco's modified Eagle medium (DMEM) (Life Technology, Gaithersburg, MD, USA) with 10% fetal bovine serum (FBS) (Life Technology, Gaithersburg, MD, USA) at 37°C, 5% CO₂, and 95% humidity. Passage occurred when the cells were about 80% full.

2.2. Cell Transfection. H9C2 cells in the growing period were inoculated the day before transfection, and the cell density should reach 80%-90% coverage on the day of transfection. On the day of transfection, Lipofectamine 2000 transfection agents (Thermo Fisher Scientific, Waltham, MA, USA) were prepared into siRNA negative control and siRNA HOTAIR/Lipofectamine complexes, according to the instructions. The H/R+si-HOTAIR+inhibitor group was cotransfected with si-HOTAIR and miR-138 inhibitor according to the instructions of Lipofectamine 2000 transfection agents. Then, the mixture after incubation was directly added to the H9C2 cell medium. Finally, the cells were placed at 37°C in a 5% CO₂ incubator for 4-6 h, and the fresh DMEM medium was replaced.

2.3. Establishment of Cell Hypoxia Reoxygenation Model. The cell hypoxic reoxygenation model was to simulate cell hypoxia and sugar-free environment *in vitro* to simulate ischemia and restore oxygen supply and saccharide environment to simulate reperfusion, so as to simulate the MIRI model. Specific steps are as follows: the cell culture medium of each group was replaced with serum-free low-glucose DMEM medium of 2 mL and put into an anoxic culture chamber full of 95% N₂+5% CO₂ mixed gas (oxygen concentration less than 1%). The anoxic culture medium was incubated at 37°C for 1 h to simulate ischemia. During the reperfusion period, the cell culture plate was taken from the anoxic culture box, and the culture medium was replaced

TABLE 1: RT-PCR primers.

Gene name	Forward (5' > 3')	Reverse (5' > 3')
IL-1 β	GCAACTGTTCTGAACTCAACT	ATCTTTTGGGTCCGTCAACT
IL-6	TAGTCCTTCCTACCCCAATTTC	TTGGTCCTAGCCACTCCTTC
TNF- α	CCTCTCTCTAATCAGCCCTCTG	GAGGACCTGGGAGTAGATGAG
IKK	GTCAGGACCGTGTCTCAAGG	GCTTCTTTGATGTTACTGAGGGC
IKB- α	GGATCTAGCAGCTACGTACG	TTAGGACCTGACGTAACACG
NF- κ B p65	ACTGCCGGGATGGCTACTAT	TCTGGATTGCTGGCTAATGG
GAPDH	ACAACCTTTGGTATCGTGGAAGG	GCCATCACGCCACAGTTTC

RT-PCR: quantitative reverse-transcription polymerase chain reaction.

with the normal DMEM medium containing serum and sugar of 2 mL. The mixed gas of 95% N₂+5% CO₂ was injected into the air inlet with the flow rate of 5 L/min and reoxygenated at 37°C for 3 h.

2.4. Western Blot Test. Cells of each group were collected, with each group containing about 4×10^6 cells, and lysed in 200 μ L lysate containing protease inhibitor, lysed at 4°C for 40 min, and centrifuged at 15,000 RPM for 20 min; then, the supernatant was taken, and protein was quantified by the bicinchoninic acid (BCA) kit (Jian Cheng, Nanjing, China). After mixing with a 4x sample buffer, the sample was boiled for 5 min. Then, the 40 μ g sample was electrophoresed in 8-10% sodium dodecyl sulphate (SDS) polyacrylamide gel for 2 h and then transferred to a polyvinylidene difluoride (PVDF, Thermo Fisher Scientific, Waltham, MA, USA) membrane. After being sealed with 5% skim milk for 2 h, the membrane was cut out according to the molecular weight, and primary antibodies (IL-1 β , Abcam, Cambridge, MA, USA, Rabbit, 1:1000; IL-6, Abcam, Cambridge, MA, USA, Rabbit, 1:3000; TNF- α , Abcam, Cambridge, MA, USA, Rabbit, 1:3000; NF- κ B p65, Abcam, Cambridge, MA, USA, Mouse, 1:2000; IKK, Abcam, Cambridge, MA, USA, Mouse, 1:2000; p-IKB α , Abcam, Cambridge, MA, USA, Rabbit, 1:3000; GAPDH, Proteintech, Rosemont, IL, USA, 1:5000) were added at 4°C overnight. After washing with phosphate-buffered saline (PBS) for 3 times, anti-rabbit or mouse IgG secondary antibody (1:1 000 dilution, Yifei Xue Biotechnology, Nanjing, China) was added for 1 h at room temperature. We used enhanced chemiluminescence (ECL) technology (Jian Cheng, Nanjing, China) to expose the target protein, and the image analysis system was used for photography and analysis.

2.5. Total RNA Extraction and Quantitative Reverse-Transcription Polymerase Chain Reaction (qRT-PCR). After the cells in each group were collected, a TRIzol reagent (Thermo Fisher Scientific, Waltham, MA, USA) was used to extract RNA from each group, complementary deoxyribose nucleic acid (cDNA) was synthesized according to the reverse transcription kit (Thermo Fisher Scientific, Waltham, MA, USA), and then, PCR reaction was performed with a PCR apparatus (Becton Dickinson, Heidelberg, Germany). The cyclic conditions were as follows: predenaturation at 95°C for 10 min, denaturation at 95°C for 15 s, and annealing at 63°C for 1 min, a total of 40 cycles. The

mRNA levels of each group were detected by SsoFast EvaGreen Supermix kit (Yi Hui, Shanghai, China), and the results were calculated by the $2^{-\Delta\Delta C_T}$ method. The primers used are shown in Table 1.

2.6. Enzyme-Linked Immunosorbent Assay (ELISA). After grouping treatment according to the test methods described above, the supernatant of cells in each group was collected, and the contents of MDA, and the activities of SOD and inflammation-related factors (TNF- α , IL-1 β , IL-6) were detected according to the instructions of the kit (Jian Cheng, Nanjing, China).

2.7. Luciferase Test. Bioinformatics analysis and prediction showed that the possible binding site of miR-138 was located in the lncRNA HOTAIR 2142~2163 bp region. The HOTAIR Lenti-reporter-Luciferase wild-type vector and its mutant vector were constructed separately (Thermo Fisher Scientific, Waltham, MA, USA). The cells were divided into four groups: HOTAIR wt-NC, HOTAIR mut-NC, HOTAIR wt+miR-138, and HOTAIR mut+miR-138 mimics. Cells were plated in 24-well plates and incubated for 24 h. The next day, the wild-type vector (200 ng) and pRL-CMV vector (20 ng) were transfected into the HOTAIR wt+NC and HOTAIR wt+miR-138 mimic groups; the mutant vector (200 ng) and the pRL-CMV vector (20 ng) were transfected into HOTAIR mut-NC and HOTAIR mut+miR-138 mimic groups. At the same time, miR-138 mimics was transfected in the HOTAIR wt+miR-138 mimic and HOTAIR mut+miR-138 mimic groups. 48 h after transfection, luciferase activity was detected using a luciferase reporter detection system (Thermo Fisher Scientific, Waltham, MA, USA).

2.8. Immunofluorescence. After the cells were fixed with 4% paraformaldehyde for 15 minutes, they were washed with 0.01 mol/L PBS buffer solution for 3 times and then sealed with 10% goat serum + 0.03% Triton X-100 blocking solution (Elabscience, Wuhan, China) at room temperature for 2 h, and then, a primary antibody (SOD1, Abcam, Cambridge, MA, USA, Rabbit, 1:3000) was added, placed in a refrigerator at 4°C overnight, and then washed with 0.01 mol/L PBS buffer solution. The sheep anti-mouse secondary antibody (Jian Cheng, Nanjing, China) was added, incubated at room temperature for 2 h, and then washed with 0.01 mol/L PBS buffer solution. The cell nucleus was stained by 4',6-diamidino-2-phenylindole (DAPI) (Jian

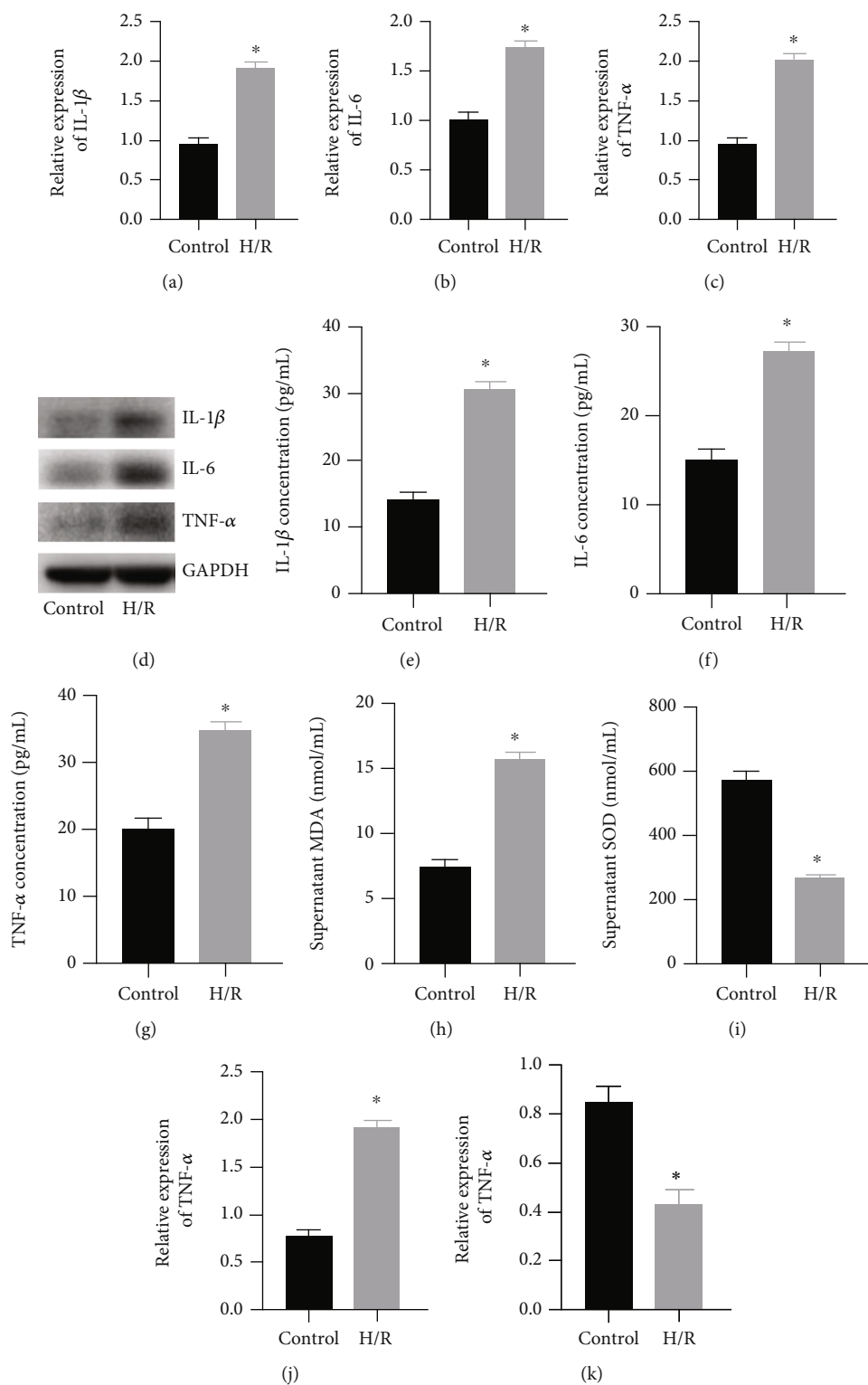


FIGURE 1: Continued.

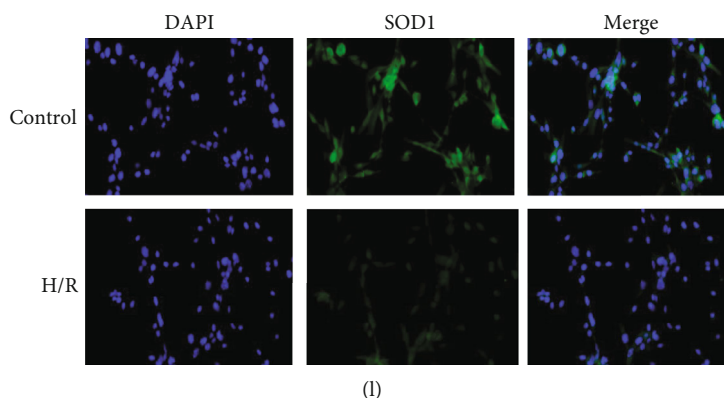


FIGURE 1: Effect of H/R on H9C2 cells. (a) qRT-PCR was used to detect the expression of IL-1 β . (b) qRT-PCR was used to detect the expression of IL-6. (c) qRT-PCR was used to detect the expression of TNF- α . (d) WB was used to detect the expression of IL-1 β , IL-6, and TNF- α . (e) ELISA was used to detect the content of IL-1 β . (f) ELISA was used to detect the content of IL-6. (g) ELISA was used to detect the content of TNF- α . (h) ELISA was used to detect the content of MDA. (i) ELISA was used to detect the activity of SOD. (j) qRT-PCR was used to detect the expression of HOTAIR. (k) qRT-PCR was used to detect the expression of miR-138. (l) Immunofluorescence staining was used to detect the expression of SOD1 (magnification: 400x). (“*” indicates statistical difference from the control group, $P < 0.05$).

Cheng, Nanjing, China) in the dark, and antifade solution (Jian Cheng, Nanjing, China) was added to the film and stored at 4°C for observation under fluorescence microscope (Keyence, Shanghai, China).

2.9. Statistical Analysis. Data analysis was performed using Statistical Product and Service Solutions (SPSS) 21.0 software (IBM, Armonk, NY, USA). Measurement data were expressed as mean \pm standard deviation. Differences between two groups were analyzed by using Student’s *t*-test. Comparison between multiple groups was done using one-way ANOVA test followed by Post Hoc Test (Least Significant Difference). Chi-square test was used for enumeration data. $P < 0.05$ was considered statistically significant.

3. Results

3.1. Effect of H/R on H9C2 Cells. Compared with the control group, H9C2 cells in the H/R group had an obvious inflammatory response. IL-1 β , IL-6, and TNF- α were detected by qRT-PCR (Figures 1(a)–1(c)). H/R induced an inflammatory response and promoted the increased expression of IL- β , IL-6, and TNF- α . At the same time, WB (Figure 1(d)) and ELISA (Figures 1(e)–1(g)) results confirm this. Next, we used the kit to detect the MDA content and SOD activity in the cell supernatant (Figures 1(h) and 1(i)) and found that H/R caused a redox imbalance, resulting in a decrease in SOD activity and an increase in MDA content. At the same time, we tested the expression of SOD1 in each group (Figure 1(j)). The results of immunofluorescence staining showed that the expression of SOD1 in the H/R group was obviously reduced. Subsequently, qRT-PCR detection revealed that the expression of lncRNA-HOTAIR increased (Figure 1(k)), while the expression of miR-138 (Figure 1(l)) decreased in the H/R group.

3.2. Effects of Silenced lncRNA-HOTAIR on H9C2 Cells. Based on the above qRT-PCR test results, we established a

transient transfected cell model of silent lncRNA-HOTAIR (si-HOTAIR) and then treated the cells with hypoxia and reoxygenation. First, we detected by qRT-PCR that HOTAIR expression in the si-HOTAIR+H/R group was obviously reduced (Figure 2(a)). At the same time, we also tested the miR-138 expression and found that the miR-138 expression was increased in the si-HOTAIR+H/R group (Figure 2(b)). Subsequently, the expression of IL-1 β , IL-6, and TNF- α was detected by qRT-PCR (Figures 2(c)–2(e)). It was found that the expression of inflammatory factors was obviously suppressed in the si-HOTAIR+H/R group. WB (Figure 2(f)) and ELISA (Figures 2(g)–2(i)) also found that silencing lncRNA-HOTAIR can reduce the H/R-induced inflammation. Next, we measured the MDA content (Figure 2(j)) and the SOD activity (Figure 2(k)) in the cell supernatant and found that silencing lncRNA-HOTAIR can alleviate the redox imbalance caused by H/R, increase the SOD activity, and inhibit the increase in MDA content. At the same time, we detected SOD1 expression by immunofluorescence and found that SOD1 expression was low in the H/R group and the H/R+siRNA NC group, while SOD1 expression was relatively high in the H/R+si-HOTAIR group (Figure 2(l)).

3.3. Effect of Silenced miR-138 on H9C2 Cells. Based on the above results and literature review, it was confirmed that miR-138 has a targeting relationship with lncRNA-HOTAIR. At the same time, the luciferase test found that compared with the HOTAIR wt+NC group, the luciferase activity of the HOTAIR wt+miR-138 mimic group was obviously reduced, and the difference was statistically significant (Figure 3(a)). There was no significant difference in luciferase activity between the HOTAIR mut+NC group and the HOTAIR mut+miR-138 mimic group. It was verified that miR-138 can target HOTAIR. So, does silencing miR-138 inhibit the effect of lncRNA-HOTAIR on H/R-induced OS and inflammation? Therefore, we divided H9C2 cells into 3 groups: H/R, H/R+si-HOTAIR, and H/R+si-HOTAIR+inhibitor. Then, the expression of IL-1 β , IL-6, and

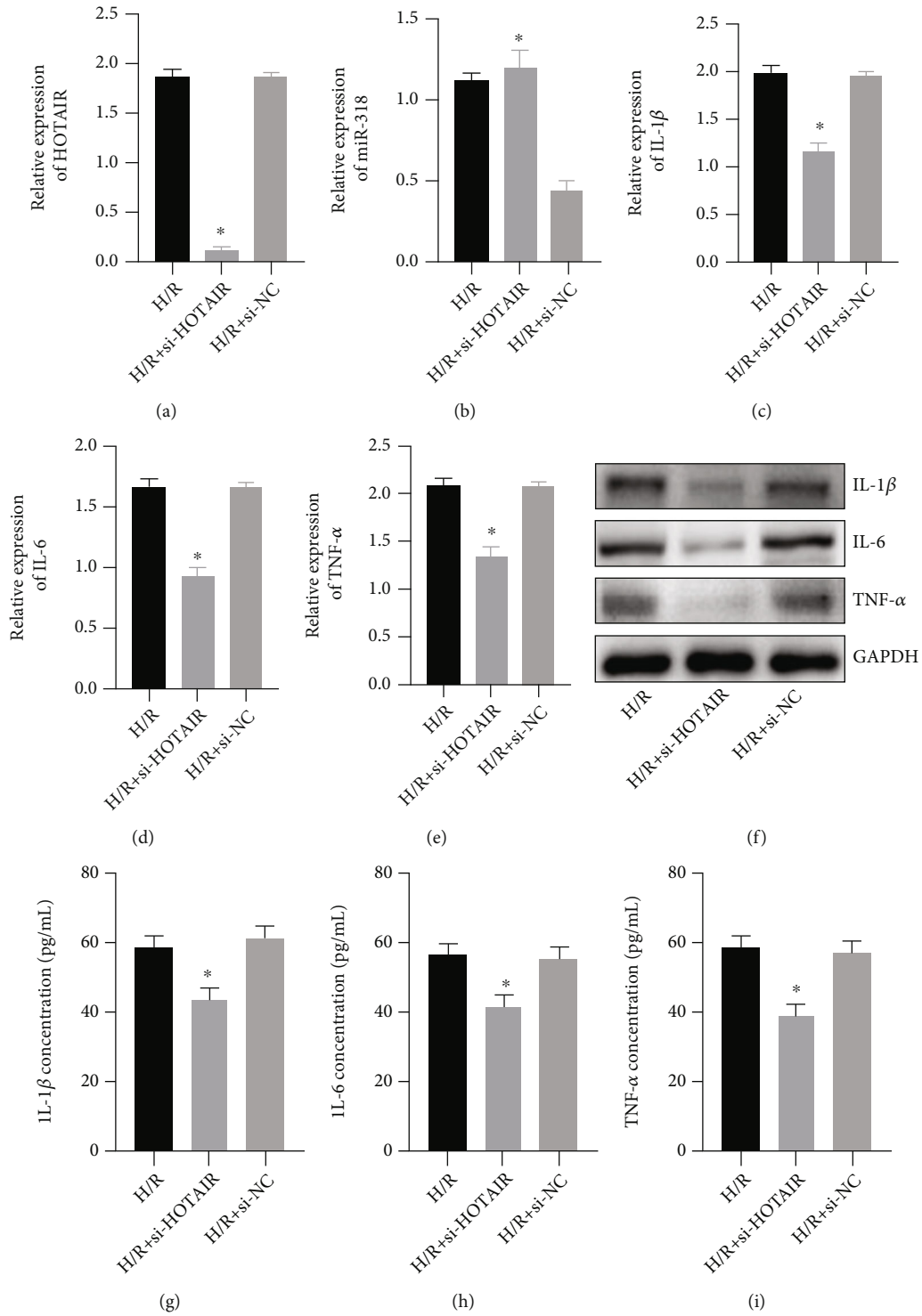


FIGURE 2: Continued.

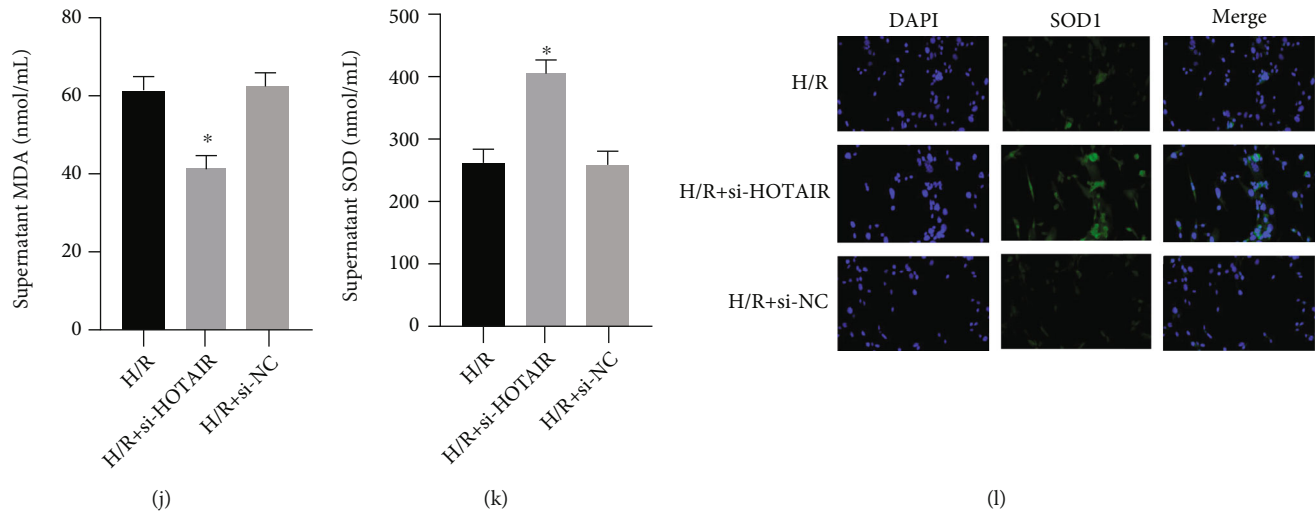


FIGURE 2: Effects of silenced lncRNA-HOTAIR on H9C2 cells. (a) qRT-PCR was used to detect the expression of HOTAIR. (b) qRT-PCR was used to detect the expression of miR-138. (c) qRT-PCR was used to detect the expression of IL-1 β . (d) qRT-PCR was used to detect the expression of IL-6. (e) qRT-PCR was used to detect the expression of TNF- α . (f) WB was used to detect the expression of IL-1 β , IL-6, and TNF- α . (g) ELISA was used to detect the content of IL-1 β . (h) ELISA was used to detect the content of IL-6. (i) ELISA was used to detect the content of TNF- α . (j) ELISA was used to detect the content of MDA. (k) ELISA was used to detect the activity of SOD. (l) Immunofluorescence staining was used to detect the expression of SOD1 (magnification: 400x). (“*” indicates statistical difference from the H/R group, $P < 0.05$).

TNF- α was detected by qRT-PCR (Figures 3(b)–3(d)), WB (Figure 3(e)), and ELISA (Figures 3(f)–3(h)). It was found that the degree of inflammation in the H/R+si-HOTAIR+inhibitor group was obviously higher than that in the H/R+si-HOTAIR group. Detection of MDA content (Figure 3(i)) and SOD activity (Figure 3(j)) in cell supernatants revealed that miR-138 inhibitor can partially inhibit the effect of si-HOTAIR, resulting in a decrease in SOD activity and an increase in MDA content. Immunofluorescence staining for SOD1 revealed that SOD1 expression was lower in the H/R+si-HOTAIR+inhibitor group than in the H/R+si-HOTAIR group (Figure 3(k)).

3.4. Silencing lncRNA-HOTAIR Inhibits NF- κ B Pathway Activation in H9C2 Cells. Compared with the control group, the protein expression levels of IKK, p-IK β , and NF- κ B p65 in the H/R group increased obviously. Compared with the H/R group, the expression levels of IKK, p-IK β , and NF- κ B p65 in the H/R+si-HOTAIR group were obviously reduced. Conversely, compared with the H/R+si-HOTAIR group, the expression levels of IKK, p-IK β , and NF- κ B p65 in the H/R+si-HOTAIR+inhibitor group were obviously increased (Figure 4(a)). At the same time, the qRT-PCR detection, IKK, and NF- κ B p65 expression were similar to WB results, and IK β - α expression was lowest in the H/R group, and the expression was increased in the H/R+si-HOTAIR group, while the inhibitor can inhibit some of the effects of si-HOTAIR (Figures 4(b)–4(d)).

4. Discussion

Previous literature has reported that HOTAIR can activate the NF- κ B signaling pathway and activate the myocardial

inflammatory response by promoting phosphorylation of the NF- κ B p65 subunit [18]. miR-138 can reduce myocardial cell apoptosis caused by hypoxia through the MLK3/JNK/c-Jun signaling pathway [19]. In addition, studies have confirmed that HOTAIR and miR-138 can interact with each other to affect LPS-induced rheumatoid arthritis *in vivo* [18]. This study was the first to explore the mechanism of the interaction between miR-138 and HOTAIR in the myocardial inflammation induced by H/R. In this study, it was found that the expression level of HOTAIR in H9C2 cells after H/R treatment was obviously increased, and the expression level of miR-138 was obviously decreased. The expression level of miR-138 was obviously increased after the silence of HOTAIR expression, indicating that HOTAIR and miR-138 did interact. Through luciferase reporter gene detection, it was found that HOTAIR could directly act on miR-138, which confirmed previous studies.

Inflammatory cytokines are involved in the MIRI process. Studies have shown that TNF- α protein and IL-1 β protein jointly initiate the inflammatory response and have a negative inotropic effect on the myocardium, while the negative regulatory effect of IL-6 on the myocardial contractility is related to each other through the protein kinase pathway [20]. In this study, it was found that the silencing of HOTAIR could inhibit the expression of inflammatory cytokines TNF- α , IL-1 β , and IL-6 in the H/R model, indicating that HOTAIR was involved in the expression of inflammatory cytokines. OS also plays a key role in MIRI, which induces excessive production of reactive oxygen species (ROS) in mitochondria, leading to an oxidation/antioxidant imbalance. ROS damage the myocardial cell membrane, leading to the production of a large amount of lipid peroxide MDA and the depletion of SOD activity. In this study, it was

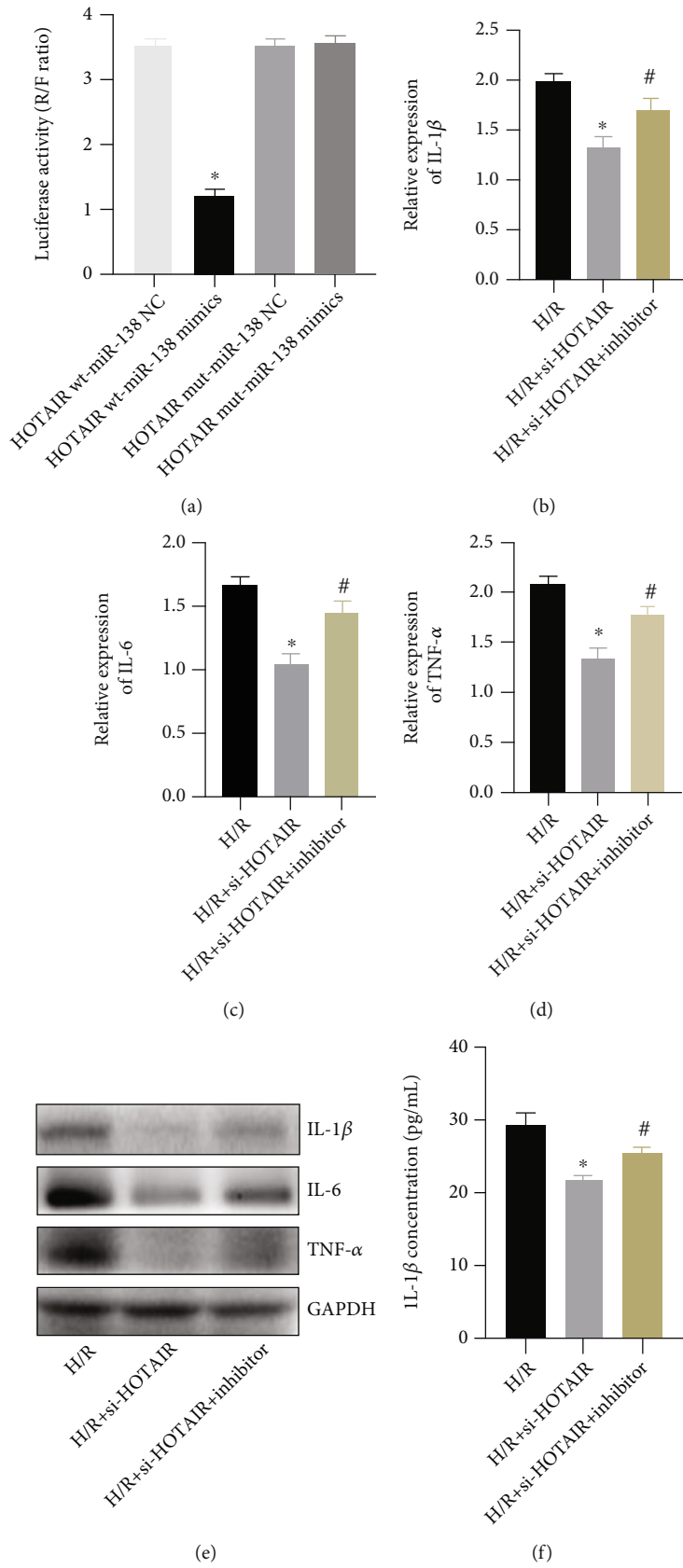


FIGURE 3: Continued.

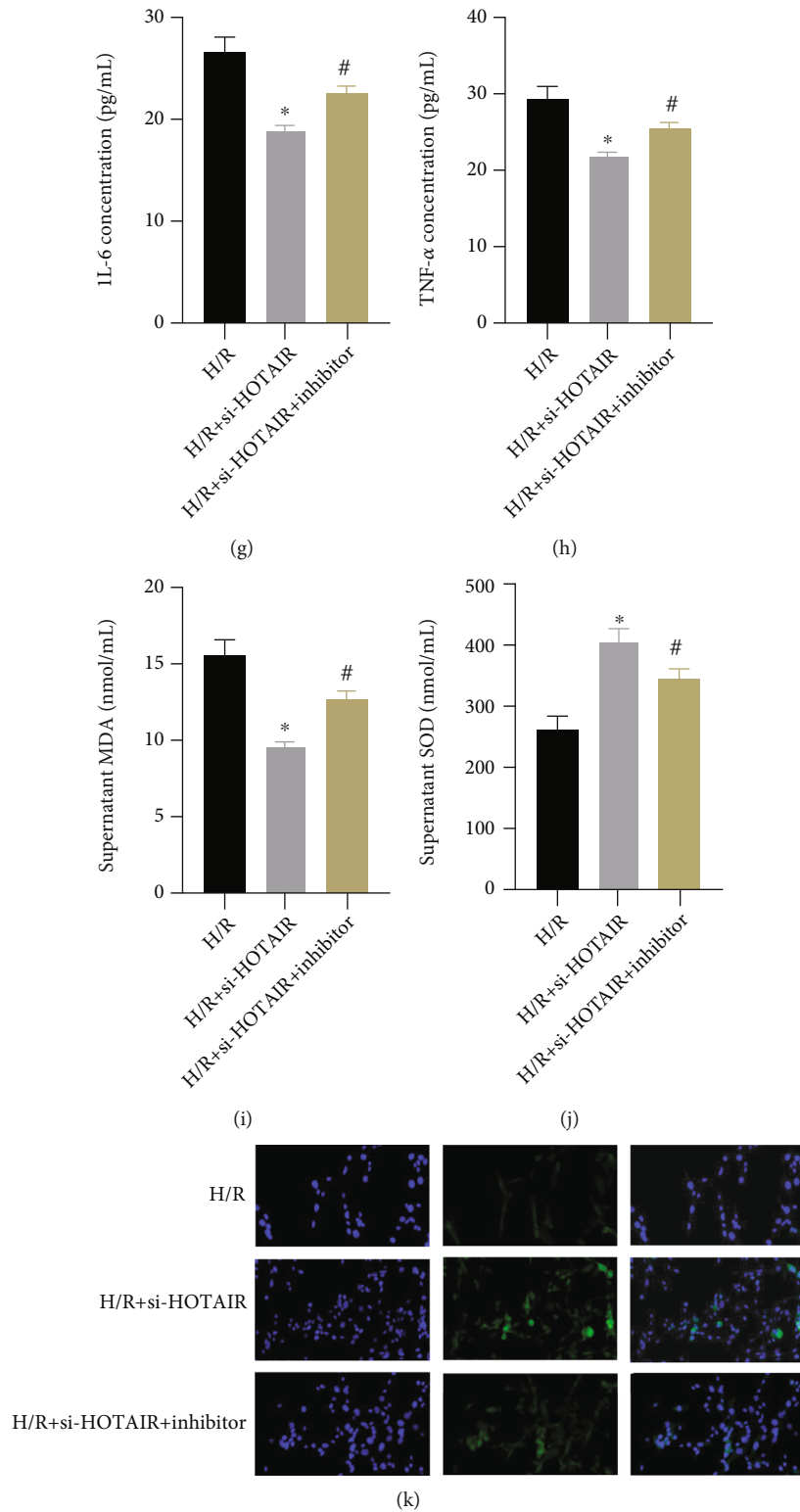


FIGURE 3: Effect of silenced miR-138 on H9C2 cells. (a) The luciferase reporter assay was used to detect the targeting relationship between miR-138 and HOTAIR. (“*” indicates statistical difference from the HOTAIR wt+miR-138 NC group $P < 0.05$.) (b) qRT-PCR was used to detect the expression of IL-1 β . (c) qRT-PCR was used to detect the expression of IL-6. (d) qRT-PCR was used to detect the expression of TNF- α . (e) WB was used to detect the expression of IL-1 β , IL-6, and TNF- α . (f) ELISA was used to detect the content of IL-1 β . (g) ELISA was used to detect the content of IL-6. (h) ELISA was used to detect the content of TNF- α . (i) ELISA was used to detect the content of MDA. (j) ELISA was used to detect the activity of SOD. (k) Immunofluorescence staining was used to detect the expression of SOD1 (magnification: 400x). (“*” indicates statistical difference from the H/R group, $P < 0.05$, and “#” indicates statistical difference from the H/R+si-HOTAIR group, $P < 0.05$).

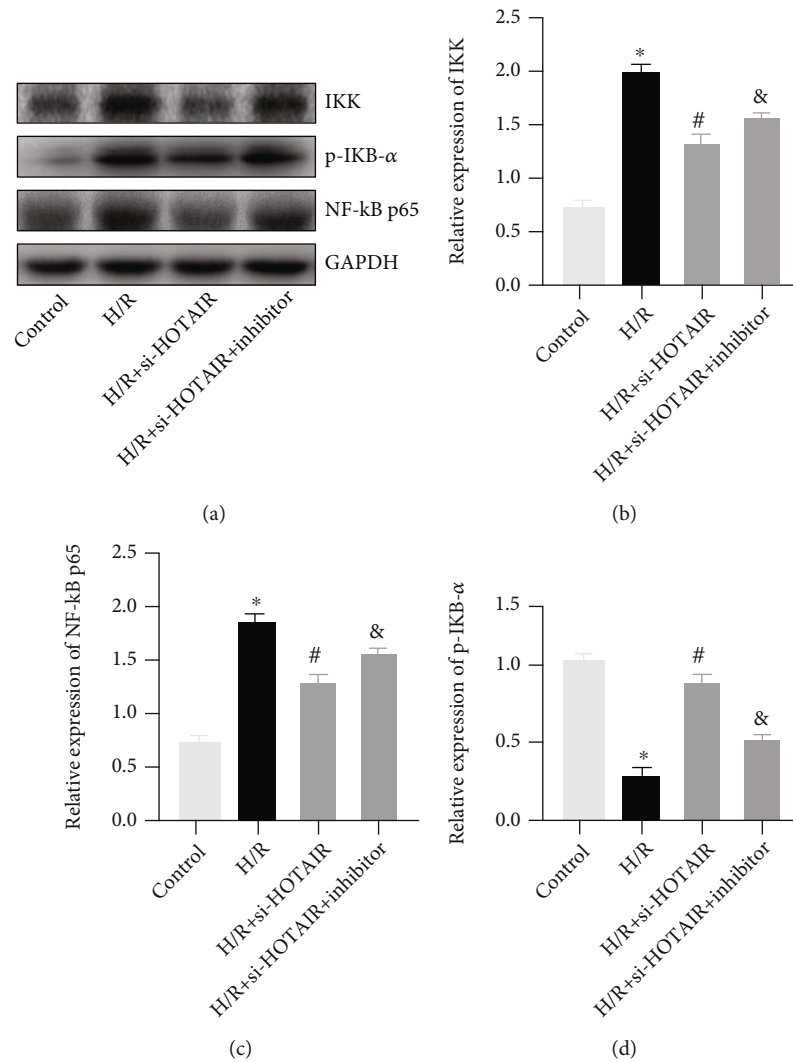


FIGURE 4: Silencing lncRNA-HOTAIR inhibits NF-κB pathway activation in H9C2 cells. (a) WB was used to detect the expression of IKK, p-IKB- α , and NF- κ B p65. (b) qRT-PCR was used to detect the expression of IKK. (c) qRT-PCR was used to detect the expression of NF- κ B p65. (d) qRT-PCR was used to detect the expression of IKB- α . (“*” indicates statistical difference from the control group, $P < 0.05$; “#” indicates statistical difference from the H/R group, $P < 0.05$; and “&” indicates statistical difference from the H/R+si-HOTAIR group, $P < 0.05$).

found that by silencing the expression of HOTAIR, the activity of SOD was restored and the content of MDA decreased, indicating that HOTAIR was involved in the OS of H9C2 cells. Further silencing of miR-138 revealed that the activity of SOD was decreased and the content of MDA was increased, indicating that miR-138 had an inhibitory effect on H/R-induced OS in H9C2 cells.

The NF- κ B signaling pathway is widely involved in various inflammatory responses. In general, NF- κ B family proteins exist in the form of isomeric p50-p65 and bind to inhibitor kappaB (IKB) in an inactivated state, which is located in the cytoplasm. In the presence of inducers such as TNF- α , IL-1, and IL-6, the IKB kinase is activated, phosphorylates IKB, causes it to release p50-p65, and is eventually degraded by proteasomes. At this time, p50-p65 exposed nuclear localization signal, transport into the nucleus, as a transcription factor to bind to various target

DNA sequences [21, 22]. In order to explore whether the NF- κ B signaling pathway was regulated by HOTAIR and miR-138 in H9C2 cells during the H/R process, in this study, the expression levels of IKK, p-IKB α , and NF- κ B p65 were detected *in vitro*. It was found that the expressions of IKK, p-IKB α , and NF- κ B p65 were obviously inhibited by the silence of HOTAIR, indicating that HOTAIR was involved in the activation of NF- κ B and promotes the inflammatory response. At the same time, we further silenced miR-138 with inhibitors and found that the expression levels of IKK, p-IKB α , and NF- κ B p65 were obviously higher than those in the H/R+si-HOTAIR group, indicating that miR-138 could inhibit the activation of NF- κ B and thus reduce the inflammatory response.

In summary, lncRNA HOTAIR was involved in the expression of inflammatory factors in cardiomyocytes induced by H/R in H9C2 cells and the occurrence of OS

and has an activation effect on NF- κ B, while miR-138 can inhibit OS and the expression of inflammatory factors by inhibiting the NF- κ B signaling pathway. HOTAIR can interact with miR-138 in H9C2 cells, resulting in miR-138 silencing. Therefore, HOTAIR can regulate the inflammatory response and OS of H9C2 cells by silencing miR-138. Furthermore, in combination with the previously reported literature, we speculated that HOTAIR and miR-138 play a regulatory role in different pathways of myocardial inflammatory response induced by H/R.

5. Conclusions

Silent HOTAIR can promote the expression of miR-138 and inhibit H/R-induced inflammatory response and OS by regulating the NF- κ B pathway, thus protecting cardiomyocytes, which provides a new therapeutic approach for the maintenance of heart function in the treatment of MIRI.

Data Availability

The datasets used and analyzed during the current study are available from the corresponding author on reasonable request.

Conflicts of Interest


The authors declare that they have no competing interests.

References

- [1] A. Fife and E. Farr, "Acute myocardial infarction," *Nursing Standard*, vol. 12, no. 26, pp. 49–56, 1998.
- [2] M. Tibaut, D. Mekis, and D. Petrovic, "Pathophysiology of myocardial infarction and acute management strategies," *Cardiovascular & Hematological Agents in Medicinal Chemistry*, vol. 14, no. 3, pp. 150–159, 2017.
- [3] A. Binder, A. Ali, R. Chawla, H. A. Aziz, A. Abbate, and I. S. Jovin, "Myocardial protection from ischemia-reperfusion injury post coronary revascularization," *Expert Review of Cardiovascular Therapy*, vol. 13, no. 9, pp. 1045–1057, 2015.
- [4] S. Wang, W. Yu, J. Chen, T. Yao, and F. Deng, "LncRNA MALAT1 sponges miR-203 to promote inflammation in myocardial ischemia-reperfusion injury," *International Journal of Cardiology*, vol. 268, p. 245, 2018.
- [5] R. B. Jennings, H. M. Sommers, G. A. Smyth, H. A. Flack, and H. Linn, "Myocardial necrosis induced by temporary occlusion of a coronary artery in the dog," *Archives of Pathology*, vol. 70, pp. 68–78, 1960.
- [6] L. D. Horwitz, D. Kaufman, M. W. Keller, and Y. Kong, "Time course of coronary endothelial healing after injury due to ischemia and reperfusion," *Circulation*, vol. 90, no. 5, pp. 2439–2447, 1994.
- [7] G. Niccoli, G. Scalone, A. Lerman, and F. Crea, "Coronary microvascular obstruction in acute myocardial infarction," *European Heart Journal*, vol. 37, no. 13, pp. 1024–1033, 2016.
- [8] J. Kim, J. Kim, H. Kook, and W. J. Park, "PICOT alleviates myocardial ischemia-reperfusion injury by reducing intracellular levels of reactive oxygen species," *Biochemical and Biophysical Research Communications*, vol. 485, no. 4, pp. 807–813, 2017.
- [9] S. Al-Salam and S. Hashmi, "Myocardial ischemia reperfusion injury: apoptotic, inflammatory and oxidative stress role of galectin-3," *Cellular Physiology and Biochemistry*, vol. 50, no. 3, pp. 1123–1139, 2018.
- [10] M. Zhai, B. Li, W. Duan et al., "Melatonin ameliorates myocardial ischemia reperfusion injury through SIRT3-dependent regulation of oxidative stress and apoptosis," *Journal of Pineal Research*, vol. 63, no. 2, 2017.
- [11] M. Kawaguchi, M. Takahashi, T. Hata et al., "Inflammasome activation of cardiac fibroblasts is essential for myocardial ischemia/reperfusion injury," *Circulation*, vol. 123, no. 6, pp. 594–604, 2011.
- [12] A. Gardini and R. Shiekhattar, "The many faces of long non-coding RNAs," *The FEBS Journal*, vol. 282, no. 9, pp. 1647–1657, 2015.
- [13] O. Khorkova, J. Hsiao, and C. Wahlestedt, "Basic biology and therapeutic implications of lncRNA," *Advanced Drug Delivery Reviews*, vol. 87, pp. 15–24, 2015.
- [14] K. Wang, T. Sun, N. Li et al., "MDRL lncRNA regulates the processing of miR-484 primary transcript by targeting miR-361," *PLoS Genetics*, vol. 10, no. 7, article e1004467, 2014.
- [15] H. Wu, J. Liu, W. Li, G. Liu, and Z. Li, "lncRNA-HOTAIR promotes TNF- α production in cardiomyocytes of LPS-induced sepsis mice by activating NF- κ B pathway," *Biochemical and Biophysical Research Communications*, vol. 471, no. 1, pp. 240–246, 2016.
- [16] D. X. Zhang, D. Y. Ma, Z. Q. Yao et al., "ERK1/2/p53 and NF- κ B dependent-PUMA activation involves in doxorubicin-induced cardiomyocyte apoptosis," *European Review for Medical and Pharmacological Sciences*, vol. 20, no. 11, pp. 2435–2442, 2016.
- [17] X. Chen, W. Yu, W. Li et al., "An anti-inflammatory chalcone derivative prevents heart and kidney from hyperlipidemia-induced injuries by attenuating inflammation," *Toxicology and Applied Pharmacology*, vol. 338, pp. 43–53, 2018.
- [18] H. J. Zhang, Q. F. Wei, S. J. Wang et al., "Retracted: lncRNA HOTAIR alleviates rheumatoid arthritis by targeting miR-138 and inactivating NF- κ B pathway," *International Immunopharmacology*, vol. 50, pp. 283–290, 2017.
- [19] S. He, P. Liu, Z. Jian et al., "miR-138 protects cardiomyocytes from hypoxia-induced apoptosis via MLK3/JNK/c-Jun pathway," *Biochemical and Biophysical Research Communications*, vol. 441, no. 4, pp. 763–769, 2013.
- [20] M. Bartekova, J. Radosinska, M. Jelemsky, and N. S. Dhalla, "Role of cytokines and inflammation in heart function during health and disease," *Heart Failure Reviews*, vol. 23, no. 5, pp. 733–758, 2018.
- [21] S. Mitchell, J. Vargas, and A. Hoffmann, "Signaling via the NF κ B system," *Wiley Interdisciplinary Reviews. Systems Biology and Medicine*, vol. 8, no. 3, pp. 227–241, 2016.
- [22] E. E. Rivera-Serrano and B. Sherry, "NF- κ B activation is cell type-specific in the heart," *Virology*, vol. 502, pp. 133–143, 2017.

Research Article

Serum Levels of lncRNA CCHE1 and TCF21 in Patients with Coronary Artery Disease and Their Clinical Significances

Miaomiao Liu , Ying Zhang, Xiantong Cao, and Xue Wang

Department of Cardiovascular Surgery, First Affiliated Hospital of Xi'an Jiaotong University, Xi'an, China

Correspondence should be addressed to Miaomiao Liu; maggielmm@xjtu.edu.cn

Received 27 October 2021; Accepted 1 December 2021; Published 21 December 2021

Academic Editor: Francesco Busard?

Copyright © 2021 Miaomiao Liu et al. This is an open access article distributed under the Creative Commons Attribution License, which permits unrestricted use, distribution, and reproduction in any medium, provided the original work is properly cited.

Objective. To detect serum level changes of CCHE1 and TCF21 in coronary artery disease (CAD) patients and to explore their clinical significances. **Patients and Methods.** A total of 150 CAD patients were divided into the mild lesion group ($n = 52$), moderate lesion group ($n = 48$), and severe lesion group ($n = 50$), respectively, according to the Gensini score. In addition, they were divided into single vessel lesion ($n = 42$), two vessel lesions ($n = 49$), and three vessel lesions group ($n = 59$), respectively. Serum levels of CCHE1 and TCF21 in CAD patients were detected by quantitative real-time polymerase chain reaction (qRT-PCR). Spearman's rank correlation was conducted to assess the relationship between levels of CCHE1 and TCF21 and severity and numbers of vessel lesions in CAD. Pearson's correlation test was used for analyzing the correlation between CCHE1 and TCF21 levels. A multivariable logistic regression test was performed to evaluate the influences of CCHE1 and TCF21 levels on CAD severity and the occurrence of cardiovascular events within 3 years of follow-up. **Results.** Significant differences in incidences of diabetes and hypertension were identified in CAD patients divided according to CAD severity. In addition, significant differences in incidences of drinking, diabetes, and hypertension were identified in CAD patients divided according to numbers of vessel lesions. The serum level of CCHE1 was positively related to CAD severity and numbers of vessel lesions, while TCF21 displayed a negative relationship. During the 3-year follow-up, the incidence of cardiovascular events was 39.3% (59/150). CAD severity, numbers of vessel lesions, and serum levels of CCHE1 and TCF21 were independent factors influencing the occurrence of cardiovascular events in CAD patients. **Conclusions.** The increased serum level of CCHE1 and decreased TCF21 level are closely related to CAD severity, which are able to influence the prognosis in CAD patients.

1. Introduction

Coronary artery disease (CAD) is one of the major reasons for global death [1]. CAD is mainly caused by atherosclerosis [2]. Phenotypes of vascular smooth muscle cells (VSMCs) are changed following injuries, and they migrate to intima and aggregate ECM. VSMCs are of significance in the development of atherosclerosis [3].

Long non-coding RNAs (lncRNAs) contain more than 200 nucleotides in length, and they are unable to encode proteins [4]. Abnormally expressed lncRNAs have been detected in the heart or circulating system of myocardial infarction (MI) patients [5, 6]. A latest study has uncovered that lncRNA LIPCAR is capable of monitoring heart failure at post-MI, serving as a promising biomarker [7]. Further, MIAT controls advanced atherosclerotic lesion formation

and plaque destabilization [8]. The SNHG1-driven self-reinforcing regulatory network promoted cardiac regeneration and repair after myocardial infarction [9]. lncRNA CCHE1 (cervical carcinoma high expressed 1) has been recently discovered [10]. Microarray analysis showed upregulated CCHE1 in breast cancer profiling, suggesting that CCHE1 may have a certain impact on breast cancer progression [11, 12]. The correlation between CCHE1 and CAD, however, is rarely reported.

TCF21 locates on 6q23-q24, which was discovered in the research on the location of chromosomal heterozygosity in 2006 by Smith et al. [13]. TCF21 is a metastasis-suppressor gene. It is reported that TCF21 is extensively expressed in stromal cells or derived cells during the development of cardiovascular system, urogenital system, and respiratory system [14]. It largely affects cell growth and differentiation.

A previous study has proposed that LINC00163 alleviates lung cancer progression by upregulating TCF21 [15]. In this paper, we mainly explored the clinical significances of CCHE1 and TCF21 in CAD patients. Our findings can provide novel ideas in clinical treatment of CAD.

2. Patients and Methods

2.1. Baseline Characteristics. A total of 150 patients admitted in our hospital from June 2017 to May 2019 because of chest tightness, chest pain, or acute MI were enrolled. All patients underwent coronary angiography and treated according to the “2012 ACCF/AHA Focused Update of the Guideline for the Management of Patients with Unstable Angina/non-ST-Elevation Myocardial Infarction” [16]. Gensini score was graded depending on the stenosis and the locations of vessel narrowing (1 grade: stenosis < 25%, 2 grades: 26%-50% stenosis, 4 grades: 51-75% stenosis, 8 grades: 76%-90%, 16 grades: 90%-98%, and 32 grades: complete stenosis) [17]. Then, the corresponding coefficients were determined by the location of different narrowing branches of coronary artery (left coronary artery: $\times 5$, proximal LAD: $\times 2.5$, mid-LAD: $\times 1.5$, and distal LAD: $\times 1$). We divided CAD patients into the mild lesion group (1.0-26.1 grades, $n = 52$), the moderate lesion group (26.2-51.4 grades, $n = 48$), and the severe lesion group (≥ 51.5 grades, $n = 50$) according to the Gensini score. In addition, patients were classified by the number of vessel lesions to the single-vessel lesion group: $\geq 50\%$ of stenosis of any single vessel in LAD, left circumflex, and right coronary artery; the two-vessel lesion group: $\geq 50\%$ of stenosis of any two vessels in LAD, left circumflex and right coronary artery; three vessel lesions group: stenosis in LAD, left circumflex and right coronary artery, or lesions in left main coronary artery combined with the right coronary artery. Patients with malignant tumors, liver or kidney insufficiency, acute/chronic infection, pregnant or lactating women, or those unwilling to participate in were excluded. The study was reviewed and approved by the Ethics Committee of First Affiliated Hospital of Xi'an Jiaotong University. All patients signed the informed consent.

2.2. Laboratory Examinations. Serum levels of TC (total cholesterol), TG (triglyceride), LDL-C (low-density lipoprotein cholesterol), and HDL-C (high-density lipoprotein cholesterol) were determined using the automatic biochemical instrument. Hcy (homocysteine) and CRP (C-reactive protein) were detected by enzyme-linked immunosorbent assay (ELISA) (R&D Systems, Minneapolis, MN, USA). LVEF (left ventricular ejection fraction) was recorded by echocardiography.

2.3. Quantitative Real-Time Polymerase Chain Reaction (qRT-PCR). Serum RNA was isolated using TRIzol and quantified by NanoDrop 2000 (Thermo Fisher Scientific, Waltham, MA, USA). RNA was reversely transcribed to complementary deoxyribose nucleic acid (cDNA) with the PrimeScript™ RT Master Mix and amplified by TBGreen® Premix Ex Taq™ II (TaKaRa, Tokyo, Japan). Thermal cycle reactions were as follows: 30 s at 95°C and 40 cycles for 5 s

at 95°C and 30 s at 60°C. Primer sequences were as follows: CCHE1—5'-AAGGTCCCAGGATACTCGC-3' (forward) and 5'-GTGTCGTGGACTGGCAAAT-3' (reverse); TCF21—5'-CCAGCTACATCGCCCACTTG-3' (forward) and 5'-CTTTCAGGTCACCTCTCGGGTTTC-3' (reverse); and GAPDH—5'-ACCACAGTCCATGCCATCAC-3' (forward) and 5'-TCCACCACCCTGTTGCTGTA-3' (reverse).

2.4. Follow-Up. Patients were followed up for three years by review, telephone, or e-mail. Cardiovascular events were recorded, including angina pectoris, MI, arrhythmia, sudden cardiac death, and stroke.

2.5. Statistical Analyses. Data were processed by SPSS 20.0. Measurement data were expressed as the mean \pm SD and compared using a *t*-test or variance analysis. Counting data were expressed as composition ratio or rate (%) and compared by a chi-square test. Spearman's rank correlation was conducted to assess the relationship between levels of CCHE1 and TCF21 and severity and numbers of vessel lesions in CAD. Pearson's correlation test was used for analyzing the correlation between CCHE1 and TCF21 levels. A multivariable logistic regression test was performed to analyze the influences of CCHE1 and TCF21 levels on CAD severity and the occurrence of cardiovascular events within 3 years of follow-up. $p < 0.05$ was statistically significant.

3. Results

3.1. Clinical Data of CAD Patients. Significant differences in incidences of diabetes and hypertension were identified in CAD patients in the mild lesion group ($n = 52$), the moderate lesion group ($n = 48$), and the severe lesion group ($n = 50$) divided according to the Gensini score. Besides, significant differences in incidences of drinking, diabetes and hypertension were identified in CAD patients in the single-vessel lesion ($n = 42$), two-vessel lesion ($n = 49$), and three-vessel lesion groups ($n = 59$) (Tables 1 and 2). It is indicated that diabetes and hypertension could affect CAD severity, while diabetes, hypertension, and drinking could affect numbers of vessel lesions.

3.2. Serum Levels of CCHE1 and TCF21 in CAD Patients with Different Severities. Serum levels of CCHE1 and TCF21 in CAD patients with different severities were detected by qRT-PCR. CCHE1 level increased with the aggravation of CAD, manifesting as the lowest level in the mild lesion group and the highest level in the severe lesion group (Figure 1(a)). On the contrary, TCF21 level decreased with the severity of CAD (Figure 1(b)).

3.3. Serum Levels of CCHE1 and TCF21 in CAD Patients with Different Numbers of Vessel Lesions. We thereafter detected CCHE1 and TCF21 levels in CAD patients classified by numbers of vessel lesions. The lowest level of CCHE1 was detected in the single-vessel lesion group, and the highest level was detected in the three-vessel lesion group (Figure 2(a)). TCF21 level gradually decreased with the increased numbers of vessel lesions (Figure 2(b)).

TABLE 1: Clinical data of CAD patients with different severities.

Variable	Mild lesion ($n = 52$)	Moderate lesion ($n = 48$)	Severe lesion ($n = 50$)	p
Male/female	25/27	24/24	27/23	0.831
Age	56.23 ± 7.85	54.91 ± 6.08	55.21 ± 5.45	0.159
BMI (kg/m ²)	24.73 ± 3.11	23.01 ± 3.65	23.83 ± 3.94	0.073
Smoking	20 (38.46%)	17 (35.42%)	23 (46%)	0.543
Drinking	12 (23.08%)	14 (29.17%)	15 (30%)	0.693
TC (mmol/L)	4.89 ± 1.07	4.08 ± 1.33	4.36 ± 1.54	0.615
TG (mmol/L)	1.64 ± 0.46	1.73 ± 0.55	1.74 ± 0.54	0.368
LDL-C (mmol/L)	1.44 ± 0.62	1.38 ± 0.56	1.43 ± 0.71	0.741
HDL-C (mmol/L)	2.56 ± 1.72	2.65 ± 1.48	2.71 ± 1.82	0.587
Hcy (mmol/L)	14.46 ± 2.88	15.84 ± 3.06	15.38 ± 2.89	0.087
CRP (mg/L)	12.27 ± 5.23	13.61 ± 5.66	13.84 ± 5.68	0.103
LVEF (%)	64.13 ± 10.22	62.33 ± 9.36	60.87 ± 8.91	0.067
Diabetes (%)	5 (9.62%)	4 (8.33%)	13 (26%)	0.021
Hypertension (%)	4 (7.69%)	7 (14.58%)	18 (16%)	0.001

BMI: body mass index; TC: total cholesterol; TG: triglyceride; LDL-C: low-density lipoprotein cholesterol; HDL-C: high-density lipoprotein cholesterol; Hcy: homocysteine; CRP: C-reactive protein; LVEF: left ventricular ejection fraction.

TABLE 2: Clinical data of CAD patients with different numbers of vessel lesions.

Variable	Single vessel ($n = 42$)	Two vessels ($n = 49$)	Three vessels ($n = 59$)	p
Male/female	23/19	22/27	31/28	0.601
Age	57.27 ± 6.95	55.68 ± 5.18	57.11 ± 6.13	0.338
BMI (kg/m ²)	22.13 ± 4.03	23.32 ± 4.53	23.12 ± 3.83	0.275
Smoking	17 (40.48%)	19 (38.78%)	24 (40.68%)	0.977
Drinking	6 (14.29%)	10 (20.41%)	25 (42.37%)	0.003
TC (mmol/L)	4.11 ± 2.37	4.41 ± 2.54	4.26 ± 2.05	0.652
TG (mmol/L)	1.77 ± 0.73	1.86 ± 0.71	1.92 ± 0.83	0.076
LDL-C (mmol/L)	1.37 ± 0.51	1.48 ± 0.56	1.43 ± 0.71	0.198
HDL-C (mmol/L)	2.56 ± 1.72	2.73 ± 1.98	2.82 ± 2.13	0.227
Hcy (mmol/L)	13.86 ± 3.18	14.21 ± 3.22	14.88 ± 3.89	0.088
CRP (mg/L)	12.57 ± 5.95	13.61 ± 5.99	14.11 ± 6.18	0.367
LVEF (%)	65.03 ± 11.73	63.13 ± 10.43	61.07 ± 9.32	0.216
Diabetes (%)	2 (4.76%)	6 (12.24%)	14 (23.73%)	0.025
Hypertension (%)	4 (9.52%)	6 (12.24%)	19 (32.2%)	0.005

BMI: body mass index; TC: total cholesterol; TG: triglyceride; LDL-C: low-density lipoprotein cholesterol; HDL-C: high-density lipoprotein cholesterol; Hcy: homocysteine; CRP: C-reactive protein; LVEF: left ventricular ejection fraction.

3.4. Relationship between Levels of CCHE1 and TCF21 and Severity and Numbers of Vessel Lesions in CAD. Spearman's rank correlation results uncovered that CCHE1 level was positively correlated to CAD severity and numbers of vessel lesions ($r = 0.388$ and 0.671 , respectively, $p < 0.05$), whereas TCF21 displayed a negative correlation to them ($r = -0.523$ and -0.397 , respectively, $p < 0.05$) (Table 3). It is further supported that CCHE1 and TCF21 were involved in the progression of CAD. In particular, CCHE1 aggravated CAD and TCF21 exerted a protective role.

3.5. Negative Interaction between CCHE1 and TCF21 in CAD Patients. Pearson's correlation test was conducted to

elucidate the potential interaction between CCHE1 and TCF21 in CAD patients. As data revealed, the serum level of CCHE1 was negatively correlated to TCF21 ($r = -0.5099$, $p < 0.001$) (Figure 3).

3.6. Influences of CCHE1 and TCF21 Levels on Cardiovascular Events in CAD Patients. During the 3-year follow-up, the incidence of cardiovascular events was 39.3% (59/150). Variables with statistical significances in Tables 1 and 2 were assigned as independent ones as follows: diabetes (yes = 1, no = 0); hypertension (yes = 1, no = 0); drinking (yes = 1, no = 0); CAD severity (mild lesion = 1, moderate and severe lesion = 2); and numbers of vessel

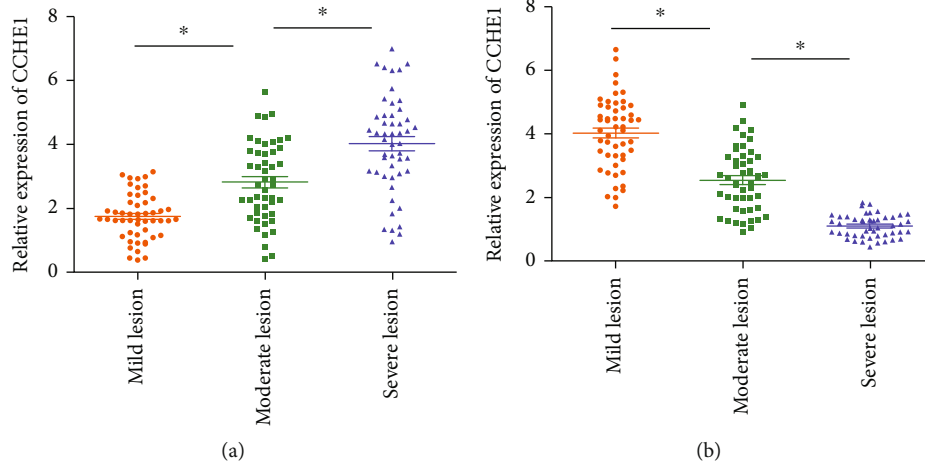


FIGURE 1: Serum levels of CCHE1 and TCF21 in CAD patients with different severities. Serum levels of CCHE1 (a) and TCF21 (b) in CAD patients of the mild lesion, moderate lesion, and severe lesion groups.

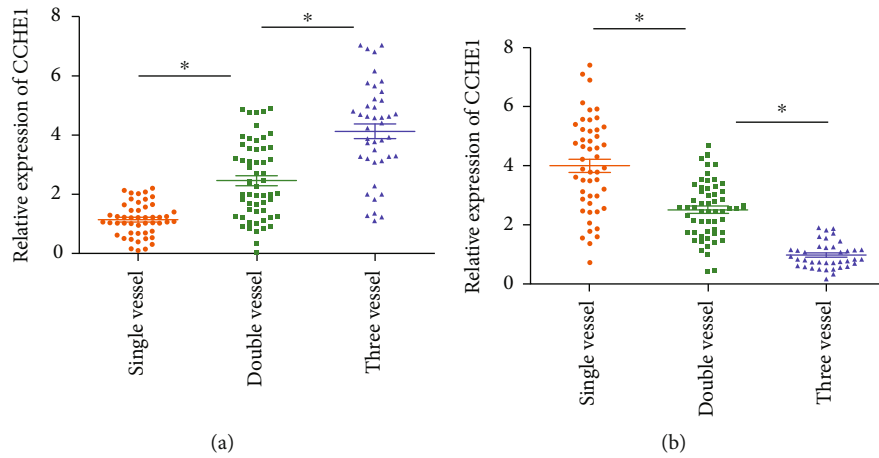


FIGURE 2: Serum levels of CCHE1 and TCF21 in CAD patients with different numbers of vessel lesions. Serum levels of CCHE1 (a) and TCF21 (b) in CAD patients of the single-vessel lesion, two-vessel lesion, and three-vessel lesion groups.

TABLE 3: Relationship between levels of CCHE1 and TCF21 and severity and numbers of vessel lesions in CAD.

	CCHE1		TCF21	
	<i>r</i>	<i>p</i>	<i>r</i>	<i>p</i>
Severity of CAD	0.388	0.041	-0.523	0.022
Numbers of vessel lesions	0.671	0.003	-0.397	<0.001

TABLE 4: Multivariable logistic analysis on potential factors influencing the occurrence of cardiovascular events in CAD patients.

Variable	OR	95% CI	<i>p</i>
Diabetes	1.733	0.614-5.332	0.142
Hypertension	0.892	0.561-2.313	0.668
Drinking	0.873	0.446-2.985	0.079
Severity of CAD	1.681	1.281-3.452	0.035
Number of vessel lesions	1.546	1.332-2.775	<0.001
CCHE1	2.387	1.654-5.872	<0.001
TCF21	0.584	0.287-1.664	0.007

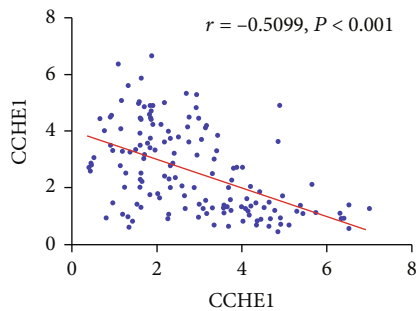


FIGURE 3: A negative correlation between serum levels of CCHE1 and TCF21 in CAD patients ($r = -0.5099, p < 0.001$).

lesions (single vessel = 1, multiple vessels = 2). Subsequently, CAD patients were divided into two groups according to the cut-off values of mRNA levels of CCHE1 and TCF21 (high level = 1, low level = 0). The occurrence of cardiovascular events during the follow-up of CAD patients was assigned as the dependent variable (yes = 1, no = 0). A multivariable logistic regression test demonstrated that severe

CAD, multiple vessel lesions, and high level of CCHE1 were independent risk factors, while the high level of TCF21 was a protective factor influencing the occurrence of cardiovascular events in CAD patients (Table 4).

4. Discussion

With the completion of the gene sequencing program and the development of molecular biology, it is found that protein-encoding mRNAs only account for 2% of the human genome. More than 95% of the transcribed sequences in the genome are noncoding RNAs [18]. These noncoding RNAs, which were initially regarded as nonfunctional, are involved in various life activities. As a family member of noncoding RNAs, lncRNAs are 200 bp long. They exert diverse functions as signal molecules, decoy molecules, and scaffold molecules. lncRNAs are involved in genetic, transcriptional, and posttranscriptional regulations [19].

lncRNAs have been identified to have a relation to vascular diseases. It is reported that lncRNA ANRIL is highly expressed in the blood of atherosclerosis patients, and the high level of ANRIL enhances the risk of MI [20, 21]. Circulating system lncRNAs are promising biomarkers for diagnosing ischemic heart diseases. For example, lncRNA LIPCAR is linked to the progression of heart failure, which serves as a molecular indicator for myocardial remodeling [22]. Upregulated plasma lncRNA CoroMarker is highly specific and sensitive for diagnosing CAD [23]. Through regulating VSMC phenotypes, lncRNAs regulate atherosclerosis development by mediating adipogenesis and lipid deposition [24].

CCHE1 is upregulated in cervical cancer specimens and correlated to tumor size, tumor staging and overall survival in cervical cancer patients. It is considered a potential therapeutic target and prognostic biomarker for cervical cancer [25]. Meanwhile, CCHE1 is highly expressed in non-small-cell lung carcinoma, which drives malignant phenotypes via the ERK/MAPK signaling [26]. Overexpression of CCHE1 triggers proliferative rate and inhibits apoptosis of gastric cancer cells [27]. Our findings detected an increased serum level of CCHE1 in CAD patients, and its level was elevated with the aggravation of CAD. The high level of CCHE1 enhanced the risk of cardiovascular events in CAD patients.

TCF21, also known as POD-1, belongs to the bHLH family. It is expressed in the mesenchymal cells of the lung, kidney, and intestine; cardiac interstitial cells [28]; and glomerular epithelial cells [29]. TCF21 is of significance in driving EMT [30–32]. Cao et al. [31] detected urine samples in 50 bladder cancer patients, 50 renal cancer patients, and 50 prostate cancer patients. They proposed that combined detection of TCF21 level and PCDH17 methylation is conducive to diagnose urinary system tumors. Ye et al. [33] showed that abnormal methylation of TCF12 is associated with the poor prognosis in clear cell renal cell carcinoma. TCF21 is also an independent factor influencing the progression of CAD [34, 35]. Consistently, we found that the serum level of TCF21 decreased in CAD patients. TCF21 exerted a protective role in CAD severity and numbers of vessel

lesions. A negative correlation was identified between serum levels of CCHE1 and TCF21. We believed that enhanced level of CCHE1 and downregulated TCF21 predict the deterioration of CAD. In summary, we uncover the relationship between CCHE1 and TCF21 in CAD; however, the lack of *in vivo* and *in vitro* assay is the shortage of this research.

5. Conclusion

Increased serum level of CCHE1 and decreased TCF21 level are closely related to CAD severity, which are able to influence the prognosis in CAD patients.

Data Availability

The datasets used and analyzed during the current study are available from the corresponding author on reasonable request.

Conflicts of Interest

The authors declared no conflict of interest.

Acknowledgments

This study is supported by the Natural Science Foundation of Shaanxi Province (2020JQ-535).

References

- [1] X. Dai, S. Wiernek, J. P. Evans, and M. S. Runge, "Genetics of coronary artery disease and myocardial infarction," *World Journal of Cardiology*, vol. 8, no. 1, pp. 1–23, 2016.
- [2] X. B. Wang, Y. D. Han, S. Sabina et al., "HDAC9 variant Rs2107595 modifies susceptibility to coronary artery disease and the severity of coronary atherosclerosis in a Chinese Han population," *PLoS One*, vol. 11, no. 8, article e160449, 2016.
- [3] S. Gao, M. Wassler, L. Zhang et al., "MicroRNA-133a regulates insulin-like growth factor-1 receptor expression and vascular smooth muscle cell proliferation in murine atherosclerosis," *Atherosclerosis*, vol. 232, no. 1, pp. 171–179, 2014.
- [4] M. Sun and W. L. Kraus, "From discovery to function: the expanding roles of long noncoding RNAs in physiology and disease," *Endocrine Reviews*, vol. 36, no. 1, pp. 25–64, 2015.
- [5] Y. Cai, Y. Yang, X. Chen et al., "Circulating "LncPPAR δ " from monocytes as a novel biomarker for coronary artery diseases," *Medicine (Baltimore)*, vol. 95, no. 6, article e2360, 2016.
- [6] J. Hou, H. Long, C. Zhou et al., "Long noncoding RNA Braveheart promotes cardiogenic differentiation of mesenchymal stem cells *in vitro*," *Stem Cell Research & Therapy*, vol. 8, no. 1, p. 4, 2017.
- [7] Z. Zhang, W. Gao, Q. Q. Long et al., "Increased plasma levels of lncRNA H19 and LIPCAR are associated with increased risk of coronary artery disease in a Chinese population," *Scientific Reports*, vol. 7, no. 1, p. 7491, 2017.
- [8] F. Fasolo, H. Jin, G. Winski et al., "Long noncoding RNA-MIAT Controls advanced atherosclerotic lesion formation and plaque destabilization," *Circulation*, vol. 144, no. 19, pp. 1567–1583, 2021.
- [9] M. Li, H. Zheng, Y. Han et al., "LncRNA Snhg1-driven self-reinforcing regulatory network promoted cardiac regeneration

- and repair after myocardial infarction,” *Theranostics*, vol. 11, no. 19, pp. 9397–9414, 2021.
- [10] M. Yang, X. Zhai, B. Xia, Y. Wang, and G. Lou, “Long noncoding RNA CCHE1 promotes cervical cancer cell proliferation via upregulating PCNA,” *Tumour Biology*, vol. 36, no. 10, pp. 7615–7622, 2015.
- [11] Y. Chen, C. X. Wang, X. X. Sun, C. Wang, T. F. Liu, and D. J. Wang, “Long non-coding RNA CCHE1 overexpression predicts a poor prognosis for cervical cancer,” *European Review for Medical and Pharmacological Sciences*, vol. 21, no. 3, pp. 479–483, 2017.
- [12] W. Peng and H. Fan, “Long noncoding RNA CCHE1 indicates a poor prognosis of hepatocellular carcinoma and promotes carcinogenesis via activation of the ERK/MAPK pathway,” *Biomedicine & Pharmacotherapy*, vol. 83, pp. 450–455, 2016.
- [13] L. T. Smith, M. Lin, R. M. Brena et al., “Epigenetic regulation of the tumor suppressor gene TCF21 on 6q23-q24 in lung and head and neck cancer,” *Proceedings of the National Academy of Sciences of the United States of America*, vol. 103, no. 4, pp. 982–987, 2006.
- [14] X. Ao, W. Ding, Y. Zhang, D. Ding, and Y. Liu, “TCF21: a critical transcription factor in health and cancer,” *Journal of Molecular Medicine*, vol. 98, no. 8, pp. 1055–1068, 2020.
- [15] X. Guo, Y. Wei, Z. Wang et al., “LncRNA LINC00163 upregulation suppresses lung cancer development through transcriptionally increasing TCF21 expression,” *American Journal of Cancer Research*, vol. 8, no. 12, pp. 2494–2506, 2018.
- [16] H. Jneid, J. L. Anderson, R. S. Wright et al., “2012 ACCF/AHA focused update of the guideline for the management of patients with unstable angina/non-ST-elevation myocardial infarction (updating the 2007 guideline and replacing the 2011 focused update): a report of the American College of Cardiology Foundation/American Heart Association Task Force on Practice Guidelines,” *Journal of the American College of Cardiology*, vol. 60, no. 7, pp. 645–681, 2012.
- [17] G. G. Gensini, “A more meaningful scoring system for determining the severity of coronary heart disease,” *The American Journal of Cardiology*, vol. 51, no. 3, p. 606, 1983.
- [18] E. Pennisi, “Shining a light on the genome’s ‘dark matter,’” *Science*, vol. 330, no. 6011, p. 1614, 2010.
- [19] J. T. Kung, D. Colognori, and J. T. Lee, “Long noncoding RNAs: past, present, and future,” *Genetics*, vol. 193, no. 3, pp. 651–669, 2013.
- [20] A. Helgadottir, G. Thorleifsson, A. Manolescu et al., “A common variant on chromosome 9p21 affects the risk of myocardial infarction,” *Science*, vol. 316, no. 5830, pp. 1491–1493, 2007.
- [21] R. Murray, J. Bryant, P. Titcombe et al., “DNA methylation at birth within the promoter of ANRIL predicts markers of cardiovascular risk at 9 years,” *Clinical Epigenetics*, vol. 8, no. 1, p. 90, 2016.
- [22] R. Kumarswamy, C. Bauters, I. Volkmann et al., “Circulating long noncoding RNA, LIPCAR, predicts survival in patients with heart failure,” *Circulation Research*, vol. 114, no. 10, pp. 1569–1575, 2014.
- [23] Y. Yang, Y. Cai, G. Wu et al., “Plasma long non-coding RNA, CoroMarker, a novel biomarker for diagnosis of coronary artery disease,” *Clinical Science (London, England)*, vol. 129, no. 8, pp. 675–685, 2015.
- [24] S. Greco, G. Zaccagnini, A. Perfetti et al., “Long noncoding RNA dysregulation in ischemic heart failure,” *Journal of Translational Medicine*, vol. 14, no. 1, p. 183, 2016.
- [25] N. Naghashi and S. Ghorbian, “Clinical important dysregulation of long non-coding RNA CCHE1 and HULC in carcinogenesis of cervical cancer,” *Molecular Biology Reports*, vol. 46, no. 5, pp. 5419–5424, 2019.
- [26] Y. Liao, S. Cheng, J. Xiang, and C. Luo, “LncRNA CCHE1 increased proliferation, metastasis and invasion of non-small lung cancer cells and predicted poor survival in non-small lung cancer patients,” *European Review for Medical and Pharmacological Sciences*, vol. 22, no. 6, pp. 1686–1692, 2018.
- [27] G. Xu, Y. Zhang, N. Li, J. B. Zhang, and R. Xu, “LncRNA CCHE1 in the proliferation and apoptosis of gastric cancer cells,” *European Review for Medical and Pharmacological Sciences*, vol. 22, no. 9, pp. 2631–2637, 2018.
- [28] S. E. Quaggin, L. Schwartz, S. Cui et al., “The basic-helix-loop-helix protein pod1 is critically important for kidney and lung organogenesis,” *Development*, vol. 126, no. 24, pp. 5771–5783, 1999.
- [29] S. E. Quaggin, G. B. vanden Heuvel, and P. Igarashi, “Pod-1, a mesoderm-specific basic-helix-loop-helix protein expressed in mesenchymal and glomerular epithelial cells in the developing kidney,” *Mechanisms of Development*, vol. 71, no. 1-2, pp. 37–48, 1998.
- [30] B. Baum, J. Settleman, and M. P. Quinlan, “Transitions between epithelial and mesenchymal states in development and disease,” *Seminars in Cell & Developmental Biology*, vol. 19, no. 3, pp. 294–308, 2008.
- [31] H. Cao, E. Xu, H. Liu, L. Wan, and M. Lai, “Epithelial-mesenchymal transition in colorectal cancer metastasis: a system review,” *Pathology, Research and Practice*, vol. 211, no. 8, pp. 557–569, 2015.
- [32] A. Mitra, L. Mishra, and S. Li, “EMT, CTCs and CSCs in tumor relapse and drug-resistance,” *Oncotarget*, vol. 6, no. 13, pp. 10697–10711, 2015.
- [33] Y. W. Ye, Z. M. Jiang, W. H. Li et al., “Down-regulation of TCF21 is associated with poor survival in clear cell renal cell carcinoma,” *Neoplasma*, vol. 59, no. 6, pp. 599–605, 2012.
- [34] C. L. Miller, D. R. Anderson, R. K. Kundu et al., “Disease-related growth factor and embryonic signaling pathways modulate an enhancer of TCF21 expression at the 6q23.2 coronary heart disease locus,” *PLoS Genetics*, vol. 9, no. 7, article e1003652, 2013.
- [35] V. L. Costa, R. Henrique, S. A. Danielsen et al., “TCF21 and PCDH17 methylation: an innovative panel of biomarkers for a simultaneous detection of urological cancers,” *Epigenetics-U.S.*, vol. 6, no. 9, pp. 1120–1130, 2011.

Research Article

miRNA-19b-3p Stimulates Cardiomyocyte Apoptosis Induced by Myocardial Ischemia Reperfusion via Downregulating PTEN

Ke Li,¹ Xujie Ya,² Xiujuan Duan,³ Yang Li,⁴ and Xuefeng Lin⁴ 

¹Department of Cardiology, Nanyang Second People's Hospital, Nanyang, China

²The First Department of Cardiology, The Eighth People's Hospital of Hengshui City, Hengshui, China

³The Second Department of Cardiology, The Eighth People's Hospital of Hengshui City, Hengshui, China

⁴Department of Cardiovascular Medicine, The First Affiliated Hospital of Baotou Medical College, Baotou, China

Correspondence should be addressed to Xuefeng Lin; 1156961689@qq.com

Received 14 October 2021; Accepted 6 December 2021; Published 16 December 2021

Academic Editor: Francesco Busardò

Copyright © 2021 Ke Li et al. This is an open access article distributed under the Creative Commons Attribution License, which permits unrestricted use, distribution, and reproduction in any medium, provided the original work is properly cited.

Objective. To clarify the function of miRNA-19b-3p in accelerating myocardial ischemia-reperfusion injury- (MIRI-) induced cardiomyocyte apoptosis by downregulating gene of phosphate and tension homology deleted on chromosome ten (PTEN), thus influencing the progression of acute myocardial infarction. **Materials and Methods.** miRNA-19b-3p and PTEN levels in HCM cells undergoing hypoxia/reoxygenation (H/R) were determined. Meanwhile, activities of myocardium injury markers [lactate dehydrogenase (LDH), malondialdehyde; malonic dialdehyde (MDA), superoxide dismutase (SOD), and glutathione peroxidase (GSH-PX)] in H/R-induced HCM cells were tested. Through dual-luciferase reporter gene assay, the binding between miRNA-19b-3p and PTEN was verified. Regulatory effects of miRNA-19b-3p and PTEN on apoptotic rate and apoptosis-associated gene expressions (proapoptotic protein Bcl-2 associated X protein (Bax), antiapoptotic protein B-cell lymphoma-2 (Bcl-2), and cytochrome C) in H/R-induced human cardiac myocytes (HCM) cells were examined. **Results.** miRNA-19b-3p was upregulated, while PTEN was downregulated in H/R-induced HCM cells. Knockdown of miRNA-19b-3p decreased activities of LDH, MDA, and GSH-PX, but increased SOD level in H/R-induced HCM cells. The binding between miRNA-19b-3p and PTEN was confirmed. More importantly, knockdown of miRNA-19b-3p reduced apoptotic rate, downregulated proapoptosis gene expressions (Bax and cytochrome C), and upregulated antiapoptosis gene expression (Bcl-2), which were reversed by silence of PTEN. **Conclusions.** miRNA-19b-3p is upregulated in HCM cells undergoing hypoxia and reoxygenation, which accelerates MIRI-induced cardiomyocyte apoptosis through downregulating PTEN.

1. Introduction

Acute myocardial infarction (AMI) is an important cause of death and disability worldwide [1–3]. Timely myocardial reperfusion is the most effective intervention for alleviating ischemia-induced myocardium injury. However, reperfusion itself induces myocardial cell death, that is, myocardial ischemia-reperfusion injury (MIRI) [4–6]. Apoptosis is a process of programmed cell death influencing MIRI and cardiomyocyte loss during cardiac remodeling at post-AMI [7]. A growing number of evidences have suggested that cardiomyocyte apoptosis occurs primarily in the surviving myocardium following ischemia [8]. It is necessary to uncover the pathogenic mechanism of

MIRI and develop effective therapeutic targets for clinical treatment of AMI.

miRNAs are a class of noncoding DNAs expressed in eukaryotic cells, ranging in length from 20 to 25 nucleotides [9–11]. Mature miRNAs are processed by primary transcripts through various nucleases, which are then assembled into an RNA-induced silencing complex (RISC). Subsequently, RISC binds 3'UTR of target mRNAs through complementary base pairing, thus degrading mRNAs or inhibiting their translation [12, 13]. miRNAs are extensively distributed in different types of cells and human diseases, such as ischemic cardiomyopathy [14], cardiac remodeling [15], heart failure [16], and arrhythmia [17]. In recent years,

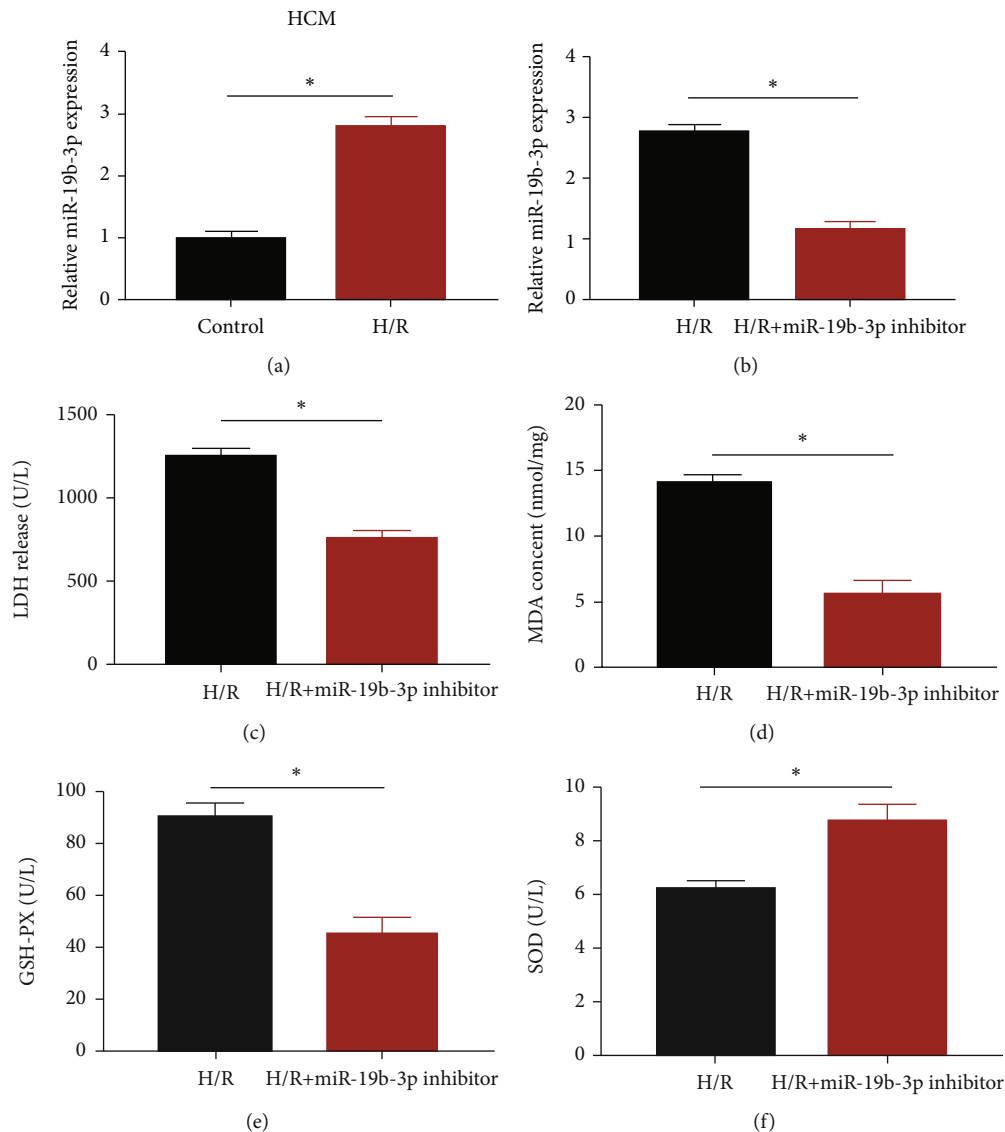


FIGURE 1: miRNA-19b-3p was upregulated in H/R-induced cells. (a) miRNA-19b-3p level in HCM cells undergoing normoxic or H/R induction. (b) Transfection efficacy of miRNA-19b-3p inhibitor. (c)–(f) Activities of LDH (c), MDA (d), GSH-PX (e), and SOD (f) in H/R-induced HCM cells or those transfected with miRNA-19b-3p inhibitor.

critical functions of miRNAs in MIRI have been identified [18–20]. These miRNAs could be utilized as therapeutic targets for clinical treatment of AMI.

miRNA-19b-3p is a member of the miR-17-92 cluster located on the human chromatin 13. Biological functions of miRNA-19b-3p have been discovered in multiple types of tumors [21–25]. In a recent study, exosomal miRNA-19b-3p of tubular epithelial cells promotes MI macrophage activation in kidney injury [26]. Further, circulating miR-19a-3p and miR-19b-3p characterize the human aging process and their isomiRs associate with healthy status at extreme ages [27]. However, the role of miR-19b-3p in AMI was unknown. In this paper, regulatory effects of miRNA-19b-3p on AMI-induced cardiomyocyte apoptosis were determined.

2. Materials and Methods

2.1. Cell Culture and H/R Induction. Human cardiac myocytes (HCM) provided by American Type Culture Collection (ATCC, Manassas, VA, USA) were cultured in Dulbecco's Modified Eagle's Medium (DMEM, Sigma, Louis, MO, USA) containing 10% fetal bovine serum (FBS, Invitrogen, Carlsbad, CA, USA). HCM cells were cultured in a humidified incubator containing 5% CO₂ and 95% N₂ for 4 h. Later, reoxygenation was conducted by cell culture in DMEM containing 10% glycerol in a humidified incubator containing 5% CO₂ and 95% air for 3 h. After normoxic culture overnight, cells were harvested for functional experiments. Normoxic-preconditioning HCM cells were harvested as controls.

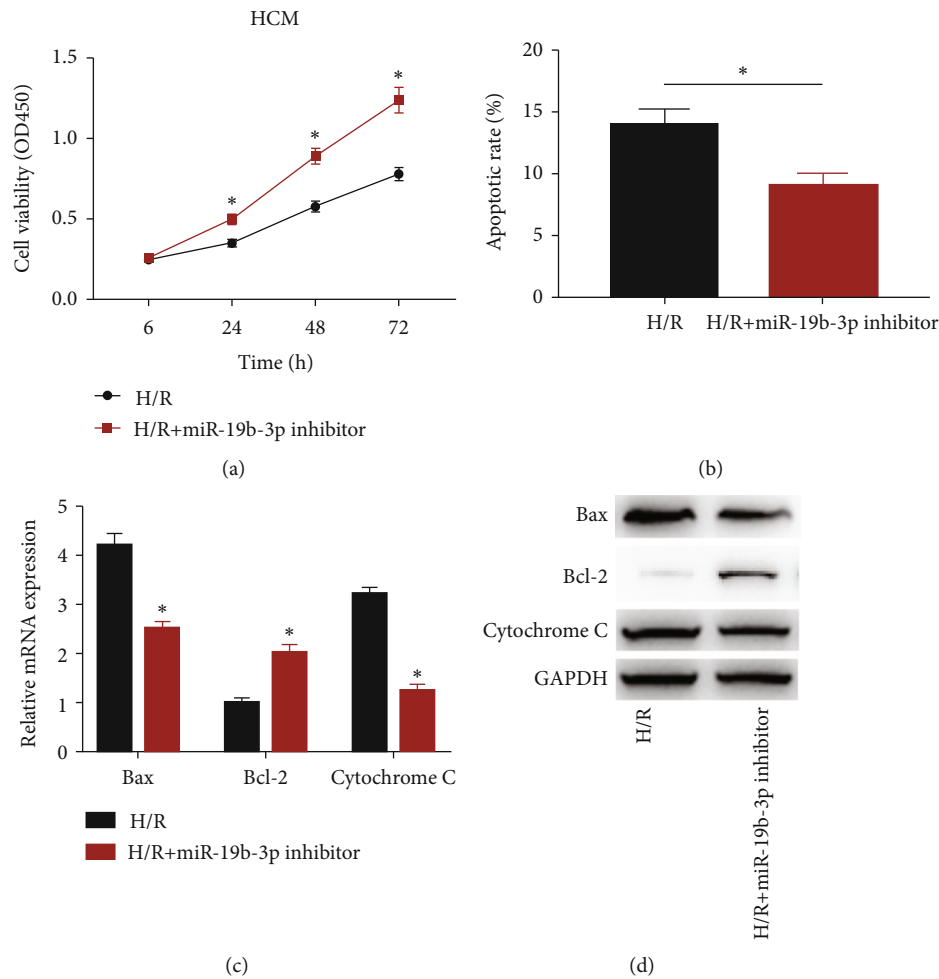


FIGURE 2: Knockdown of miRNA-19b-3p alleviated cardiomyocyte apoptosis. HCM cells were cultured in H/R environment and transfected either with miRNA-19b-3p inhibitor or not. (a) Viability. (b) Apoptotic rate. (c) The mRNA levels of Bax, Bcl-2, and cytochrome C. (d) The protein levels of Bax, Bcl-2, and cytochrome C.

2.2. Transfection. Transfection vectors were provided by GeneChem, (Shanghai, China). Cell transfection was conducted using Lipofectamine TM 2000 (Invitrogen, Carlsbad, CA, USA). Six hours later, transfection efficacy was verified. Transfected cells were collected for H/R exposure.

2.3. Real-Time Quantitative Polymerase Chain Reaction (RT-qPCR). TRIzol Reagent (Invitrogen, Carlsbad, CA, USA) was applied for isolating cellular RNA. Complementary deoxyribonucleic acids (cDNAs) was obtained by reverse transcription of 2 μ g RNA using cDNA synthesis kit (TaKaRa, Tokyo, Japan) and amplified on the MiniOpticon qPCR determination system (Bio-Rad, Hercules, CA, USA). Relative level was calculated using the $2^{-\Delta\Delta CT}$ method. miRNA-19b-3p, F: 5'-AGUUUUGCAUGGAUUUGCAC-3' and R: 5'-UUUGCAUGGAUUUGCACAUU-3'; PTEN, F: 5'-TGGT GAGTTTGTATCCGCATA-3' and R: 5'-CCCAGTCAG AGGCGCTATG-3'; Bax, F: 5'-CACAACCTCAGCGCAA CATT-3' and R: 5'-ACAGCCATCTCTCCATGC-3'; Bcl-2, F: 5'-GAAGCACAGATGGTTGATGG-3' and R: 5'-CAGCTCACAAGGTTCCAAT-3'; cytochrome C, F: 5'-

TAAATATGAGGGTGTGCGC-3' and R: 5'-AAGAATAGT TCCGTCCTG-3'.

2.4. Western Blot. Radio immunoprecipitation assay (RIPA) was applied for isolating cellular protein. Protein sample was quantified by bicinchoninic acid (BCA) method and underwent electrophoresis (Beyotime, Shanghai, China). Protein was transferred on a polyvinylidene fluoride (PVDF) membranes (Roche, Basel, Switzerland) and blocked in phosphate buffer saline (PBS) containing 5% skim milk for 2 h. Subsequently, membranes were reacted with primary antibodies at 4°C overnight and secondary antibodies for 2 h. Band exposure was achieved by enhanced chemiluminescence (ECL) and analyzed by Image Software (NIH, Bethesda, MD, USA).

2.5. Dual-Luciferase Reporter Gene Assay. Wild-type PTEN (NM_000314.8) 3' untranslated region (3'UTR) was amplified and inserted into the pGL3 vector. Predicted binding sequences between PTEN 3'UTR and miRNA-19b-3p were mutated using the QuickChange Site-Directed Mutagenesis Kit (Stratagene, Heidelberg, Germany). After cotransfection

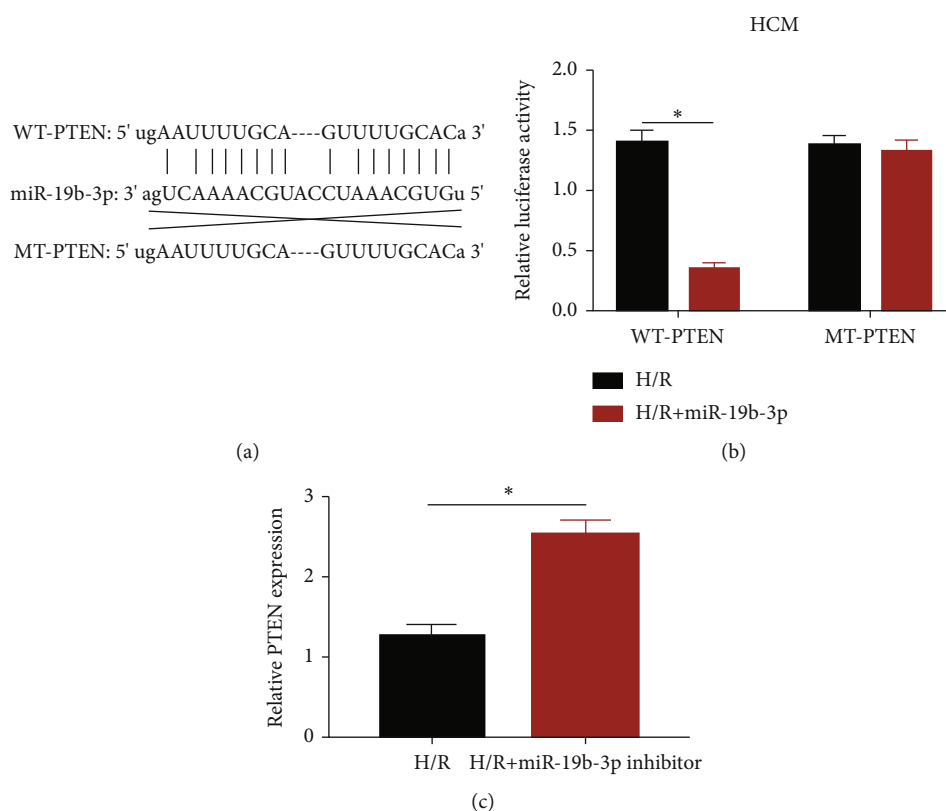


FIGURE 3: PTEN was the direct target of miRNA-19b-3p. (a) Potential binding sequences in the promoter regions of PTEN and miRNA-19b-3p. (b) Luciferase activity in HCM cells cotransfected with miRNA-19b-3p mimics/NC and WT-PTEN/MT-PTEN. (c) PTEN expression in H/R-induced HCM cells or those transfected with miRNA-19b-3p inhibitor.

with miRNA-19b-3p mimics/NC and WT-PTEN/MT-PTEN for 48 h, relative luciferase activity was determined.

2.6. Cell Counting Kit-8 (CCK-8). Cells were inoculated in a 96-well plate at 80% confluence. Viability was determined at the appointed time points using CCK-8 kit (Dojindo Laboratories, Kumamoto, Japan). Absorbance at 450 nm was recorded for plotting the viability curve.

2.7. Determination of Levels of LDH, MDA, SOD, and GSH-PX. Relative commercial kits were obtained from Sangon Biotech, (Shandong, China). Transfected cells were harvested for determining levels of myocardial injury markers based on the manufacturer's recommendations.

2.8. Flow Cytometry. Cells were digested in 0.25% trypsin, centrifuged, and washed with PBS for three times. Cells were dual-stained with Annexin-V-FITC (fluorescein isothiocyanate) and subjected to flow cytometry (FACSCalibur; BD Biosciences, Detroit, MI, USA) for measuring apoptotic rate.

2.9. Statistical Analysis. Statistical Product and Service Solutions (SPSS) 20.0 (SPSS, Chicago, IL, USA) was used for data analyses. Data were expressed as mean \pm standard deviation. The Student *t*-test was applied for analyzing differences between the two groups. $p < 0.05$ was considered statistically significant.

3. Results

3.1. miRNA-19b-3p Was Upregulated in H/R-Induced Cells. H/R was conducted in HCM cells to mimic the in vitro environment of MIRI. Compared with HCM cells under normoxic conditions, H/R induction markedly upregulated miRNA-19b-3p in HCM cells (Figure 1(a)). Subsequently, transfection of miRNA-19b-3p inhibitor markedly downregulated miRNA-19b-3p level in H/R-induced HCM cells, presenting an effective transfection efficacy (Figure 1(b)). Myocardial injury markers were determined here. As the data revealed, knockdown of miRNA-19b-3p decreased activities of LDH, MDA, and GSH-PX, but increased SOD level in H/R-induced HCM cells (Figures 1(c)–1(f)). It is demonstrated that miRNA-19b-3p was involved in MIRI.

3.2. Knockdown of miRNA-19b-3p Alleviated Cardiomyocyte Apoptosis. In H/R-induced HCM cells, transfection of miRNA-19b-3p inhibitor accelerated cell viability (Figure 2(a)). Nevertheless, apoptotic rate decreased after knockdown of miRNA-19b-3p in H/R-induced HCM cells (Figure 2(b)). Expression levels of apoptosis-associated genes, Bax, Bcl-2, and cytochrome C were determined. Both mRNA and protein levels of Bax and cytochrome C were downregulated, and Bcl-2 was upregulated in H/R-induced HCM cells transfected with miRNA-19b-3p inhibitor (Figures 2(c) and 2(d)).

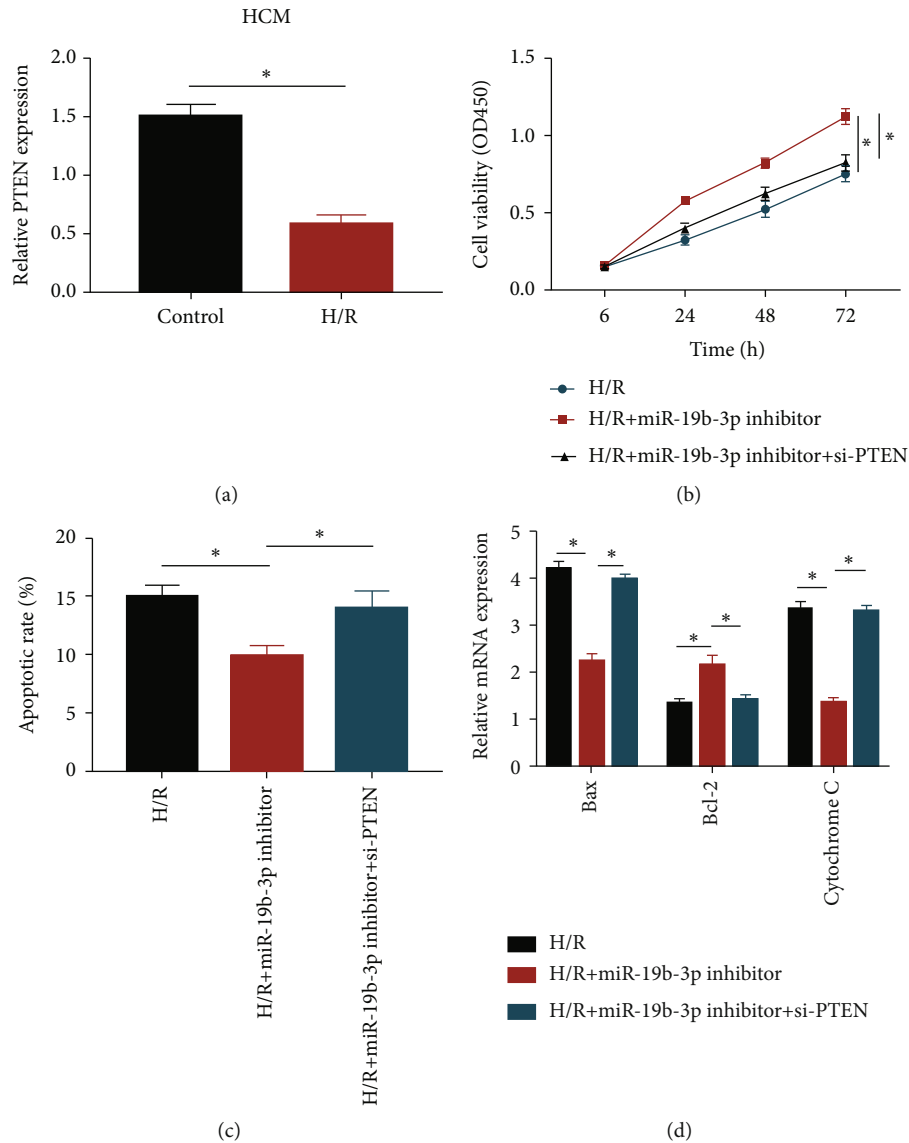


FIGURE 4: miRNA-19b-3p accelerated cardiomyocyte apoptosis by downregulating PTEN. (a) PTEN level in HCM cells undergoing normoxic or H/R induction. HCM cells were cultured in H/R environment and transfected with miRNA-19b-3p inhibitor or miRNA-19b-3p inhibitor + si-PTEN. (b) Viability. (c) Apoptotic rate. (d) The mRNA levels of Bax, Bcl-2, and cytochrome C.

3.3. PTEN Was the Direct Target of miRNA-19b-3p. To further uncover the mechanism of miRNA-19b-3p in influencing MIRI, we found potential binding sequences in the promoter regions of miRNA-19b-3p and PTEN as predicted in Targets-can (Figure 3(a)). Dual-luciferase reporter gene assay demonstrated that the overexpression of miRNA-19b-3p quenched luciferase activity in wild-type PTEN vector, while it did not affect mutant-type PTEN vector (Figure 3(b)). In addition, PTEN level was markedly upregulated in H/R-induced HCM cells transfected with miRNA-19b-3p inhibitor (Figure 3(c)). It is concluded that PTEN was the direct target of miRNA-19b-3p and negatively regulated by it.

3.4. miRNA-19b-3p Accelerated Cardiomyocyte Apoptosis by Downregulating PTEN. Compared with HCM cells cultured in the normoxic environment, PTEN was markedly downregulated in H/R-induced cells (Figure 4(a)). It is speculated that

PTEN was involved in cardiomyocyte apoptosis influenced by miRNA-19b-3p. CCK-8 assay showed that the enhanced viability in H/R-induced HCM cells with miRNA-19b-3p knock-down was partially reversed by cotransfection of si-PTEN (Figure 4(b)). Besides, decreased apoptotic rate after knock-down of miRNA-19b-3p was elevated by transfection of si-PTEN (Figure 4(c)). Similarly, regulatory effects of miRNA-19b-3p on apoptosis-associated gene expressions were reversed by silence of PTEN (Figure 4(d)). Therefore, PTEN was responsible for miRNA-19b-3p-mediated cardiomyocyte apoptosis following MIRI.

4. Discussion

Currently, thrombolysis, bypass surgery, and other interventions have been applied for reperfusion of blood flow and protection of ischemic myocardium [28].

Nevertheless, the sudden reperfusion of blood flow would result in secondary cardiovascular injury, that is, MIRI. MIRI results in cardiomyocyte apoptosis and necrosis, and even cardiac arrest [29]. Cell apoptosis is a vital event during the prognosis of MI. Inhibition of cardiomyocyte apoptosis and reduction of infarcted myocardium area could effectively alleviate the prognosis of AMI [30, 31].

Accumulating evidences have uncovered the role of miRNAs in regulating reperfusion in ischemic myocardium. In this paper, miRNA-19b-3p was upregulated in HCM cells under H/R precondition. Silence of miRNA-19b-3p markedly reduced activities of LDH, MDA, and GSH-PX and elevated SOD level in H/R-induced HCM cells. In addition, knockdown of miRNA-19b-3p resulted in viability elevation and apoptosis suppression in HCM cells. Our findings demonstrated the involvement of miRNA-19b-3p in MIRI-induced pathological changes. Furthermore, apoptosis-related genes were determined in H/R-induced HCM cells. Previous studies proposed that Bcl-2/Bax ratio is the key indicator reflecting the apoptotic level [32, 33]. Bcl-2 protein locates in the outer mitochondrial membrane, exerting an antiapoptosis function. Under normal circumstance, Bax is expressed in the cytoplasm. Once AMI occurs, apoptosis-related signaling triggers the translocation of cytoplasmic Bax into mitochondria, thus initiating the endogenous apoptosis. Here, silence of miRNA-19b-3p downregulated mRNA and protein levels of Bax and cytochrome C, and upregulated Bcl-2.

PTEN is a lipoprotein phosphatase that negatively regulates the PI3K/Akt pathway through PIP3 dephosphorylation and Akt translocation on the cell membrane [34, 35]. A recent study illustrated the crucial role of PTEN in mitochondrial-dependent apoptosis [36].

PTEN is considered to be an important pathway involved in MI. Previous studies have demonstrated that the upregulated miR-21 during MI affects collagen production by interfering with VEGF-mediated PTEN pathway [37]. In previous studies, miRNAs were reported to regulate target genes by binding to the 3'UTR area as a sponge thus to inhibit the translation of mRNA [38, 39]. In this paper, PTEN was confirmed to be the direct target of miRNA-19b-3p and negatively regulated by it. Besides, PTEN was lowly expressed in H/R-induced HCM cells. To elucidate the involvement of PTEN in HCM cell behaviors influenced by miRNA-19b-3p, gain-of-function experiments were conducted. Notably, knockdown of PTEN reversed regulatory effects of miRNA-19b-3p on apoptotic rate and apoptosis-associated gene expressions in H/R-induced HCM cells. As a result, PTEN was responsible for miRNA-19b-3p to influence MIRI-induced cardiomyocyte apoptosis.

5. Conclusions

miRNA-19b-3p is upregulated in HCM cells undergoing hypoxia and reoxygenation, which accelerates cardiomyocyte apoptosis through downregulating PTEN.

Data Availability

The datasets used and analyzed during the current study are available from the corresponding author on reasonable request.

Conflicts of Interest

The authors declared no conflict of interest.

References

- [1] A. V. Boopathy, P. L. Che, I. Somasuntharam et al., "The modulation of cardiac progenitor cell function by hydrogel-dependent Notch1 activation," *Biomaterials*, vol. 35, no. 28, pp. 8103–8112, 2014.
- [2] M. C. Acconcia, Q. Caretta, F. Romeo et al., "Meta-analyses on intra-aortic balloon pump in cardiogenic shock complicating acute myocardial infarction may provide biased results," *European Review for Medical and Pharmacological Sciences*, vol. 22, no. 8, pp. 2405–2414, 2018.
- [3] K. H. Humphries, M. Izadnegahdar, T. Sedlak et al., "Sex differences in cardiovascular disease - impact on care and outcomes," *Frontiers in Neuroendocrinology*, vol. 46, pp. 46–70, 2017.
- [4] E. Braunwald and R. A. Kloner, "Myocardial reperfusion: a double-edged sword?," *The Journal of Clinical Investigation*, vol. 76, no. 5, pp. 1713–1719, 1985.
- [5] H. M. Piper, D. Garcia-Dorado, and M. Ovize, "A fresh look at reperfusion injury," *Cardiovascular Research*, vol. 38, no. 2, pp. 291–300, 1998.
- [6] D. M. Yellon and D. J. Hausenloy, "Myocardial reperfusion injury," *The New England Journal of Medicine*, vol. 357, no. 11, pp. 1121–1135, 2007.
- [7] N. Zhao, L. Mi, X. Zhang et al., "Enhanced MiR-711 transcription by PPAR γ induces endoplasmic reticulum stress-mediated apoptosis targeting calnexin in rat cardiomyocytes after myocardial infarction," *Journal of Molecular and Cellular Cardiology*, vol. 118, pp. 36–45, 2018.
- [8] G. Olivetti, F. Quaini, R. Sala et al., "Acute myocardial infarction in humans is associated with activation of programmed myocyte cell death in the surviving portion of the heart," *Journal of Molecular and Cellular Cardiology*, vol. 28, no. 9, pp. 2005–2016, 1996.
- [9] J. Bauersachs and T. Thum, "MicroRNAs in the broken heart," *European Journal of Clinical Investigation*, vol. 37, no. 11, pp. 829–833, 2007.
- [10] V. Divakaran and D. L. Mann, "The emerging role of microRNAs in cardiac remodeling and heart failure," *Circulation Research*, vol. 103, no. 10, pp. 1072–1083, 2008.
- [11] E. van Rooij and E. N. Olson, "MicroRNAs: powerful new regulators of heart disease and provocative therapeutic targets," *The Journal of Clinical Investigation*, vol. 117, no. 9, pp. 2369–2376, 2007.
- [12] Y. Lee, C. Ahn, J. Han et al., "The nuclear RNase III Drosha initiates microRNA processing," *Nature*, vol. 425, no. 6956, pp. 415–419, 2003.
- [13] G. Hutvagner, J. McLachlan, A. E. Pasquinelli, E. Balint, T. Tuschl, and P. D. Zamore, "A cellular function for the RNA-interference enzyme dicer in the maturation of the let-

- 7 small temporal RNA," *Science*, vol. 293, no. 5531, pp. 834–838, 2001.
- [14] M. Jiao, H. Z. You, X. Y. Yang et al., "Circulating microRNA signature for the diagnosis of childhood dilated cardiomyopathy," *Scientific Reports*, vol. 8, no. 1, p. 724, 2018.
- [15] H. Harapan and C. M. Yeni, "The role of microRNAs on angiogenesis and vascular pressure in preeclampsia: the evidence from systematic review," *Egyptian Journal of Medical Human Genetics*, vol. 16, no. 4, pp. 313–325, 2015.
- [16] T. Wu, Y. Chen, Y. Du, J. Tao, Z. Zhou, and Z. Yang, "Serum exosomal MiR-92b-5p as a potential biomarker for acute heart failure caused by dilated cardiomyopathy," *Cellular Physiology and Biochemistry*, vol. 46, no. 5, pp. 1939–1950, 2018.
- [17] S. Yamada, Y. W. Hsiao, S. L. Chang et al., "Circulating microRNAs in arrhythmogenic right ventricular cardiomyopathy with ventricular arrhythmia," *Europace*, vol. 20, no. F11, pp. -f37–f45, 2018.
- [18] L. Ge, Y. Cai, F. Ying et al., "MiR-181c-5p exacerbates hypoxia/reoxygenation-induced cardiomyocyte apoptosis via targeting PTPN4," *Oxidative Medicine and Cellular Longevity*, vol. 2019, Article ID 1957920, 15 pages, 2019.
- [19] H. X. Xu, W. Pan, J. F. Qian, F. Liu, H. Q. Dong, and Q. J. Liu, "MicroRNA-21 contributes to the puerarin-induced cardioprotection via suppression of apoptosis and oxidative stress in a cell model of ischemia/reperfusion injury," *Molecular Medicine Reports*, vol. 20, no. 1, pp. 719–727, 2019.
- [20] Z. Q. Huang, W. Xu, J. L. Wu, X. Lu, and X. M. Chen, "MicroRNA-374a protects against myocardial ischemia-reperfusion injury in mice by targeting the MAPK6 pathway," *Life Sciences*, vol. 232, 2019.
- [21] L. L. Fang, X. H. Wang, B. F. Sun et al., "Expression, regulation and mechanism of action of the miR-17-92 cluster in tumor cells (review)," *International Journal of Molecular Medicine*, vol. 40, no. 6, pp. 1624–1630, 2017.
- [22] A. I. Osip'yants, E. N. Knyazev, A. V. Galatenko et al., "Changes in the level of circulating hsa-miR-297 and hsa-miR-19b-3p miRNA are associated with generalization of prostate cancer," *Bulletin of Experimental Biology and Medicine*, vol. 162, no. 3, pp. 379–382, 2017.
- [23] J. Zhang, Y. Song, C. Zhang et al., "Circulating MiR-16-5p and MiR-19b-3p as two novel potential biomarkers to indicate progression of gastric cancer," *Theranostics*, vol. 5, no. 7, pp. 733–745, 2015.
- [24] T. Huang, L. Yin, J. Wu et al., "MicroRNA-19b-3p regulates nasopharyngeal carcinoma radiosensitivity by targeting TNFAIP3/NF- κ B axis," *Journal of Experimental & Clinical Cancer Research*, vol. 35, no. 1, p. 188, 2016.
- [25] X. Zhou, W. Wen, X. Shan et al., "A six-microRNA panel in plasma was identified as a potential biomarker for lung adenocarcinoma diagnosis," *Oncotarget*, vol. 8, no. 4, pp. 6513–6525, 2017.
- [26] L. L. Lv, Y. Feng, M. Wu et al., "Exosomal miRNA-19b-3p of tubular epithelial cells promotes M1 macrophage activation in kidney injury," *Cell Death and Differentiation*, vol. 27, no. 1, pp. 210–226, 2020.
- [27] C. Morsiani, L. Terlecki-Zaniewicz, S. Skalicky et al., "Circulating miR-19a-3p and miR-19b-3p characterize the human aging process and their isomiRs associate with healthy status at extreme ages," *Aging Cell*, vol. 20, no. 7, p. 13409, 2021.
- [28] M. Ovize, R. A. Kloner, S. L. Hale, and K. Przyklenk, "Coronary cyclic flow variations "precondition" ischemic myocardium," *Circulation*, vol. 85, no. 2, pp. 779–789, 1992.
- [29] E. Murphy and C. Steenbergen, "Mechanisms underlying acute protection from cardiac ischemia-reperfusion injury," *Physiological Reviews*, vol. 88, no. 2, pp. 581–609, 2008.
- [30] M. Salto-Tellez, S. Yung Lim, R. M. el Oakley, T. P. Tang, Z. A. M. ALmsherqi, and S. K. Lim, "Myocardial infarction in the C57BL/6J mouse: a quantifiable and highly reproducible experimental model," *Cardiovascular Pathology*, vol. 13, no. 2, pp. 91–97, 2004.
- [31] E. M. Geltman, "Infarct size as a determinant of acute and long-term prognosis," *Cardiology Clinics*, vol. 2, no. 1, pp. 95–103, 1984.
- [32] P. D. Mace, S. J. Riedl, and G. S. Salvesen, "Caspase enzymology and activation mechanisms," *Methods in Enzymology*, vol. 544, pp. 161–178, 2014.
- [33] B. Leibowitz and J. Yu, "Mitochondrial signaling in cell death via the Bcl-2 family," *Cancer Biology & Therapy*, vol. 9, no. 6, pp. 417–422, 2010.
- [34] J. F. Williams, A. L. Winters, S. Lowitt, and A. Szentivanyi, "Depression of hepatic mixed-function oxidase activity by B. pertussis in splenectomized and athymic nude mice," *Immunopharmacology*, vol. 3, no. 2, pp. 101–106, 1981.
- [35] A. Gericke, M. Munson, and A. H. Ross, "Regulation of the PTEN phosphatase," *Gene*, vol. 374, pp. 1–9, 2006.
- [36] Y. Zhu, P. Hoell, B. Ahlemeyer, and J. Krieglstein, "PTEN: a crucial mediator of mitochondria-dependent apoptosis," *Apoptosis*, vol. 11, no. 2, pp. 197–207, 2006.
- [37] F. Yang, W. Liu, X. Yan et al., "Effects of mir-21 on cardiac microvascular endothelial cells after acute myocardial infarction in rats: role of phosphatase and Tensin homolog (PTEN)/vascular endothelial growth factor (VEGF) signal pathway," *Medical Science Monitor*, vol. 22, pp. 3562–3575, 2016.
- [38] L. Su, R. Li, Z. Zhang, J. Liu, J. Du, and H. Wei, "Identification of altered exosomal microRNAs and mRNAs in Alzheimer's disease," *Ageing Research Reviews*, vol. 26, article 101497, 2021.
- [39] S. Bansal, A. Arjuna, S. Perincheri et al., "Restrictive allograft syndrome vs bronchiolitis obliterans syndrome: immunological and molecular characterization of circulating exosomes," *The Journal of Heart and Lung Transplantation*, vol. 21, article 02487, 2021.

Research Article

miRNA-576 Alleviates the Malignant Progression of Atherosclerosis through Downregulating KLF5

Jing Wang,¹ Lihui Zhang,¹ Ting Wang,¹ Caige Li,¹ Lijing Jiao,¹ Zhansheng Zhao,¹ and Yongjun Li^{ID}²

¹Department of Endocrinology, The Second Hospital of Hebei Medical University, Shijiazhuang, China

²Department of Cardiology, The Second Hospital of Hebei Medical University, Shijiazhuang, China

Correspondence should be addressed to Yongjun Li; lyjbs2009@163.com

Received 10 October 2021; Accepted 16 November 2021; Published 8 December 2021

Academic Editor: Francesco Busardò

Copyright © 2021 Jing Wang et al. This is an open access article distributed under the Creative Commons Attribution License, which permits unrestricted use, distribution, and reproduction in any medium, provided the original work is properly cited.

Objective. To elucidate the role of microRNA-576 (miRNA-576) in alleviating the deterioration of atherosclerosis (AS) through downregulating krüppel-like factor 5 (KLF5). **Materials and Methods.** The AS model in mice was first constructed. Body weight, inflammation degrees, blood lipid, and relative levels of KLF5, miRNA-576, caspase-3, and bcl-2 in AS mice and control mice were compared. Dual-luciferase reporter gene assay was performed to evaluate the binding between miRNA-576 and KLF5. RAW264.7 cells were treated with 200 mg/L ox-LDL for establishing *in vitro* high-fat model. Regulatory effects of miRNA-576/KLF5 on relative levels of β -catenin and inflammatory factors in RAW264.7 cells were explored. **Results.** Body weight was heavier in AS mice than in controls. Protein levels of KLF5 and caspase-3 were upregulated, while bcl-2 was downregulated in AS mice. In particular, protein level of KLF5 was highly expressed in aortic tissues of AS mice. TC and LDL increased, and HDL decreased in AS mice compared with controls. Inflammatory factor levels were markedly elevated in AS mice. KLF5 was verified to be the target gene binding miRNA-576. Overexpression of miRNA-576 downregulated KLF5, inflammatory factors, and β -catenin in ox-LDL-treated RAW264.7 cells. Regulatory effect of miRNA-576 on the release of inflammatory factors in RAW264.7 cells could be partially abolished by KLF5. **Conclusions.** miRNA-576 alleviates malignant progression of AS *via* downregulating KLF5.

1. Introduction

Atherosclerosis (AS) is one of the most common cardiovascular diseases, posing a serious threat to human health. AS is a chronic progressive disease featured by endothelial damage, lipid deposition, monocyte infiltration, and lipid accumulation and fibrosis in the arteries [1, 2]. AS would lead to other severe cardiovascular lesions [3]. It is important to well elucidate the pathogenesis of AS.

MicroRNAs (miRNAs) are noncoding RNAs with 21-23 nucleotides long, which are extensively distributed in viruses, plants, and metazoans. They participate in posttranscriptional regulation. Abundant evidences have proven the critical role of miRNAs in the progression of AS [4]. They are responsible for regulating the formation and stability of plaques [5–7]. In a recent study, the author uncovered that miR-195-3p alleviates homocysteine-mediated atherosclerosis

by targeting IL-31 [8]. Besides, rs41291957 controls miR-143 and miR-145 expression and impacts coronary artery disease risk [9]. It is reported that miRNA-576 is a novel biomarker in renal cell carcinoma [10]. Its specific role in the progression of AS, however, remains unclear.

KLFs (krüppel-like factors) are transcription factors containing zinc finger structure, which are able to mediate DNA transcription. KLF5 is a vital mediator in the occurrence of cardiovascular diseases. It is reported that KLF5 is involved in the development of myocardial hypertrophy and fibrosis, and it could affect the pathological level of myocardial injury through activating the downstream pathways [11, 12]. In vascular smooth muscle cells, miR-9 stimulates cell phenotype changes through targeting KLF5 [13]. In addition, miRNA-152 suppresses malignant progression of AS by downregulating KLF5 [14]. In this paper, we constructed both *in vivo* and *in vitro* AS models, and the regulatory

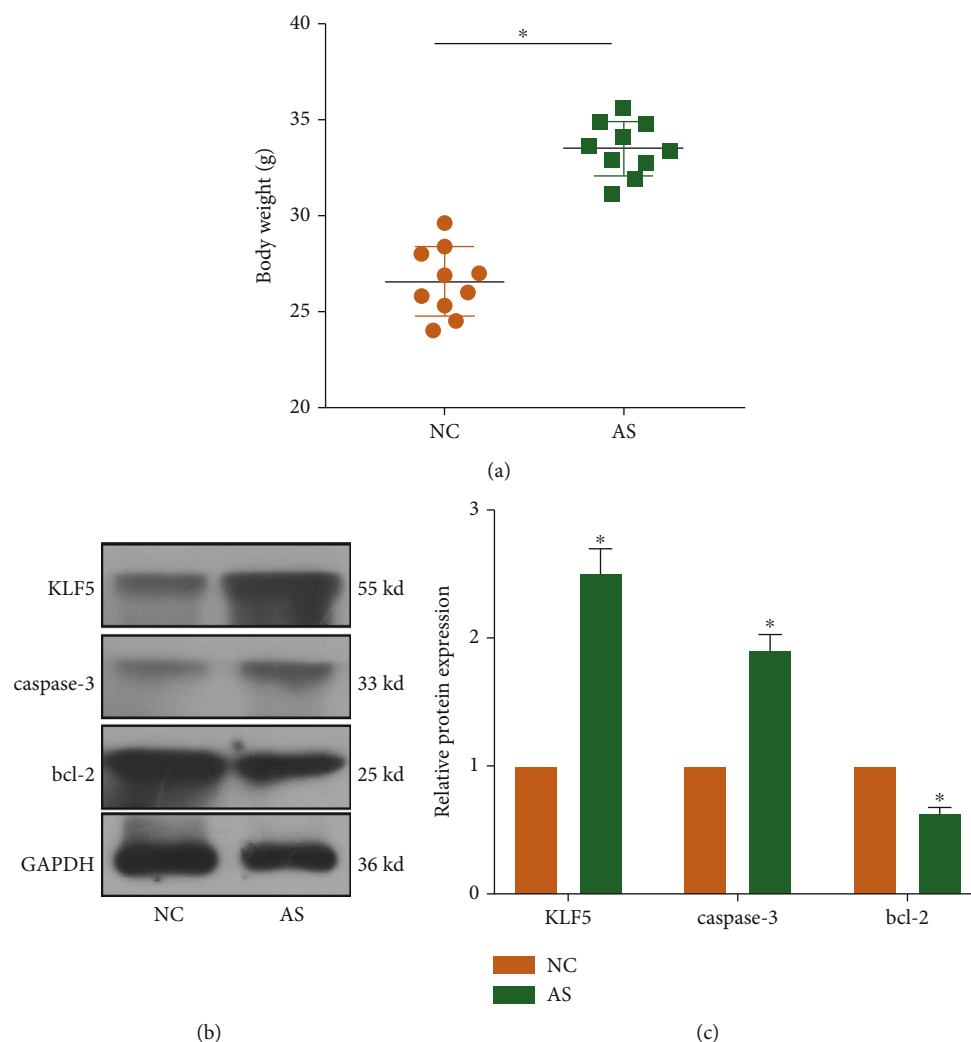


FIGURE 1: KLF5 was highly expressed in AS mice. (a) Body weight in AS mice and control mice. (b) Protein levels of KLF5, caspase-3, and bcl-2 in AS mice and control mice (c).

effects of miRNA-576 on the progression of AS were analyzed.

2. Materials and Methods

2.1. Construction of AS Model in Mice. This study was approved by the Animal Ethics Committee of Hebei Medical University Animal Center. 14 male C57BL/6J ApoE^{-/-} mice (20-25 g) were purchased from Cavens (Changzhou, Jiangsu, China). Mice were habituated in a standard environment with 12 h dark/light cycle, 55-60% humidity, and free access to food and water. They were randomly assigned into two groups, namely, AS group ($n=7$) and control group ($n=7$). Mice in the AS group were fed with high-fat diet (HFD) containing 10% custard powder, 10% lard, 1% cholesterol, 78.8% standard diet, and 0.2% sodium taurocholate for 12 consecutive weeks, while those in the control group were fed with standard diet [15].

2.2. Cell Culture. RAW264.7 cells were cultured in Roswell Park Memorial Institute 1640 (RPMI 1640) (Gibco, Rock-

ville, MD, USA) containing 10% fetal bovine serum (FBS) (Gibco, Rockville, MD, USA), 100 μ g/mL penicillin, and 100 mg/mL streptomycin. Cells were passaged for 4-5 times, and those in good condition were treated with 200 mg/L ox-LDL for 24 h.

2.3. Western Blot. Cells were lysed for isolating cellular protein and electrophoresed. Protein samples were loaded on polyvinylidene fluoride (PVDF) membranes (Roche, Basel, Switzerland). Subsequently, nonspecific antigens were blocked in 5% skim milk for 2 hours. Membranes were reacted with primary and secondary antibodies for indicated time. Band exposure and analyses were finally conducted.

2.4. Determination of Blood Lipid and Inflammatory Factors. Mice were forbidden to eat overnight before determination. Blood lipid levels and inflammatory factor levels were determined using commercial kits provided by JianKang Technology (Nanjing, China) and Abcam (Cambridge, MA, USA), respectively.

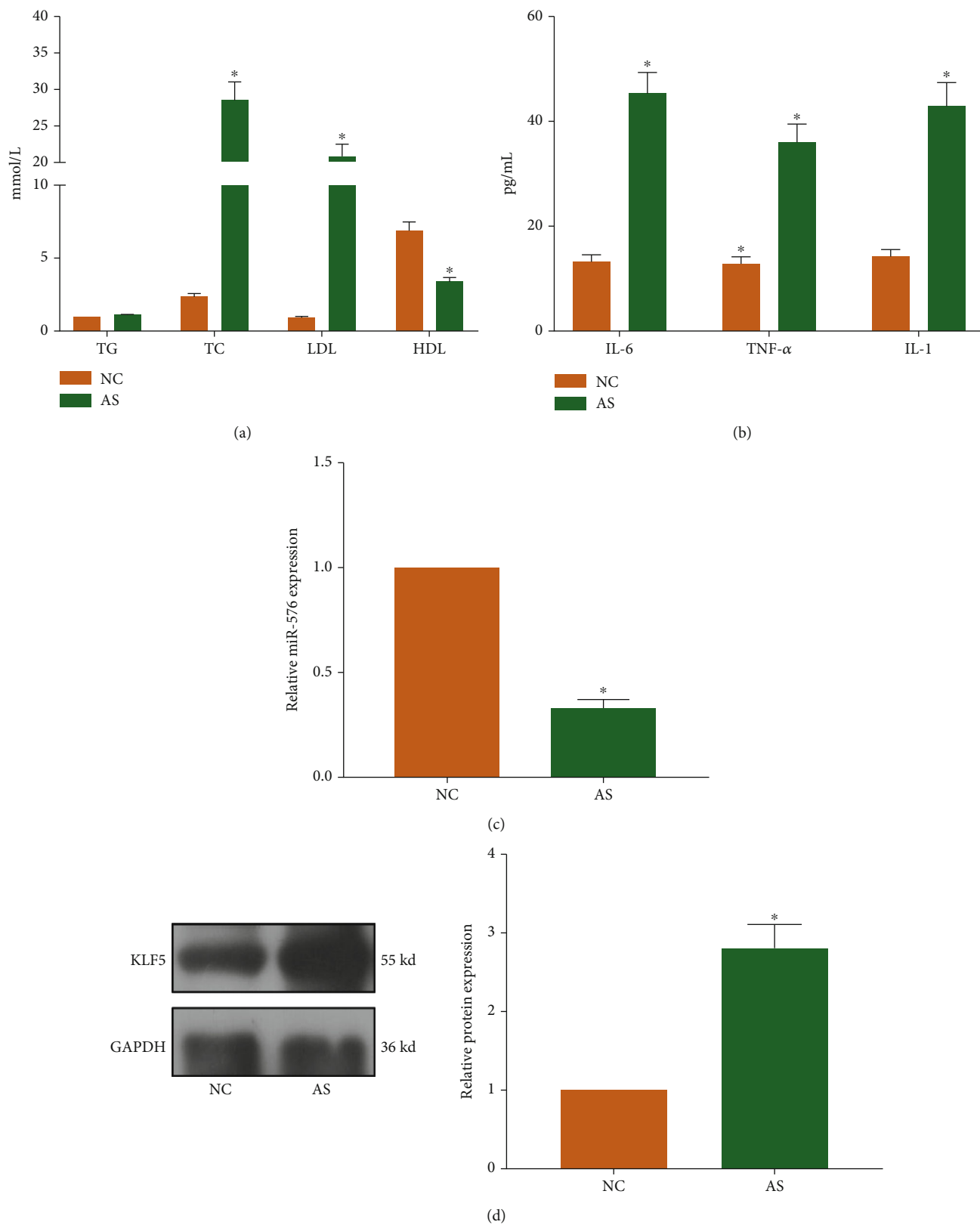


FIGURE 2: Relative levels of inflammatory factors and blood lipid increased in AS mice. (a) Serum levels of TG, TC, LDL, and HDL in AS mice and control mice. (b) Serum levels of IL-1, IL-6, and TNF-α in AS mice and control mice. (c) miRNA-576 level in AS mice and control mice. (d) Protein level of KLF5 in aortic tissues and normal tissues.

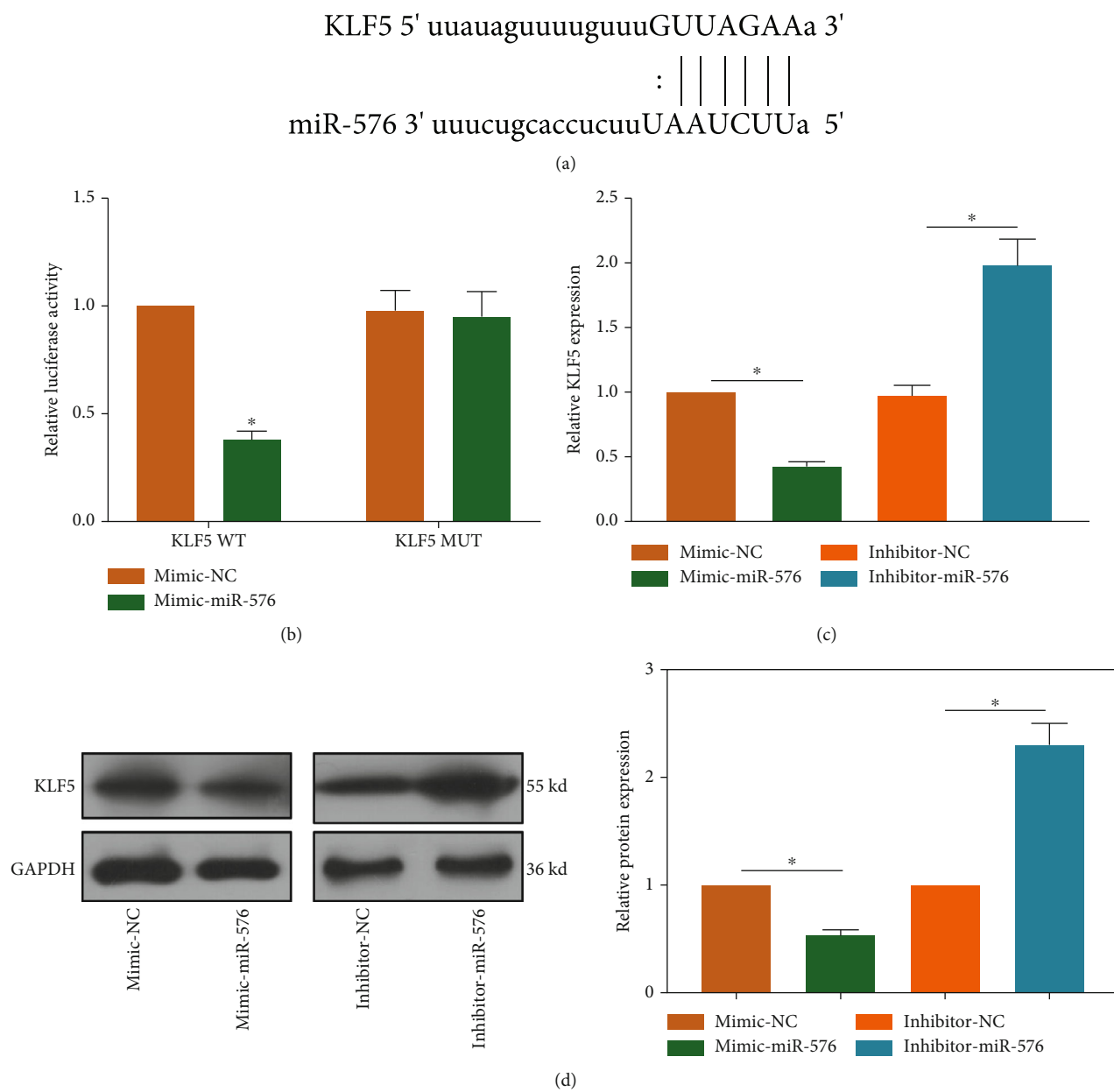
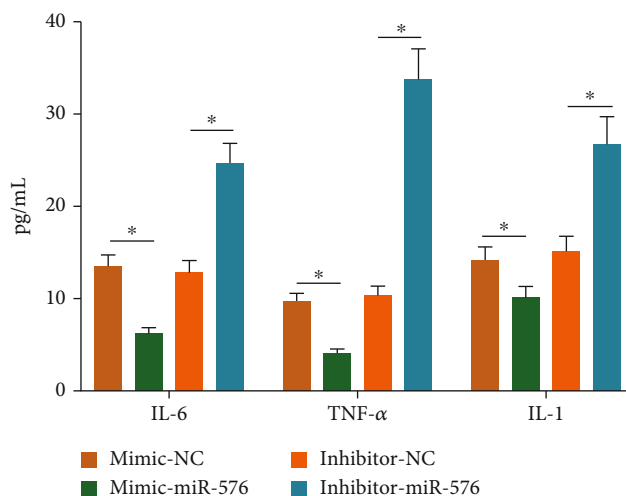


FIGURE 3: Continued.



(e)

FIGURE 3: KLF5 was the target gene binding miRNA-576. (a) Binding sequences in 3'UTR of KLF5 and miRNA-576. (b) Luciferase activity in 293T cells cotransfected with KLF5 WT/KLF5 MUT and miRNA-576 mimics/negative control, respectively. RAW264.7 cells were pretreated with 200 mg/L ox-LDL for 24 h. The (c) mRNA and (d) protein levels of KLF5 in RAW264.7 cells transfected with miRNA-576 mimic or inhibitor. (e) Relative levels of IL-1, IL-6, and TNF-α in RAW264.7 cells transfected with miRNA-576 mimic or inhibitor.

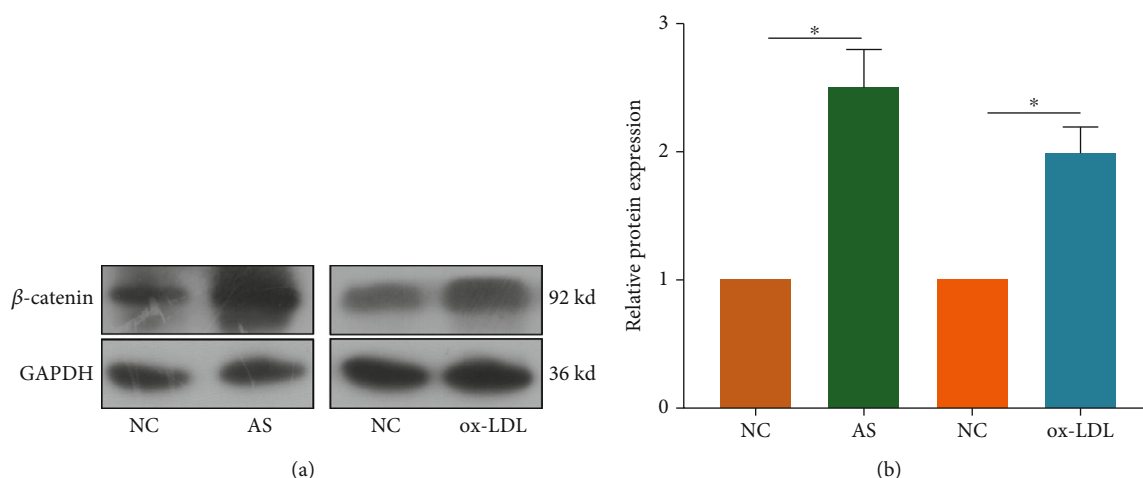


FIGURE 4: β-Catenin was upregulated in *in vivo* and *in vitro* AS models. Protein level of β-catenin in AS mice and RAW264.7 cells pretreated with 200 mg/L ox-LDL for 24 h.

2.5. Cell Transfection. RAW264.7 cells in good condition were inoculated in 6-well plates with 2×10^5 cells and transfected using Lipofectamine 2000 (Invitrogen, Carlsbad, CA, USA) at 80% confluence. Fresh medium was replaced at 6-8 h, and medium containing 2 μg/mL puromycin was applied at 48 h. Transfected cells were passaged into a new 6-well plate at 72 h. After cell culture for 1-2 weeks, positive colonies were selected for amplification.

2.6. RNA Extraction and Quantitative Real-Time Polymerase Chain Reaction (qRT-PCR). TRIzol method (Invitrogen, Carlsbad, CA, USA) was applied for isolating cellular RNA. Through reverse transcription of RNA, the extracted complementary deoxyribonucleic acid (cDNA) was used for PCR detection by SYBR Green method. Glyceraldehyde 3-phosphate dehydrogenase (GAPDH) was used as the inter-

nal reference. The primer sequences were listed as follows: GAPDH-forward: 5'-CCATGGGGAAGGTGAAGGTC-3', GAPDH-reverse: 5'-TGATGACCCTTTTGGCTCCC-3'; KLF5-forward (mouse): 5'-CGGCAGTAATGGACACCCTT-3', KLF5-reverse (mouse): 5'-ATTGTAGCGGCATAGGACGG-3'; U6-forward: 5'-CGCTTCGGCAGCACATATACTAAAATTGGAAC-3', U6-reverse: 5'-GCTTCACGAATTTGCGTGTCACTCCTTGC-3'; and miR-576-forward: 5'-TTGGGTCAAGAGTCAGAAGTTT-3', miR-576-reverse: 5'-TGGCTTCTACTTGTCTTTCC-3'.

2.7. Dual-Luciferase Reporter Gene Assay. 293T cells were inoculated in a 96-well plate with 1.5×10^4 cells. Mutant of plasmids (pGL3-KLF5-MUT and pGL3-KLF5-MUT) was generated by site-directed mutagenesis PCR reaction using

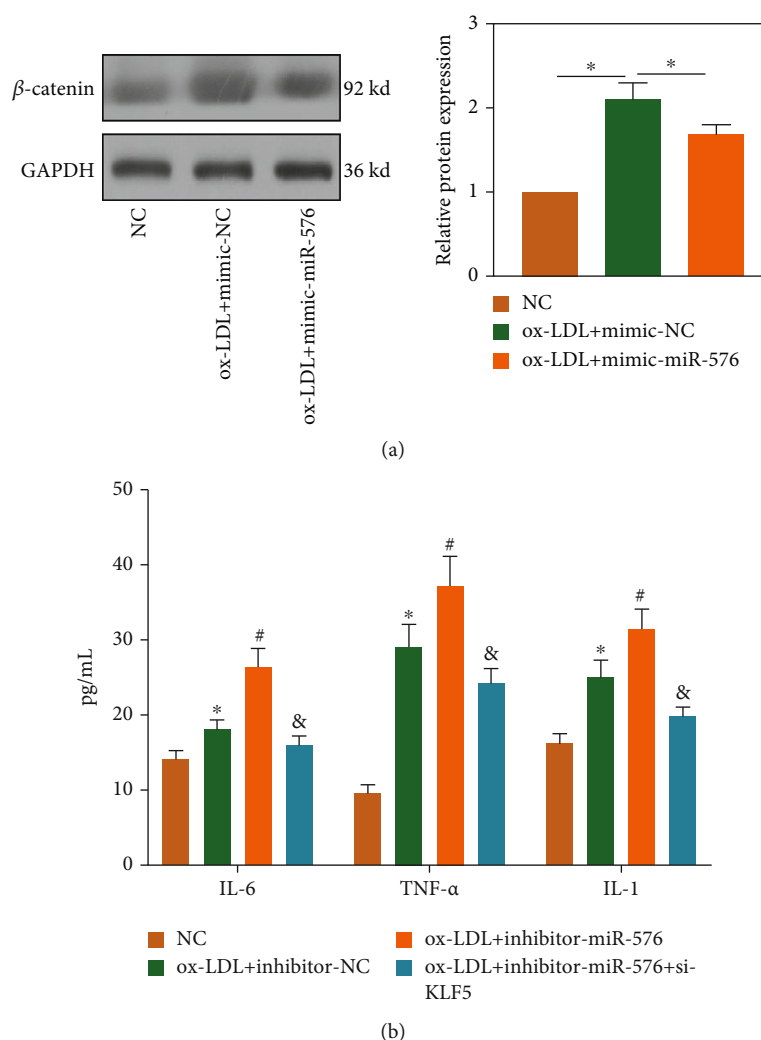


FIGURE 5: miRNA-576 downregulated β -catenin and suppressed release of inflammatory factors in RAW264.7 cells through targeting KLF5. (a) Protein level of β -catenin in ox-LDL-treated RAW264.7 cells transfected with miRNA-576 mimics or NC. (b) Relative levels of IL-1, IL-6, and TNF- α in ox-LDL-treated RAW264.7 cells transfected with NC, miRNA-576 inhibitor, or miRNA-576 inhibitor+si-KLF5.

platinum pfx DNA polymerase following the product manual. Cells were cotransfected with KLF5 WT/KLF5 MUT and miRNA-576 mimics/negative control, respectively. After transfection for 48 h, cells were lysed for measuring luciferase activity (Promega, Madison, WI, USA).

2.8. Statistical Analysis. Statistical Product and Service Solutions (SPSS) 20.0 (IBM, Armonk, NY, USA) was used for all statistical analysis. Data were expressed as mean \pm SD (standard deviation). The *t*-test was used for analyzing differences between two groups. One-way ANOVA was enrolled to comprise multigroups. $p < 0.05$ indicated the significant difference.

3. Results

3.1. KLF5 Was Highly Expressed in AS Mice. Compared with control mice, body weight was heavier in AS mice, suggesting the success construction of *in vivo* AS model (Figure 1(a)). Protein levels of KLF5 and caspase-3 were

upregulated, and bcl-2 was downregulated in AS mice (Figure 1(b)).

3.2. Relative Levels of Inflammatory Factors and Blood Lipid Increased in AS Mice. Relative levels of TC and LDL increased, and HDL decreased in AS mice, while TG level was similar in AS mice and control mice (Figure 2(a)). Furthermore, serum levels of IL-1, IL-6, and TNF- α were elevated in AS mice, verifying the stimulated inflammatory response (Figure 2(b)). Serum level of miRNA-576 was downregulated in AS mice (Figure 2(c)). Western blot analysis uncovered that protein level of KLF5 was markedly upregulated in aortic tissues than that of controls (Figure 2(d)).

3.3. KLF5 Was the Target Gene Binding miRNA-576. Through prediction in Starbase3.0, the binding sequences in 3'UTR of miRNA-576 and KLF5 were depicted (Figure 3(a)). Overexpression of miRNA-576 markedly quenched luciferase activity in wild-type KLF5 vector, confirming the binding relationship between miRNA-576 and KLF5 (Figure 3(b)). Subsequently,

RAW264.7 cells were pretreated with 200 mg/L ox-LDL for 24 h, and thus, a high-fat microenvironment was constructed. Transfection of miRNA-576 mimic markedly downregulated KLF5, and conversely, transfection of miRNA-576 inhibitor could upregulate KLF5 in ox-LDL-treated RAW264.7 cells (Figures 3(c) and 3(d)). ELISA results demonstrated that overexpression of miRNA-576 markedly downregulated inflammatory factor levels in RAW264.7 cells, and knockdown of miRNA-576 achieved the opposite trends (Figure 3(e)).

3.4. β -Catenin Was Upregulated in In Vivo and In Vitro AS Models. Interestingly, the protein level of β -catenin was markedly upregulated in AS mice than in controls. In addition, β -catenin was identically upregulated in ox-LDL-treated RAW264.7 cells (Figure 4). It is suggested that β -catenin may be involved in the pathogenesis of AS.

3.5. miRNA-576 Downregulated β -Catenin and Suppressed Release of Inflammatory Factors in RAW264.7 Cells through Targeting KLF5. The above findings have shown that β -catenin was upregulated in ox-LDL-treated RAW264.7 cells. Notably, this upregulated trend was reversed by overexpression of miRNA-576 (Figure 5(a)). Besides, knockdown of miRNA-576 triggered the release of inflammatory factors in RAW264.7 cells, which was abolished by knockdown of KLF5 (Figure 5(b)). Based on our findings, miRNA-576 downregulated β -catenin and suppressed release of inflammatory factors in RAW264.7 cells through targeting KLF5, thereafter affecting the progression of AS.

4. Discussion

Normal arterial endothelial cells have biological functions of barrier effect, anticoagulation, regulation of vascular tension, and activation of inflammatory mediators [16]. In the process of AS, vascular endothelial cells are impaired by chronic inflammation. Under the coactivation of chemokines and adhesion molecules, inflammatory cells such as monocytes and T cells migrate to the endarterium, where they are differentiated into macrophages. Eventually, monocytes and endothelial cells in the circulation are promoted to migrate and swallow lipids. Thereafter, macrophage foam cells are derived and atheromatous plaques are formed [17]. Multiple miRNAs are involved in chronic inflammatory responses in arterial endothelial cells, thus affecting the development of AS [18].

Wu et al. [19] demonstrated that miR-155 exerts an anti-AS effect on endothelial cells through a negative feedback loop. miR-125a-5p reduces the uptake of oxidized low-density lipoprotein by macrophages through downregulating ORP9. It also inhibits expression levels of inflammatory factors [20–22]. As a DNA-binding transcription factor, KLF5 could bind GT element or CACCC element in the promoter region, thus affecting transcription and expressions of downstream genes. KLF5 is involved in cancer and cardiovascular diseases [23, 24]. In recent years, KLF5 is found to be significant in the progression of AS and cardiac hypertrophy, as well as cell growth of cardiomyocytes and smooth muscle cells [25, 26]. A relevant animal experiment demon-

strated that KLF5^{-/-} mice present reduced myocardial fibrosis and hypertrophy [27].

In this paper, KLF5 was upregulated and miRNA-576 was downregulated in AS mice. We have verified that KLF5 was the downstream gene binding miRNA-576, and miRNA-576 could negatively regulate KLF5 level. Furthermore, overexpression of miRNA-576 partially reversed ox-LDL-induced upregulation of β -catenin in RAW264.7 cells. Knockdown of KLF5 abolished promotive effects of silenced miRNA-576 on the release of inflammatory factors. To sum up, miRNA-576 downregulated β -catenin and suppressed release of inflammatory factors in RAW264.7 cells through targeting KLF5, thereafter affecting the progression of AS.

5. Conclusions

miRNA-576 alleviates malignant progression of AS via downregulating KLF5.

Data Availability

The datasets used and analyzed during the current study are available from the corresponding author on reasonable request.

Conflicts of Interest

The authors declared no conflict of interest.



References

- [1] Y. Zhou, P. J. Little, H. T. Ta, S. Xu, and D. Kamato, "Lysophosphatidic acid and its receptors: pharmacology and therapeutic potential in atherosclerosis and vascular disease," *Pharmacology & Therapeutics*, vol. 204, 2019.
- [2] Department of Pediatric Gastroenterology and Metabolic Diseases, Poznań University of Medical Sciences, Poland, Institute of Human Nutrition and Dietetics, Poznań University of Life Science, Poland, M. Duś-Zuchowska et al., "The Central European diet as an alternative to the Mediterranean diet in atherosclerosis prevention in postmenopausal obese women with a high risk of metabolic syndrome - a randomized nutrition-al trial," *Acta Scientiarum Polonorum. Technologia Alimentaria*, vol. 17, no. 4, pp. 399–407, 2018.
- [3] X. Yue, D. Cao, F. Lan, Q. Pan, T. Xia, and H. Yu, "MiR-301a is activated by the Wnt/ β -catenin pathway and promotes glioma cell invasion by suppressing SEPT7," *Neuro-Oncology*, vol. 18, no. 9, pp. 1288–1296, 2016.
- [4] M. Ouimet, H. Ediriweera, M. S. Afonso et al., "MicroRNA-33 regulates macrophage autophagy in atherosclerosis," *Arteriosclerosis, Thrombosis, and Vascular Biology*, vol. 37, no. 6, pp. 1058–1067, 2017.
- [5] Y. R. Liu, J. J. Chen, and M. Dai, "Paeonol protects rat vascular endothelial cells from ox-LDL-induced injury *in vitro* via downregulating microRNA-21 expression and TNF- α release," *Acta Pharmacologica Sinica*, vol. 35, no. 4, pp. 483–488, 2014.
- [6] V. Ulrich, N. Rotllan, E. Araldi et al., "Chronic miR-29 antagonism promotes favorable plaque remodeling in atherosclerotic mice," *EMBO Molecular Medicine*, vol. 8, no. 6, pp. 643–653, 2016.

- [7] C. Zhang, L. Wang, T. Ali et al., "Hydatid cyst fluid promotes peri-cystic fibrosis in cystic echinococcosis by suppressing miR-19 expression," *Parasites & Vectors*, vol. 9, no. 1, p. 278, 2016.
- [8] J. Xiong, F. Ma, N. Ding et al., "miR-195-3p alleviates homocysteine-mediated atherosclerosis by targeting IL-31 through its epigenetics modifications," *Aging Cell*, vol. 20, no. 10, article e13485, 2021.
- [9] I. F. Hall, M. Climent, C. Viviani Anselmi et al., "rs41291957 controls miR-143 and miR-145 expression and impacts coronary artery disease risk," *EMBO Molecular Medicine*, vol. 13, no. 10, 2021.
- [10] T. Tang, X. Du, X. Zhang, W. Niu, C. Li, and J. Tan, "Computational identification and analysis of early diagnostic biomarkers for kidney cancer," *Journal of Human Genetics*, vol. 64, no. 10, pp. 1015–1022, 2019.
- [11] X. Liao, S. M. Haldar, Y. Lu et al., "Kruppel-like factor 4 regulates pressure-induced cardiac hypertrophy," *Journal of Molecular and Cellular Cardiology*, vol. 49, no. 2, pp. 334–338, 2010.
- [12] A. Clerk, T. J. Kemp, G. Zoumpoulidou, and P. H. Sugden, "Cardiac myocyte gene expression profiling during H₂O₂-induced apoptosis," *Physiological Genomics*, vol. 29, no. 2, pp. 118–127, 2007.
- [13] X. Lu, S. T. Ma, B. Zhou, and T. Li, "MiR-9 promotes the phenotypic switch of vascular smooth muscle cells by targeting KLF5," *Turkish Journal of Medical Sciences*, vol. 49, no. 3, pp. 928–938, 2019.
- [14] W. Wang, Y. Zhang, L. Wang et al., "microRNA-152 prevents the malignant progression of atherosclerosis via down-regulation of KLF5," *Biomedicine & Pharmacotherapy*, vol. 109, pp. 2409–2414, 2019.
- [15] C. Wu, H. Luan, X. Zhang et al., "Chlorogenic acid protects against atherosclerosis in ApoE^{-/-} mice and promotes cholesterol efflux from RAW264.7 macrophages," *PLoS One*, vol. 9, no. 9, article e95452, 2014.
- [16] Y. Shimizu and Y. Kuge, "Recent advances in the development of PET/SPECT probes for atherosclerosis imaging," *Nuclear Medicine and Molecular Imaging*, vol. 50, no. 4, pp. 284–291, 2016.
- [17] C. Ulrich, B. Trojanowicz, R. Fiedler et al., "Differential expression of lipoprotein-associated phospholipase A2 in monocyte subsets: impact of uremia and atherosclerosis," *Nephron*, vol. 135, no. 3, pp. 231–241, 2017.
- [18] M. C. Blaser and E. Aikawa, "Differential miRNA loading underpins dual harmful and protective roles for extracellular vesicles in atherogenesis," *Circulation Research*, vol. 124, no. 4, pp. 467–469, 2019.
- [19] X. Y. Wu, W. D. Fan, R. Fang, and G. F. Wu, "Regulation of microRNA-155 in endothelial inflammation by targeting nuclear factor (NF)- κ B p65," *Journal of Cellular Biochemistry*, vol. 115, no. 11, pp. 1928–1936, 2014.
- [20] X. Zhang, S. Shao, H. Geng et al., "Expression profiles of six circulating microRNAs critical to atherosclerosis in patients with subclinical hypothyroidism: a clinical study," *The Journal of Clinical Endocrinology and Metabolism*, vol. 99, no. 5, pp. E766–E774, 2014.
- [21] H. Yan, S. Wang, Z. Li et al., "Upregulation of miRNA-155 expression by OxLDL in dendritic cells involves JAK1/2 kinase and transcription factors YY1 and MYB," *International Journal of Molecular Medicine*, vol. 37, no. 5, pp. 1371–1378, 2016.
- [22] P. Neth, M. Nazari-Jahantigh, A. Schober, and C. Weber, "MicroRNAs in flow-dependent vascular remodelling," *Cardiovascular Research*, vol. 99, no. 2, pp. 294–303, 2013.
- [23] R. Liu, P. Shi, Z. Nie et al., "Mifepristone suppresses basal triple-negative breast cancer stem cells by down-regulating KLF5 expression," *Theranostics*, vol. 6, no. 4, pp. 533–544, 2016.
- [24] T. Shindo, I. Manabe, Y. Fukushima et al., "Kruppel-like zinc-finger transcription factor KLF5/BTEB2 is a target for angiotensin II signaling and an essential regulator of cardiovascular remodeling," *Nature Medicine*, vol. 8, no. 8, pp. 856–863, 2002.
- [25] K. Drosatos, N. M. Pollak, C. J. Pol et al., "Cardiac myocyte KLF5 regulates Ppara expression and cardiac function," *Circulation Research*, vol. 118, no. 2, pp. 241–253, 2016.
- [26] N. Takeda, I. Manabe, Y. Uchino et al., "Cardiac fibroblasts are essential for the adaptive response of the murine heart to pressure overload," *The Journal of Clinical Investigation*, vol. 120, no. 1, pp. 254–265, 2010.
- [27] K. N. Bell and N. F. Shroyer, "Krüppel-like factor 5 is required for proper maintenance of adult intestinal crypt cellular proliferation," *Digestive Diseases and Sciences*, vol. 60, no. 1, pp. 86–100, 2015.

Research Article

Cox-2 Antagonizes the Protective Effect of Sevoflurane on Hypoxia/Reoxygenation-Induced Cardiomyocyte Apoptosis through Inhibiting the Akt Pathway

Chunyan Guo,¹ Lei Zhang,² Yaoxing Gao,¹ Junzhi Sun,¹ Lingling Fan,¹ Yuguang Bai,¹ Jing Zhang,¹ Gaowa Naren,³ Jiwen Yang^{1,4} , and Libiao Li¹ 

¹Department of Anesthesiology, The Affiliated Hospital of Inner Mongolia Medical University, Hohhot, China

²Department of Ultrasound, The Affiliated Hospital of Inner Mongolia Medical University, Hohhot, China

³Department of Stomatology, Tongliao Hospital, Tongliao, China

⁴Department of Neurosurgery, The Affiliated Hospital of Inner Mongolia Medical University, Hohhot, China

Correspondence should be addressed to Jiwen Yang; yangyi19790419@163.com and Libiao Li; 20070020@immu.edu.cn

Received 12 October 2021; Accepted 16 November 2021; Published 7 December 2021

Academic Editor: Simona Pichini

Copyright © 2021 Chunyan Guo et al. This is an open access article distributed under the Creative Commons Attribution License, which permits unrestricted use, distribution, and reproduction in any medium, provided the original work is properly cited.

Objective. To uncover the protective role of sevoflurane on hypoxia/reoxygenation-induced cardiomyocyte apoptosis through the protein kinase B (Akt) pathway. **Methods.** An *in vitro* hypoxia/reoxygenation (H/R) model was established in cardiomyocyte cell line H9c2. Sevoflurane (SEV) was administrated in H9c2 cells during the reoxygenation period. Viability, layered double hydroxide (LDH) release, and apoptosis in H9c2 cells were determined to assess H/R-induced cell damage. Relative levels of apoptosis-associated genes were examined. Moreover, phosphorylation of Akt was determined. **Results.** H/R injury declined viability and enhanced LDH release and apoptotic rate in H9c2 cells. Cyclooxygenase-2 (Cox-2) was upregulated following H/R injury, which was partially reversed by SEV treatment. In addition, SEV treatment reversed changes in viability and LDH release owing to H/R injury in H9c2 cells, which were further aggravated by overexpression of Cox-2. The Akt pathway was inhibited in H9c2 cells overexpressing Cox-2. **Conclusions.** Sevoflurane protects cardiomyocyte damage following H/R *via* the Akt pathway, and its protective effect was abolished by overexpression of Cox-2.

1. Introduction

So far, ischemic heart diseases are the leading fatal cardiovascular diseases globally [1]. Myocardial ischemia/reperfusion (I/R) leads to apoptosis and necrosis of cardiomyocytes, further aggravating cardiac insufficiency, ventricular remodeling, and even heart failure [2]. Inhibition of apoptosis attributes to alleviate I/R-induced myocardial lesions, cardiomyocyte loss, and ventricular contractile dysfunction [3]. Severe hypoxia is the most typical feature of myocardial ischemia, which eventually results in ROS accumulation, intracellular calcium overload, inflammatory response, energy deficiency, and other serious lesions. Notably, reoxygenation following hypoxia may also cause secondary damage, eventually leading to cardiomyocyte death [4, 5]. It is of significance to clarify mechanisms of H/R injuries.

Protein kinase B (Akt) is a serine/threonine-specific protein kinase. Akt is extensively involved in cellular processes such as glucose metabolism, gene transcription, and cell behaviors [6, 7]. Accumulating evidences have suggested that the activated PI3K/Akt pathway following myocardial I/R injury induces a cardioprotective function [8, 9]. Cyclooxygenase-2 (Cox-2) is a cyclooxygenase isoform catalyzing the conversion of arachidonic acid to prostaglandins [10]. During the process of myocardial ischemia, Cox-2 is upregulated in myocardium [11, 12]. Besides, Cox-2 level is associated with the severity of apoptosis in myocardial infarction [13].

Sevoflurane (SEV) is an anesthetic that is widely applied in cardiac surgeries. Compared with other anesthetics, SEV has the advantages of short induction time, short recovery time, and high safety [14]. Recent studies have shown that

SEV pretreatment/posttreatment has significant protective effects on myocardial H/R injury [15, 16]. In this paper, H9c2 cells were utilized for constructing an *in vitro* H/R model. We mainly explored the potential protective role of SEV in myocardial H/R injury and the involvement of Cox-2.

2. Materials and Methods

2.1. Cell Culture. Rat embryonic cardiomyocyte cell line H9c2 was provided by Cell Bank (Shanghai, China). Cells were cultured in Dulbecco's modified eagle medium (DMEM) (Gibco, Rockville, MD, USA) containing 10% fetal bovine serum (FBS) (Gibco, Rockville, MD, USA), 100 μ g/mL penicillin, and 100 mg/mL streptomycin. Fresh medium was replaced every 2-3 days. Cell passage was performed at 80-90% confluence.

2.2. Construction of In Vitro H/R Model. H9c2 cells were cultured in low-serum medium (0.5% FBS) and exposed to 95% N₂/5% CO₂. After 2 h hypoxic culture, cells were cultured in fresh medium (10% FBS) and exposed to 95% air/5% CO₂. After reoxygenation for 1 h, the *in vitro* H/R model was constructed. Cells in the NC group were routinely cultured. SEV was administrated in cells of the H/R + SEV group during reoxygenation period.

2.3. Transfection. pcDNA3.1-Cox-2 (Cox-2 OE) (NM_017232.3) was constructed. Cells were transfected using Lipofectamine 2000 (Thermo Fisher Scientific, Waltham, MA, USA) as previously reported.

2.4. Cell Counting Kit-8 (CCK-8). Cells were inoculated in a 96-well plate. 100 μ L of 10% CCK-8 was applied in each well. At the appointed time points, absorbance value at 450 nm of each sample was recorded using the CCK-8 kit (Dojindo Laboratories, Kumamoto, Japan) for plotting the viability curves.

2.5. Layered Double Hydroxide (LDH) Release Determination. Cell supernatant was collected and incubated with 60 μ L of LDH working solution. After 30 min incubation in dark at room temperature on an oscillator, an absorbance value at 490 nm was recorded.

2.6. Flow Cytometry. Cells were collected, washed in precold PBS twice, and resuspended in 500 μ L of binding buffer containing 5 μ L of annexin V-FITC (fluorescein isothiocyanate) and 5 μ L of propidium iodide (PI) in dark. 30 min later, cell apoptosis was determined by flow cytometry at 488 nm excitation and 600 nm emission.

2.7. Quantitative Real-Time Polymerase Chain Reaction (qRT-PCR). TRIzol method (Invitrogen, Carlsbad, CA, USA) was applied for isolating cellular RNA. Through reverse transcription of RNA, the extracted complementary deoxyribose nucleic acid (cDNA) was used for PCR detection using the DBI Bestar SybrGreen qPCR Master Mix (DBI Bioscience, Shanghai, China) on Stratagene Mx3000P Real-Time PCR system (Agilent Technologies, Santa Clara, CA, USA). Glyceraldehyde 3-phosphate dehydrogenase

(GAPDH) was used as the internal reference. Cox-2: 5'-ATTGCTGGCCGGGTTGCTGG-3' (F), 5'-TCAGGGAGAAGCGTTTGCGGT-3' (R); GAPDH: 5'-TCCCTCAAGATGTTCAGCAA-3' (F), 5'-AGATCCACAACGGATACAT T-3' (R).

2.8. Western Blot. Cells were lysed for isolating cellular protein and electrophoresed. Protein samples were loaded on polyvinylidene fluoride (PVDF) membranes (Millipore, Billerica, MA, USA). Subsequently, nonspecific antigens were blocked in 5% skim milk for 2 hours. Gapdh (60004-1-Ig), Cox-2 (66351-3-Ig), Akt (60203-2-Ig), and p-Akt (66444-1-Ig) were all purchased from Proteintech. Membranes were reacted with primary and secondary antibodies for the indicated time. Band exposure and analyses were finally conducted.

2.9. Statistical Analysis. Statistical Product and Service Solutions (SPSS) 22.0 (IBM, Armonk, NY, USA) was used for all statistical analysis. Data were expressed as mean \pm SD (standard deviation). Comparison between multiple groups was done using one-way ANOVA test followed by post hoc test (Least Significant Difference). $p < 0.05$ indicated the significant difference.

3. Results

3.1. SEV Protected Cardiomyocyte Apoptosis following H/R. After establishing the H/R model in H9c2 cells, viability markedly decreased (Figure 1(a)), while LDH release (Figure 1(b)) and apoptosis increased (Figure 1(c)). Notably, SEV treatment partially reversed the above trends. Consistently, caspase-3 was markedly upregulated in the H/R group, and the increased level of caspase-3 was reduced by SEV (Figure 1(d)). Therefore, SEV markedly alleviated cardiomyocyte apoptosis following H/R injury.

3.2. Cox-2 Was Upregulated following H/R. QRT-PCR data showed that Cox-2 was upregulated at post-H/R in cardiomyocytes, and SEV treatment could partially relieve this increased trend (Figure 2(a)). Similarly, protein level changes of Cox-2 presented the same trends as its mRNA level (Figure 2(b)).

3.3. Overexpression of Cox-2 Suppressed Cardioprotective Role of SEV. To uncover the potential involvement of Cox-2 in cardioprotective role of SEV following H/R, pcDNA3.1-Cox-2 (Cox-2 OE) was constructed. Its transfection efficacy was firstly verified in H9c2 cells (Figures 3(a) and 3(b)). Interestingly, protective effects of SEV on viability enhancement (Figure 3(c)) and LDH release inhibition (Figure 3(d)) in H/R-induced cardiomyocytes were partially abolished by overexpression of Cox-2. Hence, the protective property of SEV on cardiomyocytes following H/R was largely limited by Cox-2.

3.4. Overexpression of Cox-2 Inhibited SEV-Induced p-Akt Upregulation. Accumulating evidences have proven the critical function of Akt in cardiomyocyte survival [17]. Here, p-Akt was downregulated following H/R injury. SEV treatment markedly increased protein level of p-Akt, which was

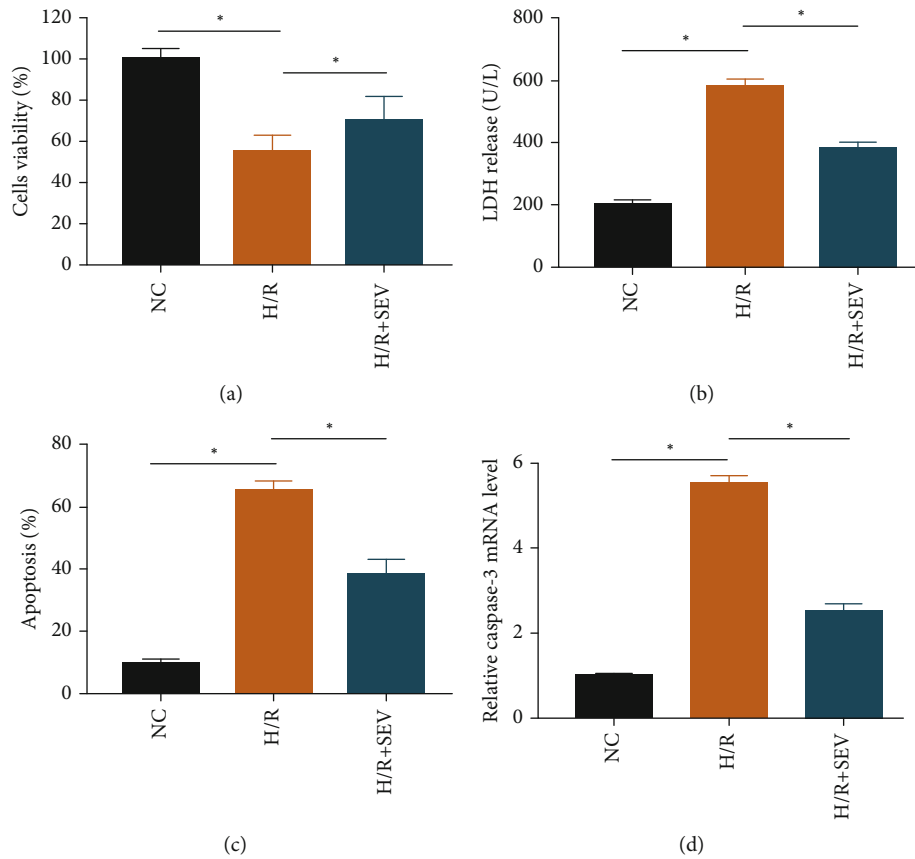


FIGURE 1: SEV protected H/R-induced cardiomyocyte apoptosis. H9c2 cells were assigned into the NC group, H/R group, and H/R + SEV group. Cell viability (a), LDH release (b), apoptotic rate (c), and mRNA level of caspase-3 (d).

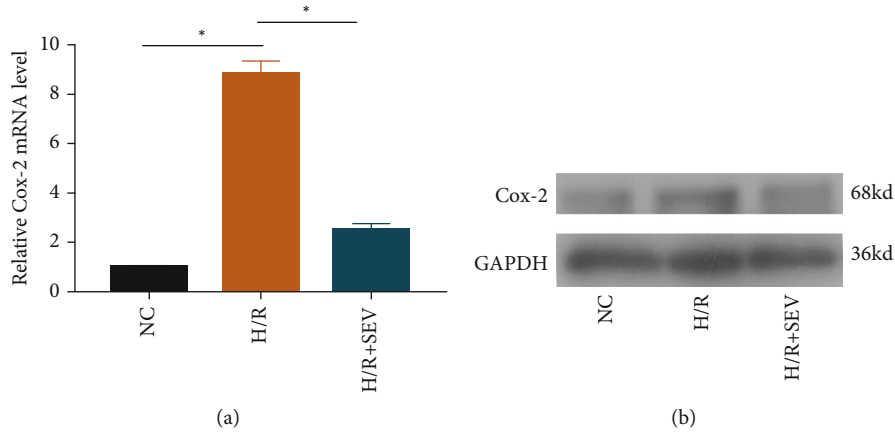


FIGURE 2: Cox-2 was upregulated following H/R. H9c2 cells were assigned into the NC group, H/R group, and H/R + SEV group. Relative mRNA (a) and protein level (b) of Cox-2.

inhibited by Cox-2 overexpression (Figures 4(a) and 4(b)). The Akt pathway was responsible for cardioprotective effect of SEV.

4. Discussion

Ischemic heart diseases pose extremely high morbidity and mortality. Blood flow reperfusion and reoxygenation follow-

ing ischemic injury are the conventional treatments. However, they may result in I/R and H/R injuries [18]. During the pathological progressions of I/R and H/R, a series of complicated events including oxidative stress, apoptosis, and inflammation significantly affect therapeutic efficacy [19, 20]. Prevention and treatment of I/R and H/R have been well concerned.

SEV is a commonly used inhalation anesthetic with multiple advantages. Animal experiments have proven that SEV

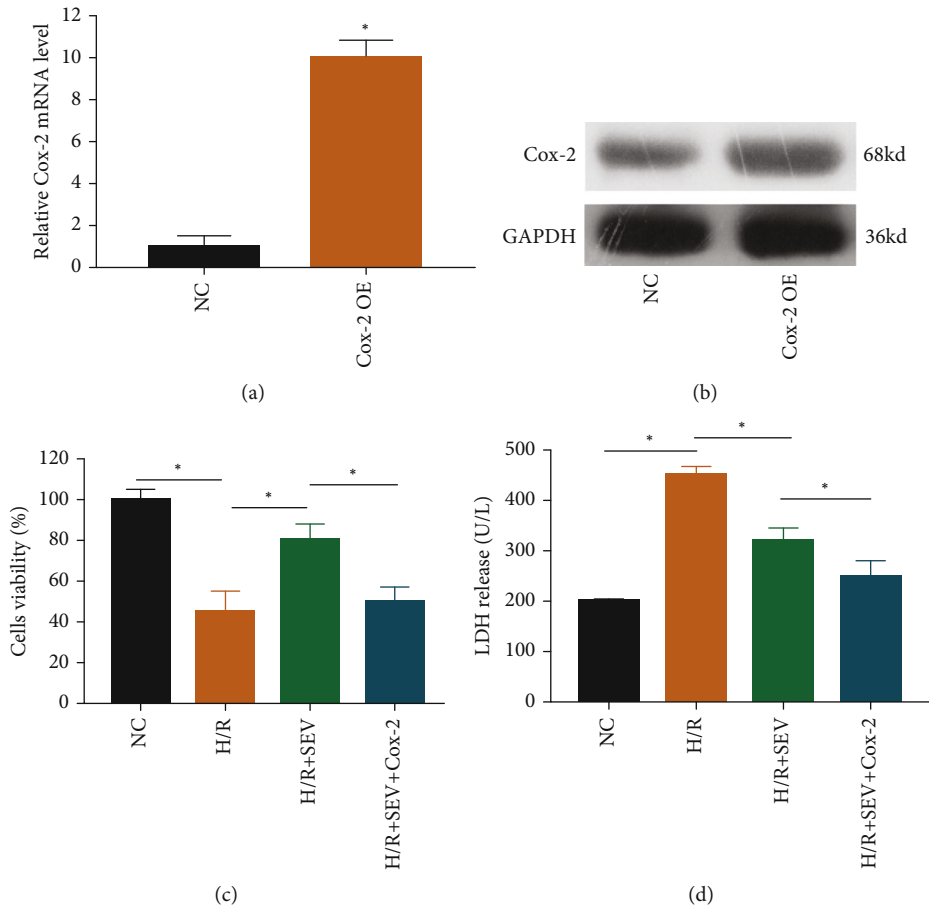


FIGURE 3: Overexpression of Cox-2 suppressed cardioprotective role of SEV. The mRNA (a) and protein level (b) of Cox-2 in H9c2 cells transfected with NC or Cox-2 OE. Cell viability (c) and LDH release (d) in H9c2 cells of NC group, H/R group, H/R + SEV group, and H/R + SEV + Cox-2 group.

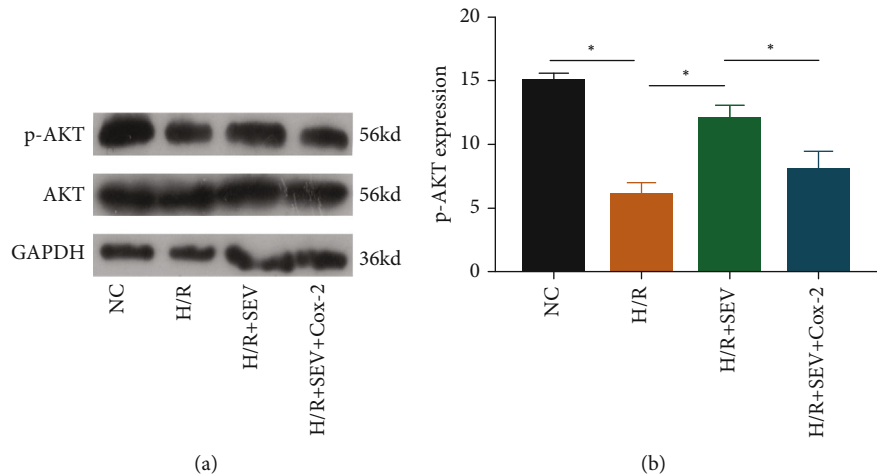


FIGURE 4: Overexpression of Cox-2 inhibited SEV-induced p-Akt upregulation. Protein levels of p-Akt and Akt in H9c2 cells of NC group, H/R group, H/R + SEV group, and H/R + SEV + Cox-2 group.

is able to alleviate myocardial I/R injury in rats [21–23]. Nevertheless, specific mechanisms underlying the protective role of SEV in I/R remain unclear. Our findings firstly showed that declined viability, enhanced LDH release, and

apoptosis in H9c2 cells undergoing H/R, suggesting the successful construction of an *in vitro* H/R model. Notably, SEV administration during reoxygenation greatly protected H/R-induced cardiomyocyte injuries.

Akt is a vital kinase involved in cell survival [24]. Acute activation of Akt markedly protects apoptosis and necrosis of cardiomyocytes under external stimuli [25]. It is reported that shikonin protects H9c2 cells against H/R *via* the PI3K/Akt pathway [26]. Through this pathway, salidroside exerts its protective role in H9c2 cells undergoing oxidative stress injury [27]. In this paper, the protein level of Akt was markedly downregulated following H/R, which was then upregulated by SEV treatment. We believed that the Akt pathway was responsible for the cardioprotective effect of SEV against H/R injury.

Cox-2 is an inducible enzyme, which could be rapidly transcribed and translated by I/R [28]. A relevant study has demonstrated that overexpression of Cox-2 is unfavorable to myocardial I/R injury [29]. Our experimental results illustrated that Cox-2 was upregulated in the H/R group. Notably, overexpression of Cox-2 partially abolished the protective property of SEV on the viability of H9c2 cells undergoing H/R injury. As previously reported, Cox-2 activation is positively correlated to Akt phosphorylation and low survival [30, 31]. Here, the downregulated protein level of p-Akt in H/R-induced cardiomyocytes was partially reversed by SEV treatment. Nevertheless, the reversed trend of the p-Akt level was abolished by overexpression of Cox-2. Cox-2 may negatively affect the protective effect of SEV on cardiomyocyte apoptosis following H/R by inhibiting Akt phosphorylation.

5. Conclusions

Sevoflurane protects cardiomyocyte damage following H/R through the Akt pathway, and its protective effect was abolished by overexpression of Cox-2. Our results proposed that inhibition of Cox-2 could assist the protective role of sevoflurane on H/R injury.

Data Availability

The datasets used and analyzed during the current study are available from the corresponding author on reasonable request.

Conflicts of Interest

The authors declare that they have no competing interests.

Authors' Contributions

Chunyan Guo and Lei Zhang contributed equally to this work.

Acknowledgments

This study was supported by Inner Mongolia Medical University Science and Technology Million Project (YKD2015KJBW022).

References

- [1] A. E. Moran, M. H. Forouzanfar, G. A. Roth et al., "The global burden of ischemic heart disease in 1990 and 2010," *Circulation*, vol. 129, no. 14, pp. 1493–1501, 2014.
- [2] S. Kumfu, S. T. Charunontakorn, T. Jaiwongkam, N. Chattipakorn, and S. C. Chattipakorn, "Humanin prevents brain mitochondrial dysfunction in a cardiac ischaemia-reperfusion injury model," *Experimental Physiology*, vol. 101, no. 6, pp. 697–707, 2016.
- [3] Y. Sun, D. Zhao, Y. Yang et al., "Adiponectin exerts cardioprotection against ischemia/reperfusion injury partially via calcitriol mediated anti-apoptotic and anti-oxidative actions," *Apoptosis*, vol. 22, no. 1, pp. 108–117, 2017.
- [4] F. Xuan, J. Jian, X. Lin et al., "17-Methoxyl-7-hydroxy-benzene-furanchalcone ameliorates myocardial ischemia/reperfusion injury in rat by inhibiting apoptosis and autophagy via the PI3K-Akt signal pathway," *Cardiovascular Toxicology*, vol. 17, no. 1, pp. 79–87, 2017.
- [5] X.-g. Chen, Y.-x. Lv, D. Zhao et al., "Vascular endothelial growth factor-C protects heart from ischemia/reperfusion injury by inhibiting cardiomyocyte apoptosis," *Molecular and Cellular Biochemistry*, vol. 413, no. 1–2, pp. 9–23, 2016.
- [6] H. Chen, D. Li, J. Chen, G. J. Roberts, T. Saldeen, and J. L. Mehta, "EPA and DHA attenuate ox-LDL-induced expression of adhesion molecules in human coronary artery endothelial cells via protein kinase B pathway," *Journal of Molecular and Cellular Cardiology*, vol. 35, no. 7, pp. 769–775, 2003.
- [7] P. Liu, M. Begley, W. Michowski et al., "Cell-cycle-regulated activation of Akt kinase by phosphorylation at its carboxyl terminus," *Nature*, vol. 508, no. 7497, pp. 541–545, 2014.
- [8] P. Zhai and J. Sadoshima, "Glycogen synthase kinase-3 β controls autophagy during myocardial ischemia and reperfusion," *Autophagy*, vol. 8, no. 1, pp. 138–139, 2012.
- [9] L. J. Marnett, S. W. Rowlinson, D. C. Goodwin, A. S. Kalgutkar, and C. A. Lanzo, "Arachidonic acid oxygenation by COX-1 and COX-2," *The Journal of Biological Chemistry*, vol. 274, no. 33, pp. 22903–22906, 1999.
- [10] C. A. Rouzer and L. J. Marnett, "Cyclooxygenases: structural and functional insights," *Journal of Lipid Research*, vol. 50, pp. S29–S34, 2009.
- [11] K. Schror, K. C. Zimmermann, and R. Tannhauser, "Augmented myocardial ischaemia by nicotine—mechanisms and their possible significance," *British Journal of Pharmacology*, vol. 125, no. 1, pp. 79–86, 1998.
- [12] S. C. Y. Wong, M. Fukuchi, P. Melnyk, I. Rodger, and A. Giaid, "Induction of cyclooxygenase-2 and activation of nuclear factor- κ B in myocardium of patients with congestive heart failure," *Circulation*, vol. 98, no. 2, pp. 100–103, 1998.
- [13] A. Abbate, D. Santini, G. G. Biondi-Zoccai et al., "Cyclo-oxygenase-2 (COX-2) expression at the site of recent myocardial infarction: friend or foe?," *Heart*, vol. 90, no. 4, pp. 440–443, 2004.
- [14] J. Cao, H. Xie, Y. Sun et al., "Sevoflurane post-conditioning reduces rat myocardial ischemia reperfusion injury through an increase in NOS and a decrease in phosphorylated NHE1 levels," *International Journal of Molecular Medicine*, vol. 36, no. 6, pp. 1529–1537, 2015.
- [15] Y. Ikeda, A. Shirakabe, C. Brady, D. Zablocki, M. Ohishi, and J. Sadoshima, "Molecular mechanisms mediating mitochondrial dynamics and mitophagy and their functional roles in

- the cardiovascular system,” *Journal of Molecular and Cellular Cardiology*, vol. 78, pp. 116–122, 2015.
- [16] P. Yu, J. Zhang, S. Yu et al., “Protective effect of sevoflurane postconditioning against cardiac ischemia/reperfusion injury via ameliorating mitochondrial impairment, oxidative stress and rescuing autophagic clearance,” *PLoS One*, vol. 10, no. 8, article e134666, 2015.
- [17] H. P. Song, Z. G. Chu, D. X. Zhang, Y. M. Dang, and Q. Zhang, “PI3K-AKT Pathway Protects Cardiomyocytes Against Hypoxia-Induced Apoptosis by MitoKATP-Mediated Mitochondrial Translocation of pAKT,” *Cellular Physiology and Biochemistry*, vol. 49, no. 2, pp. 717–727, 2018.
- [18] Y. Zhang and J. Ren, “Targeting autophagy for the therapeutic application of histone deacetylase inhibitors in ischemia/reperfusion heart injury,” *Circulation*, vol. 129, no. 10, pp. 1088–1091, 2014.
- [19] S. Rohrbach, C. Troidl, C. Hamm, and R. Schulz, “Ischemia and reperfusion related myocardial inflammation: a network of cells and mediators targeting the cardiomyocyte,” *IUBMB Life*, vol. 67, no. 2, pp. 110–119, 2015.
- [20] M. K. Tasoulis and E. E. Douzinas, “Hypoxemic reperfusion of ischemic states: an alternative approach for the attenuation of oxidative stress mediated reperfusion injury,” *Journal of Biomedical Science*, vol. 23, no. 1, p. 7, 2016.
- [21] L. Yang, P. Xie, J. Wu et al., “Sevoflurane postconditioning improves myocardial mitochondrial respiratory function and reduces myocardial ischemia-reperfusion injury by up-regulating HIF-1,” *American Journal of Translational Research*, vol. 8, no. 10, pp. 4415–4424, 2016.
- [22] C. Chen, D. Chappell, T. Annecke et al., “Sevoflurane mitigates shedding of hyaluronan from the coronary endothelium, also during ischemia/reperfusion: an ex vivo animal study,” *Hypoxia*, vol. 4, pp. 81–90, 2016.
- [23] R. C. Pasqualin, C. T. Mostarda, L. E. de Souza et al., “Sevoflurane preconditioning during myocardial ischemia-reperfusion reduces infarct size and preserves autonomic control of circulation in rats,” *Acta Cirúrgica Brasileira*, vol. 31, no. 5, pp. 338–345, 2016.
- [24] B. Wang, J. Shrivah, H. Luo, K. Raedschelders, D. D. Chen, and D. M. Ansley, “Propofol protects against hydrogen peroxide-induced injury in cardiac H9c2 cells via Akt activation and Bcl-2 up-regulation,” *Biochemical and Biophysical Research Communications*, vol. 389, no. 1, pp. 105–111, 2009.
- [25] Y. Teshima, N. Takahashi, L. C. Thuc et al., “High-glucose condition reduces cardioprotective effects of insulin against mechanical stress-induced cell injury,” *Life Sciences*, vol. 87, no. 5–6, pp. 154–161, 2010.
- [26] S. Wang, Y. Zhu, and R. Qiu, “Shikonin protects H9C2 cardiomyocytes against hypoxia/reoxygenation injury through activation of PI3K/Akt signaling pathway,” *Biomedicine & Pharmacotherapy*, vol. 104, pp. 712–717, 2018.
- [27] Y. Zhu, Y. P. Shi, D. Wu et al., “Salidroside protects against hydrogen peroxide-induced injury in cardiac H9c2 cells via PI3K-Akt dependent pathway,” *DNA and Cell Biology*, vol. 30, no. 10, pp. 809–819, 2011.
- [28] I. Morita, “Distinct functions of COX-1 and COX-2,” *Prostaglandins & Other Lipid Mediators*, vol. 68–69, pp. 165–175, 2002.
- [29] T. Saito, I. W. Rodger, H. Shennib, F. Hu, L. Tayara, and A. Giaid, “Cyclooxygenase-2 (COX-2) in acute myocardial infarction: cellular expression and use of selective COX-2 inhibitor,” *Canadian Journal of Physiology and Pharmacology*, vol. 81, no. 2, pp. 114–119, 2003.
- [30] S. Zhang, H. Bian, X. Li et al., “Hydrogen sulfide promotes cell proliferation of oral cancer through activation of the COX2/AKT/ERK1/2 axis,” *Oncology Reports*, vol. 35, no. 5, pp. 2825–2832, 2016.
- [31] S. A. Glynn, R. L. Prueitt, L. A. Ridnour et al., “COX-2 activation is associated with Akt phosphorylation and poor survival in ER-negative, HER2-positive breast cancer,” *BMC Cancer*, vol. 10, no. 1, p. 626, 2010.

Research Article

MicroRNA-146-5p Promotes Pulmonary Artery Endothelial Cell Proliferation under Hypoxic Conditions through Regulating USP3

Wei Zhang ¹, Yujuan Qi,² and Bo Wu³

¹Department of Cardiac Surgery, Tianjin Chest Hospital, Tianjin, China

²Department of Cardiac Surgery ICU, Tianjin Chest Hospital, Tianjin, China

³Department of Surgery, Tianjin Peace New Century Women and Children's Hospital, Tianjin, China

Correspondence should be addressed to Wei Zhang; zhangwei2988@hotmail.com

Received 13 October 2021; Accepted 19 November 2021; Published 7 December 2021

Academic Editor: Simona Pichini

Copyright © 2021 Wei Zhang et al. This is an open access article distributed under the Creative Commons Attribution License, which permits unrestricted use, distribution, and reproduction in any medium, provided the original work is properly cited.

Objective. MicroRNAs play a pivotal role in the progression of pulmonary hypertension (PAH). Although microRNA-146-5p is specifically expressed in many diseases, but in PAH, its role remains elusive. **Patients and Methods.** 30 patients with PAH and 20 healthy volunteers in our hospital were enrolled, and their serum samples were extracted for the detection of microRNA-146-5p and ubiquitin specific protease 3 (USP3) expression. In addition, the interaction between microRNA-146-5p and USP3 was examined by luciferase reporting assay. Furthermore, the potential mechanism was explored by cell counting kit-8 (CCK-8), 5-ethynyl-2'-deoxyuridine (EdU), and Western blotting experiments. **Results.** It was found that microRNA-146-5p was higher in PAH patients than in healthy volunteers. Meanwhile, in hypoxia-induced human pulmonary artery endothelial cell lines (HPAECs), microRNA-146-5p expression was dramatically downregulated while USP3 protein expression was conversely upregulated. Under hypoxic conditions, microRNA-146-5p mimics was able to prompt the growth of HPAECs. In addition, after overexpression of microRNA-146-5p, luciferase reporting assay revealed a reduced luciferase activity of the reporter gene containing the USP3 3'-untranslated region, and a reduction of USP3 protein expression was also confirmed. However, USP3 overexpression partially attenuated the impact of upregulated microRNA-146-5p on the proliferation capacity of HPAECs. **Conclusions.** MicroRNA-146-5p was able to enhance the proliferation ability of HPAEC cells under hypoxic conditions through targeting USP3, suggesting the microRNA-146-5p/USP3 axis may act as a target for PAH treatment.

1. Introduction

Related diseases caused by pulmonary arterial hypertension (PAH) have gradually become a serious public health problem. Hypoxia may lead to pulmonary vasoconstriction and induce PAH, which may lead to pulmonary vascular reconstruction and the occurrence of pulmonary heart disease [1, 2]. Under the current circumstances, it is of great significance to uncover the mechanism of PAH under hypoxia to improve the prognosis, survival rate, and quality of life of patients with pulmonary heart disease induced by chronic hypoxia pulmonary diseases [3, 4]. Some studies suggested that a variety of growth factors can be produced in the lung during hypoxic conditions to stimulate the proliferation of

smooth muscle cells, elastic fibers, and collagen fibers in the inner membrane, resulting in pulmonary vascular remodeling [5, 6]. PAH caused by such vascular remodeling may be relevant to a number of mechanisms such as phenotypic changes of pulmonary smooth muscle cells [7, 8].

Among many clinical molecular markers, microRNA (miRNA), due to its small molecular size and wide role, has gradually attracted wide attention from the medical community in recent years [9, 10]. miRNA is a kind of endogenous noncoding single-stranded RNA encoded by endogenous genes with a length of about 22 nucleotides, which plays a significant role in cell differentiation, proliferation, apoptosis, tumor occurrence, and drug efficiency [11, 12]. Recent studies have also demonstrated that

microRNA-146-5p, as a member of miRNA family, is also involved in various stages of cell development, including cell proliferation, apoptosis, and variation [13].

miRNAs can be engaged in the regulation of gene expression and induce protein translation inhibition by partially complementary combining with the 3' noncoding region of the mRNA of downstream gene, thereby repressing protein synthesis [14, 15]. Bioinformatics analysis demonstrated that microRNA-146-5p could regulate the expression of ubiquitin specific protease 3 (USP3) and bind to it specifically. USP3 is a member of the ubiquitin specific protease (USP) family, which can bind to its target protein through a series of steps by acting on a highly conserved small molecule protein—ubiquitin, mediating the degradation of the target protein or causing other corresponding biological effects [16, 17]. In addition, the research of ubiquitin-specific proteases in diseases is increasingly deepening, including neurodegenerative diseases, hematologic diseases, and infectious diseases, which may serve as a new treatment method for PAH and other diseases in the near future [18, 19].

In this study, we first explored the expression of microRNA-146-5p and USP3 and the interaction between them in pulmonary artery smooth muscle cells under hypoxia conditions, so as to clarify the impacts of microRNA-146-5p and USP3 in the progression and formation of PAH, which may provide a new target for the diagnosis and treatment of PAH.

2. Patients and Methods

2.1. Clinical Samples. Serum samples from 30 PAH patients aged 36.70 ± 10.31 and 20 healthy volunteers aged 33.02 ± 8.52 were collected and stored in a refrigerator at -80°C . Patients diagnosed with PAH should meet the published guidelines for the diagnosis of pulmonary hypertension: (1) mPAP ≥ 25 mmHg at rest, (2) pulmonary artery wedge pressure ≤ 15 mmHg, and (3) pulmonary vascular resistance (PVR) > 3 Wood units. Patients were excluded if associated with a definite cause, including connective tissue disease, congenital heart disease, chronic pulmonary thromboembolism, and PAH due to left heart disease, lung diseases, and hypoxemia [20–22]. According to the guidelines of the Helsinki Declaration, all subjects in this research signed informed consent, which was approved by the Ethics Committee of Tianjin Chest Hospital. This study was conducted in accordance with the Declaration of Helsinki.

2.2. Cell Culture. Human pulmonary artery endothelial cell lines (HPAECs) and human renal epithelial cell line (293T) were purchased from American Type Culture Collection (ATCC) (Manassas, VA, USA), and Dulbecco's modified eagle medium (DMEM) and fetal bovine serum (FBS) were purchased from Life Technologies (Gaithersburg, MD, USA). All cells were cultured with high glucose DMEM containing 10% FBS, penicillin (100 U/mL), and streptomycin (100 $\mu\text{g}/\text{mL}$) in a 37°C , 5% CO_2 incubator. When grown to 80%–90% confluence, cells were digested with 1x trypsin +EDTA (ethylenediaminetetraacetic acid).

2.3. Transfection and Hypoxic Treatment. The control group (miR-NC) and the overexpression vector (microRNA-146-5p mimics) containing the microRNA-146-5p lentiviral sequence were purchased from Shanghai Jima Company (Shanghai, China). Cells were plated in 6-well plates and grown to a cell density of 30–40%, and lentiviral transfection was performed according to the manufacturer's instructions. Cells were collected 48 h later for quantitative real-time polymerase chain reaction (qPCR) and Western blot experiments. In addition, HPAEC cells were exposed to hypoxia (1% O_2 and 5% CO_2) at 37°C .

2.4. Cell Proliferation Assays. The transfected cells were collected and plated into 96-well plates at 2000 cells per well. After cultured for 24 h, 48 h, 72 h, and 96 h, respectively, 10 μL of cell counting kit-8 (CCK-8) solution (Dojindo, Kumamoto, Japan) was added per well for incubation for 2 hours, and then, the optical density (OD) value of each well was measured in the microplate reader at 490 nm absorption wavelength.

2.5. 5-Ethynyl-2'-Deoxyuridine (EdU) Assay. To assess the proliferative capacity of HPAEC cells, EdU proliferation assay (RiboBio, Guangzhou, China) was performed. After transfection for 24 h, the cells were incubated with 50 μM EDU for 2 h, then stained with AdoLo and 4',6-diamidino-2-phenylindole (DAPI), and the number of EDU-positive cells was examined by fluorescence microscopy. The display rate of EDU positive was shown as the ratio of the number of EDU positive cells to the total DAPI chromogenic cells (blue cells).

2.6. Real-Time PCR. Total RNA was extracted from HPAEC cells using TRIzol reagent (Invitrogen, Carlsbad, CA, USA) and reverse transcribed into complementary deoxyribose nucleic acid (cDNA) using Primescript RT Reagent. qPCR reactions were performed using SYBR[®] Premix Ex Taq[™] (TaKaRa, Tokyo, Japan) and StepOne Plus Real-time PCR System. The following primers were used for qPCR reaction: microRNA-146-5p: forward: 5'-GCCCTCTGTGCTACTTACTC-3', reverse: 5'-GCTGGTTGTGGGTTACTCTC-3'; U6: forward: 5'-GCCCTCTGTGCTACTTACTC-3', reverse: 5'-GCTGGTTGTGGGTTACTCTC-3'; USP3: forward: 5'-TAGGTATTGTCTACTACTCTG-3', reverse: 5'-TATATCACTCTTGCTTCA-3'; and β -actin: forward: 5'-CCTGGCACCCAGCACAAT-3', reverse: 5'-TGCCGTAGGTGTCCCTTTG-3'. Data analysis was performed using the ABI Step One software (Applied Biosystems, Foster City, CA, USA), and the relative expression levels of mRNA were calculated using the $2^{-\Delta\Delta\text{Ct}}$ method [23].

2.7. Western Blot. The transfected cells were lysed using cell lysis buffer and centrifuged at $14,000 \times g$ for 15 minutes at 4°C . Total protein concentration was calculated by bicinchoninic acid (BCA) Protein Assay Kit (Pierce, Rockford, IL, USA). The extracted proteins were separated using a 10% sodium dodecyl sulphate-polyacrylamide gel electrophoresis (SDS-PAGE) gel and subsequently transferred to a polyvinylidene fluoride (PVDF) membranes (Millipore, Billerica,

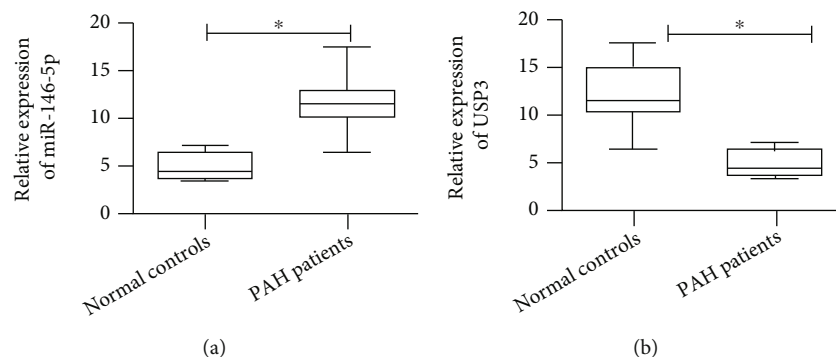


FIGURE 1: Detection of miR-146-5p and USP3 expression levels in serum from patients with pulmonary hypertension and healthy volunteers. (a) qRT-PCR was used to detect the expression level of miR-146-5p in serum of patients with pulmonary hypertension and healthy volunteers. (b) qRT-PCR was used to detect the expression level of USP3 in serum of patients with pulmonary hypertension and healthy volunteers. The data were mean \pm SD, and * indicates a significant difference compared with the normal control group ($p < 0.05$).

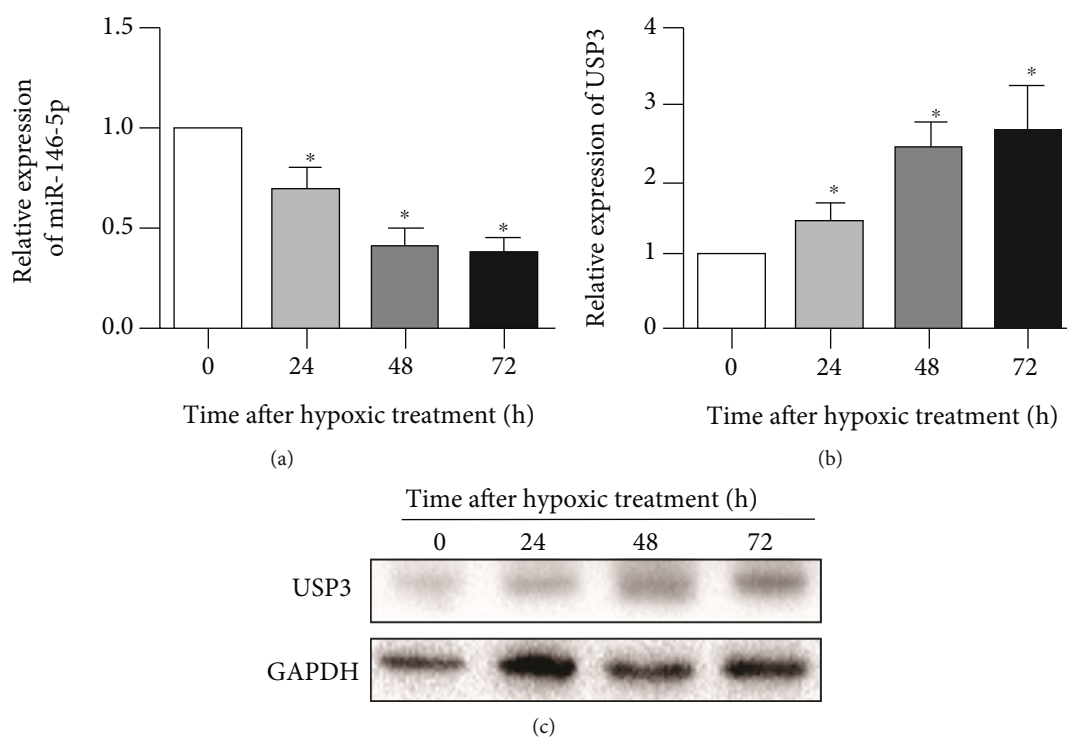


FIGURE 2: Expression of miR-146-5p and USP3 in HPAECs after hypoxia. (a) qRT-PCR was used to detect the expression levels of miR-146-5p at 0 h, 24 h, 48 h, and 72 h after hypoxia treatment. (b) Western blotting was used to detect the protein expression levels of USP3 at 0 h, 24 h, 48 h, and 72 h after hypoxia treatment. The data were mean \pm SD, and * indicates a significant difference compared with 0 h of hypoxia ($p < 0.05$).

MA, USA). Western blot analysis was performed according to standard procedures. The primary antibody against USP3 (23303S) and the internal reference GAPDH (5174T) and the secondary antibody were both purchased from Cell Signaling Technology (Danvers, MA, USA).

2.8. Dual-Luciferase Reporter Assay. 293T cells were seeded in 24-well plates and cotransfected with microRNA-146-5p mimic/NC and pMIR luciferase reporter plasmids. Prior to this, the plasmid was ligated into the pMIR by insertion of other wild-type USP3, paired with the 3'UTR of the USP3

mutation binding site. The plasmid was then introduced into the cells using Lipofectamine 2000 (Thermo Fisher Scientific, Waltham, MA, USA) according to the manufacturer's protocol. After 48 hours of transfection, the reporter luciferase activity was normalized to the control firefly luciferase activity.

2.9. Statistical Analysis. The program was processed using the Statistical Product and Service Solutions (SPSS) 22.0 program (IBM, Armonk, NY, USA), and the data were expressed as mean \pm standard deviation. $p < 0.05$ was

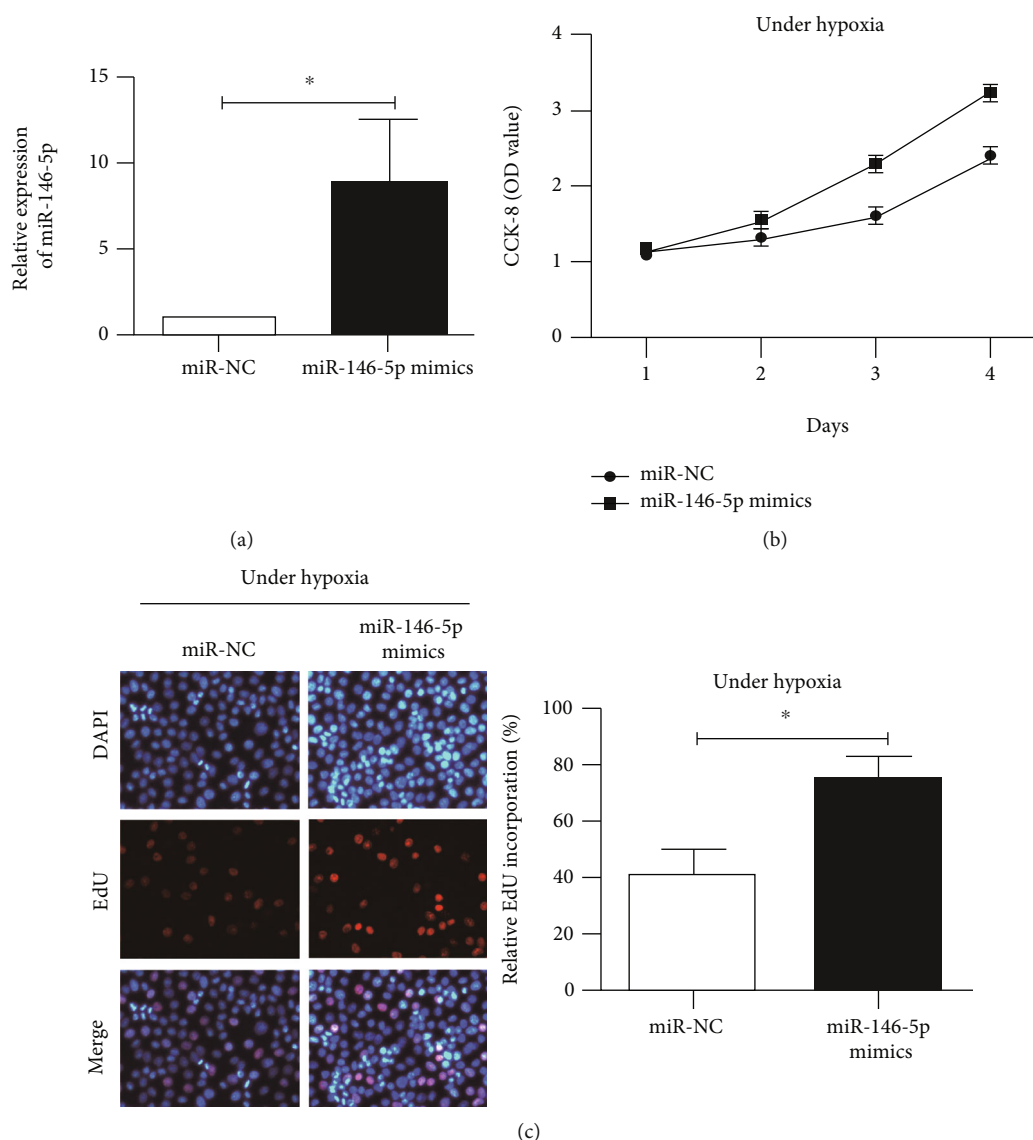


FIGURE 3: Overexpression of miR-146-5p promotes the proliferative capacity of HPAECs after 48 h of hypoxia. (a) qRT-PCR was used to detect the transfection efficiency after transfection of miR-146-5p overexpression vector after 48 h of hypoxia. (b) CCK-8 detected the proliferative capacity of HPAEC cells after transfection of miR-146-5p overexpression vector after 48 h of hypoxia. (c) The EdU assay detected the number of positive proliferating cells in HPAEC cells after overexpression of miR-146-5p after 48 h of hypoxia. The data were mean \pm SD, and * indicates a significant difference compared with the miR-NC group ($p < 0.05$).

considered to be statistically significant. The continuity variable was analyzed by t -test, and the categorical variable was analyzed by χ^2 test or Fisher's exact probability method.

3. Results

3.1. MicroRNA-146-5p and USP3 Expression in Plasma of Patients with PAH. QPCR detected that PAH patient serum contained higher microRNA-146-5p expression and lower USP3 expression compared to the healthy volunteers ($p < 0.05$; Figures 1(a) and 1(b)).

3.2. Hypoxia Decreased MicroRNA-146-5p While Increased USP3 Expression in HPAECs. To determine microRNA-146-5p and USP3 expression in HPAECs under hypoxic

conditions, we cultured HPAECs under hypoxic conditions for 0, 24, 48, and 72 h, respectively, and found a dramatic reduction in microRNA-146-5p expression in a time-dependent manner (Figure 2(a)). In addition, USP3 expression was relatively shown as 2.02 ± 0.16 , 3.38 ± 0.16 , and 3.35 ± 0.42 at 24 hours, 48 hours, and 72 hours, respectively, measured by Western blot assay, suggesting that hypoxia could dramatically induce USP3 protein expression in HPAECs (Figure 2(b)).

3.3. MicroRNA-146-5p Upregulation Accelerates Proliferation Rate of HPAECs. The microRNA-146-5p overexpression vector was constructed to further evaluate how microRNA-146-5p promotes the growth of HPAECs under hypoxic conditions. After 24 hours of transfection and 48

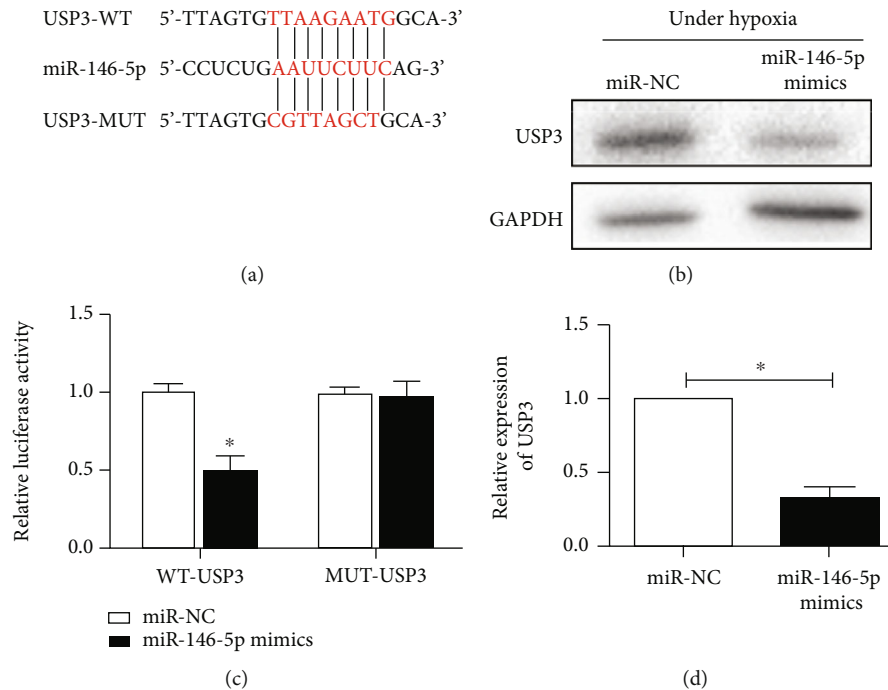


FIGURE 4: USP3 is a direct binding target gene for miR-146-5p. (a) Schematic representation of miR-146-5p sharing the same complementary seed sequence as the 3'-UTR of USP3. (b) Luciferase reporter assay detected that USP3 is the target gene for miR-146-5p. (c) Western blotting was used to detect the protein expression level of USP3 in HPAEC cells after overexpression of miR-146-5p after 48 h of hypoxia. (d) qRT-PCR was used to detect the mRNA expression level of USP3 in HPAEC cells after overexpression of miR-146-5p after 48 h of hypoxia. The data were mean \pm SD, and * indicates a significant difference compared with the miR-NC group ($p < 0.05$).

hours of exposure to hypoxia, qPCR detected an increased microRNA-146-5p level in HPAEC cells induced by overexpression of microRNA-146-5p compared to miR-NC, suggesting a successful construction model (Figure 3(a)). Subsequently, CCK-8 and EdU assays indicated that microRNA-146-5p overexpression dramatically enhanced the proliferation capacity of HPAECs exposed in hypoxia for 48 h compared to the control group (Figures 3(b) and 3(c)).

3.4. USP3 Is a Target of MicroRNA-146-5p. Bioinformatics predicted a potential binding site of microRNA-146-5p in USP3 3'-UTR (Figure 4(a)). And luciferase reporting assay verified that the luciferase activity of 293T cells transfected with WT-USP3-3'UTR vector and microRNA-146-5p overexpression vector was dramatically attenuated after 48 h of hypoxia, while the cytoluciferase activity of cells transfected with MUT-USP3-3'UTR was not affected (Figure 4(b)), which confirmed that microRNA-146-5p could directly target USP3 by binding to its 3'-UTR. In addition, overexpression of microRNA-146-5p reduced USP3 in HPAECs exposed in hypoxia for 48 h at both mRNA and protein levels (Figures 4(c) and 4(d)). The above data suggested that USP3 may act as a target for microRNA-146-5p in HPAECs under hypoxic conditions.

3.5. Overexpression of USP3 Partly Alleviates the Impacts of MicroRNA-146-5p on Cell Proliferation Ability of HPAECs under Hypoxia. To further elucidate the regulation of microRNA-146-5p and USP3 on HPAEC cell proliferation

under hypoxic conditions, we transfected miR-NC + NC, microRNA-146-5p + NC, or microRNA-146-5p + USP3 into HPAEC cells, followed by hypoxia for 48 hours. qPCR analysis revealed a significant reduction of microRNA-146-5p expression in HPAEC cells transfected with microRNA-146-5p + USP3 compared to those transfected with microRNA-146-5p + NC (Figure 5(a)). In addition, the results of CCK-8 and EdU assays indicated that the proliferation ability of HPAEC cells in the microRNA-146-5p + USP3 group was dramatically weakened compared to those in the microRNA-146-5p + NC group; however, when compared with the miR-NC + NC group, after 48 h hypoxia, the cell proliferation ability was reversed (Figures 5(b) and 5(c)). Additionally, USP3 expression was significantly higher in the microRNA-146-5p + USP3 group than in the microRNA-146-5p + NC group (Figure 5(d)). The above data suggested that USP3 overexpression partially could attenuate the influence of microRNA-146-5p upregulation on cell proliferation capacity under hypoxia.

4. Discussion

Pulmonary arterial hypertension (PAH) is a disease typically characterized by pulmonary artery contraction, progressive pulmonary vascular resistance increase, and pulmonary artery pressure rise, which can lead to fatal right heart failure [1–4]. Pulmonary arterioles are composed of endothelial cells, smooth muscle cells, and fibroblasts [5–7]; among which, pulmonary smooth muscle cells are the main

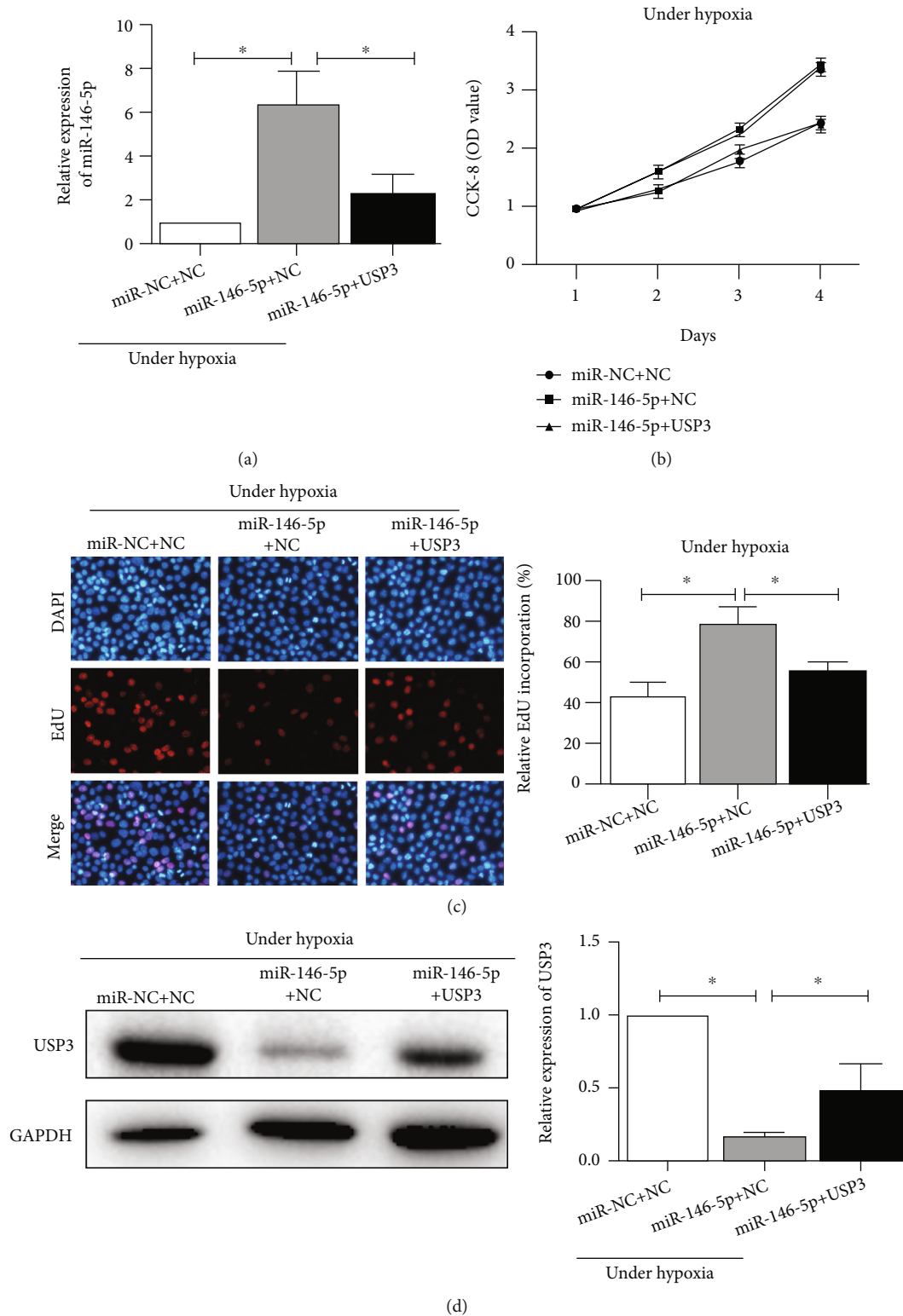


FIGURE 5: Overexpression of USP3 attenuates the effect of overexpression of miR-146-5p on the proliferative capacity of HPAEC cells after 48 h of hypoxic treatment. (a) qRT-PCR was used to detect the mRNA expression level of miR-146-5p in HPAEC cells after cotransfection of miR-146-5p and USP3 overexpression vectors after 48 h of hypoxia. (b) CCK-8 detected the proliferative capacity of HPAEC cells after cotransfection of miR-146-5p and USP3 overexpression vectors after 48 h of hypoxia. (c) The EdU assay detected the number of positive proliferating cells in HPAECs after cotransfection of miR-146-5p and USP3 overexpression vectors after 48 h of hypoxia. (d) Western blotting was used to detect the protein expression level of USP3 in HPAEC cells after cotransfection of miR-146-5p and USP3 overexpression vectors after 48 h of hypoxia. Data were mean \pm SD, and * indicates a significant difference ($p < 0.05$).

biological effector cells in the contraction process of pulmonary arterioles caused by hypoxia and also the key cells involved in the structural reconstruction of pulmonary vessels under the condition of chronic hypoxia [7, 8].

MicroRNA (miRNA), a kind of short single-stranded RNA about 18–25 bp in length, can mediate the physiological and pathological processes of almost all diseases, including cell proliferation, differentiation, migration, carcinogenesis, and apoptosis [9–11]. Previous studies uncover the key role of miRNAs in PAH. Recently, miR-182-3p/Myadm contribute to pulmonary artery hypertension vascular remodeling via a KLF4/p21-dependent mechanism [24]. Besides, miR-483 might reduce experimental pulmonary hypertension by inhibition of multiple adverse responses [25]. In this study, compared with healthy volunteers, patients with PAH had a significant higher expression of microRNA-146-5p but a lower expression of USP3. Previous studies have shown that HPAECs play a crucial role in the process of hypoxia *in vitro*, including promoting cell proliferation and apoptosis, as well as enhancing cell secretion activity. In this investigation, after hypoxia for 24 h, 48 h, and 72 h in HPAEC cells, it was found that the expression of microRNA-146-5p was markedly downregulated while USP3 expression was conversely upregulated, in a time-dependent manner. In HPAEC cells, after overexpression of microRNA-146-5p, CCK-8 and EdU assay revealed an enhanced proliferation ability of HPAEC cells and an elevated positive rate of EdU staining with the increase of time after 48 h of hypoxia culture, suggesting that overexpression of microRNA-146-5p could promote the proliferation activity of pulmonary smooth muscle cells.

miRNA genes are usually located in intron regions, and single strand mature miRNA is produced through a series of processing processes. Mature miRNA molecules form RNA-induced silencing complex (RISC) with Dicer, Argonaute protein, etc. in cells and act on the 3'UTR of specific mRNA to inhibit the translation process or directly degrade the mRNA [11, 12]. For example, microRNA-146-5p could specifically bind to USP3, confirmed in our research by bioinformatics analysis and luciferase reporter gene assay. As a new target gene of microRNA-146-5p, USP3 is found as a member of ubiquitin specific protease (DUBs), which was initially discovered for its cDNA clone fragment had one or two conserved sequences consistent with DUBs. USP3, located on human chromosome 15q22.3, is a functional ubiquitin-specific protease that inhibits ubiquitin-dependent protein degradation [16, 17]. USP can also interact with its target protein through removing the ubiquitin molecules that bind to it, thereby inhibiting the degradation or mediating downstream biological functions of the target protein [18, 19]. In addition, USP3 was dramatically downregulated after the overexpression of microRNA-146-5p. However, under hypoxia conditions, simultaneous overexpression of microRNA-146-5p and USP3 reversed the enhanced proliferation ability induced by microRNA-146-5p. In this study, we firstly uncovered the role of miR-146-5p in PAH by *in vitro* assay; however, the *in vivo* assay should be added in the future study.

5. Conclusions

In summary, microRNA-146-5p can elevate the proliferation rate of HPAEC cells under hypoxia conditions by targeted modulating USP3, suggesting that microRNA-146-5p/USP3 axis may be a potential target for PAH treatment.

Data Availability

The datasets used and analyzed during the current study are available from the corresponding author on reasonable request.

Conflicts of Interest

The authors declared no conflict of interest.

References

- [1] M. T. Harting, “Congenital diaphragmatic hernia-associated pulmonary hypertension,” *Seminars in Pediatric Surgery*, vol. 26, no. 3, pp. 147–153, 2017.
- [2] M. M. Hoeper, H. A. Ghofrani, E. Grunig, H. Klose, H. Olschewski, and S. Rosenkranz, “Pulmonary hypertension,” *Deutsches Ärzteblatt International*, vol. 114, no. 5, pp. 73–84, 2017.
- [3] H. Han, J. K. Francis, Y. Spitzer, and S. Reddy, “Anesthetic management of parturients with pulmonary hypertension undergoing cesarean deliveries,” *Journal of Clinical Anesthesia*, vol. 57, p. 79, 2019.
- [4] A. Venkateshvaran, A. Manouras, B. Kjellstrom, and L. H. Lund, “The additive value of echocardiographic pulmonary to left atrial global strain ratio in the diagnosis of pulmonary hypertension,” *International Journal of Cardiology*, vol. 292, pp. 205–210, 2019.
- [5] I. Cortés-Puch, J. Sun, A. N. Schechter et al., “Inhaled nebulized nitrite and nitrate therapy in a canine model of hypoxia-induced pulmonary hypertension,” *Nitric Oxide*, vol. 91, pp. 1–14, 2019.
- [6] B. Cockbain, L. C. Price, and M. Hind, “Bony breathlessness,” *Circulation*, vol. 140, no. 10, pp. 880–885, 2019.
- [7] S. Minatsuki, M. Hatano, H. Maki, E. Takimoto, H. Morita, and I. Komuro, “Analysis of oxygenation in chronic thromboembolic pulmonary hypertension using dead space ratio and intrapulmonary shunt ratio,” *International Heart Journal*, vol. 60, no. 5, pp. 1137–1141, 2019.
- [8] X. Cheng, Y. Wang, and L. Du, “Epigenetic modulation in the initiation and progression of pulmonary hypertension,” *Hypertension*, vol. 74, no. 4, pp. 733–739, 2019.
- [9] S. R. Mousavi, A. Ahmadi, S. A. Jamalkandi, and J. Salimian, “Involvement of microRNAs in physiological and pathological processes in asthma,” *Journal of Cellular Physiology*, vol. 234, no. 12, pp. 21547–21559, 2019.
- [10] A. Bahirae, R. Ebrahimi, R. Halabian, A. S. Aghabozorgi, and J. Amani, “The role of inflammation and its related microRNAs in breast cancer: a narrative review,” *Journal of Cellular Physiology*, vol. 234, no. 11, pp. 19480–19493, 2019.
- [11] L. Fu and Q. Peng, “A deep ensemble model to predict miRNA-disease association,” *Scientific Reports*, vol. 7, no. 1, p. 14482, 2017.

- [12] C. Backes, E. Meese, and A. Keller, "Specific miRNA disease biomarkers in blood, serum and plasma: challenges and prospects," *Molecular Diagnosis & Therapy*, vol. 20, no. 6, pp. 509–518, 2016.
- [13] A. R. Coffey, M. Kanke, T. L. Smallwood et al., "MicroRNA-146a-5p association with the cardiometabolic disease risk factor TMAO," *Physiological Genomics*, vol. 51, no. 2, pp. 59–71, 2019.
- [14] D. Wang, L. Xin, J. H. Lin et al., "Identifying miRNA-mRNA regulation network of chronic pancreatitis based on the significant functional expression," *Medicine*, vol. 96, no. 21, article e6668, 2017.
- [15] F. Afonso-Grunz and S. Muller, "Principles of miRNA-mRNA interactions: beyond sequence complementarity," *Cellular and Molecular Life Sciences*, vol. 72, no. 16, pp. 3127–3141, 2015.
- [16] X. Wu, M. Liu, H. Zhu et al., "Ubiquitin-specific protease 3 promotes cell migration and invasion by interacting with and deubiquitinating SUZ12 in gastric cancer," *Journal of Experimental & Clinical Cancer Research*, vol. 38, no. 1, p. 277, 2019.
- [17] Q. Zhou, Z. Xiao, R. Zhou et al., "Ubiquitin-specific protease 3 targets TRAF6 for deubiquitination and suppresses IL-1 β induced chondrocyte apoptosis," *Biochemical and Biophysical Research Communications*, vol. 514, no. 2, pp. 482–489, 2019.
- [18] I. Cleynen, E. Vazeille, M. Artieda et al., "Genetic and microbial factors modulating the ubiquitin proteasome system in inflammatory bowel disease," *Gut*, vol. 63, no. 8, pp. 1265–1274, 2014.
- [19] C. L. Fang, C. C. Lin, H. K. Chen et al., "Ubiquitin-specific protease 3 overexpression promotes gastric carcinogenesis and is predictive of poor patient prognosis," *Cancer Science*, vol. 109, no. 11, pp. 3438–3449, 2018.
- [20] N. Galiè, L. Rubin, M. Hoepfer et al., "Treatment of patients with mildly symptomatic pulmonary arterial hypertension with bosentan (EARLY study): a double-blind, randomised controlled trial," *Lancet*, vol. 371, no. 9630, pp. 2093–2100, 2008.
- [21] N. Galiè, M. Humbert, J. L. Vachiery et al., "2015 ESC/ERS guidelines for the diagnosis and treatment of pulmonary hypertension: the joint task force for the diagnosis and treatment of pulmonary hypertension of the European Society of Cardiology (ESC) and the European Respiratory Society (ERS): endorsed by: Association for European Paediatric and Congenital Cardiology (AEPC), International Society for Heart and Lung Transplantation (ISHLT)," *European Heart Journal*, vol. 37, no. 1, pp. 67–119, 2016.
- [22] N. Galiè, M. Humbert, J. L. Vachiery et al., "2015 ESC/ERS guidelines for the diagnosis and treatment of pulmonary hypertension," *Revista Española de Cardiología*, vol. 69, no. 2, p. 177, 2016.
- [23] K. J. Livak and T. D. Schmittgen, "Analysis of relative gene expression data using real-time quantitative PCR and the $2^{-\Delta\Delta C_T}$ method," *Methods*, vol. 25, no. 4, pp. 402–408, 2001.
- [24] L. Sun, P. Lin, Y. Chen et al., "MiR-182-3p/Myadm contribute to pulmonary artery hypertension vascular remodeling via a KLF4/p21-dependent mechanism," *Theranostics*, vol. 10, no. 12, pp. 5581–5599, 2020.
- [25] J. Zhang, Y. He, X. Yan et al., "MicroRNA-483 amelioration of experimental pulmonary hypertension," *EMBO Molecular Medicine*, vol. 12, no. 5, article e11303, 2020.

Research Article

MicroRNA-383-5p Regulates Oxidative Stress in Mice with Acute Myocardial Infarction through the AMPK Signaling Pathway via PFKM

Linlin Gao, Zhongbao Ruan, and Gecai Chen 

Department of Cardiovascular Medicine, Taizhou People's Hospital, Taizhou, China

Correspondence should be addressed to Gecai Chen; chengecai@163.com

Received 8 October 2021; Revised 5 November 2021; Accepted 7 November 2021; Published 7 December 2021

Academic Editor: Simona Pichini

Copyright © 2021 Linlin Gao et al. This is an open access article distributed under the Creative Commons Attribution License, which permits unrestricted use, distribution, and reproduction in any medium, provided the original work is properly cited.

Objective. The purpose of this study is to explore the regulating role of microRNA-383-5p (miR-383-5p) in oxidative stress after acute myocardial infarction (AMI) through AMPK pathway *via* phosphofructokinase muscle-type (PFKM). **Methods.** We established the AMI model, and the model mice were injected with miR-383-5p agomir to study the effect of miR-383-5p in AMPK signaling pathways. The target gene for miR-383-5p was reported to be PFKM, so we hypothesized that overexpression of miR-383-5p inhibits activation of the AMPK signaling pathway. **Results.** In this research, we found that overexpression of miR-383-5p decreases myocardial oxidative stress, myocardial apoptosis, the expression level of PFKM malondialdehyde (MDA), and reactive oxygen species (ROS) in the myocardial tissues after AMI, and finally, AMI-induced cardiac systolic and diastolic function could be improved. **Conclusion.** This study demonstrated that miR-383-5p could reduce the oxidative stress after AMI through AMPK signaling pathway by targeting PFKM.

1. Introduction

AMI is the main cause of persistent increases in human morbidity and mortality due to obstruction of coronary blood flow [1]. Although cTnI and cTnT are the gold standard for evaluation of myocardial ischemia, we need the search for new biomarkers. AMI can lead to the formation of scar and the remodeling of left ventricular, including cardiac dysfunction and cardiomyocyte hypertrophy and fibrosis [2]. Therefore, it causes a decrease in cardiac output and ultimately leads to heart failure (HF) [3].

MicroRNAs (miRNAs) are a small noncoding RNAs composed of unequal nucleotides that regulate gene expression by binding to a fully complementary or partially complementary target mRNAs at the posttranscriptional level [4]. miRNAs are involved in gene expression during cell differentiation, inflammation, stress response, and proliferation [5, 6]. Emerging evidences show that miRNAs are involved in the pathogenesis of cardiac diseases [7]. Therefore, it

may be possible that miRNAs have therapeutic effects [8]. In addition, some researches have shown that upregulation of miR-383-5p can inhibit cell proliferation [9, 10]. According to investigation, miR-383-5p could regulate cell viability through Wnt/ β -catenin pathway [11]. It is well known that PFKM mutation is one of the most common lesions in breast cancer [12]. Besides, a previous study has discussed that oxidative stress in cardiomyocytes after AMI can cause cell injury through activated protein kinase (AMPK) signaling pathway [13]. And this research is aimed at investigating the effect of miR-383-5p targeting PFKM *via* AMPK pathway on oxidative stress in AMI.

2. Materials and Methods

2.1. Prediction of the Target Gene of miR-383-5p Sample Collection. The target gene of miR-383-5p was predicted using the miRDB, PicTar, and TargetScan databases. Then, a correlation analysis was performed on these target genes

at the intersection using a String database. We searched for targets with known expression in cardiovascular tissues specifically.

2.2. Experimental Animal. In this study, male C57BL/6 mice, the age was six to eight weeks, and weighing 22 ± 5 g were included to be raised by the specific pathogen free (SPF) animal center. The average temperature in the animal center is 20°C , the relative humidity is 50-70%, and the light maintenance day and night cycle is 12 h. The whole process is pellet feeding, free feeding, drinking water, and single cage feeding. The cage was cleaned daily, and the cleaning pad was replaced to keep the cage clean. Mice underwent coronary artery ligation, and we use electrocardiogram measurements for the production of myocardial infarction (MI) [14]. Only mice with significant ST-elevation in the ECG were included in the research. Mice were randomly divided into 4 groups: (1) sham group, (2) AMI+PBS group (AMI mice injected with PBS *via* tail vein), (3) AMI+miR-383-5p agomir group (AMI mice with miR-383-5p agomir injected *via* tail vein), and (4) AMI+miR-383-5p agomir NC group (AMI mice with miR-383-5p agomir NC injected *via* tail vein). Seven days after AMI, echocardiography measurements were performed. This study was approved by the Ethics Committee of Taizhou People's Hospital Animal Center (18-CN-23TZ-EC031).

2.3. Echocardiography. Seven days after the AMI model was established, echocardiography was performed using ultrasound system to detect left ventricular end-diastolic volume (LVEDD), left ventricular end-systolic volume (LVESD), and left ventricular end-diastolic volume (LVEDV) and left ventricular end-systolic volume (LVESV). In this study, we evaluated cardiac function by calculating EF and FS.

2.4. Culture of H9C2 Cells. H9C2 cells were cultivated with Dulbecco's Modified Eagle Medium (DMEM) culture solution (Gibco, Rockville, MD, USA), which contained 10% fetal bovine serum (FBS) (Gibco, Rockville, MD, USA) and penicillin/streptomycin, and the H9C2 cells cultivate in a culture dish (37°C , 5% CO_2); we changed the medium every other day. The concentration of $2000 \mu\text{M}$ H_2O_2 was used for the construction of H9C2 cell injury model *in vitro* [15].

2.5. Dual Luciferase Reporter Gene Assay. We analyzed the target gene of miR-383-5p by biological prediction website. To find whether PFKM was a target gene for miR-383-5p, then in this research, we did a luciferase reporter assay for verification. Luc-PFKM-wt or Luc-PFKM-mut was cotransfected into cells with miR-383-5p mimic or its control. Luciferase activity was measured by transfection of H9C2 cardiomyocytes by dual luciferase assay system (Promega, Madison, WI, USA).

2.6. MDA Detection. The mouse serum was taken and centrifuged at 3000r for 10 minutes. After taking the supernatant, the serum MDA content was measured using a commercial kit (Jianglai, Shanghai, China).

2.7. Flow Cytometry. Detect intracellular ROS levels by flow cytometry. The mice were anesthetized by intraperitoneal injection and sacrificed. The myocardial tissues were separated and placed in 1 mL of ice PBS (Syne fisher technology, Boca Raton, FL, USA) liquid and cut. The cells were filtered through a 200-400 mesh screen and adjust the cell concentration. The prepared 1 mL single-cell suspension was incubated with $5 \mu\text{l}$ of 2',7'-dichlorofluorescein diacetate (DCF-DA), and the supernatant was removed by centrifugation and then incubated with 10% FBS. After centrifugation at 4°C , myocardial tissue suspension was prepared. The average fluorescence intensity of the intracellular marker fluorescence probe was measured by flow cytometry (BD FACSC alibur type, Becton-Dickinson (BD), Franklin Lakes, NJ, USA). In the same way, H9C2 cells were treated with H_2O_2 in 6-well plate for 4 h. Cells were collected and washed with PBS twice and then resuspended with binding buffer. Annexin V-FITC and propidium iodide (BB-4101-2; BestBio Science, Shanghai, China) staining solution were added. The apoptotic cells were detected by flow cytometry (BD FACSC alibur type, Becton-Dickinson (BD), Franklin Lakes, NJ, USA).

2.8. Real-Time qPCR. Myocardial tissue RNA was extracted using TRIzol (Thermo Fisher Scientific, Waltham, MA, USA). RNA pretreated with diethylpyrocarbonate (DEPC) (Beyotime, Shanghai, China) was dissolved in ultrapure water. The RNA concentration of the nanodroplets was measured, and the absorbance at 260 nm and 280 nm was measured. If the A260/A280 was between 1.8 and 2.1, the RNA quality was considered standard and can be used in subsequent experiments. We first synthesize complementary deoxyribose nucleic acid (cDNA) using a reverse transcription kit and then perform PCR amplification. mRNA quantitative analysis was achieved using Prism 7300 Sequence Detection System, and 25 μL reaction system was used including SYBR Green (12.5 μL , Thermo Fisher Scientific, Waltham, MA, USA), 10 μM of primers (0.5 mL each from the stock, Thermo Fisher Scientific, Waltham, MA, USA), 10.5 μL of water, and 0.5 μL of template. The data was analyzed by the SDS software, and the results were then output to EXCEL for further analysis. Glyceraldehyde 3-phosphate dehydrogenase (GAPDH) serves as an internal reference for other mRNA and U6 as an internal reference for miR-383-5p. The comparison threshold period (Ct) method, that is, the $2^{-\Delta\Delta\text{Ct}}$ method was used to calculate the folding magnification. All the primers are listed in Table 1.

2.9. Western Blotting Technology. Four groups of mouse myocardial tissue were taken in an eppendorf (EP) tube, and an appropriate amount of precooled cell lysis buffer was placed. The supernatant was taken by centrifugation at 4°C using a high-speed centrifuge. The concentration was quantified by bicinchoninic acid (BCA) kit (BCA, Construction, Nanjing, China). First, protein was separated by 10% sodium dodecyl sulfate-polyacrylamide gel electrophoresis (SDS-PAGE). The dispersed proteins were then transferred to a polyvinylidene fluoride membrane for 4 h at 4°C . Incubate with 5% skim milk for 1 h. Second, incubate the

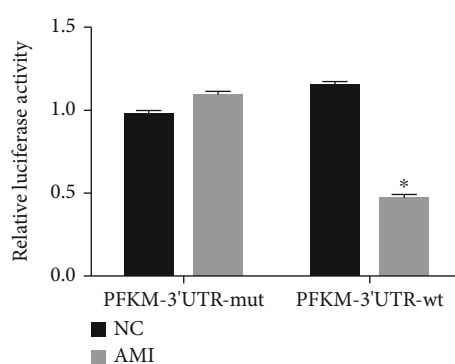
TABLE 1: Real-time PCR primers.

Gene name	Forward (5'>3')	Reverse (5'>3')
SOD1	GGTGAACCAGTTGTGTTGTC	CCGTCCTTTCCAGCAGTC
SOD2	CAGACCTGCCTTACGACTATGG	CTCGGTGGCGTTGAGATTGTT
PFKM	CATCGCCGTGTTGACCTCT	CCCGTGAAGATACCAACTCGG
miR-383-5p	GGGAGATCAGAAGGTGATTGTGGCT	CAGTGCCTGTCGTGGAGT
GAPDH	ACAACCTTTGGTATCGTGAAGG	GCCATCACGCCACAGTTTC

RT-PCR: quantitative reverse-transcription polymerase chain reaction.

	Predicted consequential pairing of target region (top) and miRNA (bottom)	Site type	Context++ score	Context++ score percentile	Weighted context++ score	Conserved branch length	P _{CT}
Position 30-36 of PFKM 3' UTR	5' ... AGGGGAUAGAUUACCUCAU ...	7mer-A1	-0.24	89	-0.24	3.614	< 0.1
hsa-miR-383-5p.1	3' UCGGUUAGUGGAA-GACUAGA						

(a)



(b)

FIGURE 1: PFKM is a target gene of miR-383-5p. (a) The predicted binding sites of miR-383-5p on the 3'UTR sequence of PFKM gene. (b) The luciferase activity of PFKM-3'UTR-wt and PFKM-3'UTR-mut; * $P < 0.05$ vs. the NC group; UTR: untranslated region; wt: wild type; mut: mutant type; miR-383-5p: microRNA-383-5p; PFKM: phosphofructokinase muscle-type; NC: negative control. The results of luciferase activity were regarded as measurement data, expressed as mean \pm SD and analyzed using the t -test, and the experiment was repeated 3 times.

membrane with a special primary antibody (PFKM, Abcam, Cambridge, MA, USA, Rabbit, 1:3000; SOD1, Abcam, Cambridge, MA, USA, Rabbit, 1:3000; SOD2, Abcam, Cambridge, MA, USA, Rabbit, 1:3000; AMPK, Abcam, Cambridge, MA, USA, Rabbit, 1:3000; and p-AMPK, Abcam, Cambridge, MA, USA, Rabbit, 1:3000). We rinse the membrane 3 times with tris buffered saline-tween (TBST) for 15 minutes each time. Next day, the membrane was bound to a second antibody for 1 h at 37°C and 3 times with TBST. Visual inspection of proteins was by the electrochemiluminescence (ECL) Plus detection system.

2.10. Statistical Analysis. All statistical results were presented as mean \pm SD. The GraphPad Prism 5 Software (La Jolla, CA, USA) was used. Student's t -test was used to analyze the comparison between the two groups. P values less than 0.05 were considered statistically significant results.

3. Results

3.1. PFKM Can Be Predicted Involving in Regulating the Oxidative Stress. The miRDB database and the TargetScan

database were used to predict the target gene of miR-383-5p. In addition, the AMPK pathway is thought to be associated with the development of AMI. We found that PFKM was located in the AMPK signaling pathway.

3.2. PFKM Is a Target Gene of miR-383-5p. We found that there is a specific binding region between the 3'UTR of PFKM and the miR-383-5p sequence through software analysis. So, we hypothesized that PFKM was a direct target gene of miR-383-5p (Figure 1(a)). We then used the dual luciferase reporter assay, and the results showed that miR-383-5p significantly downregulated PFKM-3'UT-wt luciferase activity compared to NC group ($P < 0.05$), but PFKM-3'UT-mut luciferase activity had no significant effect ($P > 0.05$). Therefore, we can obtain that miR-383-5p can specifically bind to PFKM-3'UTR, thereby inhibiting PFKM gene expression (Figure 1(b)).

3.3. H₂O₂-Induced Upregulation of miR-383-5p Expression and Increased PFKM Expression in H9C2 Cells. Real-time qPCR and western blot were used to detect the expression of miR-383-5p and PFKM in normal H9C2 cells and

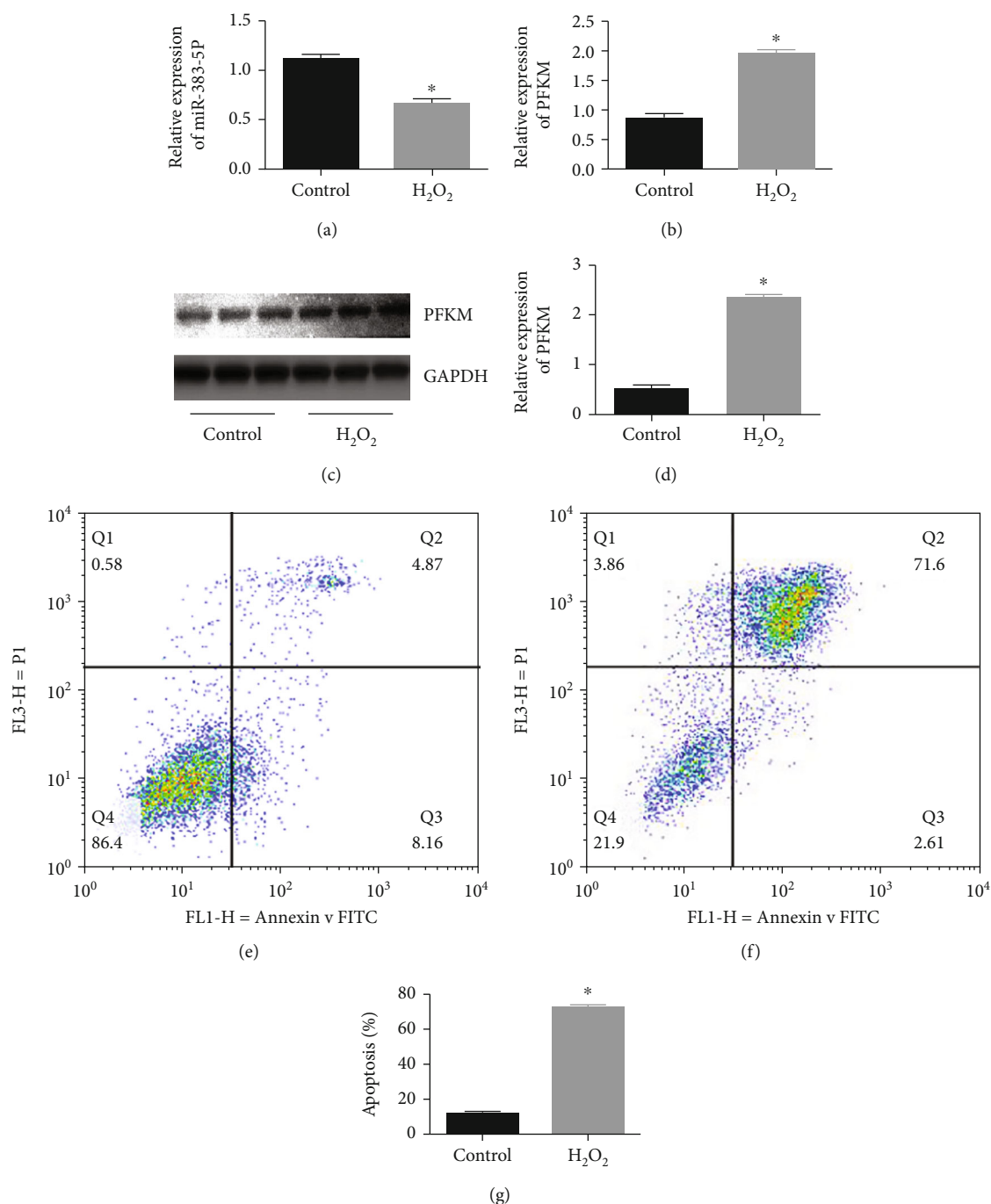


FIGURE 2: miR-383-5p expresses poorly while PFKM expresses highly in H₂O₂-induced H9C2 cells. (a, b) The expression of miR-383-5p and PFKM in normal H9C2 cells and H₂O₂-induced H9C2 cells, H9C2 cells detected by RT-qPCR. (c, d) The protein expression of PFKM in normal H9C2 cells and H₂O₂-induced H9C2 cells examined by western blot analysis, with band intensity assessed. (e) and (f) The representative images of flow cytometry using Annexin V-FITC and PI staining. (g) Statistical analysis of apoptosis rate detected *via* flow cytometry. * $P < 0.05$ vs. the control group. The data were expressed as mean \pm SD. Data at different time points were compared using repeated measurements ANOVA. The experiment was repeated 3 times. miR-383-5p: microRNA-383-5p; PFKM: phosphofructokinase muscle-type.

H₂O₂-induced H9C2 cells at 4h. And results showed that miR-383-5p expression was decreased ($P < 0.05$), but mRNA and protein expression levels of PFKM were significantly elevated in H₂O₂-induced H9C2 cells ($P < 0.05$)

(Figures 2(a)–2(d)). Also, we did flow cytometry to detect the rate of apoptosis, and the result showed that apoptosis rate significantly increased in the H₂O₂ group (Figures 2(e)–2(g)).

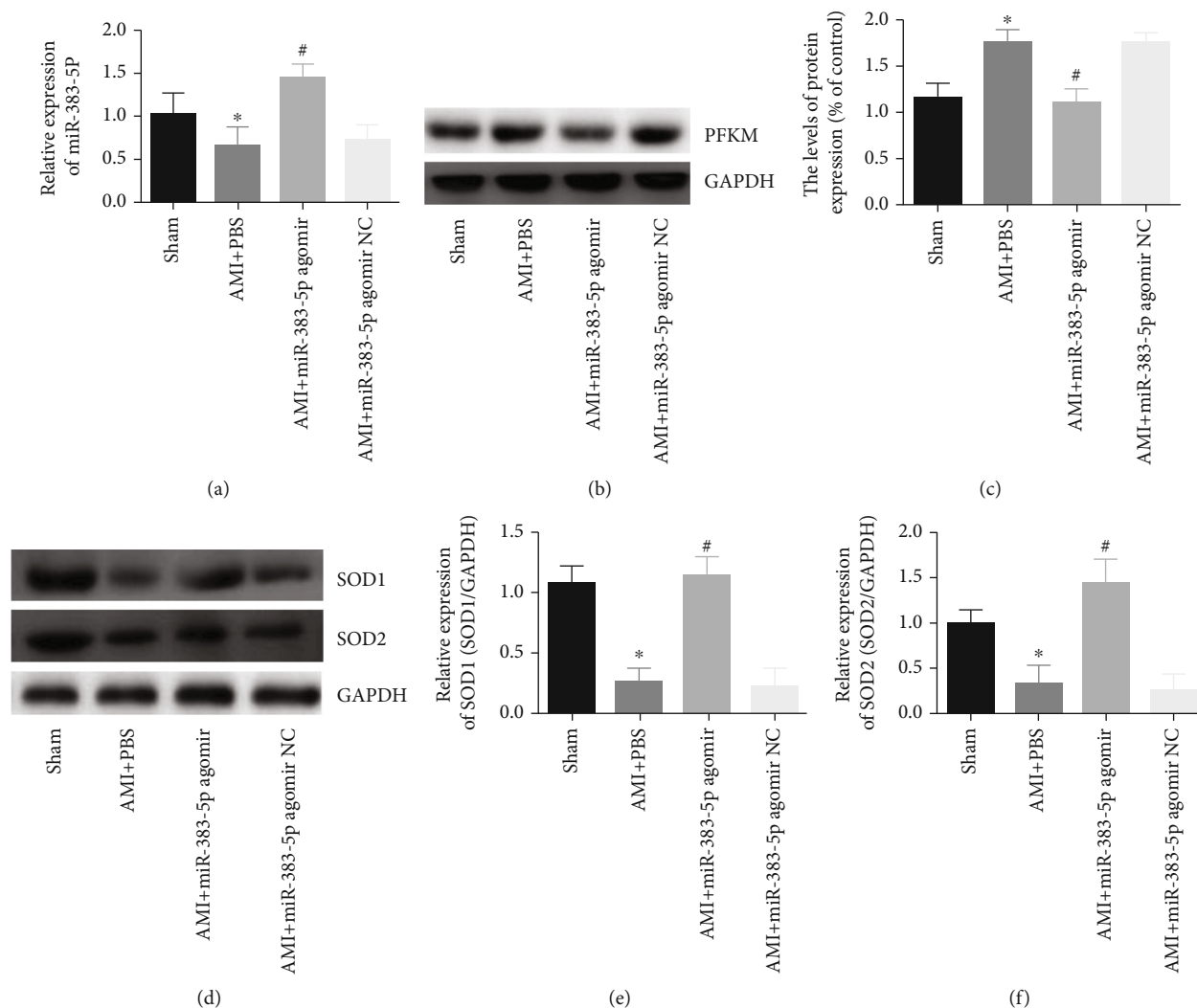


FIGURE 3: Upregulation of miR-383-5p suppresses PFKM. The myocardial tissues used for following detections were, respectively, treated with sham, AMI+PBS, AMI+miR-383-5p agomir, and AMI+miR-383-5p agomir NC. (a) miR-383-5p expression of myocardial tissue of mice by RT-qPCR. (b, c) Protein expression of PFKM in the myocardial tissue of mice by western blot analysis. (d) SOD1 and SOD2 expression by western blot. (e, f) The mRNA expression results of SOD1 and SOD2 in the three groups were determined by real-time PCR. * $P < 0.05$ vs. the sham group; # $P < 0.05$ vs. the AMI+PBS group; the results of miR-383-5p expression, PFKM mRNA, and protein expressions were regarded as measurement data, presented by mean \pm SD and analyzed by one-way ANOVA. There were 10 mice in each group, and the experiment was repeated 3 times; miR-383-5p: microRNA-383-5p; PFKM: phosphofructokinase muscle-type; AMI: acute myocardial infarction.

3.4. miR-383-5p Regulates the Expression of the AMPK Signaling Pathway Factors by Targeting PFKM. We used real-time qPCR to detect the expression of related genes to research the effect of miR-383-5p on AMPK signaling pathway. The results showed (Figure 3(a)) that compared with the sham group, the expression of miR-383-5p was significantly decreased in the AMI+PBS group ($P < 0.05$). In the AMI+miR-383-5p agomir group, miR-383-5p expression was significantly elevated ($P < 0.05$). At the same time, there was no significant difference of miR-383-5p expression in the AMI+miR-383-5p agomir NC group ($P > 0.05$). Western blot (Figures 3(b) and 3(c)) result showed that miR-383-5p agomir inhibited PFKM expression after AMI. In the miR-383-5p agomir group, the expression of SOD1 and SOD2

was increased. However, we found no significant difference in the AMI+miR-383-5p agomir NC group ($P > 0.05$) (Figure 3(d)). mRNA also obtained similar results (Figures 3(e) and 3(f)). We can conclude that miR-383-5p overexpression can inhibit oxidative stress after AMI.

3.5. miR-383-5p Reduces the Effects of Oxidative Stress after AMI through the AMPK Signaling Pathway. Moreover, the phosphorylation of AMPK was significantly increased in the AMI+miR-383-5p agomir group ($P < 0.05$). In conclusion, miR-383-5p overexpression inhibits PFKM expression after AMI and activates AMPK signaling pathway, which in turn affects downstream factors ($P < 0.05$) (Figures 4(a) and 4(b)). We all know that the level of MDA and ROS

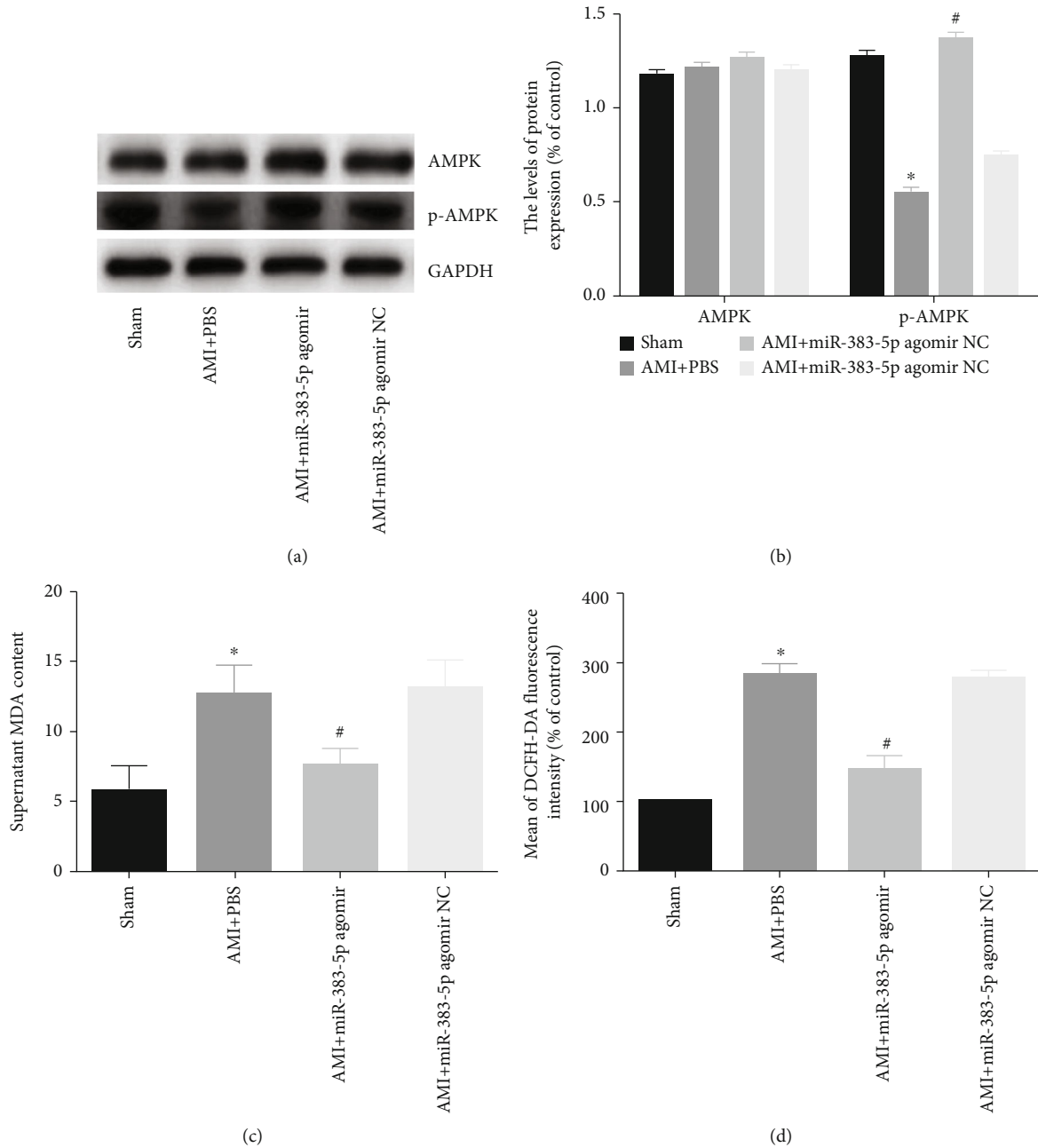


FIGURE 4: miR-383-5p reduces the effects of oxidative stress through the AMPK signaling pathway. The myocardial tissues used for following detections were, respectively, treated with sham, AMI+PBS, AMI+miR-383-5p agomir, and AMI+miR-383-5p agomir NC. (a, b) Protein expression of AMPK and p-AMPK, in the myocardial tissue of mice by western blot analysis. (c) MDA kit was used to detect the expression level of MDA in the 4 groups. (d) Flow cytometry was used to detect ROS levels in the 4 groups of myocardial tissues. * $P < 0.05$ vs. the sham group; # $P > 0.05$ vs. the AMI+PBS; AMPK and p-AMPK protein expressions were regarded as measurement data, presented by mean \pm SD and analyzed by one-way ANOVA. There were 10 mice in each group, and the experiment was repeated 3 times; miR-383-5p: microRNA-383-5p; AMPK: AMP-activated protein kinase; p-AMPK: phosphorylated AMP-activated protein kinase; MDA: malondialdehyde; ROS: reactive oxygen species.

can reflect the oxidative stress level; then, we used MDA kit to study the effect of miR-383-5p on MDA and used flow cytometry to determine the level of ROS. The results (Figure 4(c) and 4(d)) showed that MDA and ROS levels increased in the AMI+PBS group ($P < 0.05$), and by contrast, MDA and ROS levels decreased significantly in the AMI+miR-383-5p agomir group ($P < 0.05$). miR-383-5p

could decrease the levels of MDA and ROS through AMPK signaling pathway, thereby reducing oxidative stress of myocardium.

3.6. Overregulation of miR-383-5p Increased Cardiac Function in Mice. We used echocardiography to examine the heart function of mice (Figure 5(a)). The results

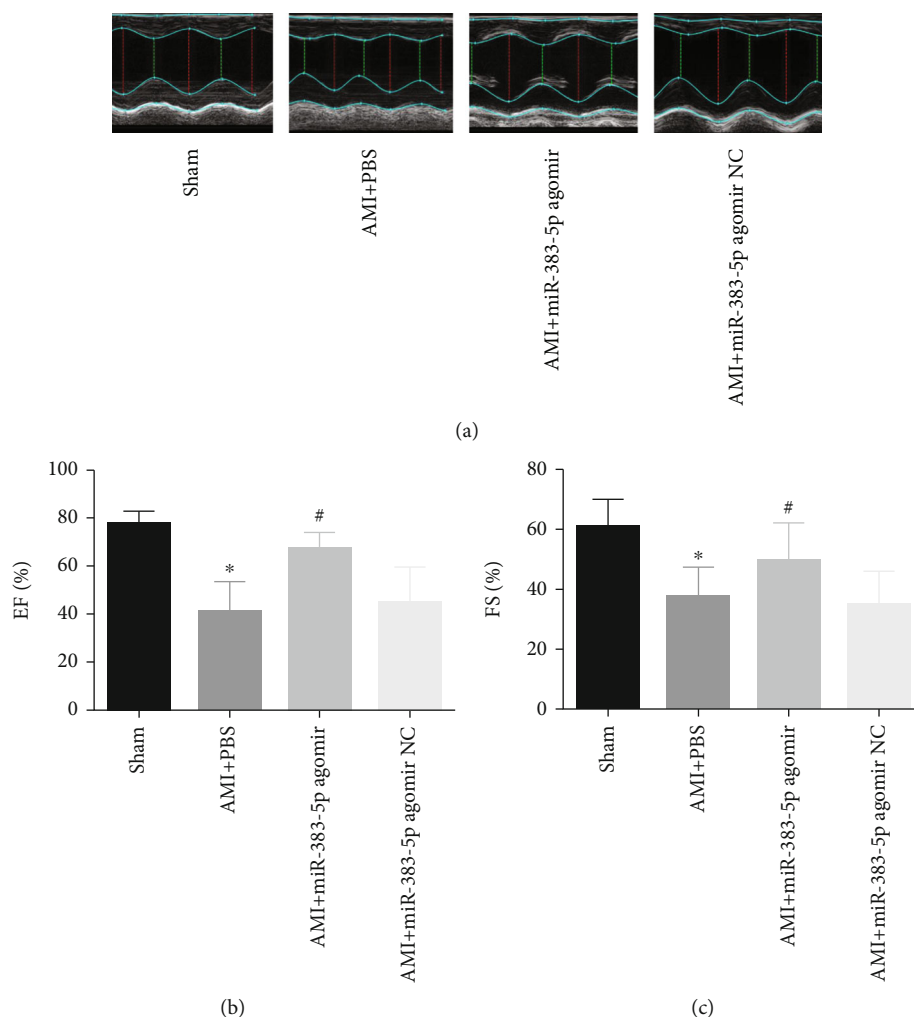


FIGURE 5: Overexpression of miR-383-p increases the cardiac function in mice. The myocardial tissues used for following detections were, respectively, treated with sham, AMI+PBS, AMI+miR-383-5p agomir, and AMI+miR-383-5p agomir NC. (a) Representative photographs in mouse echocardiography. (b) Cardiac function index EF of mice. (c) Cardiac function index FS of mice. There were 10 mice in each group, and the experiment was repeated 3 times; miR-383-5p: microRNA-383-5p; EF: ejection fraction; FS: fraction shortening.

confirmed that the AMI+miR-383-5p agomir group had a significant increase in cardiac function (Figures 5(b) and 5(c)): EF and FS ($P > 0.05$). In the AMI+miR-383-5p agomir NC group, the results had no significant difference ($P > 0.05$). And this study indicated that miR-383-5p agomir can relieve cardiac function after AMI.

4. Discussion

In this study, we demonstrated that miR-383-5p could reduce the oxidative stress after AMI through AMPK signaling pathway by targeting PFKM, thereby alleviating the redox imbalance produced by the heart after AMI and inhibiting cardiomyocyte apoptosis.

Our study demonstrated that increasing the expression of miR-383-5p may be a novel approach to AMI treatment strategies. Previous researches have found that abnormal expression of miRs was considered to play an important role in the diagnosis and treatment of various diseases such as heart disease [16–18]. miR-383-5p was known to suppress

carcinoma cell proliferation [19, 20] and could be acted as new prognostic biomarkers and therapeutic targets [21]. Furthermore, we used ROS level detection flow cytometry and immunofluorescence to detect intracellular ROS levels, and we used MDA kit to detect the effect of miR-383-5p on MDA levels. Our data suggest that miR-383-5p plays a key role in inhibiting oxidative stress in cardiomyocytes. Secondly, we successfully predicted that PFKM might be the target gene of miR-383-5p through software analysis. Therefore, we conducted a series of studies through *in vivo* and *in vitro* experiments. A lot of studies have investigated that AMPK pathway is involved in the oxidative stress progression [22–24]. And PFKM was the gene enriched in the AMPK signaling pathway by KEGG in AMI. Our study showed that miR-383-5p was decreased after AMI, and when we increased its expression in mouse's heart, cardiac function will be improved. However, decreasing the expression of miR-383-5p after AMI, we did not find the cardiac function deteriorated. And it might be explained by the fact that miR-383-5p has the low expression in the heart. We

observed that microRNA-383-5p overexpression alleviates heart injury *in vivo*. On the one hand, microRNA-383-5p reduced the level of oxidative stress and thus reduces cell apoptosis [25, 26]. In addition, microRNA-383-5p may also reduce cell apoptosis directly.

However, the research also had some limitations. First, we did not have many researches *in vitro*. Second, to detect the level of oxidative stress, we only detect the levels of MDA and ROS, and we did not do other researches in apoptosis such as TUNNEL staining *in vivo*. Finally, this study was still on the way, and the mechanism was insufficient. It needs further verification on the effects of miR-383-5p or AMPK signaling pathway on oxidative stress for the treatment of AMI.

5. Conclusions

In conclusion, our study confirmed that miR-383-5p could reduce the oxidative stress after AMI through AMPK signaling pathway by targeting PFKM.

Data Availability

The datasets used and analyzed during the current study are available from the corresponding author on reasonable request.

Conflicts of Interest

The authors declared no conflict of interest.


References

- [1] J. A. Hill and E. N. Olson, "Cardiac plasticity," *The New England Journal of Medicine*, vol. 358, no. 13, pp. 1370–1380, 2008.
- [2] N. Maulik, "Angiogenic signal during cardiac repair," *Molecular and Cellular Biochemistry*, vol. 264, no. 1/2, pp. 13–23, 2004.
- [3] M. M. Lalu, S. Mazzarello, J. Zlepzig et al., "Safety and efficacy of adult stem cell therapy for acute myocardial infarction and ischemic heart failure (SafeCell Heart): a systematic review and meta-analysis," *Stem Cells Translational Medicine*, vol. 7, no. 12, pp. 857–866, 2018.
- [4] D. P. Bartel, "MicroRNAs: genomics, biogenesis, mechanism, and function," *Cell*, vol. 116, no. 2, pp. 281–297, 2004.
- [5] G. Condorelli, M. V. Latronico, and E. Cavarretta, "MicroRNAs in cardiovascular diseases: current knowledge and the road ahead," *Journal of the American College of Cardiology*, vol. 63, no. 21, pp. 2177–2187, 2014.
- [6] E. R. Porrello, "MicroRNAs in cardiac development and regeneration," *Clinical Science (London, England)*, vol. 125, no. 4, pp. 151–166, 2013.
- [7] M. Climent, G. Viggiani, Y. W. Chen, G. Coulis, and A. Castaldi, "MicroRNA and ROS crosstalk in cardiac and pulmonary diseases," *International Journal of Molecular Sciences*, vol. 21, no. 12, p. 4370, 2020.
- [8] J. H. Park, S. Y. Shin, and C. Shin, "Non-canonical targets destabilize microRNAs in human Argonautes," *Nucleic Acids Research*, vol. 45, no. 4, pp. 1569–1583, 2017.
- [9] Z. Li and W. Li, "miR-383 inhibits proliferation of granulosa cells by down-regulation of cell cycle-related proteins in mice," *Xi Bao Yu Fen Zi Mian Yi Xue Za Zhi*, vol. 35, no. 6, pp. 518–525, 2019.
- [10] R. L. Han, F. P. Wang, P. A. Zhang, X. Y. Zhou, and Y. Li, "MiR-383 inhibits ovarian cancer cell proliferation, invasion and aerobic glycolysis by targeting LDHA," *Neoplasma*, vol. 64, no. 2, pp. 244–252, 2017.
- [11] B. Gu, J. Wang, Y. Song, Q. Wang, and Q. Wu, "MicroRNA-383 regulates cell viability and apoptosis by mediating Wnt/beta-catenin signaling pathway in non-small cell lung cancer," *Journal of Cellular Biochemistry*, vol. 120, no. 5, pp. 7918–7926, 2018.
- [12] H. Ahsan, J. Halpern, M. G. Kibriya et al., "A genome-wide association study of early-onset breast cancer identifies PFKM as a novel breast cancer gene and supports a common genetic spectrum for breast cancer at any age," *Cancer Epidemiology, Biomarkers & Prevention*, vol. 23, no. 4, pp. 658–669, 2014.
- [13] R. Kar, D. R. Kellogg, and L. J. Roman, "Oxidative stress induces phosphorylation of neuronal NOS in cardiomyocytes through AMP-activated protein kinase (AMPK)," *Biochemical and Biophysical Research Communications*, vol. 459, no. 3, pp. 393–397, 2015.
- [14] E. Gao, Y. H. Lei, X. Shang et al., "A novel and efficient model of coronary artery ligation and myocardial infarction in the mouse," *Circulation Research*, vol. 107, no. 12, pp. 1445–1453, 2010.
- [15] B. Su, S. D. Bu, B. H. Kong, R. X. Dai, and Q. Su, "Cystatin C alleviates H₂O₂-induced H9c2 cell injury," *European Review for Medical and Pharmacological Sciences*, vol. 24, no. 11, pp. 6360–6370, 2020.
- [16] A. S. Moghaddam, J. T. Afshari, S. A. Esmaeili, E. Saburi, Z. Joneidi, and A. A. Momtazi-Borojeni, "Cardioprotective microRNAs: lessons from stem cell-derived exosomal microRNAs to treat cardiovascular disease," *Atherosclerosis*, vol. 285, pp. 1–9, 2019.
- [17] B. C. Bernardo, J. Y. Ooi, R. C. Lin, and J. R. McMullen, "MiRNA therapeutics: a new class of drugs with potential therapeutic applications in the heart," *Future Medicinal Chemistry*, vol. 7, no. 13, pp. 1771–1792, 2015.
- [18] D. A. Chistiakov, A. N. Orekhov, and Y. V. Bobryshev, "Cardiac-specific miRNA in cardiogenesis, heart function, and cardiac pathology (with focus on myocardial infarction)," *Journal of Molecular and Cellular Cardiology*, vol. 94, pp. 107–121, 2016.
- [19] J. Wang, Y. Zhou, X. Fei, X. Chen, and Y. Chen, "Biostatistics mining associated method identifies AKR1B10 enhancing hepatocellular carcinoma cell growth and degenerated by miR-383-5p," *Scientific Reports*, vol. 8, no. 1, 2018.
- [20] L. Qi, C. Gao, F. Feng et al., "MicroRNAs associated with lung squamous cell carcinoma: new prognostic biomarkers and therapeutic targets," *Journal of Cellular Biochemistry*, vol. 120, no. 11, pp. 18956–18966, 2019.
- [21] J. Zhang, X. Kong, Q. Shi, and B. Zhao, "MicroRNA-383-5p acts as a potential prognostic biomarker and an inhibitor of tumor cell proliferation, migration, and invasion in breast cancer," *Cancer Biomarkers*, vol. 27, no. 4, pp. 423–432, 2020.
- [22] E. A. Queiroz, Z. B. Fortes, C. M. Da, A. M. Barbosa, N. Khaper, and R. F. Dekker, "Antiproliferative and proapoptotic effects of three fungal exocellular β -glucans in MCF-7 breast cancer cells is mediated by oxidative stress, AMP-activated protein kinase (AMPK) and the Forkhead

- transcription factor, FOXO3a," *The International Journal of Biochemistry & Cell Biology*, vol. 67, pp. 14–24, 2015.
- [23] C. H. Lin, Y. C. Cheng, C. J. Nicol, K. H. Lin, C. H. Yen, and M. C. Chiang, "Activation of AMPK is neuroprotective in the oxidative stress by advanced glycosylation end products in human neural stem cells," *Experimental Cell Research*, vol. 359, no. 2, pp. 367–373, 2017.
- [24] R. Kosuru, V. Kandula, U. Rai, S. Prakash, Z. Xia, and S. Singh, "Pterostilbene decreases cardiac oxidative stress and inflammation via activation of AMPK/Nrf2/HO-1 pathway in fructose-fed diabetic rats," *Cardiovascular Drugs and Therapy*, vol. 32, no. 2, pp. 147–163, 2018.
- [25] F. Wu, Z. Li, M. Cai et al., "Aerobic exercise alleviates oxidative stress-induced apoptosis in kidneys of myocardial infarction mice by inhibiting ALCAT1 and activating FNDC5/Irisin signaling pathway," *Free Radical Biology & Medicine*, vol. 158, pp. 171–180, 2020.
- [26] X. Hou, S. Yang, and J. Yin, "Blocking the REDD1/TXNIP axis ameliorates LPS-induced vascular endothelial cell injury through repressing oxidative stress and apoptosis," *American Journal of Physiology. Cell Physiology*, vol. 316, no. 1, pp. C104–C110, 2019.

Research Article

Protective Effect of Fasudil on Hydrogen Peroxide-Induced Oxidative Stress Injury of H9C2 Cardiomyocytes

Yu Zhang ¹, Shanxin Liu,² Xiaochun Li,³ and Jian Ye¹

¹Department of Cardiology, The Second Affiliated Hospital of Zhejiang University, School of Medicine, Hangzhou, China

²Department of Cardiology, The Affiliated Hospital of Hangzhou Normal University, Hangzhou, China

³Department of Infectious Diseases, The Second Affiliated Hospital of Zhejiang University, School of Medicine, Hangzhou, China

Correspondence should be addressed to Yu Zhang; 2311039@zju.edu.cn

Received 12 October 2021; Accepted 18 November 2021; Published 1 December 2021

Academic Editor: Simona Pichini

Copyright © 2021 Yu Zhang et al. This is an open access article distributed under the Creative Commons Attribution License, which permits unrestricted use, distribution, and reproduction in any medium, provided the original work is properly cited.

Objective. Oxidative damage is a pathological factor that causes cardiovascular damage in the clinic and is increasingly serious. This study focused on the effect of fasudil on H₂O₂-induced oxidative damage in cardiomyocytes. **Materials and Methods.** H9C2 cardiomyocytes were cultured in vitro and divided into three groups: control group (Con group), H₂O₂ treatment (H₂O₂ group), and fasudil and H₂O₂ cotreatment (H₂O₂+fasudil group). The content levels of LDH and MDA in the supernatant were detected, and the morphology of H9C2 cardiomyocytes was observed by light microscopy. 8-OHdG staining was observed by a fluorescence inversion microscope. Cell Counting Kit (CCK-8), western blotting, real-time polymerase chain reaction (RT-PCR), and enzyme-linked immunosorbent assay (ELISA) were used to investigate the effect of fasudil on the Rho/ROCK signaling pathway. **Results.** Our results showed that after H₂O₂ treatment, the H9C2 cardiomyocytes were irregular in shape and elliptical. But the morphology of the H₂O₂+fasudil group was similar to that of the Con group. The green fluorescence of the H₂O₂ group was significantly enhanced than that of the Con group, while the green fluorescence of the H₂O₂+fasudil group was weaker than those of the H₂O₂ group. By detecting the supernatant, it was found that the contents of LDH were significantly increased, and the contents of SOD and CAT in the H₂O₂ group were significantly decreased. And the expression of antioxidant indicators in the H₂O₂ group was significantly decreased by western blotting. The results of RT-PCR showed that SOD1 and SOD2 mRNA in the H₂O₂ group was significantly reduced, and the contents of GPX1 and GPX3 in the H₂O₂ group were significantly decreased by enzyme-linked immunosorbent assay (ELISA). The expression of ROCK1, ROCK2, and downstream phosphorylation of myosin phosphatase target subunit-1 (p-MYPT-1) was significantly increased in the H₂O₂ group, while fasudil inhibited the increase of ROCK1, ROCK2, and p-MYPT-1. **Conclusions.** Fasudil can inhibit the Rho/ROCK signaling pathway induced by H₂O₂ and reduce oxidative stress response, inhibit apoptosis, and improve antioxidant enzyme activity in H9C2 cardiomyocytes thereby delaying cell senescence.

1. Introduction

The rising trend of cardiovascular disease leading to human death is one of the main causes of sudden death in humans [1]. As people's quality of life improves, the incidence of many underlying diseases increases year by year, including diabetes, high blood pressure, and myocardial ischemia [2]. Among them, the incidence and mortality of cardiovascular diseases have remained at the leading level [3]. In recent years, more studies have shown that oxidative stress- (OS-) induced cardiomyocyte apoptosis plays an important role

in the development of cardiovascular diseases [4]. Cardiomyocytes are a type of highly differentiated cells. Apoptosis of cardiomyocytes leads to cardiac dysfunction, which ultimately leads to irreversible changes in the heart [5]. Therefore, the search for new drugs to inhibit OS and reduce myocardial cell apoptosis is currently a hot spot in the treatment of cardiovascular diseases.

Fasudil is a novel Rho kinase inhibitor that can inhibit OS and inflammatory responses [6]. It has been reported that fasudil can directly bind to Rho-associated protein kinase (ROCK) and inhibit Rho enzyme activity, thereby

attenuating ROS-induced abnormal activation of the Rho/ROCK signaling pathway [7]. Previous studies have found that fasudil can effectively reduce the expression of inflammatory factors in noninfarcted cardiomyocytes of rats with myocardial infarction [8]. Researches have reported that fasudil can regulate macrophage polarization and improve myocardial fibrosis in mice [9]. However, there are few researches on oxidative damage of cardiomyocytes induced by H₂O₂ in fasudil. Therefore, this research mainly discusses the effect of fasudil on H₂O₂-induced myocardial injury.

Rho protein is a small molecule guanylate binding protein, and Rho protein has GTPase activity and is expressed in mammalian tissue cells [10]. There are two states of Rho protein, one is the inactivation state bound to GDP (GDP-Rho), and the other is the activation state bound to GTP (GTP-Rho). ROCK is divided into two types: ROCK1 and ROCK2 [11]; activated ROCK can inhibit the activity of its downstream MYPT-1 through phosphorylation, while phosphorylated MYPT-1 can affect the contraction of blood vessels [12]. Studies have reported that the Rho/ROCK pathway plays an important role in cell movement, proliferation, and activation of cytokines [13]. Researches have confirmed that the Rho/ROCK signaling pathway is associated with cellular inflammation, OS, and apoptosis [14]. Therefore, fasudil has been studied as a specific inhibitor of the Rho/ROCK pathway in many fields.

2. Material and Methods

2.1. Cell Culture and Treatment. H9C2 cardiomyocytes (Cell Culture Center, Shanghai, China) were cultured in Dulbecco's modified Eagle's medium (DMEM) (Life Technology, Wuhan, China), medium containing 10% fetal bovine serum (FBS) (Life Technology, Wuhan, China) and 1% penicillin/streptomycin (Life Technology, Wuhan, China). H9C2 cardiomyocytes were evenly divided into three groups. When the cells were at the appropriate density, the H₂O₂ group and the fasudil group were treated with 200 μmol/L H₂O₂, and the Con group was added with the same amount of DMEM for 24 h. The H₂O₂+fasudil group was treated with fasudil (Qianmo Biotechnology, Hubei, China) for 3 hours before H₂O₂ treatment.

2.2. Drug Preparation. Fasudil was formulated into a stock solution with physiological saline and stored in a refrigerator at -20°C. And DMEM was diluted before use.

2.3. Cell Counting Kit (CCK-8) Assay. The optimal concentration and time of fasudil were determined by the CCK-8 (CCK-8, Construction, Nanjing, China) method. H9C2 cardiomyocytes growing in logarithmic phase were inoculated into a 96-well plate and cultured at a density of 100 μL/well for 24 h. Different concentrations of fasudil working solution were added to the plate. Each group was incubated with 10 μL of CCK-8 working solution for 1 h at 1 h, 3 h, 6 h, and 12 h, and the absorbance of the three groups was measured at 450 nm with a microplate reader.

2.4. Lactate Dehydrogenase (LDH), Malondialdehyde (MDA), and Catalase (CAT) Levels Were Determined. The supernatants of each group of cells were collected, and the supernatant was treated with a commercial kit according to

the manufacturer's instructions (Jiancheng, Nanjing, China), and the levels of LDH, MDA, and CAT were measured with a microplate reader.

2.5. Superoxide Dismutase (SOD) Detection. H9C2 cardiomyocytes were transferred to a 6-well plate; after treatment, the supernatant was collected and centrifuged. The SOD level in the cells was measured according to the SOD Assay Kit manual (Jiancheng, Nanjing, China).

2.6. RNA Isolation and Real-Time Polymerase Chain Reaction (RT-PCR). 0.5 mL of Trizol (Thermo Fisher Scientific, Shanghai, China) was added into a 24-well plate per well and shaken on ice for 10 minutes, then the liquid in each hole was collected in the EP tube without enzyme, and 0.1 mL chloroform was added to each tube, turned it upside down for 15 seconds, and placed it on top of the ice for 10 minutes. The mixture was centrifuged at 4°C (13,000 rpm, 15 min), the upper aqueous phase was aspirated, and an equal amount of isopropanol was added. The mixture was shaken for 30 seconds and allowed to stand at room temperature for 10 minutes. Then, centrifuged for another 10 minutes and discarded the supernatant. After washing the RNA pellet with 75% ethanol, it was centrifuged at 4°C (13,000 rpm, 10 min). The liquid was discarded and dissolved by the 20 μL of ribonuclease-free water. RNA concentration was measured immediately, and the absorbance at 260 nm and 280 nm was measured. If the A260/A280 was between 1.8 and 2.0, the RNA quality was considered to be standard and can be used in subsequent experiments.

mRNA quantitative analysis was achieved using the Prism 7300 Sequence Detection System, using a designed reaction system, including SYBR green, positive and negative strand primers, enzyme-free water (Thermo Fisher Scientific, Shanghai, China), and template DNA. Quantitative amplification was performed under specific PCR conditions. Data were normalized using endogenous glyceraldehyde 3-phosphate dehydrogenase (GAPDH). The comparison threshold period (Ct) method, that is, the 2^{-ΔΔCt} method was used to calculate the folding magnification, and the data was analyzed by the SDS software. RT-PCR primers are shown in Table 1.

2.7. Western Blotting. After adding 200 μL of the lysate to the 6-well plate, it was allowed to stand for 20 minutes on ice, and the liquid was collected and centrifuged (13,000 rpm, 15 min); then, the supernatant was collected. The concentration of the protein was determined by the bicinchoninic acid (BCA) (Camilo Biological, Nanjing, China) method and quantified. The protein was separated using a 10% sodium dodecyl sulfate-polyacrylamide gel, then transferred to a polyvinylidene fluoride (PVDF) membrane (Millipore, Billerica, MA, USA) for 2 hours at 4°C. 5% skim milk was prepared with Tris-buffered saline with Tween-20 (TBST) to block the specific antigen for 2 hours. After washing with TBST for 1 minute, PVDF membranes were incubated with a specific primary antibody (SOD1, Abcam, Rabbit; 1:3000; SOD2, Abcam, Rabbit, 1:3000; GPX1, US 1:1000, CST; GPX3, US 1:1000, CST; Bcl-2, Abcam, Rabbit, 1:2000; Bax, Abcam, Rabbit, 1:500; Sirt1, Bioworld, mouse, 1:500,

TABLE 1: RT-PCR primers.

Gene name	Forward (5' > 3')	Reverse (5' > 3')
Bax	CAGTTGAAGTTGCCATCAGC	CAGTTGAAGTTACCATCAGC
Bcl-2	GACTGAGTACCTGAACCGGCATC	CTGAGCAGCGTCTTCAGAGACA
Sirt1	CCAGATCCTCAAGCCATG	TTGGATTCTCGCAACCTG
SOD1	GGTGAACCAGTTGTGTTGTC	CCGTCCTTTCCAGCAGTC
SOD2	CAGACCTGCCTTACGACTATGG	CTCGGTGGCGTTGAGATTGTT
P53	CAAAATGGTGAAGGTCGGTGTG	GATGTTAGTGGGGTCTCGCTC
ROCK1	AGATATGGCAAACAGGATT	CTTCACAAGATGAGGCAC
ROCK2	CTAGAGTGCCGTAGATGCCA	GGTTCTAGGGGATGATCGGG
GAPDH	ACAAC TTTGGTATCGTGGAAGG	GCCATCAGCCACAGTTTC

qRT-PCR: quantitative reverse-transcription polymerase chain reaction.

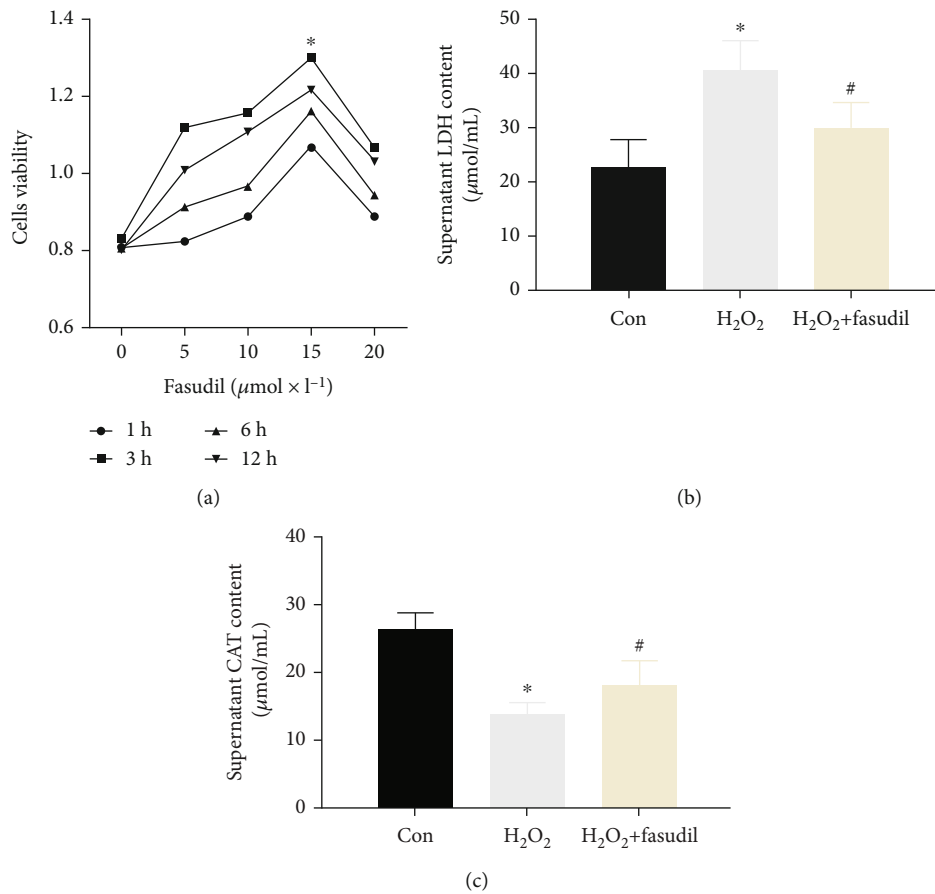


FIGURE 1: Fasudil retards degradation of H9C2 cardiomyocytes *in vitro*. (a) The optimal concentration and time of UTI were determined by the CCK-8 assay. (b) LDH kit detects the supernatant LDH content. (c) CAT kit detects the content of the supernatant CAT level (“*” indicates statistical difference from the control group $p < 0.05$, and “#” indicates statistical difference from the ischemic hypoxia group $p < 0.05$).

China; P53, Abcam, Rabbit, 1:2000; ROCK1, Abcam, Rabbit, 1:500; ROCK2, Abcam, Rabbit, 1:1000; MYPT-1, Abcam, Rabbit, 1:1000; GAPDH US 1:1000 CST) at 4°C overnight. The next day, TBST was washed for 30 minutes. Specific proteins were detected by secondary antibodies and observed by the electrochemiluminescence (ECL) (Pierce, Rockford, IL, USA) system.

2.8. *Immunofluorescence*. The plate was washed with phosphate-buffered saline (PBS) once, and H9C2 cardiomyocytes were fixed with 4% paraformaldehyde for 30 minutes, and then, goat serum was added to sealing for 1 hour. The diluted primary antibody 8-hydroxydeoxyguanosine (8-OHdG, Abcam, Rabbit, 1:500) was added to incubate at 4°C overnight. The next day, the combined secondary antibody

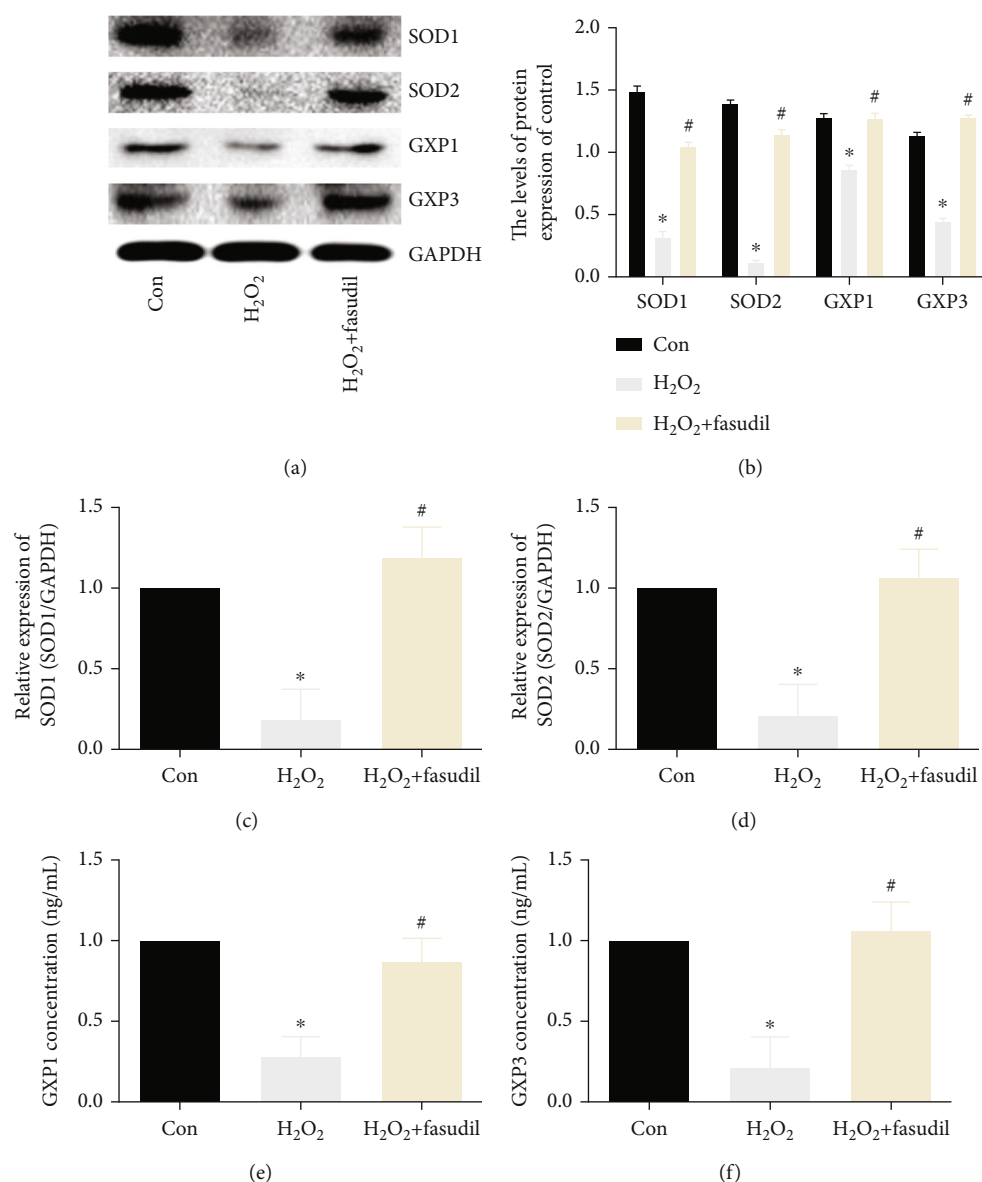


FIGURE 2: Fasudil inhibits oxidative stress induced by H₂O₂ in H9C2 cardiomyocytes. (a, b) Western blot was used to detect the expression of SOD1, SOD2, GPX1, and GPX3 in three groups. GAPDH was used as an internal control. (c, d) SOD1 and SOD2 mRNA expression was determined by real-time PCR. (e, f) ELISA detects the expression of GPX1 and GPX3 (“*” indicates statistical difference from the control group $p < 0.05$, and “#” indicates statistical difference from the ischemic hypoxia group $p < 0.05$).

was incubated for 1 hour in the dark and stained with 4',6-diamidino-2-phenylindole (DAPI) (Thermo Fisher Scientific, Shanghai, China) for nuclear staining. Finally, the film was sealed with a sealing liquid, and the image was observed under a fluorescence microscope (Olympus, Tokyo, Japan).

2.9. Enzyme-Linked Immunosorbent Assay (ELISA). H9C2 cardiomyocytes were plated at 5,000/well in 6-well plates, and the cells were treated differently. The concentration of GPX1 and GPX3 in the cell supernatant was measured according to the instructions using an ELISA kit (Elabscience, Wuhan, China).

2.10. Reactive Oxygen Species (ROS) Level Detection. Flow cytometry was used to detect intracellular ROS levels. After

different treatments of the three groups of cells, H9C2 cardiomyocytes were collected and washed with cold PBS. Total ROS levels were measured using flow cytometry (Becton Dickinson, Heidelberg, Germany) by intubation at 37°C for 20 min using DCFH-DA (10 M Kaiji, Nanjing, China).

2.11. Statistical Analysis. SPSS 21.0 statistical software (SPSS IBM, Armonk, NY, USA) was used to analyze the experimental data. Measurement data is expressed as $\bar{x} \pm s$; t -test was used for comparisons between the two groups. Comparison between multiple groups was done using the one-way ANOVA test followed by the post hoc test (least significant difference). The LSD test or SNK test was used for pairwise comparison under the condition of homogeneity of variance.

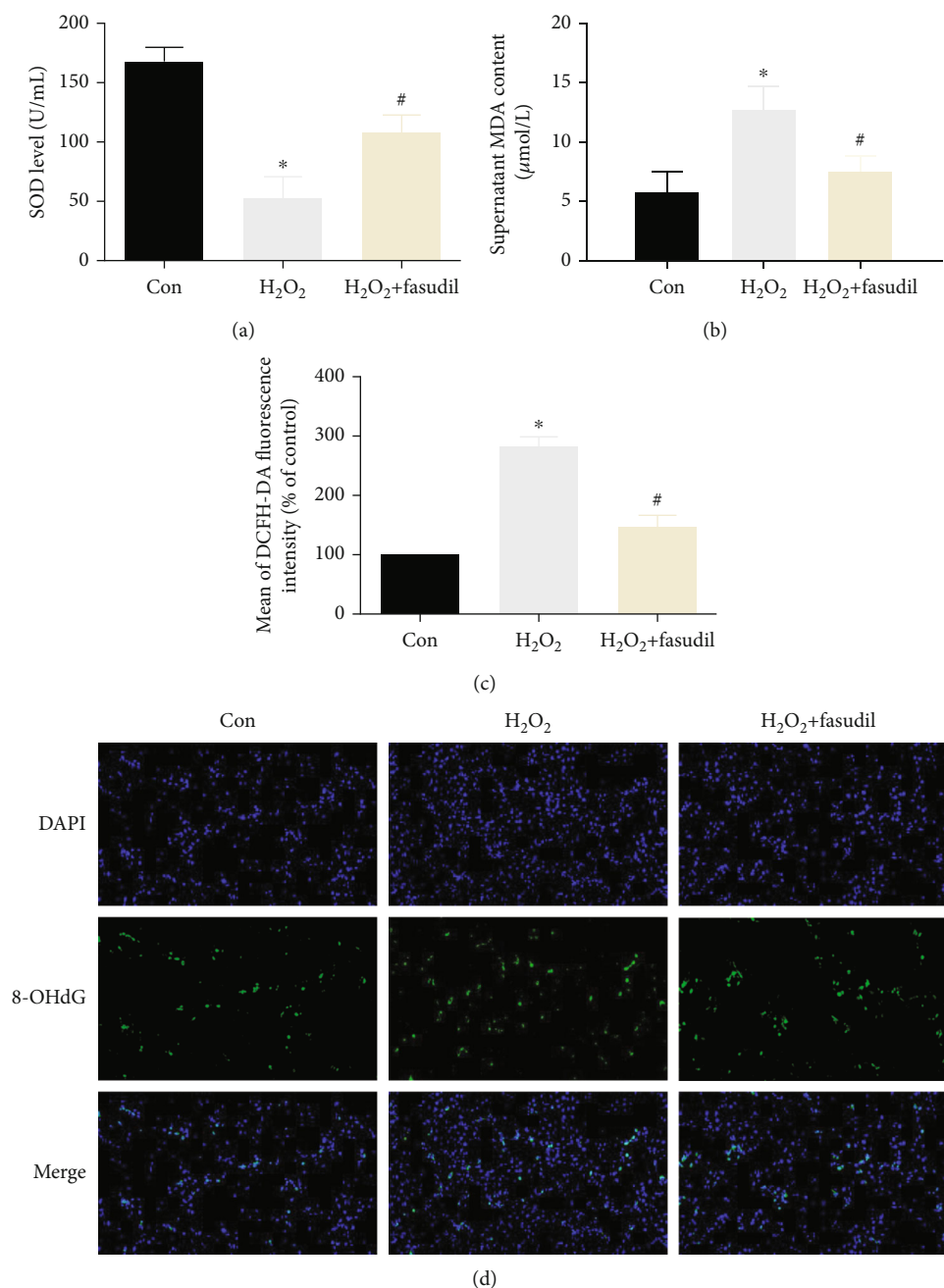


FIGURE 3: Fasudil inhibits H₂O₂-induced oxidative damage in H9C2 cardiomyocytes. (a) The SOD kit detects the level of cellular SOD. (b) The MDA kit detects the MDA content of the supernatant. (c) Flow cytometry was used to detect ROS levels. (d) Immunofluorescence was used to detect the expression of 8-OHdG in the three groups (“*” indicates statistical difference from the control group $p < 0.05$, and “#” indicates statistical difference from the ischemic hypoxia group $p < 0.05$).

$p < 0.05$ indicated the significant difference. All experiments were repeated 3 times.

3. Results

3.1. Fasudil Retards Degradation of H9C2 Cardiomyocytes In Vitro. The optimal concentration and optimal culture time point of fasudil-treated H9C2 cardiomyocytes were detected by CCK-8 (Figure 1(a)). We found that the highest cell viability was achieved after 3 hours of incubation with

20 $\mu\text{mol}\cdot\text{L}^{-1}$. LDH and CAT kits were used to detect cell supernatants. The results showed that LDH was significantly increased in the H₂O₂ group. CAT levels in the H₂O₂ group were significantly lower than in the Con group, while fasudil treatment significantly inhibited the reduction of CAT levels and inhibited the rise of LDH (Figures 1(b) and 1(c)).

3.2. Fasudil Inhibits Oxidative Stress Induced by H₂O₂ in H9C2 Cardiomyocytes. We detected antioxidant proteins by WB. Compared with the Con group, the expression of

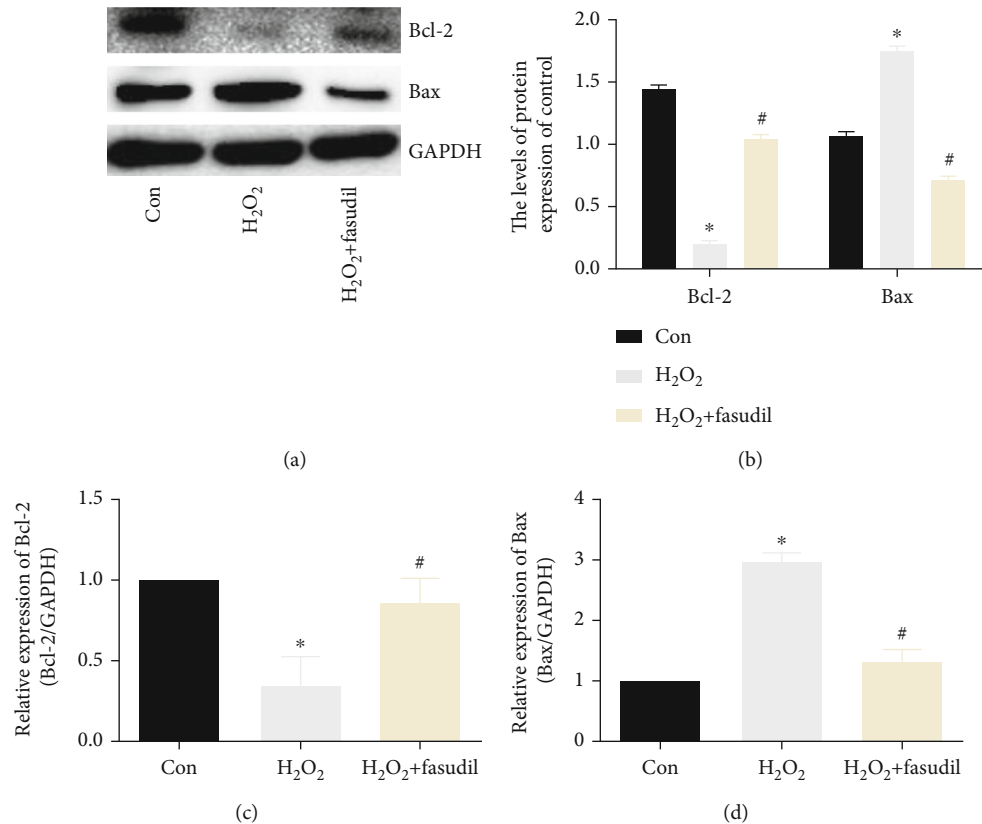


FIGURE 4: Fasudil inhibits H₂O₂-induced apoptosis of H9C2 cardiomyocytes. (a, b) Western blot was used to detect the expression of Bcl-2 and Bax in the three groups. GAPDH was used as an internal control. (c, d) Bcl-2 and Bax mRNA expression was determined by real-time PCR (“*” indicates statistical difference from the control group $p < 0.05$, and “#” indicates statistical difference from the ischemic hypoxia group $p < 0.05$).

SOD1, SOD2, GPX1, and GPX3 in the H₂O₂ group was significantly decreased, while fasudil significantly promoted the expression of SOD1, SOD2, GPX1, and GPX3 (Figures 2(a) and 2(b)). The mRNA results were similar to the former: the SOD1 and SOD2 mRNA levels were decreased in the H₂O₂ group; compared with the Con group, the SOD1 and SOD2 mRNA levels in the H₂O₂+fasudil group were significantly increased (Figures 2(c) and 2(d)). ELISA results show that GPX1 and GPX3 were decreased in the H₂O₂ group, but the expression of GPX1 and GPX3 was obviously increased in the H₂O₂+fasudil group (Figures 2(e) and 2(f)).

3.3. Fasudil Inhibits H₂O₂-Induced Oxidative Damage in H9C2 Cardiomyocytes. First, SOD and MDA levels were measured in the supernatant (Figures 3(a) and 3(b)). It was found that the SOD content was significantly decreased in the H₂O₂ group and significantly increased in the H₂O₂+fasudil group, while the MDA content was increased in the H₂O₂ group, and after fasudil treatment, the MDA content was decreased significantly. Flow cytometry results showed that the ROS levels were significantly increased in the H₂O₂ group, while ROS levels were significantly lower in the H₂O₂+fasudil group (Figure 3(c)). Immunofluorescence showed that the expression of 8-OHdG in the H₂O₂ group was significantly brighter than the Con group, while fasudil

can effectively inhibit the expression of 8-OHdG in the H₂O₂+fasudil group (Figure 3(d)).

3.4. Fasudil Inhibits H₂O₂-Induced Apoptosis of H9C2 Cardiomyocytes. WB results showed that H₂O₂ treatment could induce apoptosis of H9C2 cardiomyocytes. The expression of Bax in the H₂O₂ group was significantly increased, while the expression of Bcl-2 was significantly inhibited. The treatment of H9C2 cardiomyocytes with fasudil can effectively inhibit the increase of Bax and promote the expression of Bcl-2 (Figures 4(a) and 4(b)). Similar levels were obtained for mRNA levels (Figures 4(c) and 4(d)).

3.5. Fasudil Inhibits H₂O₂-Induced Senescence of H9C2 Cardiomyocytes. First, we detected senescence-associated proteins: Sirt1 and P53. Compared with the Con group, Sirt1 expression was significantly inhibited in the H₂O₂ group, and P53 expression was significantly promoted. In the H₂O₂+fasudil group, Sirt1 expression was significantly increased, and P53 expression was inhibited compared to the H₂O₂ group (Figures 5(a) and 5(b)). Second, Sirt1 mRNA was inhibited in the H₂O₂ group, while the P53 mRNA was significantly increased. However, in the H₂O₂+fasudil group, Sirt1 mRNA was higher than the H₂O₂ group, and P53 mRNA expression was inhibited (Figures 5(c) and 5(d)).

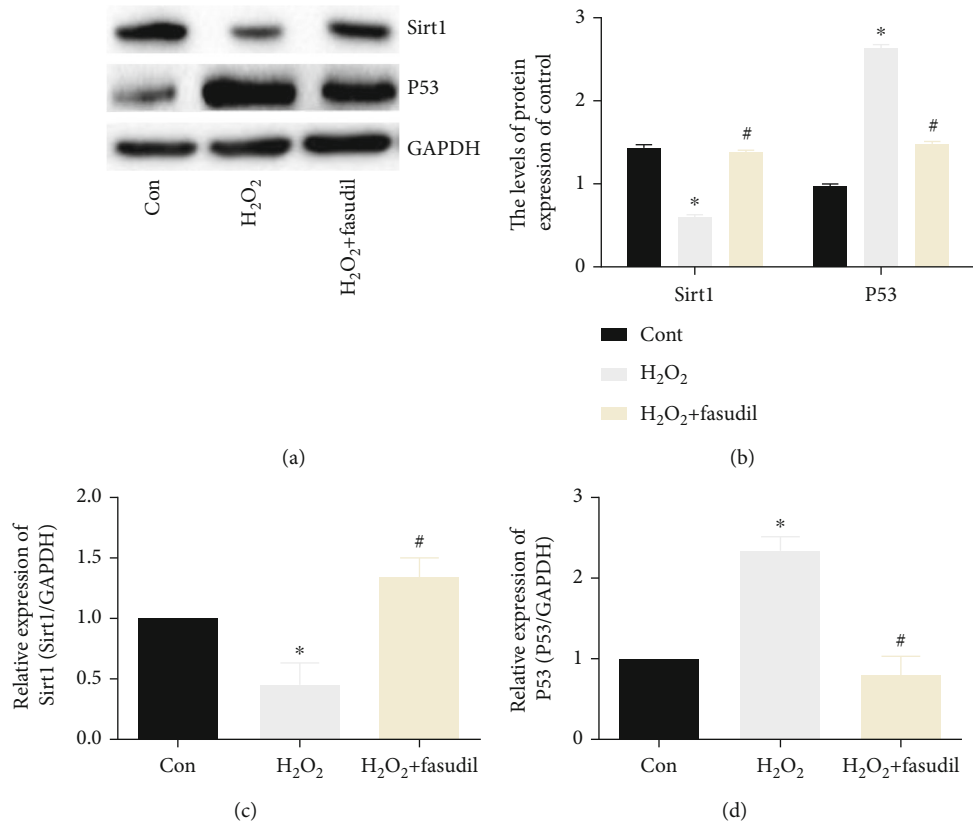


FIGURE 5: Fasudil inhibits H₂O₂-induced senescence of H9C2 cardiomyocytes. (a, b) Western blot was used to detect the expression of Sirt1 and P53 in the three groups. GAPDH was used as an internal control. (c, d) Sirt1 and P53 mRNA expression was determined by real-time PCR (“*” indicates statistical difference from the control group $p < 0.05$, and “#” indicates statistical difference from the ischemic hypoxia group $p < 0.05$).

3.6. Fasudil Inhibits Rho/ROCK Pathway Activation. We found that ROCK1 and ROCK2 expression was significantly increased in the H₂O₂ group, and the expression of ROCK1 and ROCK2 was significantly inhibited in the H₂O₂+fasudil group. Next, we detected the downstream molecule MYPT-1 and p-MYPT-1, and the results showed that the expression ratio of p-MYPT-1/MYPT-1 was significantly increased in the H₂O₂ group, while fasudil can effectively inhibit the expression ratio of p-MYPT-1/MYPT-1 (Figure 6(a)). In addition, ROCK1 and ROCK2 mRNA was significantly elevated in the H₂O₂ group but was all inhibited by fasudil (Figures 6(c) and 6(d)).

4. Discussion

Previous studies have suggested that cell necrosis and apoptosis are the main ways of myocardial damage, but in recent years, extensive research confirmed that OS is another major way of myocardial cell damage [15]. Studies have found that a large number of ROS in the central and surrounding tissues of heart disease patients with heart disease indicate that OS is also one of the main causes of myocardial infarction [16]. Therefore, inhibition of cardiomyocyte OS response is essential for the prevention of cardiovascular disease.

To further investigate the mechanism of H₂O₂-induced OS in cardiomyocytes and to explore new interventions, we constructed a model by treating H9C2 cardiomyocytes with H₂O₂. Compared with the Con group, the antioxidant capacity of the H₂O₂ group was significantly reduced, and the apoptosis and senescence were significantly increased. As an inhibitor of the Rho/ROCK pathway, fasudil significantly increases the antioxidant capacity and effectively inhibits H₂O₂-induced apoptosis and senescence, as well as DNA damage. However, the molecular mechanism of fasudil in preventing H₂O₂-induced myocardial injury and its protective effects is still unclear and further research is needed. The results confirm that fasudil reduces H₂O₂-induced H9C2 cardiomyocyte OS by three aspects: (1) Fasudil improves cell clearance of ROS. (2) Fasudil can inhibit cell apoptosis, thereby reducing cell senescence. (3) Fasudil inhibits the Rho/ROCK signaling pathway and reduces H₂O₂-induced OS, thereby protecting H9C2 cardiomyocytes.

H₂O₂ is often used in cardiovascular disease models such as myocardial ischemia and myocardial ischemia and reperfusion [17]. Studies have shown that ROS can upregulate the expression of caspase family proteins by inhibiting Bcl-2 expression and promoting the transfer of Bax to mitochondria to induce the release of cytochrome C and initiate the mitochondrial apoptosis program [18]. The results of this

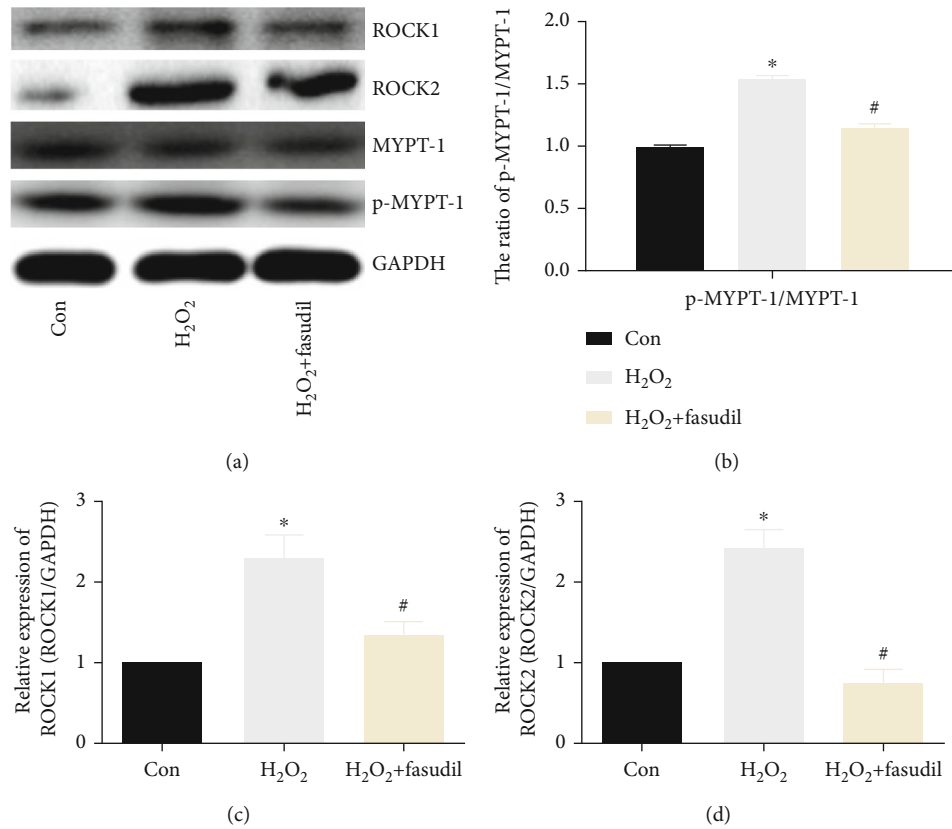


FIGURE 6: Fasudil inhibits Rho/ROCK pathway activation. (a) Western blot analysis of ROCK1, ROCK2, p-MYPT-1, and MYPT-1 expression in three groups. GAPDH was used as an internal control. (b) Protein gray value ratio of p-MYPT-1/MYPT-1. (c, d) ROCK1 and ROCK2 mRNA expression was determined by real-time PCR (“*” indicates statistical difference from the control group $p < 0.05$, and “#” indicates statistical difference from the ischemic hypoxia group $p < 0.05$).

experiment confirmed that Bax expression in the H₂O₂ group was significantly increased, but the Bax expression in the fasudil group was significantly inhibited, and the expression of antiapoptotic Bcl-2 was promoted.

Previous research confirmed that H₂O₂ produces OS damage to H9C2 cardiomyocytes. The ROS induced by H₂O₂ is cytotoxic, and ROS can cause destruction or even cleavage of DNA in the nucleus, eventually leading to apoptosis of a large number of H9C2 cardiomyocytes [19]. We confirmed by immunofluorescence that H₂O₂ treatment can significantly increase DNA damage in H9C2 cardiomyocytes, while the expression of 8-OHdG in the fasudil group was effectively inhibited, and slowing apoptosis.

A large number of articles reported that senescent was also one of the independent risk factors for cardiovascular disease. H₂O₂-induced oxidative damage can better simulate OS in the elderly, thereby promoting cell senescence [20]. This experiment verified the expression levels of senescence-associated molecule P53 and anti-senescence-related molecule Sirt1. Results show that Sirt1 expression was significantly decreased in the H₂O₂ group, while P53 expression was significantly increased. Fasudil treatment significantly inhibited the elevation of P53 and promoted the expression of Sirt1. The results showed that fasudil inhibited H₂O₂-induced H9C2 cardiomyocyte senescence, thereby alleviating H₂O₂ damage to H9C2 cardiomyocytes.

Rho kinase belongs to the serine/threonine protein kinase ACG family, which is an important effector downstream of RhoA of small GTP protein family [21]. Numerous researches have reported that the Rho/ROCK pathway is related in the regulation of inflammation and OS [22]. The results of this experiment show that H9C2 OS increased significantly after H₂O₂ treatment, which may be related to the activation of the Rho/ROCK pathway and the increase of downstream-related molecules. We confirmed that ROCK1 and ROCK2 expression in the H₂O₂ group and its downstream p-MYPT-1 was significantly prompted, while the ROCK kinase inhibitor fasudil was effective in inhibiting the increase of ROCK1, ROCK2, and p-MYPT-1 and inhibiting H₂O₂-induced H9C2 cardiomyocyte OS response.

5. Conclusions

Fasudil inhibits Rho/ROCK signaling and reduces OS, thereby inhibiting cell senescence and apoptosis. Therefore, fasudil is of great value in the intervention of hypoxic cardiomyopathy.

Data Availability

The datasets used and analyzed during the current study are available from the corresponding author on reasonable request.

Conflicts of Interest

The authors declared no conflict of interest.

References

- [1] B. Saour, B. Smith, and C. W. Yancy, "Heart failure and sudden cardiac death," *Cardiac electrophysiology clinics*, vol. 9, no. 4, pp. 709–723, 2017.
- [2] R. Naito and K. Miyauchi, "Coronary artery disease and type 2 diabetes mellitus," *International Heart Journal*, vol. 58, no. 4, pp. 475–480, 2017.
- [3] C. M. Kaneto, J. S. Nascimento, M. Prado, and L. Mendonca, "Circulating miRNAs as biomarkers in cardiovascular diseases," *European Review for Medical and Pharmacological Sciences*, vol. 23, no. 5, pp. 2234–2243, 2019.
- [4] G. A. Kurian, R. Rajagopal, S. Vedantham, and M. Rajesh, "The role of oxidative stress in myocardial ischemia and reperfusion injury and remodeling: revisited," *Oxidative Medicine and Cellular Longevity*, vol. 2016, Article ID 1656450, 14 pages, 2016.
- [5] K. Wang, Y. Yuan, X. Liu et al., "Cardiac specific overexpression of mitochondrial Omi/HtrA2 induces myocardial apoptosis and cardiac dysfunction," *Scientific Reports*, vol. 6, no. 1, article 37927, 2016.
- [6] H. Zhou, Y. Sun, L. Zhang, W. Kang, N. Li, and Y. Li, "The RhoA/ROCK pathway mediates high glucose-induced cardiomyocyte apoptosis via oxidative stress, JNK, and p38MAPK pathways," *Diabetes/Metabolism Research and Reviews*, vol. 34, no. 6, article e3022, 2018.
- [7] L. A. Ahmed, H. A. Darwish, R. M. Abdelsalam, and H. A. Amin, "Role of Rho kinase inhibition in the protective effect of fasudil and simvastatin against 3-nitropropionic acid-induced striatal neurodegeneration and mitochondrial dysfunction in rats," *Molecular Neurobiology*, vol. 53, no. 6, pp. 3927–3938, 2016.
- [8] T. Hattori, H. Shimokawa, M. Higashi et al., "Long-term inhibition of Rho-kinase suppresses left ventricular remodeling after myocardial infarction in mice," *Circulation*, vol. 109, no. 18, pp. 2234–2239, 2004.
- [9] K. Ishimaru, H. Ueno, S. Kagitani, D. Takabayashi, M. Takata, and H. Inoue, "Fasudil attenuates myocardial fibrosis in association with inhibition of monocyte/macrophage infiltration in the heart of DOCA/salt hypertensive rats," *Journal of Cardiovascular Pharmacology*, vol. 50, no. 2, pp. 187–194, 2007.
- [10] A. L. Bishop and A. Hall, "Rho GTPases and their effector proteins," *The Biochemical Journal*, vol. 348, no. 2, pp. 241–255, 2000.
- [11] H. Shimokawa, S. Sunamura, and K. Satoh, "RhoA/Rho-kinase in the cardiovascular system," *Circulation Research*, vol. 118, no. 2, pp. 352–366, 2016.
- [12] Y. N. Qiao, W. Q. He, C. P. Chen et al., "Myosin phosphatase target subunit 1 (MYPT1) regulates the contraction and relaxation of vascular smooth muscle and maintains blood pressure," *The Journal of Biological Chemistry*, vol. 289, no. 32, pp. 22512–22523, 2014.
- [13] A. Sadok and C. J. Marshall, "Rho GTPases," *Small GTPases*, vol. 5, no. 4, article e29710, 2014.
- [14] Y. Nozaki, K. Kinoshita, S. Hino et al., "Signaling Rho-kinase mediates inflammation and apoptosis in T cells and renal tubules in cisplatin nephrotoxicity," *American Journal of Physiology. Renal Physiology*, vol. 308, no. 8, pp. F899–F909, 2015.
- [15] D. A. Chistiakov, T. P. Shkurat, A. A. Melnichenko, A. V. Grechko, and A. N. Orekhov, "The role of mitochondrial dysfunction in cardiovascular disease: a brief review," *Annals of Medicine*, vol. 50, no. 2, pp. 121–127, 2018.
- [16] M. Neri, V. Fineschi, M. Di Paolo et al., "Cardiac oxidative stress and inflammatory cytokines response after myocardial infarction," *Current Vascular Pharmacology*, vol. 13, no. 1, pp. 26–36, 2015.
- [17] S. Bae, M. Park, C. Kang et al., "Hydrogen peroxide-responsive nanoparticle reduces myocardial ischemia/reperfusion injury," *Journal of the American Heart Association*, vol. 5, no. 11, article e003697, 2016.
- [18] T. J. Fan, L. H. Han, R. S. Cong, and J. Liang, "Caspase family proteases and apoptosis," *Acta Biochim Biophys Sin (Shanghai)*, vol. 37, no. 11, pp. 719–727, 2005.
- [19] C. Feng, Y. Zhang, M. Yang et al., "The matrikine N-acetylated proline-glycine-proline induces premature senescence of nucleus pulposus cells via CXCR1-dependent ROS accumulation and DNA damage and reinforces the destructive effect of these cells on homeostasis of intervertebral discs," *Biochimica et Biophysica Acta - Molecular Basis of Disease*, vol. 1863, no. 1, pp. 220–230, 2017.
- [20] A. Logan, I. G. Shabalina, T. A. Prime et al., "In vivo levels of mitochondrial hydrogen peroxide increase with age in mtDNA mutator mice," *Aging Cell*, vol. 13, no. 4, pp. 765–768, 2014.
- [21] B. Marcos-Ramiro, D. Garcia-Weber, and J. Millan, "TNF-induced endothelial barrier disruption: beyond actin and Rho," *Thrombosis and Haemostasis*, vol. 112, no. 6, pp. 1088–1102, 2014.
- [22] A. Hall, "Rho family GTPases," *Biochemical Society Transactions*, vol. 40, no. 6, pp. 1378–1382, 2012.

Research Article

Regulatory Mechanism of LINC00152 on Aggravating Heart Failure through Triggering Fibrosis in an Infarcted Myocardium

Lizhong Song,¹ Xiujuan Duan,² Xiaojuan Zeng,³ Xinglian Duan,³ and Li Li ³

¹Department of Emergency, Shanxi Cardiovascular Disease Hospital, Taiyuan, Shanxi Province, China

²Department of Cardiology, The Eighth People's Hospital of Hengshui City, Hengshui, China

³Department of Cardiology, The Third Affiliated Hospital of Chongqing Medical University, Chongqing, China

Correspondence should be addressed to Li Li; 650500@hospital.cqmu.edu.cn

Received 11 October 2021; Accepted 19 November 2021; Published 1 December 2021

Academic Editor: Francesco Busard?

Copyright © 2021 Lizhong Song et al. This is an open access article distributed under the Creative Commons Attribution License, which permits unrestricted use, distribution, and reproduction in any medium, provided the original work is properly cited.

Objective. To elucidate the role of LINC00152 in the progression of heart failure following myocardial infarction. **Patients and Methods.** Serum levels of LINC00152 in acute myocardial infarction (AMI) patients were detected by quantitative real-time polymerase chain reaction (qRT-PCR). Receiver operating characteristic (ROC) curves were depicted for assessing the diagnostic value of LINC00152 in AMI. Subsequently, an *in vivo* AMI model was generated in mice. LINC00152 level in a mouse infarcted myocardium was detected. Echocardiogram was conducted to evaluate the influence of LINC00152 on cardiac function in AMI mice. Primary cardiac fibroblasts were isolated from neonatal mice. After knockdown of LINC00152, proliferative and migratory changes in primary cardiac fibroblasts were assessed by cell counting kit-8 (CCK-8) and transwell assay, respectively. The regulatory effect of LINC00152 on Smad7 level was determined by qRT-PCR. Finally, the involvement of Smad7 in LINC00152-regulated proliferative and migratory abilities in primary cardiac fibroblasts was explored by rescue experiments. **Results.** Serum level of LINC00152 was elevated in AMI patients. ROC curves demonstrated the diagnostic potential of LINC00152 in AMI (95% CI: 0.806-0.940, $p = 0.034$). In myocardial tissues collected from AMI mice, LINC00152 level was higher than those collected from mice of the sham group. LVEF and FS markedly decreased in AMI mice overexpressing LINC00152 on the 4th week of AMI modeling. After knockdown of LINC00152 in primary cardiac fibroblasts, proliferative and migratory abilities were declined, which were abolished by Smad7 intervention. **Conclusions.** By downregulating Smad7, LINC00152 aggravates heart failure following AMI *via* promoting the proliferative and migratory abilities in cardiac fibroblasts.

1. Introduction

Heart failure (HF) is the terminal stage of most cardiovascular diseases. HF severely endangers human health because its incidence and mortality are extremely high. Globally, over 37.7 million people suffer from HF, and its incidence has annually increased. In 2003, there were 4.5 million HF patients in China, including 500,000 new onsets [1]. Acute myocardial infarction (AMI) can result in myocardial necrosis, myocardial fibrosis, and ventricular remodeling, which is an important cause of HF [2]. Although advanced progress has been made on the diagnosis and treatment of HF, the molecular mechanism of HF following AMI has

not been clarified. Effective strategies to delay or even cure HF following AMI are urgently required [3].

Long noncoding RNAs (lncRNAs) are linear transcription RNAs with 200 to 100,000 nucleotides long. As a newly discovered type of ncRNAs, lncRNAs are functional to regulate protein expressions, rather than the carries of protein translation [4]. In fact, a large number of lncRNAs are considered the direct or indirect factors influencing gene expressions [5]. Very recently, lncRNAs have been identified as biomarkers and therapeutic targets for AMI [6]. A clinical trial pointed out that expression levels of urothelial tumor-associated lncRNAs in blood circulation are downregulated at 72 h following AMI [7]. Besides,

2810403D21Rik/MirfLncRNA promotes ischemic myocardial injury by regulating autophagy through targeting Mir26a [8]. Further, ZFAS1 as a SERCA2a inhibitor to cause intracellular Ca overload and contractile dysfunction in a mouse model of myocardial infarction [9]. A microarray analysis on AMI mouse tissues showed that two transcriptional lncRNAs associated with myocardial infarction are significantly upregulated by 5 and 13 times, respectively [10].

LINC00152 is located on chromosome 2p11.2, containing 828 nucleotides. It is initially detected in hepatocellular carcinoma with a differentially low methylation level. LINC00152 is able to regulate gene expressions through epigenetic modification [11], lncRNA-miRNA interaction [12], or lncRNA-protein interaction [13]. Serving as an oncogene, LINC00152 is upregulated in many types of malignant tumors [14–16]. The biological function of LINC00152 in AMI and HF is largely unclear. This study is aimed at uncovering the influence of LINC00152 on regulating cardiac fibroblast phenotypes and cardiac function following AMI.

2. Patients and Methods

2.1. Subjects. A total of 50 eligible AMI patients who were emergently admitted within 6 h of acute chest pain and diagnosed by coronary angiography from May 2017 to December 2019 were enrolled in the AMI group. During the same period, 50 healthy subjects undergoing physical examination were enrolled in the control group. The inclusion criteria of AMI patients were as follows: (1) there are symptoms of chest pain within 6 h; (2) clinical indexes, including ECG findings, myocardial markers, and myocardial enzymes, were in accordance to 2007 ACCF/AHA guideline for the management of ST-elevation myocardial infarction [17]; (3) coronary angiography showed over 50% of coronary stenosis in more than 1 branch; and (4) this study was approved by the Ethics Committee of The Third Affiliated Hospital of Chongqing Medical University. Signed written informed consents were obtained from all participants before the study. The following are the exclusion criteria: (1) chest pain due to acute trauma, pulmonary embolism, aortic dissection, etc.; (2) complication with liver and kidney dysfunction, heart valve disease, malignant tumors, or others. Venous blood samples were collected in EDTA anticoagulation tubes from each subject and centrifuged at 3,000 r/min for 10 min. The isolated plasma was further centrifuged at 12,000 r/min for 10 min, and the upper layer was collected in RNA-free EP tubes for use.

2.2. Generation of AMI Model in Mice. This study was approved by the Animal Ethics Committee of Chongqing Medical University Animal Center. Male C57BL/6 mice (8–10 weeks old) were provided by Charles River (Beijing, China). The AMI model in mice was generated by ligating the anterior descending branch of the coronary artery. Briefly, mice were anesthetized by 1.0%–1.5% isoflurane. Endotracheal intubation connected to the small animal ventilator was conducted. Subsequently, mouse thoracic cavity was exposed from the fourth intercostal space. The parietal

pericardium was bluntly separated, and the anterior descending branch of the coronary artery was ligated using 7-0 suture. A pale myocardium in the ligation area indicated the successful modeling. The incision was closed using 5-0 suture. One week prior to AMI modeling, 1.0×10^7 TU LV-LINC00152 (150 μ L) or negative control of lentivirus was administrated into mouse tail vein. Transfection efficacy of lentivirus was examined by quantitative real-time polymerase chain reaction (qRT-PCR).

2.3. Cardiac Function Assessment. Four weeks after AMI modeling in mice, cardiac function was assessed by performing echocardiography using the Vevo 2100 Small Animal Ultrasound (probe: MS-400). LVEF (left ventricular ejection fraction) and FS (fractional shortening) in mice were recorded.

2.4. Cell Culture of Primary Cardiac Fibroblasts and Cell Transfection. The heart of neonatal C57BL/6 mouse within three days after birth was collected and cut into small pieces and digested in the mixture containing 0.08% trypsin and 0.05% collagenase II at 4°C overnight. Digestion was terminated using Dulbecco's modified Eagle medium/F-12 (DMEM/F-12) (HyClone, South Logan, UT, USA) containing 15% fetal bovine serum (FBS) (HyClone, South Logan, UT, USA). The solution was centrifuged at 1000 r for 10 min, and the collected cells were inoculated in the culture dishes for 1 h. Later, adherent cells were primary cardiac fibroblasts.

Primary cardiac fibroblasts were induced in 5 μ g/mL Polybrene (YEASEN, Shanghai, China) and transfected with 5×10^7 TU lentivirus for 24 h. Culture medium was replaced, and cells were cultivated for another 48 h. Transfection of si-LINC00152 was conducted using Lipofectamine 2000 (si-LINC00152-1#: 5'-GGGAAATAAATGACTG GAT-3'; si-LINC00152-2#: 5'-GGAGATGAAACAGGAA GCT-3') (Invitrogen, Carlsbad, CA, USA).

2.5. qRT-PCR. Total RNAs were isolated from tissues or blood samples using RNA extraction kit (ABI, Foster City, CA, USA). The concentration and purity of RNA were determined using an ultraviolet spectrophotometer (Thermo Fisher Scientific, Waltham, MA, USA). After reverse transcription, complementary deoxyribose nucleic acids (cDNAs) were amplified for qRT-PCR. Relative mRNA level was calculated by $2^{-\Delta\Delta C_t}$. Primer sequences were as follows: LINC00152 (human): 5'-TGGAATGGAGGGAAA TAAA-3' (forward) and 5'-CCAGGAAGTGTGCTGTGA AG-3' (reverse), LINC00152 (mouse): 5'-CAGCACCTC TACCTGTTG-3' (forward) and 5'-GGATTAAGACACAT AGAGACTG-3' (reverse), and GAPDH: 5'-AACGGATTT GGTCTGATTTGG-3' (forward) and 5'-TTGATTTTGGG GGGATCTCG-3' (reverse); GAPDH (mouse): 5'-CATCAC TGCCACCCAGAAGACTG-3' (forward) and 5'-ATGCCA GTGAGCTTCCCGTTCAG-3' (reverse).

2.6. Cell Counting Kit-8 (CCK-8). 1.0×10^3 cells were implanted in each well of a 6-well plate and cultured for 1

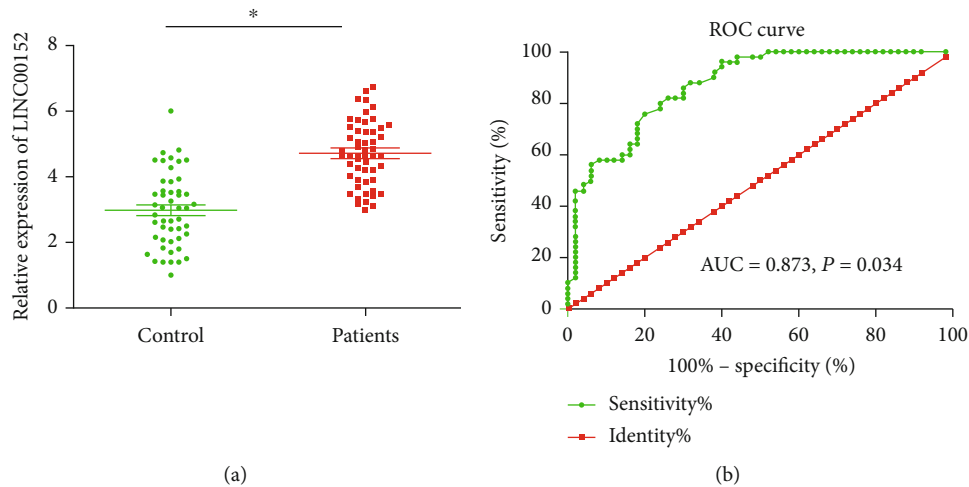


FIGURE 1: Increased serum level of LINC00152 in AMI patients. (a) Serum level of LINC00152 increased in AMI patients than healthy subjects; (b) ROC curves demonstrated the diagnostic potential of LINC00152 in AMI (AUC = 0.873, $p = 0.034$).

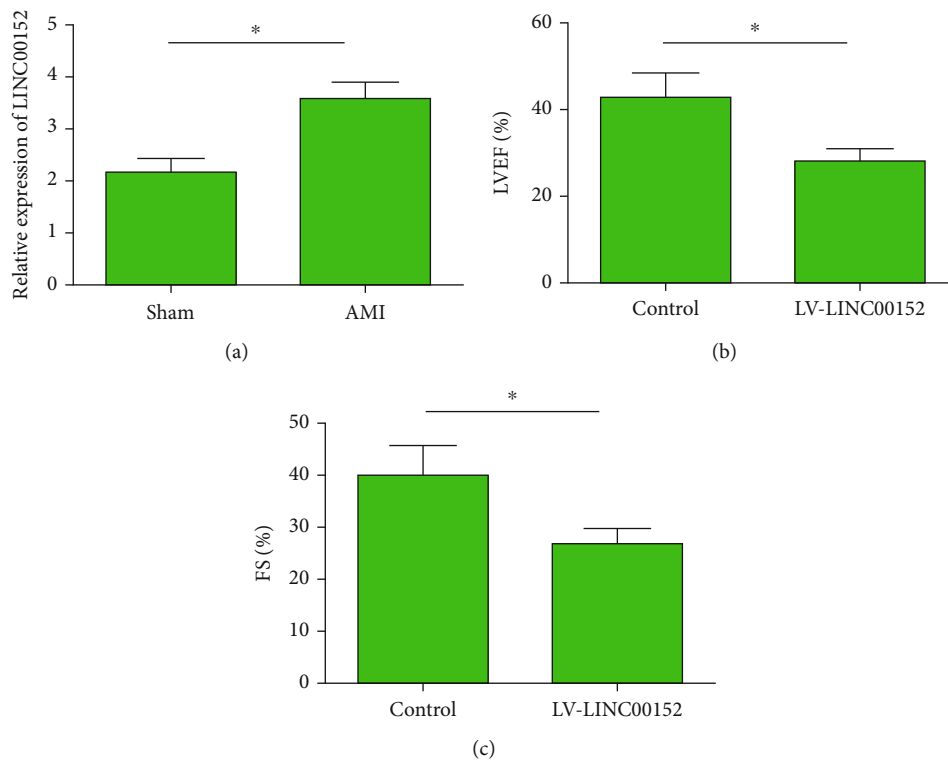


FIGURE 2: LINC00152 aggravated HF following AMI. (a) LINC00152 was upregulated in mice of AMI group than those in the sham group; (b) LVEF (%) was lower in AMI mice overexpressing LINC00152 than in AMI mice; (c) FS (%) was lower in AMI mice overexpressing LINC00152 than in AMI mice.

day, where $10 \mu\text{L}$ of CCK-8 solution was added (TaKaRa, Dalian, China). After 1 h culturing in the dark, the optical density at 450 nm was measured using a microplate reader.

2.7. Transwell Assay. $100 \mu\text{L}$ of serum-free suspension (1.0×10^5 cells/mL) and $600 \mu\text{L}$ of serum-containing medium were applied to the top and bottom transwell chamber, respectively, and cultured overnight. Cells in the bottom were

subjected to methanol fixation for 15 min and crystal violet staining for 20 min. Migratory cells were counted in 5 randomly selected fields per sample.

2.8. Statistical Analysis. Data analysis was performed using Statistical Product and Service Solutions (SPSS) 22.0 software (IBM, Armonk, NY, USA). Differences between groups were compared using Student's t -test. Receiver operating

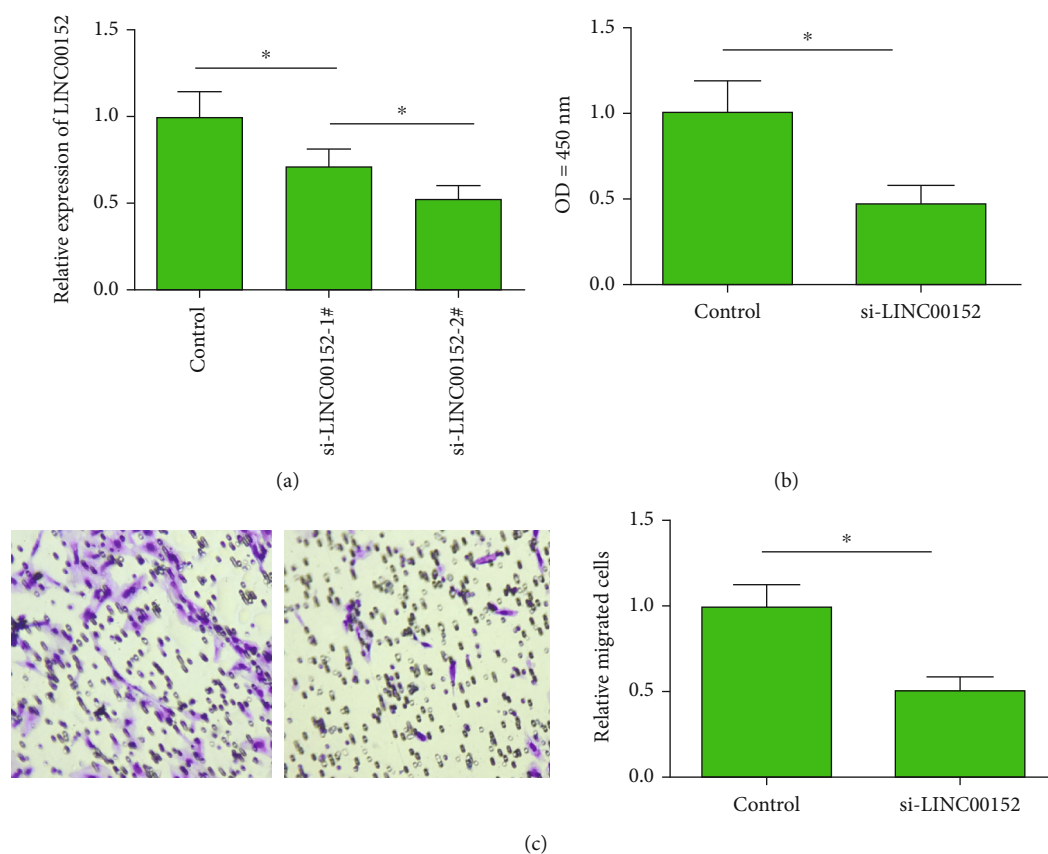


FIGURE 3: LINC00152 promoted proliferative and migratory abilities in cardiac fibroblasts. (a) Transfection of either si-LINC00152-1# or si-LINC00152-2# significantly downregulated LINC00152 in primary cardiac fibroblasts. (b) Knockdown of LINC00152 weakened proliferation in primary cardiac fibroblasts. (c) Knockdown of LINC00152 weakened migration in primary cardiac fibroblasts (magnification: 200x).

characteristic (ROC) curves were depicted for assessing the diagnostic potential of LINC00152 in AMI. $p < 0.05$ was considered statistically significant.

3. Results

3.1. Increased Serum Level of LINC00152 in AMI Patients. Compared with healthy subjects, the serum level of LINC00152 was markedly higher in AMI patients (Figure 1(a)). Subsequently, the diagnostic potential of LINC00152 in AMI was identified by the depicted ROC curves (AUC = 0.873, 95%CI = 0.806-0.940, $p = 0.034$) (Figure 1(b)). It is suggested that LINC00152 may be a potential biomarker for AMI.

3.2. LINC00152 Aggravated HF following AMI. To elucidate the influence of LINC00152 on HF following AMI, we generated an *in vivo* AMI model in mice. Myocardial tissues were collected from AMI mice and those in the sham group one week after modeling. Compared those in the sham group, LINC00152 level was much higher in infarcted myocardial tissues collected from AMI mice (Figure 2(a)). Besides, echocardiogram findings uncovered that LVEF and FS were lower in AMI mice overexpressing LINC00152 than those in AMI mice (Figures 2(b) and 2(c)). It is indi-

cated that overexpressed LINC00152 aggravated cardiac function in AMI mice.

3.3. LINC00152 Promoted Proliferative and Migratory Abilities in Cardiac Fibroblasts. We thereafter explored the *in vitro* function of LINC00152 in the process of AMI. Primary cardiac fibroblasts were used for generating the LINC00152 intervention group. Two lines of LINC00152 siRNAs were constructed. Transfection of either of them could effectively downregulate LINC00152 in primary cardiac fibroblasts (Figure 3(a)). In particular, transfection efficacy of si-LINC00152-2# was better than the other one, which was used in the following experiments. CCK-8 assay uncovered that knockdown of LINC00152 reduced viability in primary cardiac fibroblasts (Figure 3(b)). Besides, transfection of si-LINC00152 in primary cardiac fibroblasts reduced migratory cell number, indicating the attenuated migratory ability (Figure 3(c)).

3.4. LINC00152 Regulated Cardiac Fibroblast Functions by Regulating Smad7. Transfection of LV-LINC00152 markedly upregulated LINC00152 in primary cardiac fibroblasts, suggesting a great transfection efficacy (Figure 4(a)). In primary cardiac fibroblasts overexpressing LINC00152, Smad7 was downregulated (Figure 4(b)). Interestingly, enhanced

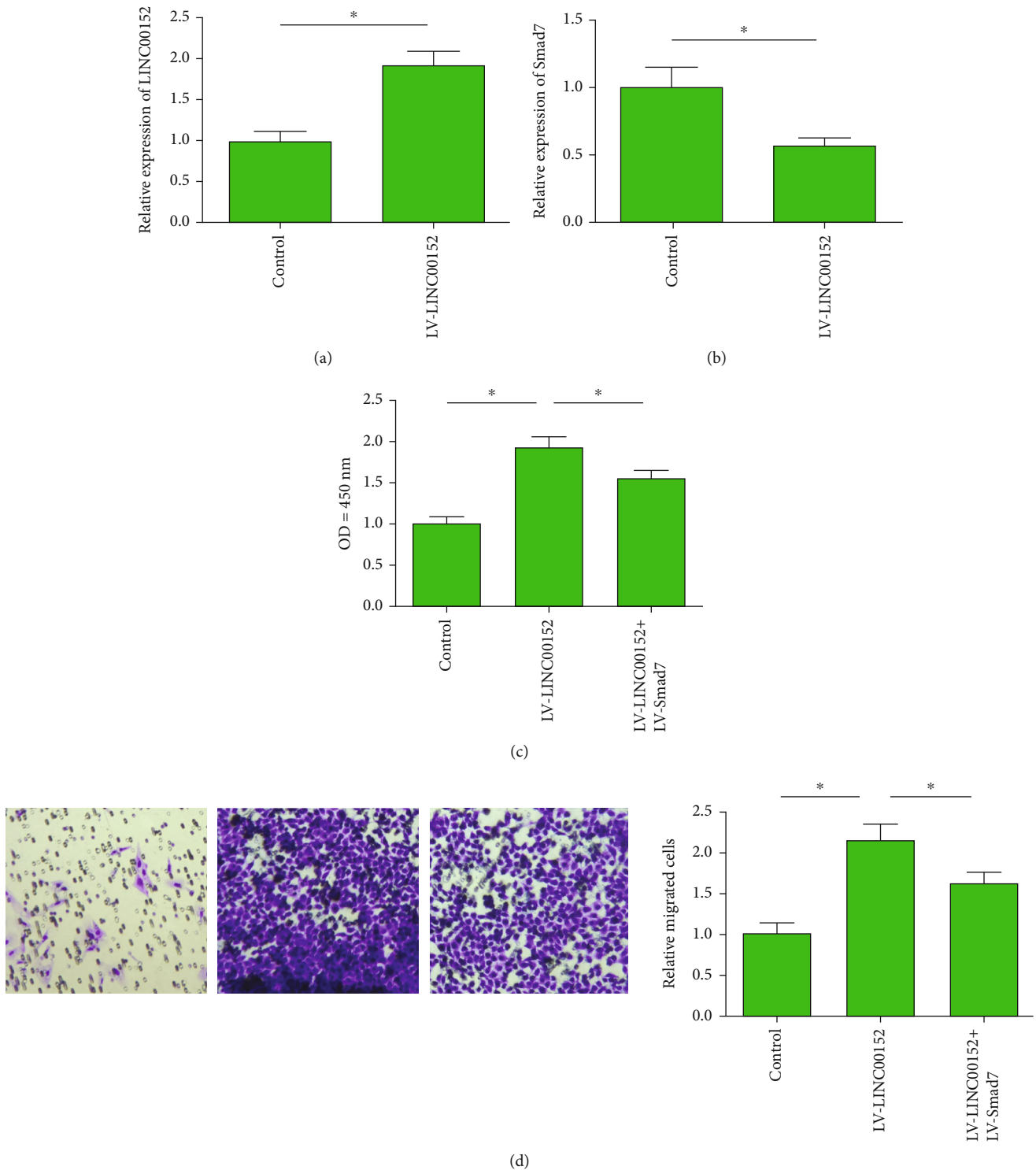


FIGURE 4: LINC00152 regulated cardiac fibroblast functions by regulating Smad7. (a) Transfection of LV-LINC00152 significantly upregulated LINC00152 in primary cardiac fibroblasts. (b) Overexpression of LINC00152 downregulated Smad7 in primary cardiac fibroblasts. (c) Enhanced proliferation in primary cardiac fibroblasts overexpressing LINC00152 was partially reversed by cooverexpression of Smad7. (d) Enhanced migration in primary cardiac fibroblasts overexpressing LINC00152 was partially reversed by cooverexpression of Smad7 (magnification: 200x).

viability and migratory cell number in primary cardiac fibroblasts overexpressing LINC00152 were partially reversed by cooverexpression of Smad7 (Figures 4(c) and 4(d)). Collec-

tively, LINC00152 promoted proliferative and migratory abilities in primary cardiac fibroblasts by negatively regulating Smad7.

4. Discussion

AMI is the major reason for death in the world [18]. At present, the diagnosis of AMI relies on examinations of previous history, chest pain symptoms, electrocardiogram (ECG) findings, and laboratory tests. Detection of cTNI/cTNT level is extensively applied in the adjuvant diagnosis of AMI. Nevertheless, cTNI/cTNT level is also elevated in non-AMI patients, including viral myocarditis, heart failure, atrial fibrillation, chronic kidney disease, and sepsis [19–21]. Moreover, ECG changes, clinical symptoms of chest pain, and previous history vary a lot in individuals, which are not specific enough for AMI diagnosis. Therefore, it is necessary to seek for serum biomarkers for AMI that can rapidly and stably diagnose AMI in the early phase, thus salvaging the lives.

At post-AMI, cardiac fibroblasts are activated and excessive ECM proteins are released. Damaged myocardial cell functions ultimately lead to interstitial fibrosis and remodeling [22]. Therefore, inhibiting the excessive secretion and deposition of ECM is an important strategy to improve the prognosis of AMI. By detecting differentially expressed lncRNAs in the infarcted myocardium collected from AMI mice at the fourth week, there are 53 upregulated lncRNAs (fold change > 2 times) and 37 downregulated ones. Among them, NONMMUT022554 is the most pronounced lncRNA that is upregulated in the infarcted myocardium, displaying a positive correlation to six upregulated genes that are interacted with ECM receptors [22]. lncRNAs are associated with the development of myocardial fibrosis as well. It is reported that overexpression of H19 triggers proliferation and fibrosis in myocardial fibroblasts [23]. LINC00152 is a cancer-associated lncRNA. In the liver cancer cell line MHCC-97H, LINC00152 is mainly distributed in the nucleus and it drives *in vitro* proliferative rate and *in vivo* cancer growth [24]. Cai et al. [25] demonstrated that LINC00152 stimulates gallbladder cells to proliferate and metastasize, whereas cell apoptosis is inhibited. Wu et al. [26] uncovered that overexpression of LINC00152 induces proliferation and invasiveness in renal cancer cells and inhibits cell cycle progression and apoptosis. In this paper, LINC00152 was upregulated in the serum of AMI patients and the infarcted myocardium of AMI mice. In addition, overexpression of LINC00152 aggravated HF severity following AMI. To clarify the mechanism of LINC00152 on myocardial fibrosis, we isolated primary cardiac fibroblasts from neonatal mice. *In vitro* experiments revealed that overexpression of LINC00152 stimulated proliferative and migratory abilities in primary cardiac fibroblasts.

Smad7 is the classical antagonistic factor for the TGF- β signaling, presenting an antifibrosis effect [27]. A previous study reported that lncRNA COL1A2-AS1 alleviates proliferative potential in scar-derived fibroblasts *via* the Smad7 signaling [28]. Here, LINC00152 negatively regulated Smad7 level in primary cardiac fibroblasts. Interestingly, overexpression of Smad7 could partially reverse the role of overexpressed LINC00152 on triggering proliferative and migratory abilities in primary cardiac fibroblasts. In this research, we uncover the role of LINC00152 in AMI *via*

in vivo and *in vitro* assay; however, the mechanism will be explored more detailed in our next research. Our findings provide experimental references for the clinical treatment of HF following AMI.

5. Conclusions

By downregulating Smad7, LINC00152 aggravates heart failure following AMI *via* promoting the proliferative and migratory abilities in cardiac fibroblasts.

Data Availability

The datasets used and analyzed during the current study are available from the corresponding author on reasonable request.

Conflicts of Interest

The authors declared no conflict of interest.

References

- [1] Y. Yu, H. Zhang, X. Li et al., “The China Patient-centered Evaluative Assessment of Cardiac Events (China PEACE) retrospective heart failure study design,” *BMJ Open*, vol. 8, no. 5, article e20918, 2018.
- [2] S. Dassanayaka and S. P. Jones, “Recent developments in heart failure,” *Circulation Research*, vol. 117, no. 7, pp. e58–e63, 2015.
- [3] F. Zhou, W. D. Fu, and L. Chen, “MiRNA-182 regulates the cardiomyocyte apoptosis in heart failure,” *European Review for Medical and Pharmacological Sciences*, vol. 23, no. 11, pp. 4917–4923, 2019.
- [4] K. C. Wang and H. Y. Chang, “Molecular mechanisms of long noncoding RNAs,” *Molecular Cell*, vol. 43, no. 6, pp. 904–914, 2011.
- [5] M. J. Hangauer, I. W. Vaughn, and M. T. McManus, “Pervasive transcription of the human genome produces thousands of previously unidentified long intergenic noncoding RNAs,” *PLoS Genetics*, vol. 9, no. 6, article e1003569, 2013.
- [6] Y. Zhang, L. Sun, L. Xuan et al., “Reciprocal Changes of Circulating Long Non-Coding RNAs ZFAS1 and CDR1AS Predict Acute Myocardial Infarction,” *Scientific Reports*, vol. 6, no. 1, p. 22384, 2016.
- [7] Y. Yan, B. Zhang, N. Liu et al., “Circulating long noncoding RNA UCA1 as a novel biomarker of acute myocardial infarction,” *BioMed Research International*, vol. 2016, Article ID 8079372, 7 pages, 2016.
- [8] H. Liang, X. Su, Q. Wu et al., “LncRNA2810403D21Rik/Mirf promotes ischemic myocardial injury by regulating autophagy through targeting Mir26a,” *Autophagy*, vol. 16, no. 6, pp. 1077–1091, 2020.
- [9] Y. Zhang, L. Jiao, L. Sun et al., “LncRNAZFAS1as a SERCA2a inhibitor to cause intracellular Ca²⁺ overload and contractile dysfunction in a mouse model of myocardial infarction,” *Circulation Research*, vol. 122, no. 10, pp. 1354–1368, 2018.
- [10] J. Zangrando, L. Zhang, M. Vausort et al., “Identification of candidate long non-coding RNAs in response to myocardial infarction,” *BMC Genomics*, vol. 15, no. 1, p. 460, 2014.

- [11] W. M. Chen, M. D. Huang, D. P. Sun et al., "Long intergenic non-coding RNA 00152 promotes tumor cell cycle progression by binding to EZH2 and repressing p15 and p21 in gastric cancer," *Oncotarget*, vol. 7, no. 9, pp. 9773–9787, 2016.
- [12] B. Yue, D. Cai, C. Liu, C. Fang, and D. Yan, "Linc00152 functions as a competing endogenous RNA to confer oxaliplatin resistance and holds prognostic values in colon cancer," *Molecular Therapy*, vol. 24, no. 12, pp. 2064–2077, 2016.
- [13] S. Wang, W. Weng, T. Chen et al., "LINC00152 Promotes Tumor Progression and Predicts Poor Prognosis by Stabilizing BCL6 From Degradation in the Epithelial Ovarian Cancer," *Frontiers in Oncology*, vol. 10, article 555132, 2020.
- [14] Y. Yu, J. Yang, Q. Li, B. Xu, Y. Lian, and L. Miao, "LINC00152: a pivotal oncogenic long non-coding RNA in human cancers," *Cell Proliferation*, vol. 50, no. 4, article e12349, 2017.
- [15] X. Zheng, S. Dong, L. Sun, J. Xu, J. Liu, and R. Hao, "LncRNA LINC00152 Promotes Laryngeal Cancer Progression by Sponging MiR-613," *Open Medicine*, vol. 15, no. 1, pp. 240–248, 2020.
- [16] D. Liu, M. Gao, K. Wu, D. Zhu, Y. Yang, and S. Zhao, "LINC00152 facilitates tumorigenesis in esophageal squamous cell carcinoma via miR-153-3p/FYN axis," *Biomedicine & Pharmacotherapy*, vol. 112, article 108654, 2019.
- [17] K. Thygesen, J. S. Alpert, and H. D. White, "Universal definition of myocardial infarction," *Journal of the American College of Cardiology*, vol. 50, no. 22, pp. 2173–2195, 2007.
- [18] C. W. Yancy, M. Jessup, B. Bozkurt et al., "2013 ACCF/AHA guideline for the management of ST-elevation myocardial infarction: executive summary: a report of the American College of Cardiology Foundation/American Heart Association Task Force on Practice Guidelines," *Catheterization and Cardiovascular Interventions*, vol. 82, no. 1, pp. E1–E27, 2013.
- [19] N. A. Abbas, R. I. John, M. C. Webb et al., "Cardiac troponins and renal function in nondialysis patients with chronic kidney disease," *Clinical Chemistry*, vol. 51, no. 11, pp. 2059–2066, 2005.
- [20] J. Finsterer, C. Stollberger, and W. Krugluger, "Cardiac and noncardiac, particularly neuromuscular, disease with troponin-T positivity," *The Netherlands Journal of Medicine*, vol. 65, no. 8, pp. 289–295, 2007.
- [21] E. Giannitsis, M. Müller-Bardorff, S. Lehrke et al., "Admission troponin T level predicts clinical outcomes, TIMI flow, and myocardial tissue perfusion after primary percutaneous intervention for acute ST-segment elevation myocardial infarction," *Circulation*, vol. 104, no. 6, pp. 630–635, 2001.
- [22] X. Qu, X. Song, W. Yuan et al., "Expression signature of lncRNAs and their potential roles in cardiac fibrosis of post-infarct mice," *Bioscience Reports*, vol. 36, no. 3, article e00337, 2016.
- [23] K. Wang, F. Liu, L. Y. Zhou et al., "The long noncoding RNA CHRF regulates cardiac hypertrophy by targeting miR-489," *Circulation Research*, vol. 114, no. 9, pp. 1377–1388, 2014.
- [24] J. Ji, J. Tang, L. Deng et al., "LINC00152 promotes proliferation in hepatocellular carcinoma by targeting EpCAM via the mTOR signaling pathway," *Oncotarget*, vol. 6, no. 40, pp. 42813–42824, 2015.
- [25] Q. Cai, Z. Q. Wang, S. H. Wang et al., "Upregulation of long non-coding RNA LINC00152 by SP1 contributes to gallbladder cancer cell growth and tumor metastasis via PI3K/AKT pathway," *American Journal of Translational Research*, vol. 8, no. 10, pp. 4068–4081, 2016.
- [26] Y. Wu, C. Tan, W. W. Weng et al., "Long non-coding RNA Linc00152 is a positive prognostic factor for and demonstrates malignant biological behavior in clear cell renal cell carcinoma," *American Journal of Cancer Research*, vol. 6, no. 2, pp. 285–299, 2016.
- [27] Z. C. Hu, F. Shi, P. Liu et al., "TIEG1 Represses Smad7 -Mediated Activation of TGF- β 1/Smad Signaling in Keloid Pathogenesis," *The Journal of Investigative Dermatology*, vol. 137, no. 5, pp. 1051–1059, 2017.
- [28] Q. Nong, S. Li, Y. Wu, and D. Liu, "LncRNA COL1A2-AS1 inhibits the scar fibroblasts proliferation via regulating miR-21/Smad7 pathway," *Biochemical and Biophysical Research Communications*, vol. 495, no. 1, pp. 319–324, 2018.

Research Article

Tanshinone IIA Improves Ventricular Remodeling following Cardiac Infarction by Regulating miR-205-3p

Peng Qiao,¹ Jie Xu,² Xueni Liu,³ and Xuehan Li⁴ 

¹Department of Traditional Chinese Medicine, Yantai Hospital, Yantai, China

²Department of Medical Security Center, PLA Rocket Force Characteristic Medical Center, Beijing, China

³Critical Care Medicine, PLA Rocket Force Characteristic Medical Center, Beijing, China

⁴Department of Geriatrics, Liaocheng People's Hospital, Liaocheng, China

Correspondence should be addressed to Xuehan Li; lixuehan@cumt.edu.cn

Received 9 October 2021; Accepted 19 November 2021; Published 29 November 2021

Academic Editor: Simona Pichini

Copyright © 2021 Peng Qiao et al. This is an open access article distributed under the Creative Commons Attribution License, which permits unrestricted use, distribution, and reproduction in any medium, provided the original work is properly cited.

Objective. To illustrate the role of tanshinone IIA (TSN) in regulating cardiac structure and function following myocardial infarction (MI) and the involvement of miR-205-3p in TSN-induced antifibrosis effect on ventricular remodeling. **Patients and Methods.** One hundred MI patients were randomly assigned into two groups, and they were treated with TSN (TSN group, $n = 50$) or conventional therapy (control group, $n = 50$). Plasma levels of miR-205-3p and TGF- β 1 were detected in each patient. Echocardiography was conducted in each patient at post-MI 1 day, 2 weeks, and 4 weeks, respectively, for recording LVIDd (left ventricular internal-diastolic diameter), LVIDs (left ventricular internal-systolic diameter), and LVEF (left ventricular ejection fraction). The interaction between miR-205-3p and TGF- β 1 was examined by the RNA-Binding Protein Immunoprecipitation (RIP) assay. After induction of TGF- β 1 and/or 10 μ L of TSN in cardiac fibroblasts, relative levels of miR-205-3p, Col1a1, and Col3a1 were detected by quantitative real-time polymerase chain reaction (qRT-PCR). **Results.** Compared with the control group, miR-205-3p and TGF- β 1 were downregulated in plasma of MI patients in the TSN group. In the TSN group, LVIDd and LVIDs were reduced, and EF was enhanced at 2 weeks and 4 weeks compared with that at post-MI 1 day. miR-205-3p could negatively interact with TGF- β 1. TSN induction abolished the regulatory effects of TGF- β 1 on downregulating miR-205-3p and upregulating Col1a1 and Col3a1 in cardiac fibroblasts. **Conclusions.** Through upregulating miR-205-3p and downregulating TGF- β 1, TSN alleviates cardiac fibrosis and improves ventricular remodeling following MI.

1. Introduction

The treatment of acute myocardial infarction (AMI) has been well concerned owing to its high incidence and mortality [1]. Due to the development of thrombolysis and interventional technology, the mortality of MI has sharply decreased. However, ventricular remodeling at post-MI should be worried. The process of ventricular processing involves multiple factors, including hypertrophy and apoptosis in cardiomyocytes and extracellular matrix (ECM) changes. Eventually, cardiac fibrosis results in heart failure, which directly affects the prognosis and life quality [1].

Tanshinone IIA (TSN) is the main liposoluble active component of *Salvia miltiorrhiza* (a traditional Chinese medicine) extracted from the dried root and rhizome of *Sal-*

via miltiorrhiza Bunge [2]. TSN is able to protect the myocardium and inhibit cardiomyocyte hypertrophy from cardiac injury [3]. Moreover, it suppresses cardiac fibroblast proliferation and collagen synthesis, thus exerting a vascular protection effect against fibrosis, improving coronary circulation and inhibiting thrombosis [4]. TSN has been extensively applied in the clinical treatment of vascular diseases, and its promising application has been reported in treating coronary disease, hypertension, cardiac ischemia-reperfusion injury, and arrhythmia [5].

miRNAs are endogenous, noncoding RNAs with 21-23 nucleotides long. They induce posttranscriptional regulation on target genes by complementary base pairing in the 3'-UTR [6]. As early as 2005, miRNAs relevant to cardiac functions have been reported [7]. With the gradual explorations

on miRNA functions, people have realized that miRNAs are important in fibrotic diseases. It is reported that miR-29 participates in the development of cardiac fibrosis at post-MI *via* regulating cardiac fibroblast functions. miR-205 is located on chromosome 1q, which is abnormally expressed in many types of tumors and involved in regulating tumor cell behaviors [8, 9]. Downregulated miR-205 has been identified in breast cancer, prostate cancer, bladder cancer, and renal cancer samples [10–13]. miR-205 contains two subtypes from the same precursor, that is, miR-205-3p and miR-205-5p. miR-205-3p serves as a tumor suppressor in ovarian cancer, which is able to attenuate proliferative and migratory capacities of cancer cells [14]. The biological functions of miR-205-3p in MI and potential mechanism are rarely reported.

TGF- β is a family of cytokines with various functions. It regulates not only physiological processes, such as embryonic development, cell growth, and differentiation, but also pathological processes, such as inflammation, fibrosis, and carcinogenesis. TGF- β is a vital regulator in the development of tissue fibrosis [15]. This study mainly detected changes of fibrosis indicators following MI and the intervention effect of TSN. The potential involvement of miR-205-3p during TSN-induced improvement of ventricular remodeling was examined. Our results provide experimental references for clinical application of TSN in treating ventricular remodeling at post-MI.

2. Patients and Methods

2.1. Subjects. This study was approved by the Ethics Committee of Qingdao Central Hospital before the study started. Besides, signed written informed consent was obtained from all participants before the study. One hundred MI patients with primary acute ST elevation of the anterior wall who were treated by percutaneous coronary intervention (PCI) within 12 h of onset in Qingdao Central Hospital from May 2017 to May 2019 were recruited. Inclusion criteria were in accordance to 2013 ACCF/AHA guideline for the management of ST-elevation myocardial infarction [16] as follows: (1) sudden ischemic chest pain symptoms, not relieved by rest or sublingual nitroglycerin; (2) ECG showing ST elevation (≥ 0.2 mV) of at least two adjacent precordial leads or left bundle branch block; (3) increase in CKI level more than twice than the normal one and/or troponin (+); (4) onset of AMI within 12 h; and (5) anterior descending artery lesion confirmed by coronary angiography and TIMI 3 graded after vascular opening. Exclusion criteria were as follows: (1) severe hepatorenal insufficiency, (2) severe valvular heart disease, (3) previous history of coronary heart disease, (4) cardiogenic shock, (5) history of major surgery or severe trauma in the past 15 days, (6) symptoms of cardiac insufficiency prior to AMI, (7) acute or chronic infection, (8) administration of NSAIDs or steroids, (9) autoimmune diseases, and (10) malignant tumors.

2.2. Grouping and Therapeutic Strategies. Patients were randomly classified into the control group ($n = 50$) and TSN group ($n = 50$). Emergency PCI was conducted in each

patient, including medications of aspirin, clopidogrel, statins, ACEI or ARB, β -blockers, spironolactone tablets, and nitrates. In the TSN group, daily intravenous administration of 60–80 mg TSN for consecutive 14 days was additionally conducted.

2.3. Blood Collection. After overnight fasting, venous blood samples (3 mL \times 2) were collected in the morning at day 1 and week 2 after admission. Samples were stored in ethylenediaminetetraacetic acid- (EDTA-) K2 anticoagulant tubes, centrifuged at 3000 rpm for 15 min and 12000 rpm for another 10 min. Plasma samples were placed in cryopreservation tubes, labeled, and stored at -80°C .

2.4. Echocardiography. Echocardiography was performed by an experienced ultrasound physician using the color Doppler ultrasound (Philips HD-15, S5-2 probe). At post-MI 1 day, 2 weeks, and 4 weeks, LVIDd (left ventricular internal-diastolic diameter), LVIDs (left ventricular internal-systolic diameter), and LVEF (left ventricular ejection fraction) were recorded as the average from three replicates.

2.5. Isolation of Rat Primary Cardiac Fibroblasts and Cell Culture. Rat primary cardiac fibroblasts were isolated and cultured as previously described [17]. Briefly, hearts of neonatal rats within 24 h were collected and washed in phosphate-buffered saline (PBS) at 4°C and 75% ethanol. Hearts were cut into small pieces and digested in 0.1% collagenase and 0.125% trypsin in a water bath at 37°C . The mixture was gently shaken every 10 min. Digestive solution was mixed in Dulbecco's modified Eagle medium (DMEM) (Gibco, Rockville, MD, USA) containing 10% fetal bovine serum (FBS) (Gibco, Rockville, MD, USA) and cultured in a culture bottle. The adherent time difference between cardiomyocytes and myofibroblasts was 60 minutes. Primary cardiac fibroblasts were regularly passaged using 0.25% trypsin, and the third generation was used for the following experiments.

2.6. TGF- β 1 and/or TSN Induction. Cardiac fibroblasts were cultured in 6-well plates until 70–80% of confluence and then cultivated in serum-free DMEM for 24 h. TGF- β 1 and/or 10 μM TSN was applied per well for 24 h.

2.7. Cell Transfection. Cardiac fibroblasts were cultured in 6-well plates with 1×10^6 cells per well in serum-free DMEM for 24 h. Until cell confluence reached 80–85%, transfection was conducted using Lipofectamine 2000 (Invitrogen, Carlsbad, CA, USA). 3 μg miR-205-3p mimics or negative control and 6 μg Lipofectamine 2000 were, respectively, suspended in 250 μL of serum-free medium. After letting them stand at room temperature for 5 min, they were mixed and maintained for 20 min. The mixture was applied per well for 36–48 cell culture.

2.8. Quantitative Real-Time Polymerase Chain Reaction (qRT-PCR). Total RNAs were isolated from plasma or cells using the RNA extraction kit (ABI, Applied Biosystems, Foster City, CA, USA). The concentration and purity of RNA

were determined using an ultraviolet spectrophotometer (Thermo Fisher Scientific, Waltham, MA, USA). After reverse transcription, complementary deoxyribose nucleic acids (cDNAs) were amplified at 92°C for 2 min, followed by 35 cycles at 95°C for 20s, 60°C for 40s, and 72°C for 2 min. Relative mRNA level was calculated by $2^{-\Delta\Delta Ct}$. Primer sequences were as follows: miR-205-3p: 5'-CGG GAT TTC AGT GGA GTG AAG TTC-3'; TGF- β 1: 5'-GCG CCT GCA GAG ATT CAA GTC AAC-3' (forward) and 5'-GTA TCA GTG GGG GTC AGC AGC C-3' (reverse); Col1a1: 5'-TTC ACC TAC AGC ACG CTT GT-3' (forward) and 5'-TTG GGA TGG AGG GAG TTT AC-3' (reverse); Col3a1: 5'-TTG AAT ATC AAA CCG CAA GGC-3' (forward) and 5'-GGT CAC TTT CAC TGG TTG ACG A-3' (reverse); and U6: 5'-CTC GCT TCG GCA GCA CA-3' (forward) and 5'-AAC GCT TCA CGA ATT TGC GT-3' (reverse).

2.9. RNA-Binding Protein Immunoprecipitation (RIP). The Magna RIP Kit (Millipore, Billerica, MA, USA) was used. Cells were lysed in RIPA and incubated with magnetic beads conjugated with anti-TGF- β 1 or anti-IgG at 4°C for 6 h. Subsequently, magnetic beads were washed and incubated with Proteinase K for clearing proteins. Purified RNAs were subjected to qRT-PCR.

2.10. Statistical Analysis. Statistical analyses were conducted using Statistical Product and Service Solutions (SPSS) 20.0 (IBM, Armonk, NY, USA). Measurement data between groups were compared using Student's *t*-test, while enumeration data were compared by the chi-square test. One-way ANOVA tests followed by the post hoc test (least significant difference) were employed for multigroup comparison. $p < 0.05$ was considered statistically significant.

3. Results

3.1. Baseline Characteristics between the Control and TSN Groups. We recruited 100 MI patients and randomly classified them into the control group ($n = 50$) and TSN group ($n = 50$). Their baseline characteristics were collected for comparison. It is shown that no significant differences in age, gender, hypertension, diabetes, smoking, LDL-C, HDL-C, and vascular opening time were found between groups ($p > 0.05$) (Table 1), suggesting that baseline characteristics were comparable.

3.2. Echocardiography Findings between the Control and TSN Groups. Echocardiography was conducted at post-MI 1 day, 2 weeks, and 4 weeks, respectively. On the first day following MI, no significant differences in LVIDd, LVIDs, and EF were found between the control and TSN groups ($p > 0.05$). These indicators were improved at post-MI 2 and 4 weeks in both groups, which were much more pronounced in the TSN group (Table 2). It is indicated that TSN treatment displayed a pronounced efficacy on improving cardiac structure and functions following MI.

TABLE 1: Baseline characteristics of myocardial infarction patients in the control group and TSN group.

Variable	Control group ($n = 50$)	TSN group ($n = 50$)	t/χ^2	p
Age	49.8 ± 5.9	48.2 ± 5.2	1.439	0.153
Sex (male/female)	37/13	34/16	0.437	0.66
TC (mmol/L)	5.66 ± 1.28	5.49 ± 1.13	0.704	0.483
LDL-C (mmol/L)	3.28 ± 0.95	3.37 ± 0.97	0.469	0.64
HDL-C (mmol/L)	1.08 ± 0.22	1.15 ± 0.24	1.52	0.132
Hypertension ($n, \%$)	17	20	0.386	0.679
Diabetes ($n, \%$)	11	8	0.585	0.611
Smoking ($n, \%$)	20	23	0.367	0.686
Vascular opening time (h)	6.92 ± 1.26	7.17 ± 1.33	0.965	0.337

TSN: tanshinone IIA; TC: total cholesterol; LDL-C: low-density lipoprotein cholesterol; HDL-C: high-density lipoprotein cholesterol.

3.3. Intervention of TSN on Plasma Levels of miR-205-3p and TGF- β 1 in MI Patients. We did not find significant differences in plasma level of miR-205-3p before treatment between groups. After two-week treatment, miR-205-3p was markedly downregulated in both groups, especially the TSN group (Figure 1(a)). Similarly, TGF- β 1 was downregulated two weeks later after treatment in the control group, which is much more pronounced in the TSN group (Figure 1(b)). It is indicated that TSN could intervene plasma levels of miR-205-3p and TGF- β 1 in MI patients.

3.4. Interaction between miR-205-3p and TGF- β 1. The RIP assay revealed that miR-205-3p was mainly enriched in anti-TGF- β 1, proving the interaction between miR-205-3p and TGF- β 1 (Figure 2(a)). Subsequently, we tested the transfection efficacy of miR-205-3p mimics in cardiac fibroblasts (Figure 2(b)). Overexpression of miR-205-3p remarkably downregulated TGF- β 1, showing a negative interaction (Figure 2(c)).

3.5. TSN Inhibited TGF- β 1-Induced Cardiac Fibroblast Fibrosis by Upregulating miR-205-3p. To explore the protective role of TSN in MI, cardiac fibroblasts were induced with TGF- β 1 and/or 10 μ L TSN. TGF- β 1 induction markedly downregulated miR-205-3p in cardiac fibroblasts, which was reversed by TSN treatment (Figure 3(a)). Moreover, Col1a1 and Col3a1 were upregulated in TGF- β 1-induced cardiac fibroblasts, and their levels were reduced by TSN treatment (Figures 3(b), 3(c)). It is demonstrated that miR-205-3p exerted a vital function during the TSN-induced antifibrotic process by mediating the TGF- β signaling.

4. Discussion

At post-MI, ventricular remodeling results in changes of ventricular volume, ventricular shape, wall thickness, and compliance. The decline in cardiac function directly influences the prognosis in MI patients [18]. At present, drugs such as ACEI, ARB, and β -blockers are used for the treatment of AMI. They are conducive to inhibiting the process

TABLE 2: Echocardiography findings in the control and TSN groups.

Variable	Control group ($n = 50$)			TSN group ($n = 50$)		
	1 d	2 w	4 w	1 d	2 w	4 w
LVIDd	51.52 ± 5.51	50.35 ± 4.98	50.27 ± 5.07	51.63 ± 6.08	$47.52 \pm 5.85^{*\&}$	$47.66 \pm 3.74^{*\&}$
LVIDs	34.82 ± 4.21	32.82 ± 4.67	32.94 ± 4.55	34.95 ± 4.38	$29.85 \pm 3.17^{*\&}$	$29.06 \pm 2.97^{*\&}$
EF (%)	42.33 ± 4.07	45.12 ± 5.51	$45.97 \pm 5.58^*$	41.82 ± 4.13	$48.72 \pm 4.82^{*\&}$	$49.57 \pm 5.03^{*\&}$

* $p < 0.05$, comparison between 1 d and 2 w; # $p < 0.05$, comparison between 1 d and 4 w; & $p < 0.05$, comparison between the control group and TSN group.

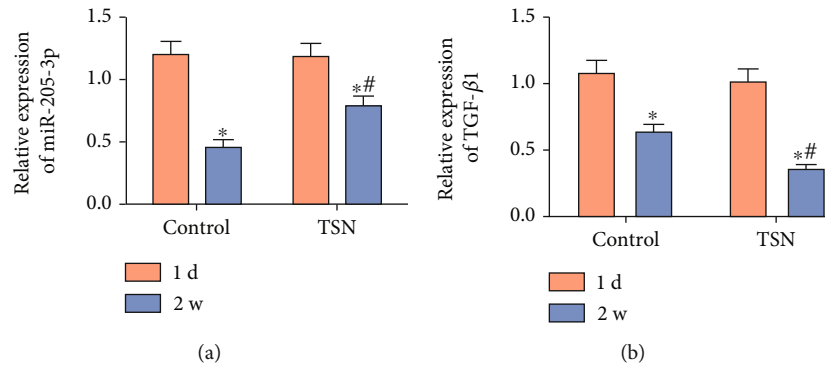


FIGURE 1: Intervention of TSN on plasma levels of miR-205-3p and TGF- β 1 in MI patients. One hundred MI patients were randomly classified into the control group ($n = 50$) and TSN group ($n = 50$). Plasma levels of miR-205-3p (a) and TGF- β 1 (b) were detected by qRT-PCR at post-MI 1 day and 2 weeks, respectively, in both groups.

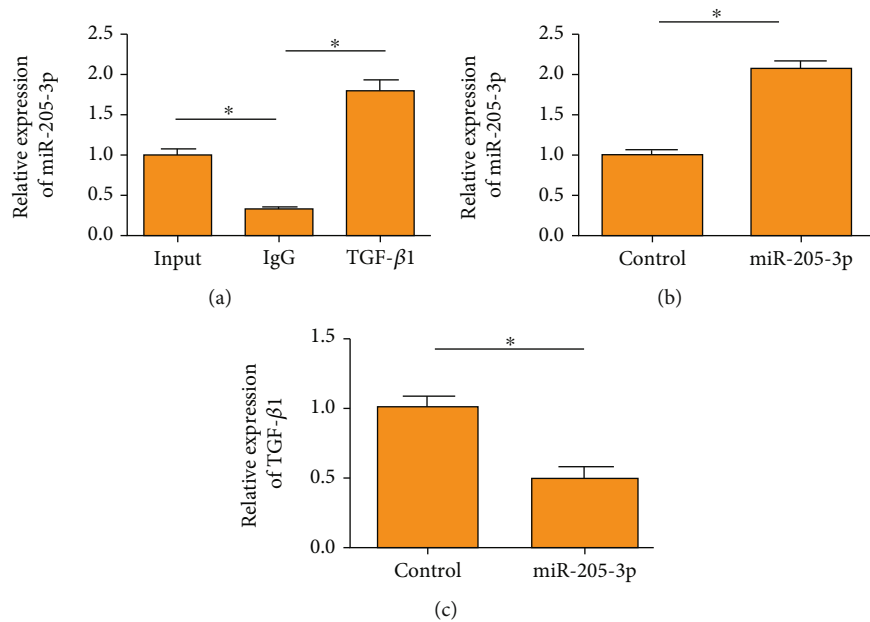


FIGURE 2: Interaction between miR-205-3p and TGF- β 1: (a) RIP assay showed the interaction between miR-205-3p and TGF- β 1; (b) transfection efficacy of miR-205-3p mimics in cardiac fibroblasts; (c) TGF- β 1 level in cardiac fibroblasts overexpressing miR-205-3p.

of myocardial fibrosis, improving ventricular remodeling, and facilitating the long-term prognosis of MI [19, 20]. However, to date, effective strategies for preventing ventricular remodeling at post-MI are lacking [21].

TSN is a fat-soluble active ingredient with clear molecular structure and molecular weight extracted from Chinese

traditional medicine *Salvia miltiorrhiza* [21]. Ouyang et al. [4] suggested that TSN inhibits RAAS overrelease in the heart, thus decreasing the synthesis and release of collagens by cardiac fibroblasts to prevent cardiac fibrosis. Our results uncovered that 2-week or 4-week TSN treatment markedly improved cardiac functions in MI patients compared with

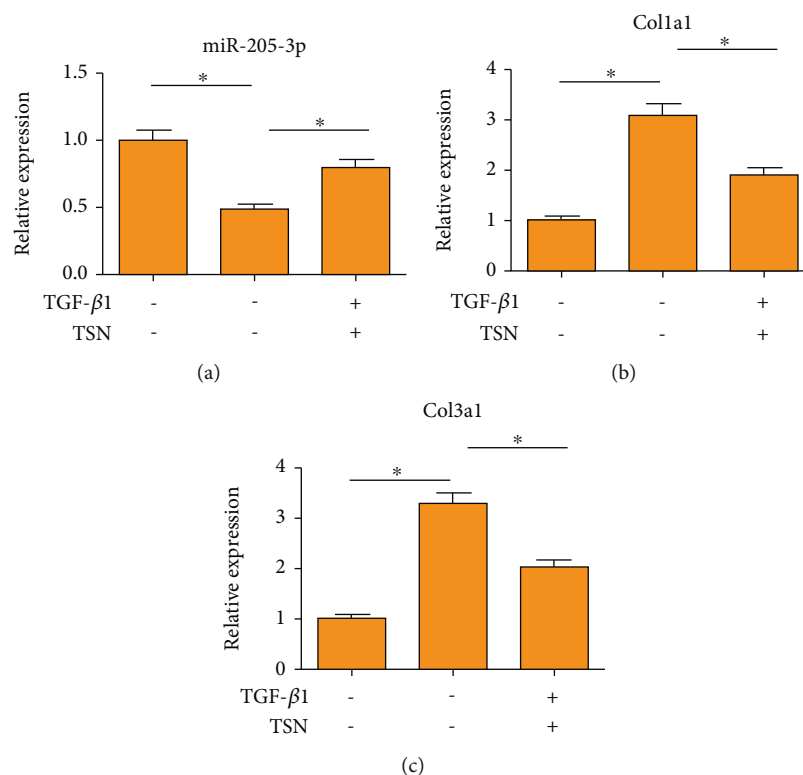


FIGURE 3: TSN inhibited TGF- β 1-induced cardiac fibroblast fibrosis by upregulating miR-205-3p. Cardiac fibroblasts were induced with TGF- β 1 and/or 10 μ L TSN. Relative levels of miR-205-3p (a), Col1a1 (b), and Col3a1 (c) were detected by qRT-PCR.

echocardiography findings on the first day of admission. It is suggested that TSN can prevent ventricular dilation and contractility decline at post-MI, displaying certain significance in improving ventricular remodeling.

TGF- β 1 exerts a key regulation in ECM metabolism [22]. It is recognized as the most important factor of fibrosis, which induces fibroblast proliferation and ECM accumulation through autocrine and paracrine [23]. Type I and III collagens are well studied. Type I collagen is featured by high tensile strength and poor stretch and retraction, which determines the rigidity of myocardial contraction and relaxation. Type III collagen has a good elasticity [24]. It is reported that increases in Col1a1 and Col3a1 lead to decreases in cardiac compliance, as well as systolic and diastolic functions [25, 26]. Accumulating evidences have highlighted the vital functions of miRNAs in ventricular remodeling at post-MI [27, 28]. In addition, the interaction between TGF- β and miRNAs is able to influence disease progression. Luna et al. [29] demonstrated that the negative interaction between TGF- β 2 and miR-29b is responsible for regulating biological functions of trabecular cells of glaucoma. Qin et al. [30] suggested that miR-29b induces renal fibrosis progression through inactivating the TGF- β /Smad3 signaling.

Our results uncovered that both plasma levels of miR-205-3p and TGF- β 1 were downregulated in MI patients. Furthermore, we have confirmed the negative interaction between miR-205-3p and TGF- β 1. The upregulated Col1a1 and Col3a1 in cardiac fibroblasts induced by TGF- β 1 were reversed by TSN treatment. To sum up, TSN upregulated

miR-205-3p and thus inhibited TGF- β 1 level, thereby improving cardiac function and alleviating cardiac fibrosis at post-MI. In this research, we uncover that TSN could improve ventricular remodeling in an in vivo and in vitro assay; however, the mechanism should be explored much more to perfect this hypothesis.

5. Conclusions

Through upregulating miR-205-3p and downregulating TGF- β 1, TSN alleviates cardiac fibrosis and improves ventricular remodeling following MI.

Data Availability

The datasets used and analyzed during the current study are available from the corresponding author on reasonable request.

Conflicts of Interest

The authors declared no conflict of interest.

References

- [1] Y. Ma, G. V. Halade, and M. L. Lindsey, "Extracellular matrix and fibroblast communication following myocardial infarction," *Journal of Cardiovascular Translational Research*, vol. 5, no. 6, pp. 848–857, 2012.

- [2] S. Gao, Z. Liu, H. Li, P. J. Little, P. Liu, and S. Xu, "Cardiovascular actions and therapeutic potential of tanshinone IIA," *Atherosclerosis*, vol. 220, no. 1, pp. 3–10, 2012.
- [3] J. Diez, B. Lopez, A. Gonzalez, and R. Querejeta, "Clinical aspects of hypertensive myocardial fibrosis," *Current Opinion in Cardiology*, vol. 16, no. 6, pp. 328–335, 2001.
- [4] X. Ouyang, K. Takahashi, K. Komatsu et al., "Protective Effect of *Salvia miltiorrhiza* on Angiotensin II-Induced Hypertrophic Responses in Neonatal Rat Cardiac Cells," *Japanese Journal of Pharmacology*, vol. 87, no. 4, pp. 289–296, 2001.
- [5] H. Shan, X. Li, Z. Pan et al., "Tanshinone IIA protects against sudden cardiac death induced by lethal arrhythmias via repression of microRNA-1," *British Journal of Pharmacology*, vol. 158, no. 5, pp. 1227–1235, 2009.
- [6] E. van Rooij, "The art of microRNA research," *Circulation Research*, vol. 108, no. 2, pp. 219–234, 2011.
- [7] Y. Zhao, E. Samal, and D. Srivastava, "Serum response factor regulates a muscle-specific microRNA that targets *Hand2* during cardiogenesis," *Nature*, vol. 436, no. 7048, pp. 214–220, 2005.
- [8] E. van Rooij, L. B. Sutherland, J. E. Thatcher et al., "Dysregulation of microRNAs after myocardial infarction reveals a role of miR-29 in cardiac fibrosis," *Proceedings of the National Academy of Sciences of the United States of America*, vol. 105, no. 35, pp. 13027–13032, 2008.
- [9] A. Y. Qin, X. W. Zhang, L. Liu et al., "miR-205 in cancer: an angel or a devil?," *European Journal of Cell Biology*, vol. 92, no. 2, pp. 54–60, 2013.
- [10] B. Guan, Q. Li, L. Shen et al., "MicroRNA-205 directly targets Krüppel-like factor 12 and is involved in invasion and apoptosis in basal-like breast carcinoma," *International Journal of Oncology*, vol. 49, no. 2, pp. 720–734, 2016.
- [11] T. Hulf, T. Sibbritt, E. D. Wiklund et al., "Epigenetic-induced repression of microRNA-205 is associated with MED1 activation and a poorer prognosis in localized prostate cancer," *Oncogene*, vol. 32, no. 23, pp. 2891–2899, 2013.
- [12] G. Wang, E. S. Chan, B. C. Kwan et al., "Expression of microRNAs in the urine of patients with bladder cancer," *Clinical Genitourinary Cancer*, vol. 10, no. 2, pp. 106–113, 2012.
- [13] X. W. Xu, S. Li, F. Yin, and L. L. Qin, "Expression of miR-205 in renal cell carcinoma and its association with clinicopathological features and prognosis," *European Review for Medical and Pharmacological Sciences*, vol. 22, no. 3, pp. 662–670, 2018.
- [14] B. Qiao, Q. Wang, Y. Zhao, and J. Wu, "miR-205-3p functions as a tumor suppressor in ovarian carcinoma," *Reproductive Sciences*, vol. 27, no. 1, pp. 380–388, 2020.
- [15] P. Stawowy, c. Margeta, h. Kallisch et al., "Regulation of matrix metalloproteinase MT1-MMP/MMP-2 in cardiac fibroblasts by TGF-beta1 involves furin-convertase," *Cardiovascular Research*, vol. 63, no. 1, pp. 87–97, 2004.
- [16] C. W. Yancy, M. Jessup, B. Bozkurt et al., "2013 ACCF/AHA guideline for the management of ST-elevation myocardial infarction: executive summary: a report of the American College of Cardiology Foundation/American Heart Association Task Force on Practice Guidelines: developed in collaboration with the American College of Emergency Physicians and Society for Cardiovascular Angiography and Interventions," *Catheterization and Cardiovascular Interventions*, vol. 82, no. 1, pp. e147–e239, 2013.
- [17] X. Zhao, K. Wang, Y. Liao et al., "MicroRNA-101a inhibits cardiac fibrosis induced by hypoxia via targeting TGFβRI on cardiac fibroblasts," *Cellular Physiology and Biochemistry*, vol. 35, no. 1, pp. 213–226, 2015.
- [18] S. R. Tiyyagura and S. P. Pinney, "Left ventricular remodeling after myocardial infarction: past, present, and future," *Mount Sinai Journal of Medicine*, vol. 73, no. 6, pp. 840–851, 2006.
- [19] H. Okada, G. Takemura, K. Kosai et al., "Postinfarction gene therapy against transforming growth factor-beta signal modulates infarct tissue dynamics and attenuates left ventricular remodeling and heart failure," *Circulation*, vol. 111, no. 19, pp. 2430–2437, 2005.
- [20] S. D. Solomon, H. Skali, N. S. Anavekar et al., "Changes in ventricular size and function in patients treated with valsartan, captopril, or both after myocardial infarction," *Circulation*, vol. 111, no. 25, pp. 3411–3419, 2005.
- [21] M. Ikeuchi, H. Tsutsui, T. Shiomi et al., "Inhibition of TGF-beta signaling exacerbates early cardiac dysfunction but prevents late remodeling after infarction," *Cardiovascular Research*, vol. 64, no. 3, pp. 526–535, 2004.
- [22] A. Leask, "TGFbeta, cardiac fibroblasts, and the fibrotic response," *Cardiovascular Research*, vol. 74, no. 2, pp. 207–212, 2007.
- [23] P. J. Lijnen, V. V. Petrov, and R. H. Fagard, "Induction of Cardiac Fibrosis by Transforming Growth Factor-β₁," *Molecular Genetics and Metabolism*, vol. 71, no. 1-2, pp. 418–435, 2000.
- [24] E. C. Miner and W. L. Miller, "A look between the cardiomyocytes: the extracellular matrix in heart failure," *Mayo Clinic Proceedings*, vol. 81, no. 1, pp. 71–76, 2006.
- [25] K. E. Porter and N. A. Turner, "Cardiac fibroblasts: at the heart of myocardial remodeling," *Pharmacology & Therapeutics*, vol. 123, no. 2, pp. 255–278, 2009.
- [26] J. I. Virag and C. E. Murry, "Myofibroblast and endothelial cell proliferation during murine myocardial infarct repair," *The American Journal of Pathology*, vol. 163, no. 6, pp. 2433–2440, 2003.
- [27] H. Liang, C. Zhang, T. Ban et al., "A novel reciprocal loop between microRNA-21 and TGFβRIII is involved in cardiac fibrosis," *The International Journal of Biochemistry & Cell Biology*, vol. 44, no. 12, pp. 2152–2160, 2012.
- [28] J. Wang, W. Huang, R. Xu et al., "MicroRNA-24 regulates cardiac fibrosis after myocardial infarction," *Journal of Cellular and Molecular Medicine*, vol. 16, no. 9, pp. 2150–2160, 2012.
- [29] C. Luna, G. Li, J. Qiu, D. L. Epstein, and P. Gonzalez, "Cross-talk between miR-29 and transforming growth factor-betas in trabecular meshwork cells," *Investigative Ophthalmology & Visual Science*, vol. 52, no. 6, pp. 3567–3572, 2011.
- [30] W. Qin, A. C. Chung, X. R. Huang et al., "TGF-β/Smad3 signaling promotes renal fibrosis by inhibiting miR-29," *Journal of the American Society of Nephrology*, vol. 22, no. 8, pp. 1462–1474, 2011.

Research Article

N-Acetylcysteine Slows Down Cardiac Pathological Remodeling by Inhibiting Cardiac Fibroblast Proliferation and Collagen Synthesis

Jin Zhou, Jing Xu, Shan Sun, Mengyuan Guo, Peng Li, and Aijuan Cheng 

Department of Cardiology, Tianjin Chest Hospital, Tianjin, China

Correspondence should be addressed to Aijuan Cheng; chengaijuan@nankai.edu.cn

Received 20 October 2021; Accepted 12 November 2021; Published 26 November 2021

Academic Editor: Francesco Busardò

Copyright © 2021 Jin Zhou et al. This is an open access article distributed under the Creative Commons Attribution License, which permits unrestricted use, distribution, and reproduction in any medium, provided the original work is properly cited.

Objective. By observing the effect of N-acetylcysteine (NAC) on the proliferation and collagen synthesis of rat cardiac fibroblasts (CFs) to explore the effect of NAC on cardiac remodeling (CR). **Methods.** *In vivo*, first, the Sprague Dawley (SD) rat myocardial hypertrophy model was constructed, and the effect of NAC on cardiac structure and function was detected by echocardiography, serological testing, and Masson staining. Western blotting (WB) and quantitative real-time polymerase chain reaction (qRT-PCR) were used to detect the expression level of antioxidant enzymes, and flow cytometry was used to detect the intracellular reactive oxygen species (ROS) content. *In vitro*, 3-(4,5-dimethylthiazol-2-yl)-2,5-diphenyl tetrazolium bromide (MTT) assay and 5-ethynyl-2'-deoxyuridine (EdU) staining were used to detect cell proliferation, and the expression level of the NF- κ B signaling pathway was detected. **Results.** Compared with the control group, the model group had disordered cardiac structure, reduced cardiac function, and obvious oxidative stress (OS) response. However, after NAC treatment, it could obviously improve the rat cardiac structure and cardiac function and alleviate redox imbalance and cardiology remodeling. At the same time, NAC can inhibit the activation of the NF- κ B signaling pathway and reduce the proliferation level of CFs and the amount of ^3H proline incorporated. **Conclusions.** NAC can inhibit AngII-induced CF proliferation and collagen synthesis through the NF- κ B signaling pathway, alleviate the OS response of myocardial tissue, inhibit the fibrosis of myocardial tissue, and thus slow down the pathological remodeling of the heart.

1. Introduction

Heart failure (HF) is the terminal stage of various heart diseases, and CR is the key pathological link of HF, which is based on myocardial hypertrophy (MH) and myocardial fibrosis (MF) [1]. In the early stage of the disease, MH is an adaptive structural change of the heart in order to maintain sufficient output function in the case of increased post-load or volume load caused by diseases such as hypertension. During the compensatory phase of the heart, physiological changes also include an increase in the volume of myocardial cells, an increase in the weight of the heart and left ventricle, and an increase in the interventricular septum and the thickness of the left ventricular wall. However, when the heart is under a high-load environment for a long time,

MH will eventually lead to a decline in ventricular function or even HF [2]. The transition from compensatory MH to decompensation or HF is a very complicated pathophysiological process. One of its main characteristics involves fibrous tissue hyperplasia, which is the occurrence of MF. In the process of pathological MH, MF will eventually lead to the attenuation of myocardial functional tissue function, ventricular expansion, or tissue sclerosis [3]. Therefore, some studies have pointed out that inhibiting MF is a promising therapeutic direction to prevent the heart from changing from compensatory MH to decompensation or HF. In addition, under various pathological conditions, the heart undergoes remodeling characterized by MF, and CR is one of the pathophysiological foundations of HF. CFs are the main effector cells of MF, and their proliferation and

collagen synthesis are important features of MF [4]. Therefore, inhibiting CF proliferation and collagen production is of great value in reversing CR.

NAC is an acetyl compound of L-cysteine, and its molecular structure contains active sulfhydryl groups. It is a strong antioxidant, which interferes with the generation of free radicals, scavenges the generated free radicals, and regulates the metabolic activity of cells [5]. In addition, NAC can also regulate gene expression and signal transduction systems, exert antiangiogenesis, inhibit the development of malignant tumors, and inhibit the generation and metastasis of new organisms, and NAC is widely used in clinical practice of respiratory and nervous systems and AIDS [6, 7]. Recently, the role of NAC in the cardiovascular system has also received wide attention from research evidence. It has been found that NAC can effectively inhibit myocardial cell apoptosis caused by ischemia-reperfusion injury (IRI) and improve cardiac function [8]. In addition, some studies have shown that NAC can play an antifibrotic role in the lungs [9], but there are few studies on the effect of NAC on cardiac fibrosis. Therefore, this study explored the effect of NAC on CFs in rats to explore their effects on CR.

The nuclear transcription factor is a type of protein that has the function of binding to a fixed nucleotide sequence in certain promoter regions to initiate gene transcription. NF- κ B is one of its important proteins, which can be found in a variety of cells, such as vascular endothelial cells, CFs, and cardiomyocytes, and is involved in the gene regulation of a variety of physiological and pathological processes such as inflammation, immunity, and cell proliferation and apoptosis [10–12]. In general, NF- κ B binds to its endogenous inhibitory protein (I κ B) in the homologous or heterodimer form to form a trimer, which exists in the cytoplasm and is inactivated. Once the I κ B is phosphorylated and dissociated from the NF- κ B/I κ B complex, the dimer and the inhibitory protein are dissociated and transferred to the nucleus, where they bind to κ B sites on DNA and participate in the transcription of multiple genes [13]. At present, a large number of studies have confirmed that the NF- κ B pathway is associated with cardiovascular disease. Therefore, we speculate that NAC may slow down MF, and MH may be regulated by the NF- κ B signaling pathway.

2. Materials and Methods

2.1. Laboratory Animal. Thirty clean four-month-old male rats, weighing 220–250 g, provided by Tianjin Chest Hospital Animal Center, were housed in cages, with room temperature 18–22°C, relative humidity 45–65%, and light and dark alternating for 12 hours. After 7 days of adaptive feeding, the rats were randomly divided into 3 groups. This study was approved by the Animal Ethics Committee of Tianjin Chest Hospital Animal Center.

2.2. Animal Model Construction. After the rats were anesthetized with 10% pentobarbital sodium, they were fixed in the supine position on the small animal thermostatic pad on the operating table, and their fur was sheared, and their skins were prepared. Next, we performed endotracheal intubation

(Zena, Shanghai, China) and mechanical ventilation by blind vision. Then, the skin of the rats' chest was cut, the thoracic tissue and aorta were separated, and the aortic arch was ligated by the insertion needle with 0.5 nonabsorbent suture (Zena, Shanghai, China) between the first and second branches. After taking out the pad and inserting the needle, we closed the chest cavity. The endotracheal intubation was removed when the rats fully resumed spontaneous breathing. Meanwhile, the sham group has only been performed thoracotomy, and the aorta was not ligated.

2.3. Experimental Animal Grouping. Experimental animals were divided into 3 groups: sham operation group (control group; $n = 15$; the rats underwent sham operation, and one week after the operation, they were intraperitoneally injected with normal saline (0.1 mL/100 g)); model group ($n = 15$; one week after aortic constriction, the rats were intraperitoneally injected with normal saline (0.1 mL/100 g)); and NAC treatment group ($n = 15$; one week after aortic constriction, rats were intraperitoneally injected with NAC (Tianpu, Guangzhou, China) (10 mg/kg/d), diluted with normal saline, and continuously administered for 2 weeks).

2.4. Echocardiography. Three weeks after the operation, MyLab30CV with a 10 MHz linear ultrasound transducer (Philips, Eindhoven, Netherlands) was used to complete the echocardiogram. The left ventricular diameter was measured on the parasternal long axis and short axis with a 50 Hz frame rate. The left ventricular end-diastolic diameter (LVEDd), left ventricular end-systolic diameter (LVESd), left ventricular ejection fraction (LVEF%), and left ventricular short-axis fractional shortening rate (LVFS%) were used to assess cardiac function.

2.5. Retention of Heart Tissue. The rats were anesthetized with intraperitoneal injection of 10% pentobarbital sodium 3 mL/kg. Then, the chest was opened along the midline incision to fully expose the heart, and blood was drawn at the root of the aorta and saved. The left ventricle was cut and weighed. Then, it was put in the refrigerator at -80°C. At the same time, the tibia of the rat was isolated and its length was measured.

2.6. Intracellular ROS Detection. The rat heart was immediately removed and placed in 1 mL of ice phosphate-buffered saline (PBS) liquid and shredded. Then, the cells were filtered with a 200–400 mesh screen, then centrifuged at 4°C, 1500 r/min for 5 minutes, and the supernatant was discarded. A cold PBS solution was added to prepare a single cell suspension, and the cell concentration was adjusted to 1×10^6 – 1.1×10^6 cells/mL. Then, 5 μ L 2',7'-dichlorofluorescein yellow diacetate (DCFH-DA, Thermo Fisher Scientific, Waltham, MA, USA) was added and mixed well, then placed in a 37°C incubator in the dark for 30 minutes. It was centrifuged again, and the supernatant was discarded; 10% fetal bovine serum (FBS, Life Technology, Wuhan, China) was added, and the mixture was incubated at 37°C for 20 minutes. Finally, it was centrifuged at 1500 r/min for 5 minutes, and a single cell suspension of heart tissue was made. The cell suspension was sent to flow cytometry within 1 hour to

detect the average fluorescence intensity of intracellular labeled fluorescent probes (Elabscience, Wuhan, China).

2.7. Masson Staining. The embedded heart tissue was cut into continuous 3-5 μm thick slices with a microtome (Camilo Biological, Nanjing, China), and then the slides were dried in an oven at 55°C for 30 minutes. Slides were first dewaxed with xylene and then placed in gradient alcohol (100%~70%) for hydration. Then, the Masson kit (Walvax, Kunming, China) was used for dyeing. After the slides were dehydrated by gradient alcohol and xylene, the neutral resin was added dropwise and the coverslips were sealed. After the slides have dried, we observed and took pictures under the microscope (Elabscience, Wuhan, China).

2.8. Serological Test. Three weeks after the operation, 3 mL of right atrial blood was collected, centrifuged at 12,500 r/min for 10 minutes at low temperature to separate serum, and stored in a refrigerator at -80°C. According to the instructions provided by the reagent supplier (Jian Cheng, Nanjing, China), the glutathione (GSH), glutathione peroxidase (GPX), superoxide dismutase (SOD), lactic dehydrogenase (LDH) activity, and malondialdehyde (MDA) content in the serum of each group were separately detected.

2.9. Cell Extraction and Cell Culture. The heart of newborn SD rats was taken under sterile conditions, cut to about 1 mm³ small pieces, added with 1 g/L type II collagenase (Jian Cheng, Nanjing, China), stirred at 37°C with a constant temperature magnetic stirrer, and assisted in the separation of cells. After 5 minutes, the cells were collected, the digestion fluid was centrifuged at 1000 r/min for 5 minutes, and the pelleted cells were resuspended and filtered. The cells were cultured in a thermostatic 5% CO₂ incubator at 37°C for 60 minutes using the differential attachment method. The supernatant was discarded, and the remaining cells were fibroblasts. Then, Dulbecco's Modified Eagle's Medium (DMEM, Life Technology, Wuhan, China) containing 10% FBS was added to continue the culture, and the medium was changed every 2-3 days. According to literature reports, 1 $\mu\text{mol/L}$ AngII (Tianpu, Guangzhou, China) was used to treat the second- to fourth-generation CFs for corresponding research.

2.10. MTT (3-(4,5-Dimethylthiazol-2-yl)-2,5-diphenyl Tetrazolium Bromide) Assay. CF cells in the logarithmic growth stage were seeded in 96-well plates with a density of $1 \times 10^5/\text{mL}$. And cells were incubated in an incubator of 5% CO₂ at 37°C. The cells were treated with 1 $\mu\text{mol/L}$ AngII for 24 hours and incubated at 37°C. After 24 hours, NAC was added to make the final concentration of NAC in each well 0, 10, 20, and 40 mmol/L, and the culture was continued to 48 hours. MTT (Yifei Xue, Nanjing, China) 20 mL of 5 mg/mL was added to each well. After the culture was continued for 4 hours, the culture medium was discarded, 150 μL dimethyl sulfoxide (DMSO) was added to each well, and the plate shaker was shaken for 10 minutes. The absorbance was measured at 490 nm with an enzyme-linked immunoassay (Kaiji, Nanjing, China).

2.11. ³H Proline Admixture Method. The cells were cultured in a 96-well plate for 48 hours according to the above treatment, and ³H proline of 1×10^3 Bq (Jian Cheng, Nanjing, China) and 50 mg/L ascorbic acid were added to each well, and the cells were further incubated for 4 hours. The number of living cells was examined by trypan blue staining. After the trypsin digested the cells into a cell suspension, the cells were collected by a cell collector onto a fiberglass filter paper. The fiberglass filter paper was placed in a scintillation counter tube, and each tube was filled with 0.5 mL of scintillation liquid. Then, we determined the radioactive intensity with a liquid scintillation counter (Jian Cheng, Nanjing, China), and the data obtained was expressed in cpm/well.

2.12. Western Blotting. Radioimmunoprecipitation assay (RIPA) protein lysate (Camilo Biological, Nanjing, China) was used to extract the cardiac tissue and CF total protein on ice, and the protein concentration of each group was detected and leveled by the bicinchoninic acid (BCA) method (Camilo Biological, Nanjing, China). Equal amounts of protein from each group were separated by sodium dodecyl sulfate-polyacrylamide gel electrophoresis (SDS-PAGE) and then transferred to the polyvinylidene difluoride (PVDF, Ye Sen, Shanghai, China) membrane. Then, the PVDF membrane was blocked with 5% skim milk at room temperature for 2 hours, and the primary antibody (GPX1, Abcam, Cambridge, MA, USA, 1:2000; GPX3, Abcam, Cambridge, MA, USA, 1:2000; NF- κ B, Abcam, Cambridge, MA, USA, 1:2000; I κ K- α , Abcam, Cambridge, MA, USA, 1:1000; I κ B- α , Abcam, Cambridge, MA, USA, 1:2000; Collagen I, Abcam, Cambridge, MA, USA, 1:2000; and GAPDH, Abcam, Cambridge, MA, USA, 1:5000) was added and incubated at 4°C overnight. The next day, after washing the PVDF membrane with PBS, the corresponding secondary antibody (Abcam, Cambridge, MA, USA, 1:1000) was added. After being incubated at room temperature for 2 hours, enhanced chemiluminescence (ECL, Yifei Xue, Nanjing, China) was added dropwise to expose in the gel imaging system.

2.13. RNA Isolation and Quantitative Real-Time Polymerase Chain Reaction (qRT-PCR). A TRIzol reagent (Thermo Fisher Scientific, Waltham, MA, USA) was used to grind and extract the total RNA of rat heart tissues and CFs in each group on ice. After quantitative analysis, the equivalent amount of RNA was transcribed into complementary deoxyribonucleic acid (cDNA) using the reverse transcription kit (Thermo Fisher Scientific, Waltham, MA, USA). The same amount of cDNA was taken for PCR amplification. Finally, cDNA was detected according to the instructions of the fluorescence quantitative PCR kit (Thermo Fisher Scientific, Waltham, MA, USA). The relative expression level of the target gene was calculated by the $2^{-\Delta\Delta C_t}$ method. And the reaction conditions were as follows: 94°C denaturation 45 seconds, 59°C annealing 45 seconds, and 72°C extension 60 seconds, a total of 35 cycles. The primer sequence is shown in Table 1.

TABLE 1: Real-time PCR primers.

Gene name	Forward (5' > 3')	Reverse (5' > 3')
α -MHC	GCCAGTACCTCCGAAAGTC	GCCTTAACATACTCCTCCTTGTC
β -MHC	ACTGTCAACACTAAGAGGGTCA	TTGGATGATTTGATCTTCCAGGG
Sirt1	CCAGATCCTCAAGCCATG	TTGGATTCTGCAACCTG
SOD1	GGTGAACCAGTTGTGTTGTC	CCGTCCTTTCCAGCAGTC
SOD2	CAGACCTGCCTTACGACTATGG	CTCGGTGGCGTTGAGATTGTT
GPX1	ATCATATGTGTGCTGCTCGGCTAGC	TACTCGAGGGCACAGCTGGGCCCTTGAG
GPX3	AGAGCCGGGGACAAGAGAA	ATTTGCCAGCATACTGCTTGA
ANP	GCTTCCAGGCCATATTGGAG	GGGGGCATGACCTCATCTT
BNP	GAGGTCACTCCTATCCTCTGG	GCCATTTCTCCGACTTTTCTC
I κ K- α	GTCAGGACCGTGTCTCAAGG	GCTTCTTTGATGTTACTGAGGGC
I κ B- α	GGATCTAGCAGCTACGTACG	TTAGGACCTGACGTAACACG
P65	ACTGCCGGGATGGCTACTAT	TCTGGATTTCGCTGGCTAATGG
GAPDH	ACAACCTTTGGTATCGTGGAAGG	GCCATCACGCCACAGTTTC

qRT-PCR: quantitative real-time polymerase chain reaction.

2.14. 5-Ethynyl-2'-deoxyuridine (EdU) Staining. Primary fibroblasts were cultured with a diluted EdU reagent (Kaiji, Nanjing, China). The next day, PBS was used to wash the cells, and after fixation, Triton X-100 (Kaiji, Nanjing, China) was used to break the membrane and 5% goat serum was used to seal it. Then, the reaction solution was prepared according to the kit instructions and incubated for half an hour at room temperature. After the cells were rinsed with PBS three times, a DAPI reagent (Thermo Fisher Scientific, Waltham, MA, USA) was used to stain the nuclei. Finally, the cells were observed and photographed under an inverted fluorescence microscope.

2.15. Statistical Analysis. Statistical Product and Service Solutions (SPSS) 20.0 software (IBM, Armonk, NY, USA) was used for statistical analysis. The experimental data were expressed as mean \pm standard deviation ($\bar{X} \pm SD$). Differences between the two groups were analyzed by using Student's *t*-test. Comparison between multiple groups was done using the one-way ANOVA test followed by the post hoc test (least significant difference). $P < 0.05$ was considered statistically significant.

3. Results

3.1. NAC Improves the Damaged Heart Structure of Rats after Aortic Constriction. To determine whether NAC protects the heart from cardiac impairment caused by overloading, the results of echocardiography showed that the diameter of ventricular dilatation of the model group was obviously higher than that of the control group, which showed that LVEDd and LVESd were obviously increased. In addition, the cardiac contractile function was obviously lower than that of the control group, which showed that the LVEF% and the LVFS% were reduced. In the NAC treatment group, the diameter of ventricular dilatation was lower than that of the model group, which showed that LVEDd and LVESd were obviously lower than those of the model group. The systolic function of the heart was obviously

higher than that of the model group, showing that the LVEF% and the LVFS% were increased compared with those of the model group (Figures 1(a)–1(d)). At the same time, we detected the ratio of Lvw/HW and Lvw/TL, and we found that the Lvw/HW and Lvw/TL values of the model group were obviously higher than those of the control group, but the Lvw/HW and Lvw/TL values of the NAC group were lower than those of the model group (Figures 1(e) and 1(f)). Then, Masson staining found that the myocardial tissue structure of the control group was normal and the fibrosis was not obvious, while the myocardial tissue structure of the model group was disordered and the fibrosis was obvious. Conversely, the myocardial tissue structure of the rats in the NAC treatment group was slightly disordered and the fibrosis area was relatively reduced (Figure 1(g)). Next, we detected the expression of Collagen I by WB and qRT-PCR and found that the expression of Collagen I in the model group was the highest, while the expression of Collagen I in the NAC group was lower than that in the model group (Figures 1(h) and 1(i)).

3.2. NAC Improves the Damaged Heart Function of Rats after Aortic Constriction. Firstly, qRT-PCR results showed that, compared with the control group, model group rats' cardiac tissue hypertrophy-related gene has obvious differences with that of the control group, including atrial natriuretic peptide (ANP), B-type natriuretic peptide (BNP), and β -myosin heavy chain (β -MHC) transcriptional expressions, which were higher than those of the control group, and α -myosin heavy chain (α -MHC) transcriptional expression was lower than that of the control group. In contrast, transcriptional expressions of the NAC group, ANP, BNP, and β -MHC, were lower than those of the model group, while transcriptional expression of α -MHC was higher than that of the model group (Figures 2(a)–2(d)). At the same time, we found through serological detection that the LDH activity and MDA content in the model group obviously increased, while the LDH activity and MDA content obviously decreased after NAC treatment (Figures 2(e) and 2(f)).

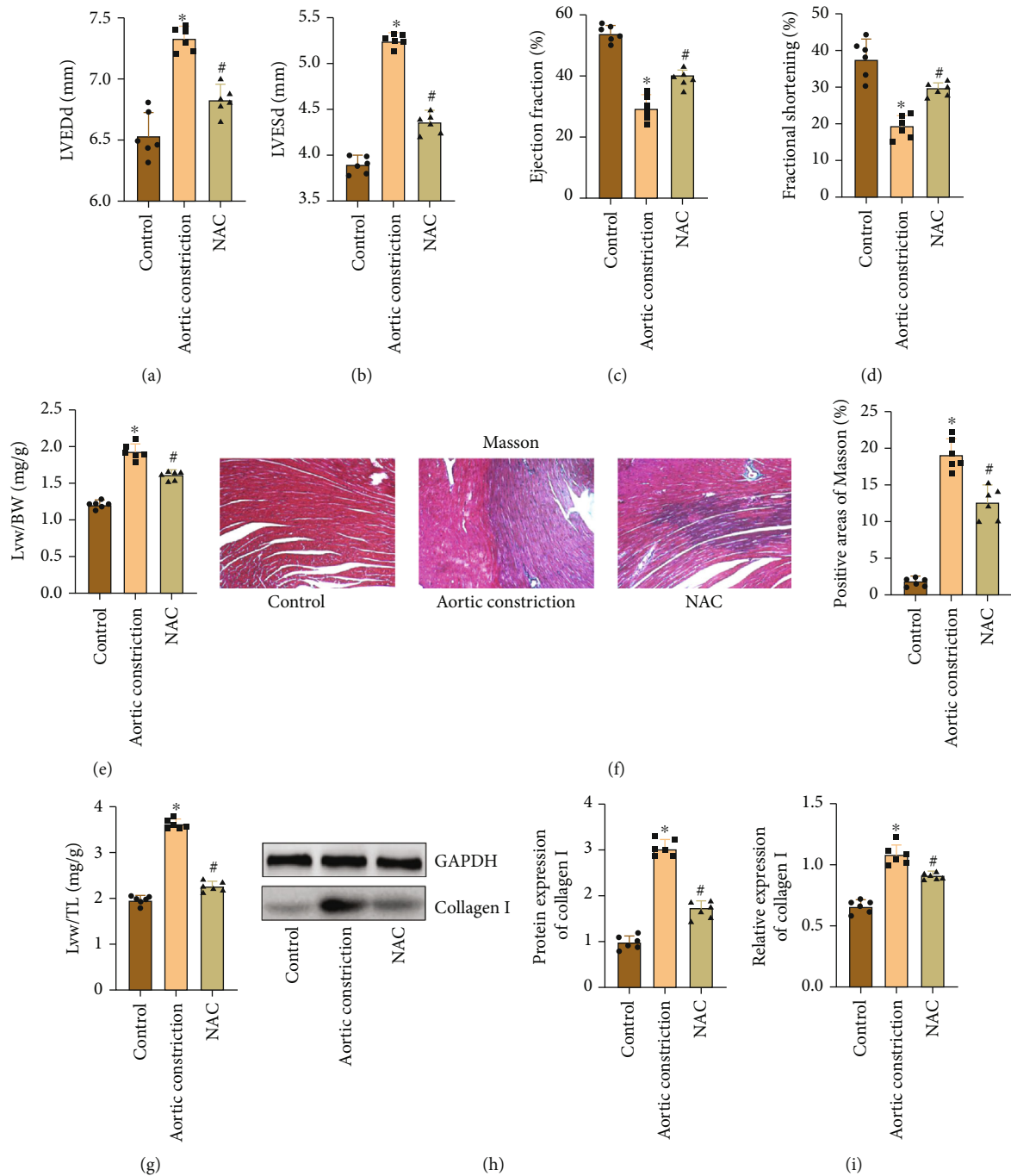


FIGURE 1: NAC improves the damaged heart structure of rats after aortic constriction. (a) Echocardiography detected the LVEDd of rats. (b) Echocardiography detected the LVESd of rats. (c) Echocardiography detected the LVEF% of rats. (d) Echocardiography detected the LVFS% of rats. (e) Ratio of Lvw/BW. (f) Ratio of Lvw/TL. (g) Masson staining and positive area analysis (magnification: 200x). (h) WB detected the Collagen I expression and gray value analysis. GAPDH was used as an internal control. (i) qRT-PCR detected the Collagen I expression. “*” indicates the statistical difference from the control group, $P < 0.05$; “#” indicates the statistical difference from the aortic constriction group, $P < 0.05$. LVEDd: left ventricular end-diastolic diameter; LVESd: left ventricular end-systolic diameter; LVEF: left ventricular ejection fraction; LVFS: left ventricular fractional shortening; Lvw: left ventricular weight; BW: body weight; TL: tibial length.

3.3. NAC Improves Oxidative Stress Response after Aortic Constriction. Firstly, we detected the expression of GPX1 and GPX3 proteins in the myocardial tissues of each group by WB (Figure 3(a)). The results showed that the expression of GPX1 and GPX3 was obviously decreased in the model group, while NAC effectively inhibited the expression of

GPX1 and GPX3 after treatment. At the same time, qRT-PCR detection of SOD1 mRNA, SOD2 mRNA, GPX1 mRNA, and GPX3 mRNA also found similar results; NAC treatment can reverse the decreased transcriptional expression of SOD1, SOD2, GPX1, and GPX3 in myocardial tissue (Figures 3(b)–3(e)). Then, we found that the activities of

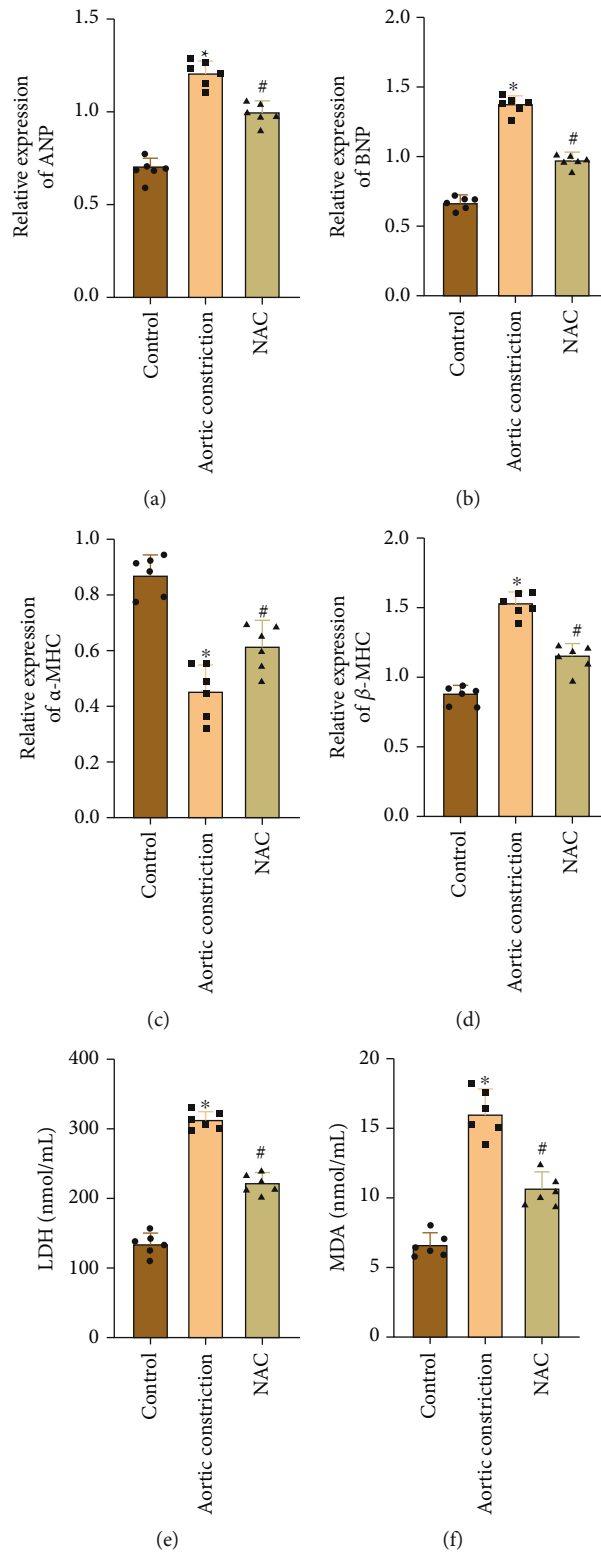


FIGURE 2: NAC improves the damaged heart function of rats after aortic constriction. (a) qRT-PCR detected the ANP expression. (b) qRT-PCR detected the BNP expression. (c) qRT-PCR detected the α -MHC expression. (d) qRT-PCR detected the β -MHC expression. (e) The kit detected the serum LDH activity. (f) The kit detected the serum MDA content. “*” indicates the statistical difference from the control group, $P < 0.05$; “#” indicates the statistical difference from the aortic constriction group, $P < 0.05$. ANP: atrial natriuretic peptide; BNP: B-type natriuretic peptide; α -MHC: α -myosin heavy chain; β -MHC: β -myosin heavy chain; LDH: lactic dehydrogenase; MDA: malondialdehyde.

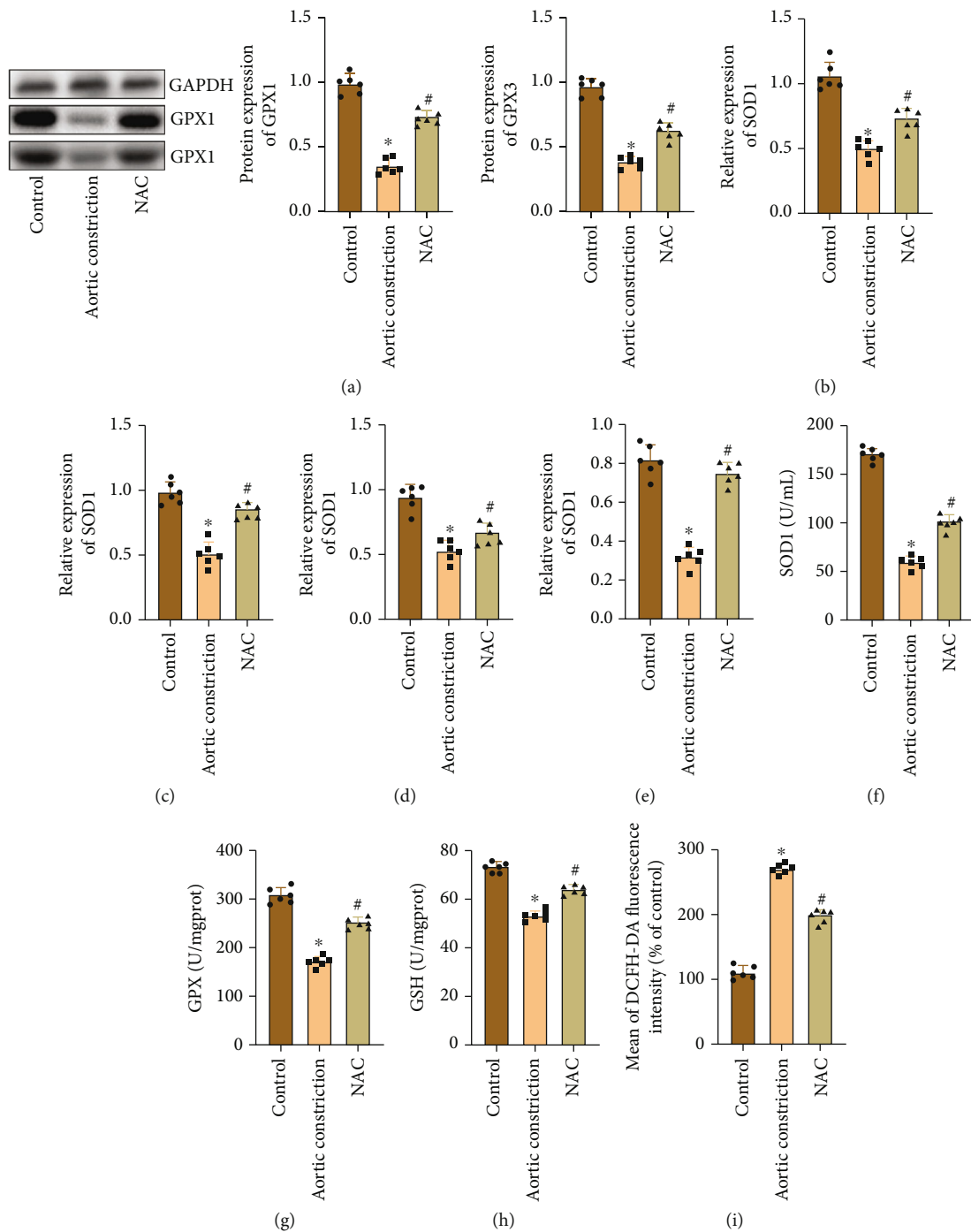


FIGURE 3: NAC improves oxidative stress response after aortic constriction. (a) WB detected the expression of GPX1 and GPX3 and gray value analysis. GAPDH was used as an internal control. (b) qRT-PCR detected the expression of SOD1. (c) qRT-PCR detected the expression of SOD2. (d) qRT-PCR detected the expression of GPX1. (e) qRT-PCR detected the expression of GPX3. (f) The kit detected the serum SOD activity. (g) The kit detected the serum GPX activity. (h) The kit detected the serum GSH activity. (i) Flow cytometry detected the intracellular ROS levels. “*” indicates the statistical difference from the control group, $P < 0.05$; “#” indicates the statistical difference from the aortic constriction group, $P < 0.05$. SOD: superoxide dismutase; GPX: glutathione peroxidase; GSH: glutathione; ROS: reactive oxygen species.

SOD, GPX, and GSH in the model group were obviously reduced by serological detection. On the contrary, we found that the expression of SOD, GPX, and GSH in the NAC group was higher than that in the model group

(Figures 3(f)–3(h)). In addition, flow cytometry detection of ROS levels in myocardial tissue revealed that ROS levels were obviously increased in the model group, while NAC can promote ROS clearance (Figure 3(i)).

3.4. NAC Inhibits the NF- κ B Signaling Pathway. In order to detect whether NAC inhibits CF proliferation and collagen synthesis through the NF- κ B signaling pathway, we investigated the effect of NAC *in vitro* by AngII treatment of CFs. First of all, the results of the MTT experiment showed that compared with the control group, NAC of 10, 20, and 40 mmol/L had an inhibitory effect on the growth of CF cells, and there were differences among groups with different concentrations (Figure 4(a)). Also, we found that when NAC concentration was at 20 mmol/L, its inhibition activity of CFs was significant. Therefore, in our subsequent experiments, we chose this concentration to treat CFs [14]. At the same time, the results of the ^3H proline incorporation method showed that compared with the control group, the synthesis of total collagen of CFs decreased obviously after NAC treatment for 48 hours, and the amount of doping also decreased with the increase of NAC concentration (Figure 4(b)). Then, we detected the proliferation of CFs by EdU staining, and the results showed that NAC treatment could significantly inhibit the proliferation of CFs induced by AngII (Figure 4(c)). In addition, WB detection found that after AngII treated CFs, the NF- κ B signaling pathway was activated, while NAC treatment can increase the levels of I κ B- α protein and decrease the levels of NF- κ B and I κ K- α protein (Figure 4(d)). At the same time, qRT-PCR also produced similar results (Figures 4(e)–4(g)).

4. Discussion

The remodeling of the heart includes myocardial parenchymal remodeling and interstitial remodeling. Parenchymal remodeling is mainly caused by pathological hypertrophy or degeneration and necrosis of cardiomyocytes, while interstitial remodeling includes activation and proliferation of fibroblasts and changes in the composition and amount of the extracellular matrix collagen network [15]. Therefore, in the process of CR, CFs and the extracellular matrix proliferate and infiltrate a lot, leading to heart fibrosis. This process is an important step in the change of heart function from decompensation to HF. Collagen I and Collagen III are secreted by CFs and are the main components of the extracellular matrix of the heart. In the process of CR, pathological hyperplasia of Collagen I and Collagen III caused an imbalance of the myocardial parenchymal and interstitial tissues, and the number of myocardial cells as working cells decreased relatively, which generally showed the body's cardiac dysfunction [16]. Our results also found that in the model group, the cardiac tissue structure was disordered, and the fibrosis area and Collagen I expression were obviously higher than those in the control group. At the same time, the heart function of rats in the model group decreased, and some hypertrophy-related indicators were obviously increased. Thus, we speculate that rational remodeling of heart disease has occurred in rats.

In the cardiovascular system, NAC has also received attention, and it can play a beneficial role in the body under the conditions of coronary atherosclerosis, myocar-

dial IRI, and hypertension and CR [17, 18]. Research studies have found that the plasma TNF- α concentration in the rat model of hypertension was obviously associated with a decrease in cardiac LVFS% and a lack of cardiac GSH. However, after NAC intervention, there was no effect on hypertension, but the plasma TNF- α concentration reached normal levels, increased LVFS% and restricted the left ventricular posterior wall hypertrophy, and inhibited the activation of matrix metalloproteinase 2 and matrix metalloproteinase 9, which reduces the collagen deposition in the left ventricle, suggesting that NAC can slow down the process of CR in hypertensive rats and effectively protect cardiac function [19]. In addition, there are research studies that believe that NAC may directly prevent blood pressure, promote the synthesis of GSH in the heart to inhibit the harmful effects of inflammatory factors on the heart, or directly inhibit the activation of NF- κ B through GSH and other mechanisms. And it can reverse the effects of hypertensive CR [20]. However, there is less relevant evidence, and its mechanism still needs further study, especially the direct effect of fibroblasts.

Studies in other systemic diseases have shown that NAC can directly affect the proliferation and collagen synthesis of mouse and human lung fibroblasts, reduce the expression of cyclin E, block cell proliferation in the G1 phase, and thus inhibit cell proliferation, and it can reduce TGF- α -induced or non-TGF- α -induced collagen synthesis [21]. The results of this experiment indicated that NAC had inhibitory effects on proliferation and collagen synthesis of rat CFs similar to those mentioned in the previous experiment, but the specific mechanism of NAC and its effect on overall cardiac fibrosis under pathological conditions still need to be further studied.

Cell pathways activated by OS led to programmed cell death, which eventually leads to cardiac dysfunction and HF. It can be seen that the signal transduction pathway mediated by OS is particularly important in the formation of MH [22, 23]. Therefore, we speculate that MF is closely related to the OS pathway. NF- κ B is a family of transcription factor proteins. And it is very sensitive to ROS produced by OS. Activated NF- κ B can cause cells to produce numerous cytokines, and research studies have shown that ROS can lead to the activation of I κ K- α , thereby promoting the activation of NF- κ B [24, 25]. Our results also found that *in vivo*, with the model group heart tissue redox imbalance, antioxidant enzyme activity decreased, prompting the accumulation of ROS in cells. *In vitro*, AngII treated CFs and induced the activation of the NF- κ B signaling pathway. NAC can restore antioxidant enzyme activity in the body and remove excess ROS in cells. At the same time, NAC can inhibit the total collagen synthesis function of cells and inhibit the excessive activation of the NF- κ B signaling pathway *in vitro*. Although the preliminary research results of this experiment suggest that NAC can be considered a potential treatment method for rational reconstruction of heart disease, it is necessary to further study the comprehensive impact of all aspects before it can provide a stronger basis for treatment.

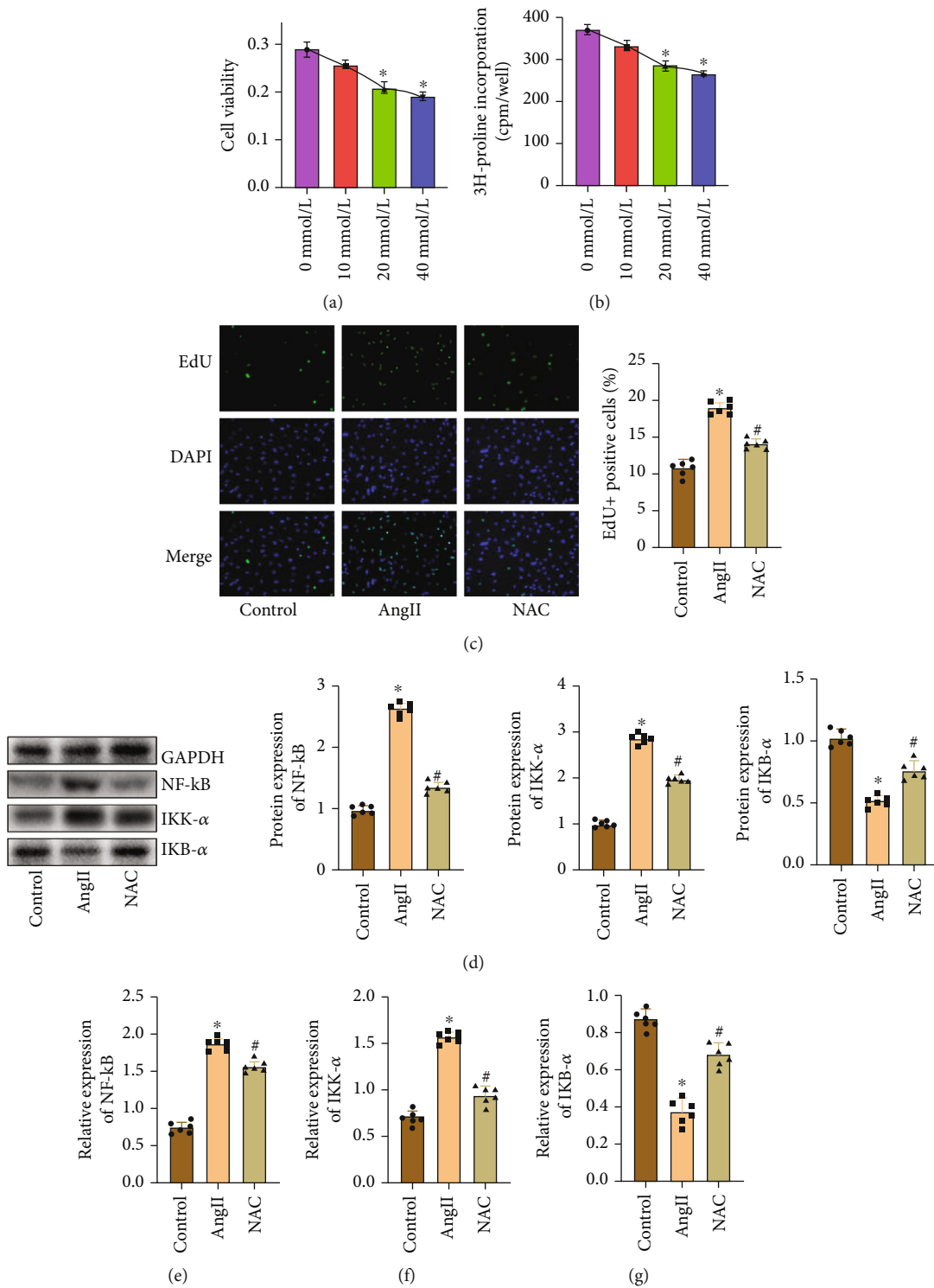


FIGURE 4: NAC inhibits the NF-κB signaling pathway. (a) MTT detected the CF activity. (b) The ³H proline incorporation method detected the cell total collagen synthesis function. (c) EdU staining detected the cell proliferation and percentage analysis of positive cells. (d) WB detected the expression of NF-κB, IκK-α, IκB-α, and gray value analysis. GAPDH is used as an internal control. (e) qRT-PCR detected the expression of NF-κB. (f) qRT-PCR detected the expression of IκK-α. (g) qRT-PCR detected the expression of IκB-α. “*” indicates the statistical difference from the control group, *P* < 0.05; “#” indicates the statistical difference from the aortic constriction group, *P* < 0.05.

Our study confirmed that *in vivo*, antioxidant enzyme activity and intracellular ROS content are closely related to myocardial remodeling, and NAC can significantly relieve OS *in vivo*, thus inhibiting MF and remodeling. Meanwhile,

in vitro, we first reported that NAC inhibits CF proliferation and collagen synthesis through the NF-κB pathway, thus providing a new research basis for the treatment of MF and remodeling.

5. Conclusions

NAC can inhibit AngII-induced CF proliferation and collagen synthesis through the NF- κ B signaling pathway, alleviate the OS response of myocardial tissue, inhibit the fibrosis of myocardial tissue, and thus slow down the pathological remodeling of the heart. This also provides a new research basis for the treatment of CR.

Data Availability

The datasets used and analyzed during the current study are available from the corresponding author on reasonable request.

Conflicts of Interest


The authors declared no conflict of interest.

References

- [1] R. A. Thandavarayan, K. R. Chitturi, and A. Guha, "Pathophysiology of acute and chronic right heart failure," *Cardiology Clinics*, vol. 38, no. 2, pp. 149–160, 2020.
- [2] T. B. Olesen, M. Pareek, J. V. Stidsen et al., "Association between antecedent blood pressure, hypertension-mediated organ damage and cardiovascular outcome," *Blood Pressure*, vol. 29, no. 4, pp. 232–240, 2020.
- [3] P. Kong, P. Christia, and N. G. Frangogiannis, "The pathogenesis of cardiac fibrosis," *Cellular and Molecular Life Sciences*, vol. 71, no. 4, pp. 549–574, 2014.
- [4] V. Talman and H. Ruskoaho, "Cardiac fibrosis in myocardial infarction—from repair and remodeling to regeneration," *Cell and Tissue Research*, vol. 365, no. 3, pp. 563–581, 2016.
- [5] G. Aldini, A. Altomare, G. Baron et al., "N-Acetylcysteine as an antioxidant and disulphide breaking agent: the reasons why," *Free Radical Research*, vol. 52, no. 7, pp. 751–762, 2018.
- [6] P. J. Millea, "N-Acetylcysteine: multiple clinical applications," *American Family Physician*, vol. 80, no. 3, pp. 265–269, 2009.
- [7] P. Santus, A. Corsico, P. Solidoro, F. Braido, F. Di Marco, and N. Scichilone, "Oxidative stress and respiratory system: pharmacological and clinical reappraisal of N-acetylcysteine," *COPD*, vol. 11, no. 6, pp. 705–717, 2014.
- [8] M. Bartekova, M. Barancik, K. Ferenczyova, and N. S. Dhalla, "Beneficial effects of N-acetylcysteine and N-mercaptopyronylglycine on ischemia reperfusion injury in the heart," *Current Medicinal Chemistry*, vol. 25, no. 3, pp. 355–366, 2018.
- [9] L. Zhang, Y. L. He, Q. Z. Li et al., "N-Acetylcysteine alleviated silica-induced lung fibrosis in rats by down-regulation of ROS and mitochondrial apoptosis signaling," *Toxicology Mechanisms and Methods*, vol. 24, no. 3, pp. 212–219, 2014.
- [10] Y. Pang, M. T. Liang, Y. Gong et al., "HGF reduces disease severity and inflammation by attenuating the NF- κ B signaling in a rat model of pulmonary artery hypertension," *Inflammation*, vol. 41, no. 3, pp. 924–931, 2018.
- [11] L. Yang and C. Gao, "miR-590 inhibits endothelial cell apoptosis by inactivating the TLR4/NF- κ B pathway in atherosclerosis," *Yonsei Medical Journal*, vol. 60, no. 3, pp. 298–307, 2019.
- [12] F. Yang, S. Jin, and Y. Tang, "Marine collagen peptides promote cell proliferation of NIH-3T3 fibroblasts via NF- κ B signaling pathway," *Molecules*, vol. 24, no. 22, p. 4201, 2019.
- [13] T. D. Gilmore, "Introduction to NF- κ B: players, pathways, perspectives," *Oncogene*, vol. 25, no. 51, pp. 6680–6684, 2006.
- [14] D. Wang, X. Yu, and P. Brecher, "Nitric oxide and N-acetylcysteine inhibit the activation of mitogen-activated protein kinases by angiotensin II in rat cardiac fibroblasts," *The Journal of Biological Chemistry*, vol. 273, no. 49, pp. 33027–33034, 1998.
- [15] L. Schirone, M. Forte, S. Palmerio et al., "A review of the molecular mechanisms underlying the development and progression of cardiac remodeling," *Oxidative Medicine and Cellular Longevity*, vol. 2017, 2017.
- [16] M. Adamcova, T. Baka, E. Dolezelova et al., "Relations between markers of cardiac remodelling and left ventricular collagen in an isoproterenol-induced heart damage model," *Journal of Physiology and Pharmacology*, vol. 70, no. 1, pp. 71–77, 2019.
- [17] B. Giam, P. Y. Chu, S. Kuruppu et al., "N-Acetylcysteine attenuates the development of cardiac fibrosis and remodeling in a mouse model of heart failure," *Physiological Reports*, vol. 4, no. 7, p. 27081162, 2016.
- [18] B. Li, Y. Sun, J. P. Wang et al., "Antioxidant N-acetylcysteine inhibits maladaptive myocyte autophagy in pressure overload induced cardiac remodeling in rats," *European Journal of Pharmacology*, vol. 839, pp. 47–56, 2018.
- [19] M. Bourraindeloup, C. Adamy, G. Candiani et al., "N-Acetylcysteine treatment normalizes serum tumor necrosis factor- α level and hinders the progression of cardiac injury in hypertensive rats," *Circulation*, vol. 110, no. 14, pp. 2003–2009, 2004.
- [20] X. Y. Wu, A. Y. Luo, Y. R. Zhou, and J. H. Ren, "N-Acetylcysteine reduces oxidative stress, nuclear factor- κ B activity and cardiomyocyte apoptosis in heart failure," *Molecular Medicine Reports*, vol. 10, no. 2, pp. 615–624, 2014.
- [21] J. M. Hu and N. S. Zhong, "A preliminary study on the mechanisms of N-acetylcysteine in the inhibition of proliferation and collagen synthesis of human pulmonary fibroblasts," *Zhonghua Jie He He Hu Xi Za Zhi*, vol. 32, no. 12, pp. 897–901, 2009.
- [22] Y. Tang, M. Guo, X. Y. Ma, W. P. Sun, M. H. Hao, and H. Y. Zhu, "Oltipraz attenuates the progression of heart failure in rats through inhibiting oxidative stress and inflammatory response," *European Review for Medical and Pharmacological Sciences*, vol. 22, no. 24, pp. 8918–8923, 2018.
- [23] C. Li, J. Zhang, M. Xue et al., "SGLT2 inhibition with empagliflozin attenuates myocardial oxidative stress and fibrosis in diabetic mice heart," *Cardiovascular Diabetology*, vol. 18, no. 1, p. 15, 2019.
- [24] A. H. Haghi, S. R. Abtahi, E. Hazrati, M. Chamanara, M. Jalili, and B. Paknejad, "Targeting of oxidative stress and inflammation through ROS/NF- κ B pathway in phosphine-induced hepatotoxicity mitigation," *Life Sciences*, vol. 232, article 116607, 2019.
- [25] Y. Liang, M. Ip, and J. Mak, "(-)-Epigallocatechin-3-gallate suppresses cigarette smoke-induced inflammation in human cardiomyocytes via ROS-mediated MAPK and NF- κ B pathways," *Phytomedicine*, vol. 58, article 152768, 2019.

Research Article

miR-190-5p Alleviates Myocardial Ischemia-Reperfusion Injury by Targeting PHLPP1

Yangxue Li,¹ Zhibo Li,¹ Jiangen Liu,¹ Yihang Liu,¹ and Guobin Miao^{1,2} 

¹Department of Cardiology, The Second Hospital of Jilin University, Changchun, China

²Department of Cardiology, Beijing Tsinghua Changgung Hospital, Tsinghua University, Beijing, China

Correspondence should be addressed to Guobin Miao; mgba01004@btch.edu.cn

Received 9 October 2021; Revised 9 November 2021; Accepted 11 November 2021; Published 25 November 2021

Academic Editor: Francesco Busardò

Copyright © 2021 Yangxue Li et al. This is an open access article distributed under the Creative Commons Attribution License, which permits unrestricted use, distribution, and reproduction in any medium, provided the original work is properly cited.

Objective. Myocardial ischemia-reperfusion (I/R) injury (MIRI) refers to the more serious myocardial injury after blood flow recovery, which seriously affects the prognosis of patients with ischemic cardiomyopathy. This study explored the new targets for MIRI treatment by investigating the effects of miR-190-5p and its downstream target on the structure and function of myocardial cells. **Methods.** We injected agomir miR-190-5p into the tail vein of rats to increase the expression of miR-190-5p in rat myocardial cells and made an I/R rat model by coronary artery occlusion. We used 2,3,5-triphenyl tetrazolium chloride staining, lactate dehydrogenase (LDH) detection, echocardiography, and hematoxylin-eosin (HE) staining to determine the degree of myocardial injury in I/R rats. In addition, we detected the expression of inflammatory factors and apoptosis-related molecules in rat serum and myocardial tissue to determine the level of inflammation and apoptosis in rat myocardium. Finally, we determined the downstream target of miR-190-5p by Targetscan system and dual luciferase reporter assay. **Results.** The expression of miR-190-5p in an I/R rat myocardium was significantly lower than that in normal rats. After treatment of I/R rats with agomir miR-190-5p, the ischemic area of rat myocardium and the concentration of LDH decreased. The results of echocardiography and HE staining also found that overexpression of miR-190-5p improved the structure and function of rat myocardium. miR-190-5p was also found to improve the viability of H9c2 cells *in vitro* and reduce the level of apoptosis of H9c2 cells. The results of Targetscan system and dual luciferase reporter assay found that miR-190-5p targeted to inhibit pleckstrin homology domain leucine-rich repeat protein phosphatase 1 (PHLPP1). In addition, inhibition of PHLPP1 was found to improve the viability of H9c2 cells. **Conclusion.** Therefore, miR-190-5p can reduce the inflammation and apoptosis of myocardium by targeting PHLPP1, thereby alleviating MIRI.

1. Introduction

Myocardial ischemia-reperfusion (I/R) injury (MIRI) means that after acute coronary artery occlusion, reperfusion leads to more serious myocardial injury than ischemia itself, including ischemia-induced injury and reperfusion injury [1]. Reperfusion of blood flow can cause damage to uninvolved myocardial cells and can also aggravate the damage of involved myocardial cells [2]. In addition, some cytokines affect nonfocal organs with blood flow, causing organ damage. Reperfusion injury can be up to 50% of the total myocardial injury, often causing serious adverse outcomes such as heart failure, arrhythmia, or even circulatory arrest [3].

Pleckstrin homology domain leucine-rich repeat protein phosphatase (PHLPP) was first discovered by Gao et al. in 2005 and is a novel intracellular serine/threonine phosphatase [4]. PHLPP1 promotes apoptosis induced by mTOR2 by interfering with the downstream signal of phosphatidylinositol-3-kinase/protein-serine-threonine kinase (PI3K/Akt) signaling pathway and rat sarcoma protein/extracellular regulatory protein kinase pathway, thereby playing a role in inhibiting tumor growth [5]. In addition to the initial inhibitory effect on tumor growth, PHLPP1 has been also found to have a close relationship with myocardial injury in recent years. A study found that luteolin can alleviate doxorubicin-induced myocardial injury by regulating PHLPP1/Akt signaling

pathway [6]. Zhang et al. found that the inhibition of PHLPP1 can alleviate myocardial dysfunction [7]. It was also revealed that PHLPP1 ablation can prevent pathological hypertrophy by promoting angiogenesis through the activation of Akt [8]. In addition, Tang et al. found that the upregulation of PHLPP1 is a key mechanism for tumor necrosis factor- (TNF-) α to participate in the course of MIRI [9]. Therefore, PHLPP1 plays an important role in heart disease.

MicroRNA (miRNA) is a class of small noncoding single-stranded RNA molecules that are sheared from precursor single-stranded RNA molecules, negatively regulating gene expression and regulating the translation and stability of specific genes [10]. A study has shown that miRNA can specifically inhibit or target the specific mRNA and participate in the regulation of cell development, proliferation, differentiation, and apoptosis and other important cell signaling pathways [11]. In recent years, significant changes of various miRNA have been found in the myocardial tissue of MIRI, suggesting that miRNA can directly or indirectly affect MIRI. miR-190-5p has been found to be involved in the occurrence and development of various diseases and to regulate the biological processes of cells, including cell proliferation, apoptosis, and metabolism [12]. Our previous study found that miR-190-5p was expressed differently in the myocardium of normal rats and I/R rats. In order to further study the effect of miR-190-5p on MIRI, we studied the effect of miR-190-5p on the viability of myocardial cells *in vivo* and *in vitro* through transfection.

2. Materials and Methods

2.1. Animals. A total of 60 male Sprague Dawley rats (8 weeks old, 200 ± 20 g) were used in this study. The animal experiments in this study were approved by the Jilin University Ethics Committee. All rats were housed in specific pathogen-free animal rooms of Jilin University Experimental Animal Center. The temperature of the animal room is $24 \pm 2^\circ\text{C}$, and the relative humidity is 40-60%. We made an I/R model by ligating the rat coronary arteries. After anesthetizing the rat with 2% sodium pentobarbital (40 mg/kg), we removed the hair from the rat's chest and disinfected it with iodophor. Then, we used a small animal ventilator (CWE SAR-830, Orange, CA, USA) to maintain the rat's breathing and observed the electrocardiogram of the rat using an electrocardiograph. During the operation, the rat was maintained under continuous anesthesia by inhalation of methoxyflurane (1.5%) on an operating table. We cut the skin and sternum of the rat's left chest. After exposing the rat heart, we gently cut the heart envelope and ligated the left anterior descending coronary artery with sutures. The elevation of the ST segment of the electrocardiogram indicated myocardial ischemia. After 30 minutes, we loosened the ligature. The decrease in the ST segment of the electrocardiogram indicated the recovery of myocardial blood flow. After 180 minutes of restoration of blood flow, we detected the rat's cardiac function and collected rat serum and myocardial tissue. The rats in the sham group were only opened the chest cavity without ligating the coronary arteries. Rats in the I/R+agomir negative control (NC) group

and the I/R+agomir miR-190-5p group were injected with agomir NC and agomir miR-190-5p via the tail vein 48 hours before modeling.

2.2. 2,3,5-Triphenyl Tetrazolium Chloride (TTC) Staining. We put the rat heart in the -20°C refrigerator for 20 minutes. The rat heart was then cut into slices with thickness of 2 mm. We used 1% TTC staining solution (Sigma-Aldrich, St. Louis, MO, USA) to stain myocardial tissue for 15 minutes. A normal myocardium was red, and an ischemic myocardium was pale.

2.3. Echocardiography. After anesthetizing rats with isoflurane, we used VEVO-2100 small animal ultrasound system to detect the cardiac function of mice. We use the MS-400 high-frequency probe to detect the long-axis view of the left ventricle and the short-axis view of the left ventricle near the sternum. The left ventricular ejection fraction (EF) and left ventricular fraction shortening (FS) were recorded.

2.4. Hematoxylin-Eosin (HE) Staining. HE staining was used to detect the structure of rat myocardial tissue. We collected rat hearts and fixed them with 4% paraformaldehyde. Then, we made the rat heart tissue into paraffin blocks. We used a microtome to make paraffin blocks into $5 \mu\text{m}$ thick paraffin sections. Before HE staining, we used xylene and gradient alcohol for dewaxing and hydration. Then, we stained the cell nucleus with hematoxylin (Beyotime, Shanghai, China) and used hydrochloric acid alcohol for differentiation. Then, we used eosin (Beyotime, Shanghai, China) to stain the cytoplasm. Finally, we dehydrated the myocardial tissue with alcohol and sealed them with neutral mounting medium.

2.5. Cell Culture. The rat myocardial cell line (H9c2) was used in this study. Dulbecco's modified Eagle medium (DMEM) (Gibco, Rockville, MD, USA) containing 10% fetal bovine serum (Gibco, Rockville, MD, USA) and 1% double antibody (Gibco, Rockville, MD, USA) was used to culture H9c2 cells. We induced the H9c2 cell injury model through hypoxia/reoxygenation (H/R). After the cells were seeded into the 6-well plate, we cultured the cells using serum-free DMEM and placed the cells in an incubator with 5% CO_2 , 1% O_2 , and 94% N_2 . After 6 hours, we changed the medium to normal DMEM and placed the cells in an incubator with 5% CO_2 , 21% O_2 , and 74% N_2 . We used lipofectamine 3000 to transfect NC mimics, miR-190-5p mimics, NC inhibitor, miR-190-5p inhibitor, siRNA-NC, or siRNA-miR-190-5p into H9c2 cells according to the manufacturer's instructions.

2.6. RNA Isolation and Quantitative Real-Time Reverse Transcription-Polymerase Chain Reaction (RT-PCR). We used the TRIzol (Invitrogen, Carlsbad, CA, USA) method to extract total RNA from myocardial tissue and H9c2 cells and dissolved the RNA with RNase-free water. Then, we used a spectrophotometer to detect the concentration of RNA. We used reverse transcriptase to reverse the mRNA to cDNA. The cDNA was stored in a -20°C refrigerator for a long time. Then, we used SYBR Green Master Mix to amplify the cDNA. We used different primers to specifically amplify the corresponding DNA fragments. The primer

TABLE 1: Primer sequence.

Name	Sense/antisense (S/AS)	Sequences (5'-3')
miR-190-5p	S	GGTCTTTGATGATGATTCTGG
	AS	CTAGGCACAGTATTGAAGGTT
PHLPP1	S	GGCCAAGGAGAAGGAGAGA
	AS	TGGTCCCCACAGCAGAA
Caspase3	S	TGGACAACAACGAAACCTC
	AS	ACACAAGCCCATTTCAGG
Bax	S	CGGCTGCTTGTCTGGAT
	AS	TGGTGAGTGAGGCAGTGAG
Bcl2	S	GTCACAGAGGGGCTACGA
	AS	GTCCGGTTGCTCTCAGG
GAPDH	S	GTTGTGGCTCTGACATGCT
	AS	CCCAGGATGCCCTTTAGT
U6	S	GCTTCGGCAGCACATATACTAAAAT
	AS	CGCTTCACGAATTTGCGTGTTCAT

sequences are shown in Table 1. $2^{-\Delta\Delta CT}$ was used to represent the relative expression of mRNA.

2.7. Cell Counting Kit-8 (CCK8) Assay. H9c2 cells were seeded on 96-well plates. After treating the cells according to the experimental requirements, we added 10 μ l of CCK8 reagent (Dojindo Molecular Technologies, Kumamoto, Japan) to each well. After incubating the 96-well plate in an incubator for 2 hours, we measured the absorbance (OD) of each well of the 96-well plate at 450 nm using a microplate reader in the dark. There was only the medium without cells in the blank wells, while the control wells had cells without treatment: cell viability = (OD sample - OD blank)/(OD control - OD blank).

2.8. Enzyme-Linked Immunosorbent Assay (ELISA). ELISA was used to detect the levels of inflammatory factors (interleukin- (IL-) 1 β , TNF- α , IL-6, and IL-8) and LDH in rat serum. The standards in the ELISA kits (R&D Systems, Emeryville, CA, USA) were diluted to different concentrations, and standards were used to make a standard curve. We then determined the LDH concentration of the inflammatory factor based on the absorbance of the sample and the standard curve. The same method was also used to detect the concentration of LDH in H9c2 cell medium.

2.9. Terminal Deoxynucleotidyl Transferase-Mediated dUTP-Biotin Nick End Labeling (TUNEL) Assay. H9c2 cells were seeded on 24-well plates and treated according to experimental requirements. Then, we used 4% paraformaldehyde and 0.1% TritonX-100 to sequentially treat H9c2 cells. We used the TUNEL kit (Sigma-Aldrich, St. Louis, MO, USA) for staining according to the manufacturer's instructions. Apoptotic cells were positive, and the number of positive cells was proportional to the level of apoptosis.

2.10. Dual Luciferase Reporter Assay. We used the Targets-can system (http://www.targets-can.org/vert_72/) to predict

the potential targets of miR-190-5p. PHLPP1 was found to be a target downstream of miR-190-5p. Therefore, we used the HEK 293T cell line to detect the interaction between miR-190-5p and PHLPP1. We constructed wild type (WT) mRNA 3'-UTR and mutation (MUT) mRNA 3'-UTR. Then, we used the dual luciferase reporter assay kit (R&D Systems, Emeryville, CA, USA) to detect the fluorescence intensity of WT and MUT combined with miR-190-5p according to the manufacturer's instructions.

2.11. Statistical Analysis. Statistical Product and Service Solutions (SPSS) 21.0 statistical software was used to analyze the results of this study. We used a *t*-test to analyze the difference between the two groups of data and used one-way analysis of variance to analyze the difference between multiple groups. $P < 0.05$ was considered statistically significant. All experiments were repeated three times.

3. Results

3.1. miR-190-5p Expression Was Reduced in I/R Rats. We made a rat I/R model by coronary artery occlusion. HE staining detected the structure of rat myocardial tissue (Figure 1(a)). The structure of the myocardial tissue of the rats in the control group and the sham group was intact, while the myocardial cells of the I/R group were disorderly arranged and there were inflammatory cell infiltrations in the intercellular substance. TTC staining detected the ischemic area (Figure 1(b)). The ischemic area of rats in I/R group was significantly larger than that in the control group and sham group. The results of the LDH detection also showed that the serum of the I/R group of rats contained a large amount of LDH (Figure 1(c)). The results of rat cardiac function detection showed that EF (Figure 1(d)) and FS (Figure 1(e)) of I/R rats were significantly reduced. These results indicated that the I/R model was successfully made in rats. We detected the expression of miR-190-5p in rats

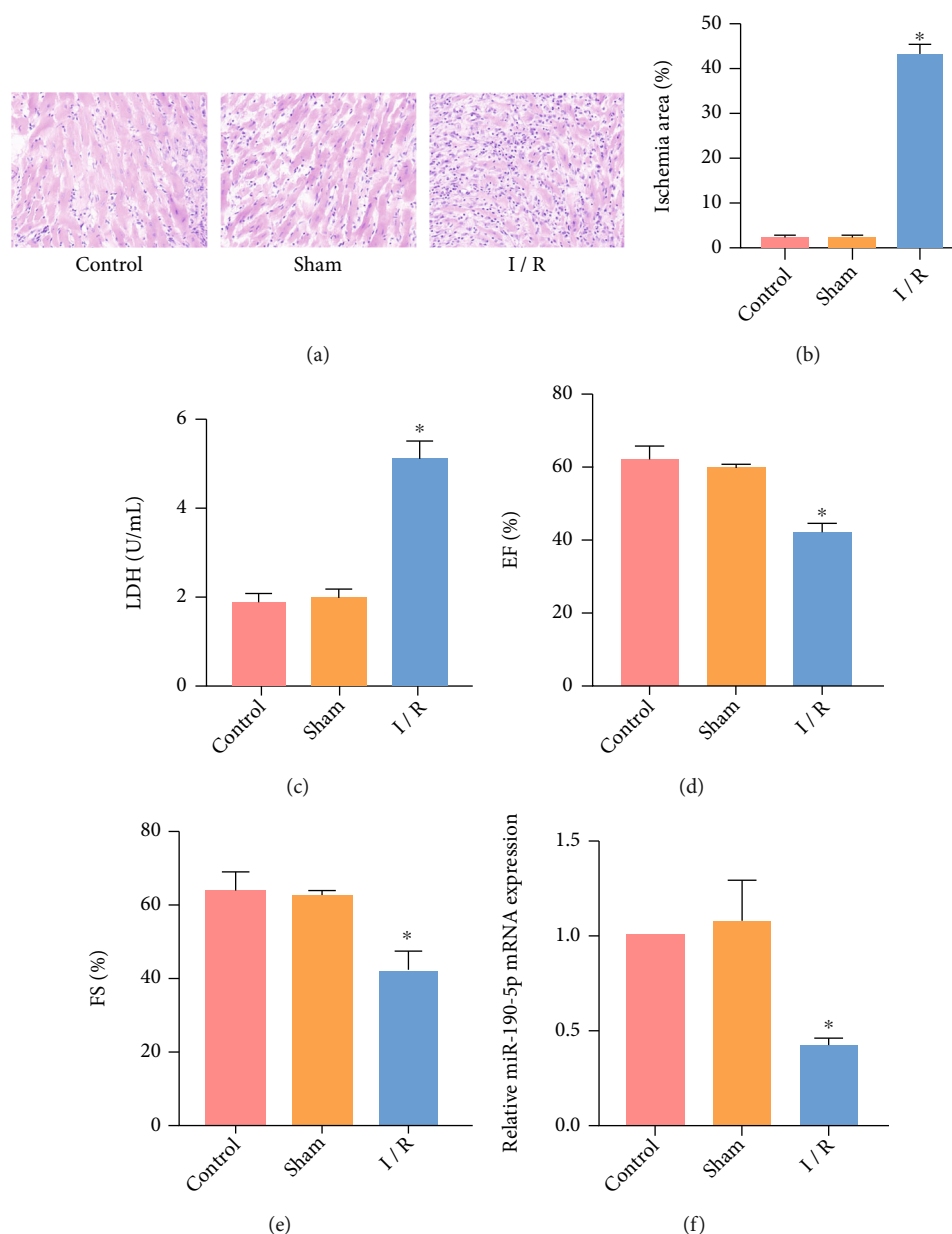


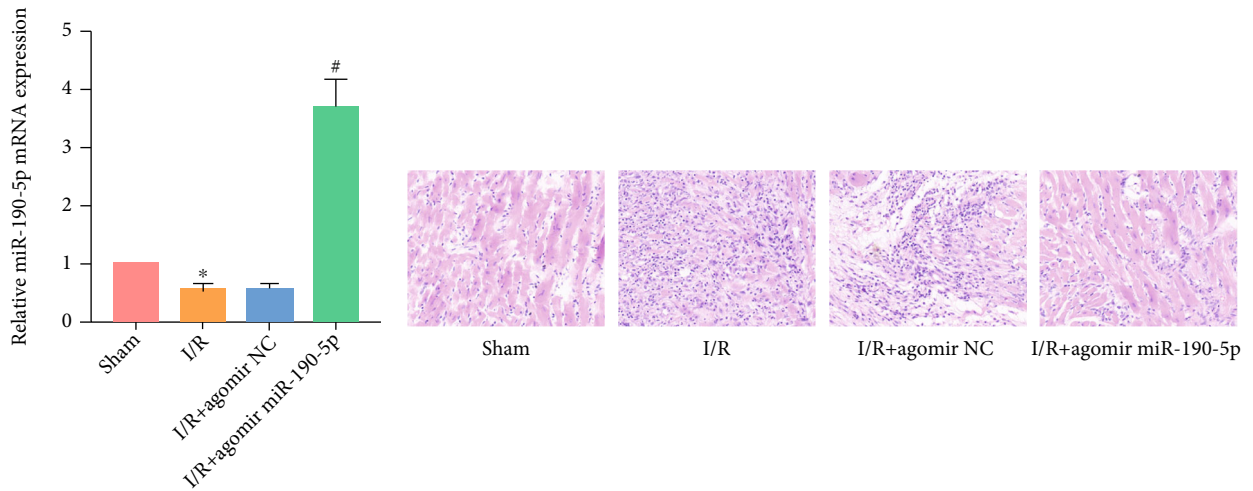
FIGURE 1: miR-190-5p expression was reduced in I/R rats. (a) HE staining of rat myocardium (200 \times); (b) Myocardial ischemic area of rats; (c) LDH level in rat serum; (d, e). EF and FS of rats; (f) miR-190-5p expression in a rat myocardium. (“*” means $P < 0.05$ vs. the sham group).

by RT-PCR. The expression of miR-190-5p in myocardial tissue of I/R rats was significantly lower than that in the control group and sham group (Figure 1(f)).

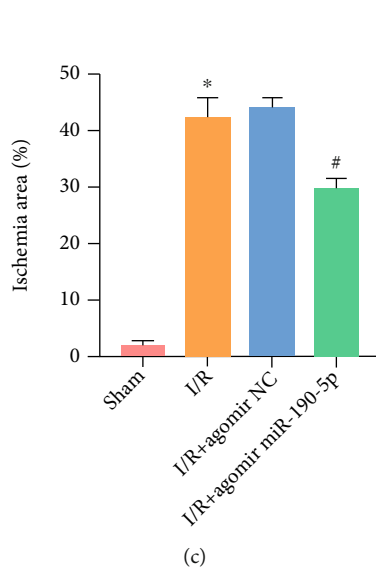
3.2. Overexpression of miR-190-5p Alleviated Myocardial Injury in I/R Rats. We increased the expression of miR-190-5p in rats by agomir NC and agomir miR-190-5p transfection. We identified the overexpression of miR-190-5p in rat myocardial tissue by RT-PCR (Figure 2(a)). HE staining detected changes in a rat myocardial tissue structure (Figure 2(b)). After using agomir miR-190-5p to promote the expression of miR-190-5p in rat myocardial tissue, we found that the structure of rat myocardial tissue was significantly improved. The results of TTC staining also showed

that miR-190-5p reduced the myocardial ischemic area in rats (Figure 2(c)). The results of LDH detection showed that miR-190-5p can reduce the level of LDH in rat serum (Figure 2(d)). Cardiac function detection results showed that miR-190-5p increased EF (Figure 2(e)) and FS (Figure 2(f)) in rats. ELISA detected the expression of inflammatory factors (IL-1 β , TNF- α , and IL-6) in rat serum. The levels of inflammation in rats treated with agomir miR-190-5p were significantly reduced (Figures 2(g)–2(i)).

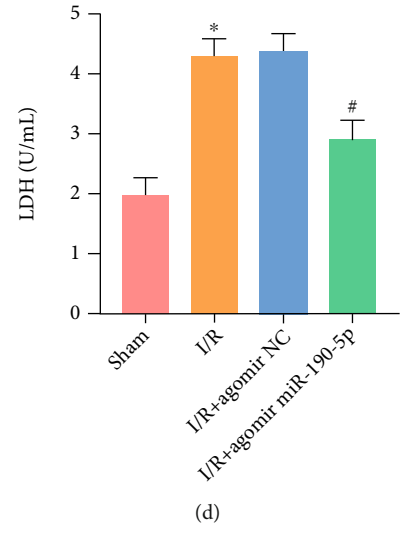
3.3. Overexpression of miR-190-5p Alleviated H/R-Induced H9c2 Cell Injury. To determine the effect of miR-190-5p on cardiomyocytes, we used miR-190-5p mimics to transfect H9c2 cells. RT-PCR results showed that miR-190-5p mimics



(a)

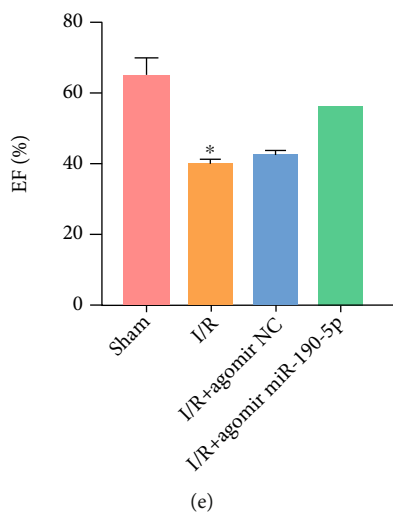


(b)

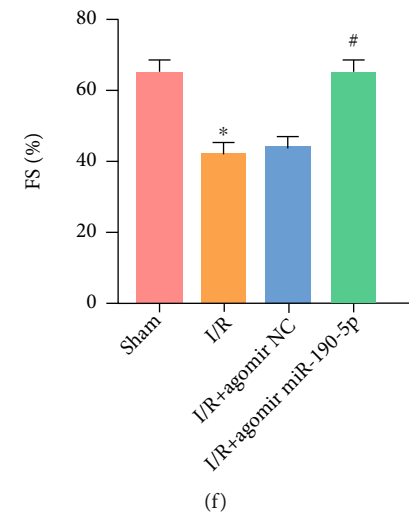


(c)

(d)



(e)



(f)

FIGURE 2: Continued.

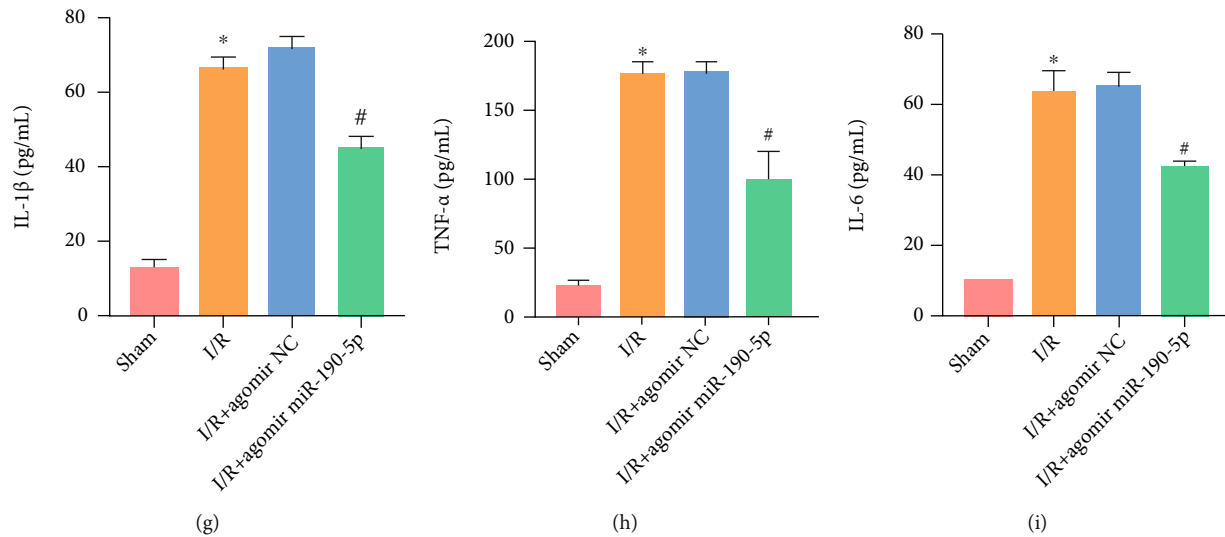


FIGURE 2: Overexpression of miR-190-5p alleviated myocardial injury in I/R rats. (a) miR-190-5p expression in rat myocardium; (b) HE staining of rat myocardium (200 \times); (c) Myocardial ischemic area of rats; (d) LDH level in rat serum; (e, f) EF and FS of rats; (g–i) ELISA results of IL-1 β , TNF- α , and IL-6 in rat serum. (“*” means $P < 0.05$ vs. the sham group; “#” means $P < 0.05$ vs. the I/R+agomir NC group).

significantly increased the expression of miR-190-5p in H9c2 cells (Figure 3(a)). We detected the proliferation ability of H9c2 cells by CCK8 assay. The proliferation ability of cells in the H/R group decreased significantly, and miR-190-5p mimics were found to increase the proliferation ability of H9c2 cells (Figure 3(b)). Furthermore, we detected the level of LDH in the cell medium. The LDH level in the H/R group was higher than that in the control group, while the LDH level in the H/R+miR-190-5p mimics group decreased (Figure 3(c)). TUNEL staining detected the apoptosis level of H9c2 cells. The apoptosis level of the H/R group increased significantly while miR-190-5p mimics decreased the apoptosis level of H9c2 cells (Figure 3(d)). RT-PCR detected the expression of proapoptotic molecules caspase3 and Bax, and antiapoptotic molecule Bcl2. miR-190-5p mimics were also found to reduce the mRNA expression of caspase3 and Bax and increase the mRNA expression of Bcl2 (Figures 3(e)–3(g)).

3.4. miR-190-5p Targets PHLPP1, and the Deficiency of PHLPP1 Alleviates H/R-Induced Cell Injury. We predicted the potential binding site of miR-190-5p and PHLPP1 through the Targetscan system (Figure 4(a)). Then, we clarified the effect of miR-190-5p on PHLPP1 by dual luciferase reporter assay. It was found that miR-190-5p can significantly reduce the fluorescence intensity of WT without affecting the MUT (Figure 4(b)). This indicated that miR-190-5p can degrade PHLPP1 mRNA. Then, we used siRNA-PHLPP1 to reduce the expression of PHLPP1 in H9c2 cells to clarify the effect of PHLPP1 on H9c2 (Figure 4(c)). The results of CCK8 assay indicated that the deficiency of PHLPP1 can increase the viability of H9c2 cells (Figure 4(d)). In addition, LDH detection results also found that the deficiency of PHLPP1 reduced the LDH level in H9c2 cell medium (Figure 4(e)). The result of TUNEL staining proved that the deficiency of PHLPP1 can reduce the

apoptosis level of H9c2 cells (Figure 4(f)). RT-PCR results revealed that the deficiency of PHLPP1 reduced the expression of caspase3 and Bax and increased the expression of Bcl2 (Figures 4(g)–4(i)).

4. Discussion

MIRI is a common clinical pathological phenomenon in the cardiovascular department. It often occurs in the process of revascularization of acute myocardial infarction. It is also seen in blood flow blockage, organ transplantation, and shock treatment during surgery [13]. MIRI involves calcium overload, inflammation, oxidative stress, endoplasmic reticulum stress, mitochondrial dysfunction, and protease activation [14]. miRNA has been found to be involved in the course of MIRI in recent years and affect various aspects of myocardial injury. A study has found that miR-24-3p can target RIPK1 to inhibit MIRI in mice. miR-24-3p was found to be lowly expressed in myocardial tissues of I/R rats and overexpression of miR-24-3p protected myocardial cells from I/R injury [15]. Another study also found that miR-374 can protect myocardial cells by inhibiting SP1 and activating PI3K/Akt signaling pathway [16]. Our study focused on miR-190-5p. miR-190 has been extensively studied in many diseases, such as Parkinson’s disease, chronic kidney disease, and various tumor diseases. Sun et al. found that miR-190 can alleviate nerve injury and reduce nerve inflammation in Parkinson’s disease model mice [17]. Rudnicki et al. [18] found that miR-190 was lowly expressed in the kidney tissue of patients with chronic kidney disease. In our study, we made an I/R rat model by ligating coronary arteries and detected the difference in the expression of miR-190-5p in a rat myocardium. After ligating the rat coronary arteries, the expression of miR-190-5p in rat myocardial tissue was significantly reduced, suggesting that miR-190-5p was involved in the process of myocardial injury and

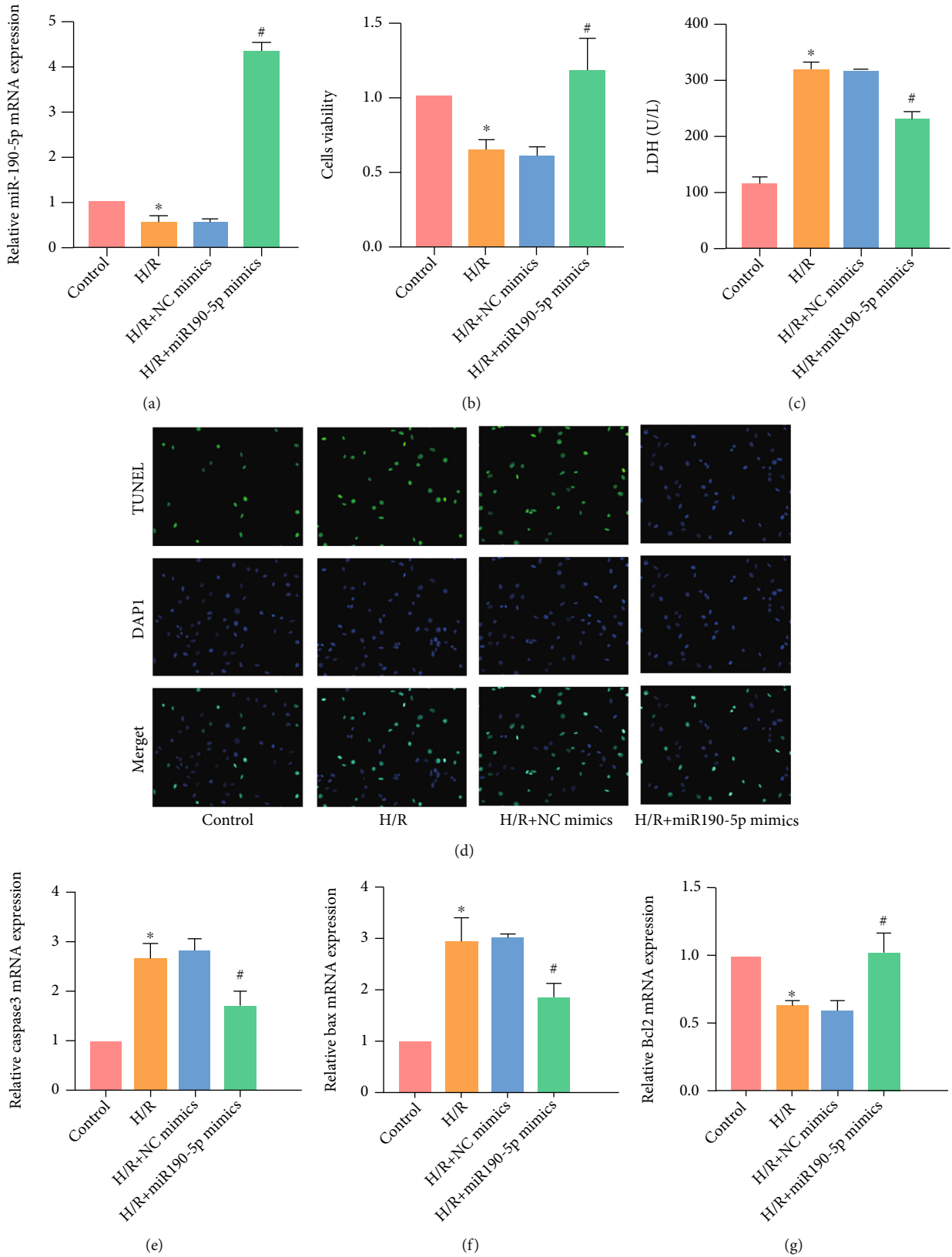


FIGURE 3: Overexpression of miR-190-5p alleviated H/R-induced H9c2 cell injury. (a) miR-190-5p expression in H9c2 cells; (b) CCK8 assay results of H9c2 cells; (c) LDH level in DMEM of H9c2; (d) TUNEL staining results in H9c2 cells (200x); (e-g) mRNA expression of caspase3, Bax, and Bcl2 in H9c2 cells. (“*” means $P < 0.05$ vs. the control group; “#” means $P < 0.05$ vs. the I/R+NC mimics group).

	Predicted consequential pairing of target region (top) and miRNA (bottom)		Site type	Context++ score
Position 230-237 of PHLPP1 3' UTR	5'	... UAACUUCUUUCCGUAACAUAUCA ...	8mer	-0.35
hno-miR-190b-5p	3'	UUGGAUUAUAGUUUGUAUACU		

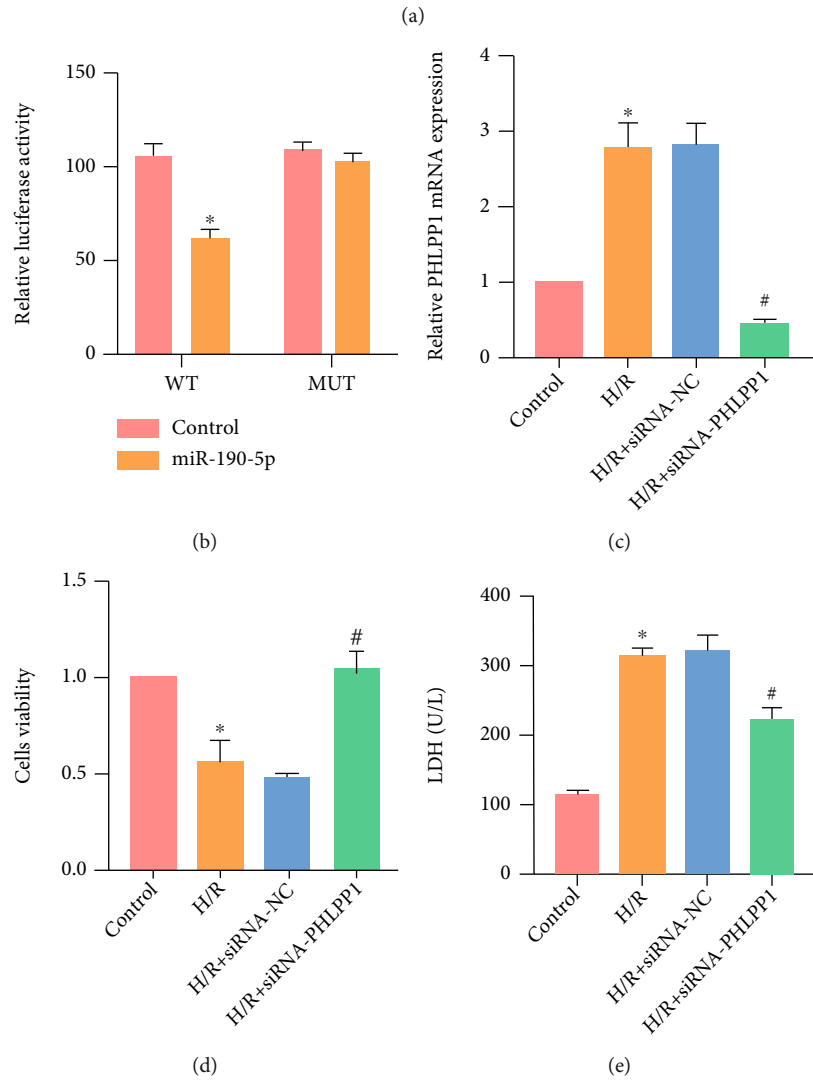


FIGURE 4: Continued.

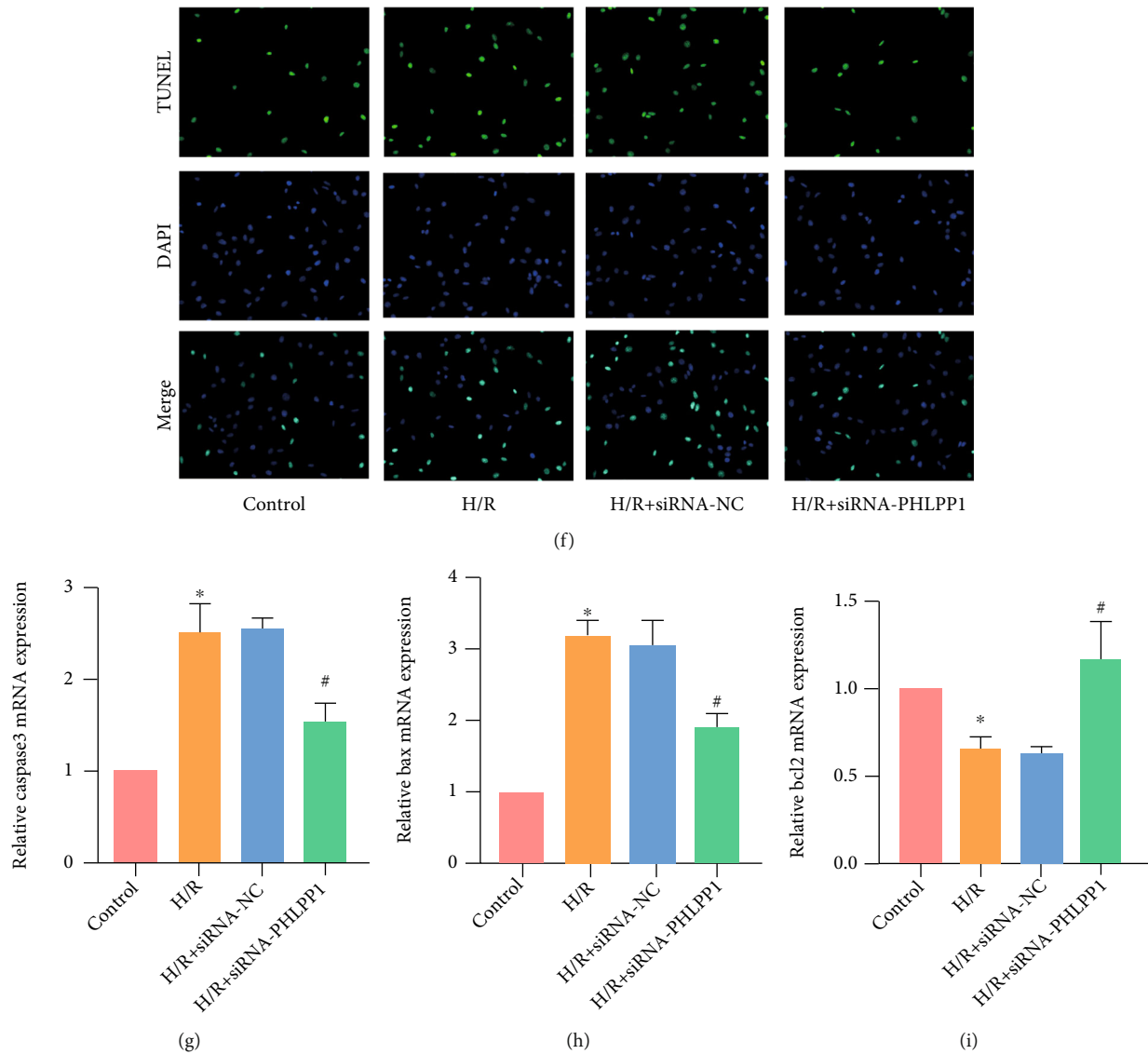


FIGURE 4: miR-190-5p targets PHLPP1 and the deficiency of PHLPP1 alleviates H/R-induced cell injury. (a) miR-190-5p has potential binding sites with PHLPP1. (b) The mRNA of PHLPP1 was degraded by miR-190-5p. (c) PHLPP1 mRNA expression in H9c2 cells. (d) CCK8 assay results of H9c2 cells. (e) LDH level in DMEM of H9c2. (f) TUNEL staining results in H9c2 cells (200 \times); (g-i). mRNA expression of caspase3, Bax, and Bcl2 in H9c2 cells. (“*” means $P < 0.05$ vs. the control group; “#” means $P < 0.05$ vs. the I/R+siRNA-NC group).

the decreased expression of miR-190-5p may be one of the factors of MIRI. After injection of agomir miR-190-5p through the tail vein, the myocardial structure and cardiac function of the rats were significantly improved. Moreover, the level of inflammation in rats also decreased with the treatment of agomir miR-190-5p. This suggested that the increase of miR-190-5p alleviated myocardial injury in rats. In addition, in order to clarify the specific effect of miR-190-5p on myocardial cells, we used miR-190-5p mimics to treat H9c2 cells and found that the increase of miR-190-5p improved the proliferation ability of H9c2 cells and reduced its apoptosis level, which suggested that miR-190-5p can regulate the damage process of myocardial cells. The results of the Targetscan system and dual luciferase reporter assay indicated that miR-190-5p can target to

inhibit PHLPP1. This may be an important mechanism by which miR-190-5p exerted myocardial protection.

The PHLPP gene is located on chromosomes 18 and 16 of the human body. The PHLPP proteins (PHLPP1 and PHLPP2) are protein phosphatases. Their physiological role is to specifically dephosphorylate phosphorylated Akt and inactivate the protein kinase activity, thereby inhibiting the growth promoting effect of Akt [5]. Brognard and Newton [19] found that when PHLPP1 is not expressed, the phosphorylation level of Akt in cells can be increased by 30-fold under the induction of agonists. A study has shown that inhibition of PHLPP1 can improve diabetic cardiomyopathy by activating PI3K/Akt signaling pathway [7]. In addition, a study has found that the deficiency of PHLPP1 can promote the proliferation of chondrocytes by increasing the expression

of fibroblast growth factor 18 [20]. Therefore, we used H9c2 cells to study the effect of PHLPP1 on the viability of myocardial cells. We used siRNA to reduce the expression of PHLPP1 in H9c2 cells. The results of experiments such as CCK8 and TUNEL showed that the deficiency of PHLPP1 can increase the proliferation ability of H9c2 cells and reduce apoptosis, thus alleviating H/R-induced cell injury. Therefore, the degree of myocardial cell injury is positively correlated with the expression of PHLPP1, and targeted inhibition of PHLPP1 may be one of the methods to alleviate myocardial injury.

During myocardial I/R, aseptic inflammation is generated, which activates the innate immune response and adaptive immune response, leading to the production of a large number of inflammatory cells, as well as inflammatory reactions in other organs [21]. Excessive inflammatory stimulation leads to the activation of apoptotic cascade pathway in myocardial cells and promotes the expression and activation of caspase3. The activated caspase3 hydrolyzes various intracellular proteins and causes apoptosis. In addition, the ratio of the expression levels of Bax and Bcl2 in myocardial cells also increases with the increase of inflammation level, thereby promoting the apoptosis of myocardial cells [22]. After overexpressing miR-190-5p in rat myocardial cells or knocking down PHLPP1 in H9c2 cells, we found that the expression of caspase3 and Bax in myocardial cells decreased, while the expression of Bcl2 increased. Results of TUNEL staining also showed that the overexpression of miR-190-5p and the knockdown of PHLPP1 can inhibit the apoptosis of myocardial cells. Therefore, miR-190-5p targeted and inhibited PHLPP1 and alleviated the level of inflammation and apoptosis in myocardial tissue, which may provide a new target for clinical MIRI treatment.

5. Conclusions

This is the first study to investigate the miR-190-5p targeting and inhibiting PHLPP1 to regulate MIRI. miR-190-5p reduced the expression of inflammatory factors in a rat myocardium and serum by targeting PHLPP1, thereby reducing the apoptosis of rat myocardial cells. Therefore, miR-190-5p can improve the structure and function of myocardial tissue and may become a potential therapeutic target of MIRI.

Data Availability

The datasets used and analyzed during the current study are available from the corresponding author on reasonable request.

Conflicts of Interest

The authors declared no conflict of interest.

References

- [1] A. Mokhtari-Zaer, N. Marefati, S. L. Atkin, A. E. Butler, and A. Sahebkar, "The protective role of curcumin in myocardial ischemia-reperfusion injury," *Journal of Cellular Physiology*, vol. 234, no. 1, pp. 214–222, 2019.
- [2] I. Russo, C. Penna, T. Musso et al., "Platelets, diabetes and myocardial ischemia/reperfusion injury," *Cardiovascular Diabetology*, vol. 16, no. 1, p. 71, 2017.
- [3] Z. Chen, D. Wu, L. Li, and L. Chen, "Apelin/APJ system: a novel therapeutic target for myocardial ischemia/reperfusion injury," *DNA and Cell Biology*, vol. 35, no. 12, pp. 766–775, 2016.
- [4] T. Ran, Y. Zhang, N. Diao et al., "Enhanced neutrophil immune homeostasis due to deletion of PHLPP," *Frontiers in Immunology*, vol. 10, p. 2127, 2019.
- [5] A. J. Smith, Y. A. Wen, P. D. Stevens, J. Liu, C. Wang, and T. Gao, "PHLPP negatively regulates cell motility through inhibition of Akt activity and integrin expression in pancreatic cancer cells," *Oncotarget*, vol. 7, no. 7, pp. 7801–7815, 2016.
- [6] Y. Zhang, C. Ma, C. Liu, and F. Wei, "Luteolin attenuates doxorubicin-induced cardiotoxicity by modulating the PHLPP1/AKT/Bcl-2 signalling pathway," *PeerJ*, vol. 8, article e8845, 2020.
- [7] M. Zhang, X. Wang, M. Liu et al., "Inhibition of PHLPP1 ameliorates cardiac dysfunction via activation of the PI3K/Akt/mTOR signalling pathway in diabetic cardiomyopathy," *Journal of Cellular and Molecular Medicine*, vol. 24, no. 8, pp. 4612–4623, 2020.
- [8] M. Li and E. Hirsch, "Akt activation by PHLPP1 ablation prevents pathological hypertrophy by promoting angiogenesis," *Cardiovascular Research*, vol. 105, no. 2, pp. 129–130, 2015.
- [9] B. Tang, J. Ma, X. Ha, Y. Zhang, and Y. Xing, "Tumor necrosis factor- α upregulated PHLPP1 through activating nuclear factor- κ B during myocardial ischemia/reperfusion," *Life Sciences*, vol. 207, pp. 355–363, 2018.
- [10] K. W. Witwer and M. K. Halushka, "Toward the promise of microRNAs - enhancing reproducibility and rigor in microRNA research," *RNA Biology*, vol. 13, no. 11, pp. 1103–1116, 2016.
- [11] D. Tiwari, K. Peariso, and C. Gross, "MicroRNA-induced silencing in epilepsy: opportunities and challenges for clinical application," *Developmental Dynamics*, vol. 247, no. 1, pp. 94–110, 2018.
- [12] Y. Yu and X. C. Cao, "miR-190-5p in human diseases," *Cancer Cell International*, vol. 19, no. 1, p. 257, 2019.
- [13] S. Cadenas, "ROS and redox signaling in myocardial ischemia-reperfusion injury and cardioprotection," *Free Radical Biology & Medicine*, vol. 117, pp. 76–89, 2018.
- [14] M. Kunecki, W. Plazak, P. Podolec, and K. S. Golba, "Effects of endogenous cardioprotective mechanisms on ischemia-reperfusion injury," *Postępy Higieny i Medycyny Doświadczalnej (Online)*, vol. 71, pp. 20–31, 2017.
- [15] H. Tan, J. Qi, B. Y. Fan, J. Zhang, F. F. Su, and H. T. Wang, "MicroRNA-24-3p attenuates myocardial ischemia/reperfusion injury by suppressing RIPK1 expression in mice," *Cellular Physiology and Biochemistry*, vol. 51, no. 1, pp. 46–62, 2018.
- [16] S. B. Zhang, T. J. Liu, G. H. Pu, B. Y. Li, X. Z. Gao, and X. L. Han, "MicroRNA-374 exerts protective effects by inhibiting SP1 through activating the PI3K/Akt pathway in rat models of myocardial ischemia-reperfusion after sevoflurane preconditioning," *Cellular Physiology and Biochemistry*, vol. 46, no. 4, pp. 1455–1470, 2018.
- [17] Q. Sun, S. Wang, J. Chen et al., "MicroRNA-190 alleviates neuronal damage and inhibits neuroinflammation via Nlrp3 in MPTP-induced Parkinson's disease mouse model," *Journal of Cellular Physiology*, vol. 234, no. 12, pp. 23379–23387, 2019.

- [18] M. Rudnicki, P. Perco, B. D'haene et al., "Renal microRNA- and RNA-profiles in progressive chronic kidney disease," *European Journal of Clinical Investigation*, vol. 46, no. 3, pp. 213–226, 2016.
- [19] J. Brognard and A. C. Newton, "PHLiPPing the switch on Akt and protein kinase C signaling," *Trends in Endocrinology and Metabolism*, vol. 19, no. 6, pp. 223–230, 2008.
- [20] E. W. Bradley, L. R. Carpio, A. C. Newton, and J. J. Westendorf, "Deletion of the PH-domain and leucine-rich repeat protein phosphatase 1 (Phlpp1) increases fibroblast growth factor (Fgf) 18 expression and promotes chondrocyte proliferation," *The Journal of Biological Chemistry*, vol. 290, no. 26, pp. 16272–16280, 2015.
- [21] D. J. Hausenloy and D. M. Yellon, "Myocardial ischemia-reperfusion injury: a neglected therapeutic target," *The Journal of Clinical Investigation*, vol. 123, no. 1, pp. 92–100, 2013.
- [22] Y. Yang, Y. Sun, W. Yi et al., "A review of melatonin as a suitable antioxidant against myocardial ischemia-reperfusion injury and clinical heart diseases," *Journal of Pineal Research*, vol. 57, no. 4, pp. 357–366, 2014.

Research Article

RRM2 Improves Cardiomyocyte Proliferation after Myocardial Ischemia Reperfusion Injury through the Hippo-YAP Pathway

Huamin Yu,¹ Haiyan Tang,² Chaochao Deng,³ Qing Lin,³ Peng Yu,³ Shaowen Chen,⁴ and Jingming Ruan ³

¹Department of Cardiology, The First People's Hospital of Linping District, Hangzhou, China

²Catheterization Room, The First People's Hospital of Linping District, Hangzhou, China

³Department of Cardiovascular, Fujian Provincial Hospital South Branch, Fuzhou, China

⁴Department of Cardiovascular, Longyan First Hospital, Longyan, China

Correspondence should be addressed to Jingming Ruan; fareast1973@hotmail.com

Received 14 October 2021; Accepted 9 November 2021; Published 25 November 2021

Academic Editor: Simona Pichini

Copyright © 2021 Huamin Yu et al. This is an open access article distributed under the Creative Commons Attribution License, which permits unrestricted use, distribution, and reproduction in any medium, provided the original work is properly cited.

Objective. Ribonucleotide reductase M2 (RRM2) as an enzyme that catalyzes the deoxyreduction of nucleosides to deoxyribonucleoside triphosphate (dNTP) has been extensively studied, and it plays a crucial role in regulating cell proliferation. However, its role in ischemia-reperfusion injury (I/RI) is still unclear. **Methods.** SD rats were used as the research object to detect the expression of RRM2 in the myocardium by constructing an I/RI model. At the same time, primary SD neonatal rat cardiomyocytes were extracted, and hypoxia/reoxygenation (H/R) treatment simulated the I/RI model. Using transfection technology to overexpress RRM2 in cardiomyocytes, quantitative Real-Time Polymerase Chain Reaction (qRT-PCR) was used to detect the expression of RRM2, Cell Counting Kit-8 (CCK-8) assay was used to detect cell viability, and immunofluorescence staining was used to detect Ki67 and EdU-positive cells. Western blot (WB) technology was used to detect YAP and its phosphorylation expression. **Results.** qRT-PCR results indicated that the expression of RRM2 was inhibited in the model group, and cardiomyocytes overexpressing RRM2 can obviously promote the proliferation of primary cardiomyocytes and improve the damage of cardiac structure and function caused by I/R. At the same time, RRM2 can promote the increase of YAP protein expression and the increase of Cyclin D1 mRNA expression. **Conclusion.** RRM2 expression was downregulated in myocardial tissue with I/R. After overexpression of RRM2, cardiomyocyte proliferation was upregulated and the Hippo-YAP signaling pathway was activated.

1. Introduction

With the improvement of the national economy and the aging of the population, the number of patients suffering from cardiovascular diseases (CVD) in China is also increasing year by year. Acute myocardial infarction (AMI) has always been one of the diseases with high mortality and prevalence in CVD, and it has been increasing year by year [1, 2]. In recent years, with the development of interventional and thrombolytic therapy, the blood vessels of AMI have been opened in an early and timely manner, which has obviously reduced the mortality rate of AMI. However, cell metabolism dysfunction and structural damage will occur after myocardial I/R [3]. The nonrenewable nature of myocardial cells

leads to the recognition, phagocytosis and elimination of necrotic cardiomyocytes in the ischemic area by the immune system, and their replacement by collagen tissue, while the myocardial structure, function, and morphology in the non-ischemic area are remodeled and eventually develop into heart failure. Apoptosis of myocardial cells in nonischemic areas, hypertrophy, and fibrosis of myocardial tissues leads to pathological remodeling of ischemia-related tissues and myocardial dysfunction [4, 5]. Therefore, how to reduce myocardial reperfusion injury and promote myocardial cell proliferation has always been the focus of cardiovascular clinicians.

Ribonucleotide reductase (RR) was first discovered in tumors. It is a specialized enzyme that catalyzes the

deoxygenation of nucleosides to dNTPs, and dNTPs are important raw materials for DNA damage repair and replication. More and more studies have suggested that the large and small subunits of RR are separated from each other in the resting state of cells, and only their specific combination with each other can perform the RR function [6]. At present, RR has been proven to regulate the proliferation and migration of tumor cells in many studies [7, 8], but there are not many studies on it in the heart. Regnier M's study found that the heart-specific overexpression of RRM2 can enhance myocardial contractility and flaccidity [9, 10]. So whether RRM2 has a similar effect in I/R, it is worth exploring.

Previous studies have proved that the Hippo-YAP signaling pathway is a crucial pathway for myocardial regeneration. Hippo cascade kinase inhibits cell proliferation and organ growth by inhibiting YAP through phosphorylation. As a transcriptional coactivator, YAP's proliferation and oncogenic activity are driven by the association of its transcription factor TEAD family, which upregulates genes that promote cell growth and inhibit cell apoptosis. When the Hippo-YAP pathway is activated, YAP is phosphorylated by serine residues and sequestered in the cytoplasm. When the Hippo pathway is not activated, YAP enters the nucleus and regulates gene expression [11, 12]. Therefore, we speculated that RRM2 can participate in the regulation of cardiomyocyte proliferation through the Hippo-YAP signaling pathway.

2. Methods

2.1. Experimental Animal. Specific-pathogen-free (SPF) grade healthy Sprague Dawley (SD) rats, clean grade healthy SD newborn rats, were provided by the animal center of Fujian Provincial Hospital. The experimental design and surgical operation engineering strictly abide by the relevant regulations of the Chinese Laboratory Animal Management Regulations. The breeding room was kept at a constant temperature of $22 \pm 2^\circ\text{C}$, with alternating light and dark cycles for 12 hours. This study was approved by the Animal Ethics Committee of Fujian Provincial Hospital.

2.2. Construction of Rat I/RI Model. According to reports in the literature, a rat I/RI model was constructed using reversible left anterior descending coronary artery ligation. Before the operation, the rats were fasted and water for 12 hours. The next day, the rats were anesthetized by intraperitoneal injection of 2% sodium pentobarbital (2 mL/100 g). After anesthesia, they were fixed on the dissection table, and the trachea was intubated. Then, connect the small animal ventilator and connect the ECG record to observe the ST segment changes. Later, a thoracotomy was performed. After iodophor disinfection, an incision was made along the 3-4th rib of the left chest wall to expose the heart, and a threading ligation was performed at the left atrial appendage 2-3 mm (the sham operation group only performed threading but not ligation). The sign of successful I/RI construction was obvious cyanosis of the myocardial wall and ST-segment elevation in more than two leads of the ECG. After 30

minutes of ischemia, the ligature was cut and the model was successfully constructed after 2 hours of reperfusion.

2.3. RRM2-RNA Adenovirus Treatment. The adenovirus (Ad) RRM2 vector and the empty vector were synthesized by Shanghai Jikai Gene Chemical Company (Shanghai, China). 1 mL of the packaged adenovirus was added to normal saline to dissolve and mix, and an Ad mixture with a final volume of $200 \mu\text{L}/\text{mL}$ was prepared. During the construction of the rat I/RI model, the rats in the Ad-RRM2 group were injected with 0.5 mL of the mixture, and the rats in the empty vector group were injected with an equal volume of the Ad empty vector mixture.

2.4. Cardiac Function Detection. The MAC 1200ST ECG analyzer and GE Logic E9 echocardiography instrument were used to detect cardiac function in rats. The rats were anesthetized by intra-abdominal injection of 2% sodium pentobarbital, then the rats were fixed on the table supine for chest depilation, and then echocardiography was performed to obtain indexes such as left ventricular end diastolic diameter (LVEDD), left ventricular end systolic diameter (LVESD), left ventricular ejection fraction (LVEF%), and left ventricular fractional shortening (LVFS%).

2.5. Tissue Specimen Collection. The blood and heart of each rat were collected immediately after the cardiac function test was completed. For blood collection, blood was drawn from the abdominal aorta with a 10 mL syringe and then divided into 1.5 mL centrifuge tubes after collection. After 4000 r/min centrifugation, the serum was collected and placed in a low-temperature refrigerator for storage. Then, the heart tissue was taken out, half of the heart was transected and placed in the 4% paraformaldehyde, and the rest of the heart tissue was placed in a low temperature refrigerator for later use.

2.6. Detection of Serum Lactate Dehydrogenase (LDH) and Creatine Kinase MB (CK-MB). The determination of serum myocardial enzyme indexes CK-MB and LDH was carried out strictly in accordance with the instructions provided by the kits (Rongjin, Shenzhen, China), and the content of CK-MB and LDH was measured by a spectrophotometer (Life Technology, Wuhan, China).

2.7. H&E Staining. After the myocardial tissue was fixed with tissue fixative for 24-72 hours, it was removed from the fixative and washed with running water for 1 hour. According to the method reported in the literature, the heart tissue was sliced, and the H&E kit (Jiancheng, Nanjing, China) was used for staining. After mounting with neutral resin, the image was observed under a microscope (Thermo Fisher Scientific, Waltham, MA, USA).

2.8. Primary Cardiomyocyte Extraction. 30 newborn SD rats were taken and soaked them in 75% ethanol for about 1 minute. After removal, the heart was quickly removed from the ultraclean workbench and placed in a petri dish filled with D-Hank solution (Thermo Fisher Scientific, Waltham,

MA, USA). The heart was washed in D-Hank solution for 2-3 times and cut off the excess tissue, then transferred to a penicillin bottle and cut it into pieces, about 1 mm³ in size. An appropriate amount of D-Hank solution was used to wash away the remaining blood, and the supernatant was discarded after standing. Then, the tissue block was transferred to a 15 mL centrifuge tube, an appropriate amount of mixed enzymes was added into the tube at the same time, and the tube was placed in a 37°C water bath for 15 minutes. After the digestion was over, the centrifuge tube was taken out, the supernatant was discarded, an appropriate amount of complete medium was added and pipetted to mix, and then, the supernatant was transferred to a clean centrifuge tube. D-Hank solution was used to pipette the cells, and the supernatant was discarded after standing. The supernatant obtained after 3 digestions was filtered with a 200-mesh cell sieve, and the filtered supernatant was placed in a petri dish in a 5% CO₂ 37°C incubator for differential adherence culture for 1.5 hours. After incubation, the culture dish was taken out, and the supernatant was transferred to the culture flask. Brdu solution (Thermo Fisher Scientific, Waltham, MA, USA) with a final concentration of 0.1 mmol/L was added to inhibit the growth of fibroblasts and then placed in an incubator, and the first medium change was performed after 24 hours.

2.9. Cell Transfection and Processing. Cardiomyocytes were seeded in a 12-well plate (5×10^5 cells/well) and transfected after the cells adhered to the wall. Ad-NC and Ad-RRM2 were transfected for 8 hours. The model group cells were cultured in a hypoxic box for 2 hours, 4 hours, 6 hours, and 8 hours and then reoxygenated for 3 hours. The control group cells were cultured in a normal incubator.

2.10. Cell Counting Kit-8 Assay. Cardiomyocytes of each group were seeded in 96-well plates at a density of 2×10^3 cells per well, and the cardiomyocytes were treated with hypoxia and reoxygenation according to the above operation. The CCK-8 kit (Ye Sen, Shanghai, China) was used to evaluate cell proliferation at each time point.

2.11. Immunofluorescence. Cardiomyocytes were seeded on slides at 5×10^5 cells/well. After treatment, cardiomyocytes in each group were fixed with 4% paraformaldehyde. Phosphate-buffered saline (PBS) was used to wash the slides, 0.2% Triton X-100 (Jian Cheng, Nanjing, China) was used to permeate the cell membrane for 10 minutes, and then, PBS was used to wash the cardiomyocytes. Next, goat serum was used for blocking for 30 minutes. Primary antibody Ki67 (Abcam, Cambridge, MA, USA, Rabbit, 1:1000) was added and incubated overnight at 4°C. The next day, PBS was used to wash the slides. FITC-labeled secondary antibody was incubated at 37°C in the dark for 2 hours. After washing with PBS, 4',6-diamidino-2-phenylindole (DAPI) dye solution (Thermo Fisher Scientific, Waltham, MA, USA) was used to stain the nuclei for 10 minutes. Next, glycerin was used to mount the slide, and the slide was placed under a fluorescent microscope to observe and take pictures.

2.12. EdU Staining. The transfected cardiomyocytes and control cells were cultured overnight with EdU reagent (Ye Sen, Shanghai, China). The next day, the proliferating cells were labeled with EdU DNA cell proliferation reagent. Randomly count EdU positive rate from 5 areas = EdU-positive nucleus/DAPI-positive nucleus.

2.13. Western Bolt. The total protein extraction kit was used to extract the total protein of cardiomyocytes. The bicinchoninic acid (BCA) protein quantification kit (Pierce, Rockford, IL, USA) was used to quantify the protein; then 10% sodium dodecyl sulphate-polyacrylamide gel electrophoresis (SDS-PAGE) electrophoresis were carried out and transferred the protein to a polyvinylidene fluoride (PVDF) membrane (Roche, Basel, Switzerland), the membrane in 5% skim milk at room temperature for 30 minutes was blocked, and then it was incubated with primary antibody (YAP, Abcam, Cambridge, MA, USA, Rabbit, 1:2000; p-YAP, Abcam, Cambridge, MA, USA, Mouse, 1:2000; GAPDH, Abcam, Cambridge, MA, USA, Rabbit, 1:5000) at 4°C overnight. Then, horseradish peroxidase-labeled secondary antibody was incubated at room temperature for 2 hours at room temperature. After incubation with enhanced chemiluminescence (ECL, Elabscience, Wuhan, China) solution, it was developed on the chemiluminescence imaging system. ImageJ software was used to analyze protein bands.

2.14. Total RNA Extraction and Quantitative Real-Time Polymerase Chain Reaction. TRIzol reagent (Thermo Fisher Scientific, Waltham, MA, USA) was used to extract total RNA from rat myocardial tissue and primary myocardial cells. The RNA extracted by reverse transcription using PrimeScript RT reagent kit (Thermo Fisher Scientific, Waltham, MA, USA) was cDNA, and qRT-PCR was performed using TaqMan microRNA Assay Kit (Thermo Fisher Scientific, Waltham, MA, USA). The total reaction volume was 20 μ L. SYBR Premix Ex Taq was used to perform qRT-PCR analysis on ABI Prism fast 7500 fluorescent quantitative PCR instrument, with GAPDH as the internal reference gene. The PCR reaction conditions were as follows: predenaturation at 95°C for 3 minutes, denaturation at 95°C for 30 seconds, annealing at 60°C for 30 seconds, extension at 72°C for 30 seconds, 30 cycles, and extension at 72°C for 5 minutes. The $2^{-\Delta\Delta CT}$ method was used to calculate the relative expression level. The primer sequence of the target gene after reverse transcription is shown in Table 1.

2.15. Statistical Analysis. Statistical Product and Service Solutions (SPSS) 20.0 statistical software (IBM, Armonk, NY, USA) were used for processing, measurement data were expressed as the mean \pm standard deviation ($\bar{X} \pm SD$), a variance test was used for comparison between groups, a *t*-test was used for comparison between two groups, and *P* < 0.05 means the difference was statistically significant.

3. Results

3.1. Cardiac I/R Causes Changes in Cardiac Function and Structure. On the first day after the establishment of the rat I/R model, the pathological staining of cardiac tissue

TABLE 1: Primer sequences of quantitative reverse transcription-polymerase chain reaction.

Oligo name		Sequence (5'-3')
RRM2 (rat)	Forward	TGGCTGACAAGGAGAACACG
	Reverse	AGGCGCTTTACTTTCCAGCTC
Cyclin D1 (rat)	Forward	GCGTACCCTGACACCAATCTC
	Reverse	CTCCTCTTCGCACTTCTGCTC
GAPDH (rat)	Forward	CAACTCCCTCAAGATTGTCAGCAA
	Reverse	GGCATGGACTGTGGTCATGA

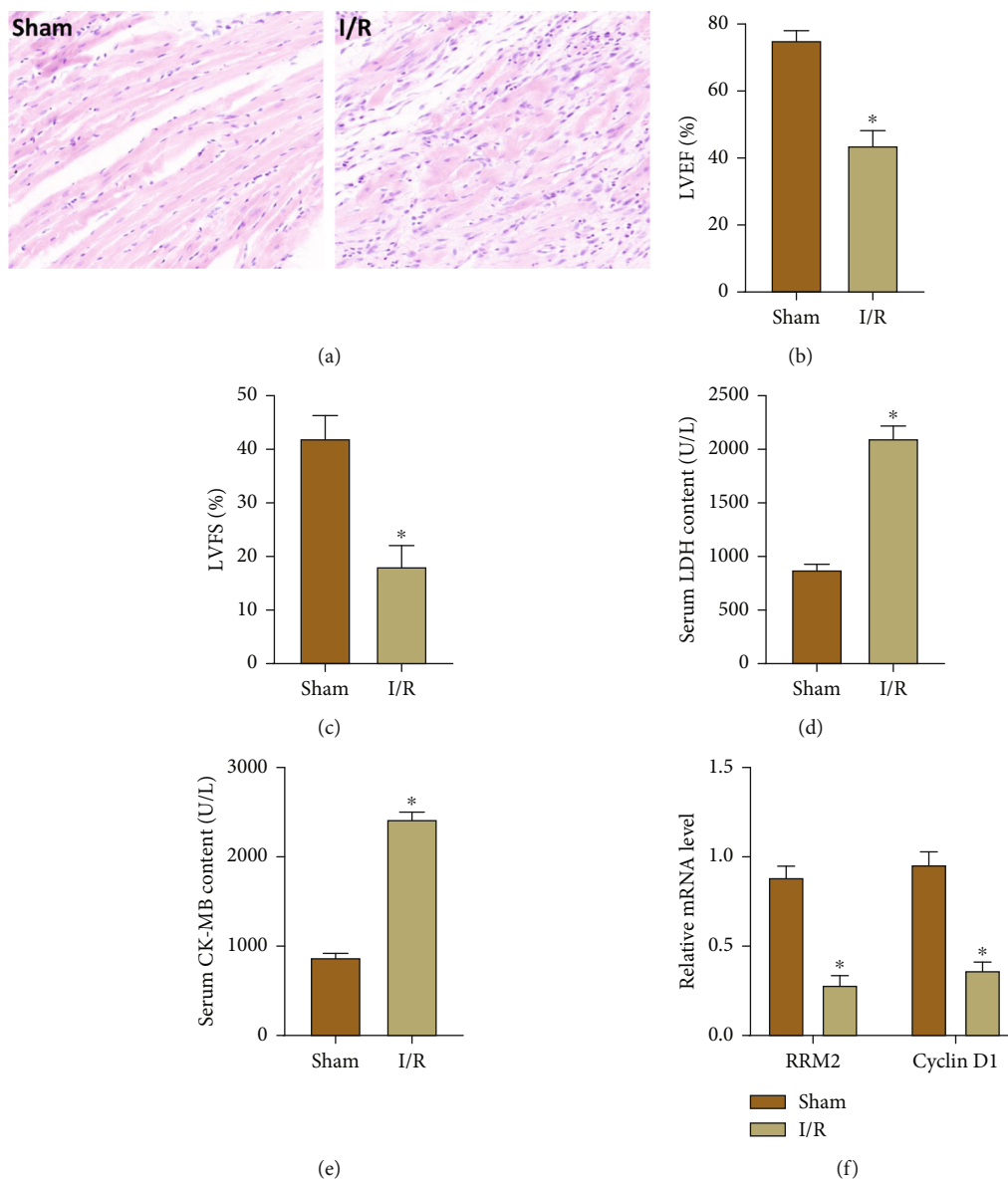


FIGURE 1: Cardiac I/R causes changes in cardiac function and structure. (a) The structural changes of heart were observed by H&E staining. (b, c) The cardiac function changes of heart were observed by echocardiography. (d, e) The serum levels of CK-MB and LDH were measured in two groups of rats. (f) The mRNA levels of RRM2 and Cyclin D1 in myocardial tissue were detected by qRT-PCR. * $P < 0.05$ vs. the Sham group.

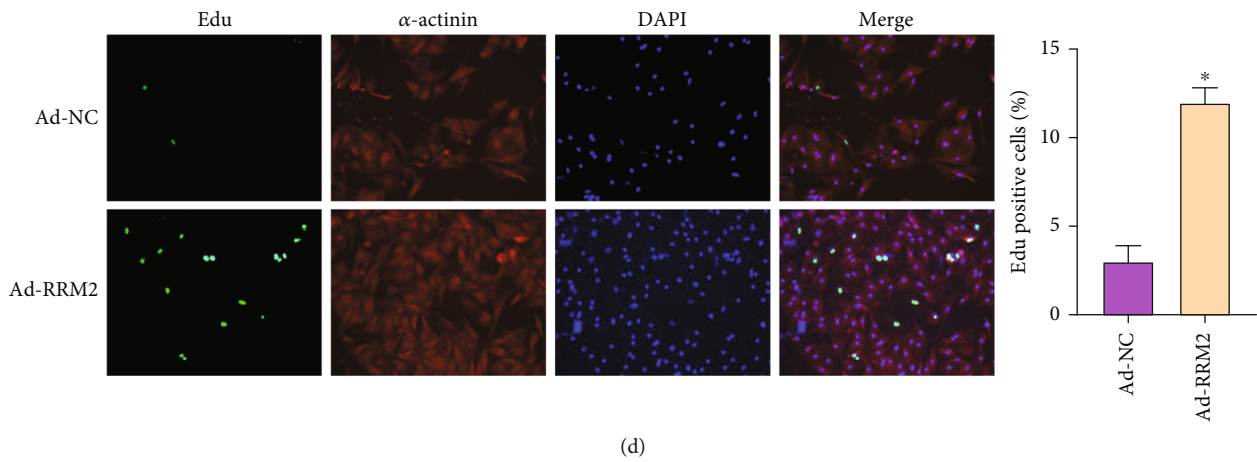
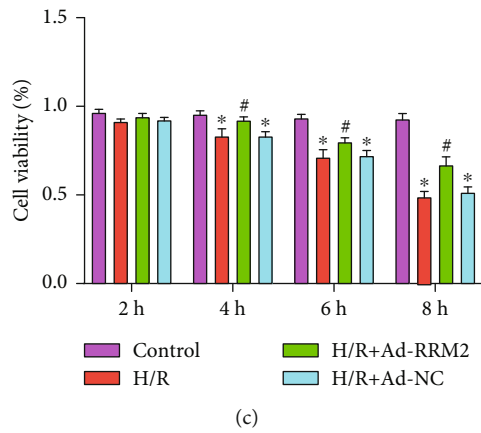
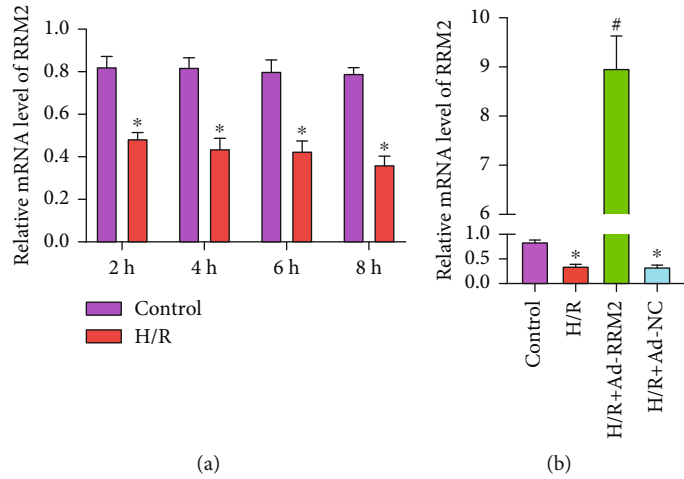
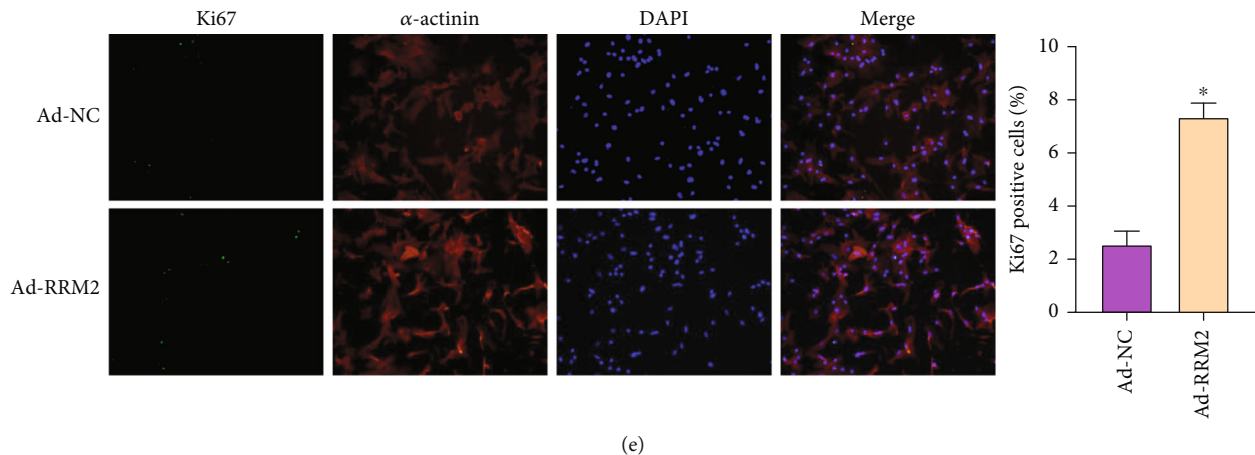


FIGURE 2: Continued.



(e)

FIGURE 2: Overexpression of RRM2 in cardiomyocytes in vitro can inhibit the reduction of proliferation induced by H/R. (a) The mRNA levels of RRM2 were detected in cardiomyocytes after 2, 4, 6, and 8 h hypoxia. $*P < 0.05$ vs. the Control group. (b) qRT-PCR was used to detect transfection efficiency. (c) The cell activity of four groups was measured by CCK-8 assay. $*P < 0.05$ vs. the Control group; $*P < 0.05$ vs. the H/R+Ad-NC group. (d) EdU immunofluorescence staining was used to detect cell proliferation and quantitative analysis. (e) Ki67 immunofluorescence staining was used to detect cell proliferation and quantitative analysis. $*P < 0.05$ vs. the Ad-NC group.

showed that the myocardial tissue structure of the I/R group was obviously disordered; the myocardium was broken (Figure 1(a)). At the same time, echocardiography was used to detect the cardiac function of each group of rats; the results showed that the LVEF% and LVFS% of rats in the I/R group were obviously reduced (Figures 1(b) and 1(c)). However, the heart function of rats in the sham group was normal, and the pathological staining of the heart tissue also showed a normal structure. Next, the serum LDH and CK-MB levels were detected within 24 hours after blood collection (Figures 1(d) and 1(e)). The results showed that the LDH and CK-MB levels were in the normal range in the sham group, while the I/R group LDH and CK-MB levels were obviously higher. Subsequently, we used qRT-PCR technology to detect the expression of RRM2 and Cyclin D1 from the collected heart tissue (Figure 1(f)). The results showed that the expression of RRM2 and Cyclin D1 was inhibited in the I/R group, compared with the sham group.

3.2. Overexpression of RRM2 in Cardiomyocytes In Vitro Can Inhibit the Reduction of Proliferation Induced by H/R. In order to explore the expression of RRM2 on the H/R cardiomyocyte model, the cardiomyocytes were hypoxia for 2, 4, 6, and 8 hours and then reoxygenation for 3 hours. qRT-PCR was used to evaluate the expression of RRM2 (Figure 2(a)). The results showed that the expression of RRM2 decreased obviously after H/R treatment, and the expression of RRM2 in the myocardium after H/R was time-dependent. In order to further explore the function of RRM2 in cardiomyocyte H/R, overexpression of RRM2 was used to detect its role in cell proliferation. qRT-PCR was used to evaluate the transfection efficiency (Figure 2(b)). At the same time, CCK-8 assay detected the cell viability of 4 groups, and the results showed that cardiomyocyte overexpression of RRM2 can obviously inhibit the reduction of cell viability induced by H/R (Figure 2(c)). Then, EdU and Ki67 immunofluores-

cence staining were used to assess the proliferation level of cardiomyocyte (Figures 2(d) and 2(e)). The staining results showed that the number of EdU- and Ki67-positive cells in Ad-RRM2 group was significantly increased compared with that in Ad-NC group.

3.3. Overexpression of RRM2 in Cardiomyocytes In Vivo Can Inhibit the Reduction of Proliferation Induced by I/R. After the SD rat I/R model was constructed, adenovirus was injected from the pericardium. The control group was injected with Ad-NC, and the model group was injected with Ad-RRM2. One day later, we detected the expression of RRM2 in the heart of rats. qRT-PCR detection found that the expression of RRM2 in the heart of the I/R+Ad-RRM2 group was obviously increased (Figure 3(a)). At the same time, H&E staining showed that overexpression of RRM2 can alleviate myocardial tissue structural disorder, myocardial rupture, and inflammatory factor infiltration caused by I/R (Figure 3(b)). And the results of echocardiography showed that the LVEF% and LVFS% of rats in the I/R+Ad-RRM2 group were improved (Figures 3(c) and 3(d)). The levels of LDH and CK-MB in rat serum also showed a significant decrease in the I/R+Ad-RRM2 group (Figures 3(e) and 3(f)). In addition, the qRT-PCR detection of Cyclin D1 expression found that, compared with that in the I/R+Ad-NC group, the expression of Cyclin D1 in the myocardial tissue of the I/R+Ad-RRM2 group increased (Figure 3(g)).

3.4. RRM2 Promotes Cardiomyocyte Proliferation through the Hippo-YAP Pathway. Primary cardiomyocytes were randomly divided into two groups, one of which was the H/R+Ad-NC group and the other was the H/R+Ad-RRM2 group. WB detection found that the expression of YAP in the H/R+Ad-RRM2 group was obviously increased, while the phosphorylation of YAP was reduced (Figures 4(a) and

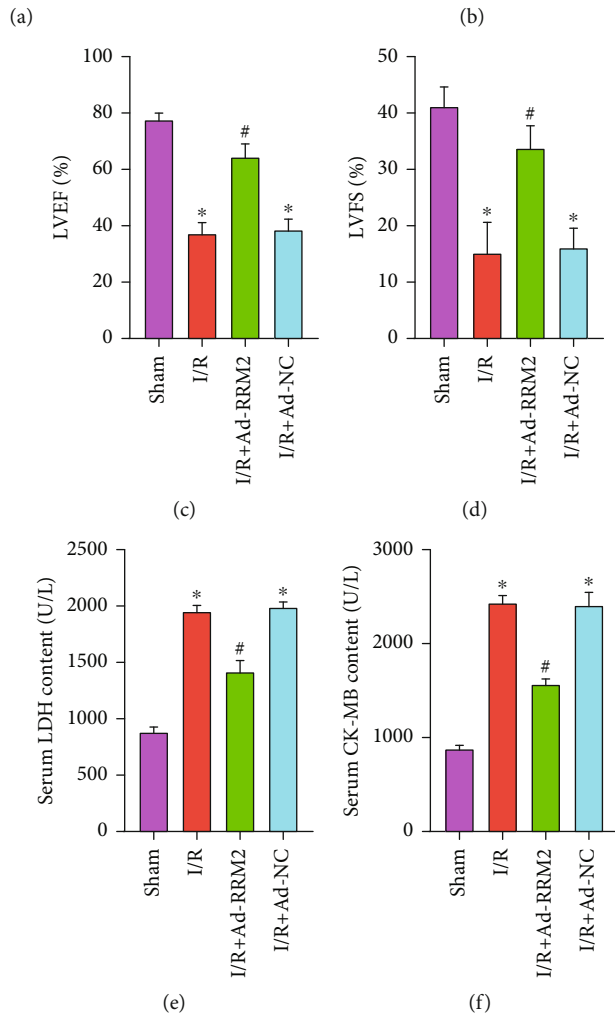
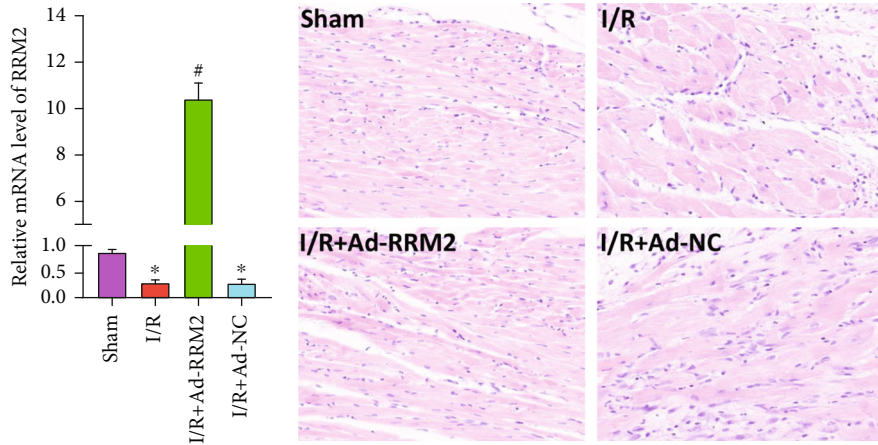


FIGURE 3: Continued.

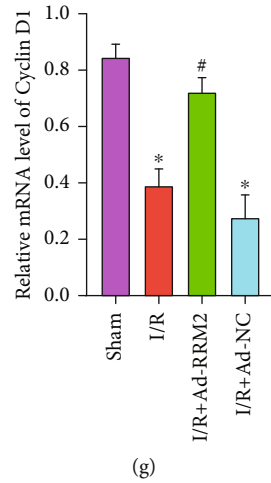


FIGURE 3: Overexpression of RRM2 in cardiomyocytes in vivo can inhibit the reduction of proliferation induced by I/R. (a) qRT-PCR was used to detect transfection efficiency. (b) The structural changes of heart were observed by H&E staining. (c, d) The cardiac function changes of heart were observed by echocardiography. (e, f) The serum levels of CK-MB and LDH were measured in four groups of rats. (g) The mRNA levels of Cyclin D1 in myocardial tissue were detected by qRT-PCR. * $P < 0.05$ vs. the Sham group; # $P < 0.05$ vs. the I/R+Ad-NC group.

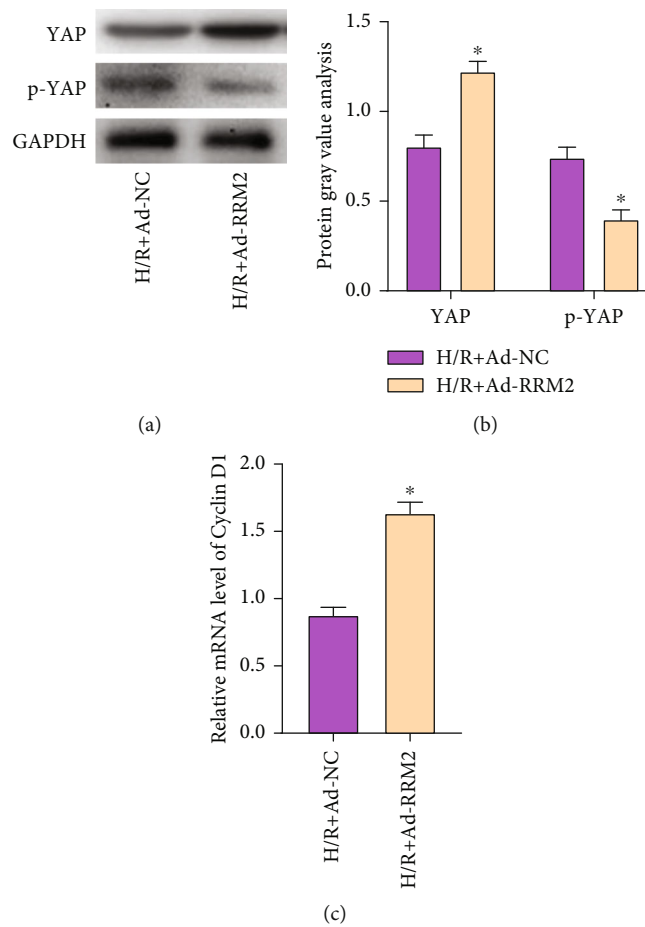


FIGURE 4: RRM2 promotes cardiomyocyte proliferation through the Hippo-YAP pathway. (a) The protein expression level of YAP and p-YAP was detected by WB. (b) Protein gray value analysis. (c) The mRNA levels of Cyclin D1 in cardiomyocyte were detected by qRT-PCR. * $P < 0.05$ vs. the H/R+Ad-NC group.

4(b)). Subsequently, qRT-PCR detection of Cyclin D1 expression found that the Cyclin D1 expression in the H/R +Ad-RRM2 group was obviously higher than that in the H/R+Ad-NC group (Figure 4(c)).

4. Discussion

CVD has become the leading cause of death worldwide, and its damage to human health and economy is unmatched by other diseases [13]. Studies have shown that myocardial I/RI may lead to myocardial ischemic necrosis [14, 15]. In addition, I/RI are also common in CVD systems and patients undergoing cardiopulmonary bypass and cardiac surgery transplantation [16]. Therefore, seeking new treatment methods to improve the I/RI prognosis of patients with AMI and cardiopulmonary bypass and to avoid or reduce myocardial damage caused by organ or tissue I/RI has become a top priority for clinicians.

Studies have confirmed that the cardiomyocyte H/R model can be used as an effective method to simulate myocardial I/RI in the cardiomyocyte culture model [17]. And the duration of hypoxia is a crucial factor for the success of the H/R model. In order to determine the appropriate hypoxia time, we choose hypoxia for 2, 4, 6, and 8 hours, followed by reoxygenation for 3 hours. Cell viability decreases with the time of hypoxia. The results showed that we successfully constructed an in vitro H/R model of cardiomyocytes.

There are relatively few studies on RRM2 in the cardiovascular field. The traditional view is that RRM2 is mainly involved in the S-phase DNA synthesis process and is strictly regulated by the cell cycle [18]. Regnier M's research pointed out that RRM2 is expressed in the heart, and overexpression of RRM2 can effectively improve the cardiac function of mice after MI. Combining the two, we speculated that RRM2 also has a similar mechanism for cardiac ischemic diseases.

This study confirmed that the expression of RRM2 decreased in the myocardium of I/RI model. At the same time, LDH and CK-MB induced by I/RI are released in large quantities, inhibiting cell proliferation. Overexpression of RRM2 can obviously inhibit the levels of LDH and CK-MB in serum and promote the increase of Cyclin D1 expression. Cyclin D is a member of the cyclin family and is involved in the regulation of the cell cycle process. The synthesis of Cyclin D starts in the G1 phase and drives the G1/S transition [19]. In order to observe the effect of RRM2 on the proliferation of cardiomyocytes, we selected primary cardiomyocytes as the research object to observe their proliferation after the expression of RRM2 increased. Then, we found that the expression of RRM2 in the cardiomyocyte of H/R model also decreased. And overexpression of RRM2 can increase cell viability and promote proliferation. The results of immunofluorescence staining showed that after the expression of RRM2 increased, the proportion of Ki67 in the nucleus of cardiomyocytes increased, and the proportion of EdU also increased obviously. Ki67 is a relatively positive nuclear proliferation marker [20]. It is only expressed during the proliferation phase and is closely

related to cell division. It maintains the stability of the DNA structure during cell mitosis and indicates the number of cells entering the division phase. EdU is a thymidine analogue, which can be incorporated into the replicating DNA molecule during cell proliferation. By detecting the EdU label, the DNA replication activity can be detected and accurately reflect the cell proliferation. In our study, both results indicated that overexpression of RRM2 in vitro can promote the proliferation of cardiomyocytes after H/R.

Besides, we found that RRM2 can regulate the proliferation of cardiomyocytes by influencing Hippo-YAP signal and the expression of cell cycle-related factors. The Hippo pathway and its downstream transcriptional coactivator YAP regulate organ growth and cell plasticity during animal development and regeneration. Activation of YAP in mice can promote the regeneration of adult hearts with poor regenerative capacity [21]. In mammals, the core of the Hippo pathway is cascade kinase, including LATS1 and MST1. LATS1 can bind and phosphorylate the transcription regulatory factor YAP in vitro and in vivo. At the same time, LATS1, after phosphorylation of YAP, inhibits its transcriptional regulation of cell genes by fixing YAP in the cytoplasm [22]. And we found in in vitro experiments that overexpression of RRM2 can obviously increase the expression of YAP protein, inhibit its phosphorylation expression, and promote the increase of Cyclin D1 mRNA expression. Therefore, the above results all suggested that RRM2 can be used as a potential target for the treatment of myocardial I/RI.

5. Conclusion

The expression of RRM2 was downregulated in the ischemia-reperfusion injury model. Overexpression of RRM2 in cardiomyocytes can promote cell proliferation, and this may be related to the activation of the Hippo-YAP pathway. This will also provide a new therapeutic target for the treatment of myocardial ischemia-reperfusion injury.

Data Availability

The datasets used and analyzed during the current study are available from the corresponding author on reasonable request.

Conflicts of Interest

The authors declare that they have no competing interests.

Authors' Contributions

Huamin Yu and Haiyan Tang contributed equally to this work.

Acknowledgments

This study was supported by Nature Fund of Fujian Province (2018J01237, project name: Effects of Apelin and its receptor on the expression of inflammatory factors in rat

hypertrophic cardiomyocytes through mTOR signaling pathway).

References

- [1] M. A. Fares, "Introduction: challenges and advances in cardiovascular disease," *Cleveland Clinic Journal of Medicine*, vol. 84, 12 Supplement 3, p. 11, 2017.
- [2] N. Kazemian, M. Mahmoudi, F. Halperin, J. C. Wu, and S. Pakpour, "Gut microbiota and cardiovascular disease: opportunities and challenges," *Microbiome*, vol. 8, no. 1, p. 36, 2020.
- [3] Z. Yang, L. Zhang, J. Gao et al., "Giant coronary artery fistula complicated with coronary artery aneurysm and acute myocardial infarction: a case report," *BMC Cardiovascular Disorders*, vol. 20, no. 1, p. 136, 2020.
- [4] S. H. Lim, J. Lee, and M. J. Han, "Comprehensive analysis of the cardiac proteome in a rat model of myocardial ischemia-reperfusion using a TMT-based quantitative proteomic strategy," *Proteome Science*, vol. 18, no. 1, 2020.
- [5] H. Zhou, B. Hu, and X. Liu, "Thyroid hormone metabolite 3-iodothyronamine (T1AM) alleviates hypoxia/reoxygenation-induced cardiac myocyte apoptosis via Akt/FoxO1 pathway," *Medical Science Monitor*, vol. 26, article e923195, 2020.
- [6] A. L. Chabes, C. M. Pflieger, M. W. Kirschner, and L. Thelander, "Mouse ribonucleotide reductase R2 protein: a new target for anaphase-promoting complex-Cdh1-mediated proteolysis," *Proceedings of the National Academy of Sciences of the United States of America*, vol. 100, no. 7, pp. 3925–3929, 2003.
- [7] V. K. Grolmusz, K. Karácsi, T. Micsik et al., "Cell cycle dependent RRM2 may serve as proliferation marker and pharmaceutical target in adrenocortical cancer," *American Journal of Cancer Research*, vol. 6, no. 9, pp. 2041–2053, 2016.
- [8] N. Huang, W. Guo, K. Ren et al., "LncRNA AFAP1-AS1 suppresses miR-139-5p and promotes cell proliferation and chemotherapy resistance of non-small cell lung cancer by competitively upregulating RRM2," *Frontiers in Oncology*, vol. 9, p. 1103, 2019.
- [9] F. S. Korte, J. Dai, K. Buckley et al., "Upregulation of cardiomyocyte ribonucleotide reductase increases intracellular 2 deoxy-ATP, contractility, and relaxation," *Journal of Molecular and Cellular Cardiology*, vol. 51, no. 6, pp. 894–901, 2011.
- [10] S. J. Kolwicz, G. L. Odom, S. G. Nowakowski et al., "AAV6-mediated cardiac-specific overexpression of ribonucleotide reductase enhances myocardial contractility," *Molecular Therapy*, vol. 24, no. 2, pp. 240–250, 2016.
- [11] M. Ponnusamy, P. F. Li, and K. Wang, "Understanding cardiomyocyte proliferation: an insight into cell cycle activity," *Cellular and Molecular Life Sciences*, vol. 74, no. 6, pp. 1019–1034, 2017.
- [12] Y. Zheng and D. Pan, "The hippo signaling pathway in development and disease," *Developmental Cell*, vol. 50, no. 3, pp. 264–282, 2019.
- [13] A. G. Thrift, G. Howard, D. A. Cadilhac et al., "Global stroke statistics: an update of mortality data from countries using a broad code of "cerebrovascular diseases"," *International Journal of Stroke*, vol. 12, no. 8, pp. 796–801, 2017.
- [14] S. F. Yang and P. H. Huang, "Mir-25 is a potential treatment target for myocardial ischemic-reperfusion injury," *Journal of the Chinese Medical Association*, vol. 83, no. 5, pp. 419–420, 2020.
- [15] M. Neri, I. Riezzo, N. Pascale, C. Pomara, and E. Turillazzi, "Ischemia/reperfusion injury following acute myocardial infarction: a critical issue for clinicians and forensic pathologists," *Mediators of Inflammation*, vol. 2017, Article ID 7018393, 2017.
- [16] L. Zhou, G. Zang, G. Zhang et al., "MicroRNA and mRNA signatures in ischemia reperfusion injury in heart transplantation," *PLoS One*, vol. 8, no. 11, article e79805, 2013.
- [17] M. Dou, Z. Ma, X. Cheng et al., "Intrathecal lentivirus-mediated RNA interference targeting nerve growth factor attenuates myocardial ischaemia-reperfusion injury in rat," *British Journal of Anaesthesia*, vol. 123, no. 4, pp. 439–449, 2019.
- [18] C. W. Chen, Y. Li, S. Hu et al., "DHS (_trans_ -4,4'-dihydroxystilbene) suppresses DNA replication and tumor growth by inhibiting RRM2 (ribonucleotide reductase regulatory subunit M2)," *Oncogene*, vol. 38, no. 13, pp. 2364–2379, 2019.
- [19] T. Mohamed, Y. S. Ang, E. Radzinsky et al., "Regulation of cell cycle to stimulate adult cardiomyocyte proliferation and cardiac regeneration," *Cell*, vol. 173, no. 1, pp. 104–116.e12, 2018.
- [20] J. Bullwinkel, B. Baron-Luhr, A. Ludemann, C. Wohlenberg, J. Gerdes, and T. Scholzen, "Ki-67 protein is associated with ribosomal RNA transcription in quiescent and proliferating cells," *Journal of Cellular Physiology*, vol. 206, no. 3, pp. 624–635, 2006.
- [21] Y. Morikawa, T. Heallen, J. Leach, Y. Xiao, and J. F. Martin, "Dystrophin-glycoprotein complex sequesters Yap to inhibit cardiomyocyte proliferation," *Nature*, vol. 547, no. 7662, pp. 227–231, 2017.
- [22] N. Furth and Y. Aylon, "The LATS1 and LATS2 tumor suppressors: beyond the hippo pathway," *Cell Death and Differentiation*, vol. 24, no. 9, pp. 1488–1501, 2017.

Research Article

FOXC2 Alleviates Myocardial Ischemia-Reperfusion Injury in Rats through Regulating Nrf2/HO-1 Signaling Pathway

Rui Wang , Yonggang Wu, and Shoutao Jiang

Department of Cardiology, Guangzhou Hospital of Integrated Chinese and Western Medicine, Guangzhou, China

Correspondence should be addressed to Rui Wang; 1812170199@e.gzhu.edu.cn

Received 15 October 2021; Accepted 12 November 2021; Published 23 November 2021

Academic Editor: Simona Pichini

Copyright © 2021 Rui Wang et al. This is an open access article distributed under the Creative Commons Attribution License, which permits unrestricted use, distribution, and reproduction in any medium, provided the original work is properly cited.

Objective. Myocardial ischemia-reperfusion injury (MIRI) is the leading cause of death in patients with cardiovascular disease. The purpose of this study is to investigate the effect and mechanism of forkhead box C2 (FOXC2) on MIRI in rats. **Methods.** We made ischemia-reperfusion (I/R) models for rats by performing I/R surgery. After 3 hours, 3 days, and 7 days of reperfusion, we detected the structure and function of rat myocardium by 2, 3, 5-triphenyl tetrazolium chloride staining, echocardiography, lactate dehydrogenase kit, and haematoxylin-eosin staining. The change of FOXC2 expression in myocardial tissue was also detected. Then, we increased the expression of FOXC2 in rats by adenovirus transfection to clarify the effect of FOXC2 on changes of oxidative stress and inflammation of rat myocardium. In addition, we detected the effect of FOXC2 overexpression plasmid on the function of H9c2 cells *in vitro*. The expression changes of Nrf2/HO-1 in myocardial cells were also detected to clarify the mechanism of action of FOXC2. **Results.** The expression of FOXC2 in I/R rats was significantly lower than that in the sham group. After overexpressing FOXC2 in I/R rats, we found that the expression of SOD1/2 of rat myocardium and inflammatory factors in the serum were significantly reduced. Overexpression of FOXC2 also increased the viability and antioxidant capacity of H9c2 cells. In addition, FOXC2 was found to increase the activity of the Nrf2/HO-1 signaling pathway in myocardial cells, and the inhibition of Nrf2/HO-1 signaling pathway attenuated the protective effect of FOXC2 on myocardial cells. **Conclusions.** MIRI in rats was accompanied by low expression of FOXC2 in myocardial tissue. Overexpression of FOXC2 reduces the level of inflammation and oxidative stress in myocardial tissue by promoting the Nrf2/HO-1 signaling pathway, thereby alleviating MIRI.

1. Introduction

Acute myocardial infarction is the acute manifestation of coronary heart disease and the main cause of death. Its basic pathological changes include rupture of coronary plaques, thrombosis, and decreased blood supply, which eventually leads to severe ischemia in myocardial tissues [1]. Timely reperfusion therapy, such as drug thrombolysis, percutaneous coronary intervention, and coronary artery bypass grafting treatment, is beneficial to recanalize occlusive vessels as early as possible and reduce infarct size [2]. However, with further research on the process of myocardial ischemia and reperfusion, the researchers found that although reperfusion therapy can make the ischemic heart regain blood perfusion in a short period of time, the reperfusion therapy itself can also lead to severe dysfunction and structural injury [3]. This

phenomenon is called myocardial ischemia-reperfusion injury (MIRI). After myocardial ischemia reperfusion, although the blood supply is restored, the increase in the generation of oxygen free radicals of myocardial cells and the overload of calcium ions during ischemia will initiate the programmed apoptosis of myocardial cells, resulting in structural and functional damage of myocardial cells [4].

Forkhead box C2 (FOXC2) belongs to the forkhead transcription factor family [5]. The role of FOXC2 was first confirmed in lymphedema-distichiasis syndrome. FOXC2 protein is expressed in various tissues such as bone, fat, and tumor and plays an important role in the development of the cardiovascular system, lymphatic system, and axial bone system [6]. A study showed that FOXC2 can regulate angiopoietin-like protein 2, thereby affecting the level of apoptosis and inflammation of macrophages [7]. FOXC2

has also been found to promote bone marrow mesenchymal differentiation by regulating Wnt- β -catenin signaling pathway [8]. In addition, Kume et al. revealed that FOXC1 and FOXC2 are both required for cardiovascular development and somitogenesis [9]. However, the role of FOXC2 in MIRI is still unclear. Therefore, we used rats to make MIRI models to detect changes in FOXC2 expression in myocardial tissue. Then, we studied the effect of FOXC2 on the MIRI of rats by adenovirus transfection.

2. Materials and Methods

2.1. Animals and Grouping. Sixty male Sprague Dawley rats (8-10 weeks, 180-200 g) were used in this study. All rats were provided by Guangzhou Hospital of Integrated Chinese and Western Medicine Animal Center and housed in specific pathogen-free animal rooms. The room temperature of the animal rooms was 22-24°C, and the relative humidity was 50-60%. We used rats to make the ischemia-reperfusion (I/R) model and detected the structure and function of the rat heart after 3 hours, 3 days, and 7 days. This study was approved by the Animal Ethics Committee of Guangzhou Hospital of Integrated Chinese and Western Medicine Animal Center.

2.2. Procedure of Ischemia-Reperfusion (I/R) Model. After anesthetizing the rat with 2% sodium pentobarbital (40 mg/kg), we fixed the rat on the operating table and removed the fur from rat's chest. We cut the skin and trachea of rat's neck and then use the animal ventilator (CWE SAR-830, Orange, CA, USA) to maintain rat's breathing. The ventilator was set to the heart rate of 80-100 times/min, the respiratory rate of 60 times/min, the breathing ratio of 1:1.5, and the tidal volume of 70 mL. Then, we cut the skin of rat's left chest and bluntly separated the muscles. After the heart was exposed, we cut the pericardium and ligated the left anterior descending coronary artery. The cyanosis of the epicardium distal to the ligation site and the ST segment elevation of the electrocardiogram indicated myocardial ischemia. After 30 minutes, we loosened the ligature. Hyperemia of myocardial tissue and the ST segment depression of the electrocardiogram indicated successful myocardial reperfusion [10]. We measured cardiac structure and function at 3 hours, 3 days, and 7 days after reperfusion.

2.3. Adenovirus Transfection. Seven days before making the I/R model, we fixed the rats on the operating table. Then, we wiped the tail vein of the rats with 75% alcohol to fully dilate the tail vein. We used a microsyringe (Molecular Devices, Santa Clara Valley, MD, USA) to inject 20 μ L of purified adenovirus (Genepharma, Shanghai, China), including negative control (NC) adenovirus and FOXC2 overexpressing adenovirus, into the tail vein of rats. Adenovirus was constructed in Genepharma (Genepharma, Shanghai, China) with the titer of 1×10^{11} plaque forming unit.

2.4. 2, 3, 5-Triphenyl Tetrazolium Chloride (TTC) Staining. We collected rat hearts and rinsed them with normal saline. Then, we put the rat hearts in the -20°C refrigerator for

20 minutes. The heart tissue was cut into 5 pieces with the thickness of 2 mm. Then, we put the slices in 1% TTC staining solution (Sigma-Aldrich, St. Louis, MO, USA) for 15 minutes. Finally, we used the camera to take pictures and analyze the results. Normal tissues appeared red, while ischemic tissues appeared pale. Area at risk (AAR) was expressed as the percentage of the left ventricle.

2.5. Echocardiography. We tilted rat's body 30° to the left and placed the ultrasound probe on rat's left chest. Left ventricular ejection fraction (LVEF), left ventricular fractional shortening (LVFS), left ventricular end-diastolic volume (LVEDV), left ventricular end-systolic volume (LVESV), left ventricular end-diastolic diameter (LVEDd), and left ventricular end-systolic diameter (LVESd) were detected.

2.6. Detection of Lactate Dehydrogenase (LDH). We took 2 mL of rat aortic blood and separated the serum. The LDH kit (R&D Systems, Emeryville, CA, USA) was used to detect the LDH level in serum. Matrix buffer and 5 μ L of coenzyme 1 were added to the serum. We placed the mixture in a 37°C incubator for 15 minutes. Then, we added 25 μ L of 2, 4-dinitrophenylhydrazine and continued to incubate for 15 minutes. Finally, we added 250 μ L of 0.4 M NaOH and measured the absorbance of the mixture at 450 nm with a spectrophotometer. The same method was also used to detect LDH level in H9c2 cells.

2.7. Enzyme Linked Immunosorbent Assay (ELISA). We used ELISA kits (R&D Systems, Emeryville, CA, USA) to detect the levels of inflammatory factors, interleukin (IL)-1 β , and tumor necrosis factor (TNF)- α in rat serum. Standards were used to make standard curves. Then, we detected the absorbance of the sample and calculated the concentration of the sample according to the standard curve.

2.8. Haematoxylin-Eosin (HE) Staining. We collected rat hearts and fixed them with 4% paraformaldehyde. Then, we made them into paraffin blocks and used a microtome to cut the paraffin block into paraffin slices. HE staining was used to detect the morphology of rat myocardial tissue. We used xylene for dewaxing and alcohol solution for hydration. Then, we stained the cell nucleus with hematoxylin (Beyotime, Shanghai, China) and stained the cytoplasm with eosin (Beyotime, Shanghai, China). Finally, we used an optical microscope to observe the morphology of myocardial tissue.

2.9. Immunohistochemical (IHC) Staining. We used xylene and alcohol solutions for dewaxing and hydration. Then, we used citrate buffer to repair the antigen. 3% H₂O₂ was used to remove peroxidase. We then used 10% goat serum to block nonspecific antigens. After adding the primary antibody dilution (FOXC2, ab65141; SOD1, ab13498; SOD2, ab13533. Abcam, Cambridge, MA, USA) to myocardial tissue, we placed the slices in a 4°C refrigerator overnight. Then, we used secondary antibody dilution (Abcam, Cambridge, MA, USA) to incubate myocardial tissue and used diaminobenzidine (DAB) for color development.

Finally, we used an optical microscope to observe the staining results.

2.10. Cell Culture. The rat myocardial cell line, H9c2 cells, was used in this study. Dulbecco's modified eagle medium (Gibco, Rockville, MD, USA) containing 10% fetal bovine serum (Gibco, Rockville, MD, USA) and 1% penicillin plus streptomycin (Gibco, Rockville, MD, USA) was used to culture H9c2 cells. H9c2 cells were cultured in an incubator with 37°C and 5% CO₂.

2.11. Procedure of Hypoxia Reoxygenation (H/R) Model. The H/R model was used to simulate rat I/R *in vitro*. After washing the cells with PBS, we added simulated ischemic fluid and placed the cells in an incubator with 95% N₂ and 5% CO₂ for 10 hours. Then, we recultivated the cells under normal conditions for 24 hours.

2.12. RNA Isolation and Quantitative Real-Time Reverse Transcription-Polymerase Chain Reaction (RT-PCR). TRIzol reagent (Invitrogen, Carlsbad, CA, USA) was used to extract total RNA from rat myocardium and H9c2 cells. We used a spectrophotometer to detect the concentration of total RNA. We used the reverse transcription kit (Vazyme, Nanjing, China) to configure the reverse transcription system according to manufacturer's instructions and reversed the mRNA to complementary deoxyribose nucleic acid (cDNA) using a PCR machine. Then, we used SYBE Green Master Mix (Vazyme, Nanjing, China) and primers to amplify the cDNA. Primer sequences were shown in Table 1. The expression level of glyceraldehyde 3-phosphate dehydrogenase (GAPDH) was used as reference. The ratio of the RNA concentration of each group to the sham group or control group was used to represent the relative concentration of RNA ($2^{-\Delta\Delta Ct}$).

2.13. Plasmid Transfection. We seeded H9c2 cells into six-well plates. When the cell growth density reached 30%, we used Lipofectamine 3000 reagent (Sigma-Aldrich, St. Louis, MO, USA) to transfect NC plasmid and FOXC2 overexpression plasmid into H9c2 cells. RT-PCR was used to detect the transfection efficiency.

2.14. Cell Counting Kit-8 (CCK-8) Assay. The CCK-8 assay was used to detect the viability of H9c2 cells. We used 96-well plates to culture H9c2 cells with 5000 cells per well. After treating the cells, we added 10 μ L of CCK-8 reagent (Dojindo Molecular Technologies, Kumamoto, Japan) to each well. After putting the cells into the incubator for 2 hours, we used a microplate reader to detect the absorbance of each well at 450 nm.

2.15. Immunofluorescent (IF) Staining. We used 24-well plates to culture cells. Then, we discarded the medium and fixed the cells with 4% paraformaldehyde. Then, we used 0.2% TritonX-100 to treat the cells for 15 minutes. 10% goat serum was used to block nonspecific antigens. We used primary antibody dilution (SOD1, ab13498; SOD2, ab13533; Nrf2, ab31163; HO-1, ab13248. Abcam, Cambridge, MA, USA) to incubate cells at 4°C overnight and fluorescent sec-

TABLE 1: RT-PCR primers sequences.

Name	Sense/antisense (S/AS)	Sequence(5'-3')
FOXC2	S	CACAGCGGGGACCTGAA
	AS	CAGCCGGTGGGAGTTGA
SOD1	S	CAATGTGGCTGCTGGAA
	AS	TGATGGAATGCTCTCCTGA
SOD2	S	GCCGTGTTCTGAGGAGAG
	AS	GTCGTAAGGCAGGTCAGG
Nrf2	S	ATTCCCAGCCACGTTGAGAG
	AS	TCCTGCCAAACTTGCTCCAT
HO-1	S	CCATCCCTTACACACCAGCC
	AS	GCGAGCACGATAGAGCTGTT
IL-1 β	S	CCCTTGACTTGGGCTGT
	AS	CGAGATGCTGCTGTGAGA
TNF- α	S	CAGCCAGGAGGGAGAAC
	AS	GTATGAGAGGGACGGAACC
GAPDH	S	GTTGTGGCTCTGACATGCT
	AS	CCCAGGATGCCCTTTAGT

ondary antibody dilution (Abcam, Cambridge, MA, USA) to incubate cells at room temperature. After staining the cell nucleus with 4',6-diamidino-2-phenylindole (DAPI), we used a fluorescence microscope to observe the staining results.

2.16. Statistical Analysis. Statistical Product and Service Solutions 20.0 statistical software (IBM, Armonk, NY, USA) was used to analyze the results of this study. All data were represented as mean \pm standard deviation. Differences between two groups were analyzed by using Student's *t*-test. Comparison between multiple groups was done using one-way ANOVA test followed by post hoc test (least significant difference). $P < 0.05$ indicated that the difference was statistically significant. All experiments were repeated 3 times.

3. Results

3.1. Expression of FOXC2 Decreased in Myocardial Tissue after I/R. After making the I/R model for rats, we reperfused them for 3 hours, 3 days, and 7 days and collected the rat heart tissue for TTC staining to observe the changes of rat AAR (Figure 1(a)). After reperfusion, the AAR of rat myocardium increased significantly, and the AAR after 3 days was greater than that after 3 hours. There was no significant difference between AAR after 7 days and AAR after 3 days. In addition, we detected changes in rat cardiac function by echocardiography. After I/R, LVEDV (Figure 1(b)), LVESV (Figure 1(c)), LVEDd (Figure 1(d)), and LVESd (Figure 1(e)) of rats increased significantly, while LVEF (Figure 1(f)) and LVFS (Figure 1(g)) decreased. We also detected the concentration of myocardial injury marker LDH in the serum of rats and found that the concentration

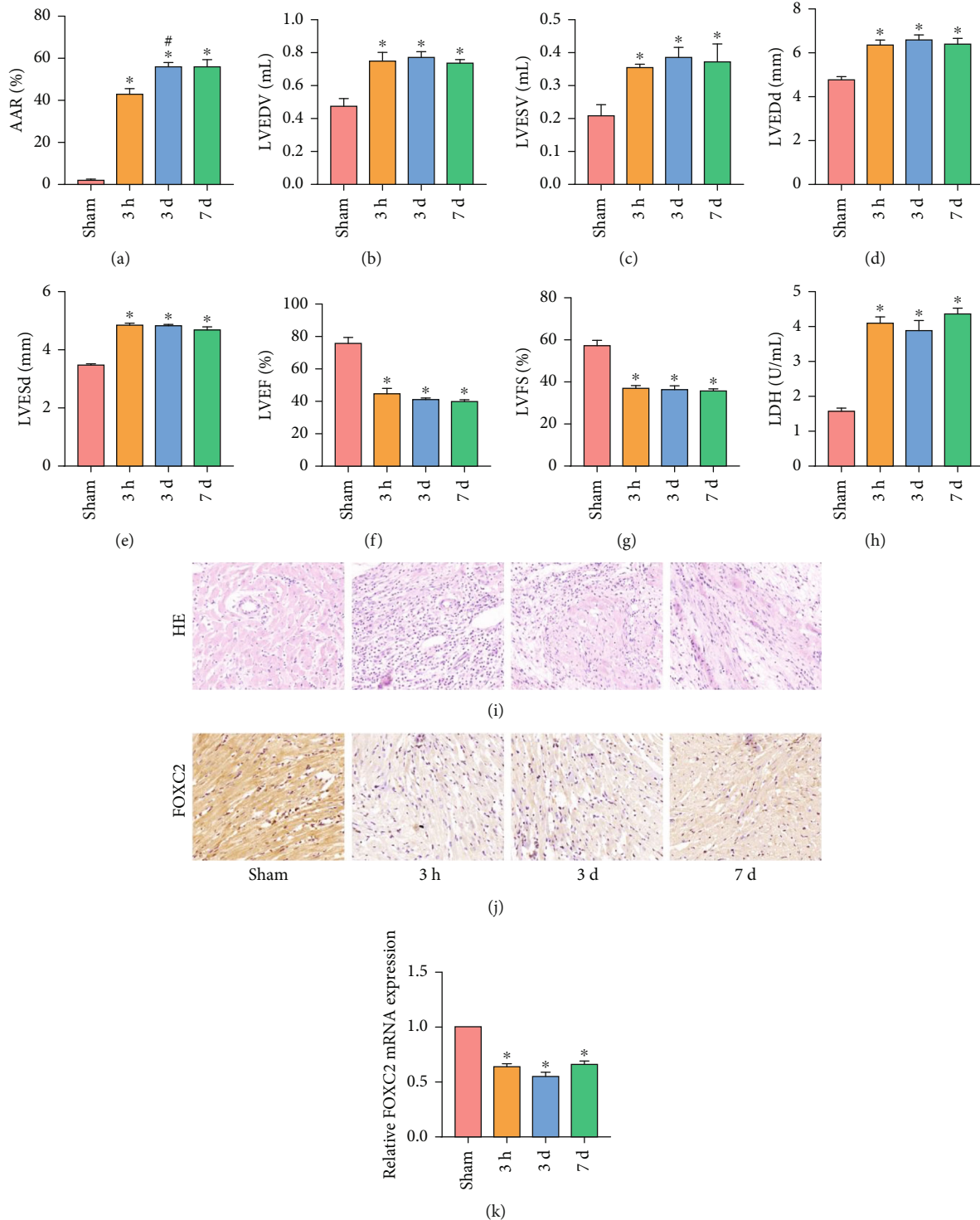


FIGURE 1: Expression of FOXC2 decreased in myocardial tissue after I/R. (a) AAR of rats; (B–G) cardiac function (LVEDV, LVESV, LVEDd, LVESd, LVEF, and LVFS) in rats; (h) LDH level of rat serum; (i) HE staining of rat myocardium (200x); (j) IHC staining results of FOXC2 expression of rat myocardium (200x); (k) mRNA expression of FOXC2 in rat myocardium (“*” means $P < 0.05$ vs. sham group; “#” means $P < 0.05$ vs. 3 d group).

of LDH was increased in the serum of the I/R rats (Figure 1(h)). The results of HE staining also showed that the structure of myocardial tissue of I/R rats was disordered (Figure 1(i)). These results indicated that the I/R model was

successfully established. We detected the FOXC2 in rat myocardial tissue by IHC staining (Figure 1(j)) and RT-PCR (Figure 1(k)). After I/R, the expression of FOXC2 mRNA and protein in rat myocardium was significantly reduced.

3.2. Overexpression of FOXC2 Reduced Inflammation and Oxidative Stress in I/R Rat Myocardium. To detect the effect of FOXC2 on MIRI, we used adenovirus to overexpress FOXC2 in rats. The rats with reperfusion for 3 hours showed significant myocardial injury, so we took the rats with reperfusion for 3 hours as the study object. The rats were divided into sham group, I/R group, I/R + negative control (NC) group, and I/R + FOXC2 group. Rats in the I/R + NC group and the I/R + FOXC2 group were injected with NC and FOXC2 overexpressing adenovirus from the tail vein one week before the I/R model was made. RT-PCR detected the expression of FOXC2 mRNA in rat myocardial tissue and found that FOXC2 adenovirus effectively increased the expression of FOXC2 in rat myocardial tissue (Figure 2(a)). We detected the degree of myocardial injury in rats by TTC staining (Figure 2(b)) and LDH (Figure 2(c)) measurement. After overexpressing FOXC2, AAR and LDH of rats were significantly reduced. We detected the expression of inflammatory factors IL-1 β and TNF- α in rat serum by ELISA (Figures 2(d) and 2(e)) and RT-PCR (Figures 2(f) and 2(g)). FOXC2 has been found to reduce inflammation level in rats. In addition, we determined the change of oxidative stress level in rat myocardial tissue by detecting the expression of superoxide dismutase (SOD)1/2 in myocardium. The results of RT-PCR (Figures 2(h) and 2(i)) and IHC staining (Figure 2(j)) showed that overexpression of FOXC2 effectively increased the expression of SOD1/2 in rat myocardium.

3.3. Overexpression of FOXC2 Alleviated H/R-Induced H9c2 Cell Injury by Promoting the Nuclear Factor-Erythroid 2-Related Factor 2 (Nrf2)/Heme Oxygenase (HO)-1 Signaling Pathway. We induced H9c2 cell injury through H/R and transfected cells with FOXC2 overexpression plasmid. RT-PCR results showed that FOXC2 overexpression plasmid significantly increased FOXC2 expression in H9c2 cells (Figure 3(a)). The CCK-8 assay detected the viability of H9c2 cells. The viability of H9c2 cells decreased significantly after H/R, and the overexpression of FOXC2 could increase the viability of H9c2 cells (Figure 3(b)). We examined the level of LDH in H9c2 cells and found that overexpression of FOXC2 can reduce the LDH level (Figure 3C). In addition, we examined the effect of FOXC2 on the level of oxidative stress in H9c2 cells. RT-PCR and IF staining found that FOXC2 can promote the expression of SOD1/2, Nrf2, and HO-1 in H9c2 cells (Figures 3(d)–3(h)).

3.4. Inhibition of Nrf2/HO-1 Signaling Pathway Attenuated the Protective Effect of FOXC2 on H9c2 Cells. In order to verify the mechanism of FOXC2 protecting myocardial cells, we used Nrf2/HO-1 signaling pathway inhibitor ML385 to treat H9c2 cells based on FOXC2 transfection. The results of IF staining showed that after treatment of H9c2 cells with ML385, the expression of SOD1/2 in H9c2 cells was reduced, indicating that the antioxidant capacity of the cells was reduced (Figure 4(a)). The CCK-8 assay also found that ML385 attenuated the promoting effect of FOXC2 on cell viability (Figure 4(b)). RT-PCR results also showed that

ML385 reduced the expression of SOD1/2 mRNA in H9c2 cells (Figures 4(c) and 4(d)).

4. Discussion

MIRI is the pathophysiological disorder that mainly occurs during the transition from the ischemic phase to the reperfusion phase [11]. The mechanism of MIRI has not been fully elucidated, but a large number of studies have shown that MIRI may be involved in excessively generated oxygen free radicals, cytoplasmic and mitochondrial calcium overload, endothelial cell dysfunction, inflammation, and myocardial necrosis and apoptosis [12–14]. FOXC2, as a multifunctional cytokine *in vivo*, was found to play an important role in MIRI [15]. We found that the expression of FOXC2 in the rat myocardium group after I/R was reduced. After using adenovirus to increase the expression of FOXC2 in rat myocardium, the activity of SOD1/2 in rat myocardium increased, and the expression of inflammatory factors decreased, indicating that FOXC2 can reduce the level of oxidative stress and inflammation in rats. After increasing the expression of FOXC2 in H9c2 cells by plasmid transfection, we also found that FOXC2 can relieve H/R-induced myocardial cells injury *in vitro*. FOXC2 has been found to activate the Nrf2/HO-1 signaling pathway, which may allow FOXC2 to protect myocardial cells.

Studies have shown that the inflammatory response is activated during the myocardial ischemia stage, and reperfusion further exacerbates the inflammatory response of the myocardium [16]. Inflammation mainly caused by neutrophil infiltration is one of the important mechanisms. In addition, a clinical study found that after revascularization of myocardial infarction, inflammatory factors in patients' serum including TNF- α , IL-1 β , IL-6, and IL-8 were significantly increased [17]. Niermann et al. [18] used oligophrenin1 to treat I/R rats and found that oligophrenin1 reduced myocardial cells apoptosis by regulating the inflammation level of myocardial tissue, thereby alleviating MIRI. Another study found that recombinant human IL-1 β receptor inhibitors can alleviate myocardial injury in I/R rats by inhibiting IL-1 β activity [19]. After treating I/R rats with FOXC2 overexpression adenovirus, we found that the expression of inflammatory factors in rat serum and myocardial tissue was significantly reduced through ELISA and RT-PCR.

Previous studies have shown that the imbalance between oxidation and antioxidation caused by myocardial ischemia can aggravate the damage of cardiac function and the degree of inflammatory response [20]. The increase of oxygen free radicals and the decrease of the activity of free radical scavenging enzymes are the direct causes of oxidative stress damage [21]. SOD, as a key enzyme for scavenging oxygen free radicals in the body, can directly reflect the level of oxygen free radicals in the body [22]. Sedova et al. [23] examined the level of oxidative stress in I/R rats and found that SOD activity in I/R rats was significantly lower than that in normal rats. After the treatment of rats with the antioxidant melatonin, the cardiac function of the rats was significantly improved. Loo et al. [24] found that oxidative damage to

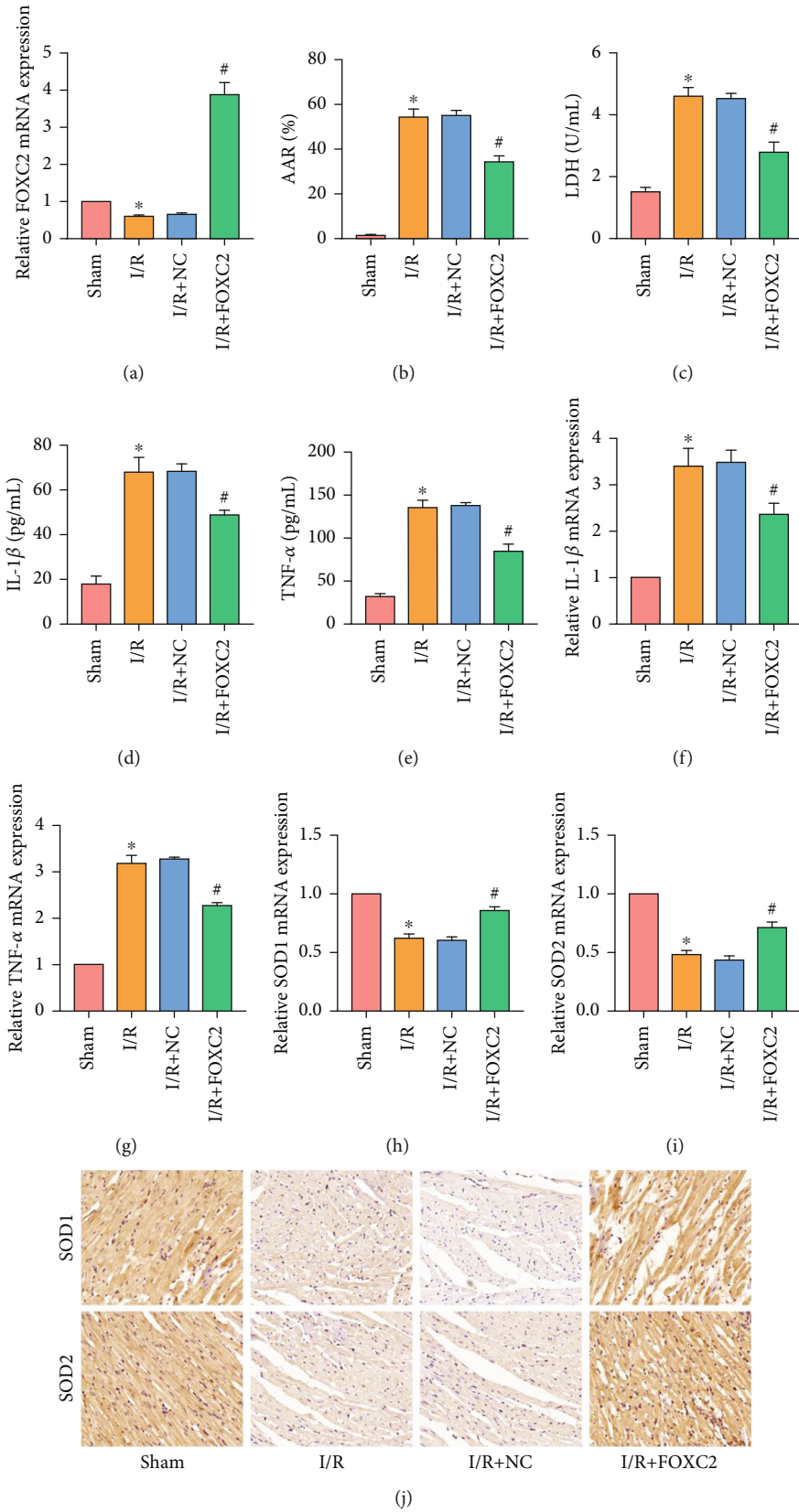


FIGURE 2: Overexpression of FOXC2 reduced inflammation and oxidative stress in I/R rat myocardium. (a) mRNA expression of FOXC2 in rat myocardium; (b) AAR of rats; (c) LDH level of rat serum; (d, e) ELISA results of IL-1 β and TNF- α in rat serum; (f-i) mRNA expression of IL-1 β , TNF- α , SOD1, and SOD2 in rat myocardium. (j) IHC staining results of SOD1/2 expression of rat myocardium (200x) (“*” means $P < 0.05$ vs. sham group; “#” means $P < 0.05$ vs. I/R+NC group).

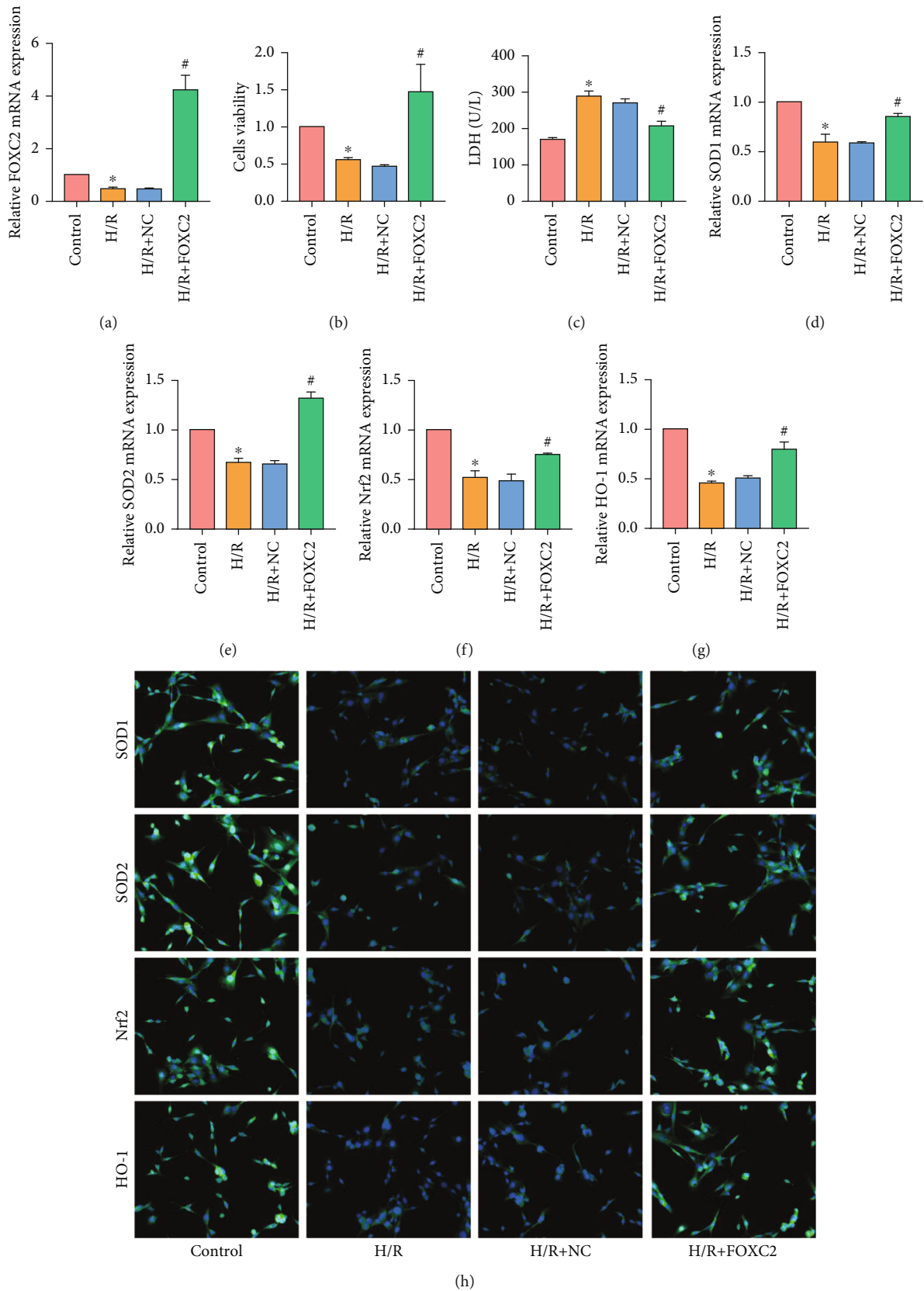


FIGURE 3: Overexpression of FOXC2 alleviated H/R-induced H9c2 cell injury by promoting the Nrf2/HO-1 signaling pathway. (a) mRNA expression of FOXC2 in H9c2 cells; (b) CCK-8 assay results of H9c2 cells; (c) LDH level of H9c2 cells; (d-g) mRNA expression of SOD1/2, Nrf2, and HO-1 in H9c2 cells; (h) IF staining results of SOD1/2, Nrf2, and HO-1 in H9c2 cells (200x) (“**”) means $P < 0.05$ vs. control group; “#” means $P < 0.05$ vs. H/R+NC group).

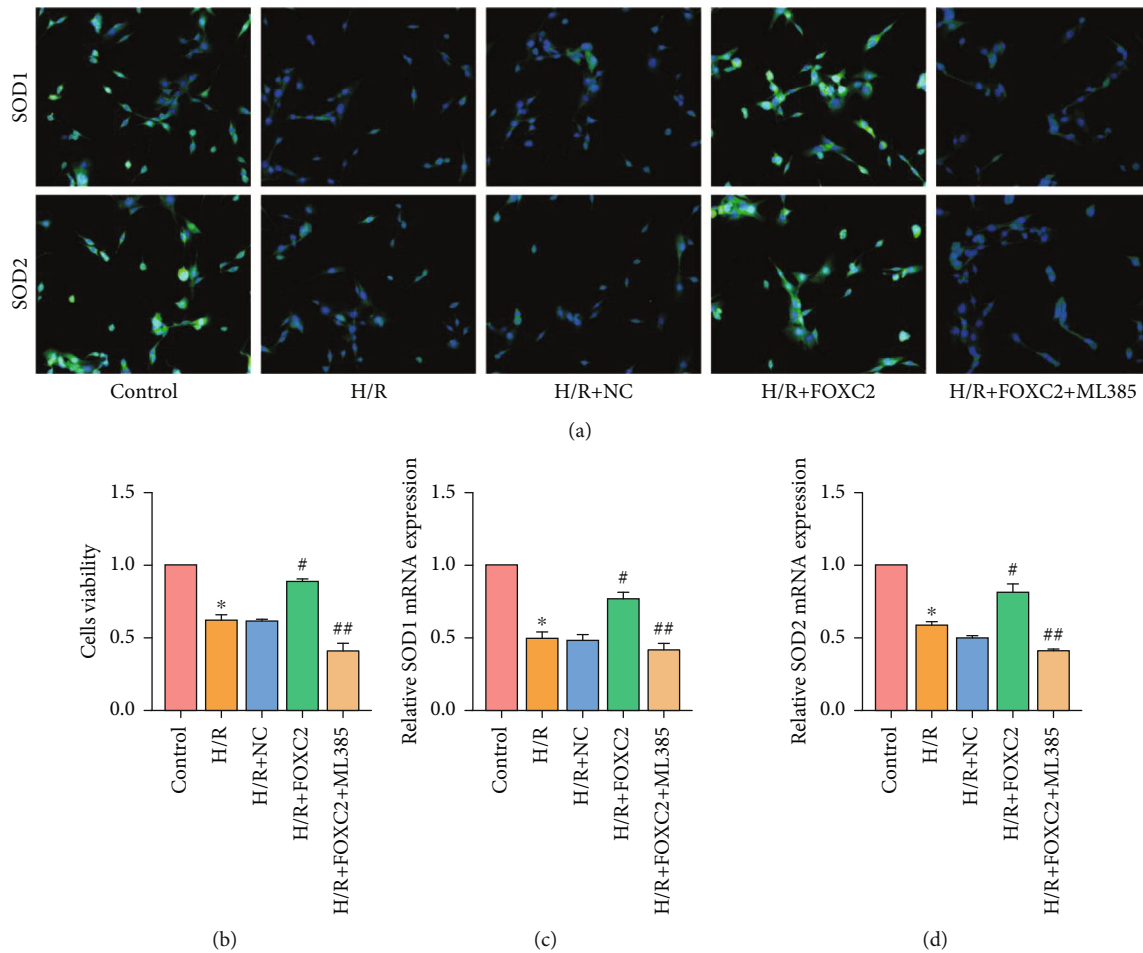


FIGURE 4: Inhibition of Nrf2/HO-1 signaling pathway attenuated the protective effect of FOXC2 on H9c2 cells. (a) IF staining results of SOD1/2 in H9c2 cells (200x); (b) CCK-8 assay results of H9c2 cells; (c, d) mRNA expression of SOD1/2 in H9c2 cells (“*” means $P < 0.05$ vs. control group; “#” means $P < 0.05$ vs. H/R+NC group; “##” means $P < 0.05$ vs. H/R+FOXC2 group).

mitochondria is an important factor in cell death of MIRI. Mitochondria in ischemic myocardial cells produce reactive oxygen species through Bax/Bak-independent pathways, triggering mPTP activation, mitochondrial depolarization, and cell death. The FOXC family has been found to alleviate oxidative damage in rat models of chronic obstructive pulmonary disease [25]. FOXC2 has also been found to be related to oxidative stress-related pathways in cancer research [26]. We detected the expression of SOD1/2 in rat myocardial tissue and H9c2 cells by IHC staining and RT-PCR and found that FOXC2 can promote the activity of SOD1/2, thereby improving the antioxidant capacity of cardiomyocytes. Nrf2/HO-1 is an important pathway for the body to resist oxidative stress. When oxidative stress occurs in the body, the Nrf2 gene is activated and transcribed, which initiates the expression of downstream antioxidant proteins, oxidases, and phase II detoxification enzymes [27]. We found that FOXC2 can promote the expression of Nrf2 and HO-1 in H9c2 cells, and Nrf2/HO-1 signaling pathway inhibitor ML385 attenuated the protective effect of FOXC2 on H9c2 cells, suggesting that the activation of Nrf2/HO-1 may be an important mechanism by which FOXC2 protected myocardial cells. To our knowledge, this

is the first study to investigate the effect of FOXC2 on MIRI. We hope to provide new targets for clinical MIRI treatment through this study.

5. Conclusions

After I/R, the expression of FOXC2 in the myocardium of rats was significantly reduced. Overexpression of FOXC2 reduced the level of inflammation and oxidative stress in myocardial tissue. In addition, FOXC2 promoted the activity of Nrf2/HO-1 signaling pathway in myocardial cells, and the inhibition of Nrf2/HO-1 signaling pathway attenuated the protective effect of FOXC2 on myocardial cells, indicating that FOXC2 alleviated MIRI by regulating the Nrf2/HO-1 pathway.

Data Availability

The datasets used and analyzed during the current study are available from the corresponding author on reasonable request.

Conflicts of Interest

The authors declared no conflict of interest.

References

- [1] G. W. Reed, J. E. Rossi, and C. P. Cannon, "Acute myocardial infarction," *Lancet*, vol. 389, no. 10065, pp. 197–210, 2017.
- [2] M. Hartman, H. E. Groot, I. M. Leach, J. C. Karper, and P. van der Harst, "Translational overview of cytokine inhibition in acute myocardial infarction and chronic heart failure," *Trends in Cardiovascular Medicine*, vol. 28, no. 6, pp. 369–379, 2018.
- [3] I. M. Seropian, C. Sonnino, B. W. Van Tassel, L. M. Biasucci, and A. Abbate, "Inflammatory markers in ST-elevation acute myocardial infarction," *European Heart Journal Acute Cardiovascular Care*, vol. 5, no. 4, pp. 382–395, 2016.
- [4] J. B. Cabello, A. Burls, J. I. Emparanza, S. E. Bayliss, T. Quinn, and Cochrane Heart Group, "Oxygen therapy for acute myocardial infarction," *Cochrane Database of Systematic Reviews*, vol. 2016, no. 12, p. D7160, 2016.
- [5] M. Castaneda, L. Chen, L. Pradhan et al., "A forkhead box protein C2 inhibitor: targeting epithelial–mesenchymal transition and cancer metastasis," *Chembiochem*, vol. 19, no. 13, pp. 1359–1364, 2018.
- [6] Y. Shimoda, Y. Ubukata, T. Handa et al., "High expression of forkhead box protein C2 is associated with aggressive phenotypes and poor prognosis in clinical hepatocellular carcinoma," *BMC Cancer*, vol. 18, no. 1, p. ???, 2018.
- [7] L. Yang, T. Li, and L. Zha, "Foxc2 alleviates ox-LDL-induced lipid accumulation, inflammation, and apoptosis of macrophage via regulating the expression of Angptl2," *Inflammation*, vol. 43, no. 4, pp. 1397–1410, 2020.
- [8] P. Zhou, Y. Li, R. di et al., "H19 and Foxc2 synergistically promotes osteogenic differentiation of BMSCs via Wnt- β -catenin pathway," *Journal of Cellular Physiology*, vol. 234, no. 8, pp. 13799–13806, 2019.
- [9] T. Kume, H. Jiang, J. M. Topczewska, and B. L. Hogan, "The murine winged helix transcription factors, Foxc1 and Foxc2, are both required for cardiovascular development and somitogenesis," *Genes & Development*, vol. 15, no. 18, pp. 2470–2482, 2001.
- [10] M. Yang, D. Y. Kong, and J. C. Chen, "Inhibition of miR-148b ameliorates myocardial ischemia/reperfusion injury via regulation of Wnt/ β -catenin signaling pathway," *Journal of Cellular Physiology*, vol. 234, no. 10, pp. 17757–17766, 2019.
- [11] Y. Shen, X. Liu, J. Shi, and X. Wu, "Involvement of Nrf2 in myocardial ischemia and reperfusion injury," *International Journal of Biological Macromolecules*, vol. 125, pp. 496–502, 2019.
- [12] H. J. Chi, M. L. Chen, X. C. Yang et al., "Progress in therapies for myocardial ischemia reperfusion injury," *Current Drug Targets*, vol. 18, no. 15, pp. 1712–1721, 2017.
- [13] S. Sanada, I. Komuro, and M. Kitakaze, "Pathophysiology of myocardial reperfusion injury: preconditioning, postconditioning, and translational aspects of protective measures," *American Journal of Physiology. Heart and Circulatory Physiology*, vol. 301, no. 5, pp. 1723–1741, 2011.
- [14] H. M. Piper, K. Meuter, and C. Schäfer, "Cellular mechanisms of ischemia-reperfusion injury," *The Annals of Thoracic Surgery*, vol. 75, no. 2, pp. S644–S648, 2003.
- [15] D. Nilsson, M. Heglind, Z. Arani, and S. Enerback, "Foxc2 is essential for podocyte function," *Physiological Reports*, vol. 7, no. 9, article e14083, 2019.
- [16] N. J. Pluijmer, M. C. den Haan, V. L. van Zuylen et al., "Hypercholesterolemia affects cardiac function, infarct size and inflammation in APOE*3-Leiden mice following myocardial ischemia-reperfusion injury," *PLoS One*, vol. 14, no. 6, article e217582, 2019.
- [17] J. C. Tardif, S. Kouz, D. D. Waters et al., "Efficacy and safety of low-dose colchicine after myocardial infarction," *The New England Journal of Medicine*, vol. 381, no. 26, pp. 2497–2505, 2019.
- [18] C. Niermann, S. Gorressen, M. Klier et al., "Oligophrenin1 protects mice against myocardial ischemia and reperfusion injury by modulating inflammation and myocardial apoptosis," *Cellular Signalling*, vol. 28, no. 8, pp. 967–978, 2016.
- [19] A. Varma, A. Das, N. N. Hoke, D. E. Durrant, F. N. Salloum, and R. C. Kukreja, "Anti-inflammatory and cardioprotective effects of tadalafil in diabetic mice," *PLoS One*, vol. 7, no. 9, article e45243, 2012.
- [20] S. Al-Salam and S. Hashmi, "Myocardial ischemia reperfusion injury: apoptotic, inflammatory and oxidative stress role of galectin-3," *Cellular Physiology and Biochemistry*, vol. 50, no. 3, pp. 1123–1139, 2018.
- [21] S. B. Ansari and G. A. Kurian, "Hydrogen sulfide modulates sub-cellular susceptibility to oxidative stress induced by myocardial ischemic reperfusion injury," *Chemico-Biological Interactions*, vol. 252, pp. 28–35, 2016.
- [22] M. Hao and R. Liu, "Molecular mechanism of CAT and SOD activity change under MPA-CdTe quantum dots induced oxidative stress in the mouse primary hepatocytes," *Spectrochimica Acta. Part A, Molecular and Biomolecular Spectroscopy*, vol. 220, article 117104, 2019.
- [23] K. A. Sedova, O. G. Bernikova, J. I. Cuprova et al., "Association between antiarrhythmic, electrophysiological, and antioxidative effects of melatonin in ischemia/reperfusion," *International Journal of Molecular Sciences*, vol. 20, no. 24, p. 6331, 2019.
- [24] G. Loor, J. Kondapalli, H. Iwase et al., "Mitochondrial oxidant stress triggers cell death in simulated ischemia-reperfusion," *Biochimica et Biophysica Acta*, vol. 1813, no. 7, pp. 1382–1394, 2011.
- [25] S. Xia, J. Qu, H. Jia et al., "Overexpression of forkhead box C1 attenuates oxidative stress, inflammation and apoptosis in chronic obstructive pulmonary disease," *Life Sciences*, vol. 216, pp. 75–84, 2019.
- [26] K. M. Hargadon, B. Györffy, E. W. Strong et al., "The FOXC2 transcription factor promotes melanoma outgrowth and regulates expression of genes associated with drug resistance and interferon responsiveness," *Cancer Genomics Proteomics*, vol. 16, no. 6, pp. 491–503, 2019.
- [27] J. S. Kang, L. B. Nam, O. K. Yoo, and Y. S. Keum, "Molecular mechanisms and systemic targeting of NRF2 dysregulation in cancer," *Biochemical Pharmacology*, vol. 177, article 114002, 2020.